



**HAL**  
open science

# Rôle du compartiment stromal et des macrophages dans le cancer du pancréas

Kevin Thierry

► **To cite this version:**

Kevin Thierry. Rôle du compartiment stromal et des macrophages dans le cancer du pancréas. Immunology. Université Claude Bernard - Lyon I, 2023. English. NNT : 2023LYO10228 . tel-04792836

**HAL Id: tel-04792836**

**<https://theses.hal.science/tel-04792836v1>**

Submitted on 20 Nov 2024

**HAL** is a multi-disciplinary open access archive for the deposit and dissemination of scientific research documents, whether they are published or not. The documents may come from teaching and research institutions in France or abroad, or from public or private research centers.

L'archive ouverte pluridisciplinaire **HAL**, est destinée au dépôt et à la diffusion de documents scientifiques de niveau recherche, publiés ou non, émanant des établissements d'enseignement et de recherche français ou étrangers, des laboratoires publics ou privés.

**THESE de DOCTORAT DE  
L'UNIVERSITE CLAUDE BERNARD LYON 1**

**Ecole Doctorale N° 340  
Biologie Moléculaire, Intégrative et Cellulaire**

**Discipline : Immunologie**

Soutenue publiquement le 21/11/2023, par :

**Kevin THIERRY**

---

**The role of the stromal compartment  
and macrophages in pancreatic cancer**

---

Devant le jury composé de :

Pr. VALCOURT Ulrich	Professeur des Universités Lyon	Président
Dr. TOMASINI Richard	Directeur de Recherche Inserm Marseille	Rapporteur
Dr. MILLET Arnaud	Chargé de Recherche Inserm Grenoble	Rapporteur
Dr. SALMON Hélène	Chargé de Recherche Inserm Paris	Examinatrice
Pr. BALKWILL Frances	Professeur des Universités Londres	Examinatrice
Dr. CASANOVA-ACEBES Maria	Chercheur Madrid	Examinatrice
Dr. WALZER Thierry	Directeur de Recherche Inserm Lyon	Examineur
Dr. HENNINO Ana	Chargé de Recherche Inserm Lyon	Directrice de thèse





# TABLE OF CONTENT

TABLE OF CONTENT	4
ACKNOWLEDGEMENTS	8
RESUME DE LA THESE	11
ABSTRACT	12
FIGURE LIST	13
I. Introduction and conclusion	13
II. Results	14
A. Pericyte stem cells induce Ly6G <sup>+</sup> cell accumulation and immunotherapy resistance in pancreatic cancer	14
a. Figure	14
b. Supplementary figure	14
i. Expanded View (EV)	14
ii. Appendix	15
B. CD169 <sup>+</sup> macrophages orchestrate immune reaction and matrix deposition in pancreatic cancer.	15
a. Figure	15
b. Supplementary figure	15
LIST OF ABBREVIATIONS	16
INTRODUCTION	22
I. Pancreatic ductal adenocarcinoma (PDAC)	22
A. Pancreatic cancers : State of the art	22
a. Pancreas structure and function	22
b. Pancreatic cancer epidemiology	22
c. Clinical features	23
d. Current treatments	25
B. Pathophysiology of PDAC	26
a. Genetical abnormalities and classification	26
C. Early development of PDAC	31
a. Acinar to ductal metaplasia (ADM) : a tipping point	31
b. Pancreatic intraepithelial neoplasia	34
II. PDAC is both a stromal and immune disease	34
A. The close relationship between the tumor microenvironment and cancer cells	34

a.	Tumor microenvironment keystones: the concepts of “ <i>seed and soil</i> ” and “ <i>a wound that do not heal</i> ”.	34
b.	Cancer-associated fibroblasts in PDAC	36
i.	Origins	36
ii.	CAFs subtypes and functions	39
iii.	CAFs targeting	43
c.	The stroma	46
i.	Collagen	46
ii.	Hyaluronic acid	47
iii.	$\beta$ ig-h3	48
iv.	Fibronectin	51
v.	Mechanical forces	51
B.	The immune system in PDAC	53
a.	Introduction	53
b.	The actors of the immune system in PDAC	56
i.	Good and bad immunity	56
ii.	T lymphocytes	56
iii.	B Lymphocytes	59
iv.	Myeloid-derived suppressor cells	60
c.	Immune escape mechanisms in PDAC	60
i.	Priming and T cells trafficking	60
ii.	Effector T cells inhibition	61
d.	Current immunotherapy status in PDAC	62
i.	Immune ckeckpoint based strategy	62
ii.	Adoptive transfer immunotherapy	63
III.	Macrophages are the pillars of the pancreatic TME	66
A.	Macrophages development and maintenance	66
a.	Introduction	66
b.	Macrophages development and maintenance	66
i.	Mononuclear Phagocyte System	66
ii.	Embryonic origin of tissue-resident macrophages	68
iii.	Colony-stimulating-factor as a key regulator of macrophages development	71
B.	Role of tumor associated macrophages in PDAC	72
a.	“M1” vs “M2” macrophages... and beyond !	72

b.	Exploring TAMs and MDSCs functions in the context of cancer and wound healing	74
i.	Introduction	74
ii.	Inflammation	74
iii.	Tissue remodelling	75
iv.	Injury resolution	76
c.	Macrophages based therapies.	79
i.	Introduction	79
ii.	Recruitment	79
iii.	Survival and reprogramming	80
iv.	Phagocytosis	80
v.	Cellular therapy	81
C.	CD169 <sup>+</sup> macrophages	84
a.	Introduction	84
i.	CD169 macrophage function in non-cancerous condition	84
b.	Emerging role of intra tumoral CD169 <sup>+</sup> macrophages in cancer	87
i.	Pro-tumoral role	87
ii.	Anti-tumoral role	88
	OBJECTIVES	91
	RESULTS	92
I.	Pericyte stem cells induce Ly6G <sup>+</sup> cell accumulation and immunotherapy resistance in pancreatic cancer	92
II.	CD169 <sup>+</sup> macrophages orchestrate immune reaction and matrix deposition in pancreatic cancer.	138
A.	Summary	140
B.	Material and methods	141
C.	Introduction	147
D.	Results	148
E.	Discussion	153
F.	Figure legend	155
G.	Figure	158
H.	Supplementary figure	168
I.	References	172
III.	Stiffness-induced cancer-associated fibroblasts are responsible for immunosuppression in a PDGF ligand-dependent manner	175
	DISCUSSION	214

I. The discovery of CD169 <sup>+</sup> and PeSC in PDAC	214
II. The Janus-faced of PDAC stroma	217
III. Personalized medicine in pancreatic cancer	221
CONCLUSION	224
Appendices	225
A. Posters	225
B. Oral Presentations	225
C. List of publications	226
a. Published manuscript	226
b. Submitted manuscript	226
c. Published abstract	226
D. Participant paper results	226
REFERENCES	243

# ACKNOWLEDGEMENTS

I spent more than 20 years building the scientist that I am today by meeting people and professors who impacted my choices and mindset. While our career paths took different directions many years ago, I would like to thank all the professors who transferred their knowledge and guided me. Although this signals the end of my graduate studies, I hope that I'll never stop learning new concepts, skills, and beyond throughout my life and career.

First, I would like to express my deepest appreciation to all the members of my PhD committee: Prof. BALKWILL Frances, Dr. CASANOVA-ACEBES Maria, Dr. MILLET Arnaud, Dr. SALMON H  l  ne, Dr. TOMASINI Richard, Prof. VALCOURT Ulrich, and Dr. WALZER Thierry. You have influenced the exact content of this thesis, and I am grateful and honored for your presence at my PhD defense.

I would also like to highlight the two members of my monitoring PhD committee: Prof. VALCOURT Ulrich and Prof. LAWRENCE Toby. You followed my work from the very beginning and provided me with the tools to overcome difficulties and doubts. Your comments were always constructive and well-received.

Anca, it's been more than 4 years since I joined you in this adventure! What started as a 2-month internship ended up in a PhD thesis. Who would have thought? I cannot express my gratitude enough for your unfailing support in making this PhD project possible. I believe you are the most optimistic person I have ever met, both in life and science. I might take some of your optimism for the future, haha! I couldn't have asked for a better PhD mentor than you: open-minded, kind, and dynamic. You always found a way to spark my interest, and I enjoyed spending time with you discussing science and other topics. Your love for immunology and fundamental knowledge impressed me, and I am deeply grateful for your trust. I hope that I have acquired some of your resilience and creativity. I wish you many more years of success in both life and science.

Sophie, I know that you were not excited when you were told that another master student was arriving! Despite that, you taught me many technical skills without which I couldn't have completed my project. One day, you told me not to give up on an experiment, and you were right! Despite being far from the best in mathematics and the wet lab, you showed impressive patience, and I am grateful for that! I also thank you for the many laughs we shared during lunchtime and in the lab!

Zhichong, we shared an office for three years, but we also travelled all the way to Japan together ! I thank you for your many advice about my project and my PhD. I was always impressed by your ability to stay motivated and produce high standard science despite being far from your family. I enjoyed spending time with you talking about both Chinese and French culture. I really hope you enjoyed your PhD in France and your "Tour de France" despite the Covid-19 situation and 我与你稍后再见在上海!

Pia, I thank you for your expertise and insightful advice in flow cytometry! Your rigor and organizational skills were exemplary for me. I wish that I could have learned German with you!

Melissa, I appreciate the many hours you spent with me during in vivo experiments! You taught me a lot, and I hope that I also shared some of my knowledge with you. I'm afraid that I won't be available anymore to set up the flow cytometer after my PhD, but I am confident that you will develop a love for flow cytometry by the end of your PhD. With your skills and mindset, I am certain that you will succeed in both your PhD and your career. I wish you good luck for the remaining years of your PhD—hold on to it!

Louis-Antoine, I won't go so far as to say you were a "Bol d'air frais," but you provided me with six excellent months that were more than needed! You were an outstanding master's degree intern—highly motivated and kind. I trusted you and discovered many shared passions. I hope I successfully conveyed to you what a PhD entails. Over time, you became a friend. I wish for you the experience of witnessing your favorite driver's victory one day. Well, if only it were that simple. At least you have a cap from him!

I also want to thank all present and old members of our group that evolved through time ; Tiffanie, Clémentine, Philippe, Marie, Gerald, Audrey, Moitza and Hélène. Despite not being in my group of research, many people in the institute directly or indirectly helped me to go through this PhD ; Trang, Ivan, Clara, Enzo, Quentin, Léa and both Olivier, Saidi, Chloé, Meigge, Delphine, Valentin and finally and special thanks to Dr. DUMONTET Charles, Dr. JORDHEIM Lars Petter for your input during lab meeting as team leader.

Maman, Papa, Aurélie. Je vous remercie infiniment pour votre patience et votre compréhension. Je vous remercie pour le soutien sans faille dont vous m'avez fait preuve dès le 1er jour de mes études jusqu'à la fin de cette thèse. Cette thèse et ces 8 années d'études ont été signe de beaucoup de sacrifice qui j'espère font de moi un fils et un frère dont vous êtes fière.

All PhD student or PhD graduate will tell you that having a relationship while doing a PhD is not possible or extremely challenging. Well... I want to write some word for a person who supported me for the past 5 years in everything I did in my daily life but also in my professional choices, Morgane. You are a pillar of this PhD thesis, your insight and feedback were always valuable. You succeeded to help me manage my effort during what was a marathon ! I cannot remember the countless time you asked me at what time I was leaving the lab. I am grateful for your immense patience seeing me working late and weekends. My mind was always occupied, and you knew it but accepted it. The tiny things in life can become big, it represents what you did during my PhD ; helping me to think about something else or making me laugh during bad times. I know that it was 3 very long years. We managed to build our relationship despite my PhD, and I am extremely lucky to have you. I love you and I am excited for the years to come with you. You and I against the rest of the world.

# RESUME DE LA THESE

L'adénocarcinome canalaire pancréatique est associé à une réaction stromale très importante puisqu'elle représente jusqu'à 90% du volume tumoral. La contribution du stroma tumoral à l'évolution du cancer a été décrite ces dernières années à la fois chez l'Homme et chez la souris en l'identifiant comme un nouvel acteur important dans l'initiation et la progression néoplasique.

L'activation des cellules du stroma ainsi que le recrutement des cellules immunitaires contribuent à l'immunosuppression et à la résistance au thérapie dans le cancer du pancréas portant le taux de survie sur 5 ans à moins de 10%. Parmi les cellules immunitaires les plus importantes se trouvent les macrophages et les lymphocytes T CD8. L'objectif principal de cette étude est de déterminer le rôle de la communication entre le compartiment stromal et les macrophages ainsi que les conséquences sur la réponse immunitaire antitumoral dans le cancer du pancréas. La première partie de cette thèse a permis l'identification d'une population stromale ayant des caractéristiques de type souche et pericytaire appelé "Pericyte Stem Cell" PeSC. Nous montrons que cette populations permet d'induire une résistance au traitement anti-PD-1 via le recrutement de cellules immunitaires myéloïdes suppressive. Dans une deuxième partie, nous montrons qu'une sous population de macrophages présente dans l'environnement tumoral, les macrophages CD169<sup>+</sup>, peuvent être différenciés par les PeSC à la fois *in vivo* et *in vitro*. Enfin, nous montrons que les macrophages CD169<sup>+</sup> sont nécessaires au recrutement des lymphocytes T CD8<sup>+</sup> au sein de l'environnement tumoral mais sont également nécessaire à la mise en place de la complexité stromale. Enfin, dans la troisième partie de cette étude, nous montrons que la rigidité tissulaire peut induire une communication entre les cellules cancéreuses et les fibroblastes de manière dépendante de la signalisation PDGF. Pour terminer, nous montrons pour la première fois que cibler cette signalisation permet de réduire l'agressivité de la tumeur.

**Mots clefs :** Adénocarcinome canalaire pancréatique, Macrophages, Stroma, Microenvironnement tumoral, Fibroblaste associées au cancer

# ABSTRACT

Pancreatic ductal adenocarcinoma is characterized by a substantial stromal reaction, constituting as much as 90% of the tumor volume. Recent years witnessed the elucidation of the tumor stroma's contribution to the advancement of cancer in both human and murine contexts, pinpointing it as a significant novel participant in the initiation and evolution of neoplastic processes. The activation of stromal cells and the recruitment of immune cells collectively foster immunosuppression and resistance to therapeutic interventions in pancreatic cancer, leading to a 5-year survival rate below 10%. Since macrophages and CD8<sup>+</sup> T lymphocytes emerge as pivotal constituents among the immune cells, the principal aim of this research is to ascertain the interplay between the stromal compartment and macrophages. In the first part of this thesis discerned a stromal population displaying stem-like attributes and pericyte traits, called Pericyte Stem Cells (PeSC). We showcase the capacity of this population to support tumor progression but also to confer resistance to anti-PD-1 treatment through the recruitment of suppressive myeloid immune cells. In the second part, we illustrate that CD169<sup>+</sup> macrophages are present in both human and murine pancreatic tumor microenvironment. We show that CD169<sup>+</sup> macrophages can be differentiated by PeSC both in vivo and in vitro contexts. Lastly, we underscore the indispensability of CD169<sup>+</sup> macrophages for the recruitment of CD8<sup>+</sup> T lymphocytes into the tumor milieu, in addition to their pivotal role in establishing the complexity of stromal architecture. In the third part, we show that the tissue stiffness to influence fibroblast phenotype and function. We show that during cancer cell expansion, they secrete PDGF-AA ligand that is captured by fibroblasts. This communication leads to fibroblast differentiation with increased extracellular matrix protein deposition properties leading to modified anti-tumoral immune response, leading to a reduction tumor microenvironment complexity.

To conclude, this thesis provides a comprehensive exploration of the distinct roles played by individual stromal components in pancreatic cancer, unveiling a plethora of interconnected communications among these elements during the progression of the disease.

**Key words** : Pancreatic Adenocarcinoma, Macrophages, Stroma, Tumor microenvironment  
Microenvironnement tumoral, Cancer-associated Fibroblast

# FIGURE LIST

## I. Introduction and conclusion

Figure 1. Survival rates of different cancers.	23
Figure 2. Cancer patient timeline.	25
Figure 3. Pancreatic cancer treatment diagram.	26
Figure 4. Pancreatic cancer development.	28
Figure 5. Pancreatic cancer classification according to transcriptomic data.	30
Figure 6. Acinar to ductal metaplasia in different pancreatic context.	33
Figure 7. Cancer-associated fibroblast ontogeny in pancreatic cancer.	38
Figure 8. CAFs development and heterogeneity.	40
Figure 9. $\beta$ ig-h3 structure	49
Figure 10. $\beta$ ig-h3 in pancreas pathology.	50
Figure 11. 3e hypothesis in pancreatic cancer	54
Figure 12. Cancer-immunity cycle applied to pancreatic cancer.	55
Figure 13. Immune checkpoint summary	57
Figure 14. Mononuclear Phagocyte System.	68
Figure 15. Embryonic origin of macrophages	70
Figure 16. Macrophages polarization concept.	73
Figure 17. Macrophages orchestrate wound healing like process in pancreatic cancer.	79
Figure 18. CD169 <sup>+</sup> role in spleen and lymph-node.	86
Figure 19. Effect of CD169 <sup>+</sup> macrophages on cancer progression in human.	90
Figure 20. Determinant parameters of stroma role in PDAC	219
Figure 21. Personalized medicine to treat PDAC	223

## II. Results

### A. Pericyte stem cells induce Ly6G<sup>+</sup> cell accumulation and immunotherapy resistance in pancreatic cancer

#### a. Figure

Result I Fig.1 The CD106<sup>+</sup> population is uniquely localized in pancreatic injury and precancerous lesions.

Result I Fig.2 Single-cell RNAseq analysis reveals a cell population distinct from the PanIN signature population.

Result I Fig.3 The CD106<sup>+</sup> population shares pericyte, stem cell and stromal features.

Result I Fig.4 Stem properties of PeSCs and their impact on tumor cell proliferation on vessel formation.

Result I Fig.5 In vivo injection of PeSCs in the context of epithelial tumors induce Ly6G<sup>+</sup> MDSCs in the microenvironment.

Result I Fig.6 Tumor-PeSCs crosstalk induces Ly6G<sup>+</sup> MDSC differentiation.

Result I Fig.7 PeSCs drive PD-1 resistance in the tumor microenvironment.

#### b. Supplementary figure

##### i. Expanded View (EV)

Result I Fig. EV1 The CD106<sup>+</sup> population is uniquely localized in pancreatic injury and precancerous lesions.

Result I Fig. EV2 PeSC signature in human cancer single-cell data.

Result I Fig. EV3 Chimera approach identifies the origin of PeSC.

Result I Fig. EV3 Chimera approach identifies the origin of PeSC.

Result I Fig. EV4 Stem properties of PeSCs and their impact on tumor cells.

Result I Fig. EV5 Tumor-PeSC crosstalk affects the immune system.

ii. Appendix

Result I Appendix Fig.S1 The CD106<sup>+</sup> population is uniquely localized in pancreatic injury and precancerous lesions.

Result I Appendix Fig.S2 Gating strategy for FACS sorting and single cell RNAseq.

Result I Appendix Fig.S3 Generation of the PeSC line and its phenotype.

Result I Appendix Fig.S4 Single cell analysis reveals a distinct cluster 7 with PeSC signature.

Result I Appendix Fig.S5 Tumor-PeSC crosstalk affects the immune system.

Result I Appendix Fig.S6 In vivo depletion of Ly6G<sup>+</sup> MDSCs diminishes tumor growth

Result I Appendix Fig.S7 Interaction of CD106<sup>+</sup> PeSCs with CD11b<sup>+</sup> myeloid stem cells in the neoplastic microenvironment of PDAC

B. CD169<sup>+</sup> macrophages orchestrate immune reaction and matrix deposition in pancreatic cancer.

a. Figure

Result II Fig. 1 CD169 <sup>+</sup> macrophages are expressed in both human and mouse pancreatic cancer	158
Result II Fig. 2 Pericyte stem cells potentiate CD169 expression on macrophages <i>in vitro</i> .	159
Result II Fig. 3 $\beta$ ig-h3 secreted by macrophages activate PeSC to attract and inhibit CD8 <sup>+</sup> T cells.	160
Result II Fig. 4 Depletion of CD169 <sup>+</sup> macrophages inhibit CD8 <sup>+</sup> T cell recruitment in the tumor microenvironment.	161
Result II Fig. 5 Depletion of CD169 <sup>+</sup> macrophages reshape the extracellular matrix in the tumor microenvironment.	162
Result II Fig. 6 CD169 <sup>+</sup> macrophages allow collagen deposition and architecture	163
Result II Fig. 7 CD169 <sup>+</sup> macrophages structure the fibrotic response in PDAC	165

b. Supplementary figure

Result II supplementary Fig. 1 CD169 <sup>+</sup> macrophages are expressed in both human and mouse pancreatic cancer	168
Result II supplementary Fig. 3 $\beta$ ig-h3 secreted by macrophages activate PeSC to attract and inhibit CD8 <sup>+</sup> T cells.	169
Result II supplementary Fig. 4 Depletion of CD169 <sup>+</sup> macrophages inhibit CD8 <sup>+</sup> T cell recruitment in the tumor microenvironment.	170
Result II supplementary Fig. 5 Depletion of CD169 <sup>+</sup> macrophages reshape the extracellular matrix in the tumor microenvironment.	171

## LIST OF ABBREVIATIONS

<b>ADM</b>	Acinar to Ductal Metaplasia	<b>CAR-M</b>	Chimeric Antigen Receptor macrophage
<b>Acvr1b</b>	Activin receptor type-1B	<b>CAR-T Cells</b>	Chimeric Antigen Receptor T Cells
<b>ADCC</b>	antibody-dependant cellular cytotoxicity	<b>Cav1</b>	Caveolin 1
<b>ADCP</b>	antibody-dependent cellular phagocytosis	<b>CCL2,8</b>	C-C Motif Chemokine Ligand 2,8
<b>ADEX</b>	Aberrantly Differentiated Endocrine Exocrine	<b>CCR2,5</b>	C-C chemokine receptor type 2,5
<b>apCAFs</b>	Antigen Presenting Cancer-Associated Fibroblasts	<b>CDKN2A</b>	Cyclin-Dependent Kinase Inhibitor 2A
<b>APCs</b>	Antigen Presenting Cells	<b>CDPs</b>	Common Dendritic Cell Progenitors
<b>aPSC</b>	Activated Pancreatic Stellate Cells	<b>ClT</b>	Clinical trial
<b>ATRA</b>	All-Trans Retinoic Acid	<b>cMoPs</b>	Common Monocyte Progenitors
<b>BCR</b>	B cells-cell receptor	<b>CMsPs</b>	Common Myeloid Progenitors
<b>Bregs</b>	Regulatory B cells	<b>CNS</b>	Central nervous system
<b>BTK</b>	Bruton's Tyrosine Kinase	<b>CR</b>	Complete response
<b>CA19-9</b>	Cancer Antigen 19-9	<b>CRD</b>	Cysteine Rich Domain
<b>CAFs</b>	Cancer-Associated Fibroblasts	<b>CSF1/2 (R)</b>	Colony-Stimulating Factor 1/2 (Receptor)

<b>CT</b>	Central region	<b>Fabp4</b>	Fatty Acid-Binding Protein 4
<b>CTLA4</b>	Cytotoxic T-Lymphocyte-Associated Protein 4	<b>FAK</b>	Focal Adhesion Kinase
<b>CXCL1/8/12/14/16</b>	CXC motif chemokine ligand 1/8/12/14/16	<b>FAP</b>	Fibroblast Activated Protein
<b>CXCR7</b>	CXC chemokine receptor 7	<b>FL</b>	Fetal Liver
<b>DAMPs</b>	Damage-Associated Molecular Patterns	<b>FOXP3</b>	Forkhead Box P3
<b>DCs</b>	Dendritic cells	<b>Gas6</b>	Growth Arrest-Specific Gene 6
<b>DDR1</b>	Discoidin domain receptor 1	<b>GBM</b>	Glioblastoma
<b>Dpp4</b>	Dipeptidyl Peptidase-4	<b>GFAP</b>	Glial Fibrillary Acidic Protein
<b>DPT</b>	Dermatopontin	<b>Gli1</b>	GLI Family Zinc Finger 1
<b>DTR</b>	Diphtheria Toxin Receptor	<b>GM-CSF</b>	Granulocyte-Macrophage Colony-Stimulating Factor
<b>ECM</b>	Extracellular Matrix	<b>GMPs</b>	Granulocyte-Macrophage Progenitors
<b>EGF</b>	Epidermal Growth Factor	<b>Gpm6a</b>	Glycoprotein M6A
<b>EMPs</b>	Erythro-Myeloid Precursors	<b>HA</b>	Hyaluronic Acid
<b>EMT</b>	Epithelial-Mesenchymal Transition	<b>HCC</b>	Hepatocellular carcinoma
<b>ENG</b>	Endoglin	<b>HER2</b>	Human Epidermal Growth Factor Receptor-2

<b>HNC</b>	Head and Neck Cancer	<b>Klf4</b>	Kruppel-Like Factor 4
<b>Hoxb6</b>	Homeobox B6	<b>Kras</b>	Kirsten Rat Sarcoma Viral Oncogene Homolog
<b>HSCs</b>	Hematopoietic Stem Cells	<b>Lgals7</b>	Galectin 7
<b>iCAFs</b>	Inflammatory Cancer- Associated Fibroblasts	<b>LIF</b>	Leukaemia Inhibitory Factor
<b>ICAM1</b>	Intercellular adhesion molecule 1	<b>LN</b>	Lymph nodes
<b>ICI</b>	Immune Checkpoint Inhibitors	<b>LOX (1/2)</b>	Lysyl Oxidase (1/2)
<b>IFP</b>	Interstitial Fluid Pressure	<b>LPS</b>	Lipopolysaccharides
<b>IFN(<math>\gamma</math>)</b>	Interferon (gamma)	<b>LRRC15</b>	Leucine Rich Repeat Containing 15
<b>Igf1</b>	Insulin-Like Growth Factor One	<b>Lrrn4</b>	Leucine Rich Repeat Neuronal 4
<b>Igfbp4</b>	Insulin-Like Growth Factor Binding Protein 4	<b>Lyve1</b>	Lymphatic vessel endothelial hyaluronan receptor 1
<b>IM</b>	Invasive margin	<b>MAPK</b>	Mitogen-Activated Protein Kinase
<b>iNKT</b>	Invariant Natural Killer T	<b>MCN</b>	Mucinous Cystic Neoplasm
<b>iNOS</b>	Nitric oxide synthase	<b>MDPs</b>	Macrophage and Dendritic Cell Precursors
<b>IPMN</b>	Intraductal Papillary Mucinous Neoplasm	<b>MDSCs</b>	Myeloid Derived Suppressor Cells
<b>JAK-STAT</b>	Janus kinase-signal transducer and activator of transcription	<b>MEPs</b>	Megakaryocyte and Erythrocyte Progenitors

<b>MHC- (I-II)</b>	Major Histocompatibility Complex I or II	<b>PAMPs</b>	Pathogen-Associated Molecular Patterns
<b>MMP11</b>	Matrix Metalloproteinase 11	<b>PanIN</b>	Pancreatic Intraepithelial Neoplasia
<b>MMPs</b>	Matrix Metalloproteinases	<b>PD-1</b>	Programmed Cell Death Protein 1
<b>MPS</b>	Mononuclear Phagocyte System	<b>PDAC</b>	Pancreatic Ductal Adenocarcinoma
<b>Msln</b>	Mesothelin	<b>pDCs</b>	Plasmacytoid DCs
<b>MUC16</b>	Mucin-16	<b>PDGF-BB</b>	Platelet-Derived Growth Factor-BB
<b>myCAFs</b>	Myofibroblastic Cancer-Associated Fibroblasts	<b>PDGFRa</b>	Platelet-Derived Growth Factor Receptor
<b>MYL9</b>	Myosin Light Chain 9	<b>PDK1</b>	Phosphoinositide-Dependent Kinase 1
<b>N/A</b>	Non-applicable	<b>PD-L1</b>	Programmed Cell Death Ligand 1
<b>Nab-Pac</b>	Nab-Paclitaxel	<b>PDPN</b>	Podoplanin
<b>NO</b>	Nitric oxide	<b>PDX1</b>	Pancreatic and Duodenal Homeobox 1
<b>Nfkb</b>	nuclear factor-kappa B	<b>p-ERK</b>	Phosphorylated Extracellular Signal-Regulated Kinase
<b>NK</b>	Natural Killer	<b>Pi16</b>	Peptidase Inhibitor 16
<b>Nr5a2</b>	Nuclear Receptor Subfamily 5, Group A, Member 2	<b>PI3K(γ)</b>	Phosphoinositide 3-Kinase gamma
<b>Notch</b>	Neurogenic locus notch homolog		
<b>OP/OP</b>	Osteopetrotic		

<b>POSTN</b>	Periostin	<b>SOX9</b>	SRY (Sex-Determining Region Y)-Box 9
<b>PR</b>	Partial response		
<b>Pre-macs</b>	Pre-Macrophages	<b>USP18</b>	Ubiquitin specific peptidase 18
<b>PSCs</b>	Pancreatic Stellate Cells	<b>TAGLN</b>	Transgelin
<b>PTF1a</b>	Pancreas Transcription Factor 1 Alpha	<b>TAMs</b>	Tumor-Associated Macrophages
<b>Ptn</b>	Pleiotrophin	<b>T-bet</b>	T-Box Expressed in T Cells
<b>qPSC</b>	Quiescent Pancreatic Stellate Cells	<b>TCR</b>	T-cell receptor
<b>RAS</b>	Rat sarcoma virus	<b>CD8<sup>+</sup> T<sub>eff</sub></b>	CD8 <sup>+</sup> Effector T Cells
<b>ROCK</b>	Rho-Associated Coiled Coil-Containing Protein Kinase	<b>TERT</b>	Telomerase Reverse Transcriptase
<b>RORGT</b>	RAR-Related Orphan Receptor Gamma	<b>CD8<sup>+</sup> T<sub>ex</sub></b>	Exhausted CD8 <sup>+</sup> T Cells
<b>SAA3</b>	serum amyloid A3	<b>TF</b>	Transcription Factor
<b>SARS-CoV-2</b>	Severe acute respiratory syndrome coronavirus 2	<b>TGF<math>\alpha</math></b>	Transforming Growth Factor Alpha
<b>SCS</b>	Subcapsular Sinus	<b>TGF<math>\beta</math></b>	Transforming Growth Factor beta
<b>SH</b>	Sonic Hedgehog	<b>TGF<math>\beta</math>-i</b>	TGF- $\beta$ -Induced
<b>SIGLEC-1</b>	Sialic acid-binding immunoglobulin-like lectin-1	<b>Th</b>	Thelper
<b>SMAD (2,3,4)</b>	SMAD Family Member 2,3 or 4	<b>Thbd</b>	Thrombomodulin
<b>SMO</b>	Smoothened	<b>TLS</b>	Tertiary lymphoid structure
		<b>TME</b>	Tumor Microenvironment

<b>TNF</b>	Tumor necrosis factor	<b>Vim</b>	Vimentin
<b>TP53</b>	Tumor Protein 53	<b>VSV</b>	Vesicular Stomatitis Virus
<b>Tregs</b>	Regulatory T Cells	<b>YS</b>	Yolk Sac
<b>VCAM1</b>	Vascular cell adhesion molecule 1	<b>ZEB1</b>	Zinc finger E-box- binding homeobox 1
<b>VEGFR</b>	Vascular Endothelial Growth Factor	<b>αSMA</b>	Alpha Smooth Muscle Actin

# INTRODUCTION

## I. Pancreatic ductal adenocarcinoma (PDAC)

### A. Pancreatic cancers : State of the art

#### a. Pancreas structure and function

The pancreas is a mixed gland composed of exocrine and endocrine compartments. The exocrine compartment is composed of acinar and ductal cells organized in acini and ductal structures. The exocrine component of the pancreas is responsible for producing essential enzymes that are vital for the process of digestion.

The endocrine component of the pancreas consists of Langerhans islets that produce and release important hormones into the bloodstream. The main hormones secreted by the endocrine gland in the pancreas are insulin and glucagon, which regulate the level of glucose in the blood, and somatostatin, which prevents the release of the other two hormones.

#### b. Pancreatic cancer epidemiology

Cancers are a major public health problem both internationally and nationally. According to the latest data from the International Agency for Research on Cancer, the incidence of cancer (the number of new cases diagnosed each year) is estimated to be more than 19 million, highlighting the importance of these diseases. Cancers are responsible of almost 10 million deaths per year (Sung et al., 2021). The World Health Organisation estimates that these numbers will double by 2040. In France, 433 000 patients were diagnosed with cancer in 2023 which represents a twofold increase compared to 1990.

Pancreatic cancer is a multifactorial and heterogeneous type of disease characterized by the uncontrolled and aberrant proliferation of cells due to dysregulation of cellular processes. The majority of pancreatic cancer (95%) affects the exocrine compartment, while neuroendocrine cancer represents only 5%. Throughout this thesis, I will solely refer to PDAC unless mentioned otherwise. PDAC is among

the deadliest cancers, with a five-year survival rate between 5% to 10% (Figure 1). According to GLOBOCAN 2020, almost half a million cases of PDAC worldwide were registered in 2020, with a corresponding high mortality rate among patients (Sung et al., 2021). The incidence of PDAC is higher in developed countries (Sung et al., 2021). PDAC is expected to become the second deadliest cancer behind lung cancer by 2024 in the United States (Rahib et al., 2021). Factors associated with PDAC development are intrinsic ((e.g., genetic factors such as Peutz-Jeghers and Lynch syndrome) (Benzel and Fendrich, 2018), age) and extrinsic factors (alcohol and tobacco, chronic pancreatitis).

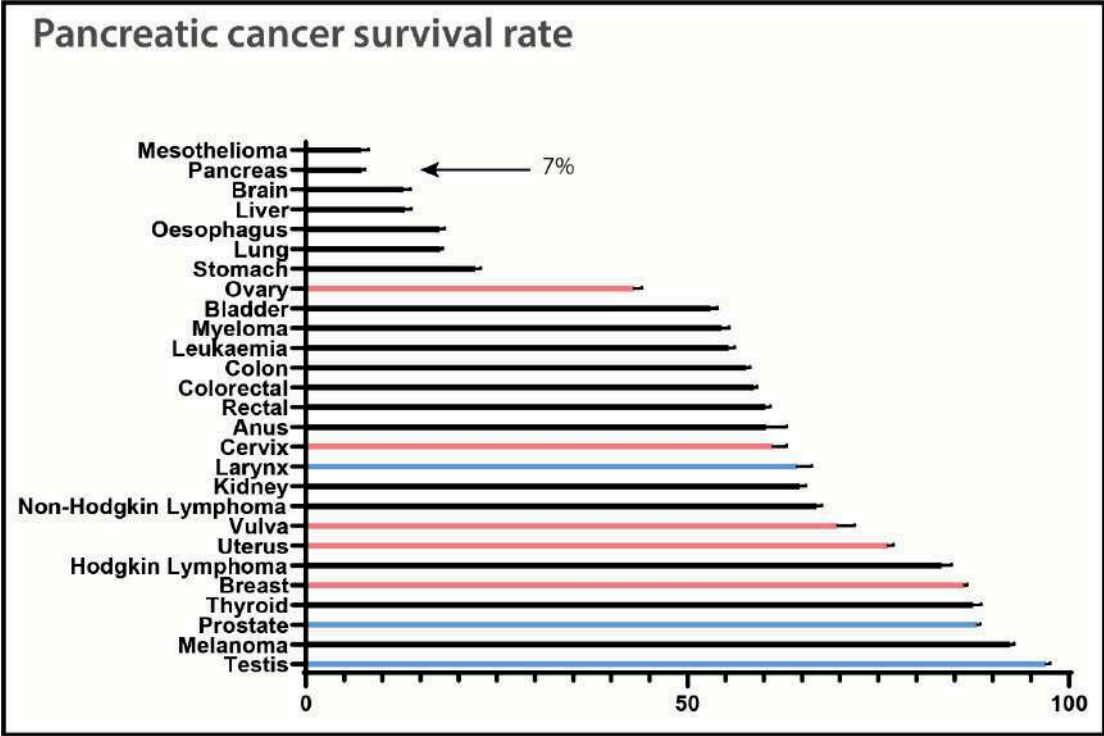


Figure 1 Survival rates of different cancers.

5-year cancer survival estimates for adults (aged 15-99 years) in England diagnosed between 2014 and 2018 and followed up to 2019. Black - All sexes, Pink - Female only, Blue - Male only. Source: Public Health England.

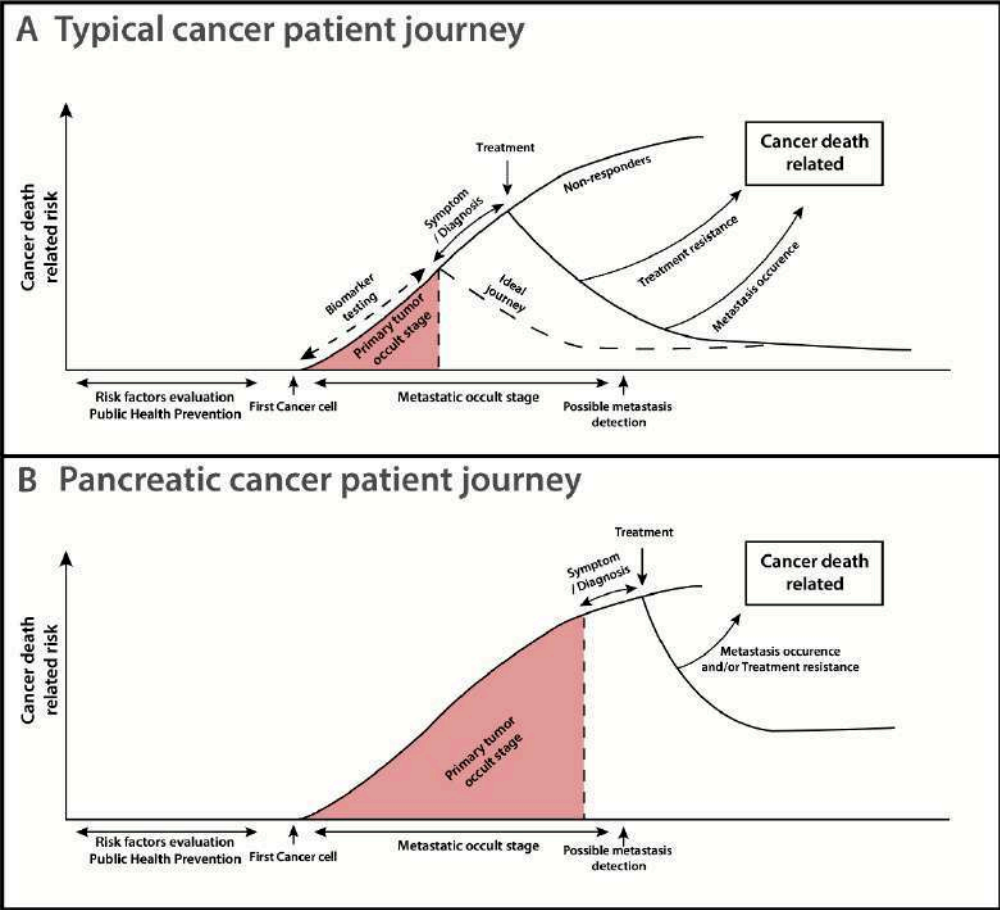
c. Clinical features

According to the American Cancer Society, the typical age of diagnosis for PDAC is 72 years old. The age at diagnosis plays a critical role in survival, as patients between 20 and 40 years old have a survival rate almost three times higher than those older than 40 (Wang et al., 2020).+

Furthermore, the survival rate of patients significantly declines with the advancement of the disease stage. The Surveillance, Epidemiology, and End Results database from the National Cancer Institute categorizes PDAC into three stages: localized, regional, and distant. The 5-year survival rate for localized PDAC patients is 44%. For regional PDAC patients, the rate drops to 15%, while for those with

distant (metastatic) PDAC, the survival rate falls to 3% over a 5-year period. This particularity distinguishes PDAC from other cancers that can be detected through clinical manifestation or imaging.

Due to the lack of obvious clinical symptoms, PDAC diagnosis is usually made at an already advanced metastatic stage. Another particularity of PDAC is that there are currently no biomarkers that would predict the disease. The most prominent biomarker in PDAC is Cancer Antigen 19-9 (CA19-9), which is released by tumor cells. It has been shown that CA19-9 could be detected 2 years before clinical symptoms (Fahrman et al., 2021). The specificity of CA19-9 has been reported to be around 80% (Ballehaninna and Chamberlain, 2012). The American Health Institutes underline that general screening of the population is not a solution, given the lack of specificity of such a biomarker. More importantly, it was recently shown in a pivotal study that most human individuals harbor pre-cancerous lesions that do not progress into invasive tumors (Carpenter et al., 2023). A solution for the lack of specificity is to screen only high-risk patients



(Legend next-page)

## Figure 2 Cancer patient timeline.

A The general population is subject to preventive measures before cancer initiation (e.g., smoke-free campaigns). Biomarkers can be tested before and during the primary tumor silent stage. This phase is the timeframe when the primary tumor is not detectable by conventional imaging and/or is not associated with clinical symptoms. Ideally, cancer should be detected as soon as possible to reduce the risk of cancer-related death. When a patient is treated, there are four different outcomes: non-responders, partial response but show resistance, partial response but show metastasis, and complete response. There is a metastatic silent phase in which the patient can respond to the treatment but given the necessary time for a secondary tumor to grow, some patients show metastasis years after treatment and/or complete response. B In pancreatic cancer, the primary tumor silent stage is longer, meaning that the tumor is already advanced when clinical symptoms appear. As a consequence, pancreatic cancer is often metastatic, as the primary tumor silent phase is almost as long as the metastatic silent phase, resulting in a higher risk of cancer-related death. The primary tumor silent stage sets the difficulty for pancreatic cancer patient diagnosis and early treatment.

### d. Current treatments

At diagnosis, PDAC is divided into three different categories: resectable, borderline resectable, and advanced (**Figure 3**). Resectable PDAC represents a localized tumor type not spreading nearby blood vessels or other organs. Patients with resectable PDAC are eligible for surgery, but they represent only 20% of diagnosed patients (**Figure 3**). Borderline resectable and advanced tumors are tumors with cancer cells spread in organs nearby arteries and in other organs. These two categories represent 80% of patients (**Figure 3**). Patients with borderline resectable tumors undergo neo-adjuvant therapy, which consists of a treatment (Chemotherapy and/or radiotherapy (RT)) that will shrink the tumor to make it resectable. It has been reported that patients have a better survival rate after tumor resection (Cloyd et al., 2017).

Although resection shows a better survival rate than chemotherapeutic agents, it was reported that around 75% of a 700-patients cohort showed metastatic recurrence in the liver or in the lung 1 year after pancreatectomy, indicating an active metastatic phase (Groot et al., 2018). If the tumor is not resectable, patients undergo palliative chemotherapy (FOLFIRINOX, Gemcitabine (Gem), paclitaxel) (Conroy et al., 2011) (Von Hoff et al., 2013) (**Figure 3**).

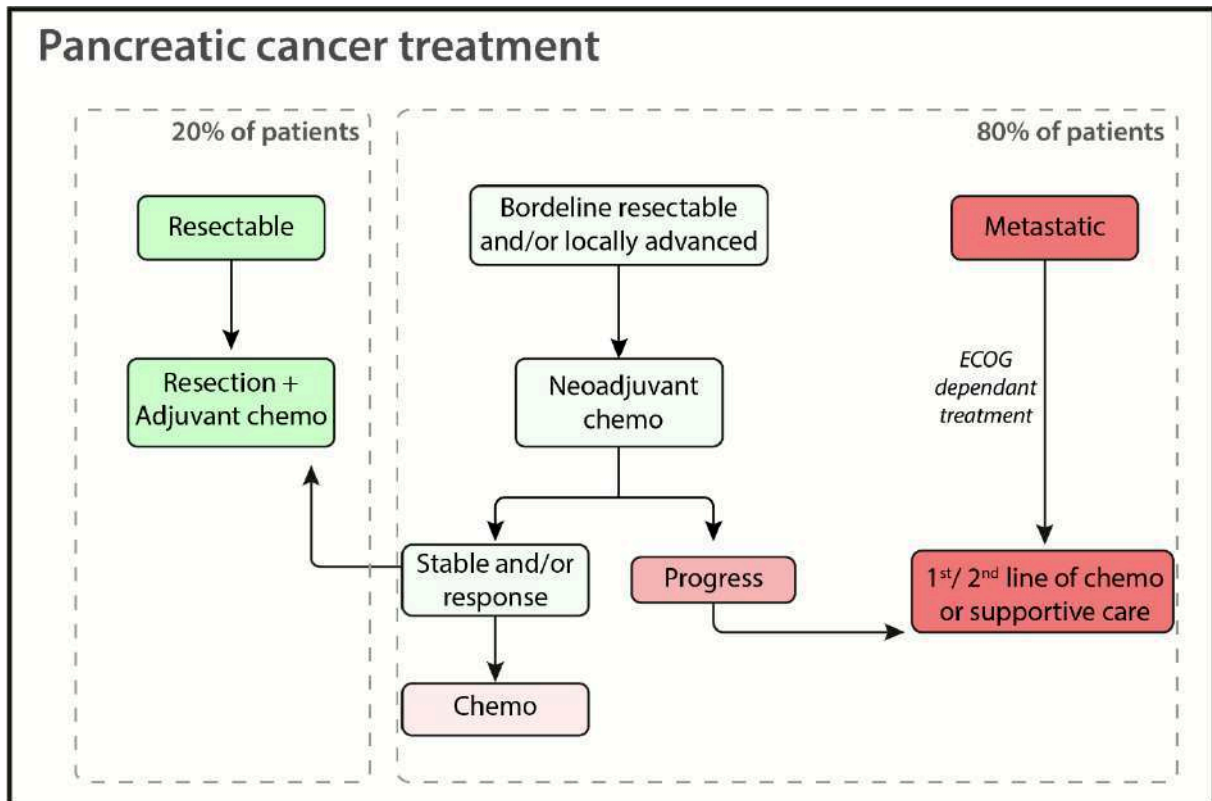


**Figure 3. Pancreatic cancer treatment diagram.**

20% of patients undergo surgery to have a tumor resection. 80% of patients have borderline resectable/locally advanced or metastatic pancreatic cancer. In the case of successful neoadjuvant therapy, the patients can undergo tumor resection. Green indicates good prognosis, and red indicates a bad prognosis.

## B. Pathophysiology of PDAC

### a. Genetical abnormalities and classification

PDAC displays the 14 different hallmarks of cancer described over the years (Hanahan, 2022; Hanahan and Weinberg, 2011, 2000) : genome instability and mutation, resistance to cell death, cellular metabolism dysregulation, phenotypic plasticity, sustained proliferation, growth suppression escape, epigenetic reprogramming, immune escape, replicative immortality, tumor-promoting inflammation, polymorphic microbiomes, invasiveness, angiogenesis. Indeed, although PDAC is characterized by a relatively lower number of mutations per megabase compared to other types of cancers. (Bruni et al., 2020), These mutations have been extensively described. There are four different driver mutations that directly contribute to cell malignant behavior: Kirsten Rat Sarcoma Viral Oncogene Homolog (KRAS), Cyclin-Dependent Kinase Inhibitor 2A (CDKN2A), Tumor Protein 53 (TP53), and SMAD Family Member 4 (SMAD4) (**Figure 4**). These mutations are at the basis of the genetically engineered mice recapitulating human pathology (**Table 1**).

**Table 1.**

Name	Promotor	Mutation	Lesions	Survival	Reference
KC	<i>p48</i>	<i>Kras</i> <sup>G12D</sup>	Neoplastic in 4 weeks	>1year	(Hingorani et al., 2003)
KIC	<i>Pdx1</i>	<i>Kras</i> <sup>G12D</sup> , <i>Ink4a/Arf</i> <sup>flox/flox</sup>	Cancer in 5 weeks	2 m	(Aguirre et al., 2003)
KPC	<i>Pdx1</i>	<i>Kras</i> <sup>G12D</sup> , <i>TP53</i> <sup>R172H</sup>	Cancer in 16 weeks	5m	(Hingorani et al., 2005)
4KC	<i>p48</i>	<i>Kras</i> <sup>G12D</sup> , <i>Acvr1b</i> <sup>flox/flox</sup>	Neoplastic in 3 weeks	6 m	(Ripoche et al., 2013)

This table is not exhaustive: KC, KIC, KPC are the most used model for PDAC. 4KC is a model developed in our group. Acvr1b Activin receptor type-1B, m Months.

Rat sarcoma virus (RAS) proteins are GTPases that allow the activation of downstream signaling for cell proliferation. Specifically, KRAS gene mutation is present in 90% of PDAC patients due to Single Nucleotide Variations, mostly G12D and G12V. It is important to note that mutation of KRAS alone is not sufficient to develop a malignant tumor. Additional loss of the CDKN2A gene (homozygous deletion) leads to the transformation of neoplasia into a tumor. This gene codes for both P16 and P14arf, which regulate the cell cycle as tumor suppressor proteins. TP53, an essential actor in DNA repair and apoptosis of abnormal cells, is also lost in 80% of PDAC patients (Figure 4). This loss triggers the transformation of neoplastic cells into cancer cells. Finally, SMAD4 (a downstream protein of transforming growth factor-beta (TGFβ) signaling) alteration occurs in 50% of cases.

However, PDAC is not only caused by intrinsic factors alone. KRAS mutation allows the transition from chronic pancreatitis (i.e., inflammation of the pancreas) to PDAC in mice. It is important to note that although embryonic *Kras* mutation leads to 50% of PDAC 12 months after birth, it does not lead to any PDAC lesions when *Kras* is mutated in adult mice (Guerra et al., 2007). Inducible activation of *Kras* in adult mice leads to cancer lesions only in conjunction with pancreatitis (Guerra et al., 2007). This study highlights the limitations of widely used mouse models, as the cellular kinetics of pancreatic cell transformation differ from those in humans, given that the vast majority of KRAS mutations in humans occur during adulthood.

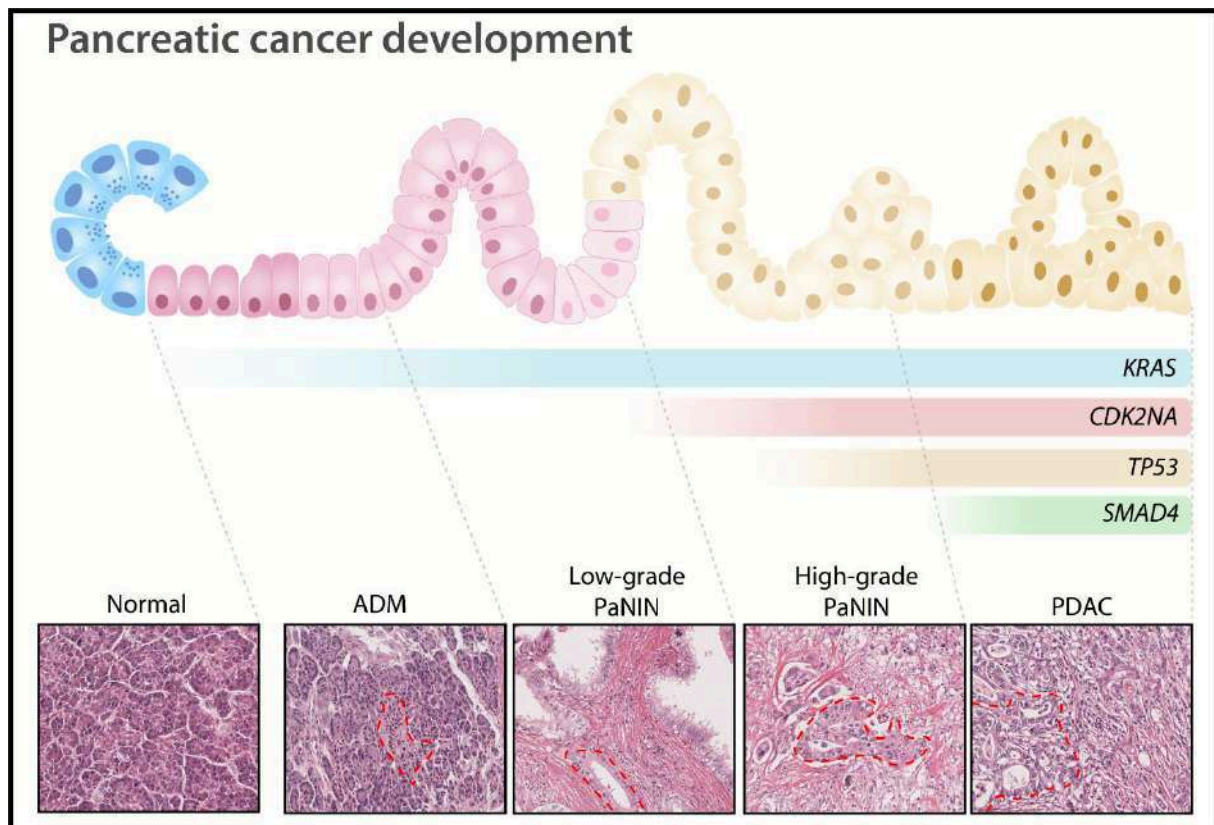


**Figure 4. Pancreatic cancer development.**

Pancreatic cancer is a multistep disease that mainly derives from acinar cells becoming ductal-like cells through acinar to ductal metaplasia. The main driver mutation is *Kras*, but accumulation of cell cycle mutations later in the disease (*CDK2NA* or *TP53*) leads to adenocarcinoma lesions. Hematoxylin and eosin staining of human tissue sections show the different stages of human pancreatic cancer.

PDAC has been categorized into several subtypes based on various parameters and technological approaches (**Figure 5**). One such classification, conducted by Bailey and colleagues identified four distinct subtypes through bulk transcriptomic analysis (Bailey et al., 2016) :

- squamous subtype: characterized by an inflammatory, hypoxic, and  $TGF\beta$  pathway signature.
- pancreatic progenitor subtype: associated with the upregulation of a set of pancreatic lineage genes mutation, such as Pancreatic and Duodenal Homeobox 1 (*PDX1*) or Motor Neuron And Pancreas Homeobox 1 (*MNX1*), related to the exocrine compartment.
- Aberrantly Differentiated Endocrine Exocrine (ADEX) subtype: defined by a gene network important in the late development of pancreatic tumor progenitors.
- immunogenic subtype: linked to an immune infiltration of  $CD4^+$ ,  $CD8^+$  T cells and B cells.

Additionally, other classifications have been described by Collisson and Moffitt including classical (adhesion and epithelial genes), basal (mesenchymal genes), and exocrine (high digestive enzyme) subtypes (Collisson et al., 2011; Moffitt et al., 2015). However, the ADEX subtype's validity was

challenged since. Recent data suggest that previous classifications were biased by normal tissue contamination taken into account in the analysis (Hwang et al., 2022; Puleo et al., 2018). To address the complexity of PDAC subtype, a more integrated classification based on both tumoral, and stromal components was established in a study involving over 300 patients, resulting in the following subtypes (**Figure 5**):

- pure classical subtype: characterized by a well-differentiated tumor, low cellular infiltration, and a good prognosis.
- immune classical subtype: dominated by infiltration of T and B cells.
- desmoplastic subtype: exhibiting immune cell and fibroblast infiltration.
- stroma activated subtype: featuring low immune infiltration but high fibroblast infiltration.
- pure-basal-like subtype: consisting of poorly differentiated tumors with low immune cell presence and a poor prognosis.

More recently, both molecular specificities were considered using spatial transcriptomics (Williams et al., 2023). The existence of classical and basal subtypes was confirmed, but most patients exhibited heterogeneity between classical and basal subtypes, referred to as "mixed," which correlated with an intermediate survival rate. Furthermore, cancer cells can transition between classical, mixed, and basal subtypes. Additionally, it was demonstrated that small biopsies yielded results consistent with larger tissue sections, suggesting the potential diagnostic utility of these methods (Williams et al., 2023). For a summarized overview of all PDAC classifications, refer to **Figure 5**.

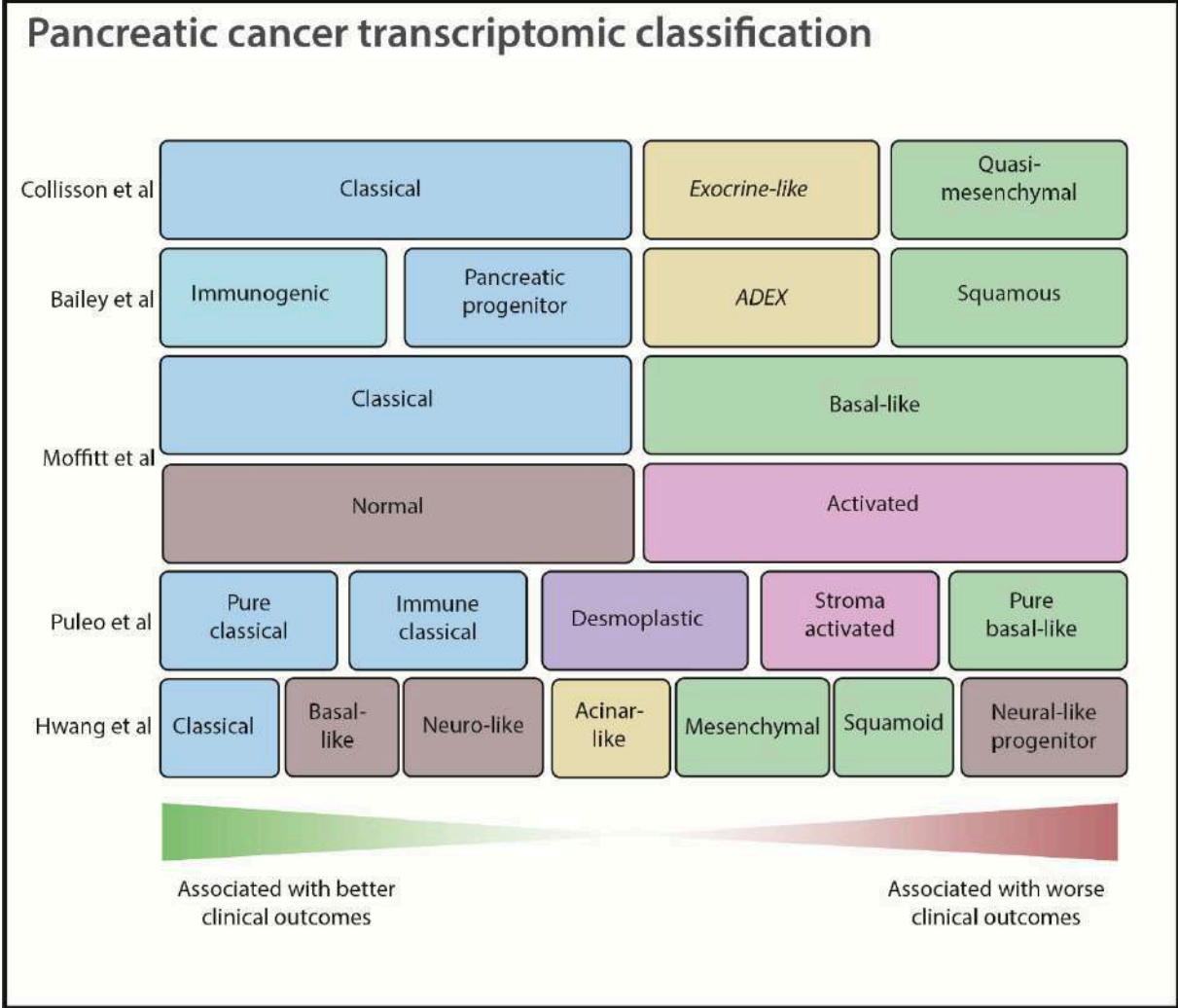


Figure 5. Pancreatic cancer classification according to transcriptomic data.

Classical pancreatic cancer is associated with good clinical outcomes whereas mesenchymal/squamous is associated with poor clinical outcomes. The stroma can also be considered in the classification as normal stroma is associated with good prognosis compared to activated stroma (Bailey et al., 2016; Collisson et al., 2011; Hwang et al., 2022; Moffitt et al., 2015; Puleo et al., 2018).

## C. Early development of PDAC

### a. Acinar to ductal metaplasia (ADM) : a tipping point

The ductal-like shape of PDAC cells initially led to the belief that the cell of origin was the ductal cell. However, it was shown that Neurogenic locus notch homolog (Notch) signalling in acinar cells can trigger a process called Acinar to Ductal metaplasia (ADM) where acinar cells transform into ductal-like cells. Cell-lineage tracing studies in PDAC mouse models demonstrated that neoplastic lesions arise from acinar cells through the activation of Notch pathway (Miyamoto et al., 2003; Shi et al., 2009). Furthermore, mutations in the *Kras* gene in acinar cells lead to more increased neoplastic lesions than mutations in ductal cells (Kopp et al., 2012).

The molecular changes in acinar cells have been extensively studied under various pancreatic pathological conditions, and these are outlined in the provided **Figure 6**. PDAC can originate from Pancreas Transcription Factor 1 Alpha positive (*Ptf1a*<sup>+</sup>) acinar cells or SRY (Sex-Determining Region Y)-Box 9 (*Sox9*<sup>+</sup>) ductal cells, but they are associated with different cancer subtypes in mice. Indeed, PDAC originating from acinar cells is linked to the classical subtype, while cancer derived from ductal cells is associated with the basal-like subtype. In mouse models, the cell of origin appears clear, but studying it in humans presents challenges. Nevertheless, human acinar cells can change their cellular identity *in vitro* and adopt a ductal-like state (Houbracken et al., 2011). Single-cell analysis in humans material using prediction algorithms indicated that PDAC cell transformation might originate from acinar cells through the ADM mechanism, as an intermediary state between acinar and ductal-like cells is observed.

Normal acinar cells become ductal-like cells when treated with Transforming Growth Factor Alpha (TGF $\alpha$ ). This transformation involves the activation of normal KRAS, Phosphoinositide-Dependent Kinase 1 (PDK1), and finally NOTCH that triggers a ductal-like program (**Figure 6**). In the case of *Kras* mutation, TGF $\alpha$  is no longer necessary, as *Kras* continuously stimulates the PDK1-NOTCH pathway. The regulation of the acinar and ductal-like states involves various genes, such as *Sox9*, that is expressed in both normal ductal cells and neoplastic pancreatic lesions (Liou et al., 2015a). Induction of neoplastic lesions from acinar cells is *Sox9*-dependent, as the absence of *Sox9* in acinar cells prevents the development of neoplastic lesions in mutated acinar cells (Kopp et al., 2012). Furthermore, Nuclear Receptor Subfamily 5, Group A, Member 2 (*NR5A2*) gene was also reported to be involved in this process in human PDAC. (**Figure 6**).

However, the conjunction of *Kras* mutation in acinar cells and inflammation leads to an irreversible loss of acinar cell state towards a ductal-like state (von Figura et al., 2014). Both alleles of *Nr5a2* are

necessary to maintain acinar state. Indeed, heterozygous *Nr5a2*<sup>+/-</sup> in conjunction with *Kras* mutation and inflammation can cooperate to promote tumor development (**Figure 6**). Other factors have been reported to play a role in regulating acinar cell identity, such as Kruppel-Like Factor 4 (*Klf4*), and the *Mist1* genes. Induction of *Klf4* or loss of *Mist1* expression is associated with a ductal-like program, through NOTCH activation (**Figure 6**) (Wei et al., 2016).

Recently, a specific acinar cell population with high levels of Telomerase reverse transcriptase (TERT ) (TERThi clone) was described (Neuhöfer et al., 2021). This clone has the ability to restore the identity of the metaplastic acini, even after experiencing damage like acute pancreatitis. However, if this clone undergoes mutation, it accelerates the development of neoplastic lesions through the Mitogen-Activated Protein Kinase (MAPK) pathway (Phosphorylated Extracellular Signal-Regulated Kinase (p-ERK)). Mutated clones containing p-ERK positive foci can be found in both pathological and non-pathological conditions in humans, suggesting that early clonal expansion may occur in the disease due to *Kras* mutation in specific clones, creating a spectrum of carcinogenesis in the tissues, increasing the likelihood of additional oncogenic mutations affecting acinar cells and leading to tissue transformation (Neuhöfer et al., 2021). The factors regulating acinar to ductal metaplasia are described in **Figure 6**.

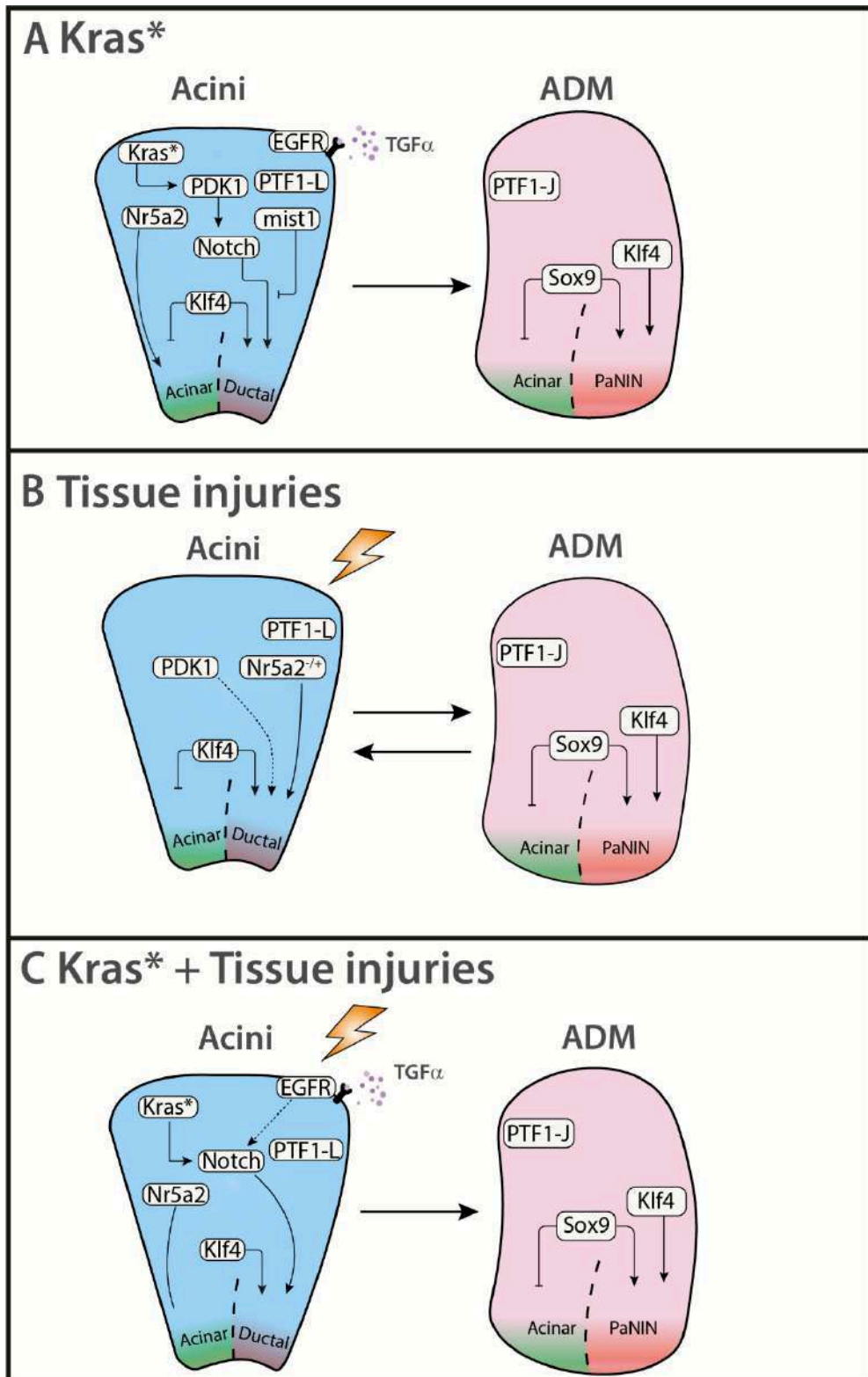


Figure 6. Acinar to ductal metaplasia in different pancreatic context.

## b. Pancreatic intraepithelial neoplasia

Three precursor lesions of PDAC have been described : pancreatic intraepithelial neoplasia (PanIN), Intraductal Papillary Mucinous Neoplasm (IPMN), and Mucinous Cystic Neoplasm (MCN) that differ in developmental pathway and histological structure. However, throughout this manuscript, we will focus on PanIN as they are the most common precursors lesions of PDAC in mouse models. They are non-cystic lesion that cannot be identifies using conventional imaging as there size is under 0.5 cm. They are classified into two grades based on the degree of cellular atypia (Basturk et al., 2015).

- Low grade PanIN show non-papillary lesion, columnar cells, and a preserved nuclear polarity (**Figure 3**).
- High grade PanIN show papillary lesions, loss of nuclear polarity and the nuclei are pleomorphic and mis-oriented (**Figure 3**) (Basturk et al., 2015).

PanIN lesions are relatively small compared to IPMN (> 1 cm). However, the size criterion is limited since small IPMN lesions can show PanIN size.

Although precursor lesions lead to PDAC, an increased number of studies show that individuals without any clinical signs of PDAC have precursor lesions in the healthy pancreas (Carpenter et al., 2023; Matsuda et al., 2017). The incidence of PanIN lesions appear much higher than PDAC incidence emphasizing that PanIN to PDAC transition may need extracellular stimuli to occur.

## II. PDAC is both a stromal and immune disease

### A. The close relationship between the tumor microenvironment and cancer cells

- a. Tumor microenvironment keystones: the concepts of “*seed and soil*” and “*a wound that do not heal*”.

As previously stated, most humans will develop pre-cancerous lesions in the pancreas (low-grade PanIN) (Carpenter et al., 2023; Matsuda et al., 2017). However, PDAC incidence does not correlate with low-grade PanIN incidence which indicate that PDAC may be more than a single-hit disease (Carpenter et al., 2023). Indeed, cancer has been considered for a long time as a genetic and unicellular disease where a single hit (e.g., a mutation) could cause malignant cancer. Considering the large number of cells present in the human organism and that most humans will not die from cancer-related causes, it is unlikely that a single-cell mutation occurrence would lead to cancer-related death. The statistician Richard Peto explained that the number of cells in an organism does not correlate with cancer incidence but rather that natural selection operates to select anti-tumoral mechanisms in larger

organisms (e.g., whales, elephants) (Peto et al., 1975). One hypothesis is that pre-cancerous cells can receive signals from the microenvironment.

The tumor microenvironment (TME) is composed of cellular and acellular components located between the tumor lesions within a specific organ. It goes without saying that a primary tumor has a different TME than a secondary tumor (i.e., metastasis). Those differences have been evaluated and shown to be dependent on the primary tumor, although differences between primary tumor and metastatic cancer cells can exist and are tissue-specific (Martínez-Jiménez et al., 2023). The cellular components of the TME are represented by blood vessels, pericytes, fibroblasts, mesenchymal cells, adipocytes, neural and/or immune cells. The acellular components are represented by secreted factors (e.g., growth factors, cytokines, and chemokines). Components of the extracellular matrix (ECM) (e.g., collagens, fibronectin, elastin) are highly abundant in the TME and form a network that structures the tissue (Gamradt et al., 2021). Given the prominent place of the TME in the tissue, we can raise the question about its function.

Bissel and Hines proposed a model in which the TME may have a protective role in the initial events of oncogenesis but evolves toward a tumor-promoting role, explaining why most humans do not develop cancerous lesions despite harboring pre-cancerous lesions (Bissell and Hines, 2011). The functions of the TME are explained by two main theories, i) "Seed and Soil" from Paget and ii) "Tumors: wounds that do not heal" from Dvorak. More than a century ago, Paget stated the "Seed and soil" theory (Paget, 1889) where the TME is seen as a soil and cancer cells as seeds. This hypothesis was originally stated to explain why metastasis occurs in a selected organ rather than in a random occurrence. Indeed, it was thought that cancer cells (i.e., seeds) only grow in a suitable environment (i.e., soil). It is not unreasonable to apply this hypothesis to primary tumor growth since it may explain why some cancers derive from inflamed tissue.

More recently, Dvorak (Dvorak, 1986) postulated that cancer was a replicating wound-healing process indefinitely in order to progress. His hypothesis has been validated by numerous studies (Dolberg et al., 1985; Schuh et al., 1990). Wound healing process can be summarized in 3 steps : inflammation, tissue remodelling, injury resolution (Schäfer and Werner, 2008). These steps are made possible by the involvement of fibroblasts, ECM proteins, and immune cells.

Therefore, in the next two parts, we will focus on the involvement of fibroblasts and ECM in PDAC establishment and progression and how these actors shape the tumoral tissue. Finally, we will discuss the question of whether these actors can be targeted in order to improve cancer outcomes.

b. Cancer-associated fibroblasts in PDAC

i. Origins

Cancer-associated fibroblasts (CAFs) refer to a heterogeneous group of activated spindle-shaped fibroblasts that are primarily found in the TME. They constitute the major non-immune cells in the pancreatic TME (Steele et al., 2020). CAFs are detected in the pancreas microenvironment as early as the emergence of ADM or PanIN lesions (Carpenter et al., 2023; Provenzano et al., 2012) and they positively correlate with ECM deposition. For many years, CAFs were believed to emerge exclusively from lipid-associated fibroblasts that are resident in healthy tissue termed pancreatic stellate cells (PSCs).

SCs are found in the healthy pancreas in a quiescent state (qPSCs). qPSCs are mainly defined by the expression of cytoskeleton markers such as DESMIN and Glial Fibrillary Acidic Protein (GFAP) but also by the retention of lipid droplets in the cytoplasm by the Fatty Acid-Binding Protein 4 (FABP4) (Apte et al., 1998). qPSC are activated during perturbed states (e.g., inflammation). In humans, there is a communication between transforming cells and inactive PSCs, resulting in the formation of activated PSC (aPSCs) characterized by the expression of Alpha Smooth Muscle Actin ( $\alpha$ SMA<sup>+</sup>) and their ability to produce collagens (Apte et al., 2004). aPSCs are characterized by the loss of Fabp4 expression as the lipid droplets are released in the environment and captured by cancer cells (Auciello et al., 2019; Sherman et al., 2014).

Based on this, it has been postulated that CAFs mostly originate from qPSCs. However, this assumption is not accurate since tracing the origin of CAFs is challenging in both mouse and human settings. Most of the initial data were based on the *in vitro* isolation of qPSCs by density gradient protocols (Apte et al., 1998). With the emergence of single cell technologies and cell lineage tracing in *in vivo* models, a more complex picture of CAFs diversity emerged in PDAC (**Figure 7**). A recent study showed that only 15% of CAFs (Platelet-derived growth factor receptor positive (PDGFR $\alpha$ <sup>+</sup>), Podoplanin positive (PDPN<sup>+</sup>) were originating from qPSC in PDAC using different orthotopic models (Helms et al., 2022). This observation is in line with the fact that fibroblasts were shown to contribute up to 50% of  $\alpha$ SMA<sup>+</sup> CAF pool (Garcia et al., 2020). Indeed, the latter study took an interest in perivascular Gli1<sup>+</sup> fibroblasts. Gli1<sup>+</sup> fibroblasts are a mesenchymal stem cell-like population responsible for fibrosis in various organs upon injury through expansion and differentiation (Kramann et al., 2015). In mouse PDAC model (*Ptf1a*<sup>FipO/+</sup>; *Kras*<sup>FSF-G12D/+</sup>; *Trp53*<sup>FRT-STOP-FRT/+</sup>), resident *Gli1*<sup>+</sup> fibroblast were able to proliferate and represent around 40% of CAFs (**Figure 7**) (Garcia et al., 2020). Furthermore, the authors also showed that *Hoxb6*<sup>+</sup> resident fibroblasts represent only 5% of CAFs, indicating that not all resident fibroblast has the same CAFs-contribution capacity (**Figure 7**). It is possible that other resident fibroblast

populations not yet determined might contribute to CAF contingent. Despite those discoveries, the indicated proportions of CAFs origin may not reflect the situation in human pathological condition in which it is impossible to do tracing experiments.

The different ability of resident fibroblasts to be activated and to differentiate into CAFs can be influenced by two types of factors. First, extrinsic cues such as the variability of resident fibroblast location but also the type of precursor lesions may have a role since it is possible that PanIN and IPMN/MCN have different secretomes. The second type of factors is the intrinsic cues. Indeed, different sensitivity of resident fibroblasts to external cues may be displayed in the resident fibroblast pools. Comforting this hypothesis is a pivotal piece of information pointing out that the vast majority of resident fibroblasts come from the splanchnic mesenchyme (70% of PDPN<sup>+</sup> and 90% of PDGFR $\alpha$ <sup>+</sup>) as well as  $\alpha$ SMA<sup>+</sup> CAFs (Han et al., 2023).

CAFs can also originate from recruited mesenchymal cells from the bone-marrow and from the differentiation of epithelial cancer cells into mesenchymal state through EMT. Through irradiation and cell lineage tracing in murine models, both origins are believed to contribute to around 10% of CAFs in PDAC (Dominguez et al., 2020; Han et al., 2023) (**Figure 7**).

Although it has been shown in other organs that CAFs can originate from adipocytes (Bochet et al., 2013), endothelial cells (Zeisberg et al., 2007) or pericytes (Hosaka et al., 2016), up to date, there are no clear *in vivo* evidences that those mechanisms occur during PDAC development.

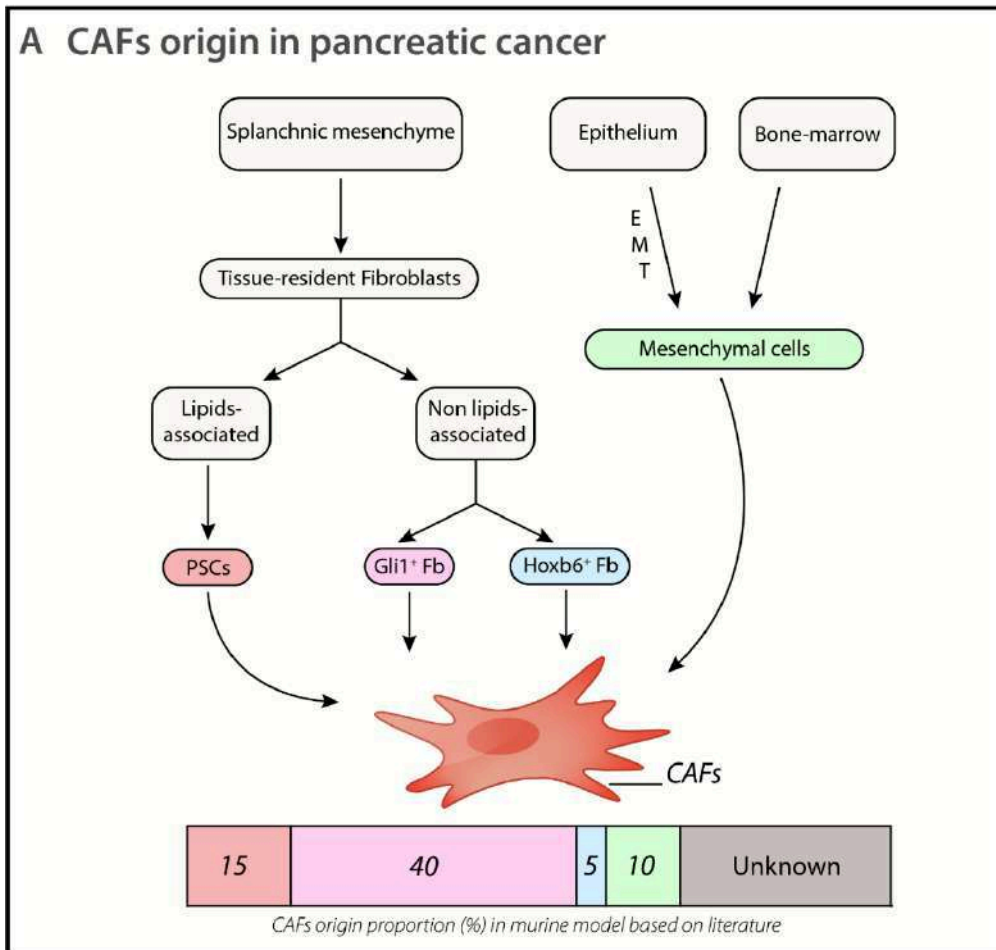


**Figure 7 Cancer-associated fibroblast ontogeny in pancreatic cancer.**

CAFs have numerous origins in pancreatic cancer. The stacked bar chart shows the relative percentage of the different origins of CAFs in pancreatic cancer. PSCs, Gli1<sup>+</sup>, Hoxb6b<sup>+</sup>, mesenchymal cells contribute to 15%, 40%, 5%, 10% of total CAFs, respectively. Gli1 Zinc finger protein GLI1, Hoxb6 Homeobox protein Hox-B6.

## ii. CAFs subtypes and functions

Classification of CAFs in PDAC is complicated considering the large number of markers that can define a fibroblast (Elyada et al., 2019; Luo et al., 2022).

A recent report from Buchler et al. shows that healthy organs are composed of two types of fibroblasts: i) universal fibroblasts conserved between tissues and ii) specialized fibroblasts (e.g., Fibroblastic Reticular Cells in lymph nodes, Red Pulp Fibroblasts in spleen). During a perturbed state (e.g., cancer, auto-immune disease), tissues are composed of activated fibroblasts (Buechler et al., 2021). More importantly, pancreatic resident fibroblasts can be distinguished into two main populations: one that differentiates into immunomodulatory CAFs and another one that becomes ECM/Chemoattractant-producing CAFs (**Table 2**) (**Figure 8A**) (Dominguez et al., 2020). As a matter of fact, resident fibroblasts are selected to develop into CAFs since it was shown that universal Dermatopontin positive (DPT<sup>+</sup>), Peptidase Inhibitor 16 (PI16<sup>+</sup>) fibroblasts (fibroblast that are expressed in the pancreas but also across many tissues at steady state) contribute to the majority of CAFs compared to another universal fibroblast population (COL15A1<sup>+</sup>) (**Figure 8B**) (Buechler et al., 2021).

Indeed, DPT<sup>+</sup> PI16<sup>+</sup> fibroblasts gradually shift toward Leucine Rich Repeat Containing 15 (LRRC15<sup>+</sup>) CAFs during cancer progression (**Figure 8B**) (Buechler et al., 2021). At least 50% of LRRC15<sup>+</sup> also emerge from ECM organizing resident fibroblasts (Dominguez et al., 2020). Those fibroblasts are pro-tumoral since: i) they are associated with anti-tumoral response by suppressing CD8<sup>+</sup> T lymphocyte response in mouse models (Buechler et al., 2021), ii) They are upregulated in many cancers and associated with immunotherapy restraint in humans. (Dominguez et al., 2020).

CAFs phenotype can vary through PDAC development and are different from neoplastic lesions to the PDAC-stage CAFs (Bernard et al., 2019). Alongside with healthy tissue heterogeneity, CAFs in PDAC have recently been classified in three main subtypes : Myofibroblastic CAFs (myCAF), inflammatory CAFs (iCAF) and antigen presenting CAFs (apCAF) (**Figure 8C-E**) (Elyada et al., 2019; Öhlund et al., 2017). Those subtypes can be found in both human and mouse pancreatic cancer. Myo-fibroblasts or « myCAF » are CAFs found in the peri-glandular region nears cancer cells. They are defined as  $\alpha$ SMA<sup>+</sup> fibroblasts and express ECM genes (Elyada et al., 2019) (**Table 2**). Chen and colleagues elegantly showed that  $\alpha$ SMA<sup>+</sup> fibroblasts in PDAC were the main producers of type I collagen among the three main subtypes (Chen et al., 2021). Inflammatory CAFs or "iCAF" are found far from cancer cells and secrete cytokines, including IL-6 and IL-11 (**Table 2**). Despite being distinct, myCAF and iCAF share common markers such as COL1A1, Fibroblast Activated Protein (FAP), Vimentin (VIM), PDPN (Elyada et al., 2019). Antigen-presenting CAFs or "apCAF" do not have a specific location but express the antigen-presenting complex (**Table 2**).

It is important to note that myCAFs and iCAFs are family of CAFs since there are subpopulation of CAFs. For example, among myCAFs are the Fibroblast activation protein- $\alpha$  CAFs (FAP<sup>+</sup> CAFs) that represent a large portion of myCAFs (Feig et al., 2013).

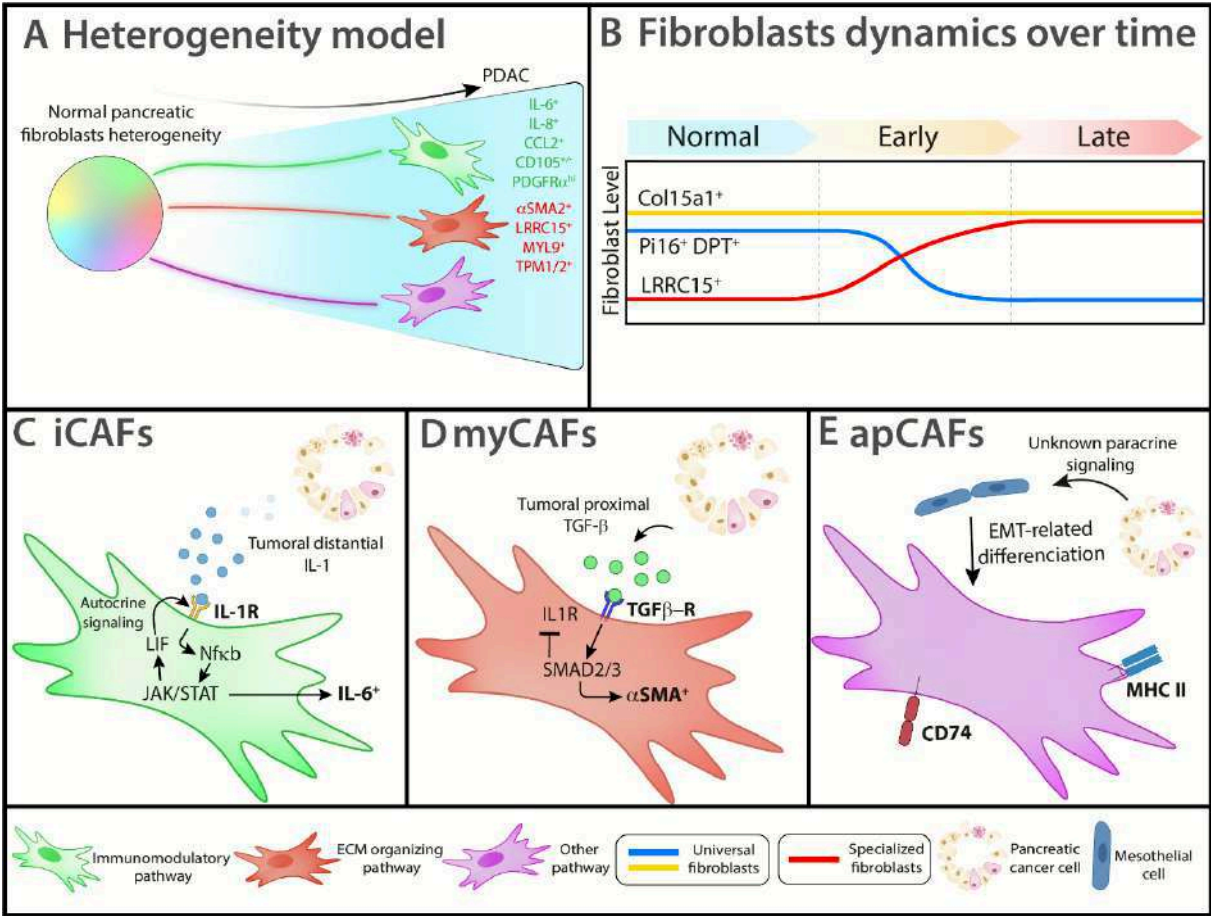


Figure 8. CAFs development and heterogeneity.

**A** Normal pancreatic fibroblasts are heterogeneous at steady state and are selected to give rise to specialized CAFs in pancreatic cancer. **B** Pi16<sup>+</sup> universal fibroblasts are replaced by LRRC15<sup>+</sup> CAFs during pancreatic cancer progression. **C** iCAFs are differentiated with IL-1 from cancer cells leading to the activation of JAK-STAT signalling through NFκB. Downstream signalling lead to LIF expression. LIF act as an autocrine activator of IL-1R. iCAFs are defined by IL-6 secretion. **D** myCAFs are activated by TGFβ. TGFβ signalling inhibit IL-1R expression and induce αSMA expression. **E** apCAFs are differentiated from mesothelial cells through EMT-like process. They are defined by the expression of MHC-II. MYL9 Myosin Light Chain 9, TPM Tropomyosin, MHC-II major histocompatibility complex.

iCAFs and myCAFs and have different activation mechanisms related to their location in the TME (Elyada et al., 2019). iCAFs are activated by IL-1 cytokine secreted by distant cancer cells, binding to IL-1 receptor on fibroblasts (**Figure 8C**). The downstream signalling activates nuclear factor-kappa B (NF $\kappa$ B) pathway and Janus kinase-signal transducer and activator of transcription (JAK-STAT) leading to the secretion of IL-6 cytokine (Biffi et al., 2019; Öhlund et al., 2017). In the same time, the Leukaemia inhibitory factor (LIF) (Hilton et al., 1988) which is part of IL-6 cytokine family, is expressed and have an autocrine effect through IL-1R (**Figure 8C**). Transcriptomic single-cell analysis revealed that myCAFs were sensitive to TGF- $\beta$  (Biffi et al., 2019; Dominguez et al., 2020; Elyada et al., 2019). Locally secreted TGF- $\beta$  by tumor cells binds to TGF- $\beta$  receptor on fibroblasts and activates the SMAD pathway (SMAD2/3), leading to  $\alpha$ SMA expression upregulation (Figure 8D). Interestingly, TGF- $\beta$  signaling occurring in myCAFs has an antagonist effect to IL-1 signaling, suggesting that in a given niche, both iCAFs and myCAFs are unlikely to coexist (**Figure 8D**)(Biffi et al., 2019). However, myCAFs and iCAFs can transdifferentiate, as specific JAK-STAT pathway inhibition in iCAFs can turn them into myCAFs, and hybrid states of CAFs were reported (Biffi et al., 2019). Finally, apCAFs have recently been shown to have gene signature similarities with mesothelial cells (Dominguez et al., 2020). This was confirmed by a large cell lineage analysis of mesothelial cells during PDAC progression (Huang et al., 2022).

Mesothelial cells that surround the pancreas organ, upon PDAC progression, downregulate their mesothelial gene (e.g., Mesothelin (Msln)) while activating EMT-related genes (Vim, Snai1/2, Zinc finger E-box-binding homeobox 1 (Zeb1)), suggesting an activation of the embryonic program during cancer progression (**Figure 8E**). This differentiation is led by both IL-1 and TGF $\beta$ .

While myCAFs, iCAFs, and apCAFs represent the most used and recognized CAFs classification system in PDAC, it is important to note that other groups have reported alternative classifications. Specifically, a CAFs classification was established in the human context based on the expression of other markers (Neuzillet et al., 2022). The authors proposes subtype A, B and D to be associated with a poor prognosis in human patients. They are respectively defined as : POSTN<sup>+</sup>,  $\alpha$ SMA<sup>low</sup>, Vimentin<sup>Low</sup> (Subtype A) ; MYHII<sup>+/-</sup>,  $\alpha$ SMA<sup>high</sup>, Vimentin<sup>high</sup> (Subtype B/D). Subtype C is defined as PDPN<sup>+</sup> CAFs<sup>+</sup> are associated with a good prognosis. This classification has not been confirmed in mouse models making mechanistic analysis difficult.

Name	Location	Methods of analysis	Characterized markers	Function	Reference
myCAFs	Peri-glandular region		$\alpha$ SMA	Myofibroblast genes, TGF $\beta$ response, ECM genes	(Öhlund et al., 2017)
iCAFs	Distantly from cancer cells		IL6, IL11, LIF	Interleukins, Chemokines, JAK-STAT	
apCAFs	(Mesothelium ?)		MHC cl II, CD74, SAA3	Antigen-presentation and processing, fatty-acid metabolism	(Elyada et al., 2019)
myCAFs	Peri-glandular region	Single cell on human and KPC murine tumor	$\alpha$ SMA, TAGLN, MMP11, MYL9, POSTN	<u>Human</u> : Smooth muscle contraction, focal adhesion, ECM organization, and collagen formation. <u>Mouse</u> : EMT, myogenesis, ECM receptor interaction, and focal adhesion	
iCAFs	Distantly from cancer cells		PDGFR $\alpha^{hi}$ , IL-6, IL-8, CCL2, CXCL12	<u>Human</u> : IFN $\gamma$ response, TNF/NF- $\kappa$ B, IL2/STAT5, IL6/JAK-STAT3, and the complement pathway	
LRRC15 <sup>+</sup>	N/A	Single-cell and LRRC15 <sup>DTR/DTR</sup> model	MMP11, COL10A1, COL11A	Impair CD8 T cell immune response	(Krishnamurthy et al., 2022)
C8	N/A	Single cell and trajectory analysis	Ly6C, PDGFR $\alpha^{hi}$ , ENG <sup>+/-</sup> , CXCL1	Immune modulation (Thbd, CD55, IL33, Dpp4, and Cxcr7)	(Dominguez et al., 2020)
C2			LRRC15, PDGFR $\alpha^{low}$ , Col11a <sup>+</sup> , $\alpha$ SMA <sup>+</sup>	ECM et chemoattractant (Col4a1, Col6a6) (Ccl11, Cxcl14, and Cxcl16)	
FB1	N/A	Single cell on Normal pancreas, Early and late KIC mouse model	CXCL14, Ptn, IGF1, IGFBP4/7, IL6, CCL2/7, CXCL12, PDGFR $\alpha$ , Ly6a, Ly6c1, Nov, Pi16	Similar to iCAFs	(Hosein et al., 2019)
FB2			Lrrn4, Gas6, Cav1, Cdh11,	Physiological function	
FB3			Gpm6a, Msln, Lgals7	Similar to myCAFs	

---

SAA3 Serum Amyloid A3, TAGLN Transgelin, MMP11 Matrix Metalloproteinase 11, POSTN Periostin, ENG Endoglin, CXCL1 CXC motif chemokine ligand 1, CCL2 C-C Motif Chemokine Ligand 2, CXCL12 CXC motif chemokine ligand 12, IFN $\gamma$  Interferon gamma, TNF Tumor necrosis factor, Thbd Thrombomodulin, Dpp4 dipeptidyl peptidase-4, CXCR7 CXC chemokine receptor 7, Ptn Pleiotrophin, Igf1 Insulin-like Growth Factor One, Igfbp4/7 insulin like growth factor binding protein 4/7, Lrrn4 Leucine Rich Repeat Neuronal 4, Gas6 growth arrest-specific gene 6, Cav1 Caveolin 1, Gpm6a Glycoprotein M6A, Lgals7 Galectin 7, DTR Diphtheria Toxin Receptor

---

### iii. CAFs targeting

CAFs targeting in PDAC can be achieved by focusing on different aspects of the CAFs life cycle, despite the fact that it is utterly difficult to dissociate the relationship between CAFs and desmoplasia given their interdependent nature. One of the main CAFs-related signaling pathways that has been targeted is the Sonic Hedgehog (SH) pathway. SH ligands are secreted by tumor cells, and it has been reported that the SH pathway induces the activation of pancreatic fibroblasts into desmoplastic CAFs (Bailey et al., 2008). Indeed, hedgehog ligands binding to their receptors on fibroblasts result in Smoothened (SMO) protein activation and GLI transcription factor activity in stromal cells during PDAC development (Tian et al., 2009). A pivotal study showed that SMO inhibitors in PDAC allow transient better tissue vascularization, higher drug delivery, lower collagen content, and  $\alpha$ SMA<sup>+</sup> cell proliferation with minimal effect on tumor size (Olive et al., 2009). Brought to humans, SH inhibitors failed to show therapeutic benefits due to an increase in metastasis compared to the standard of care (Catenacci et al., 2015; Kim et al., 2014). This failure can be explained by several reasons. The first reason is that CAFs are highly heterogeneous and can display pro or anti-tumoral behaviors (Hutton et al., 2021). Therefore, depleting CAFs in their wholeness may disrupt the equilibrium between tumor restricting or permissive signalling in the TME. The second reason might be that the desmoplasia implemented by  $\alpha$ SMA<sup>+</sup> CAFs is not exclusively tumor-permissive (Lee et al., 2014) which is in contradiction with the common idea that mechanical forces are fueling cancer progression in many indications (Northey et al., 2017).

Supporting the latter idea, by depleting  $\alpha$ SMA<sup>+</sup> cells (i.e. Cells differentiated by SH pathway), Kalluri's group showed that tumors are more developed, less differentiated and are associated with a lower survival rate emphasizing a perhaps tumor-restricting role of the stroma instructed by  $\alpha$ SMA<sup>+</sup> fibroblasts (Özdemir et al., 2014). Although their model also depleted pro-tumoral CAFs such as LRR15C<sup>+</sup> CAFs (Krishnamurthy et al., 2022),  $\alpha$ SMA<sup>+</sup> cell depletion correlates with less type I collagen, softer tissue and higher invasive properties of cancer cells (Özdemir et al., 2014).  $\alpha$ SMA<sup>+</sup> cells seems to have a tumor protecting role through type I collagen secretion (Bhattacharjee et al., 2021; Chen et al., 2021) while having a tumor-promoting role through the secretion of Hyaluronic Acid (HA) and Matrix Metalloproteinases (MMPs). This highlights the importance of not radically disrupting the

stroma but rather fine-tuning the therapy by targeting CAFs more precisely. For example, it has recently been brought up that specifically depleting  $\alpha\beta3$ -expressing cells (fibroblast and cancer cells) in the PDAC context in mice were resorbing collagen deposition and increasing drug delivery by releasing interstitial pressure (Turaga et al., 2021). Also, the depletion of FAP<sup>+</sup> CAFs can enhance the anti-tumoral immunity in PDAC (Feig et al., 2013; Kraman et al., 2010). Of greater importance, FAP<sup>+</sup> CAFs depletion in PDAC reduces desmoplasia and tumor size (Lo et al., 2015). Considering that  $\alpha$ SMA<sup>+</sup> CAFs<sup>+</sup> can also express FAP (Öhlund et al., 2017), It is possible that there are two distinct populations:  $\alpha$ SMA<sup>+</sup> FAP<sup>+</sup> CAFs and  $\alpha$ SMA<sup>+</sup> FAP<sup>-</sup>, each having tumor-permissive and tumor-restricting effects, respectively. Finally, we cannot rule out the hypothesis that periglandular  $\alpha$ SMA<sup>+</sup> CAFs-derived collagen has different effects on tumor architecture than distant  $\alpha$ SMA<sup>+</sup> CAFs-derived collagen. Indeed, local collagen architecture can impact cancer cell aggressiveness independently of the total collagen content in PDAC (Laklai et al., 2016).

Recently, there has been a growing interest in Focal Adhesion Kinase (FAK) signaling in CAFs. Low FAK signaling activity in CAFs has been associated with better survival in PDAC patients (Zaghdoudi et al., 2020). However, FAK activity is not specific to CAFs, as a recent report stated that FAK signaling lowers the expression of MHC-I on tumor cells in PDAC patients, allowing immune evasion (Canel et al., 2023). Similar results were reported showing that FAK expression in neoplastic cells allows for stroma remodelling with an increased collagen deposition (Jiang et al., 2016).

Independently of desmoplasia, CAF reprogramming might represent an attractive therapeutic alternative. CAFs can be reprogrammed both *in vitro* and *in vivo* with the use of specific pharmaceutical agents such as vitamin D analog or tretinoin (Chronopoulos et al., 2016; Sherman et al., 2014) (**Table 3**). CAFs reprogramming is associated with a decrease  $\alpha$ SMA and ECM gene expression. More importantly, in line with the concept of solid stress compression of blood vessels (Chauhan et al., 2014), CAF reprogramming treatment with a vitamin D analog combined with Gem in mice leads to better vascularization, ultimately resulting in reduced tumor volume (Sherman et al., 2014). CAF reprogramming impacts the paracrine communication with cancer cells, leading to decreased cancer cell invasion (Chronopoulos et al., 2016). To conclude, although CAF reprogramming is still new and challenging, it represents a promising avenue for PDAC therapy. Indeed, the past 10 years have highlighted that CAF targeting requires precision and refinement. Therefore, identifying markers that would selectively identify tumor-permissive CAFs should be a priority, as tumor-restricting CAFs are necessary.

<b>Table 3. CAFs targeting in pancreatic cancer</b>				
<b>Drug</b>	<b>Clinical stage</b>	<b>Targeting family</b>	<b>Results</b>	<b>Reference</b>
SH inhibitors	I/II	Direct targeting	No benefits compared to standard of care	(Catenacci et al., 2015) (Kim et al., 2014)(NCT01064622)(NCT01195415)
FAP <sup>+</sup> depletion	Pre-clinical	Direct targeting	Reduced tumor-permissive desmoplasia	(Lo et al., 2015)
FAP <sup>+</sup> depletion	Pre-clinical	Indirect targeting	Increased effector CD8 <sup>+</sup> T cell infiltration	(Feig et al., 2013)
SOM-230	I	Direct targeting	Increased drug sensitivity	(Duluc et al., 2015)
ROCK inhibition	Pre-clinical	Indirect targeting	Reduced tumor-progression	(Whatcott et al., 2017)
Paricalcitol	Pre-clinical and I	Reprogramming	Reprogrammed CAFs in qPSC	(Sherman et al., 2014) (NCT04524702)
Pro-Agio	Pre-clinical and I	Direct targeting	Reduced collagen deposition and increased drug delivery	(Turaga et al., 2021) (NCT05085548)
IPI-926	I	Direct targeting	No benefits compared to standard of care	(Ko et al., 2016) (NCT01383538)
ATRA	I/II	Reprogramming	Safe and tolerable	(Kocher et al., 2020) (NCT03307148) (NCT04241276)

ROCK Rho-associated coiled coil-containing protein kinase, ATRA all-trans retinoic acid.

c. The stroma

i. Collagen

Desmoplasia is defined by the accumulation of ECM proteins in the microenvironment. Collagen is among the most abundant proteins secreted in the stroma during PDAC progression (Tian et al., 2019). Collagen synthesis is a well-known multi-step mechanism that is conserved across tissues. Approximately 90% of ECM proteins consist of collagens, with 90% of these being type I and III collagens (Tian et al., 2019). Type I collagen is a heterodimer fiber composed of two  $\alpha 1$  and one  $\alpha 2$  chains and is present across all tissues (**Table 4**).

<b>Table 4. Type of collagen across tissues at steady state</b>				
Structure	Type	Chains	Genes	Distribution
Fibrillar	I	$[\alpha 1(I)]_2 \alpha 2(I)$	<i>COL1A1, COL1A2</i>	Dermis, cornea, ligaments
	II	$[\alpha 1(II)]_3$	<i>COL2A1</i>	Cartilage, vitreous body
	III	$[\alpha 1(III)]_3$	<i>COL3A1</i>	Skin, vessel wall
	V	$[\alpha 1(V)]_2 \alpha 2(V) ; \alpha 1(V)_2 \alpha 2(V) \alpha 3(V)$	<i>COL5A1, COL5A2, COL5A3</i>	Lung, cornea, bone
Network forming	IV	$[\alpha 1(IV)]_2 \alpha 2(IV) ; \alpha 1-\alpha 6$	<i>[COL4A1; COL4A6]</i>	Basement membranes

*Adapted from (Gelse, 2003)*

Collagen is mainly produced by activated fibroblasts that proliferate throughout the disease evolution (Bachem et al., 2005). Type I collagen production by tumor cells in the PDAC context has a tumor-restricting role independently of  $\alpha$ SMA<sup>+</sup> cell production (Bhattacharjee et al., 2021). While the tumor-restricting role of collagen has been reported, the exact mechanism behind it is poorly understood. Collagen is partially responsible for the establishment of tissue stiffness in the TME (Jiang et al., 2016). In particular, thick collagen fibers are associated with cancer cell aggressiveness and a lower survival rate in patients (Laklai et al., 2016). It is also important to note that PSCs can be activated by mechanical forces, indicating that activated PSCs may exert an indirect mechanical loop by secreting collagen (Lachowski et al., 2017).

Interestingly, a high level of type I collagen is associated with higher survival rates in patients, while a high level of  $\alpha$ SMA<sup>+</sup> is associated with a lower survival rate (Erkan et al., 2008; Ogawa et al., 2021) although there are contradictory data showing that high collagen content is also associated with lower survival rate (Miller et al., 2015). This observation is a reminder of the three described stroma subtypes in human PDAC : i) Collagen-rich, ii)  $\alpha$ SMA-dominant and iii) FAP-dominant stroma (Ogawa et al., 2021). It is important to note that the effect of collagen on tumor cells and patient prognosis is not entirely clear. Recently, an innovative study showed that type I collagen can be remodeled in the

microenvironment (Su et al., 2022). Indeed, intact and cleaved type I collagen in PDAC have different effects on tumor cells. This study may explain the controversial observation between  $\alpha$ SMA<sup>+</sup> CAFs infiltration and type I collagen in pancreatic cancer. Type I collagen might be biochemically remodeled and cleaved by MMPs, allowing an enhancement of cancer cell metabolism and growth, whereas intact collagen might inhibit mitochondrial synthesis in tumor cells. Since human patients displaying a high cleaved type I collagen content have lower survival, stroma sub-type may be considered a prognostic marker (Su et al., 2022).

Moreover, although the large majority of collagen is produced by fibroblast in an heterodimeric form ( $\alpha$ 1 $\alpha$ 2), there are evidence of homotrimeric form secretion of type I collagen by cancer cell in PDAC (Chen et al., 2022). The homotrimeric form induces cancer cell proliferation through Discoidin domain receptor 1 (DDR1) signaling, which the heterodimeric form is not capable of (Chen et al., 2022; Su et al., 2022). More importantly, deletion of cancer cell-derived type I collagen appears to delay cancer initiation and progression, indicating a tumor-permissive role of the homotrimeric form. It appears, then, that several parameters are important to define the tumor-permissive or restrictive role of collagen fibers in pancreatic cancer: biochemical state, location, abundance, thickness, and alignment of the fibers, as well as tumor genotype.

Direct targeting of collagen has been assessed by inhibiting the Lysyl Oxidase (LOX) enzyme. This enzyme permits the cross-linking of collagen fibers, making the tissue stiffer. In pre-clinical studies, LOX inhibitors showed promising results by restraining cancer cell invasion and, more importantly, increasing drug delivery within the tumor bed, which became more vascularized (Miller et al., 2015).

## ii. Hyaluronic acid

Hyaluronic acid (HA) is a glycosaminoglycan structured of repeated sequence of glucuronic acid and N-acetylglucosamin:  $[-\beta(1,4)\text{-GlcUA}-\beta(1,3)\text{-GlcNAc-}]_n$ . is synthesized by the hyaluronan synthases enzyme and extruded toward the ECM without being modified in the endoplasmic reticulum or Golgi apparatus. Once secreted in the ECM, HA is cleaved by hyaluronidase. HA has several receptors (CD44, Lymphatic vessel endothelial hyaluronan receptor 1 (Lyve1)) and plays a role in cell signaling, tissue architecture, and angiogenesis (Toole, 2004). HA can be secreted by several cell types and have been shown to be in excess in many cancer indications (Jacobetz et al., 2013; Toole, 2004). HA is found in normal pancreas but is abnormally accumulated during PDAC development alongside with  $\alpha$ SMA<sup>+</sup> fibroblasts (Jacobetz et al., 2013; Provenzano et al., 2012). It was shown that HA is responsible of interstitial fluid pressure (IFP) increase in PDAC, causing vessel shrinkage. However, it was proposed

that HA does not increase IFP but rather solid stress, referring to the mechanical force exerted by proliferating cells as they exert pressure on their surrounding environment (Chauhan et al., 2014). As previously explained, drug delivery is impaired in PDAC due to the poor vascularization of the tissue. This is a major limitation of chemotherapy efficiency; therefore, there is a need to develop therapies that relieve the pressure applied on the blood vessels to increase cytotoxic agent concentration in the tumor bed.

Recently, a drug has been developed called PEGPH20 to degrade HA molecule in the stroma. The combination of PEGPH20 with Gem confirmed the physical barrier role of HA, as the tumor exhibited a lower interstitial fluid pressure (IFP) or solid stress, resulting in increased drug delivery (Jacobetz et al., 2013; Provenzano et al., 2012). However, when brought to human, HA depleting therapy by PEGPH20 showed increased metastasis and toxicity and/or no benefits compared to the standard of care (Ramanathan et al., 2019; Van Cutsem et al., 2020).

The reason of such therapeutical failure may be multiple, including that one of the clinical trial did not select patient based on HA level (Hakim et al., 2019). Also, as discussed previously, the role of stroma architecture in PDAC is variable, and disrupting the entire acellular environment in a highly heterogeneous patient cohort with different stroma subtypes may explain why PEGPH20 failed to show benefits. To support this claim, it has been shown that HA compresses vessels in collagen-rich stroma only, indicating a putative relationship between HA and collagen that is still not elucidated (Chauhan et al., 2013)

### iii. $\beta$ ig-h3

$\beta$ ig-h3 or TGF $\beta$ -i (TGF- $\beta$ -induced) is a 68 kDa extracellular protein coded by chromosome 13 and 5 in mouse and human, respectively. The structure of  $\beta$ ig-h3 comprises an N-terminal secretory signal, a cysteine-rich domain (CRD), four fascilin-1 domains, and a C-terminal cell attachment site (**Figure 9**)(Ween et al., 2012). The term  $\beta$ ig-h3 will be uniquely used since it refers to the original name of the protein identified in the late 20th century “TGF- $\beta$  induced gene human clone 3” (Skonier et al., 1992).  $\beta$ ig-h3 is secreted by many cell types (Thapa et al., 2007) and its secretion is induced by TGF $\beta$  but also IL-4, IL-10 and IL-13 (Lecker et al., 2021). This protein is expressed in many normal tissues at basal level (Ivanov et al., 2008) and as early as embryonic development in mouse (Schorderet et al., 2000). To date, there is only one known disease based on a  $\beta$ ig-h3 mutation; the corneal dystrophy (Kheir et al., 2019). The physiological role of  $\beta$ ig-h3 is mainly restricted to cell adhesion, migration process through signalling pathway action (FAK activation) or ECM binding (Kheir et al., 2019). Indeed,  $\beta$ ig-h3 can bind to cellular receptors, mainly integrins ( $\beta$ 1,  $\beta$ 3, and  $\beta$ 5). It can also bind to ECM macromolecules such

as fibronectin, laminin, and type I, II, IV, and VI collagens, although its binding is limited to triple-helical collagens (Hashimoto et al., 1997).

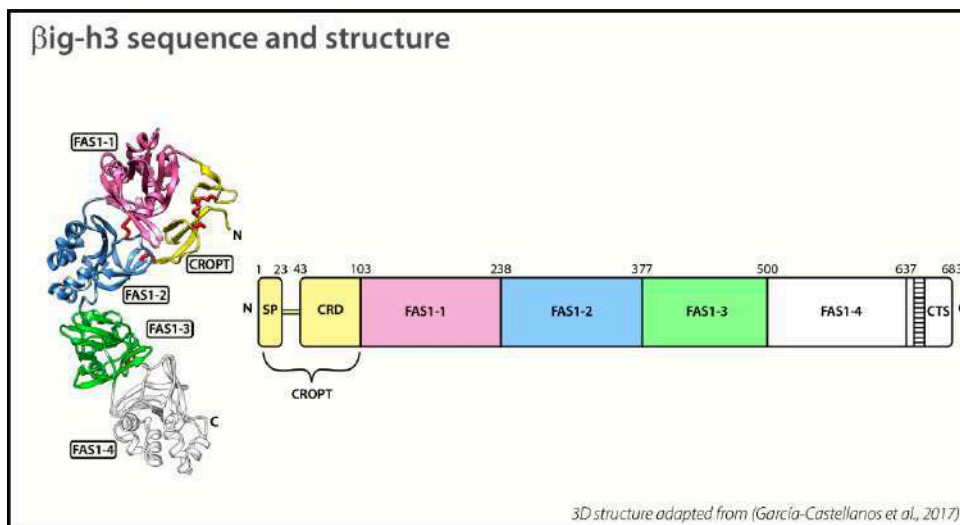


**Figure 9.  $\beta$ ig-h3 structure**

$\beta$ ig-h3 structure is shown on a Ribbon plot.  $\beta$ ig-h3 is composed of a CROPT domain and 4 different FAS1 domains with a CTS. CROPT is yellow, FAS1-1 is pink, FAS1-2 in blue, FAS1-3 in green, FAS1-4 in white. Red indicates disulfide bonds. CROPT cysteine-rich domain of periostin and TGF $\beta$ 1p, SP Signal Peptide, FAS fasciclin domain, CTS C-terminal segment. Hatched segment is an integrin-recognition motif.

$\beta$ ig-h3 is upregulated in many cancer types, including PDAC (Ivanov et al., 2008). In the pancreas, it was shown that  $\beta$ ig-h3 preserves the function and integrity of pancreatic islets during diabetes (Han et al., 2014, 2011). More importantly, our group showed that  $\beta$ ig-h3 expression was altered during type I diabetes and that  $\beta$ ig-h3 was able to inhibit autoreactive CD8<sup>+</sup> T cells by lowering granzyme B release (**Figure 10A**)(Patry et al., 2015). We showed that  $\beta$ ig-h3 treated CD8<sup>+</sup> T cells were less diabetogenic compared to untreated CD8<sup>+</sup> T cells, resulting in a restoration of insulin secretion by  $\beta$ -cells associated with lower glycemia (Patry et al., 2015) (**Figure 10A**). In pancreatic cancer,  $\beta$ ig-h3 is present in the ECM as early as ADM lesions stage and accumulates in the stroma in mouse models and humans but is also detected in the blood of patients throughout the disease progression (**Figure 10B**)(Costanza et al., 2019; de la Fouchardière et al., 2022; Goehrig et al., 2019). Given the early secretion of  $\beta$ ig-h3, it is considered as a potential biomarker for PDAC combined with CA 19-9 marker (de la Fouchardière et al., 2022; Yang et al., 2020) although there are no published data about  $\beta$ ig-h3 detection specificity and sensitivity,  $\beta$ ig-h3 was reported to be secreted by CAFs. Targeting  $\beta$ ig-h3 with a monoclonal antibody showed in vivo response by lowering pancreatic tumor growth in both implanted and spontaneous PDAC models. More importantly,  $\beta$ ig-h3 depletion is associated with an increase in effector CD8<sup>+</sup> T cell response and thinner collagen fibers without perturbing the total collagen content (**Figure 10C**)(Goehrig et al., 2019).

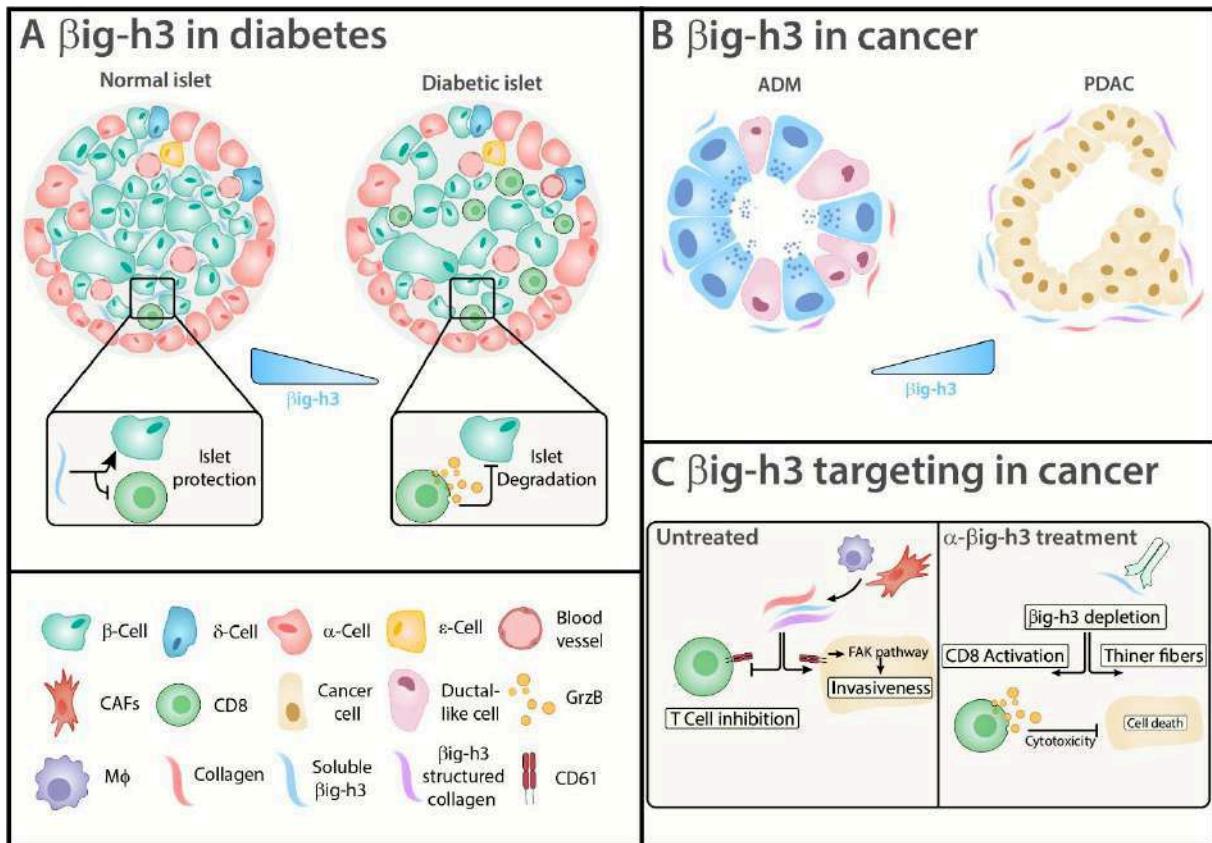


**Figure 10. βig-h3 in pancreas pathology.**

**A** In diabetes, βig-h3 is downregulated, allowing CD8+ T cells to exert cytotoxic activity on insulin-producing β-cells.

**B** In pancreatic cancer, βig-h3 is upregulated and can exist in soluble form or bind to collagen fibers.

**C** Both forms of βig-h3 can inhibit T cells and induce cancer cell invasiveness. βig-h3 can be targeted in pancreatic cancer with a monoclonal antibody, unleashing CD8+ T cells' potential, but also inducing a restructuring of the collagen fibers

Although it is reported that βig-h3 is mainly secreted by CAFs (Goehrig et al., 2019), there are evidence of βig-h3 secretion from a proportion of cancer cells in PDAC (Costanza et al., 2019). βig-h3 can bind to β5 integrin on cancer cells and induce FAK pathway activation leading to invasive phenotype (Costanza et al., 2019). Accumulated evidence shows that βig-h3 is not only secreted by CAFs and cancer cells. Indeed, in both ovarian cancer and glioblastoma (Lecker et al., 2021; Peng et al., 2022), IL-4 stimulated macrophages were shown to secrete βig-h3 to support tumor progression. More importantly, anti-βig-h3 targeting was also efficient in ovarian cancer (Lecker et al., 2021). Finally, we demonstrate (results section) that βig-h3 can also be secreted by macrophages in both mouse and human PDAC.

#### iv. Fibronectin

Although this work is mainly focused on the ECM proteins mentioned above, it is important to note that other proteins structure the ECM. One of them is the glycoprotein fibronectin, which is found at higher levels in PDAC compared to the normal pancreas (Tian et al., 2019). There are two main forms of fibronectin: soluble fibronectin found in the bloodstream and insoluble fibronectin found in the ECM. Fibronectin has binding sites for various cell surface receptors, such as integrins, and it helps anchor cells to the ECM (Gamradt et al., 2021). This is essential for processes like tissue development, wound healing, and cell migration. In PDAC, the presence of fibronectin is associated with chemotherapy resistance (Amrutkar et al., 2019). Fibronectin is mainly produced by CAFs. In a landscape study, it was demonstrated that fibronectin promotes metastatic dissemination to the liver. Indeed, the authors showed that PDAC exosomes are captured by Kupffer cells (Costa-Silva et al., 2015). In return, Kupffer cells secrete TGF- $\beta$  and induce fibronectin secretion by hepatic stellate cells. Additionally, the role of structuring the ECM network, fibronectin can directly impact immune cells through integrin pathway (Gamradt et al., 2021).

#### v. Mechanical forces

The deposition of ECM proteins is intrinsically associated with tissue stiffness. Tissue stiffness is the property of a tissue to be easily compressed or stretched. Tissue stiffness is rarely directly measured; instead, the elastic modulus is measured. The elastic modulus is a fundamental mechanical property that quantifies a material's resistance to deformation when subjected to an applied stress, providing a measure of how stiff or rigid a material is. The elastic modulus (E) is typically defined as the ratio of stress ( $\sigma$ ) to strain ( $\epsilon$ ) within the elastic deformation range:  $E = \sigma/\epsilon$ , where  $\sigma$  is the force applied per unit area (force/area), and  $\epsilon$  is the relative change in length or deformation of the material. It is important not to confound tissue stiffness with solid stress and/or IFP, which are interconnected but different.

Cells are sensitive to mechanical signals in both pathological and steady-state conditions (Northey et al., 2017). Cells have mechano-receptors capable of sensing mechanical changes in the environment. The most common pathways activated by these changes are the YAP and FAK pathways through integrin–ECM contact (Northey et al., 2017).

In PDAC, qPSC are capable of becoming activated CAFs due to increased mechanical forces in the matrix (Lachowski et al., 2017). The same group showed that pancreatic cancer cells were also sensitive to mechanical forces resulting in the process of EMT (Rice et al., 2017). Finally, what is considered a

landscape study in the field of mechanobiology applied to PDAC showed that mechanical forces can be modeled by cancer cells. They demonstrated that increased contractibility of pancreatic cancer cells directly affects local collagen structure and impacts tissue stiffness. As a consequence, cancer cells experience higher mechano-signaling locally through the activation of the YAP pathway (Laklai et al., 2016).

To date, there are no studies reporting the role of tissue stiffness on macrophages and T cells in PDAC, although both populations are mechano-sensitive (Adu-Berchie et al., 2023; Meng et al., 2020; Solis et al., 2019). This lack of information is mainly due to the absence of models to study mechanical forces. Indeed, studies on mechanical forces are often limited to artificial matrices with distinct stiffness. While it is interesting to analyze the pathways involved in mechano-sensitivity, it does not fully recapitulate the physiological events. Tissue stiffness is constantly evolving during tumorigenesis in PDAC and can vary significantly from one location to another. Therefore, dynamic ECM models that mimic *in vivo* changes are needed.

## B. The immune system in PDAC

### a. Introduction

Our tissues contain patrolling immune cells that maintain the integrity of the tissue, divided into two categories: innate and adaptive immune cells. On one hand, innate immune cells such as macrophages, dendritic cells (DCs), and natural killer (NK) cells exhibit non-specific responses and lack memory capabilities. They promptly respond to invading pathogens or aberrant cells without the ability to undergo clonal expansion. These cells recognize molecular patterns, known as DAMPs (damage-associated molecular patterns) and PAMPs (pathogen-associated molecular patterns). This broad recognition allows innate immune cells to detect a wide range of pathogens, enabling rapid and diverse responses against potential threats. Innate immunity serves as the first line of defense in a tissue, responsible for secreting inflammatory cytokines (IL-1, IL-6, TNF $\alpha$ ) and chemokines (CCL2) to activate and recruit other innate and adaptive immune cells. On the other hand, adaptive immune cells (CD8<sup>+</sup>, CD4<sup>+</sup> T cells, and B cells) are late responders but highly specific and can undergo clonal expansion. They are recruited to the tissue if the inflammatory response is long-lasting, although there is tissue resident CD8<sup>+</sup> T cells and  $\gamma\delta$  T cells.

We know that tumors are monitored by the immune system, as mice lacking an immune system are more sensitive to tumor development (Shankaran et al., 2001). Another proof of that concept is the regression of melanoma in patients with skin auto-immune disease (e.g., Vitiligo) (Zitvogel et al., 2021). As a cancer initiates, both the innate and adaptive immune systems can induce cancer cell death or cancer cell senescence (Dunn et al., 2004). It can either be sufficient to stop the tumor growth or not. The immune surveillance is supported by the **3Es** theory: **E**limination, **E**quilibrium, **E**scape (**Figure 11**)(Dunn et al., 2004).

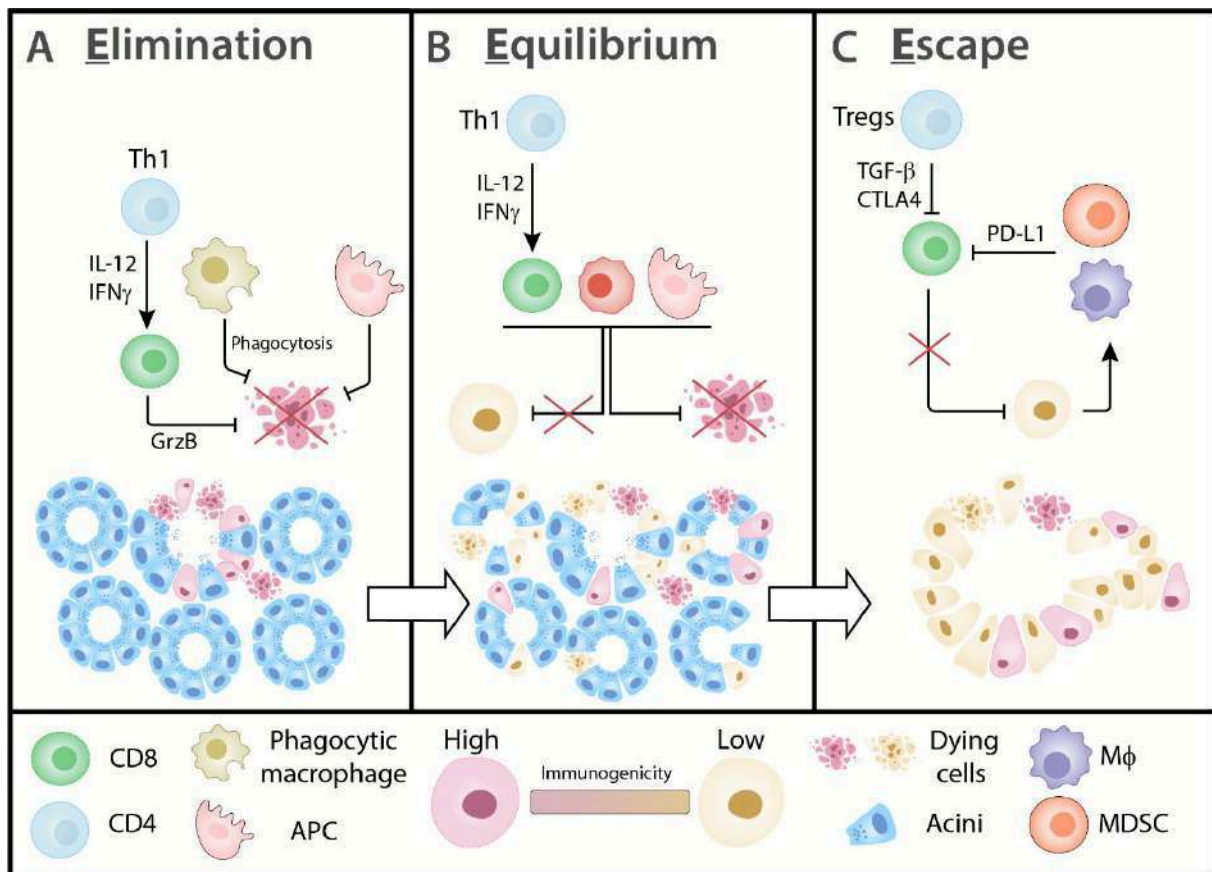


Figure 11. 3e hypothesis in pancreatic cancer

**A** Elimination phase. Neoplastic pancreatic cancer cells are rapidly eliminated by the innate and adaptive immune systems but are selected over time. **B** Equilibrium phase. Through selection, some pancreatic cancer cell clones resist immune surveillance and establish an equilibrium between cancer cell clearance and cancer cell emergence. This phase lasts for years. **C** Escape phase. The number of pancreatic cancer cell clones with low immunogenicity and the recruitment of immune suppressive populations allow the tumor to escape from the immune system and grow.

APC Antigen presenting cell, MDSC Myeloid Derived Suppressor cells

The Elimination phase refers to the mobilization of both innate and adaptive immunity during the early stage of cancer. Through various immunological mechanisms that will be discussed, they eliminate the abnormal cells from the tissue (**Figure 11A**). In PDAC, both CD8<sup>+</sup> and CD4<sup>+</sup> T cells increase as early as PanIN lesions and expand throughout PDAC progression (Clark et al., 2007), however, these T lymphocytes are not necessarily effective.

The Equilibrium phase is long and occurs prior to cancer detection (**Figure 11B**). It happens when the elimination phase fails. In this phase, there is constant communication between cancer cells and the immune system. This communication is based on the fundamental model called the 'cancer-immunity cycle.' The latter explains step by step how the immune system can restrain cancer progression through cancer cell elimination (**Figure 12**). (Chen and Mellman, 2013). When dying, cancer cells release antigens (**Figure 12.1**). Antigen-Presenting cells (APCs), mainly DCs, undergo

maturation and uptake tumoral antigens to prime and activate T cells (**Figure 12.2,3**). Attracted by danger signals, activated T cells traffic and infiltrate the tumor site (**Figure 12.4,5**). They recognize their target and kill the cancer cell (**Figure 12.6,7**), leading to more cancer cell antigen releasing (**Figure 12**). One evidence of the equilibrium phase is the observation that transplanted organs apparently cancer-free emerge as cancer in the recipient under immune-suppressive treatment (Mackie et al., 2003). It shows that cancer cells in the donor were indeed in an equilibrium phase for years. This concept of immunoediting was recently elaborated in human PDAC (Łuksza et al., 2022).

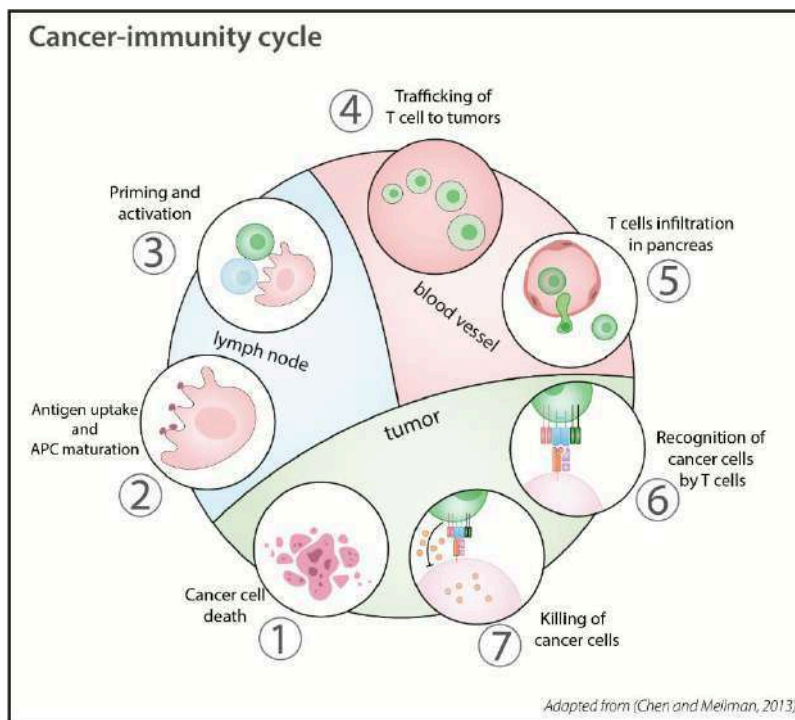


**Figure 12. Cancer-immunity cycle applied to pancreatic cancer.**

Cancer-immunity cycle rule the immune response in cancer and is composed of 7 steps. 1, Cancer cells death occurring in pancreatic tissue ; 2, DCs uptake antigens and mature during lymphoid tissue migration; 3, T cells are primed by APCs; 4, T cells are attracted by danger signals in the tumoral tissue and traffic in blood stream; 5, T cells invade pancreatic tissue through extravasation; 6, antigen specific T cells recognize cancer cells; 7, T cells exert cytotoxic activities on cancer cells.

The Escape phase usually occurs at the same time as clinical symptoms (Figure 11C). While the cycle is occurring, cancer cells are 'immunoselected.' In other words, they are immune-resistant clones emerging in the intra-tumoral heterogeneity mosaic. Cancer cells acquire a repertoire of immune evasion mechanisms and adaptation mechanisms because of immune system pressure (Tsai et al., 2023). MHC-I loss, physical inaccessibility caused by the ECM, immunological editing, and recruitment of immune suppressive populations are the main escape mechanisms.

In this chapter, we will discuss the main immune actors in pancreatic cancer, how PDAC is the realm of immune escape mechanisms, and finally, the state of immunotherapy in pancreatic cancer.

b. The actors of the immune system in PDAC

i. Good and bad immunity

Due to the wide range of immune cells present in tumors and the diverse extracellular signaling within the TME, immune cells can exhibit both positive and negative effects on tumor progression. Researchers have classified immune cells as either beneficial or detrimental in cancer based on their function and behavior (Galon and Bruni, 2020). The abundance of immune cell populations varies greatly across different cancer types, stages, and individuals (Thorsson et al., 2018). For instance, NK cells are plentiful in breast cancer but are scarce in the PDAC TME (Steele et al., 2020). To assess clinical outcomes, an alternative to the traditional TNM (Tumor – Lymph Node – Metastasis) classification has been proposed. This alternative, known as the Immunoscore, involves histopathological analysis of CD8<sup>+</sup> T cells and CD3<sup>+</sup> T cells found in both the central region (CT) and invasive margin (IM) of the tumor. The Immunoscore gained international recognition following a study involving over 2500 patients with colorectal cancer, which revealed that patients with high Immunoscore had a significantly lower risk of recurrence after 5 years (Pagès et al., 2018).

Although there have been no studies evaluating the relevance of the Immunoscore in pancreatic cancer, the immune composition has been well-characterized. The immune cell landscape in PDAC is primarily composed of T cells and myeloid cells (macrophages and Myeloid-Derived Suppressor Cells (MDSCs)). Additionally, there are DCs, B cells, plasma cells, and NK cells, although their presence is relatively minor compared to the aforementioned cell types.

In the next parts, we will discuss about lymphoid cells (T and B cells). It's noteworthy that given the major contribution of macrophages in PDAC and their central place in this thesis, they will be discussed in a following separate chapter (Chapter III).

ii. T lymphocytes

T lymphocytes, referred to as T cells, are a vital component of the immune system as white blood cells. Their primary function entails identifying and combating external intruders like viruses, bacteria, cancer cells, and others anomalous cells within the body. These cells originate in the bone marrow and undergo maturation in the thymus gland, hence their designation as "T" cells. Within the immune system, T cells encompass various types, each possessing a distinct role.

Given the vital role of T cells, their regulation is tailor-made to avoid any disruption of immune homeostasis that are responsible of some diseases. Immune homeostasis is defined by the balance between immune tolerance and immune activation.

Immune tolerance is a prevalent physiological state wherein the immune system refrains from developing a response against self-antigen expressing cells. This state of tolerance is actively induced prior exposure to the antigen. There are two main types of tolerance: central and peripheral. Central tolerance, also known as negative selection, occurs in the thymus and is responsible for eliminating self-reactive T cells (Murphy and Weaver, 2016). Peripheral tolerance occurs in tissues to regulate self-reactive T cells in peripheral tissues. These mechanisms include co-stimulatory receptors, immune-suppressive populations, and, notably, immune checkpoints that play a crucial role in modulating the immune response. Immune checkpoints are divided into stimulatory or inhibitory checkpoints; there are numerous checkpoints, mainly expressed by T cells and APCs, as described in Figure 15. Immune checkpoints have been at the center of cancer biology for the last three decades, as we discovered that immune checkpoint hijacking was one of the main immune escape mechanisms (Leach et al., 1996). Both immune checkpoint and associated therapies will be further discussed in the context of pancreatic cancer.

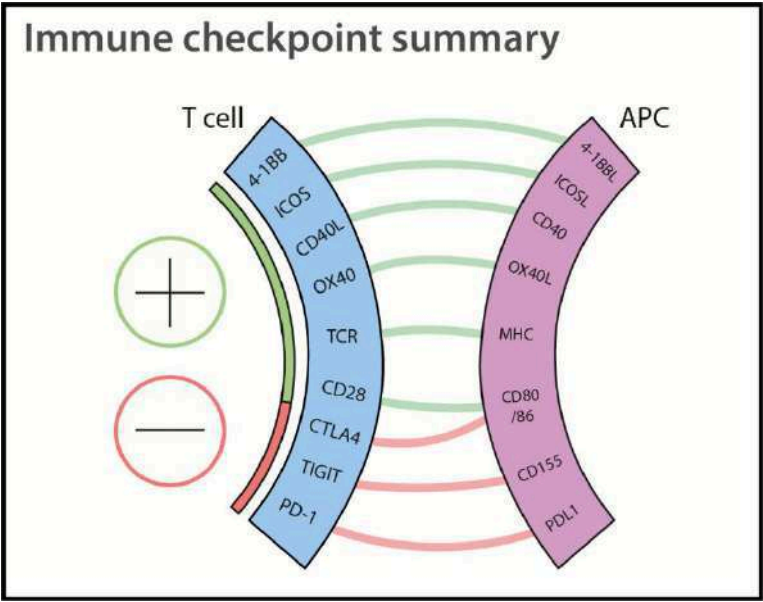


Figure 13. Immune checkpoint summary

T cells express a large amount of immune checkpoint that rule their activities. They have either positive (+) or negative (-) effect on T cells activation. Most of T cell immune checkpoint are dictated by APCs.

**CD8<sup>+</sup> T cells cytotoxic T cells:** These cells directly attack and kill infected or abnormal cells in the body. T cells utilize their T-cell receptor (TCR) to identify specific targets by interacting with the MHC-I complex. Once activated, they release cytotoxic agents (e.g., granzyme B, perforin) into the targeted cell. High infiltration of CD8<sup>+</sup> T cells is associated with a better prognosis in human PDAC. (Ino et al., 2013). However, the quality of the effector T cell matters. Caused by mutations during proliferation, cancer cells generate new antigens that are only expressed in tumor cells, called neoantigens. In pancreatic cancer, it has been reported that long-term survivors have higher quality neoantigens compared to short-term survivors (Balachandran et al., 2017; Łuksza et al., 2022). Indeed, some neoantigens confers a higher immunogenicity (e.g., Mucin-16 (MUC16)).

**CD4<sup>+</sup> Helper T cells (Th):** These cells help activate other cells in the immune system, including B cells and cytotoxic T cells, to fight off infections, through the recognition of the MHC-II complex. They are defined by the CD4 TCR. CD4<sup>+</sup> T cells are precursors to a large variety of helper T cells (Th) (**Table 5**). The most common ones are Th1 and Th2, but there are also Regulatory T Cells (Tregs), Th17, and others (**Table 5**). The fate of CD4<sup>+</sup> T cells is mainly decided by environmental cytokines, triggering specific transcription factors (**Table 5**).

Name	Associated cytokine	Master regulator TF	Secreted cytokine
Th1	IL-12 IFN $\gamma$	T-bet	IFN $\gamma$ TNF $\alpha$
Th2	IL-4	GATA-3	IL-4 IL-5 IL-13
Tregs	IL-2 TGF $\beta$	FOXP3	IL-10 TGF $\beta$
Th17	IL-6 IL-1b TGF $\beta$	RORGT	IL-17A IL-22

TF Transcription factor, T-bet T-box expressed in T cells, FOXP3 Forkhead Box P3, RORGT RAR-related orphan receptor gamma. Adapted from (Gelse, 2003)

**CD4<sup>+</sup> regulatory T cells :** These cells are differentiated from CD4<sup>+</sup> T cells and are mainly characterized by the expression of the transcription factor (TF) FoxP3. Tregs are necessary for peripheral tolerance as they restrain self-reactive T cells and excessive immune response. They are associated with a poor prognosis in PDAC and the majority of cancers (Fridman et al., 2017). The differentiation of CD4<sup>+</sup> T cells is thought to be partially driven by TGF $\beta$  secreted by PDAC cells (Moo-Young et al., 2009). Despite their poor prognosis association, the depletion of Tregs did not yield favourable outcomes (Zhang et al., 2020). In this study, the authors made an unforeseen discovery when they found that the depletion of Tregs led to tumor progression. They observed that the depletion of Tregs was associated with a decline in  $\alpha$ SMA<sup>+</sup> CAFs and collagen, thought to be tumor-restricting, while simultaneously increasing the presence of immunosuppressive myeloid cells (Zhang et al., 2020). An additional interaction between CAFs and Tregs was demonstrated in a recent study. Given that apCAF<sup>s</sup> express the MHC-II complex but lack a co-stimulatory receptor, they induce CD4<sup>+</sup> T cell anergy and provoke Tregs differentiation (Huang et al., 2022). Importantly, the levels of apCAF<sup>s</sup> were found to correlate with the levels of Tregs in human PDAC (Huang et al., 2022).

**$\gamma\delta$ -T cells :**  $\gamma\delta$  T cells are a unique subset of T cells expressing a TCR composed of  $\gamma$  and  $\delta$  chains instead of  $\alpha\beta$ . They also develop in the thymus but are not restricted to MHC-I or MHC-II cognate peptides (Vantourout and Hayday, 2013). This trait enables a faster response compared to the normal kinetics of adaptive immunity (Zeng et al., 2012), It may indicate that  $\gamma\delta$  T cells are somehow related to innate immunity. It has been reported that  $\gamma\delta$  T cells are significantly more prevalent in human PDAC

compared to CD8<sup>+</sup> T cells. Depletion of  $\gamma\delta$  T cells led to infiltration and activation of CD4<sup>+</sup> and CD8<sup>+</sup> T cells, ultimately resulting in tumor reduction

### iii. B Lymphocytes

B lymphocytes are mostly found in secondary lymphoid organs (spleen and lymph nodes) and are characterized by a specific expression of the B-cell receptor (BCR). B cells have numerous functions in TME. One of their functions is to secrete soluble forms of their BCR as antibodies when they are activated. B cells can take up tumor-specific antigens through the internalization of their BCR. Once activated, they become plasma cells and release their BCR. Many mechanisms are associated with antibody secretion in cancer. Tumor-specific antigens can be targeted by antibodies, leading to several processes: antibody-dependent cellular phagocytosis (ADCP) mediated by macrophages, and antibody-dependent cellular cytotoxicity (ADCC) mediated by NK cells. While T cells have been extensively studied in cancer, we lack a good understanding of the ins and outs of B cell biology in PDAC. Indeed, the effect of B cell infiltration on PDAC prognosis is currently being discussed (Laumont et al., 2022; Wouters and Nelson, 2018). "While some studies show that B cell infiltration is associated with a good prognosis, others demonstrate a neutral or negative association. The poor understanding of B lymphocyte function in PDAC may stem from the fact that there are fewer infiltrated B cells in the KPC golden standard model than in human pathology (Elyada et al., 2019). However, we know that B cells infiltrate pancreatic tissue during the neoplastic stage (Pylayeva-Gupta et al., 2016). The question of B cells in cancer more is linked to the presence of Tertiary lymphoid structure (TLS) or regulatory B cells (Bregs).

On one hand, TLS are lymphoid-like structures organized in the peripheral tissue, resulting from specific cytokine and chemokine signaling occurring in the TME (Sautès-Fridman et al., 2019). They are organized as a germinal center with a B cell area, a T cell area, and differentiated DCs, allowing the activation of effector CD8<sup>+</sup> T cells next to tumor cells (Sautès-Fridman et al., 2019). These structures allow for a quicker CD8<sup>+</sup> T cell response. In pancreatic cancer, the presence of TLS is associated with a good prognosis (Castino et al., 2016; Hiraoka et al., 2015; Kinker et al., 2023). In PDAC, tertiary lymphoid structures (TLS) may be formed by sustained TGF $\beta$ -stimulated T cells that secrete the B cell chemoattractant CXCL13 (Kinker et al., 2023) although the majority of CXCL13 is secreted by CAFs (Pylayeva-Gupta et al., 2016).

On the other hand, there is evidence showing that B cells can have an immune suppressive role in PDAC. Specifically, CD19<sup>+</sup>CD1dHiCD5<sup>+</sup>(CD21Hi) cells have been reported as regulatory Bregs (Mirlekar et al., 2018; Pylayeva-Gupta et al., 2016). Bregs secrete the IL-35 cytokine and inhibit CD8<sup>+</sup> T cell function and recruitment through STAT-3 activation in CD8<sup>+</sup> T cells (Mirlekar et al., 2020, 2018). More

importantly, the equilibrium between Bregs and plasma cells plays a crucial role in pancreatic cancer. A master regulator of this equilibrium is IL-35, which drives the transcriptional reprogramming of naïve B cells into Bregs while inhibiting plasma cell differentiation (Mirlekar et al., 2022). IL-35 is considered a potential therapeutic target in PDAC, as preclinical results have shown promising outcomes (Mirlekar et al., 2022, 2020, 2018; Pylayeva-Gupta et al., 2016).

#### iv. Myeloid-derived suppressor cells

MDSCs are cells that emerge from the bone marrow, sharing a common precursor with macrophages and DCs. In the context of cancer, myelopoiesis is impaired, and myeloid progenitors are more prone to become MDSCs than macrophages or DCs (Groth et al., 2019). They can be differentiated from monocytes by various mechanisms, such as the secretion of extracellular cues by PSCs (Mace et al., 2013). Their survival in pancreatic was shown to be dependent on PDAC cells (Stromnes et al., 2014). They are divided into two categories : Monocytic ( $CD11b^+, Ly6G^-, Ly6C^{Hi}$ ) and granulocytic ( $CD11b^+, Ly6G^+, Ly6C^{Low}$ ) but both types suppress  $CD8^+$  T cells. Throughout the progression of PDAC, there is an accumulation of infiltrating MDSCs in the tissue, impairing an effective immune response against cancer cells (Clark et al., 2007). Additionally, cancer cells secrete granulocyte-macrophage colony-stimulating factor (GM-CSF), which regulates the recruitment and immunosuppressive functions of MDSCs, in turn inhibiting  $CD8^+$  T cells (Bayne et al., 2012). MDSCs have been shown to exhibit high heterogeneity in human PDAC (Gulhati et al., 2023).

#### c. Immune escape mechanisms in PDAC

##### i. Priming and T cells trafficking

###### **Priming**

The uptake of antigen to prime T cells can be impaired. Indeed, DCs are unable to uptake neoantigens in PDAC for several reasons. First, they are not mobilized during PDAC development and are present in low numbers. More importantly, cross-presenting  $CD103^+CD24^{Hi}$  dendritic cells (cDC1s) at the tumor site express low levels of both co-stimulatory and maturation markers (CD86, TIM-3, OX40-L, MHC-I) in PDAC compared to lung cancer (Hegde et al., 2020). Despite the proper loading of neoantigens, these DCs are not capable of priming  $CD8^+$  T cells in secondary lymphoid organs (Hegde et al., 2020). DCs are not only weakened on the tumor site but also during development stage, where DCs precursors are favored to become MDSCs (Meyer et al., 2018).

## Trafficking

T cells trafficking and infiltration into the TME in PDAC is difficult. Lymphocytes infiltration can be impaired by blood vessel compression induced by desmoplasia (Olive et al., 2009; Provenzano et al., 2012). More importantly, the ECM can serve as a physical barrier. It was shown in both murine and human PDAC that CD8<sup>+</sup> T cells are trapped in the ECM, preventing them from cancer cells (Ene-Obong et al., 2013; Hartmann et al., 2014). Also, one of the main tumor escape mechanisms in cancer is the loss of MHC-I making cancer cells invisible to CD8<sup>+</sup> T cells. This mechanism has been reported in PDAC (Pommier et al., 2018; Ryschich et al., 2005). Specifically, the loss of MHC-I in PDAC cells is thought to be mediated by autophagy (Yamamoto et al., 2020).

### ii. Effector T cells inhibition

Most immune-escape mechanisms occurring in the tumor microenvironment (TME) act directly on effector T cells. The mechanisms organizing the inhibition of effector T cells are complex, highly diverse, and rely on several factors, such as immune checkpoints, extracellular cues, or the recruitment of immunosuppressive cells.

Within the context of cancer, CD8<sup>+</sup> T cells are commonly referred to as effector CD8<sup>+</sup> T cells (CD8<sup>+</sup> Teff) due to their active cellular state. However, as cancer persists (i.e., the cancer-immunity cycle runs indefinitely), CD8<sup>+</sup> T cells encounter repeated recognition of the same antigen (Chow et al., 2022). This repetitive stimulation leads to a gradual loss of their ability to proliferate and perform cytotoxic activities, resulting in their functional exhaustion. These exhausted CD8<sup>+</sup> T cells (CD8<sup>+</sup> Tex) predominantly upregulate the programmed cell death 1 (PD-1) immune checkpoint (Chow et al., 2022). When PD-1 binds to Programmed Cell Death Ligand 1 (PD-L1) expressed on APCs (**Figure 13**), it eventually leads to T cell death. Abnormal expression of PD-L1 by cancer cells and other immune cells (e.g., macrophages) (Diskin et al., 2020) hijack this mechanism to inhibit CD8<sup>+</sup> Teff. Of note, it has been reported that CD8<sup>+</sup> T cells can also express PD-L1 and suppress their neighboring macrophages and T cells (Diskin et al., 2020). CD11b<sup>+</sup> Ly6G<sup>+</sup> MDSCs have been shown to enable PDAC maintenance, but more importantly, it has been reported that myeloid cells express PD-L1 and induce PD-L1 expression on cancer cells to inhibit CD8<sup>+</sup> T cells in PDAC (Stromnes et al., 2014; Zhang et al., 2017).

While PD-1 exerts an immune suppressive activity in the tumoral tissue, it is thought that Cytotoxic T-lymphocyte-Associated protein 4 (CTLA-4) also inhibits the anti-tumoral immune response but not at the same place and time point. Indeed, CTLA-4 is an immune checkpoint found on the surface of T cells. CTLA-4 binds to the CD80/CD86 co-stimulatory molecules and outcompetes the CD28 co-stimulator since it has a much higher affinity with CD80/86. In PDAC, CTLA-4 is abundantly found on

the surface of Tregs (Gulhati et al., 2023; Steele et al., 2020). In PDAC, tregs are mainly found in the draining lymph nodes and may regulate CD4<sup>+</sup> T cell infiltration into the tumor through CTLA-4 expression, at least in mouse models (Bengsch et al., 2017).

d. Current immunotherapy status in PDAC

i. Immune checkpoint based strategy

Monoclonal antibodies have been created to target various immune checkpoints that regulate the immune response, especially the response of CD8<sup>+</sup> T cells. Antagonist antibodies or Immune Checkpoint Inhibitors (ICIs) are used to target negative immune checkpoints (e.g., PD-1, CTLA-4, and TIGIT) to inhibit their signaling. By targeting CTLA-4, the competition between CD28 and CTLA-4 to bind to the CD80/86 co-stimulatory molecule is weakened (Figure 13). PD-1/PD-L1 signaling targeting can be achieved with the use of anti-PD-1 or anti-PD-L1, allowing the decrease of the CD8<sup>+</sup> T cell activation threshold. Although anti-PD-1 and anti-PD-L1 targeting may seem similar, they target two different biological compartments, as PD-1 is expressed on T cells and PD-L1 on cancer cells and myeloid cells. More importantly, anti-CTLA-4 and anti-PD-1/PD-L1 are thought to act during the priming and effector phases, respectively. This observation may explain why the combination of anti-CTLA-4 with anti-PD-1/PD-L1 shows greater results than monotherapy (Hodi et al., 2018). In PDAC, anti-CTLA-4, anti-PD1 or the combination showed no benefits in patient compared to standard of care (O'Reilly et al., 2019; Royal et al., 2010; Wainberg et al., 2020).

These observations can be explained by several reasons: i) as previously described, PDAC is infiltrated with a great amount of immune suppressive cells, ii) drug delivery efficiency is impaired, iii) T<sub>H</sub>1 are physically blocked and cannot reach the cancer cells, iv) immune checkpoint ligand expression is heterogeneous across patients, v) PDAC cells do not produce enough antigens to stimulate and prime the immune response. Since mono and combination therapies of ICI failed, there are multiple ongoing attempts to combine ICI with other therapies (**Table 6**). Given the desmoplastic nature of pancreatic cancer, stroma-based therapies are the most commonly associated with ICI. Most combined therapies with stroma-based therapies showed greater results than monotherapy (**Table 6**). These observations are in line with the idea that ICI efficiency in PDAC is mainly limited by the stroma. However, some therapies showed no benefit, such as the combination between anti-PD-1 and PEGPH20. (Zhen et al., 2022).

Conversely, agonist antibodies are employed to target positive immune checkpoints (e.g., CD40, GITR, OX40, CD28) and induce T cell proliferation and survival. Agonist therapies are less frequent than antagonist therapies for many reasons. Indeed, co-stimulatory receptors that are targeted are usually

expressed in a specific time window during T cell activation. Finally, one of the most challenging aspects of agonist therapies is understanding the duration and number of cycles of agonist administration. Indeed, agonist antibodies can induce CD8<sup>+</sup> T cell exhaustion as T cells are constantly stimulated. There have been investigations to evaluate the synergic effect of  $\alpha$ PD-1 combined with CD40 agonist, and no benefits have been observed compared to  $\alpha$ PD-1 monotherapy (Padrón et al., 2022) although encouraging results are observed in pre-clinical studies when  $\alpha$ PD-1 is combined with  $\alpha$ TIGIT and CD40 agonist (**Table 6**).

ii. Adoptive transfer immunotherapy

Another path of immunotherapy is chimeric antigen receptor T cells (CAR-T cells), which involves genetically modifying a patient's T cells to recognize and attack cancer cells. Patient's T cells are extracted from the blood and modified to recognize specific neoantigens when reinfused into the bloodstream. This approach was initially developed for non-solid cancers (Maude et al., 2014; Schuster et al., 2019). However, despite early limitations of CAR-T cells in solid cancers, encouraging data are observed in human PDAC (Leidner et al., 2022). In a groundbreaking study conducted by Allen et al. (Allen et al., 2022), The impact of CAR-T cells equipped with a synthetic IL-2 secretion circuit upon binding to cancer cell antigens was assessed. The results demonstrated that localized secretion of IL-2 combined with CAR-T cells exhibited improved survival rates and reduced toxicity compared to systemic injection of IL-2 in conjunction with CAR-T cells. Notably, the study also revealed that locally delivered IL-2 from CAR-T cells facilitated autocrine expansion of T cells and enhanced the recruitment of CD8<sup>+</sup> T cells (Allen et al., 2022).

<b>Table 6. Combined ICI based immunotherapy in PDAC</b>			
<b>ICT</b>	<b>Phase</b>	<b>Results</b>	<b>Reference</b>
αPD-1 + CD40 agonist + αTIGIT	pre-clinical	Show significant benefits compared to monotherapy	(Freed-Pastor et al., 2021)
αPD1 + CD40 agonist	II	Show less benefit compared to αPD1 monotherapy	(Padrón et al., 2022) (NCT03214250)
αPD1 + αCTLA4 + FAKi + chemo	pre-clinical	Show better survival rate compared to monotherapy alone with less Tregs infiltration	(Jiang et al., 2016)
αPD1 + FAKi	II	Ongoing	(NCT03727880)
αPD1 + Homotrimer collagen depletion	pre-clinical	Increase survival compared to αPD1 monotherapy or collagen depletion only. Correlate with less Tregs	(Chen et al., 2022)
αCTLA4 + myCAFs depletion	pre-clinical	Combined therapy showed better survival rate than monotherapy associated with less aggressive tumor and less tregs	(Özdemir et al., 2014)
αPD-L1 + LRRC15 CAFs depletion	pre-clinical	Combined therapy led to smaller tumor volume and CD8 <sup>+</sup> T <sub>eff</sub> infiltration compared to control	(Krishnamurty et al., 2022)
αPD-1 + CXCR4i	II	Trial suspended, no published results yet	(NCT02907099)
αPD-1 + CXCR4i + chemo	II	Increase disease stabilization	(Bockorny et al., 2020) (NCT02826486)
αPD-1 + PEGPH20	II	Combination showed no benefits compared to historical data	(Zhen et al., 2022) (NCT03634332)
αPD-L1 + CV301	I/II	Ongoing	(NCT03376659)

(Continue next page)

$\alpha$ PD-L1 + AMD3100	pre-clinical	Show reduced tumor growth with higher CD8 infiltration	(Feig et al., 2013)
$\alpha$ PD-L1 + IL-35 depletion	pre-clinical	Showed higher CD8 infiltration and activities with lower tumor weight	(Mirlekar et al., 2018)
$\alpha$ CD40 + GEM	pre-clinical		(Long et al., 2016)

As discussed, one of the main reasons for therapeutic failure in PDAC is the massive immune suppression ongoing in the TME. The immune cell population that is most represented in the PDAC TME is macrophages. We will explore how the plastic and tissue-remodeling nature of macrophages can support PDAC development and impair therapeutic approaches. More importantly, we will delve into the cross-communication between the stromal compartment, the lymphoid compartment, and macrophages.

### III. Macrophages are the pillars of the pancreatic TME

#### A. Macrophages development and maintenance

##### a. Introduction

It all started with an observation in starfish larvae of cells engulfing others. Discovered at the end of the 19th century by Ilya Ilyich Metchnikoff (Metchnikoff, 1887), phagocytes (from the Greek phagein, 'to eat,' and -cyte, 'cells') are the pivots of the adaptive immune response, tissue architecture, and homeostasis. Alterations in macrophage development in humans can lead to leukoencephalopathy caused by non-functional brain tissue-resident macrophages (Oosterhof et al., 2019; Rademakers et al., 2011). Phagocytes are generally classified into two types: macrophages and DCs, although monocytes and granulocytes can be categorized as phagocytes. Macrophages differ from DCs in several aspects. On one hand, macrophages are long-lived specialized immune cells that reside in almost all tissues and organs, playing a crucial role in the innate immune response as the first line of defense against pathogens. They are capable of recognizing and engulfing foreign particles, pathogens, and cellular debris through phagocytosis; they function as cleaners. Macrophages also release cytokines, regulating inflammation and facilitating immune cell recruitment in the tissue. On the other hand, DCs, like macrophages, are responsible for capturing antigens. However, their specificity lies in their ability to present the antigen to other immune cells by maturing and migrating to secondary lymphoid organs.

Macrophages are highly sensitive to their environment; therefore, they have a central role in steady-state homeostasis and in many altered states (e.g., cancer, obesity, infection). Throughout this chapter, we will delve into the developmental pathway and maintenance state of macrophages in tissues at steady state and in cancer. We will particularly focus on macrophages in PDAC and how they can establish a niche within the TME.

##### b. Macrophages development and maintenance

###### i. Mononuclear Phagocyte System

Macrophages are part of what is called the Mononuclear Phagocyte System (MPS). Stated by Furth and collaborators (van Furth et al., 1972), the MPS is a network of cells consisting of circulating monocytes differentiating into macrophages or DCs (**Figure 14**). These macrophages are referred to as monocyte-derived macrophages. Understanding the development pathway of monocytes is crucial for comprehending the regulation of macrophages during adulthood. The development of monocytes is

highly intricate, and our understanding is constrained by reliance on specific markers and the chosen model. Consequently, the following developmental pathways may not provide an exact representation of reality, as certain precursors may exhibit overlapping functions.

During adulthood, circulating monocytes are produced in the bone marrow from hematopoietic stem cells (HSCs). Specifically, common myeloid progenitors (CMPs) arise from HSCs and give rise to various cell lineages. CMPs have been identified as the source of megakaryocyte and erythrocyte progenitors (MEPs) as well as granulocyte-macrophage progenitors (GMPs) that give rise to neutrophils, eosinophils, and basophils (**Figure 14**). Additionally, GMPs are also involved in the emergence of macrophage and DCs precursors (MDPs) (Fogg et al., 2006) although MDPs can develop directly from CMPs (Yáñez et al., 2017). MDPs further differentiate into two distinct progenitor populations: CD135<sup>low</sup> common monocyte progenitors (cMoPs) (Hettinger et al., 2013) and c-kit<sup>low</sup> common dendritic cell progenitors (CDPs) (Naik et al., 2007)(Onai et al., 2007). CDPs give rise to pre-DCs (Liu et al., 2009), which subsequently circulate and differentiate exclusively into DCs within tissues (**Figure 14**).

Meanwhile, cMoPs give rise to two types of monocytes: Ly6C<sup>hi</sup> (also known as "classical monocytes"), equivalent to CD16<sup>-</sup> human monocytes, and Ly6C<sup>low</sup> monocytes (referred to as "non-classical monocytes"), equivalent to CD16<sup>+</sup> human monocytes. Classical monocytes are involved in the initial stages of the immune response and differentiate in monocyte-derived-macrophages. It is important to consider the complexity of this developmental pathway, as intermediate cell states exist and shared markers can be observed among different populations (Guilliams et al., 2018).

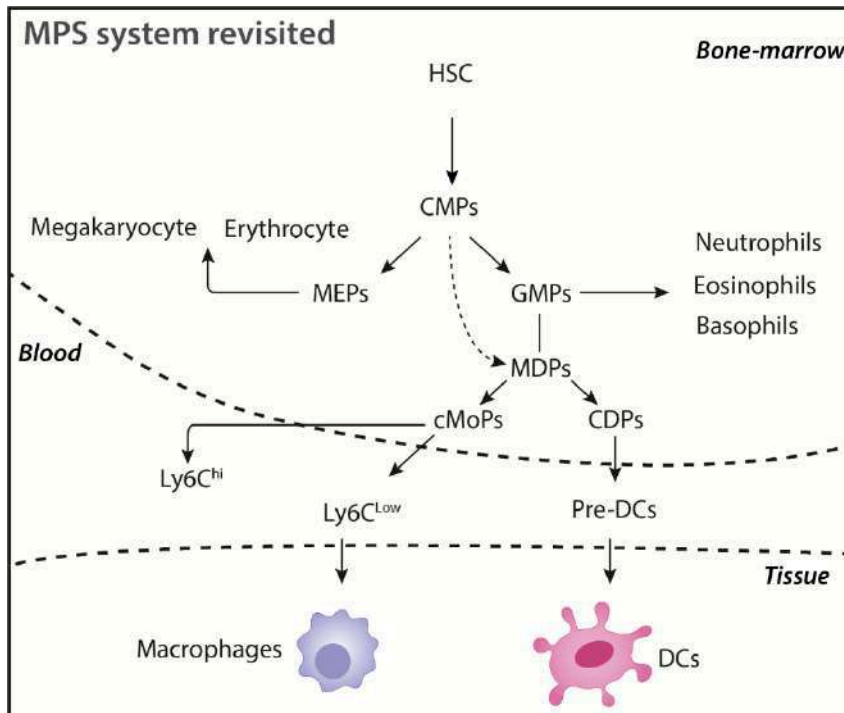


Figure 14. Mononuclear Phagocyte System.

The MPS system describe how HSC progenitors can lead to macrophages and DCs development in tissues.

Evidence showing that monocytes or bone marrow-derived cells can undergo macrophage differentiation *in vitro*, and also that blood monocytes can be recruited and differentiate into macrophages during inflammation, has reinforced the idea that circulating monocytes contribute to macrophage homeostasis in adult tissue. It should be noted that accurately assessing the contribution of circulating monocytes to tissue macrophages was challenging before the development of accurate cell lineage tracing techniques (Ginhoux and Guilliams, 2016). The development of monocyte-derived macrophages is highly intricate, and our understanding is constrained by reliance on specific markers that can be influenced by the chosen model.

While circulating monocytes can differentiate into tissue macrophages, they are not the only precursors contributing to macrophage development, as the contribution of circulating monocytes can vary drastically between tissues.

ii. Embryonic origin of tissue-resident macrophages

A pioneering study demonstrated that Langerhans cells could maintain themselves in skin tissue independently from circulating monocytes (Merad et al., 2002). The striking observation made at that time has been subsequently validated in numerous tissues (Schulz et al., 2012), to name: brain (Ajami et al., 2007; Ginhoux et al., 2010), lung (Guilliams et al., 2013; Hashimoto et al., 2013; Jakubzick et al., 2013), dermis (Tamoutounour et al., 2013), heart (Epelman et al., 2014; Molawi et al., 2014) and intestine (Bain et al., 2014). Those studies also showed that most tissue-resident macrophages could originate from the prenatal stage during embryonic development, as reviewed by Ginhoux and Guilliams (Ginhoux and Guilliams, 2016). Embryonic development of macrophages is a step-wise event,

Indeed, the development of macrophage precursors during embryonic haematopoiesis involves three distinct waves. The first wave, known as the "primitive" wave, occurs in the embryonic yolk sac (YS) and gives rise to primitive blood cells (**Figure 15A**). While it has been proposed that microglia solely originate from this first wave of embryonic haematopoiesis (Ginhoux et al., 2010), this topic remains of ongoing discussion (Lazarov et al., 2023).

The second wave, referred to as the 'transient definitive' wave, gives rise to erythro-myeloid precursors (EMPs). Near the end of the wave (**Figure 15A**), these precursors migrate to the fetal liver (FL) and differentiate into pre-macrophages (Pre-Macs). (Gomez Perdiguero et al., 2015).

Finally, the third wave involves the migration of HSCs to the fetal liver, where they colonize the bone marrow prior to birth (**Figure 15A**). It is crucial to emphasize that the majority of tissue-resident macrophages have been demonstrated to originate from the first and second waves of embryonic haematopoiesis although there are different proposed models of fetal macrophage ontogeny (Ginhoux and Guilliams, 2016).

Tissue-resident macrophages possess the ability to self-renew, and the extent to which they can be replaced by bone marrow-derived macrophages is largely tissue-specific (Figure 15B). They are long-lived cells, but the exact mechanism of their self-renewal remains unknown. It is still unclear whether they renew themselves through mitosis or if they arise from a tissue-resident progenitor cell population. Further research is needed to uncover the precise mechanisms by which tissue-resident macrophages are maintained during homeostasis or inflammation.

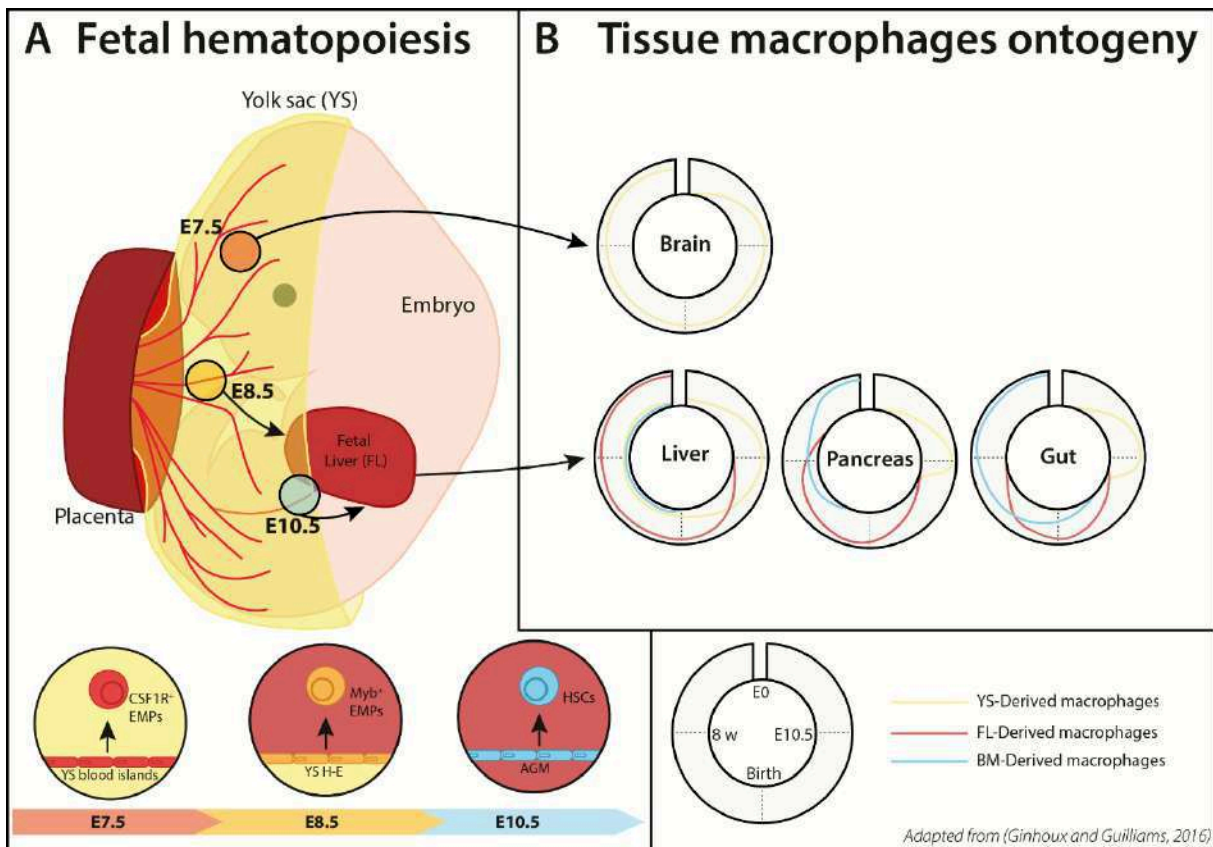


**Figure 15. Embryonic origin of macrophages**

**a** Macrophages Fetal haematopoiesis is composed of three distinct waves. EMPs derived from YS blood islands at E7.5 can migrate in the YS to give rise to microglia. At E8.5, YS-H-E give rise to *myb*<sup>+</sup> EMPs migrating in the fetal liver and giving rise to FL monocytes that populate most of adult tissues. At E10.5, bloodstream is in place and AGM give rise to HSCs to produce blood circulating monocytes. These sequential waves may not represent the reality in human but also, the contribution of each wave to EMPs production is still discussed. **b** Resident macrophages in tissue have different origin. Brain remains the only organ which is composed of pre-natal macrophages from the YS only at steady state. In the digestive system (e.g., Liver, Pancreas, Gut) the contribution of different compartment is age and organs dependant. H-E Hemogenic Endothelium, AGM Aorta-gonad-mesonephros, BM Bone-marrow, E Embryonic Day.

Certain macrophage populations, such as microglia are considered resident cells of "closed" organs (**Figure 15B**)(Ginhoux and Guilliams, 2016), meaning they are not significantly replaced by bone marrow-derived macrophages through time.

The pancreas is considered "slow" in terms of macrophage replacement (**Figure 15B**)(Ginhoux and Guilliams, 2016), as it allow for a gradual and slow turnover of bone marrow-derived macrophages during adulthood. More specifically, islet macrophages are exclusively derived from the bone marrow, whereas stromal macrophages come from both origins but are completely replaced by circulating monocytes after genotoxic stress (Calderon et al., 2015).

iii. Colony-stimulating-factor as a key regulator of macrophages development

The development and survival of macrophages are primarily dependent on two key factors: Colony-stimulating factor 1 (CSF1 or Macrophage-CSF) and CSF2 (GM-CSF). These factors act through their respective receptors, CSF1R and CSF2R. In mice, the absence of CSF1R leads to a monocytopenia and a reduced number of macrophages in all tissues (Dai et al., 2002). The latter observation is explained by the fact MDPs massively express CSF1R which is confirmed since CSF-1 is sufficient to generate bone marrow derived macrophages *in vitro* in 7 days (Toda et al., 2021). Additionally, alveolar macrophages have been shown to rely on CSF2R signalling (Guilliams et al., 2013).

Interestingly, osteoporotic mice with a natural CSF-1 deficiency do not have altered alveolar macrophages or microglia but have a reduced number of other tissue-resident macrophages (Cecchini et al., 1994). This suggests that CSF1R may have another ligand involved in the regulation of these macrophages. Several studies have revealed that IL-34 shares the CSF1 receptor with CSF1 (Lin et al., 2008; Ma et al., 2012). Notably, the absence of IL-34 leads to a decrease in the number of Langerhans cells and microglia indicating that IL-34 plays a critical role in the prenatal development of tissue macrophages in the yolk sac and their maintenance (Greter et al., 2012). In the pancreas, islet macrophages are CSF1-1 dependent, whereas stromal macrophages are both CSF-1 and IL-34 independent at 8 weeks of age (Calderon et al., 2015)

Altogether, these findings show that whether they are bone marrow-derived or originate from prenatal development, trophic factors are of great importance. Therefore, it is crucial to understand how they maintain steady states to comprehend plausible dysregulation during perturbed states (e.g., cancer)

Cellular source of CSF-1/2 and IL-34 are extremely different and tissue specific (Guilliams et al., 2020). Two different mechanisms currently explain how trophic factors (CSF1/2, IL-34) can maintain and develop macrophage in tissue : i) by entering the tissue from the blood or ii) by local production in the vicinity of macrophages. The latter idea is supported by the recent findings showing that fibroblasts and macrophages express growth factors (CSF1 and PDGF ligand, respectively) allowing the stability of fibroblast – macrophage interaction in a contact-dependant manner (Zhou et al., 2018). It has been described that macrophages constantly consume CSF-1. CSF-1 levels can increase locally due to macrophage death or acute expression of CSF-1, leading to macrophage proliferation and expansion (Guilliams et al., 2020). This expansion occurs as macrophages consume the excess CSF-1 until they reach a threshold necessary for their survival at lower level of CSF-1. This model suggests that the

availability of CSF-1 plays a crucial role in regulating macrophage population dynamics or survival and might be used to target macrophages.

## B. Role of tumor associated macrophages in PDAC

### a. “M1” vs “M2” macrophages... and beyond !

Macrophages (or tumor associated macrophages (TAMs) in cancer) are inherently adaptable cells that can sense and integrate external signals through many sensors ; Pressure (Solis et al., 2019), pH (Tcymbarevich et al., 2019), oxygen availability (Fang et al., 2009) or ECM organisation (McWhorter et al., 2013). Through different integrative signal they can change their phenotype and function. This process is known as macrophage polarization.

The initial observation regarding the differential response of macrophages to external stimuli revealed that IFN $\gamma$  inhibits the expression of CD206, while IL-4 enhances the expression of CD206 (Stein et al., 1992). The concept of macrophage polarization was then fully demonstrated through a study involving typical Th1 (C57BL/6) and Th2 (BALB/c) mouse strains. It was observed that Th1-produced IFN $\gamma$  activated macrophages to produce nitric oxide (NO), while Th2 macrophages expressed the enzyme arginase to facilitate the transformation of L-Arginine into L-ornithine (Mills et al., 2000).

The initial observations of distinct phenotypes in macrophages, termed M1 and M2 suggested that macrophages can exhibit different functional states during an inflammatory response. Importantly, macrophage polarization can occur independently of T cells, as similar polarization results have been observed in mouse models lacking T cells (Mills et al., 2000).

M1 are considered as immune-regulatory and anti-tumoral macrophages. They are typically activated by IFN $\gamma$  or lipopolysaccharides (LPS) (**Figure 16**). They express the enzyme nitric oxide synthase (iNOS) and are involved in promoting a Th1 immune response, which is effective against intracellular pathogens and the elimination of abnormal cells (e.g., cancer cells) (Klug et al., 2013; Mantovani et al., 2004). Additionally, M1 macrophages secrete high levels of cytokines like IL-12 and TNF (**Figure 16**).

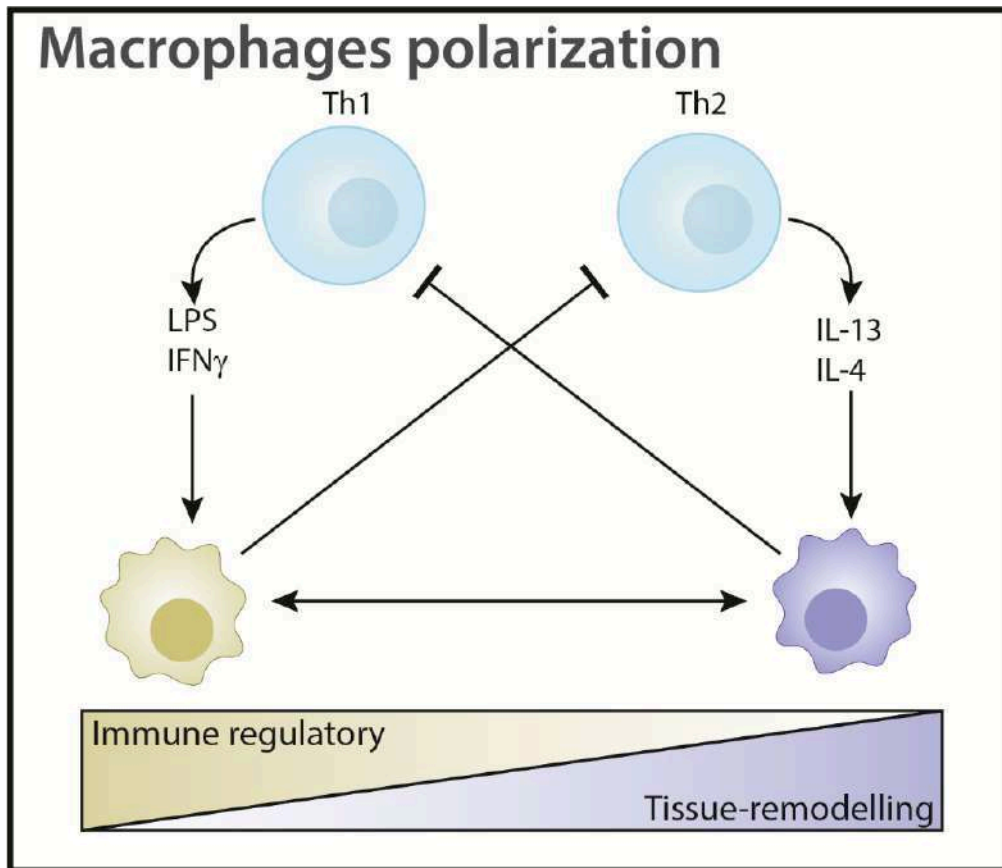


Figure 16. Macrophages polarization concept.

Macrophages can be immune-regulatory and tissue-remodelling depending on external stimuli. Immune regulatory macrophages are activated by LPS and IFN $\gamma$  whereas tissue-remodelling macrophages are activated by IL-13 or IL-4 that can be secreted by Th1 and Th2 cells, respectively. A large diversity of macrophages subtype exists between the two extremes phenotype so as others external stimuli.

On the other hand, M2 macrophages are classified as tissue-remodeling and pro-tumoral macrophages. They are mainly activated by IL-4 and IL-13. M2 macrophages express the enzyme Arginase and contribute to a Th2 immune response, which is associated with tissue remodeling and anti-inflammatory signaling.

It is important to note that the M1 and M2 nomenclature oversimplifies macrophage biology *in vivo*. Indeed, there are intermediate phenotypes between the "M1" and "M2" extremes since there can be overlapping states of macrophage phenotypes (Palma et al., 2018). This complexity has led to discussions about the nomenclature used for macrophages (Murray et al., 2014). The use of the M1 and M2 markers can be misleading because markers classified as "M2" can also be expressed by "M1" macrophages, we often refer to "M2-like" macrophages for those cells. The current consensus among researchers is to describe macrophages using a combination of markers rather than relying solely on the M1 or M2 classification. Indeed, this simple classification, in itself, cannot recapitulate the

complexity of macrophage subtypes existing in human tissue at steady state (Gautier et al., 2012) or in cancer (Franklin et al., 2014; Movahedi et al., 2010)

The concept of M1 and M2 macrophages, while flawed in the context of an inflammatory response, faces even greater limitations in the context of cancer. The TME is incredibly complex, with specialized niches where macrophages regulate the immune response in different ways (Casazza et al., 2013). The role of macrophages in the TME is primarily influenced by their specific location within the TME (Rivera and Bergers, 2013) and also by their developmental origin.

b. Exploring TAMs and MDSCs functions in the context of cancer and wound healing

i. Introduction

TAMs infiltrate most of solid cancers (Galon and Bruni, 2020). They are either recruited due to inflammatory signals from the tumor or are resident from prenatal development. TAMs have a dual potential role in cancer: they can phagocytize tumor cells, or they can inhibit the antitumoral immunity. Their fate necessarily depends on their molecular environment and surrounding niche within the TME. Given the role of macrophages in maintaining tissue homeostasis and the established connection between wound healing and cancer (Dvorak, 1986), we will now explore this parallel in the context of TAMs. Specifically, we will focus on the stages of inflammation initiation, tissue remodelling, and closure of the injury.

ii. Inflammation

One of the initial roles of resident macrophages following an injury is to eliminate potential pathogens through phagocytosis and induce an inflammatory cascade.

In the context of cancer, macrophages are recruited very early in the pancreas (**Figure 17A**)(Dixit et al., 2022) (Linde et al., 2018). TAMs are highly heterogeneous in PDAC and can vary between early and late stage of the disease (Hosein et al., 2019). TAMs rely on monocyte-derived macrophages for their maintenance in the tissue (Franklin et al., 2014) and it is now clear that macrophages are mainly recruited through CCL2 – C-C chemokine receptor type 2 (CCR2) axis (**Figure 17A**)(Dixit et al., 2022; Sanford et al., 2013; Tu et al., 2021). However, it is worth mentioning that several groups demonstrated in various cancer including PDAC that macrophages have variable origin and that TAMs ontogeny have crucial impact on their functions (Bowman et al., 2016; Loyher et al., 2018; Zhu et al., 2017). CCL2 is mainly secreted by pancreatic neoplastic cells and cancer cells but also by iCAFs and myCAFs (**Figure 17A**)(Dixit et al., 2022). Macrophages can also be recruited by other chemoattractant since it was recently brought up that necrotic PDAC cells can release CXCL1 chemokine and attract

macrophages to reduce their inflammatory capacities (Seifert et al., 2016). It was also shown that macrophages can be recruited by intercellular adhesion molecule-1 (ICAM1) that is secreted by *Kras* mutated acinar cells (Liou et al., 2015b).

Once recruited, macrophages play a crucial role in clearing cellular debris and dying cells through a process called efferocytosis, which involves recognizing "eat-me" signals. Once activated, macrophages release pro-inflammatory cytokines (such as IL-1 $\beta$ , TNF $\alpha$ , IL-6, and IL-12) and chemokines (such as CXCL8 and CCL2) to attract other immune cells. TNF $\alpha$  derived macrophages indirectly reduce CD103<sup>+</sup> DCs by lowering chemoattractant secreted by cancer cells (Dixit et al., 2022). Circulating monocyte-derived macrophages constitute a significant portion of the TAM population (Zhu et al., 2017). However, other TAMs are originated from pre-natal stage can expand during PDAC progression (Zhu et al., 2017)

Although inflammatory macrophages are generally associated with a better prognosis (Galon and Bruni, 2020), their impact is typically evaluated later in the immune response. This raises the question of whether the phagocytosis of cancer cells contributes to effective immunity. Indeed, it is important to consider that as macrophages eliminate cancer cells, the cancer cells can acquire "don't eat-me" signals such as CD47 (Steele et al., 2020). The binding of CD47 to its receptor, SIRP $\alpha$ , expressed on macrophages can abort phagocytosis (Jaiswal et al., 2009).

Altogether, these observations show that macrophages in PDAC follow the same behavioural pattern as in the first steps of wound healing process.

### iii. Tissue remodelling

Tissue remodelling refers to the process of modifying the structure (e.g., ECM, cellular composition) and function of tissues in response to various stimuli, such as injury. In the context of wound healing, tissue remodelling is an important stage where new blood vessels are formed, the ECM is modified, and the immune response is slowed down to prevent tissue damage.

In cancer, macrophages can mimic the inflammation resolution process observed in wound healing by changing their phenotype through polarization (**Figure 17B**)(Sanford et al., 2013). In cancer, this polarization can be induced through various mechanisms, including cell-cell interactions, signals from intra-tumoral Th2 and ECM organization (Bachy et al., 2022; DeNardo and Ruffell, 2019). Specifically, in PDAC, IL-1 $\beta$  and mesenchymal stem cells have been shown to promote macrophage polarization (Das et al., 2020; Mathew et al., 2016). The mechanisms underlying macrophage polarization in the TME are complex and involve multiple signals, but it is generally accepted that tissue-remodelling macrophages play a dominant role in PDAC and are associated with a poor prognosis (Ino et al., 2013).

TAMs can actively participate in ECM reorganization. Indeed, embryonic-derived macrophages derived are responsible for the fibrotic response, while circulating monocyte-derived macrophages are associated with immune-regulatory responses (Baer et al., 2023; Zhu et al., 2017). TAMs send signals, such as Platelet-Derived Growth Factor-BB (PDGF-BB), to induce collagen deposition by myofibroblasts (Kaneda et al., 2016). Tissue-remodelling macrophages predominantly express the surface marker CD206, which has been shown to interact with cancer cells and contribute to their evasion of anti-tumoral immunity (Allavena et al., 2010; Mantovani et al., 2004). In PDAC, CD206<sup>+</sup> tissue-remodelling macrophages can take up degraded collagen, leading to differentiation of PSCs into myofibroblasts in vivo (LaRue et al., 2022). Additionally, TAMs can be educated by the ECM to promote fibrosis, with  $\beta$ 1-g3 structured collagen being shown to enhance the differentiation of tissue-remodelling macrophages (Bachy et al., 2022).

TAMs play a crucial role in angiogenesis, which is a hallmark of cancer (Hanahan, 2022). They secrete soluble factors that promote the formation of new blood vessels (**Figure 17A**) (Palma et al., 2005; Sierra et al., 2008). While not specifically shown in PDAC, Vascular Endothelial Growth Factor positive (VEGFR<sup>+</sup>) TAMs are specifically guided to hypoxic areas. Once in hypoxic areas, macrophages promote local angiogenesis, highlighting the importance of the microenvironment niche for TAM function (Casazza et al., 2013).

As mentioned earlier, tissue-remodelling macrophages express immune checkpoints that inhibit the response of CD8<sup>+</sup> T cells. Myeloid cells in general are also responsible for PD-L1 expression on cancer cells through Epidermal Growth Factor (EGF) secretion (Zhang et al., 2017). PD-L1, in particular, is highly expressed by TAMs and hinders the activities of CD8<sup>+</sup> T cells (Zhu et al., 2014). Consequently, blocking the CSF1R receptor to deplete TAMs has shown promising results when combined with anti-PD-1 and anti-CTLA-4 therapies (Zhu et al., 2014). TAMs can also directly inhibit the activities of CD8<sup>+</sup> T cells by expressing specific surface markers, such as Dectin-1, and by impeding their infiltration into the TME (Beatty et al., 2015; Daley et al., 2017).

These observations demonstrate that macrophages in PDAC exhibit an immune-resolutive phenotype and perform functions related to angiogenesis, fibrosis, and inhibition of CD8<sup>+</sup> T cell responses. Ultimately, these characteristics contribute to PDAC's resistance to conventional immunotherapy.

#### iv. Injury resolution

The final step of wound healing is the injury closing by the re-epithelisation. In this process, epithelial cells undergo intermediate EMT in order to migrate through the wound.

On the other hand, in cancer, epithelial cells typically undergo a complete EMT, which is associated with increased invasion through the basal membrane and metastasis (**Figure 17C**). There is a bidirectional communication between cancer cells and macrophages that enhances the invasiveness of cancer cells. Firstly, resident macrophages at the metastatic site can be influenced by PDAC exosomes, creating a favourable environment for cancer cells dissemination (Costa-Silva et al., 2015; Quaranta et al., 2018). Additionally, macrophages can be recruited to metastatic tissues and activate resident fibroblasts into  $\alpha$ SMA<sup>+</sup> myofibroblasts, promoting local fibrosis (Nielsen et al., 2016). Furthermore, blocking the recruitment of circulating monocytes through CCR2 blockade has been associated with reduced incidence of metastasis (Dixit et al., 2022).

The direct promotion of EMT in PDAC cells has been observed through the action of tissue-remodelling macrophages (Liu et al., 2013). Importantly, macrophages-derived tumor necrosis factor-alpha (TNF $\alpha$ ) play a partial role in inducing subtype switching in pancreatic cancer, leading to the upregulation of EMT-related genes in cancer cells and facilitating the transition between classical and basal subtypes (**Figure 17**)(Tu et al., 2021). Furthermore, tissue-remodelling macrophages contribute to the extravasation of PDAC cells by modifying the structure of the ECM by expressing LOX2. In an elegant study, the depletion of macrophages was shown to result in a defect of collagen alignment and the failure of metastatic dissemination (**Figure 17C**)(Alonso-Nocelo et al., 2023).

Collectively, these observations indicate that the functions performed by macrophages during wound healing are hijacked and utilized in the context of carcinogenesis to sustain the maintenance and malignant progression of the cancer ecosystem.

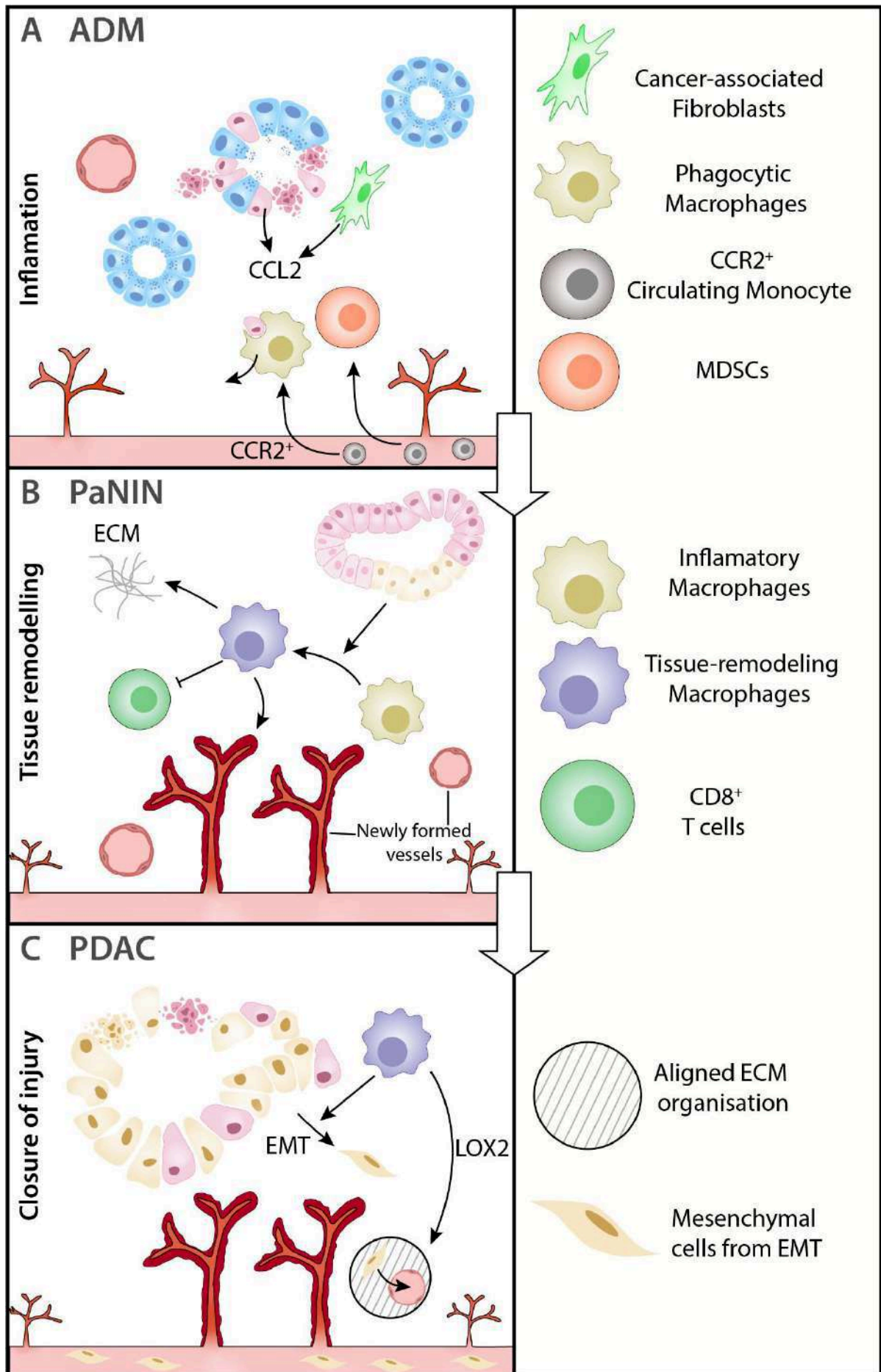


**Figure 17 Macrophages orchestrate wound healing like process in pancreatic cancer.**

**A** First step is inflammation when the neoplasia kicks. Neoplastic cells and CAFs are among the producers of CCL2 chemokine recruiting CCR2<sup>+</sup> circulating monocytes. These latter are differentiated into macrophages or MDSCs. Macrophages phagocyte cancer cells expressing “eat-me” signal. **B** The second step is tissue remodelling. Given the immunosuppressive environment, macrophages are polarized into tissue-remodelling macrophages and have a wide spectrum of functions. Tissue-remodelling macrophages promote angiogenesis, ECM production and T cells inhibition. **C** The final step of wound healing is the closure of the injury. In pancreatic cancer, macrophages are a sine qua non condition for metastasis as they promote EMT but also re-organize the ECM alignment to favour cancer cells migration.

c. Macrophages based therapies.

i. Introduction

Due to the various mechanisms that actively or indirectly contribute to the development of PDAC and cancer overall, these mechanisms present a key target within the TME. More importantly, it is important to note that macrophages are also responsible for resistance to conventional therapies, therefore, most of macrophages-based therapy are combined with others conventional and/or immune checkpoint-based therapy. There are four main approaches to macrophage-based therapy: i) inhibiting their recruitment, ii) regulating their differentiation, iii) enhancing their phagocytic activity, and iv) utilizing cellular therapy. In the subsequent sections, we will explore the application of macrophage-based therapy in the context of cancer in general, with a focus on its relevance to PDAC whenever applicable.

ii. Recruitment

Numerous studies investigated the effect of macrophages recruitment inhibition. CCL2-CCR2 axis is the main axis for circulating monocytes recruitment in pancreatic cancer. Recruitment of macrophages is responsible for the resistance of conventional RT in PDAC, as inhibiting monocytes recruitment through anti-CCL2 antibody allow RT efficacy enhancement (Kalbasi et al., 2017). Moreover, targeting CCR2 in PDAC show promising data in both pre-clinical and clinical studies as the inhibition of CCR2 reduced metastasis incidence and enhanced an anti-tumoral immunity (Nywening et al., 2016; Sanford et al., 2013). Others clinical trials are ongoing evaluating the safety and efficiency of CCR5 inhibition in combination with ICI (**Table 7**). Although CCL2-CCR2 axis was targeted in other indications than PDAC (Qian et al., 2011), it was shown to have some limitation in breast cancer. Bonapace et al., observed that cessation of anti-CCL2 monotherapy induces an increase of blood vessel formation associated with metastasis (Bonapace et al., 2014). Upon treatment with anti-CCL2, monocytes are blocked and accumulate in the blood circulation since their development is not impaired. When the therapy stops, monocytes are recruited in larger number than before therapy (Keklikoglou and De Palma, 2014)

### iii. Survival and reprogramming

Macrophage reprogramming as a therapy aims in pushing macrophages phenotype toward an inflammatory phenotype. In PDAC, the use of anti-CSF1 allows macrophages reprogramming through CD206<sup>+</sup> macrophages death but also a shift between tissue-remodelling macrophages and inflammatory-macrophages (Zhu et al., 2014). Similar observation were also made in glioma (Pyonteck et al., 2013). Macrophages reprogramming actually occur very rapidly and in a transient manner before cells death. This short-term reprogramming is sufficient to induce a proper anti-tumoral immune response (Hoves et al., 2018).

Macrophages can also be targeted by impairing their development and survival through the targeting of CSF-1. Indeed, pancreatic neuroendocrine tumors are reduced in CSF1<sup>OP/OP</sup> mice (Pyonteck et al., 2012). However, the use of CSF1<sup>OP/OP</sup> may not represent the reality as it is impairing embryonic-derived macrophages. CSF-1 level is abnormally elevated in human PDAC and a low CSF1R signature is associated with a better prognosis. CSF-1/CSF1R axis as a target has been elegantly studied in PDAC (Zhu et al., 2014). Blockade of these axis permit CD8<sup>+</sup> T cells activation but induce PD-L1 expression on cancer cells. Therefore, combined therapy with anti-PD-L1 has been used to overcome this mechanism. The combined treatment induced Tregs decrease and a better survival (Zhu et al., 2014). The efficacy of anti-CSF1R therapy was assessed in phase I/II in combination with chemotherapy and anti-PD-1, the clinical trial did not show sufficient anti-tumoral activities to further evaluate the potential therapeutic role of the combination although the combination were shown to be safe and tolerated (Razak et al., 2020).

TAMs mainly express a specific  $\gamma$  isoform of the Phosphoinositide 3-Kinase gamma enzyme (PI3K $\gamma$ ) that has been targeted in pre-clinical study and showed great benefit in monotherapy. Genetic ablation or pharmacological targeting of PI3K $\gamma$  in macrophages is associated with CD8<sup>+</sup> T cells infiltration in the TME and less metastasis (Kaneda et al., 2016). PI3K $\gamma$  pro-tumoral action was shown to activate Bruton's tyrosine kinase (BTK) enzyme (Gunderson et al., 2016). Although BTK targeting showed significant benefits in combination with chemotherapy in mouse models (Gunderson et al., 2016), it failed to show benefit in a phase III clinical trial (**Table 7**)

### iv. Phagocytosis

Since most of PDAC patients are diagnosis at late stage, TAMs in the TME have very low phagocytic activities due to immune selection. Therapies has been developed to bypass “don't eat-me” signals expressed by cancer cells (e.g., CD47).  $\alpha$ CD47 therapy has been shown to have great results in Non-Hodgkin's Lymphoma with around 50% of complete or partial response (**Table 7**). To date, in PDAC,

there are no clinical trials ongoing for the evaluation of anti-CD47 treatment (Jiang et al., 2021). However, pre-clinical studies showed promising data since anti-CD47 treatment was associated with TME remodulation and synergy with anti-PD-L1 therapy (Pan et al., 2019).

v. Cellular therapy

As CAR-T cells show more and more results, Chimeric Antigen Receptor macrophage (CAR-M) have been developed to specifically recognize tumoral antigen (Klichinsky et al., 2020). In the latter innovative study, CAR-M are injected and show a sustain inflammatory phenotype and Human Epidermal Growth Factor Receptor-2 (HER2) expressing cells specific clearance and was inducing endogenous tissue-remodelling TAMs to inflammatory TAMs conversion (Klichinsky et al., 2020). These advances in macrophages engineering are currently tested in HER2 overexpressing solid tumors clinical trials (**Table 7**). Macrophages can also be genetically modified by mRNA technology. Indeed, master regulator gene Interferon regulatory factor 5 (*IFR5*) induction by mRNA nanocarrier in macrophages led to tumour rejection and reduce metastasis (Zhang et al., 2019). Finally, the injection of macrophages with an IFN $\gamma$  “backpacks” allow the sustains presence of inflammatory TAMs and led to tumor reduction (Shields et al., 2020)

<b>Table 7. Macrophages targeting in cancer</b>					
Agent	Mono/combined(agent)	Cancer	Clinical status	Observation	References and NCT identifiers
<b>Recruitment based therapy</b>					
$\alpha$ CCL2	Monotherapy	Breast	Pre-clinical	Increase survival and Reduce metastasis	(Qian et al., 2011)
$\alpha$ CCL2	Combined (RT)	PDAC	Pre-clinical	Bypass RT resistance induced by TAMs	(Kalbasi et al., 2017)
CCR2 antagonist	Monotherapy	PDAC	Pre-clinical, Phase I	Decrease tumor growth, reduce metastasis, enhance anti-tumor immunity	(Sanford et al., 2013), (Nywening et al., 2016) (NCT01413022)
CCR2 inhibitors	Combined (CXCR2 inhibitors and/or Gem)	PDAC	Pre-clinical	Improve antitumour immunity through neutrophils recruitment impairment	(Nywening et al., 2018)
CCR2/CCR5 antagonist	Combined (Chemo $\pm$ $\alpha$ PD1)	PDAC	Phase I/II	Ongoing CT	(NCT03184870)
CCR5 Antagonist	Combined ( $\alpha$ PD1+ $\alpha$ CTLA4)	PDAC	Phase I	Ongoing CT	(NCT04721301)
<b>Survival and Reprogramming</b>					
$\alpha$ CSF1R	Combined (Oxaliplatin or Cisplatin)	Breast	Pre-clinical	Enhancement of chemo	(Salvagno et al., 2019)
$\alpha$ CSF1/ $\alpha$ CSF1R	Combined ( $\alpha$ PD-L1/ $\alpha$ CTLA4)	PDAC	Pre-clinical	Overcome ICI resistance	(Zhu et al., 2014)
Csf1 <sup>op/op</sup>	Monotherapy	Pancreatic neuroendocrine	Pre-clinical	Tumor shrinkage with lower angiogenic islet	(Pyonteck et al., 2012)
$\alpha$ CSF1R	Combined (Chemo)	PDAC	Phase I/II	Ongoing CT	(NCT03193190)
$\alpha$ CSF1R	Combined ( $\alpha$ PD-1)	PDAC	Phase I/II	Tolerable drug but the efficiency was not sufficient	(Razak et al., 2020) (NCT02713529)
PI3K $\gamma$ inhibitors	Combined (Gem)	PDAC	Pre-clinical	Enhancement of chemo	(Kaneda et al., 2016) (Gunderson et al., 2016)
BTK inhibitors	Combined therapy (Nab-Pac + Gem)	PDAC	Pre-clinical, Phase III	Phase III showed no benefits	(NCT02436668)

[\(Continue next page\)](#)

TLR4 analog + IFN $\gamma$	Monotherapy	Breast	Pre-clinical	Turn tissue-remodelling TAMs into effective tumor-restricting TAMs	(Sun et al., 2021)
<b>Phagocytosis</b>					
$\alpha$ CD47	Combined (Rituximab)	Non-Hodgkin's Lymphoma	Phase I/II	50% of patient with CR/PR	(Advani et al., 2018)(NCT02953509)
$\alpha$ CD47	Monotherapy	PDAC	Pre-clinical	Increase of pancreatic cancer cells clearance	(Michaels et al., 2018)
$\alpha$ CD47	Monotherapy and combined ( $\alpha$ PD-L1)	PDAC	Pre-clinical	Overcome ICI resistance and remodel TME	(Pan et al., 2019)
<b>Cellular therapy</b>					
CAR-M (HER2)	Monotherapy	HER2 <sup>+</sup> solid tumors	Phase I	Ongoing CT	(NCT04660929)
Backpack macrophages	Monotherapy	Breast	Pre-clinical	Polarize TAMs into inflammatory TAMs	(Shields et al., 2020)
mRNA nanocarrier	Monotherapy	Ovarian	Pre-clinical	TAMs phenotype reversing with tumor regression	(Zhang et al., 2019)
Chemo Chemotherapy, CIT Clinical Trial, Nab-Pac Nab-Paclitaxel, CR Complete Response, PR Partial Response.					

## C. CD169<sup>+</sup> macrophages

### a. Introduction

#### i. CD169 macrophage function in non-cancerous condition

CD169<sup>+</sup> macrophages are characterized by the expression of sialic acid-binding immunoglobulin-like lectin-1 (Siglec-1 which is part of the Siglec family). CD169 denomination will be use throughout this thesis. CD169 is a type I lectin composed of 16 C2-set immunoglobulin domain and 1 V-set immunoglobulin domain binding to sialic-acid (Crocker et al., 2007). CD169<sup>+</sup> macrophages studying has been facilitated with the generation of a conditional depletion model. In this model, diphtheria toxin receptor is expressed only in CD169 expressing-cells (Miyake et al., 2007). The use of diphtheria toxin allows for CD169 depletion across tissues without impairing other myeloid populations (Miyake et al., 2007). CD169<sup>+</sup> macrophages can be found in both lymphoid and non-lymphoid tissue at steady state. Indeed, CD169<sup>+</sup> expression define Marginal zone metallophilic macrophages in the spleen and both Subcapsular sinus macrophages (SCS) or Medullary macrophages in the lymph nodes (Gordon et al., 2015). Moreover, they also define resident macrophages in the liver, intestine, bone-marrow, lung or in the pancreas (Asano et al., 2015; Chittezhath et al., 2019; Chow et al., 2011; Gordon et al., 2015; Ural et al., 2020).

In the pancreas, CD169<sup>+</sup> macrophages are present under normal condition since the use of CD169<sup>+</sup> macrophages with CD169-DTR model reduces the number of macrophages in pancreatic islet (Chittezhath et al., 2019). However, up to date, there are no evidence about the origin of CD169<sup>+</sup> macrophages in the pancreas as no fate-mapping has been done. More specifically, CD169<sup>+</sup> macrophages are upregulated in diabetes and can remodel pancreatic islets vasculature leading to glucose decrease in blood. Their survival may depend on CSF1 as targeting CSF1R allows the reduction of CD169<sup>+</sup> macrophages in pancreatic islets (Chittezhath et al., 2019).

CD169<sup>+</sup> macrophages are capable of dead cells associated antigen clearance (Miyake et al., 2007). CD169<sup>+</sup> macrophages have a strategic location as they are localized at the interface between antigen afferent area and T/B cells area in spleen and lymph node (**Figure 18**). Their location mainly depend on sialoglycan expression and density on lymphatic vessels (D'Addio et al., 2021). Given their location, CD169<sup>+</sup> macrophages are exposed to antigens and their antigens specific function has been deeply evaluated.

Specifically, SCS macrophages can capture lipid antigens and retain the antigen at their surface in association with C1d. This mechanism was shown to be necessary for the activation of invariant natural killer T (iNKT) *in vivo* (Barral et al., 2010). In infection context, CD169<sup>+</sup> macrophages capture Vesicular

Stomatitis Virus (VSV) particles and protect nerves from being infected as CD169<sup>+</sup> macrophages depletion induce nerves infection (Iannacone et al., 2010). CD169<sup>+</sup> macrophages are able to recruit plasmacytoid DCs (pDC) to secrete type I IFN and protect nerves, hematopoietic cells, and stromal cells from lethal infection. CD169<sup>+</sup> macrophages are therefore often called central nervous system (CNS) gatekeeper (Iannacone et al., 2010). More precisely, CNS macrophages (i.e., CD169<sup>+</sup>) are considered as a “Flypaper” (**Figure 18A**). Indeed, they are capable of translocating viral particle to B cells and inducing anti-viral humoral response against pathogens (Junt et al., 2007). Similar observation has been made in listeria monocytogene infection as CD169<sup>+</sup> macrophages protect from lethal infection by translocating antigen in B and T cells area through the trans-infection of CD8a DCs (**Figure 18A**) (Perez et al., 2017). Specifically, CD169<sup>+</sup> macrophages do not directly cross-present antigens to CD8<sup>+</sup> T cells. They rely on DCs as CD169<sup>+</sup> macrophages and DCs co-localize in lymphoid tissue (**Figure 18A**) (van Dinther et al., 2018). Those latter observations contradict a study showing that CD169<sup>+</sup> macrophages can cross-present antigens to T cells in absence of DC through MHC-I (Bernhard et al., 2015).

A pivotal information is that CD169<sup>+</sup> macrophages are more than a “flypaper” but rather a viral replication “sink” (**Figure 18B**) (Ludewig and Cervantes-Barragan, 2012). Indeed, in a VSV model, Honke and colleagues showed that marginal zone CD169<sup>+</sup> macrophages capture VSV virus and inducing Ubiquitin specific peptidase 18 (USP18) upregulation. USP18 compete with JAK1 and inhibit type I IFN signalling pathway from inhibiting viral replication. In this way, CD169<sup>+</sup> macrophages are producers of viral load and enhance T cells priming from DCs but also present more antigens to B cells leading to a better systemic anti-viral response (**Figure 18B**) (Honke et al., 2012).

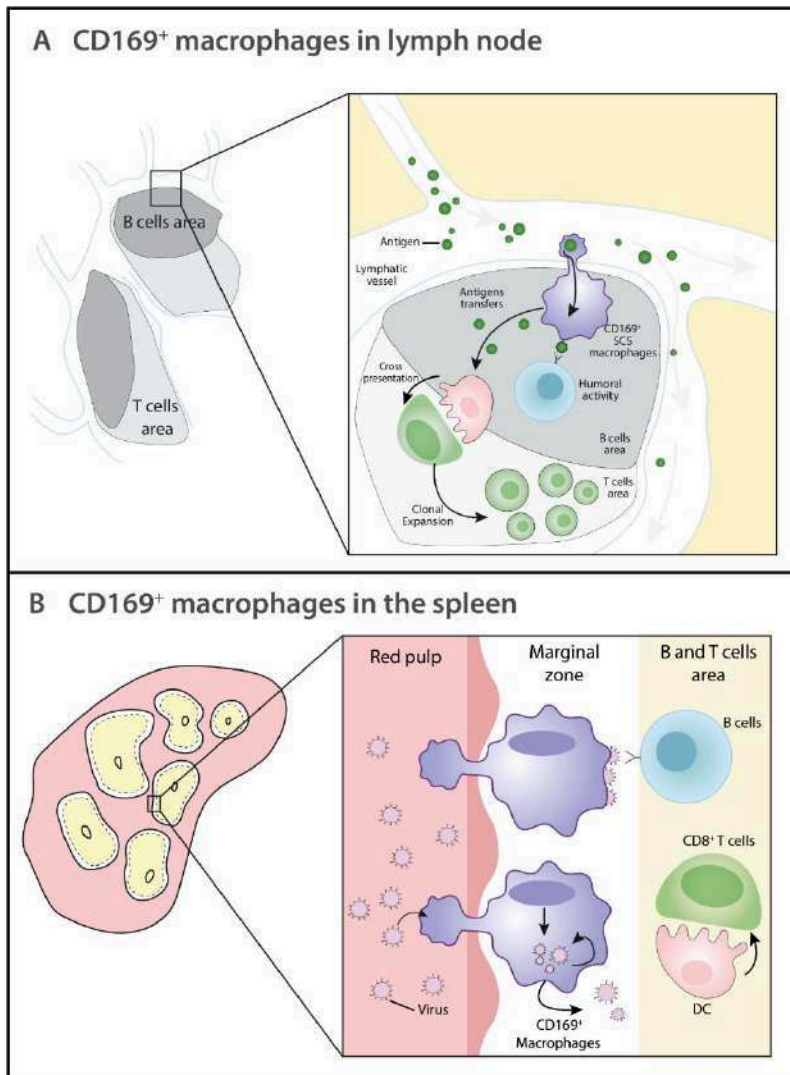


Figure 18. CD169<sup>+</sup> role in spleen and lymph-node.

**a** CD169<sup>+</sup> macrophages capture antigens circulating in lymphatic vessel to translocate them to B cells and pDC in order to cross-present CD8<sup>+</sup> T cells that will expand. **b** CD169<sup>+</sup> macrophages are located in the marginal zone of the spleen between the red pulp and lymphoid cells area. They are capable of capturing circulating viruses and allow viral replication to enhance anti-viral response activation in the spleen.

More recently, they have been associated with severe acute respiratory syndrome coronavirus 2 (SARS-CoV-2) infection severity and outcomes. Since they express SARS-CoV-2 receptor and can be infected, they've been shown to impair anti-viral immunity in lymphoid tissue. More generally, CD169 molecule is upregulated on monocytes during infection and is considered as a biomarker (Feng et al., 2020; Gatti et al., 2023; Roussel et al., 2021).

CD169<sup>+</sup> macrophages can also be found in the bone marrow in mouse and human. They have a crucial role in retaining HSCs progenitor by secreting protein factor and activating mesenchymal stromal cell in the bone marrow to secrete CXCL12 in nestin positive niche (Chow et al., 2011). CD169<sup>+</sup> macrophages also have been shown to retain HSCs in the spleen (Dutta et al., 2015). CD169<sup>+</sup> macrophages also regulate erythropoiesis as the depletion of CD169<sup>+</sup> macrophages reduce erythroblast island number but also erythroblast maturation. More importantly, vascular cell adhesion

molecule 1 positive (VCAM1<sup>+</sup>) CD169<sup>+</sup> macrophages allow recovery after haemolytic anaemia (Chow et al., 2013).

These results show that CD169<sup>+</sup> macrophages can have multiple functions at steady state and in infection context. Their role seems to be antigen-restricted in lymphoid organ but more complex in non-lymphoid tissue. Although there are also macrophages niches in lymphoid tissue (Bellomo et al., 2020), there are more complex niche in non-lymphoid organ (Guilliams et al., 2020). Macrophages can be maintained in a stromal niche and exert a reciprocal secretion of growth factor to regulate immune cells migration across tissue. Given their capacity to communicate with other cell type, CD169<sup>+</sup> macrophages may have a particular role in cancer. Therefore, in the following parts, the specific role of CD169<sup>+</sup> macrophages in cancer will be discussed.

b. Emerging role of intra tumoral CD169<sup>+</sup> macrophages in cancer

i. Pro-tumoral role

The involvement of CD169<sup>+</sup> macrophages within the TME has been assessed in various primary tumors. In breast cancer, a high level of CD169<sup>+</sup> macrophages is associated with a lower survival rate and is correlated with the expression of CD163 (Cassetta et al., 2019; Gunnarsdottir et al., 2023). Notably, CD169<sup>+</sup> macrophages in breast cancer are linked to the secretion of CXCL12, which leads to the inhibition of T cells, resembling the macrophage niche in the bone marrow (Gunnarsdottir et al., 2023). The expression of CD169<sup>+</sup> macrophages in breast cancer can be induced by factors such as type I interferon (TNF $\alpha$ ), CSF1, and/or IL-1 $\beta$  secreted by breast cancer cells (Cassetta et al., 2019). In turn, CD169<sup>+</sup> macrophages secrete CCL8 to recruit more monocytes and induce transcriptional changes in cancer cells.

The pro-tumoral role of CD169<sup>+</sup> macrophages in breast cancer have been confirmed, as the depletion of CD169<sup>+</sup> macrophages led to a slowdown in tumor progression and reduced the number of lung metastases. Moreover, it has been observed that CD169<sup>+</sup> macrophages inhibit CD8<sup>+</sup> T cells through the PD-1 – PD-L1 axis in breast cancer (Jing et al., 2020).

A pivotal study conducted by Casanova-Acebes and colleagues (Casanova-Acebes et al., 2021) investigated the impact of macrophages ontogeny on the progression of non-small cell lung cancer. The study revealed that the heterogeneity of macrophages in murine models closely resembles the one observed in humans. Of particular significance, they identified a subset of macrophage in the lung that does not originate from the bone marrow but rather derives from the embryonic stage. These resident macrophages, originating during the pre-natal stage, express both CD169 and CD206 receptors. During the early stages of tumor initiation, these macrophages establish close contact with

cancer cells. As the tumor progresses, CD169<sup>+</sup> macrophages form a distinct structure around the tumor. In culture, lung cancer cells exhibit more invasive protrusions when exposed to tissue-resident macrophages expressing CD169 compared to those cultured with macrophages derived from circulating monocytes. The invasiveness of cancer cells is EMT-related, induced by resident CD169<sup>+</sup> macrophages. The researchers also observed that depleting CD169<sup>+</sup> macrophages was associated with fewer cancer lesions in the lung and a significant infiltration of CD3<sup>+</sup> T cells. However, this effect was only observed when CD169<sup>+</sup> macrophages were depleted during tumor initiation and not after the tumor was already established. This highlights the crucial role of tissue-resident CD169<sup>+</sup> macrophages during the early stages of tumor development. (Casanova-Acebes et al., 2021).

The role of CD169<sup>+</sup> macrophages has been assessed in different cancers. In myeloma, depleting CD169<sup>+</sup> macrophages has been found to act as a preventive measure, effectively hindering the development of myeloma (Opperman et al., 2019). Furthermore, patients with colorectal cancer display elevated levels of CD14<sup>+</sup>CD169<sup>+</sup> monocytes in their bloodstream. Interestingly, it has been observed that intra-tumoral CD169<sup>+</sup> macrophages exhibit anti-inflammatory properties (Li et al., 2015).

Taken together, these findings suggest that intra-tumoral CD169<sup>+</sup> macrophages can play diverse pro-tumoral roles in various tissues. However, in the subsequent section, we will delve into the anti-tumoral role of intra-tumoral CD169<sup>+</sup> macrophages.

#### ii. Anti-tumoral role

CD169<sup>+</sup> macrophages level is lower in hepatocellular carcinoma (HCC) than in normal liver. Patients with high CD169<sup>+</sup> macrophages infiltration in HCC have a better survival rate (Li et al., 2017; Liao et al., 2022; Zhang et al., 2016). More precisely, high CD169<sup>+</sup> macrophages infiltration lead to IFN $\gamma$  and IL-2 secretion which ultimately correlate with higher CD8<sup>+</sup> T cells activation. Bone-marrow derived monocytes can differentiate into CD169<sup>+</sup> macrophages when treated with tumoral supernatant. More precisely, type I IFN (IFN $\alpha$ ) induces CD169<sup>+</sup> differentiation in HCC (Liao et al., 2022)

Lastly, it was recently brought up that CD169<sup>+</sup> is expressed glioblastoma (GBM) macrophages but not in microglia. A parabiosis experiment highlighted that CD169<sup>+</sup> macrophages in GBM originate from circulating monocyte in a CCR2 dependant manner but also that depleting CD169<sup>+</sup> macrophages accelerate GBM progression. CD169<sup>+</sup> macrophages in GBM are located in tumoral core and are in physical contact with T lymphocytes and NK cells. NK cells were shown to secrete IFN $\gamma$  to induce monocytes differentiation into CD169<sup>+</sup> macrophages. CD169<sup>+</sup> macrophages depletion in GBM reshaped the TME with microglia expansion. More importantly, CD169<sup>+</sup> depletion led to a decrease of cytotoxic T cells and less phagocytosis activities from macrophages.

While intra-tumoral CD169<sup>+</sup> macrophages have distinct role depending on primary tumor location. It is widely accepted that CD169<sup>+</sup> macrophages level in lymph node of cancerous patients is associated with a good prognosis (**Figure 19**). Indeed, high CD169<sup>+</sup> level in regional lymph node of many cancer (e.g., Bladder, Breast, Gastric, Colorectal, Melanoma, Prostate) correlate with high CD8<sup>+</sup> T cells in TME and a better prognosis (**Figure 19**).

Altogether, these observations highlight that intra-tumoral CD169<sup>+</sup> macrophages in cancer are of different origins. More importantly, it appears that intra-tumoral CD169<sup>+</sup> macrophages role in cancer is not defined by ontogeny but rather is tissue specific. TAMs are mostly associated with a negative or mixed prognosis in all tissues (Galon and Bruni, 2020). Further investigation should be performed to evaluate the specific niche that rule CD169<sup>+</sup> macrophages behaviour in a tissue specific manner. Also, CD169 marker is not a specific marker for embryonically or circulating monocyte derived macrophages.

A dichotomy is observed in some cancer (e.g., Breast, Gastric) where intra-tumoral CD169<sup>+</sup> macrophages support tumor progression while infiltrating lymph nodes CD169<sup>+</sup> macrophages inhibit tumor progression. That is one of the reasons why CD169 targeting therapy should be use with caution but also because CD169<sup>+</sup> macrophages are expressed in various organs as resident macrophages (e.g., Lung, bone-marrow).

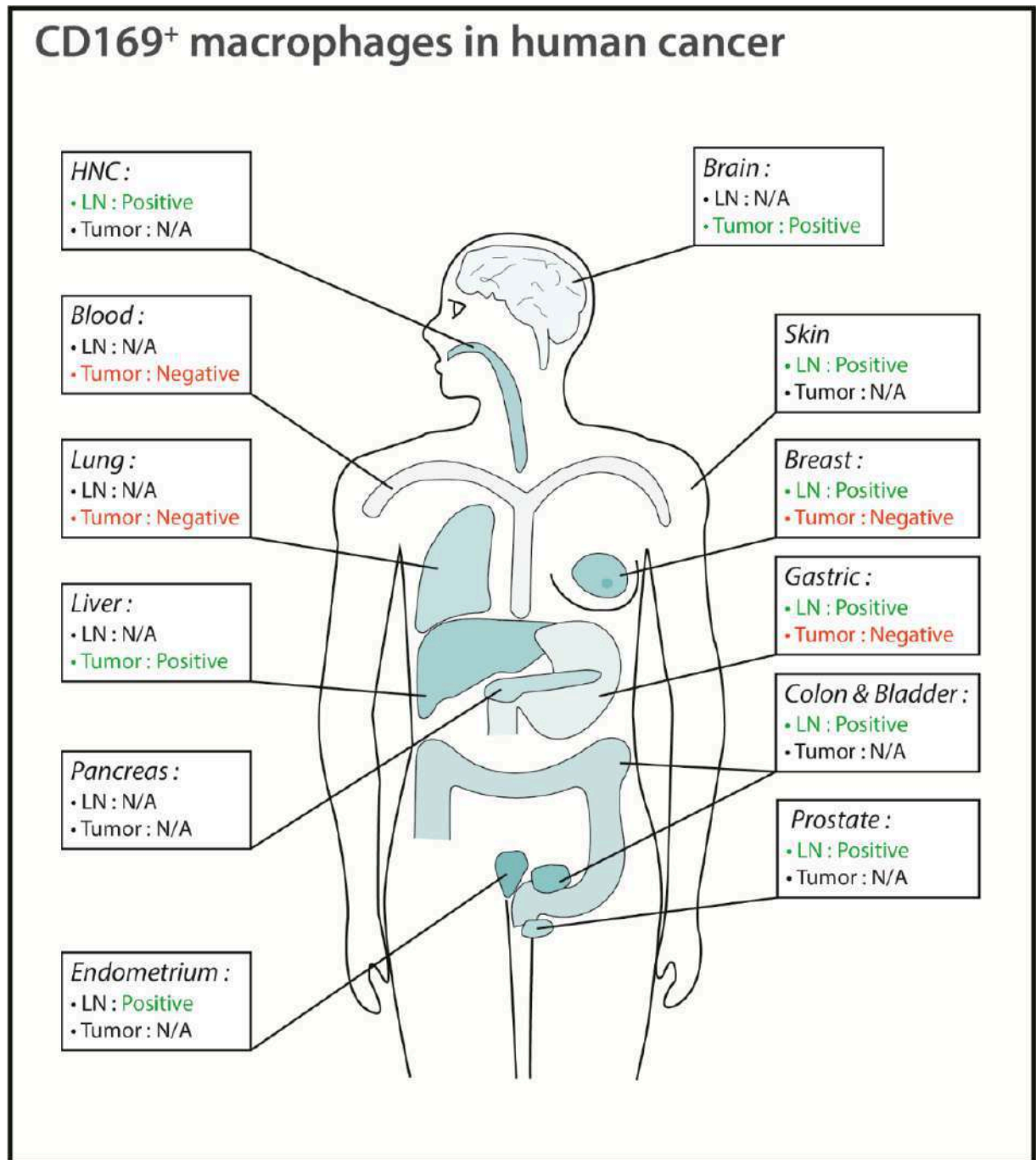


Figure 19. Effect of CD169<sup>+</sup> macrophages on cancer progression in human.

CD169<sup>+</sup> macrophages have anti-tumoral (Positive) and/or pro-tumoral (Negative) role depending on organs in tumor. CD169<sup>+</sup> have only anti-tumoral role in lymph nodes (Asano et al., 2018; Kumamoto et al., 2021; Ohnishi et al., 2016, 2013; Pucci et al., 2016; Stromvall et al., 2017; Tacconi et al., 2021; Topf et al., 2019; Zhang et al., 2016). CD169<sup>+</sup> in pancreas are evaluated in this thesis. N/A Non-Applicable. LN Lymph Nodes , HNC Head and Neck Cancer

# OBJECTIVES

PDAC primarily comprises stromal components such as CAFs, pericytes, immune cells, and ECM proteins. These elements collectively shape the TME. The TME is characterized by a desmoplastic reaction that results in elevated tissue rigidity and significant immune suppression. The pancreatic TME displays remarkable diversity, yet the mechanisms through which stromal components interact to orchestrate the desmoplastic and immune-inhibitory responses remain incompletely understood. Notably, immune suppression predominantly stems from macrophages, the most prominent infiltrating cell population, owing to their adaptable phenotype. Similar to their roles in other tissues, macrophages collaborate with mesenchymal cells to structure the cellular environment.

Consequently, comprehending the interplay between tissue-resident macrophages and stromal cells holds paramount importance in devising novel therapeutic strategies. In addition to their interactions with macrophages, stromal cells have been implicated in fostering the development of tissue stiffness in pancreatic cancer, a factor linked to unfavourable prognoses. Despite this, the mechanisms governing *in vivo* tissue stiffness establishment in PDAC remain insufficiently explored. Therefore, our project aimed to investigate in an integrative manner how stromal cell-macrophage communication contributes to the TME and, concurrently, delve into the processes by which CAFs contribute to the generation of tissue stiffness within the context of PDAC.

Specifically, the objectives of my thesis were to :

- I. Studying the role of a newly described stromal population in pancreatic cancer : Pericyte Stem Cells *in vitro* and *in vivo*.
- II. Identifying the cross talk between macrophages and Pericyte Stem Cells with a focus on macrophages role *in vitro* and *in vivo*.
- III. Understanding how tissue stiffness is generated and the consequent impact on the local anti-tumoral immune response.

# RESULTS

## I. Pericyte stem cells induce Ly6G<sup>+</sup> cell accumulation and immunotherapy resistance in pancreatic cancer

I actively participated to the study of Dr. Wu in Dr. Hennino's group. This study entitled " Pericyte stem cells induce Ly6G<sup>+</sup> cell accumulation and immunotherapy resistance in pancreatic cancer " was published in EMBO reports journal in February 2023. This study was part of Dr. Wu PhD work and lasted during the first two years of my PhD thesis. I participated in the conceptualization and performance of experiments, both *in vivo* and *in vitro*. In the reviewing process of the paper, I also evaluated the role of PeSC in supporting cancer cell progression through Ly6G accumulation in an orthotopic model.

This study was done in a context of identifying stromal cell population in early lesion of pancreatic cancer that communicate with blood vessel. Indeed, blood vessels and specifically pericytes that physically support endothelial cells are the first encounters of immune cells that are recruited in the TME. Therefore, we questioned whether pericytes were capable of shaping the immune profile of recruited immune cells. In an effort to answer this question, we questioned the presence of Vascular Cell Adhesion Molecule 1 (VCAM-1) in PDAC stroma.

We identified a stromal cell population defined as CD106<sup>+</sup>CD24<sup>+</sup>CD44<sup>+</sup>CD31<sup>-</sup>CD45<sup>-</sup>EPCAM<sup>-</sup>. We could generate a cell line based on these markers that can be identified by RNAseq single cell analysis in pre-cancerous genetical engineered mouse model. We showed through *in vitro* and *in silico* analysis that this cell population had both stem and pericyte properties. Therefore, this cell population was named Pericyte Stem Cell (PeSC). We demonstrated that PeSC were not of tumoral origin but were rather recruited from the bone marrow early in the steps of tumorigenesis. Given that PeSC were present only in pre-cancerous model but not in the healthy pancreas, we evaluated the role of PeSC in supporting cancer progression. Through multiple *in vivo* models, we showed that PeSC were supporting tumour progression through the accumulation of Ly6G<sup>+</sup> MDSC. Our study also demonstrated that in our model, PeSC were responsible for anti-PD1 resistance.

While the role of mesenchymal stem cells and pericytes is documented in pancreas, our data support the idea that both mesenchymal stem cells and pericytes are interconnected in pathological conditions and shape the immune response in pancreatic cancer.

**(See published paper next page)**

SOURCE  
DATATRANSPARENT  
PROCESSOPEN  
ACCESS

# Pericyte stem cells induce Ly6G<sup>+</sup> cell accumulation and immunotherapy resistance in pancreatic cancer

Zhichong Wu<sup>1,2,3,4,†</sup> , Kevin Thierry<sup>1,2,3,†</sup> , Sophie Bachy<sup>1,2,3</sup>, Xinyi Zhang<sup>1,2,3</sup>, Pia Gamradt<sup>1,2,3</sup>, Hector Hernandez-Vargas<sup>1,2,3</sup> , Ivan Mikaelian<sup>1,2,3</sup>, Laurie Tonon<sup>1,2,3</sup>, Roxanne Pommier<sup>1,2,3</sup>, Yajie Zhao<sup>1,2,3,5</sup>, Philippe Bertolino<sup>1,2,3</sup>  & Ana Hennino<sup>1,2,3,\*</sup> 

## Abstract

We report the identification of a cell population that shares pericyte, stromal and stemness features, does not harbor the *Kras*<sup>G12D</sup> mutation and drives tumoral growth *in vitro* and *in vivo*. We term these cells pericyte stem cells (PeSCs) and define them as CD45<sup>-</sup>EPCAM<sup>-</sup>CD29<sup>+</sup>CD106<sup>+</sup>CD24<sup>+</sup>CD44<sup>+</sup> cells. We perform studies with *p48-Cre;Kras*<sup>G12D</sup> (KC), *pdx1-Cre;Kras*<sup>G12D</sup>;*Ink4a/Arf*<sup>fl/fl</sup> (KIC) and *pdx1-Cre;Kras*<sup>G12D</sup>;*p53*<sup>R172H</sup> (KPC) and tumor tissues from PDAC and chronic pancreatitis patients. We also perform single-cell RNAseq analysis and reveal a unique signature of PeSC. Under steady-state conditions, PeSCs are barely detectable in the pancreas but present in the neoplastic microenvironment both in humans and mice. The coinjection of PeSCs and tumor epithelial cells leads to increased tumor growth, differentiation of Ly6G<sup>+</sup> myeloid-derived suppressor cells, and a decreased amount of F4/80<sup>+</sup> macrophages and CD11c<sup>+</sup> dendritic cells. This population induces resistance to anti-PD-1 immunotherapy when coinjected with epithelial tumor cells. Our data reveal the existence of a cell population that instructs immunosuppressive myeloid cell responses to bypass PD-1 targeting and thus suggest potential new approaches for overcoming resistance to immunotherapy in clinical settings.

**Keywords** myeloid-derived suppressor cells; pancreatic cancer; PD-1 therapy; pericyte stem cells

**Subject Categories** Cancer; Immunology; Stem Cells & Regenerative Medicine

DOI 10.15252/embr.202256524 | Received 22 November 2022 | Revised 23

January 2023 | Accepted 1 February 2023 | Published online 21 February 2023

EMBO Reports (2023) 24: e56524

## Introduction

The pancreatic tumor stroma consists of a variety of components, including fibroblasts, myofibroblasts, blood vessels, inflammatory and immune cells, extracellular matrix (ECM) and matricellular proteins (Neesse *et al*, 2011; Gore & Korc, 2014). High stromal activity, as assessed by  $\alpha$ -smooth muscle actin ( $\alpha$ -SMA) expression, is associated with poor prognosis in patients with pancreatic cancer (Erkan *et al*, 2008). Nevertheless, the depletion of  $\alpha$ -SMA-expressing cells (Ozdemir *et al*, 2014) also resulted in undifferentiated PDA tumors and decreased survival in mice, suggesting that solely this parameter is not defining the whole complexity of the stromal activity. Fibrous proteins, such as collagens, laminin, and fibronectin, and noncollagenous proteins, such as glycoproteins, proteoglycans, and glycosaminoglycans, together make up the ECM that constitutes the stromal component. The cellular component of the stroma includes immune cells such as lymphocytes, macrophages, mast cells, and myeloid-derived suppressor cells (MDSCs) along with vascular and neural elements (endothelial cells and neurons, respectively).

Accumulating evidence indicates the presence of a close and complex interplay of paracrine interactions between tumor cells and the stroma that facilitates cancer progression (Gore & Korc, 2014). Because the stromal compartment evolves rapidly starting from the beginning of the neoplastic reaction, we investigated the existence and role of stromal stem cells within the neoplastic microenvironment that are capable of driving the stromal reaction. Since the discovery of cancer stem cells (CSCs) in 1997 by Bonnet and Dick in leukemia (Bonnet & Dick, 1997), these cells have been found in several other types of solid tumors, including colon, breast, brain, skin, and pancreatic tumors. Here, we describe the identification of a cell population that shares pericyte, stem, and stromal and properties within the neoplastic microenvironment of pancreatic cancer. We have named these cells pericyte stem cells (PeSCs). We generated primary cell lines of PeSCs

1 Cancer Research Center of Lyon, UMR INSERM 1052, CNRS 5286, Lyon, France

2 Université Lyon 1, Lyon, France

3 Centre Léon Bérard, Lyon, France

4 Department of General Surgery, Pancreatic Disease Center, Ruijin Hospital, Shanghai Jiao Tong University School of Medicine, Shanghai, China

5 Department of Geriatrics, Ruijin Hospital, Shanghai Jiao Tong University School of Medicine, Shanghai, China

\*Corresponding author. Tel: +33469166669; E-mail: ana.hennino@inserm.fr

<sup>†</sup>These authors contributed equally to this work

from mouse pancreatic neoplasms that stably express a fluorescent tag to assess the impact of the stromally elicited signals on tumor growth and the response to immunotherapy in pancreatic cancer.

## Results

### The CD106<sup>+</sup> population is uniquely localized in pancreatic injury and precancerous lesions

CD106 has been proposed as a specific marker for defining mesenchymal stem cells in tissue repair and regeneration (Dominici *et al*, 2006; Acharya *et al*, 2013). Therefore, we performed IHC staining for CD106 in human PDAC samples (stages II and III). We found that CD106 positive cells were exclusively localized in the tumor adjacent stroma rather than in the tumor core (Fig 1A and Appendix Fig S1). We also observed CD106 positive cells in the intraductal papillary mucinous tumor (IPMT). No staining was detected in the normal pancreas or in the tumor core of PanIN III and IPMT (Fig EV1A and B). By identifying the tumor core versus the adjacent region of paired surgical samples, we verified that CD106 positive cells were labeled in all the adjacent regions of Pancreatic Intraepithelial Neoplasia (PanIN) I to PanIN III and of IPMT (Fig EV1B). Immunohistology staining of human tumor microarray (TMA) for CD106 further indicated that these cells were uniquely present in pancreatitis and precancerous early lesions PanINs rather than at the PDAC stage (Fig EV1C and Appendix Table S1), which is similar to the results obtained from our patient samples (Figs 1A and EV1B, and Appendix Fig S1). Next, we took advantage of the *p48-Cre*; *Kras*<sup>G12D</sup> (KC) mouse model, which develops PanINs from the age of 1.5 months (Hingorani *et al*, 2003). We found that the CD106<sup>+</sup> population was in close contact with  $\alpha$ SMA<sup>+</sup> cells (Fig 1B left) and absent in the CK19<sup>+</sup> nascent duct region (Fig 1B right). To obtain further insights into their precise phenotype and frequencies, we used FACS staining to determine their presence in the pancreas of KC mice compared with that of WT mice. In our analysis, we excluded CD45<sup>+</sup> cells (hematopoietic cells) and CD31<sup>+</sup> cells (endothelial cells). The gated CD106<sup>+</sup> cells represented 1.5% of the CD45<sup>-</sup>CD31<sup>-</sup> population and 0.15% of the total population of pancreatic cells but were not detected in the WT mice (Fig 1C). Furthermore, CD45<sup>-</sup>CD31<sup>-</sup>CD106<sup>+</sup>CD29<sup>+</sup> cells also exhibited positive CD44 and CD24 expression and expressed no EPCAM and low levels of PDGFR $\alpha$  (which define duct cells and cancer-associated fibroblasts, respectively; Fig 1C). Previous studies noted the expression of CD24, CD44, and EPCAM at the cell surface and identified CSCs in the pancreas (Li *et al*, 2007). This suggests that the CD106<sup>+</sup>

population might carry both stemness and stromal properties. Therefore, we next perform double immunofluorescence staining for CD24 and CD44 and we identified a population of cells located within the stromal compartment of the pancreas of KC mice that displayed a spindle-shaped morphology (Fig 1D, left). This population was diminished in mice with PDAC, that is, *pdx1-Cre*; *Kras*<sup>G12D</sup>; *Ink4a/Arf*<sup>fl/fl</sup> (KIC; Unpublished observations, Wu), and *pdx1-Cre*; *Kras*<sup>G12D</sup>; *p53*<sup>R172H</sup> (KPC) mice (Fig 1D, right), which develop adenocarcinoma beginning at 5 and 16 weeks of age, respectively (Aguirre *et al*, 2003; Hingorani *et al*, 2005).

To get further insight into the phenotype of this population, we then performed RNAseq single-cell analysis. We have performed first a FACS sorting to obtain a fibroblast-enriched fraction and a tumor duct forming PanINs. Pancreatic cells from 5 KC (2 months of age) mice were dissociated into single cells. From the pooled cells we isolated two fractions of cells by FACS: (i) a viable cell population of fibroblasts-enriched population and (ii) a viable cell population of PanIN-enriched population (Fig 2A and Appendix Fig S2). Sorted cells were subjected to the same droplet-based protocol for single-cell capture and library preparation. Since the identified CD106<sup>+</sup> population was associated with PanINs, we analyzed the sequencing data from the viable cell PanIN enriched population (2,000 cells) isolated from the pooled KC pancreases were clustered in 10 clusters (Fig 2B). We analyzed the most expressed genes of each cluster (Fig 2C) and performed Wiki pathway identification\_2019 and identified a unique population (cluster 7) that have stem properties, focal adhesion, and inflammatory response pathways (Fig 2D).

### The CD106<sup>+</sup> population shares pericyte, stem, and stromal features

Because the frequency of the CD106<sup>+</sup> cells was low in the neoplastic pancreas, we thought to amplify the cells by serum deprivation as previously described (Ferro *et al*, 2019). KC pancreases from 2.5-month-old mice were recovered and digested with collagenase, and a single-cell suspension was cultured for 14 days in the absence of serum. After 14 days of serum starvation, the CD106<sup>+</sup> population represented approximately 4% of the CD45<sup>-</sup>EPCAM<sup>-</sup>CD31<sup>-</sup> population (Appendix Fig S3A). We obtained similar results from two different pancreata of KC mice (Unpublished observations, Wu). To further characterize their properties, we decided to generate a primary cell line via several successive passages (up to passage 20) and infected the cells to stably express the mCherry tag (Figs 3A and EV1D, and Appendix Fig S3A and B). During passaging from P0 to P20, the cells underwent spontaneous dynamic selection of the

**Figure 1. The CD106<sup>+</sup> population is uniquely localized in pancreatic injury and precancerous lesions.**

- Representative IHC staining of tumor core and adjacent region in PDAC patient (stage II) for CD106<sup>+</sup>. The corresponding magnification insets of the tumor core (red dotted line) or adjacent region (green dotted line) are displayed on the right. Scale bar, 500  $\mu$ m in gross, 20  $\mu$ m in magnification.
- Immunofluorescence staining of the pancreas obtained from a 2.5-month-old KC mouse for CD106 (red),  $\alpha$ -SMA (green) or CK19 (green), and DAPI (blue). Scale bar, 50  $\mu$ m, 10  $\mu$ m.
- Gating strategy for the identification of the CD106<sup>+</sup>CD24<sup>+</sup>CD44<sup>+</sup> population in KC and WT mice. FACS analysis of the percentage of CD106<sup>+</sup> among CD45<sup>-</sup>CD31<sup>-</sup> cells; each dot represents one mouse. The bars are representing the mean. The *P*-values were calculated using Student's *t*-test.
- Immunofluorescence staining of pancreases obtained from a KC mouse (left) and a 2.5-month-old KPC mouse (right) for CD44 (green), CD24 (red), and DAPI (blue). Scale bar, 50, 10  $\mu$ m.

Source data are available online for this figure.

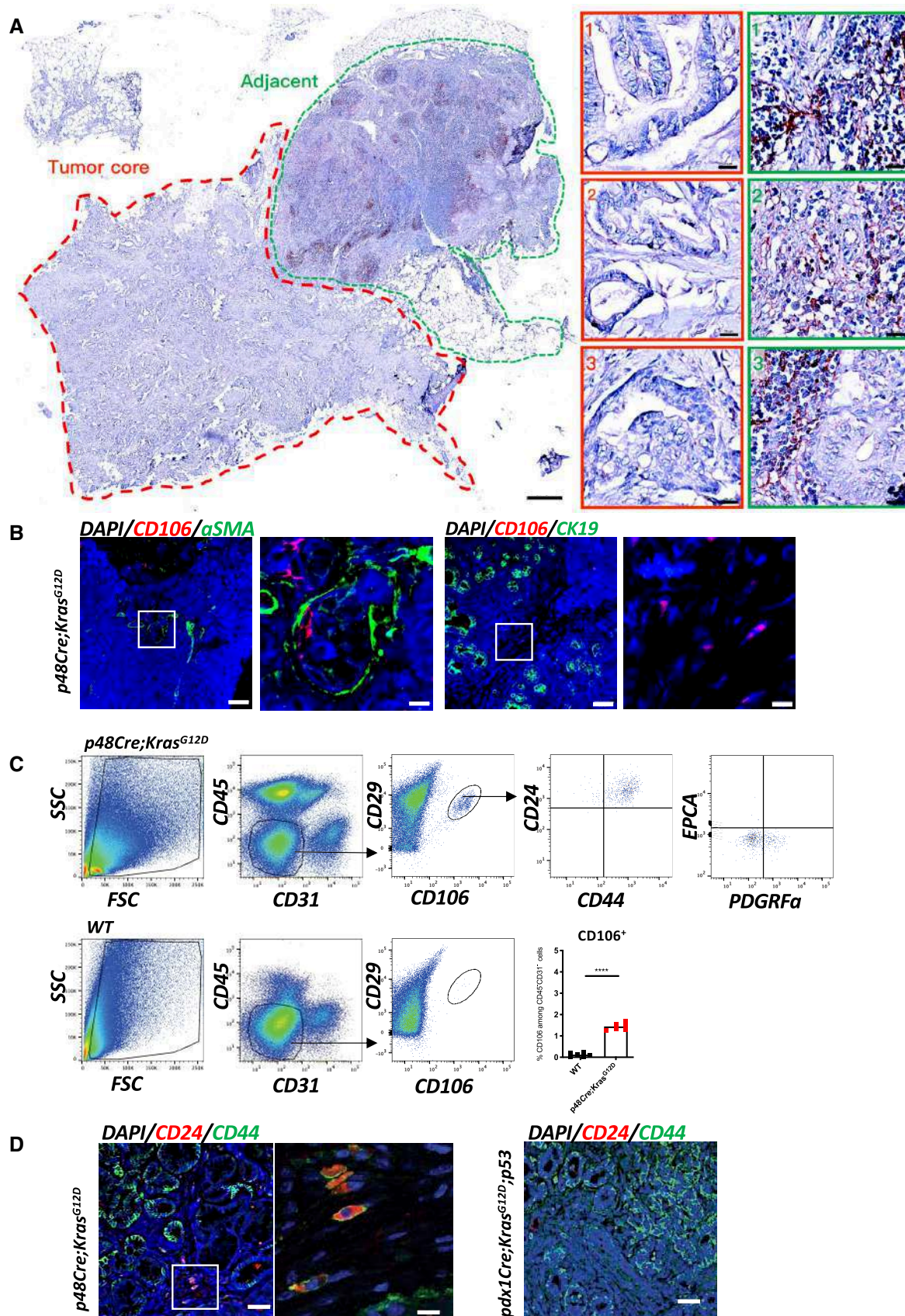


Figure 1.

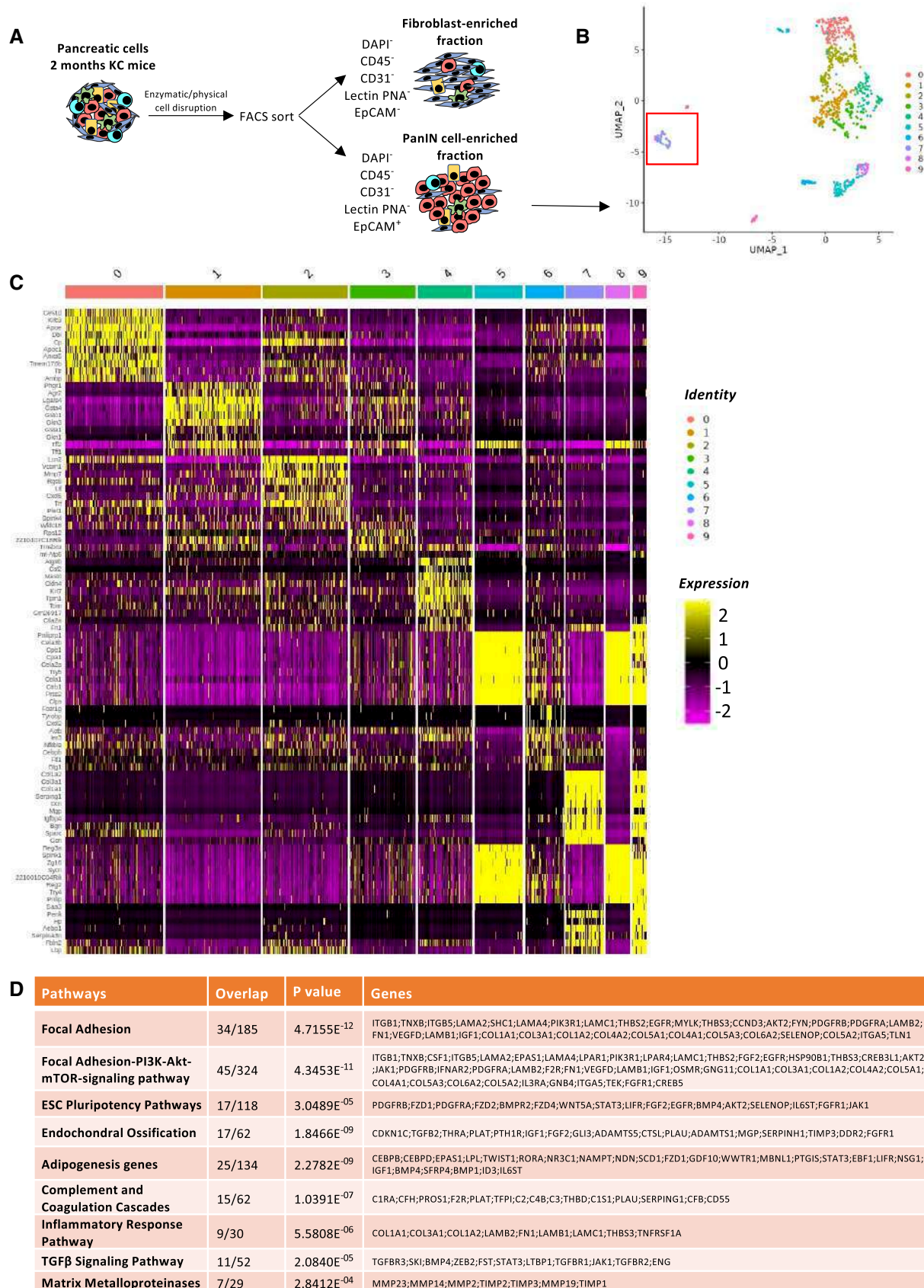


Figure 2.

**Figure 2. Single-cell RNAseq analysis reveals a cell population distinct from the PanIN signature population.**

- A Graphical scheme describing the workflow. Murine 2-month KC pancreases were dissociated into single cells. Two fractions of cells were collected by FACS from each sample: (i) viable cell fraction (DAPI<sup>-</sup>) fibroblast-enriched fraction (DAPI<sup>-</sup>, CD45<sup>-</sup>, CD31<sup>-</sup>, Lectin PNA<sup>-</sup> and EPCAM<sup>-</sup>) and (ii) viable cell fraction (DAPI<sup>-</sup>) PanIN-enriched fraction (DAPI<sup>-</sup>, CD45<sup>-</sup>, CD31<sup>-</sup>, Lectin PNA<sup>-</sup>, and EPCAM<sup>-</sup>). The sorted cells from each fraction were subjected to single-cell capture, barcoding, and reverse transcription using the 10X Genomics platform.
- B Unsupervised clustering UMAP representation of the PanIN enriched fraction. The red square is indicating cluster 7.
- C Heat map showing scaled normalized expression of discriminative marker genes between the nine subclusters, with cells as columns and genes as rows.
- D Wiki pathway identification\_2019 analysis reveals nine most up-regulated pathways. The number of overlapped genes of the pathways are indicated, as well as the *P*-value and the names of the genes detected.

Source data are available online for this figure.

CD106<sup>+</sup> population from 15 to 90% (Figs 3A and EV1D, and Appendix Fig S3A–C). We defined these cells as PeSCs. We also generated an epithelial tumoral PanIN cell line (defined as Epi) and a lung metastasis cell line (defined as Meta) from the pancreas and lung of 2-month-old KIC mice, respectively, that express an eGFP tag (Appendix Fig S3D and E). We tested the presence of the floxed *Kras*<sup>G12D</sup> allele in the three cell lines and showed that the PeSCs, in contrast to the Epi and Meta cell lines, did not carry the recombined *Kras*<sup>G12D</sup> gene, which confirmed that the PeSCs were not of tumoral origin (Fig 3B). We also confirmed that PeSC does not express the *Kras*<sup>G12D</sup> mutated protein by Western Blot approach using an anti-*Kras*<sup>G12D</sup>-specific Ab (Fig 3C). A FACS phenotypic analysis confirmed that the PeSCs were CD44<sup>+</sup>CD24<sup>low</sup>, whereas the Epi and Meta cells were CD44<sup>+</sup>CD24<sup>high</sup> and CD44<sup>+</sup>CD24<sup>-</sup>, respectively, and clustered differently on a CD24 CD44 and CD24 CD106 dot plot (Fig 3D and Appendix Fig S3F). We further investigated their transcriptomic profile by RNA sequencing. The principal component analysis (PCA) and gene expression profile of the RNA-seq data showed that the PeSCs exhibited an upregulated stemness and interferon gene signature compared with the Epi and Meta cells (Fig 3E and F). Furthermore, the PeSCs presented downregulated cell cycle genes compared with the Epi and Meta cells and did not exhibit epithelial characteristics (Fig 3F). We confirmed the RNAseq data through a qPCR analysis of several upregulated genes detected in the transcriptomic analysis (Fig 3G). We confirmed that *Nanog* and *Oct3/4* were specifically upregulated in PeSCs and not in Epi and Meta cells. Furthermore, we detected an upregulation of genes associated with the pericyte signature in the PeSCs (Armulik *et al*, 2011). The transcriptomic analysis revealed that the RNA expression levels of *NKX3.2*, *Anpep* (encoding Anpep [alanine aminopeptidase]), *Cd248*, *Eng* (encoding endoglin), *Pdgfrb* (encoding PDGFRβ), and *Rgs5* (encoding RGS5 [regulator of G-protein signaling 5]) were higher in the PeSCs than in the Epi and Meta cells and

we then confirmed their expression by qPCR and FACS staining (Fig 3G and Appendix Fig S3C). To define if the cells obtained were reflecting the population observed *ex vivo*, we have generated a PeSC score from the RNAseq data of the PeSC cell line and applied the score to the single-cell RNAseq analysis. As shown in Fig 3H, the highest PeSC score is displayed by cluster 7 (Fig 2B). Cluster 7 stands for the minority population in this PanIN enriched fraction and their distribution indeed diverges from the other major clusters (cluster 1–6, 8, 9, Fig 2B and C). The detailed genes of the PeSC score are depicted in plots in Appendix Fig S4. We further checked the expression of EPCAM in the PeSC fraction and found that cluster 7 (PeSC fraction) had no expression of EPCAM (Appendix Fig S3G). As PeSC is in close contact with the PanIN lesions according to the staining on the tissue section (Figs 1B and EV1B), these cells are sorted with the ductal enriched fraction as contamination. Moreover, we show now that, in addition to our PeSC score, cluster 7 is enriched in pericyte scores independently (Fig EV2A and B) obtained from the literature (ovarian cancer pericytes; Sinha *et al*, 2016) as well as brain pericytes (Oudenaarden *et al*, 2022). More interestingly, we checked the distribution of this PeSC in the human PDAC context by applying the PeSC score to the public data of human PDAC single-cell RNAseq. The database contains 35 samples (24 PDAC and 11 nontumor) and altogether over 80 k cells (Chen *et al*, 2021; Fig EV2C). The general identities of cell type were annotated based on Muraro's single-cell dataset as a reference (Muraro *et al*, 2016; Fig EV2D). Unsupervised clustering showed 23 different clusters of cells in the integration of whole samples (Fig EV2E), as well as in grouping samples into normal pancreas or PDAC, respectively (Fig EV2F). Consistent with our findings in GEMMs, the PeSC population is significantly clustering in human PDAC with the highest PeSC scores among the mesenchymal populations (Fig EV2D) compared to the normal pancreas (Fig 3I). Altogether these data point out the existence of a new defined population both

**Figure 3. The CD106<sup>+</sup> population shares pericyte, stem cell and stromal features.**

- A Schematic representation of the experimental setting for PeSC line generation.
- B PCR for genomic *Kras* and *Kras*<sup>G12D</sup>.
- C Western Blot analysis for tubulin and mutated *Kras*<sup>G12D</sup> proteins in total proteins extracts of PeSC, Epi, and Meta cells.
- D Representative dot plot of the CD44 and CD24 staining of PeSCs and Epi and Meta cells.
- E Principal component analysis (PCA) of RNA-seq data from the indicated cell populations (*n* = 3).
- F Pathway enrichment of a list of genes.
- G qPCR analysis of several genes identified in the RNAseq analysis. Treatment was performed in biological triplicates and qPCR analysis was performed by technical duplicates. The bars are representing the mean ± SD. \**P* < 0.05, \*\**P* < 0.01, \*\*\**P* < 0.001, and \*\*\*\**P* < 0.0001. The *P*-values were calculated using Student's *t*-test.
- H Definition of the PeSC score (bulk RNAseq) applied to the single-cell RNAseq analysis and identification of cluster 7.
- I Application of PeSC score to the human PDAC public single-cell RNAseq database and identification of a cluster with the highest PeSC (red square) among the mesenchymal population (Fig EV2D) in either Normal Pancreas (left) or Human PDAC (right).

Source data are available online for this figure.

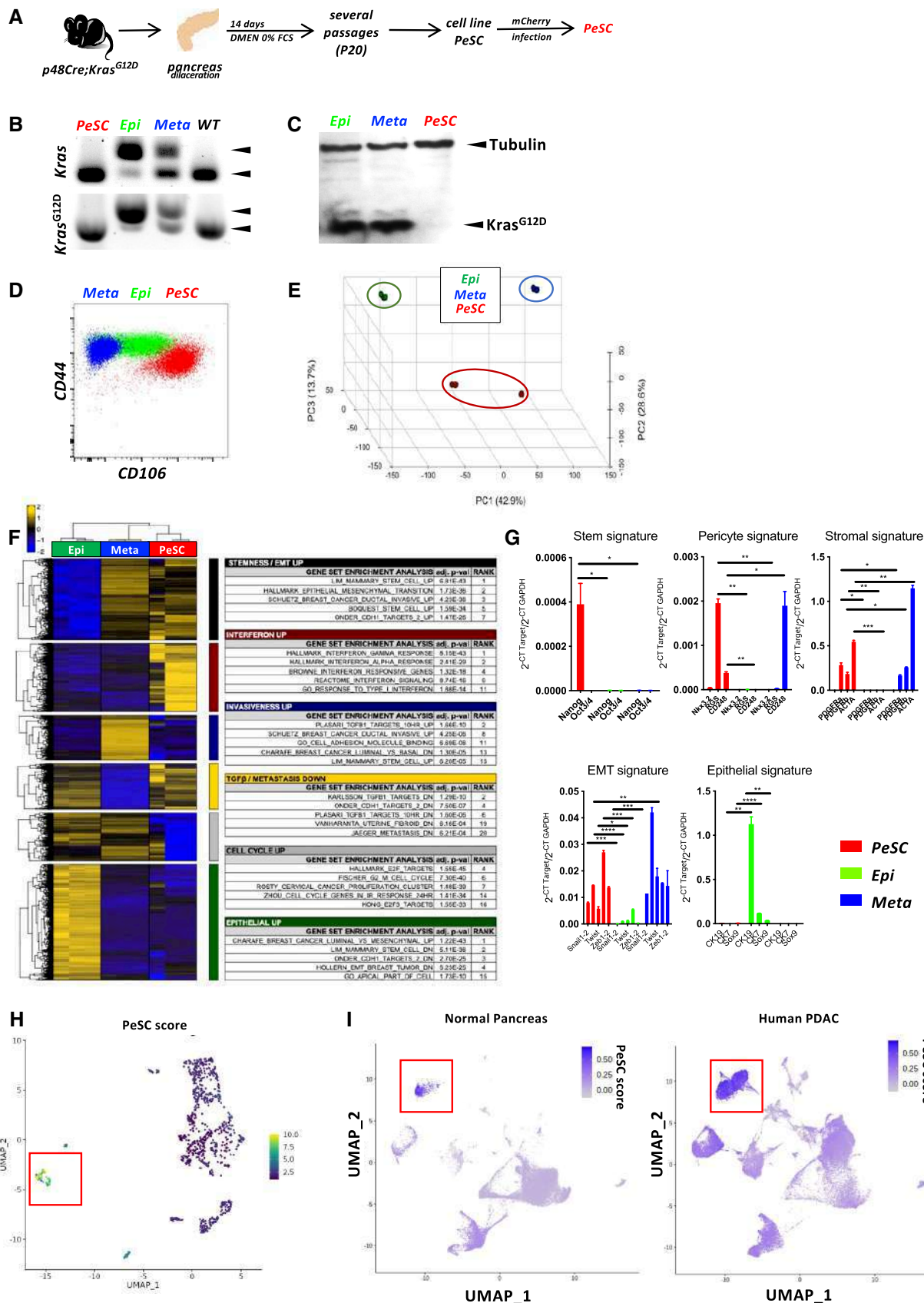


Figure 3.

in PDAC GEMMs and human PDAC, distinct from PanIN epithelial cells and from fibroblast enriched fractions with unique stem properties. To determine their origin, we performed bone marrow chimeras. For this purpose, 3 weeks KC mice were irradiated and *iv* injected with bone marrow cells from a Tomato expressing mouse and sacrificed at day 60 (Fig EV3A). We found that the efficiency of reconstitution in the generated chimeras was around 50% of donor bone marrow in the periphery (Fig EV3B) and around 30% in the pancreas (Fig EV3B). We further analyzed the % CD106<sup>+</sup> in the pancreas. We gated on CD45<sup>-</sup>CD106<sup>+</sup> cells, and then quantified % of the Tomato<sup>+</sup> cells. The % of Tomato<sup>+</sup> among CD106<sup>+</sup> cells was around 20–30% (Fig EV3C) in the pancreas, which is consistent with the % of the above-mentioned reconstituted Tomato<sup>+</sup> cells in the pancreas of the chimeras (Fig EV3B), suggesting that the majority of CD106 were of bone marrow origin. We verified by immunofluorescence staining that CD106 was coexpressed with Tomato in the stroma around PanIN lesions demonstrating the bone marrow origin of this population (Fig EV3D). Generally, stem cells are continuously losing their stemness during conventional *ex vivo* 2-D culture (Banerjee & Bhonde, 2006). Hanging drop spheroid assay has been described to verify cell stemness *in vitro* (Banerjee & Bhonde, 2006), indicating that only stem cells are capable of forming spheroids. Furthermore, by seeding these stem cells trypsinized from spheroids in the culture plates, their proliferation to confluency indicates retention of their self-duplication capacity. We performed 2-D and 3-D hanging drop combination assay using PeSC cell lines in both early and late passages. We showed that either PeSC early passages (P1) or late passages (P20) were able to form spheroids by hanging drop assay (Fig 4A and B), while the Epi cells did not (Fig 4B). Moreover, with the notion that PeSC shares stem cell characteristics in the gene expression profile, we tested their ability to differentiate into multiple cell lineages. We cultured the cells in specific chondrogenic and osteogenic media and determined that PeSCs had the potential to differentiate into cartilage and bone cells (Fig 4C). We then questioned whether the PeSCs influenced the proliferation of tumor cells *in vitro*. For this purpose, we cocultured PeSCs with the Epi cell line *in vitro* at different ratios to determine the impact of PeSCs on tumor epithelial cell growth. We observed that PeSCs significantly potentiated Epi cell proliferation when the cells were cocultured at Epi cells:PeSC ratios as low as 10:1 or 100:1 (Figs 4D and EV4A). These IncuCyte analyses were confirmed by Ki67 intracellular staining and FACS analysis (Fig EV4B). In contrast, we found that the Epi cell line had no

impact on PeSC proliferation under the same conditions (Fig EV4C and D). Because pericytes are mural cells capable of sustaining vessel formation, we performed an *in vitro* analysis of vessel formation using C57BL/6 mouse primary pancreatic microvascular endothelial cells under 3D conditions (Fig 4E). PeSCs had the potential to sustain vessel formation in 3D cell culture conditions. Moreover, in the presence of Epi cells, PeSC was able to structure the vessel in structures containing the three cell types (Fig 4E inset Endo-Epi-PeSC). A large variety of anti- and pro-angiogenic growth factors, extracellular matrix proteins, proteases, and adhesion molecules interacting with multiple cells and tissues are required for angiogenesis. It has been described that the vasculature was reinforced and the endothelial cells were protected by maintaining a balance between the endothelial cells and pericytes controlled by the PDGF-BB signaling pathway operating in a paracrine manner to keep pericytes in the quiescent state. Pericytes turned into an activated state to migrate by the cause of PDGF-BB expression disruption, dissociating pericyte-endothelial connections in injury (Wong *et al*, 2015). To further study the impact of PDGF-BB on PeSCs, we treated PeSCs with PDGF-BB + TGF- $\beta$  for 7 days and perform q-PCR together with FACS analysis. We found that the expression of stroma/CAF-related genes and markers, that is, PDGFR $\alpha$ , PDGFR $\beta$ ,  $\alpha$ -SMA, Desmin and CD61 were significantly diminished after the treatment at both RNA (Fig 4F) and protein level (Fig 4G). Furthermore, several EMT-related genes were also down-regulated by the treatment (Fig EV4E). This indicated that PeSCs could be transformed to the quiescent state to sustain the vasculature by PDGF-BB as described in the literature.

Altogether, these data suggest the identification of a pericyte stromal cell with stemness, self-renewal, asymmetric division and differentiation character and the ability to increase epithelial tumor cell proliferation *in vitro*.

#### PeSCs lead to increased tumor growth and the accumulation of Ly6G<sup>+</sup> myeloid-derived suppressor cells *in vivo*

Because PeSCs potentiated the *in vitro* proliferation of Epi cells, we subsequently sought to investigate the impact of PeSCs on epithelial tumor growth *in vivo*. To explore this issue, we injected s.c. Epi cells alone (one flank) or in the presence of PeSCs (the other flank) in Matrigel plugs (Fig 5A) at a 1:1 ratio in Rag2<sup>KO</sup> recipient mice. We sacrificed the mice 10 days after the injection and found that the coinjection of Epi with PeSCs induced an increased tumor weight

**Figure 4. Stem properties of PeSCs and their impact on tumor cell proliferation on vessel formation.**

- Representative image of PeSC spheroid in early passages (P1) performed by hanging drop approach after 6 days. Scale bar, 100  $\mu$ m. Quantification of PeSC spheroids surface area. Unit,  $\mu$ m<sup>2</sup>.
- Representative images of spheroid formed by PeSCs and cell clusters formed by Epi cells, respectively, in late passages (P20). Scale bar, 100  $\mu$ m.
- Representative Alizarin Red S staining (left) and Alcian blue staining (right) of PeSCs in a 12-well culture plate observed with a 10 $\times$  optical lens. Scale bar, 200  $\mu$ m.
- Representative full-well view (upper Scale bar, 1.4 mm) and 5 $\times$  magnification (lower) of cocultures of Epi cells + PeSCs at the indicated ratio in 96-well plates observed by IncuCyte after 48 h.
- Pericyte property of PeSCs impact tube vessel formation. Representative 3D culture illustration of the cell lines in the indicated condition: primary pancreatic endothelial cells (Endo), Endo + Epi, Endo + PeSC, and Endo + Epi + PeSC. The tube forming test has been performed twice. Scale bar, 500  $\mu$ m, insets 1,500  $\mu$ m.
- qPCR analysis of stroma/CAF-related genes expressed by PeSCs after the treatment of PDGF-BB + TGF- $\beta$ . Treatment was performed in biological triplicates and qPCR analysis was performed by technical duplicates. The bars are representing the mean  $\pm$  SD.
- FACS analysis of stroma/CAF-related surface markers expressed by PeSC after the treatment of PDGF-BB + TGF- $\beta$ . Treatment and FACS analysis were both performed by biological triplicates. The bars are representing the mean  $\pm$  SD. \* $P$  < 0.05, \*\*\* $P$  < 0.001, and \*\*\*\* $P$  < 0.0001. The  $P$ -values were calculated using Student's  $t$ -test.

Source data are available online for this figure.

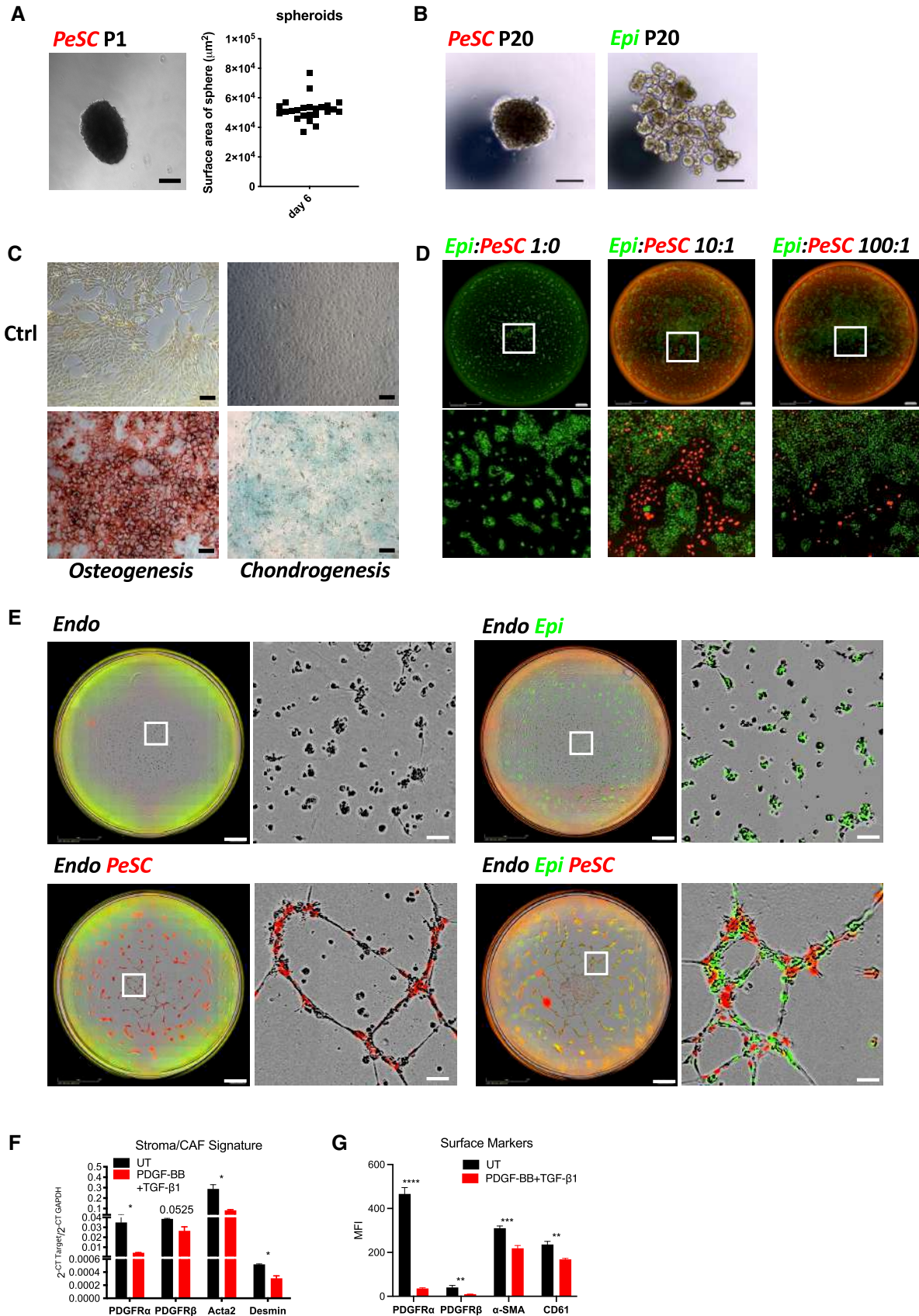


Figure 4.

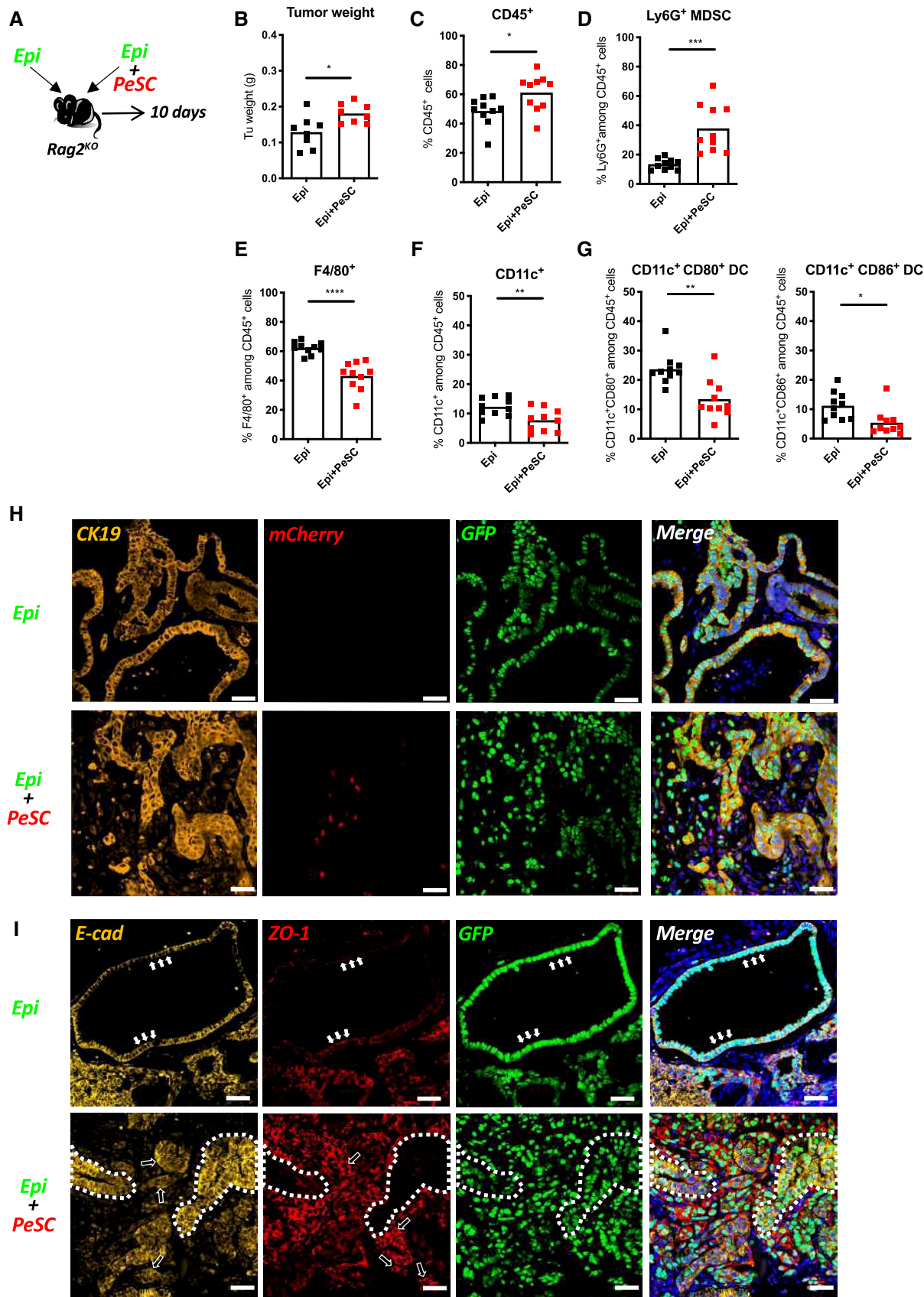


Figure 5.

### Figure 5. *In vivo* injection of PeSCs in the context of epithelial tumors induce Ly6G<sup>+</sup> MDSCs in the microenvironment.

- A Experimental setting.
- B–G (B) Tumor weight. FACS analysis of the percentages of CD45<sup>+</sup> cells (C), Ly6G<sup>+</sup>CD45<sup>+</sup> MDSCs (D), F4/80<sup>+</sup>CD45<sup>+</sup> Macrophages (E), CD11c<sup>+</sup>CD45<sup>+</sup> DCs (F), and CD11c<sup>+</sup>CD80<sup>+</sup>/CD11c<sup>+</sup>CD86<sup>+</sup> DCs (G). The results shown are cumulative from three independent experiments (each dot represents one mouse, 12–15 mice per group).
- H, I Representative immunofluorescence staining of implanted tumors in Rag2<sup>KO</sup> mice for CK19, mCherry, GFP and DAPI (H) and E-cadherin, ZO-1 and GFP (I). Solid white arrows indicated the representative cells which expressed E-cadherin and ZO-1 in the cell junctions. Hollow white arrows indicated the representative cells whose E-cadherin or ZO-1 expression was shifting to the cytoplasm. The white dotted line indicated two representative areas where E-cadherin and ZO-1 were reversely expressed. Scale bar, 50 μm. \**P* < 0.05, \*\**P* < 0.01 and \*\*\**P* < 0.001. The *P*-values were calculated using Student's *t*-test.
- Source data are available online for this figure.

compared with the injection of Epi cells alone (Fig 5B). By quantifying the number of grafted cells on day 10, we found that although we injected the equivalent number of cells of both Epi and PeSC, the amount of PeSC is about 1% of the Epi cells, which is similar to the observed level of PeSC in KC pancreas (Figs EV4F and 1C). This confirmed that the increase in graft weight is predominantly due to the proliferation of Epi cells in both Epi alone and Epi + PeSC condition rather than the proliferative contribution by PeSCs. The percentage of recruited CD45<sup>+</sup> hematopoietic cells obtained with the coinjection of Epi cells PeSCs were higher than those obtained with the injection of Epi cells alone (Fig 5C), and among the CD45<sup>+</sup> recruited cells, a markedly higher proportion of Ly6G<sup>+</sup> MDSCs (defined as CD11b<sup>+</sup>Ly6G<sup>+</sup>) was obtained with the coinjection of Epi cells and PeSCs (Fig 5D). As described in the literature, PDAC is characterized by abundant myeloid cell infiltrates that predominantly include monocytes, granulocytes, and macrophages (Mitchem *et al*, 2013). These infiltrates are associated with immunosuppression, fibrosis, T-cell dysfunction, and poor prognosis in patients with PDAC (DeNardo *et al*, 2011; Nywening *et al*, 2018). The F4/80<sup>+</sup> macrophage and CD11c<sup>+</sup> dendritic cell populations were strongly reduced (Fig 5E and F), and the expression of the costimulatory molecules CD80 and CD86 on the surface of macrophages and dendritic cells were also markedly decreased (Fig 5G). The effect on the Ly6G MDSC, F4/80, and CD11c populations was observed even with very low numbers of injected PeSCs (i.e., Epi cell:PeSC ratio of 100:1, Unpublished observations, Wu). Furthermore, we performed immunofluorescence staining with anti-CK19 Ab to label epithelial PanIN duct cells and anti-mCherry and anti-GFP Abs to identify implanted cells (PeSCs and Epi) on graft sections (Fig 5H). We observed that Epi cells formed PanIN structures similar to those found on the pancreas of KC mice (Figs 5H and 1B right). In the presence of PeSCs, PanIN structures displayed a loss of nuclear polarity, which suggested the development of more

advanced lesions (Fig 5H). We confirmed the change in PanIN structures by immunofluorescence using ZO-1 and E-cad staining. As previously described (Polette *et al*, 2007), we found that ZO-1 and Ecad expression shifted from tight junctions to the cytoplasm of duct cells (Fig 5I). Altogether, these results indicate that PeSCs influence tumor progression with a concomitant loss of nuclear polarization in epithelial tumor cells *in vivo* by inducing reprogramming of the innate immune cell microenvironment, and this reprogramming was characterized by increases in Gr-MDSCs and reductions in F4/80<sup>+</sup> macrophages and mature CD11c<sup>+</sup> dendritic cells. Because these three populations share CD11b expression, we hypothesized that PeSCs might impact CD11b differentiation upon recruitment to the tumor microenvironment. To test this hypothesis, we sought to determine whether PeSCs promote the differentiation of monocytes into Gr-MDSCs expressing Ly6G<sup>+</sup> rather than macrophages and dendritic cells. For this purpose, we isolated and cultured mouse bone marrow precursors (Fig 6A) and tested the effects of coculturing PeSCs, Epi cells or Epi cells + PeSCs with bone marrow precursors. After the coculture of bone marrow cells in the presence of PeSCs or Epi cells alone, approximately 15–20% of the bone marrow cells were Ly6G<sup>+</sup>CD11b<sup>+</sup>, whereas this population was strongly increased in the coculture with Epi cells + PeSCs (Fig 6B and C). Extended analysis of the cytokine/chemokine production by LegendPlex assay pointed out an increased production of CCL2 and CCL5 but also CCL20, CXCL1, CXCL5, and CXCL10 (Appendix Fig S5A–H).

Furthermore, we analyze the accumulation of the Ly6G<sup>+</sup>CD11b<sup>+</sup> population in three s.c. grafting condition, respectively, that is, Epi, PeSC, or Epi + PeSC, in the Rag2<sup>KO</sup> mice. The result revealed that the increased amount of Ly6G<sup>+</sup>CD11b<sup>+</sup> was only obtained in the Epi + PeSC condition (Fig 6D), and these Ly6G<sup>+</sup> cells were in close contact with the mCherry<sup>+</sup> PeSCs observed by IF staining of the graft section (Fig 6E) and express Nanog (Fig 6F). Furthermore, the use of anti-CCL5-depleting Ab did not affect Ly6G<sup>+</sup>CD11b<sup>+</sup>

### Figure 6. Tumor-PeSCs crosstalk induces Ly6G<sup>+</sup> MDSC differentiation.

- A Experimental setting of bone marrow differentiation.
- B Representative dot plots of CD11b and Ly6G staining in bone marrow cells cultured in the presence of Epi cells, PeSCs or both Epi cells, and PeSCs.
- C Quantification of the percentage of Ly6G<sup>+</sup> cells among CD11b<sup>+</sup> cells (cumulative from three independent experiments). The bars are representing the mean ± SD.
- D Experimental setting for *in vivo* injection. FACS analysis of the percentages of Ly6G<sup>+</sup>CD45<sup>+</sup> cells (each dot represents one mouse per group).
- E, F Representative immunofluorescence staining of coimplanted Epi cells + PeSCs for Ly6G, mCherry, Nanog, and DAPI. Scale bar, 50 μm.
- G–M *In vivo* depletion of Ly6G<sup>+</sup> MDSCs diminishes tumor growth. (G) Experimental setting. (H) Tumor weight. FACS analysis of the percentage of CD45<sup>+</sup> cells (I), and Ly6G<sup>+</sup> MDSCs (J) derived from the tumor. (K) Representative dot plots of Ly6G- and F4/80-stained CD45<sup>+</sup> cells. FACS analysis of the percentage of F4/80<sup>+</sup> cells. (L) Representative dot plots of CD45- and CD11c-stained cells. FACS analysis of the percentage of CD11c<sup>+</sup> cells among CD45<sup>+</sup> cells. (M) FACS analysis of GrzB<sup>+</sup>, TNFα<sup>+</sup>, and IFNγ<sup>+</sup> cells among CD45<sup>+</sup> cells. Eight mice in each group, five for FACS analysis and three for histological analysis. Each dot represents one mouse.

Data information: \**P* < 0.05, \*\**P* < 0.01, and \*\*\**P* < 0.001. The *P*-values were calculated using Student's *t*-test.  
Source data are available online for this figure.

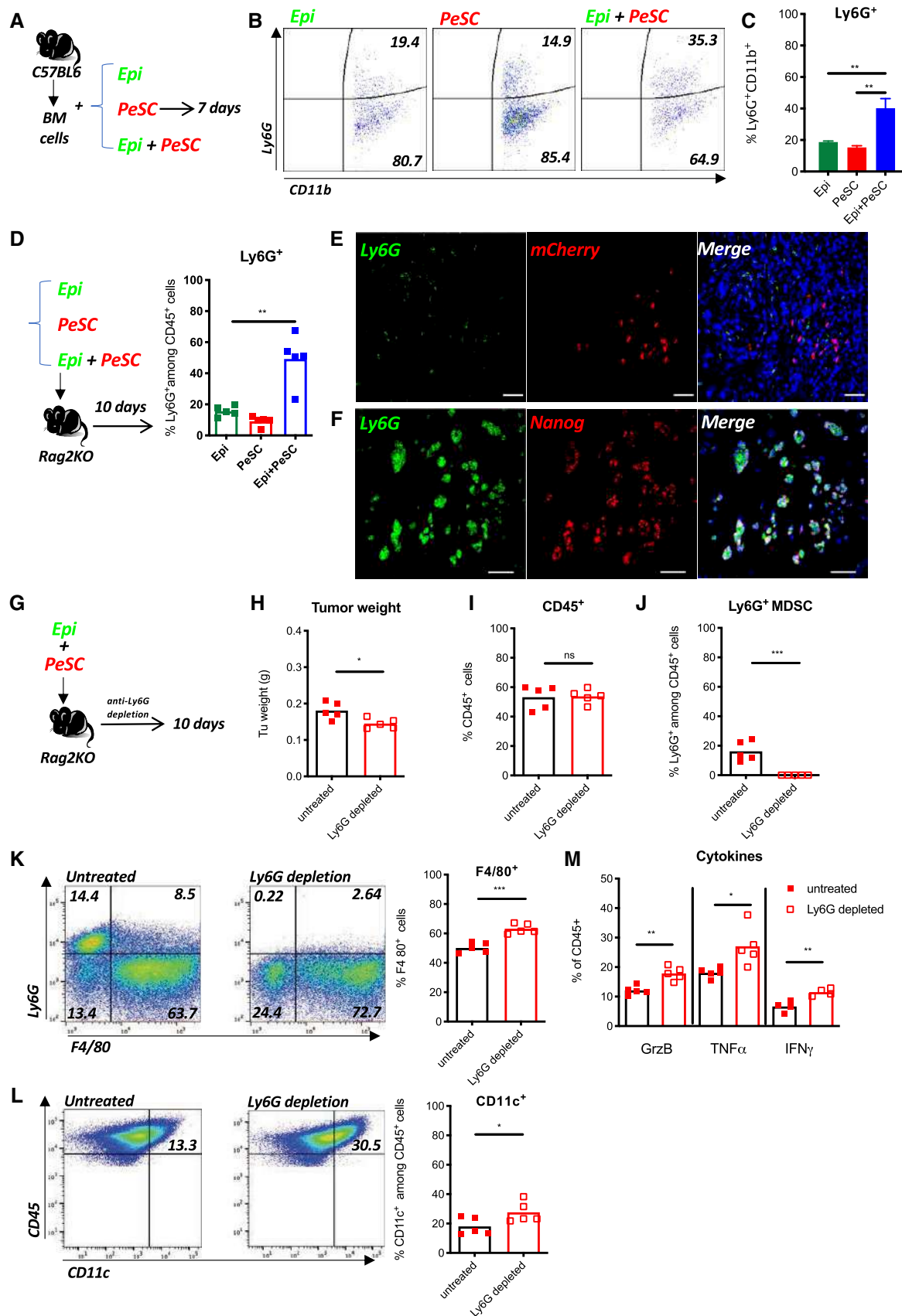


Figure 6.

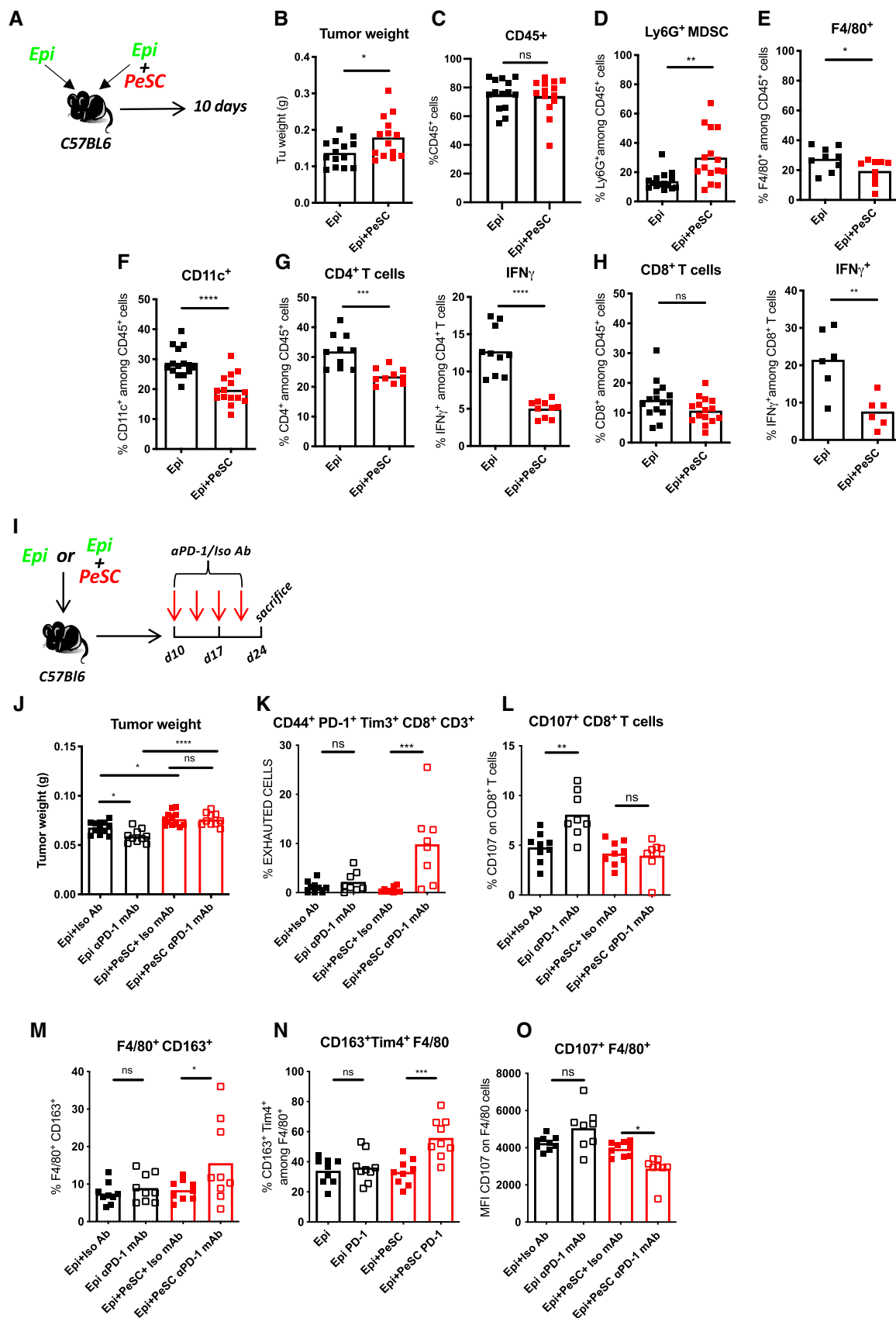


Figure 7.

**Figure 7. PeSCs drive PD-1 resistance in the tumor microenvironment.**

- A Experimental setting.  
 B–H (B) Tumor weight. FACS analysis of the percentage of CD45<sup>+</sup> cells derived from the tumor (C), Ly6G<sup>+</sup> MDSCs (D), F4/80<sup>+</sup>CD45<sup>+</sup> cells (E), CD11c<sup>+</sup>CD45<sup>+</sup> cells (F), CD4<sup>+</sup>CD45<sup>+</sup> and IFN $\gamma$ <sup>+</sup>CD4<sup>+</sup> (G) and CD8<sup>+</sup>CD45<sup>+</sup> and IFN $\gamma$ <sup>+</sup>CD8<sup>+</sup> (H). The results shown are cumulative from three independent experiments (each dot represents one mouse, 12–15 mice per group).  
 I Experimental setting.  
 J–O (J) Tumor weight. FACS analysis of CD44<sup>+</sup>PD-1<sup>+</sup>Tim3<sup>+</sup>CD8<sup>+</sup>CD3<sup>+</sup> T cells (K), CD107<sup>+</sup>CD8<sup>+</sup> T cells (L), F4/80<sup>+</sup>CD163<sup>+</sup> Macrophages (M), CD163<sup>+</sup> Tim4<sup>+</sup> Macrophages (N) and CD107<sup>+</sup> Macrophages (O). The results shown are cumulative from three independent experiments (each dot represents one mouse, 9–12 mice per group).  
 Data information: \**P* < 0.05, \*\**P* < 0.01, \*\*\**P* < 0.001, and \*\*\*\**P* < 0.0001. The *P*-values were calculated using Student's *t*-test.  
 Source data are available online for this figure.

differentiation but did affect macrophage differentiation, which expressed less CD103<sup>+</sup> *in vitro* and *in vivo* (Appendix Fig S5I and J), and these findings suggest a role for CCL5 in the local instruction of macrophages and residency. The use of anti-CD106-depleting Ab did not affect Ly6G<sup>+</sup>CD11b<sup>+</sup> differentiation or macrophage differentiation but reduced the tumor weight and number of PeSC and Epi GFP tumor cells in the tumor graft (Fig EV5A and B). Altogether, these data demonstrate that the presence of PeSCs increased the tumor weight and favored the accumulation of Ly6G<sup>+</sup>CD11b<sup>+</sup> within the tumor microenvironment. To determine whether Ly6G<sup>+</sup> MDSCs are required for the *in vivo* effects of PeSCs, we coinjected Epi cells and PeSCs subcutaneously and treated the mice with an anti-Ly6G-depleting Ab (Fig 6G). We observed a significant decrease in the tumor weight (Fig 6H) with a similar PeSC amount (Appendix Fig S6D). The depletion was effective because we detected no Ly6G<sup>+</sup> cells in the tumor grafts (Fig 6J). Similar percentages of CD45<sup>+</sup> cells were observed in both conditions (Fig 6I). In contrast, we detected increased populations of F4/80<sup>+</sup> macrophages and CD11c<sup>+</sup> dendritic cells (Fig 6K and L). We also detected increases in the populations of NKp46<sup>+</sup> and Ly6C<sup>+</sup> cells, whereas the percentage of CD206<sup>+</sup> among F4/80 cells were decreased (Appendix Fig S6A–C). More importantly, we detected increased antitumoral cytokine production, including TNF $\alpha$ , IFN $\gamma$ , and cytotoxic GrzB (Fig 6M). Altogether, these results indicate that Ly6G<sup>+</sup> MDSCs play an important role in the immunosuppressive role of PeSCs.

Previous studies have shown that the targeted depletion of MDSCs unmasks pancreatic ductal adenocarcinoma to adaptive immunity (Stromnes *et al*, 2014). We then questioned whether PeSCs impact the innate immune response in fully immune-competent mice. To explore this hypothesis, we injected s.c. Epi cells alone (one flank) or in the presence of PeSCs (the other flank) in Matrigel plugs (Fig 7A) at a 1:1 ratio in C57BL/6 immunocompetent recipient mice. Similar to the results obtained with Rag2KO recipient mice, we found that the coinjection of Epi cells with PeSCs induced an increase in the tumor weight compared with that obtained with the injection of Epi cells alone (Fig 7B). Although the percentage of CD45<sup>+</sup> hematopoietic cells was not increased with the injection of Epi cells + PeSC as previously found in Rag2<sup>KO</sup> mice (Figs 7C and 5C), the percentage of Ly6G<sup>+</sup> MDSC population was unanimously increased (Fig 7D). Moreover, as previously described, the populations of F4/80<sup>+</sup> macrophages and CD11c<sup>+</sup> dendritic cells expressing the costimulatory molecule CD86 were strongly reduced (Fig 7E and F). Furthermore, a markedly lower percentage of CD4<sup>+</sup> T cells and a lower production of IFN $\gamma$  were obtained with the injection of Epi cells + PeSCs compared with the injection of Epi cells alone (Fig 7G). The CD8<sup>+</sup> T cell compartment was also affected but

to a lesser extent (nonsignificant reduction in the percentage of CD8<sup>+</sup> T cells), and a significant reduction in the percentage of IFN $\gamma$  among CD8<sup>+</sup> T cells was detected (Fig 7H). This effect was partially due to the local accumulation of the CCL5 chemokine because the depletion of this chemokine *in vivo* diminishes PD-L1 expression in F4/80 cells and decreases CD8<sup>+</sup> T cells without affecting the Ly6G<sup>+</sup>CD11b<sup>+</sup> compartment (Fig EV5C–L). Altogether, these results suggest that the presence of PeSCs in the tumor microenvironment reprogram CD11b<sup>+</sup> monocyte differentiation to result in diminished T cell priming and activation.

**PeSCs drive resistance to PD-1 treatment in pancreatic cancer**

Extensive immunosuppressive myeloid cell infiltration in PDAC (Bayne *et al*, 2012; Pylayeva-Gupta *et al*, 2012; Stromnes *et al*, 2014) tissues has been shown to be associated with resistance to immunotherapy (Blair *et al*, 2019). Strategies that target monocyte or granulocyte trafficking or macrophage survival (Zhu *et al*, 2014) in combination with checkpoint immunotherapies have shown promise in preclinical studies, and these studies have transitioned into ongoing clinical trials for the treatment of pancreatic and other cancer types. Because the presence of PeSCs in the tumor microenvironment suppressed the T cell response, the next step was to determine whether PeSCs influence the response to immune therapy, that is, anti-PD-1 Ab treatment.

To test this hypothesis, we injected s.c. Epi cells alone or in the presence of PeSCs at a ratio of 1:1 into the same C57BL/6 recipient mice. Ten days later, we injected anti-PD1 or ctrl isotype Ab twice a week for 2 weeks and sacrificed the mice 14 days later (Fig 7I).

We found that mice injected with Epi cells alone responded to anti-PD-1 therapy because they displayed a diminished tumor weight compared to isotype ctrl-treated animals in contrast to the coinjection of Epi + PeSC with led to equivalent tumor weight (Fig 7J). The analysis of the immune compartment in each condition showed that CD8<sup>+</sup> T cells displayed an exhausted phenotype characterized by concomitant expression of CD44, PD-1, and Tim-3 (Fig 7K). Furthermore, CD8<sup>+</sup> T cells have an increased ability to produce CD107a upon anti-PD1 treatment solely in Epi conditions but not in combo conditions (Fig 7L). With respect to the macrophage response, we observed increased percentages of F4/80 expressing CD163 as well as both CD163 and Tim4 in anti-PD-1 treated combo condition (Fig 7M and N). These macrophages were expressing less CD107a (Fig 7O). Altogether these data suggest that PeSC drives PD-1 resistance by affecting the monocyte differentiation *in situ*.

## Discussion

The role of the stromal compartment in regulating antitumoral immune responses and tumoral growth is indisputable (Hanahan & Weinberg, 2011), but this “ménage-à-trois” tumor–stromal–immune cell interaction is a difficult process to fine-tune with the aim of achieving a positive therapeutic outcome. Here, we describe the existence of a cell population that emerges very early during the process of transformation, shares features of pericyte, stromal, and stem cells and is able to modulate and pervert the interaction between tumor cells and the innate immune system from the beginning of neoplasia. This population is defined by the expression of CD106, CD29, CD24, and CD44 and the exclusion of CD45 and EPCAM. This population, which harbors neoplastic lesions in mice and humans, has the capacity to instruct recruited monocytes to become granulocytic MDSCs “*in situ*” and skew the outcome of the antitumoral T cell response by reducing their inflammatory cytokine production and therefore sustaining exhaustion and ultimately driving resistance to conventional anti-PD-1 therapy.

Pericytes of perivascular cells are important cells that have been previously described to regulate the T cell response in different locations (in the brain and lung; Balabanov *et al*, 1996) and pathophysiological contexts (acute respiratory distress syndrome). However, their role in the tumoral progression is not well understood. In the context of glioblastoma, pericytes are able to support tumor growth through immune suppression (Valdor *et al*, 2017; Guerra *et al*, 2018; Sena *et al*, 2018). Recent studies revealed that the cancer burden is controlled by mural cells expressing integrin  $\beta 3$  in the context of an implanted B16 melanoma model (Wong *et al*, 2020). The researchers showed that CCL2 secretion is important for MEK1 and ROCK2 activity in tumor cells. In our context, even though both CCL2 and CCL5 were secreted by PeSCs in the proximity of tumor cells, CCL5 appears to play a more important local effect because the neutralization of CCL5 led to decreased CD103 and PD-L1 expression on F4/80 macrophages. CCL20, CXCL1, CXCL5, and CXCL10 were also found increased suggesting a complex orchestration of chemokines that needs further investigation. Our data showed that PeSCs were able to structure the vessels *in vitro* similarly to the pericyte functions in tissue repair related to pancreatic injury in our model. These CD106<sup>+</sup> cells likely play an important role in the context of neoplastic transformation because we detected them in a human pancreas TMA and in the GEMM mice in the PanIN areas. One limitation of the study comes from the fact that we coinject Epi cells with PeSC at a ratio of 1:1 which does not reflect the biological cellular relationships within the tissue. Nevertheless, the percentage of PeSC in the grafts represented about 1% of the Epi cells amount at day 10 when the mice are sacrificed. This level is similar to the *in vivo* PeSC observation in the KC pancreas. Because tumors evolve as heterogeneous *in vivo*, our preliminary IHC staining on human samples verified that the majority of CD106<sup>+</sup> cells are indeed distributed in the tumor adjacent regions, indicating their contribution greatly correlated to tumor initiation from the early stage.

One important feature of the identified PeSC population is their “stem” cell property, which allows these cells to adapt to the local signals in the tumor microenvironment. We demonstrated that these cells were able to directly increase the proliferation of tumor cells,

whereas the tumor cells did not have feedback on their proliferation status, at least *in vitro*. Furthermore, the cells were able to differentiate into chondrocytes and osteoblasts, and the choice of the cell was highly related to their location in the pancreas (Van Noorden *et al*, 1995; Pilarsky *et al*, 2008).

Because these cells are present at the beginning of the transformation in the pancreas, the next question was related to the crosstalk of PeSCs with the early actors of the immune response, that is, the innate immune response. The early bone marrow recruitment of monocyte precursors in the context of neoplasia is a well-documented process (Movahedi *et al*, 2010; Franklin *et al*, 2014). The plasticity of PeSCs cells in the tumor microenvironment represents a double-edged sword mechanism. Recent data demonstrate that the reprogramming of the innate immune compartment by CD11b agonism can render tumors more sensitive to checkpoint blockade (Panni *et al*, 2019), which indicates the importance of early events in the kinetics of the immune response. CD11b<sup>+</sup>Ly6G<sup>+</sup> MDSCs are associated with immune suppression in several cancer types, and the GM-CSF cytokine plays an important role as a driver mechanism (Pylayeva-Gupta *et al*, 2012; Stromnes *et al*, 2014). IL6 production also plays an important role in the observed effect (Weber *et al*, 2020). Our data revealed no differences in the production of those cytokines from PeSCs in the TME. The suppressive function of MDSCs has previously been linked to their immature state (Gabrilovich *et al*, 2012). In our model, we found that a vast majority of the Ly6G<sup>+</sup> cells are Nanog<sup>+</sup>, which sustains their immature phenotype (Fig 6F). The depletion of the Ly6G<sup>+</sup> population through an Ab approach led to increased antitumoral cytokine production and a decrease in tumor weight. Furthermore, this depletion was accompanied by restoration of the F4/80<sup>+</sup> and CD11c<sup>+</sup> percentages in the TME, which suggests that the CD11b<sup>+</sup> precursors of these three populations play a key role in mediating the effect of PeSCs on the modulation of the tumor microenvironment.

Last but not least, we discovered that this initial interaction between PeSCs and innate CD11b<sup>+</sup> precursors has an impact on the adaptive immune response by impacting the quantity and quality of the T cell immune response. We found a drastic reduction in the percentage of CD4<sup>+</sup> T cells and the production of IFN $\gamma$  by CD8<sup>+</sup> T cells in the presence of PeSCs in the tumor microenvironment. This reduction was associated with an increase in the Ly6G<sup>+</sup>CD11b<sup>+</sup> population in the tumor microenvironment and led to anti-PD1 resistance. One important finding is that Epi tumor cells respond to anti-PD1 treatment, which suggests that PD-1 resistance in pancreatic cancer is not driven by the paucity of tumor antigen presentation but rather local immune suppressive signals, which include MDSCs (Stromnes *et al*, 2014) and stromal exclusion (Jiang *et al*, 2016, 2020).

Our study provides the first demonstration that CD106<sup>+</sup> PeSCs are able to target the innate CD11b compartment to drive the differentiation of Ly6G<sup>+</sup> MDSCs and inhibit the antitumoral differentiation of F4/80 macrophages and CD11c<sup>+</sup> dendritic cells, which ultimately leads to PD-1 immunotherapy resistance (Appendix Fig S7). Further studies should identify strategies for targeting this population in the tumor microenvironment to unleash the potential of existing immunotherapy for pancreatic cancer.

## Materials and Methods

### Reagents and Tools table

Reagent/Resource	Reference or Source	Identifier or Catalog Number
<b>Experimental Models</b>		
Pericyte stem cells	This paper	N/A
Tumoral epithelial cells (Epi)	Goehrig <i>et al</i> (2019)	Goehrig <i>et al</i> (2019)
Lung metastatic cells (Meta)	This paper	N/A
C57BL/6 mouse primary pancreatic microvascular endothelial cells	Cell Biologics	Cat#C57-6206
C57BL/6 mice (wild type)	Envigo	C57bL/6J OlaHsd
Rag2 <sup>KO</sup> mice	Charles Rivers	
P48 <sup>+Cre</sup> ;Kras <sup>G12D</sup> (KC) mice	Hingorani <i>et al</i> (2003)	See reference
pdx1 <sup>+Cre</sup> ;Kras <sup>G12D</sup> ;p53 <sup>R172H</sup> (KPC) mice	Hingorani <i>et al</i> (2005)	See reference
pdx1 <sup>+Cre</sup> ;Kras <sup>G12D</sup> ;lnk4a/Arf <sup>fl/fl</sup> (KIC) mice	Aguirre <i>et al</i> (2003)	See reference
<b>Recombinant DNA</b>		
H2B-GFP	Addgene	Cat#25999, RRID:Addgene_25999
H2B-mCherry	Addgene	Cat#20972, RRID:Addgene_20972
<b>Antibodies</b>		
Mouse monoclonal anti-CD24 antibody (clone SN3b)	Invitrogen/Thermo Fisher Scientific	Cat# MA5-11833, RRID:AB_10985938
Rabbit polyclonal anti-CD44 antibody	Abcam	Cat# ab157107, RRID:AB_2847859
Rabbit monoclonal recombinant anti-VCAM1 (CD106) antibody (clone EPR5047)	Abcam	Cat# ab134047, RRID:AB_2721053
Goat polyclonal anti-alpha smooth muscle actin antibody, N-term	GeneTex	Cat# GTX89701, RRID:AB_10721877
Rat monoclonal anti-mouse cytokeratin 19 antibody, unconjugated	DSHB	Cat# TROMA-III, RRID:AB_2133570
Rabbit monoclonal recombinant anti-ZO1 tight junction protein antibody (clone EPR19945-296)	Abcam	Cat# ab221547, RRID:AB_2892660
Rat monoclonal anti-E-cadherin antibody (clone ECCD-2)	Invitrogen/Thermo Fisher Scientific	Cat# 13-1900, RRID:AB_2533005
Rabbit polyclonal anti-mCherry antibody	Abcam	Cat# ab167453, RRID:AB_2571870
Goat polyclonal anti-GFP antibody	Abcam	Cat# ab6673, RRID:AB_305643
Rat monoclonal purified anti-mouse Ly-6G antibody (clone 1A8)	BioLegend	Cat# 127602, RRID:AB_1089180
Rabbit polyclonal StemAb™ anti-mouse Nanog antibody	ReproCell Incorporated	Cat# RCAB002P-F
Horse anti-goat IgG antibody (H+L), biotinylated	Vector Laboratories/Eurobio Scientific	Cat# BA-9500, RRID:AB_2336123
Goat anti-mouse IgG antibody (H+L), biotinylated	Vector Laboratories/Eurobio Scientific	Cat# BA-9200, RRID:AB_2336171
Horse anti-rabbit IgG antibody (H+L), biotinylated	Vector Laboratories/Eurobio Scientific	Cat# BA-1100, RRID:AB_2336201
Goat anti-rat IgG antibody, mouse adsorbed (H+L), biotinylated	Vector Laboratories/Eurobio Scientific	Cat# BA-9401, RRID:AB_2336208
Chicken polyclonal anti-Rat IgG (H+L) Cross-Adsorbed Secondary Antibody, Alexa Fluor 647	Invitrogen/Thermo Fisher Scientific	Cat# A-21472, RRID:AB_2535875
Donkey polyclonal anti-Rat IgG (H+L) Highly Cross-Adsorbed Secondary Antibody, Alexa Fluor 488	Invitrogen/Thermo Fisher Scientific	Cat# A-21208, RRID:AB_2535794
Donkey polyclonal anti-Rabbit IgG (H+L) Highly Cross-Adsorbed Secondary Antibody, Alexa Fluor 555	Invitrogen/Thermo Fisher Scientific	Cat# A-31572, RRID:AB_162543
Donkey polyclonal anti-Rabbit IgG (H+L) Highly Cross-Adsorbed Secondary Antibody, Alexa Fluor 488	Invitrogen/Thermo Fisher Scientific	Cat# A-21206, RRID:AB_2535792
Donkey polyclonal anti-Goat IgG (H+L) Cross-Adsorbed Secondary Antibody, Alexa Fluor 488	Invitrogen/Thermo Fisher Scientific	Cat# A-11055, RRID:AB_2534102

Reagents and Tools table (continued)

Reagent/Resource	Reference or Source	Identifier or Catalog Number
Donkey polyclonal anti-Mouse IgG (H+L) Highly Cross-Adsorbed Secondary Antibody, Alexa Fluor 555	Invitrogen/Thermo Fisher Scientific	Cat# A-31570, RRID:AB_2536180
Rat monoclonal anti-mouse CD45 (clone 30-F11), APC/Cyanine7 conjugated	BioLegend	Cat# 103116, RRID:AB_312981
Rat monoclonal anti-mouse CD45 (clone 30-F11), APC conjugated, eBioscience	Invitrogen/Thermo Fisher Scientific	Cat# 17-0451-82, RRID: AB_469392
Rat monoclonal anti-mouse CD31 (clone 390), Brilliant Violet 421 conjugated	BioLegend	Cat# 102423, RRID:AB_2562186
Rat monoclonal anti-mouse/rat CD29 (clone HM $\beta$ 1-1), PerCP/Cyanine5.5 conjugated	BioLegend	Cat# 102228, RRID:AB_2572079
Rat monoclonal anti-mouse CD106 (clone 429 [MVCAM.A]), Alexa Fluor 647 conjugated	BioLegend	Cat# 105712, RRID:AB_493429
Rat monoclonal anti-mouse CD24 (clone M1/69), PE/Cyanine7 conjugated	BioLegend	Cat# 101822, RRID:AB_756048
Rat monoclonal anti-mouse/human CD44 (clone IM7), Alexa Fluor 700 conjugated	BioLegend	Cat# 103026, RRID:AB_493713
Rat monoclonal anti-mouse PDGFR $\alpha$ (clone AP45), Super Bright 600 conjugated, eBioscience	Invitrogen/Thermo Fisher Scientific	Cat# 63-1401-82, RRID: AB_2734880
Rat monoclonal anti-mouse CD326 (Ep-CAM) (clone G8.8), Brilliant Violet 510 conjugated	BioLegend	Cat# 118231, RRID:AB_2632774
Rat monoclonal anti-mouse PDGFR $\beta$ (clone APB5), Super Bright 780 conjugated	Invitrogen/Thermo Fisher Scientific	Cat# 78-1402-80, RRID: AB_2784899
Armenian hamster monoclonal anti-mouse CD34 (clone HM34), PE conjugated	BioLegend	Cat# 128610, RRID:AB_2074601
Rat monoclonal anti-mouse CD90.2 (clone 30-H12), Brilliant Violet 570 conjugated	BioLegend	Cat# 105329, RRID:AB_10917055
Rat monoclonal anti-mouse CD105 (clone MJ7/18), Pacific Blue conjugated	BioLegend	Cat# 120412, RRID:AB_2098890
Rat monoclonal anti-mouse CD146 (clone ME-9F1), PerCP/Cyanine5.5 conjugated	BioLegend	Cat# 134710, RRID: AB_11203708
Mouse monoclonal anti-mouse/human/rat $\alpha$ SMA (clone 1A4), eFluor 570 conjugated, eBioscience	Invitrogen/Thermo Fisher Scientific	Cat# 41-9760-82, RRID: AB_2573631
Armenian hamster monoclonal anti-mouse/rat CD61 (clone 2C9.G2 [HM $\beta$ 3-1]), PE/Cyanine7 conjugated	BioLegend	Cat# 104318, RRID:AB_2687361
Rat monoclonal anti-mouse Ly-6G (clone 1A8), Brilliant Violet 785 conjugated	BioLegend	Cat# 127645, RRID:AB_2566317
Rat monoclonal anti-mouse Ly-6C (clone HK1.4), PE conjugated	BioLegend	Cat# 128008, RRID:AB_1186132
Rat monoclonal anti-mouse F4/80 (clone BM8), PE/Cyanine7 conjugated	BioLegend	Cat# 123114, RRID:AB_893478
Rat monoclonal anti-mouse F4/80 (clone BM8), PerCP/Cyanine5.5 conjugated	BioLegend	Cat# 123128, RRID:AB_893484
Armenian hamster monoclonal anti-mouse CD11c (clone N418), Alexa Fluor 700 conjugated, eBioscience	Invitrogen/Thermo Fisher Scientific	Cat# 56-0114-82, RRID: AB_493992
Armenian hamster monoclonal anti-mouse CD80 (clone 16-10A1), Brilliant Violet 605 conjugated	BioLegend	Cat# 104729, RRID: AB_11126141
Rat monoclonal anti-mouse CD86 (clone GL-1), APC/Cyanine7 conjugated	BioLegend	Cat# 105030, RRID:AB_2244452
Rat monoclonal anti-mouse/human CD11b (clone M1/70), Brilliant Violet 421 conjugated	BioLegend	Cat# 101251, RRID: AB_2562904
Human/mouse monoclonal anti-human/mouse Granzyme B (clone GB11), Alexa Fluor 647 conjugated	BioLegend	Cat#515406, RRID:AB_2566333
Rat monoclonal anti-mouse Granzyme B (clone 16G6), Biotin, eBioscience	Invitrogen/Thermo Fisher Scientific	Cat# 13-8822-80, RRID: AB_466954
Rat monoclonal anti-mouse TNF- $\alpha$ (clone MP6-XT22), Brilliant Violet 605 conjugated	BioLegend	Cat# 506329, RRID:AB_11123912
Rat monoclonal anti-mouse IFN- $\gamma$ (clone XMG1.2), Brilliant Violet 650 conjugated	BioLegend	Cat#505831, RRID:AB_11142685

**Reagents and Tools table** (continued)

Reagent/Resource	Reference or Source	Identifier or Catalog Number
Rat monoclonal anti-mouse CD4 (clone RM4-5), Brilliant Violet 510 conjugated	BioLegend	Cat# 100553, RRID:AB_2561388
Rat monoclonal anti-mouse CD8a (clone 53-6.7), Brilliant Violet 421 conjugated	BioLegend	Cat# 100738, RRID: AB_11204079
Rat monoclonal anti-mouse CD279 (PD-1) (clone 29F.1A12), PE conjugated	BioLegend	Cat# 135206, RRID:AB_1877231
Rat monoclonal anti-mouse CD366 (Tim-3) (clone B8.2C12), APC conjugated	BioLegend	Cat# 134008, RRID:AB_2562998
Rat monoclonal anti-mouse CD3 (clone 17A2), Brilliant Violet 711 conjugated	BioLegend	Cat# 100241, RRID:AB_2563945
Rat monoclonal anti-mouse CD107a (LAMP-1) (clone 1D4B), PE/Cyanine7 conjugated	BioLegend	Cat# 121619, RRID:AB_2562146
Rat monoclonal anti-mouse CD163 (clone TNKUPJ), PE conjugated, eBioscience	Invitrogen/Thermo Fisher Scientific	Cat# 12-1631-82, RRID: AB_2716924
Rat monoclonal anti-mouse Tim-4 (clone RMT4-54), Alexa Fluor 647 conjugated	BioLegend	Cat# 130008, RRID:AB_2271648
Armenian Hamster monoclonal anti-mouse CD103 (clone 2E7), Brilliant Violet 510 conjugated	BioLegend	Cat# 121423, RRID:AB_2562713
Rat monoclonal anti-mouse CD335 (Nkp46) (clone 29A1.4), Brilliant Violet 421 conjugated	BioLegend	Cat# 137611, RRID:AB_10915472
Rat monoclonal anti-mouse CD206 (MMR) (clone C068C2), Brilliant Violet 650 conjugated	BioLegend	Cat# 141723, RRID:AB_2562445
Rat monoclonal anti-mouse CD115 (CSF-1R) (clone AFS98), PerCP/Cyanine5.5 conjugated	BioLegend	Cat# 135526, RRID:AB_2566462
Rat monoclonal anti-mouse CD274 (B7-H1, PD-L1) (clone 10F.9G2), PerCP/Cyanine5.5 conjugated	BioLegend	Cat# 124334, RRID:AB_2629832
Lectin PNA from arachis hypogaea (peanut), Alexa Fluor 647 conjugate	Invitrogen/Thermo Fisher Scientific	Cat# L32460
<i>InVivo</i> Mab mouse IgG1 isotype control (clone MOPC-21)	Bio X cell	Cat# BE0083, RRID:AB_1107784
<i>InVivo</i> Mab anti-mouse CD106 (VCAM-1)	Bio X Cell	Cat# BE0027, RRID:AB_1107572
<i>InVivo</i> Plus anti-mouse PD-1 (CD279)	Bio X Cell	Cat# BE0146, RRID: AB_10949053
<i>InVivo</i> Plus anti-mouse Ly6G antibody	Bio X Cell	Cat# BE0075-1, RRID: AB_1107721
Mouse IgG2A isotype control (clone 20102)	R&D systems	Cat# MAB003, RRID:AB_357345
Mouse CCL5/RANTES Antibody	R&D Systems	Cat# MAB478, RRID:AB_2290968
Ras (G12D Mutant Specific) (D8H7) Rabbit mAb	Cell Signaling	Cat# 14429S, RRID:AB_2728748
Peroxidase-AffiniPure donkey anti-rabbit IgG (H+L) antibody	Jackson ImmunoResearch	Cat# 711-035-152, RRID: AB_10015282
<b>Oligonucleotides and other sequence-based reagents</b>		
Primers for Nanog: Forward: 5'-TCTCTCAGCCAGCTGTGT-3' and Reverse: 5'-GCTTGCACTTCATCCTTTG-3'	Intergrated DNA Technologies	N/A
Primers for Oct3/4: Forward: 5'-GCCCTGCAGAAGGAGCTAGAAC-3' and Reverse: 5'-GGAATACTCAATACTTGATCT-3'	Intergrated DNA Technologies	N/A
Primers for Nkx3.2: Forward: 5'-AGATGTCAGCCAGCGTTTC-3' and Reverse: 5'-AGGGCTAACGCTGTCATCCT-3'	Intergrated DNA Technologies	N/A
Primers for RGS: Forward: 5'-GCTTTGACTTGCCAGAAA-3' and Reverse: 5'-CCTGACCAGATGACTACTTGATTAGCT-3'	Intergrated DNA Technologies	N/A
Primers for PDGFR $\alpha$ : Forward: 5'-TCTGTGACTTTAAGGATGCTTCA-3' and Reverse: 5'-GATGCCCACATAGCCTTCATTC-3'	Intergrated DNA Technologies	N/A
Primers for PDGFR $\beta$ : Forward: 5'-TCATGAAGCCAGCAAGAGTG-3' and Reverse: 5'-GTGGTAATCCCGTCAGCATC-3'	Intergrated DNA Technologies	N/A
Primers for ACTA2: Forward: 5'-GCCAGTCGCTGTCAGGAACCC-3' and Reverse: 5'-AGCCGGCCTTACAGAGCCCA-3'	Intergrated DNA Technologies	N/A

Reagents and Tools table (continued)

Reagent/Resource	Reference or Source	Identifier or Catalog Number
Primers for Prominin1: Forward: 5'-GCCCAAGCTGGAAGAAATATG-3' and Reverse: 5'-CAGCAGAAAGCAGACAATCAA-3'	Intergrated DNA Technologies	N/A
Primers for Snail1: Forward: 5'-CTTGTGTCTGCACGACCTGT-3' and Reverse: 5'-CAGGAGAATGGCTTCTCACC-3'	Intergrated DNA Technologies	N/A
Primers for Snail2: Forward: 5'-CATTGCCTTGTGTCTGCAAG-3' and Reverse: 5'-AGAAAGGCTTTTCCCCAGTG-3'	Intergrated DNA Technologies	N/A
Primers for Sparc: Forward: 5'-AGAGGAAACGGTCGAGGAG-3' and Reverse: 5'-CTCACACACCTTGCCATGTT-3'	Intergrated DNA Technologies	N/A
Primers for Twist: Forward: 5'-AGCTACGCCTTCTCCGTCT-3' and Reverse: 5'-TCCTTCTCTGAAACAATGACA-3'	Intergrated DNA Technologies	N/A
Primers for Zeb2: Forward: 5'-CCAGAGGAAACAAGGATTTTTCAG-3' and Reverse: 5'-AGGCCTGACATGTAGTCTTGTG-3'	Intergrated DNA Technologies	N/A
Primers for Zeb1: Forward: 5'-TGAGCACACAGGTAAGAGGCC-3' and Reverse: 5'-GGCTTTTCCCCAGAGTGCA-3'	Intergrated DNA Technologies	N/A
Primers for Col6a: Forward: 5'-GCAAGGATGAGCTGGTCAA-3' and Reverse: 5'-GTCCACGTCTCTTGCATC-3'	Intergrated DNA Technologies	N/A
Primers for Epcam: Forward: 5'-GATTCTGCAGCTGAGACCTG-3' and Reverse: 5'-GATACCAAGTCAAACCGAGAATT-3'	Intergrated DNA Technologies	N/A
Primers for Fn1: Forward: 5'-CGGAGAGAGTGCCTACTA-3' and Reverse: 5'-CGATATTGGTGAATCGCAGA-3'	Intergrated DNA Technologies	N/A
Primers for Krt19: Forward: 5'-TCCCAGCTCAGCATGAAAGCT-3' and Reverse: 5'-AAAACCGCTGATCACGCTCTG-3'	Intergrated DNA Technologies	N/A
Primers for Krt7: Forward: 5'-CACGAACAAGGTGGAGTTGGA-3' and Reverse: 5'-TGTCTGAGATCTGCGACTGCA-3'	Intergrated DNA Technologies	N/A
Primers for Sox9: Forward: 5'-CAAGACTCTGGCAAGCTCTG-3' and Reverse: 5'-TCCGCTTGCCGTTCTTAC-3'	Intergrated DNA Technologies	N/A
Primers for GAPDH: Forward: 5'-CAACGACCCCTTCATTGACC-3' and Reverse: 5'-GGTCTCGCTCCTGGAAGATG-3'	Intergrated DNA Technologies	N/A
PrimePCR™ SYBR® Green Assay CD248 for Mouse	Bio-Rad	Cat#10025636
Kras <sup>G12D</sup> conditional primers for PCR: con1: 5'-GTC TTTCCCCAGCACAGTGC-3'; con2: 5'-CTCTTGCTACGCCACCAGCT C-3'; con3: 5'-AGCTAGCCACCATGGCTTGTAGTAAGTCTGCA-3'	Intergrated DNA Technologies	<a href="https://jacks-lab.mit.edu/protocols/genotyping/kras_cond">https://jacks-lab.mit.edu/protocols/genotyping/kras_cond</a>
<b>Chemicals, Enzymes and other reagents</b>		
Complete mouse endothelial cell medium	Cell Biologics	Cat# M1168
Phosphate-buffered saline (PBS) 10×	Gibco/Thermo Fisher Scientific	Cat# 14190-144
Dulbecco's Modified Eagle Medium (DMEM)	Gibco/Thermo Fisher Scientific	Cat# 61965059
Fetal calf serum (FCS)	Eurobio Scientific	Cat# CVFSVF00-01
Penicillin-Streptomycin (P/S)	Gibco/Thermo Fisher Scientific	Cat# 15140-122
Collagenase P	Roche/Sigma-Aldrich	Cat# 11213865001
16% Formaldehyde solution (PFA)	Termo Fisher	Cat# 28908
10% Neutral buffered formalin	Diapath S.p.A.	REF: F0043
Triton X-100	Sigma-Aldrich	Cat# T8787
Antigen Unmasking Solution, Citrate-Based	Vector Laboratories/Eurobio Scientific	Cat# H-3300
DAB Substrate Kit, Peroxidase (HRP), with Nickel, (3,3'-diaminobenzidine)	Vector Laboratories/Eurobio Scientific	Cat# SK-4100
Mayer Hematoxylin	Diapath S.p.A.	REF: C0303
Antibody diluent Reagent	Life Techno/Thermo Fisher	Cat# 003218
Vectashield mounting medium with DAPI	Vector Laboratories/Eurobio Scientific	Cat# H-1200
NuPAGE 4-12% Bis-Tris polyacrylamide gel	Invitrogen/Thermo fischer	Cat# NP0335BOX
Immune-Blot PVDF membrane	BIO-RAD	Cat# 1620177
Tris buffered saline (TBS)	Euromedex	Cat# ET220

Reagents and Tools table (continued)

Reagent/Resource	Reference or Source	Identifier or Catalog Number
Tween 20	VWR	Cat# 28829.296
Bovine serum albumin (BSA)	Sigma	Cat# A2153-100G
RIPA buffer	Pierce/Thermo Fisher	Cat# 89900
Protease complete EDTA-free	Roche/Sigma-Aldrich	Cat# 04 693 159 001
Phosphatase phoSTOP	Roche/Sigma-Aldrich	Cat# 04 906 837 001
Cell Activation Cocktail (w/o Brefeldin A)	BioLegend	Cat# 423301
Brefeldin A solution	BioLegend	Cat# 420601
Corning® Matrigel® Basement Membrane Matrix High Concentration	Corning	Cat# 354248
Corning® Matrigel® Growth Factor Reduced (GFR) Basement Membrane Matrix, Phenol Red-free, LDEV-free	Corning	Cat# 356231
Recombinant Murine PDGF-BB	PeproTech/Thermo Fisher Scientific	Cat# 315-18
TGF-β1	Biotechne	Cat#7666-MB
IncuCyte® Zoom live-cell analysis system	Essen Bioscience	
<b>Other</b>		
PA485: Pancreatitis and matched pancreatic cancer tissue array	US Biomax, Inc.	<a href="https://www.biomax.us/tissue-arrays/pancreas/PA485">https://www.biomax.us/tissue-arrays/pancreas/PA485</a>
BIC14011a: Pancreas intraepithelial neoplasia, pancreatitis and cancer tissue array	US Biomax, Inc.	<a href="https://www.biomax.us/tissue-arrays/pancreas/BIC14011a">https://www.biomax.us/tissue-arrays/pancreas/BIC14011a</a>
StemPro® Osteogenesis Differentiation Kit	Gibco/Thermo Fisher Scientific	Cat#10072-01
StemPro® Chondrogenesis Differentiation Kit	Gibco/Thermo Fisher Scientific	Cat#10071-01
Alizarin Red S Staining Kit	ScienCell Research Laboratories	Cat#0223
Alcian Blue 8GX	Sigma-Aldrich	Cat#A3157-10G
True-Nuclear™ Transcription Factor Buffer Set	BioLegend	Cat#424401
NucleoSpin® RNA Plus kit	MACHEREY-NAGEL	REF 740984
CellTrace™ CFSE Cell Proliferation Kit	Invitrogen/Thermo Fisher Scientific	Cat#C34554
LEGENDplex™ Custom Mouse 5-plex Panel	BioLegend	Cat# B285861
ECL Western Blotting Substrate	Pierce/Thermo Fisher Scientific	Cat# 32106

## Methods and Protocols

### Mice

The *Ptf1a/p48-Cre;Kras<sup>G12D</sup>* (KC), *Pdx1-Cre;Kras<sup>G12D</sup>;Ink4a/Arf<sup>fl/fl</sup>* (KIC), and *Pdx1-Cre;Kras<sup>G12D</sup>;Tp53<sup>R172H</sup>* (KPC) mice have been previously described (Aguirre *et al*, 2003; Ascher *et al*, 2003; Hingorani *et al*, 2005). *Rag2<sup>KO</sup>* and C57BL/6 mice were obtained from The Charles River Laboratories and Envigo (France) and used as hosts in the s.c. tumor implantation experiments. All mice were kept under specific pathogen-free conditions at the Animale en Cancérologie (AniCan) platform at the Cancer Research Center of Lyon (CRCL). All animal procedures and experiments were performed in compliance with the ethical guidelines of the CRCL Animal Care and Use Committee, with approval of the Experimental Animal Ethics Committee of the Rhône-Alpes region (CECCAPP; CECCAPP\_CLB\_2019\_002).

### Mouse primary cell lines

The isolation and culture of cells were performed using a protocol adapted from a previously published protocol (Bayne *et al*, 2012; Goehrig *et al*, 2019). PeSCs were obtained from the pancreas of 2.5-month-old neoplastic KC mice and dissociated. Tumor primary

cell lines (Epi) and metastatic lung cell lines (Meta) were obtained from the pancreas of 2-month-old KIC mice respectively, using the same protocol. The cells were then plated in six-well plates with serum-free DMEN (Gibco), and after 2 weeks, the media was changed to DMEN-complete. The *Kras<sup>G12D</sup>* mutation was detected by PCR and WB. After several passages as indicated in Fig 3A and Appendix Fig S3D, the cells were infected with a lentivector expressing H2B-mCherry (PeSC) or H2B GFP (Epi or Meta cells) as previously described (Deygas *et al*, 2018). C57BL/6 mouse primary pancreatic microvascular endothelial cells were purchased from Cell Biologics.

### Matrigel tube formation assay

The assay of tube formation performed with endothelial cells based on Matrigel embodiment has been previously described (Sorrell *et al*, 2009; Zhang *et al*, 2015; Kutikhin *et al*, 2020). Briefly, Matrigel (Growth Factor-Reduced Basement Membrane Matrix, Phenol Red-Free, LDEV-free) was melted on ice and then paved onto a 96-well plate. Subsequently, 20 ml of Matrigel was distributed into each well, and the plate was then centrifuged at 500 g for 1 min to ensure uniform coverage. Afterward, the plate was immediately placed in an incubator for 30 min for gel formation. C57BL/6 mouse primary

pancreatic microvascular endothelial cells (Endo) were trypsinized and then seeded on the polymerized gel in a complete endothelial culture medium (Cell Biologicals) at a density of 10,000 cells/cm<sup>2</sup>. For the coculture with the Endo cells, Epi cells and PeSCs were seeded at the same condition and above-mentioned density. A monolayer culture with no Matrigel polymer was used as a control. Each condition was performed in triplicate. The cultures were monitored using IncuCyte Zoom<sup>®</sup>, and photographs were captured every 2 h after initiation of the assay. Endothelial cells were observed under phase contrast, whereas combined phase contrast with green and red fluorescence optics was used for the analysis of the Epi cells and/or PeSCs in coculture conditions.

### Cell culture, proliferation and differentiation

Cells were cultured in DMEM supplemented with 10% FCS and 1% penicillin/streptomycin for proliferation. PeSCs were cocultured with Epi cells at the indicated ratios, and these cell lines were then observed through the red and green channels, respectively, using IncuCyte Zoom<sup>®</sup>. The proliferation curves of the Epi cells were depicted based on the total green object area count (μm<sup>2</sup>/well) analyzed and exported from the IncuCyte<sup>®</sup> system. For the PeSC differentiation experiments, the cells were plated using StemPro<sup>®</sup> differentiation kits (Gibco) for osteogenesis and chondrogenesis in accordance with the provided instructions. Alizarin Red S staining for osteogenic lineages and Alcian Blue staining for chondrogenic lineages were also performed according to the protocols recommended by the above-mentioned commercial kits. For the PDGF-BB treatment assay, PeSCs were stimulated by PDGF-BB (10 ng/ml) and TGF-β1 (2 ng/ml). PDGF-BB and TGF-β1 were replenished every 2 days for 7 days. After 7 days, the cells were recovered for FACS analysis and mRNA is subject to RT-qPCR for stemness, epithelial, fibroblast, and mesenchymal-related genes.

### Short-term PeSC and tumor cell implantation studies

PeSC or Epi cells (1 × 10<sup>5</sup>) were embedded as plugs in a 1:1 Matrigel-PBS mix (Matrigel<sup>®</sup> Basement Membrane Matrix High Concentration, HC) into the flanks of C57BL/6 or Rag2<sup>KO</sup> mice. The mice were then monitored and sacrificed at the indicated time points. The tumor grafts were weighed, measured, and processed for staining prior to flow cytometry analysis. Ly6G<sup>+</sup> cells were depleted *in vivo* by administering two consecutive i.p. injections of anti-Ly6G mAbs to the mice (8.5 mg/kg) at the indicated time points. The anti-PD-1 strategy involved the i.p. injection of anti-PD-1 into the mice (5 mg/kg) twice a week at the indicated time points for 2 weeks. CCL5 depletion was administrated by pre-mixing anti-CCL5 mAbs (5 μg/kg or 0.5 μg/ml) in the Matrigel<sup>®</sup> (HC) plugs before implanting. Control mice were treated with anti-IgG2A (5 μg/kg or 0.5 μg/ml).

### Reverse transcription and qPCR

RNA from pelleted islets was extracted using a NucleoSpin<sup>®</sup> RNA Plus kit according to the manufacturer's instructions. The RNA concentrations were measured using a Nanodrop spectrophotometer. Reverse transcription (RT) was performed using equivalent quantities of extracted RNAs (greater than 300 ng), and cDNA was used for quantitative polymerase chain reaction (qPCR) analyses with SsoAdvanced Universal SYBR<sup>®</sup> Green Supermix (Bio-Rad). The following primers were used: Nanog, Oct3/4, Nkx3.2, RGS, PDGFRα,

PDGFRβ, Acta2, Desmin, Prominin, Snail1, Snail2, Sparc, Twist, Zeb1, Zeb2, Col6a, EpCAM, Fn-1, Krt19, Krt, Sox9, and PrimePCR<sup>™</sup> SYBR<sup>®</sup> Green Assay CD248 for Mouse (Bio-Rad).

### RNAseq analysis

Raw sequencing data quality controls were performed with FastQC (v 0.11.5). Salmon (0.10.0) was used for the quantification of gene expression from the raw sequencing reads, and the reference mouse genome GRCm38 and the annotations of protein-coding genes from gencode vM20 were utilized as an index. Unless otherwise specified, the analyses were performed using R (v3.5.1). Starting from the Salmon transcript quantification, we used the R packages tximport (Soneson *et al*, 2015; v1.10.1) and DESeq2 (Love *et al*, 2014; v1.22.2) to perform the differential expression analyses (Wald test and *P*-value correction with the Benjamini–Hochberg method). We used the R packages clusterProfiler (Yu *et al*, 2012; v 3.10.1) and msgidbr (v 6.2.1) to test the pathway enrichment of a list of genes. We tested the list of genes against pathways from the msgidb hallmark, C2 and C5 gene sets. Overrepresentation *P*-values were corrected with the Benjamini–Hochberg method.

### Single cell RNA sequencing (scRNAseq)

CAFs and ductal tumor cells were obtained from a pool of 5 KC mice, as described above.

After tissue dissection and dissociation, FACS purified suspended cells were partitioned into nanoliter-scale Gel Bead-In-Emulsions (GEMs) with the Chromium Single Cell Controller (10XGenomics) at the Single Cell Platform (CLB/CRCL). After cell encapsulation and barcoding, library preparation followed the standard 10XGenomics 3' scRNAseq protocol comprising reverse transcription, amplification and indexing. Sequencing was performed using a NovaSeq Illumina device (Illumina). Illumina bcl files were basecalled, demultiplexed and aligned to the mouse mm10 genome using the cellranger software (10XGenomics). All downstream analyses were performed using R/Bioconductor/CRAN packages, R version 4.0.3 (2020-10-10) —“Bunny-Wunnies Freak Out” [<https://cran.r-project.org/>; <http://www.bioconductor.org/>; <https://cran.r-project.org/>] on a linux platform (x86\_64-pc-linux-gnu [64-bit]). Filtered barcoded matrices were used to create a Seurat object (Stuart *et al*, 2019) for CAFs and Ducts cells that were subsequently merged. A total of 4,949 cells (4,072 CAFs and 877 Ducts) remained after filtering for quality parameters (number of features per cell < 6,000, fraction of mitochondrial genes < 10%). SCTransform was used to simultaneously normalize, identify variable features, and scale the data. Following dimension reduction with PCA, the first 20 dimensions were used to construct a shared nearest neighbor (SNN) graph using the FindNeighbours function. Clusters were identified with a resolution of 0.5 and projected in two-dimensional plots using Uniform Manifold Approximation and Projection (UMAP; arXiv:1802.03426v3).

Differentially expressed genes for each cluster were identified using the FindMarkers function. In addition, a list of PeSC markers obtained from bulk RNAseq data was used to calculate a PeSC score. This permitted the identification of a common cluster between CAFs and Ducts with a high PeSC score. This putative PeSC cluster was isolated and pathway analysis was performed in its full list of unique markers using EnrichR R (Kuleshov *et al*, 2016) and pathfindR (Ulgen *et al*, 2019) CRAN packages. Significant markers and pathways were selected with a threshold of adjusted *P*-value (FDR) below 0.05.

### Immunohistochemistry and immunofluorescence

BIC14011a and PA485 human tissue microarrays (TMAs) were obtained from a commercial source (US Biomax, Inc.). BIC14011a is a pancreas array that contains 22 pancreatitis cases, 18 pancreatic intraepithelial neoplasia cases, and eight pancreatic adenocarcinoma cases. PA485 is pancreatitis and matching pancreatic adenocarcinoma array containing 43 cases of pancreatitis and five matched pancreatic adenocarcinomas. Mouse tumor grafts were harvested, fixed overnight in 10% neutral buffered formalin, embedded in paraffin, and sectioned at 4  $\mu$ m. All immunohistochemical (IHC) staining procedures were performed following heat-induced epitope retrieval (Antigen-unmasking solution), and the sections were incubated with the primary antibodies overnight at 4°C. IHC staining was revealed using 3,3'-diaminobenzidine (DAB kit), and the sections were counterstained with hematoxylin. The CD106 positivity was visually quantified by the identification of at least one positive cell within each individual TMA spot. IF staining was performed using a standard protocol, and the sections were counterstained with VECTASHIELD® Antifade Mounting Medium with DAPI for nuclear counterstaining. The primary antibodies used were the following: anti-CD24, anti-CD44, anti-CD106 (VCAM-1), anti- $\alpha$ SMA, anti-CK19 (Troma III), anti-ZO-1, anti-E-cadherin, anti-Nanog, anti-Ly6G, anti-mCherry, and anti-GFP. Specific anti-F(ab')<sub>2</sub>-Alexa Fluor 647, anti-F(ab')<sub>2</sub>-Alexa Fluor 555 and anti-F(ab')<sub>2</sub>-Alexa Fluor 488 antibodies were used as secondary antibodies.

### Western blot

WB is performed among Epi, Meta and PeSC cells for *Kras*<sup>G12D</sup> detection. Cells were collected by scratching in 10 ml of PBS. After centrifugation, the proteins were isolated using RIPA buffer supplemented with protease and phosphatase inhibitors. Twenty microliters of the obtained lysate were separated by NuPAGE 4–12% Bis-Tris Gel electrophoresis system and transferred to an Immune-Blot PVDF membrane. After transfer, the immune blots were blocked by incubating with 5% BSA in Tris-buffered saline (TBS) containing 0.05% Tween 20. The blots were then probed overnight with Ras (G12D) mAb at 1:1,000. After washing in TBS-Tween 0.05%, the membranes were revealed with secondary antibodies for 1 h at room temperature. After washing, the blots were developed using the ECL chemiluminescence method according to the manufacturer's protocol (Pierce™ ECL Western Blotting Substrate). HRP-conjugated anti-rabbit Ab was used for primary antibody binding.

### FACS analysis

Cells were collected by trypsinizing from the culture plate and then distributed into the 96-well plate for FACS staining. In the case of tumor implantation, the tumor grafts were excised, weighed, and measured. The tumor grafts were then digested in 1% PBS supplemented with collagenase at 1 mg/ml for 20 min at 37°C. The digested tissue was homogenized by passage through a 100  $\mu$ m cell strainer. Single-cell suspensions derived from tumor grafts were stained with fluorescently labeled antibodies for 20 min at 4°C. For cytokine analysis and intracellular staining, single-cell suspensions were incubated with a complete culture medium containing a cell activation cocktail (PMA + ionomycin + Brefeldin A) for 2–4 h at 37°C prior to surface staining to retain intracellular proteins. After surface staining, cells were fixed and permeabilized using the True-Nuclear™ Transcription

Factor Buffer Set according to the manufacturer's protocol. Intracellular staining was performed for 30 min at 4°C. Fluorescently labeled cells were acquired on a BD Fortessa Flow Cytometer (BD; Franklin Lakes/NJ/USA) and analyzed using FlowJo. The monoclonal Abs used in flow cytometry were summarized in the key resources table.

### Bone marrow chimera approach

Briefly, recipient mice were sublethally irradiated with 7 Gy via a cesium  $\gamma$  source 2 days prior to transplantation. Bone marrow cells were harvested from the femurs and tibias of donor mice in RPMI-1640. Recipient mice were administered approximately  $2 \times 10^6$  bone marrow cells in 0.2 ml medium via iv injection. Five weeks after transplantation, recipient mice were subjected to whole blood sampling to determine the degree of chimerism by flow cytometry determination of Tomato expression.

### Quantification and statistical analysis

The *P*-values were calculated using Student's *t*-test with GraphPad Prism as indicated in the figure legends: \**P* < 0.05, \*\**P* < 0.01, \*\*\**P* < 0.001, and \*\*\*\**P* < 0.0001. One-way ANOVA with Tukey's *post hoc* test was used for multiple comparisons. The contingency analysis was performed using Fisher's exact test.

## Data availability

The scRNAseq data from this publication have been deposited to the Gene Expression Omnibus (GEO) with the identifier GSE220687 (<https://www.ncbi.nlm.nih.gov/geo/query/acc.cgi?acc=GSE220687>).

**Expanded View** for this article is available [online](#).

## Acknowledgements

The authors thank the staff at ANICAN (Cancer Research Center of Lyon) staff for the maintenance of the mouse strains and Christophe Vanbelle for the helpful assistance with the confocal microscopy experiments. This study was supported by grants from La Ligue Contre le Cancer (AH and PB), Bristol Meyers Squibb Foundation (AH), INSERM Transfert (AH), Sanofi iAward (AH), Institut National du cancer (INCA) AAP 2019, and Fondation de France (AH and PG), ZCW and YJZ were both supported by a Chinese Scholarship Council (CSC) Fellowship. ZCW was supported by Science and Technology Commission of Shanghai Municipality (Shanghai Administration of Foreign Experts Affairs), no. 21430711900.

## Author contributions

**Zhichong Wu:** Investigation; writing – original draft; writing – review and editing. **Kevin Thierry:** Investigation; writing – review and editing. **Sophie Bachy:** Investigation. **Xinyi Zhang:** Investigation. **Pia Gamradt:** Investigation. **Hector Hernandez-Vargas:** Formal analysis. **Ivan Mikaelian:** Investigation. **Laurie Tonon:** Software; formal analysis. **Roxanne Pommier:** Data curation; software; formal analysis. **Yajie Zhao:** Investigation. **Philippe Bertolino:** Writing – original draft. **Ana Hennino:** Conceptualization; supervision; funding acquisition; writing – original draft; project administration; writing – review and editing.

## Disclosure and competing interests statement

The authors declare that they have no conflict of interest.

## References

- Acharya C, Cline RA, Jaligama D, Noel P, Delany JP, Bae K, Furlan A, Baty CJ, Karlsson JM, Rosario BL *et al* (2013) Fibrosis reduces severity of acute-on-chronic pancreatitis in humans. *Gastroenterology* 145: 466–475
- Aguirre AJ, Bardeesy N, Sinha M, Lopez L, Tuveson DA, Horner J, Redston MS, DePinho RA (2003) Activated Kras and Ink4a/Arf deficiency cooperate to produce metastatic pancreatic ductal adenocarcinoma. *Genes Dev* 17: 3112–3126
- Armulik A, Genove G, Betsholtz C (2011) Pericytes: developmental, physiological, and pathological perspectives, problems, and promises. *Dev Cell* 21: 193–215
- Ascher E, Markevich N, Schutzer RW, Kallakuri S, Jacob T, Hingorani AP (2003) Cerebral hyperperfusion syndrome after carotid endarterectomy: predictive factors and hemodynamic changes. *J Vasc Surg* 37: 769–777
- Balabanov R, Washington R, Wagnerova J, Dore-Duffy P (1996) CNS microvascular pericytes express macrophage-like function, cell surface integrin alpha M, and macrophage marker ED-2. *Microuasc Res* 52: 127–142
- Banerjee M, Bhonde RR (2006) Application of hanging drop technique for stem cell differentiation and cytotoxicity studies. *Cytotechnology* 51: 1–5
- Bayne LJ, Beatty GL, Jhala N, Clark CE, Rhim AD, Stanger BZ, Vonderheide RH (2012) Tumor-derived granulocyte-macrophage colony-stimulating factor regulates myeloid inflammation and T cell immunity in pancreatic cancer. *Cancer Cell* 21: 822–835
- Blair AB, Kim VM, Muth ST, Saung MT, Lokker N, Blouw B, Armstrong TD, Jaffee EM, Tsujikawa T, Coussens LM *et al* (2019) Dissecting the stromal signaling and regulation of myeloid cells and memory effector T cells in pancreatic cancer. *Clin Cancer Res* 25: 5351–5363
- Bonnet D, Dick JE (1997) Human acute myeloid leukemia is organized as a hierarchy that originates from a primitive hematopoietic cell. *Nat Med* 3: 730–737
- Chen K, Wang Q, Li M, Guo H, Liu W, Wang F, Tian X, Yang Y (2021) Single-cell RNA-seq reveals dynamic change in tumor microenvironment during pancreatic ductal adenocarcinoma malignant progression. *EBioMedicine* 66: 103315
- DeNardo DG, Brennan DJ, Rexhepaj E, Ruffell B, Shiao SL, Madden SF, Gallagher WM, Wadhvani N, Keil SD, Junaid SA *et al* (2011) Leukocyte complexity predicts breast cancer survival and functionally regulates response to chemotherapy. *Cancer Discov* 1: 54–67
- Deygas M, Gadet R, Gillet G, Rimokh R, Gonzalo P, Mikaelian I (2018) Redox regulation of EGFR steers migration of hypoxic mammary cells towards oxygen. *Nat Commun* 9: 4545
- Dominici M, Le Blanc K, Mueller I, Slaper-Cortenbach I, Marini F, Krause D, Deans R, Keating A, Prockop D, Horwitz E (2006) Minimal criteria for defining multipotent mesenchymal stromal cells. The international society for cellular therapy position statement. *Cytotherapy* 8: 315–317
- Erkan M, Michalski CW, Rieder S, Reiser-Erkan C, Abiatari I, Kolb A, Giese NA, Esposito I, Friess H, Kleeff J (2008) The activated stroma index is a novel and independent prognostic marker in pancreatic ductal adenocarcinoma. *Clin Gastroenterol Hepatol* 6: 1155–1161
- Ferro F, Spelat R, Shaw G, Duffy N, Islam MN, O'Shea PM, O'Toole D, Howard L, Murphy JM (2019) Survival/adaptation of bone marrow-derived mesenchymal stem cells after long-term starvation through selective processes. *Stem Cells* 37: 813–827
- Franklin RA, Liao W, Sarkar A, Kim MV, Bivona MR, Liu K, Pamer EG, Li MO (2014) The cellular and molecular origin of tumor-associated macrophages. *Science* 344: 921–925
- Gabrilovich DI, Ostrand-Rosenberg S, Bronte V (2012) Coordinated regulation of myeloid cells by tumours. *Nat Rev Immunol* 12: 253–268
- Goehrig D, Nigri J, Samain R, Wu Z, Cappello P, Gabiane G, Zhang X, Zhao Y, Kim IS, Chanal M *et al* (2019) Stromal protein betaig-h3 reprogrammes tumour microenvironment in pancreatic cancer. *Gut* 68: 693–707
- Gore J, Korc M (2014) Pancreatic cancer stroma: friend or foe? *Cancer Cell* 25: 711–712
- Guerra DAP, Paiva AE, Sena IFG, Azevedo PO, Silva WN, Mintz A, Birbrair A (2018) Targeting glioblastoma-derived pericytes improves chemotherapeutic outcome. *Angiogenesis* 21: 667–675
- Hanahan D, Weinberg RA (2011) Hallmarks of cancer: the next generation. *Cell* 144: 646–674
- Hingorani SR, Petricoin EF, Maitra A, Rajapakse V, King C, Jacobetz MA, Ross S, Conrads TP, Veenstra TD, Hitt BA *et al* (2003) Preinvasive and invasive ductal pancreatic cancer and its early detection in the mouse. *Cancer Cell* 4: 437–450
- Hingorani SR, Wang L, Multani AS, Combs C, Deramandt TB, Hruban RH, Rustgi AK, Chang S, Tuveson DA (2005) Trp53R172H and KrasG12D cooperate to promote chromosomal instability and widely metastatic pancreatic ductal adenocarcinoma in mice. *Cancer Cell* 7: 469–483
- Jiang H, Hegde S, Knolhoff BL, Zhu Y, Herndon JM, Meyer MA, Nywening TM, Hawkins WG, Shapiro IM, Weaver DT *et al* (2016) Targeting focal adhesion kinase renders pancreatic cancers responsive to checkpoint immunotherapy. *Nat Med* 22: 851–860
- Jiang H, Liu X, Knolhoff BL, Hegde S, Lee KB, Jiang H, Fields RC, Pachter JA, Lim KH, DeNardo DG (2020) Development of resistance to FAK inhibition in pancreatic cancer is linked to stromal depletion. *Gut* 69: 122–132
- Kuleshov MV, Jones MR, Rouillard AD, Fernandez NF, Duan Q, Wang Z, Koplev S, Jenkins SL, Jagodnik KM, Lachmann A *et al* (2016) Enrichr: a comprehensive gene set enrichment analysis web server 2016 update. *Nucleic Acids Res* 44: W90–W97
- Kutikhin AG, Tupikin AE, Matveeva VG, Shishkova DK, Antonova LV, Kabilov MR, Velikanova EA (2020) Human peripheral blood-derived endothelial Colony-forming cells are highly similar to mature vascular endothelial cells yet demonstrate a transitional transcriptomic signature. *Cell* 9: 876
- Li C, Heidt DG, Dalerba P, Burant CF, Zhang L, Adsay V, Wicha M, Clarke MF, Simeone DM (2007) Identification of pancreatic cancer stem cells. *Cancer Res* 67: 1030–1037
- Love MI, Huber W, Anders S (2014) Moderated estimation of fold change and dispersion for RNA-seq data with DESeq2. *Genome Biol* 15: 550
- Mitchem JB, Brennan DJ, Knolhoff BL, Belt BA, Zhu Y, Sanford DE, Belaygorod L, Carpenter D, Collins L, Piwnicka-Worms D *et al* (2013) Targeting tumor-infiltrating macrophages decreases tumor-initiating cells, relieves immunosuppression, and improves chemotherapeutic responses. *Cancer Res* 73: 1128–1141
- Movahedi K, Laoui D, Gysemans C, Baeten M, Stange G, Van den Bossche J, Mack M, Pipeleers D, In't Veld P, De Baetselier P *et al* (2010) Different tumor microenvironments contain functionally distinct subsets of macrophages derived from Ly6C(high) monocytes. *Cancer Res* 70: 5728–5739
- Muraro MJ, Dharmadhikari G, Grun D, Groen N, Dielen T, Jansen E, van Gorp L, Engelse MA, Carlotti F, de Koning EJ *et al* (2016) A single-cell transcriptome atlas of the human pancreas. *Cell Syst* 3: 385–394
- Neesse A, Michl P, Frese KK, Feig C, Cook N, Jacobetz MA, Lolkema MP, Buchholz M, Olive KP, Gress TM *et al* (2011) Stromal biology and therapy in pancreatic cancer. *Gut* 60: 861–868

- Nywenning TM, Belt BA, Cullinan DR, Panni RZ, Han BJ, Sanford DE, Jacobs RC, Ye J, Patel AA, Gillanders WE *et al* (2018) Targeting both tumour-associated CXCR2(+) neutrophils and CCR2(+) macrophages disrupts myeloid recruitment and improves chemotherapeutic responses in pancreatic ductal adenocarcinoma. *Gut* 67: 1112–1123
- Oudenaarden C, Sjolund J, Pietras K (2022) Upregulated functional gene expression programmes in tumour pericytes mark progression in patients with low-grade glioma. *Mol Oncol* 16: 405–421
- Ozdemir BC, Pentcheva-Hoang T, Carstens JL, Zheng X, Wu CC, Simpson TR, Laklai H, Sugimoto H, Kahlert C, Novitskiy SV *et al* (2014) Depletion of carcinoma-associated fibroblasts and fibrosis induces immunosuppression and accelerates pancreas cancer with reduced survival. *Cancer Cell* 25: 719–734
- Panni RZ, Herndon JM, Zuo C, Hegde S, Hogg GD, Knolhoff BL, Breden MA, Li X, Krisnawan VE, Khan SQ *et al* (2019) Agonism of CD11b reprograms innate immunity to sensitize pancreatic cancer to immunotherapies. *Sci Transl Med* 11: eaau9240
- Pilarsky C, Ammerpohl O, Sipos B, Dahl E, Hartmann A, Wellmann A, Braunschweig T, Lohr M, Jesenofsky R, Friess H *et al* (2008) Activation of Wnt signalling in stroma from pancreatic cancer identified by gene expression profiling. *J Cell Mol Med* 12: 2823–2835
- Polette M, Mestdagt M, Bindels S, Nawrocki-Raby B, Hunziker W, Foidart JM, Birembaut P, Gilles C (2007) Beta-catenin and ZO-1: shuttle molecules involved in tumor invasion-associated epithelial-mesenchymal transition processes. *Cells Tissues Organs* 185: 61–65
- Pylayeva-Gupta Y, Lee KE, Hajdu CH, Miller G, Bar-Sagi D (2012) Oncogenic Kras-induced GM-CSF production promotes the development of pancreatic neoplasia. *Cancer Cell* 21: 836–847
- Sena IFG, Paiva AE, Prazeres P, Azevedo PO, Lousado L, Bhutia SK, Salmina AB, Mintz A, Birbrair A (2018) Glioblastoma-activated pericytes support tumor growth via immunosuppression. *Cancer Med* 7: 1232–1239
- Sinha D, Chong L, George J, Schluter H, Monchgesang S, Mills S, Li J, Parish C, Bowtell D, Kaur P *et al* (2016) Pericytes promote malignant ovarian cancer progression in mice and predict poor prognosis in serous ovarian cancer patients. *Clin Cancer Res* 22: 1813–1824
- Soneson C, Love MI, Robinson MD (2015) Differential analyses for RNA-seq: transcript-level estimates improve gene-level inferences. *F1000Res* 4: 1521
- Sorrell JM, Baber MA, Caplan AI (2009) Influence of adult mesenchymal stem cells on *in vitro* vascular formation. *Tissue Eng Part A* 15: 1751–1761
- Stromnes IM, Brockenbrough JS, Izeradjene K, Carlson MA, Cuevas C, Simmons RM, Greenberg PD, Hingorani SR (2014) Targeted depletion of an MDSC subset unmasks pancreatic ductal adenocarcinoma to adaptive immunity. *Gut* 63: 1769–1781
- Stuart T, Butler A, Hoffman P, Hafemeister C, Papalexi E, Mauck WM, Hao Y, Stoeckius M, Smibert P, Satija R (2019) Comprehensive integration of single-cell data. *Cell* 177: 1888–1902
- Ulgen E, Ozisik O, Sezerman OU (2019) pathfindR: an R package for comprehensive identification of enriched pathways in omics data through active subnetworks. *Front Genet* 10: 858
- Valdor R, Garcia-Bernal D, Bueno C, Rodenas M, Moraleda JM, Macian F, Martinez S (2017) Glioblastoma progression is assisted by induction of immunosuppressive function of pericytes through interaction with tumor cells. *Oncotarget* 8: 68614–68626
- Van Noorden CJ, Jonges GN, Vogels IM, Hoeben KA, Van Urk B, Everts V (1995) Ectopic mineralized cartilage formation in human undifferentiated pancreatic adenocarcinoma explants grown in nude mice. *Calcif Tissue Int* 56: 145–153
- Weber R, Riester Z, Huser L, Sticht C, Siebenmorgen A, Groth C, Hu X, Altevogt P, Utikal JS, Umansky V (2020) IL-6 regulates CCR5 expression and immunosuppressive capacity of MDSC in murine melanoma. *J Immunother Cancer* 8: e000949
- Wong SP, Rowley JE, Redpath AN, Tilman JD, Fellous TG, Johnson JR (2015) Pericytes, mesenchymal stem cells and their contributions to tissue repair. *Pharmacol Ther* 151: 107–120
- Wong PP, Munoz-Felix JM, Hijazi M, Kim H, Robinson SD, De Luxan-Delgado B, Rodriguez-Hernandez I, Maiques O, Meng YM, Meng Q *et al* (2020) Cancer burden is controlled by mural cell-β3-integrin regulated crosstalk with tumor cells. *Cell* 181: 1346–1363
- Yu G, Wang LG, Han Y, He QY (2012) clusterProfiler: an R package for comparing biological themes among gene clusters. *OMICS* 16: 284–287
- Zhang Y, Huang Q, Tang M, Zhang J, Fan W (2015) Complement factor H expressed by retinal pigment epithelium cells can suppress neovascularization of human umbilical vein endothelial cells: an *in vitro* study. *PLoS ONE* 10: e0129945
- Zhu Y, Knolhoff BL, Meyer MA, Nywenning TM, West BL, Luo J, Wang-Gillam A, Goedegebuure SP, Linehan DC, DeNardo DG (2014) CSF1/CSF1R blockade reprograms tumor-infiltrating macrophages and improves response to T-cell checkpoint immunotherapy in pancreatic cancer models. *Cancer Res* 74: 5057–5069



**License:** This is an open access article under the terms of the [Creative Commons Attribution-NonCommercial-NoDerivs](https://creativecommons.org/licenses/by-nc-nd/4.0/) License, which permits use and distribution in any medium, provided the original work is properly cited, the use is non-commercial and no modifications or adaptations are made.

## Expanded View Figures

**Figure EV1. The CD106<sup>+</sup> population is uniquely localized to pancreatic injury and precancerous lesions.**

- A Representative IHC staining for CD106<sup>+</sup> in normal pancreas. Scale bar, 50  $\mu$ m.
- B Representative IHC staining for CD106<sup>+</sup> in IPMN+PanIN I-III and IPMT human samples. The adjacent region (above) and tumor core (below) were paired from the same patient respectively, corresponding to the diagnosis. The red arrow indicated the CD106<sup>+</sup> spindle-like cells. Scale bar, 50  $\mu$ m.
- C Representative IHC staining of pancreatic lesions of human TMA for CD106<sup>+</sup>. The magnification region indicates representative CD106<sup>+</sup> cells. Scale bar, 200, 50  $\mu$ m. Quantification of CD106 expression in pancreatitis, PanIN and PDAC lesions according to patients' pathological references of TMA (Appendix Table S1). \* $P < 0.05$  and \*\* $P < 0.01$ . \*\*\*\* $P < 0.0001$ . The  $P$ -values were calculated using Student's  $t$ -test.
- D Representative IF staining of the PeSC cell line on a coverslip for CD106 (green), mCherry (red), and DAPI (blue). Scale bar, 50  $\mu$ m.

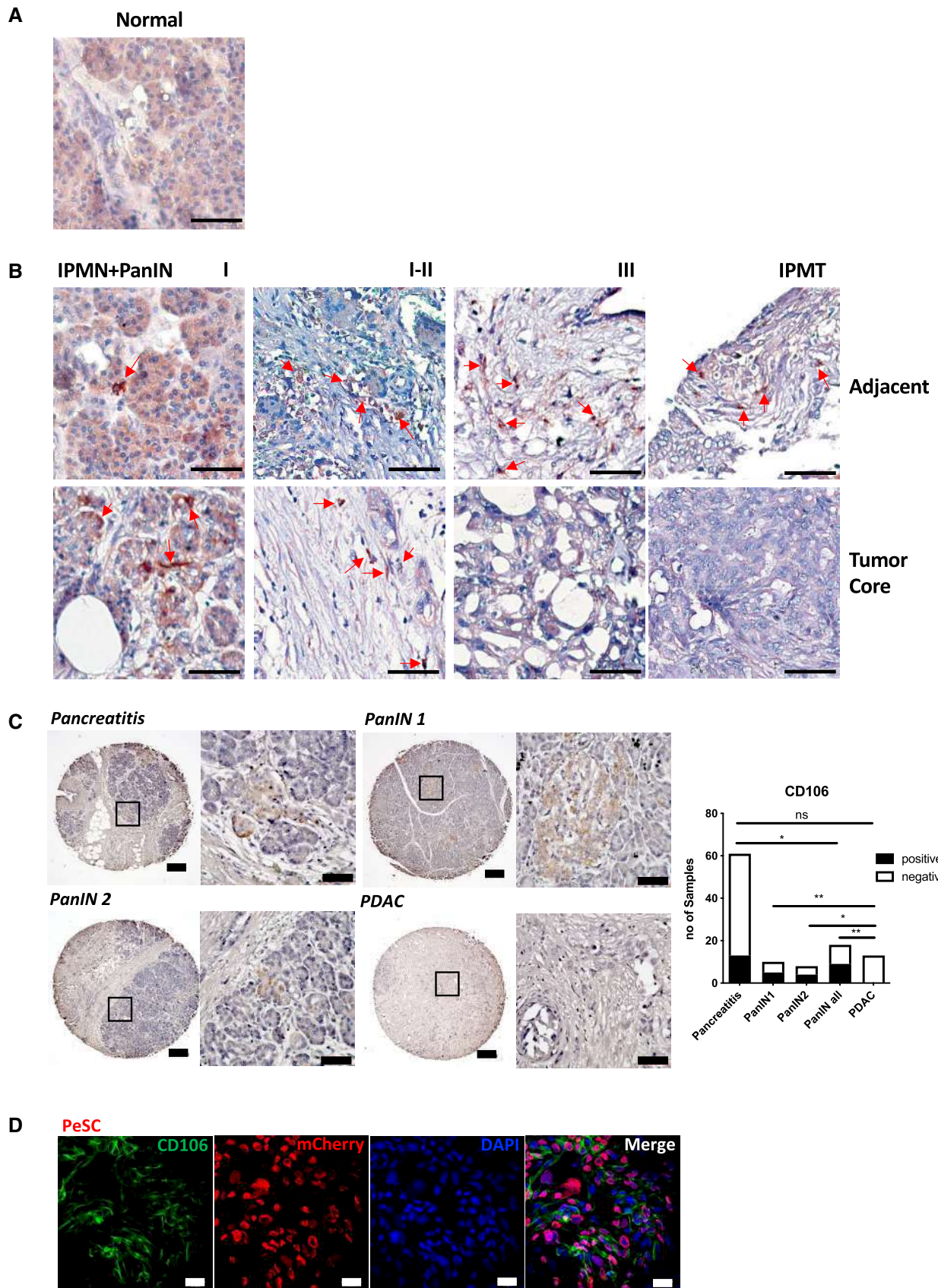


Figure EV1.

**Figure EV2. PeSC signature in human cancer single-cell data.**

- A, B Application of ovarian cancer pericyte (A) and brain cancer pericyte score (B) to our mouse single-cell RNAseq analysis showing enrichment in the unique cluster of PeSC.
- C Pooled single-cell RNAseq data to UMAP analysis from 35 samples (11 normal pancreas and 24 PDAC patients), including a total number of over 80,000 cells. The UMAP shows the distribution of each cell cluster.
- D Cell types of each cluster were identified based on Muraro's single-cell dataset as a reference.
- E, F Unsupervised clustering UMAP analysis distinguishes 23 subclusters in the integration of whole 35 samples (E), pooled from 11 normal pancreas samples and 24 PDAC samples (F).

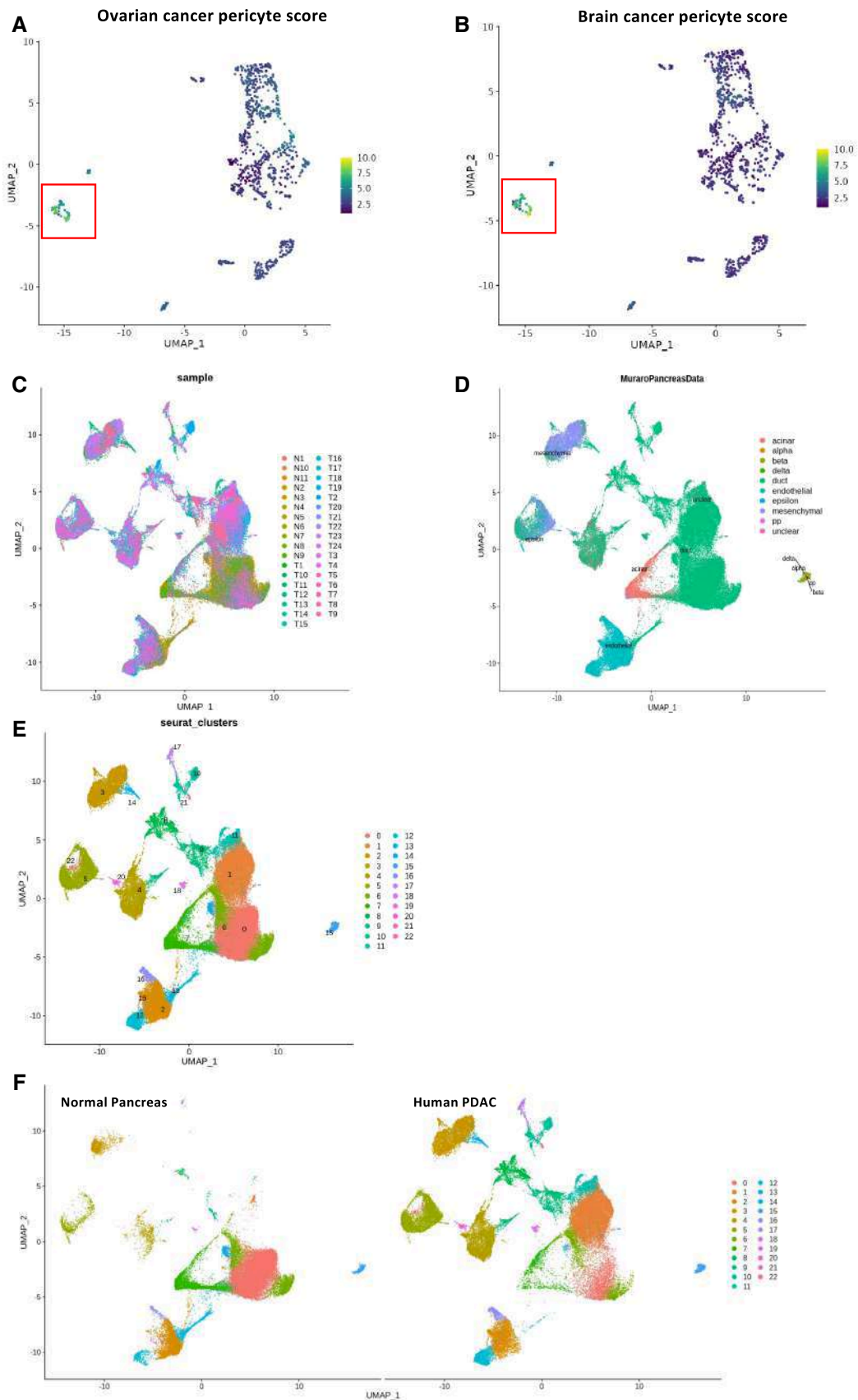


Figure EV2.

**Figure EV3. Chimera approach identifies the origin of PeSC.**

- A Experimental protocol for bone marrow chimeras. One month old KC mice were sublethally irradiated and reconstituted with bone marrow cells from a Tomato expressing mouse. After reconstitution, the chimeras were sacrificed on day 60.
- B Representative dot plots of reconstituted bone marrow cells (Tomato<sup>+</sup>) in KC chimeras compared to the nonreconstituted KC mice as control by FACS analysis. Quantification of reconstituted cells (Tomato<sup>+</sup>) among CD45<sup>+</sup> immune cells in either pancreas or periphery of KC chimeras compared to the control. Three mice in each condition.
- C Representative dot plots and gating strategy of distinguishing the reconstituted CD106<sup>+</sup> cells (Tomato<sup>+</sup>) and nonreconstituted CD106<sup>+</sup> cells (Tomato<sup>-</sup>) in KC chimeras. Three mice in the group, each dot represents one mouse.
- D Representative IF staining for CD106 (green) and Tomato (red) in the pancreas of chimera mice. Inset shows colocalization of CD106- and Tomato-stained cells. Scale bar, 50  $\mu$ m (upper), 10  $\mu$ m (lower).

Data information: ns not significant, \* $P < 0.05$ , \*\* $P < 0.01$ , \*\*\* $P < 0.001$  and \*\*\*\* $P < 0.0001$ . The  $P$ -values were calculated using Student's  $t$ -test.

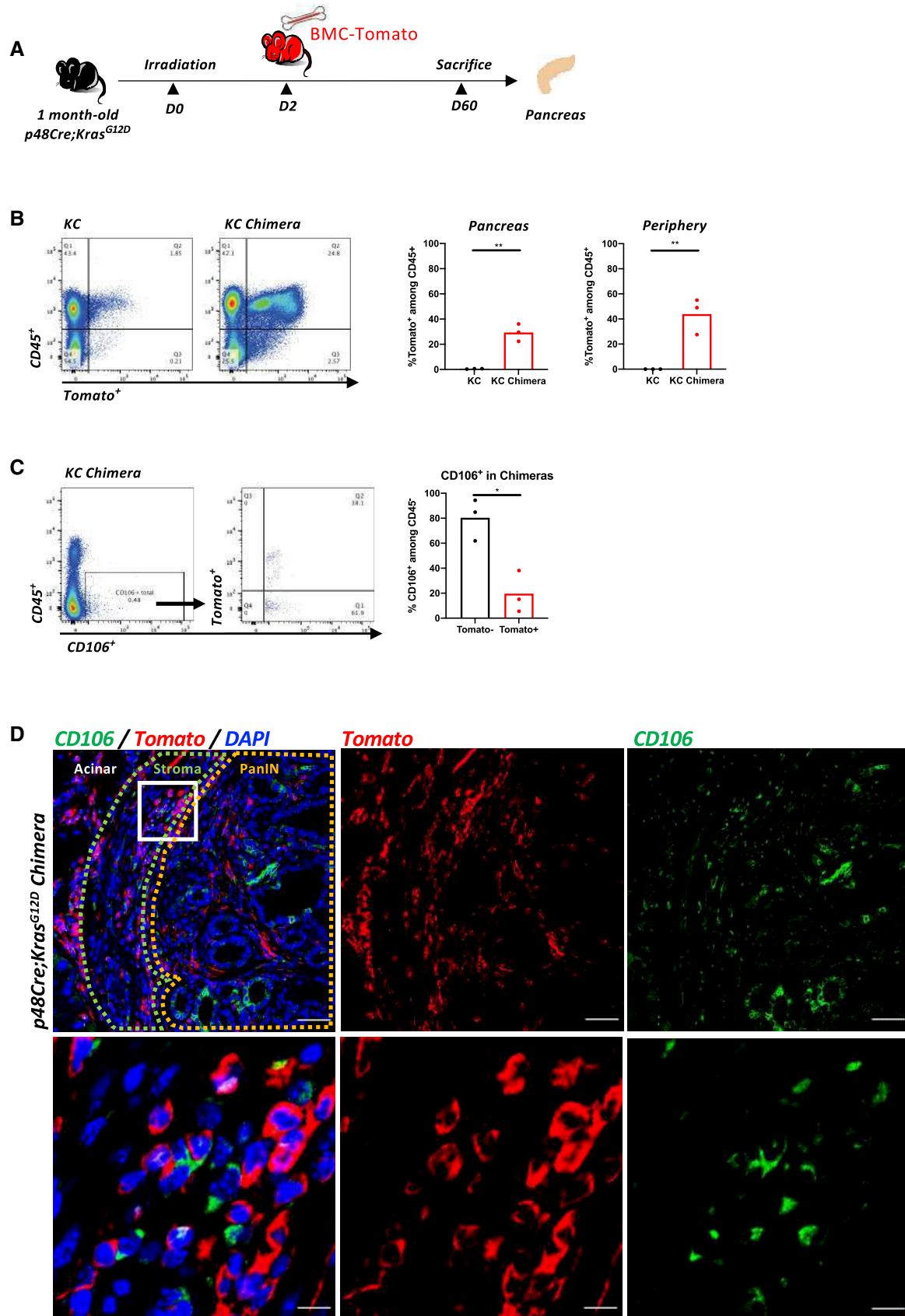


Figure EV3.

**Figure EV4. Stem properties of PeSCs and their impact on tumor cells.**

- A Proliferation curves of Epi cells in the indicated culture conditions based on the analysis of total green (GFP) object area in each well observed by IncuCyte. The data of each curve are summarized from six biological replicates of each condition. The bars are representing the mean  $\pm$  SD.
- B FACS analysis of the percentage of Ki67<sup>+</sup> Epi cells in each culture condition at 48 h. FACS analysis was performed by biological triplicates corresponding to the indicated culture condition.
- C, D The bars are representing the mean  $\pm$  SD (C, D) Proliferation curves of PeSCs in the indicated culture conditions based on the analysis of the total red (mCherry) object area in each well observed by IncuCyte. The data of each curve are summarized from six biological replicates of each condition. The bars are representing the mean  $\pm$  SD.
- E qPCR analysis of EMT-related genes expressed by PeSCs after the treatment of PDGF-BB and TGF- $\beta$  compared to the untreated ones (UT). Treatment was performed in biological triplicates and qPCR analysis was performed by technical duplicates. The bars are representing the mean  $\pm$  SD.
- F Quantification of Epi (GFP<sup>+</sup>) or PeSC (mCherry<sup>+</sup>) cells in the s.c. tumor grafts in the indicated conditions based on FACS analysis. Five mice in each group.

Data information: \* $P < 0.05$ , \*\* $P < 0.01$ , \*\*\* $P < 0.001$ , and \*\*\*\* $P < 0.0001$ . The  $P$ -values were calculated using Student's  $t$ -test.

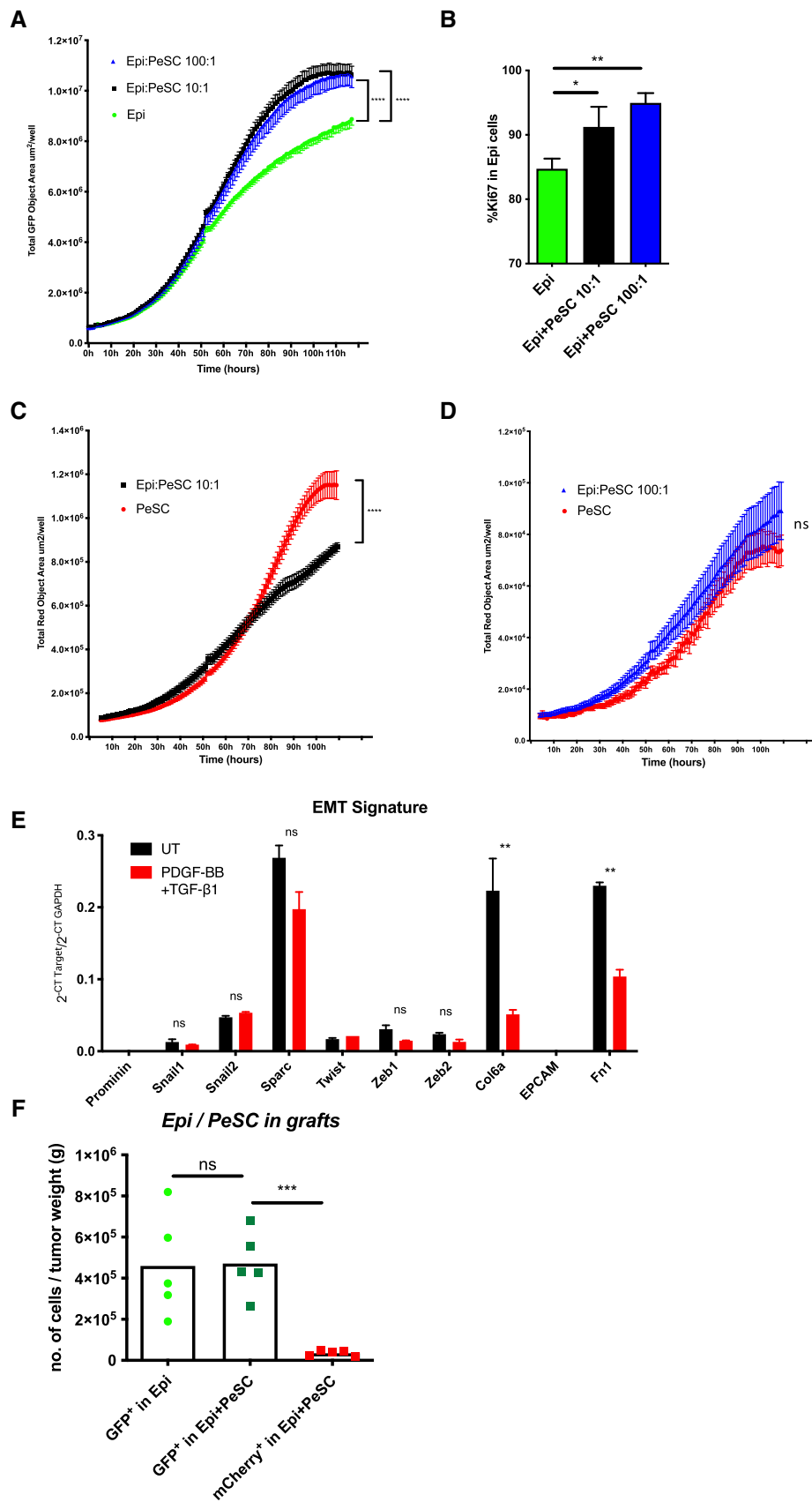


Figure EV4.

**Figure EV5. Tumor-PeSC crosstalk affects the immune system.**

- A, B *In vivo* neutralization of CD106: (A) Experiment setting. (B) Tumor weight, FACS analysis of % PeSC<sup>+</sup> among CD45<sup>-</sup> cells, % Epi<sup>+</sup> among CD45<sup>-</sup> cells, % CD11b<sup>+</sup> among CD45<sup>+</sup> cells, % Ly6G<sup>+</sup>CD11b<sup>+</sup> among CD45<sup>+</sup> cells, % CD11b<sup>+</sup>F4/80<sup>+</sup> among CD45<sup>+</sup> cells, % CD11b<sup>+</sup>F4/80<sup>+</sup>CD103<sup>+</sup> among CD45<sup>+</sup> cells (eight mice in each group, five for FACS analysis, and three for histological analysis. Quantification of PeSCs and Epi cells were cumulative from two FACS panels as technical duplicates).
- C–L *In vivo* depletion of CCL5 impact the macrophages differentiation: (C) Experimental setting. (D) Tumor weight of the grafts formed by Epi + PeSC in CCL5-depleted conditions compared with undepleted conditions. FACS analysis of the percentage of CD11b<sup>+</sup> cells (E), Ly6G<sup>+</sup>CD11b<sup>+</sup> (F), F4/80<sup>+</sup>CD11b<sup>+</sup> (G), F4/80<sup>+</sup>CSFR1<sup>+</sup> (H), F4/80<sup>+</sup>CD163<sup>+</sup> (I), F4/80<sup>+</sup>CD11b<sup>+</sup>CD103<sup>+</sup> (J), F4/80<sup>+</sup>CD11b<sup>+</sup>PD-L1<sup>+</sup> (K) and CD8<sup>+</sup> cells (L) among CD45<sup>+</sup> cells derived from the tumor grafts. Ten mice in each group, six for FACS analysis and four for histological analysis.

Data information: \* $P < 0.05$ , \*\* $P < 0.01$ , \*\*\* $P < 0.001$ , and \*\*\*\* $P < 0.0001$ . The  $P$ -values were calculated using Student's  $t$ -test.

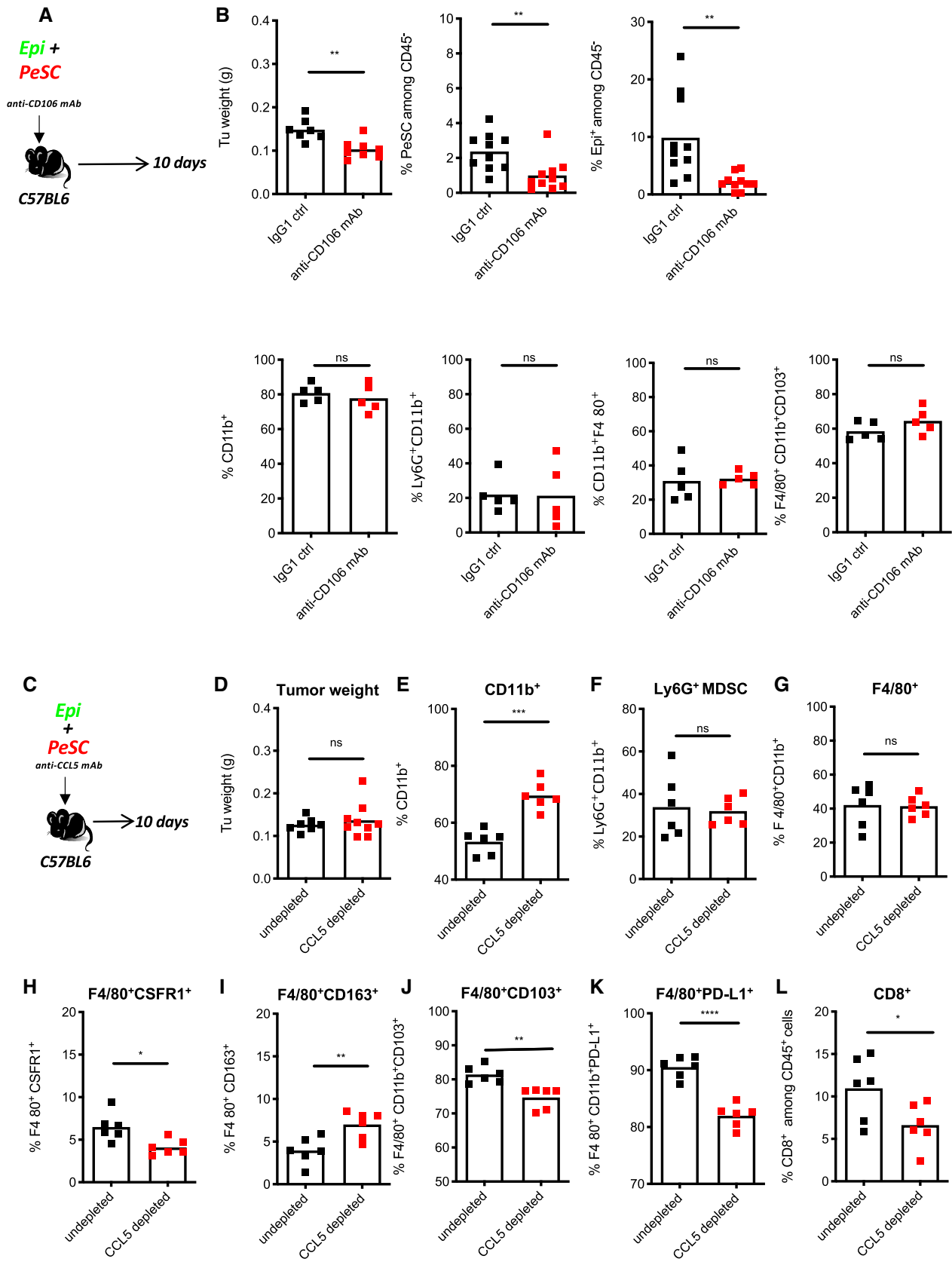
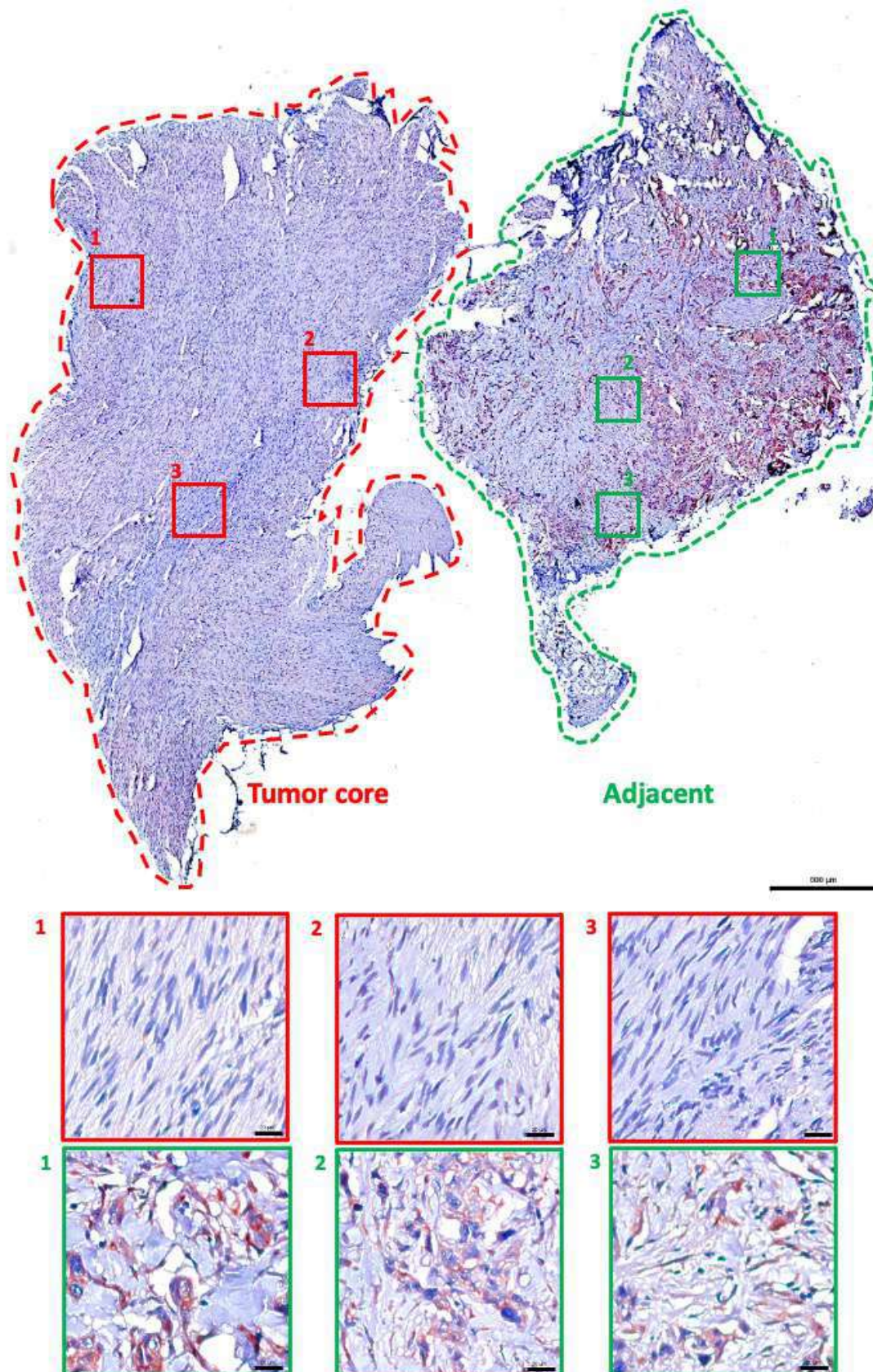


Figure EV5.

Appendix for  
"CD106<sup>+</sup> pericyte stem cells induce Ly6G<sup>+</sup> cell accumulation and resistance to immunotherapy in pancreatic cancer"

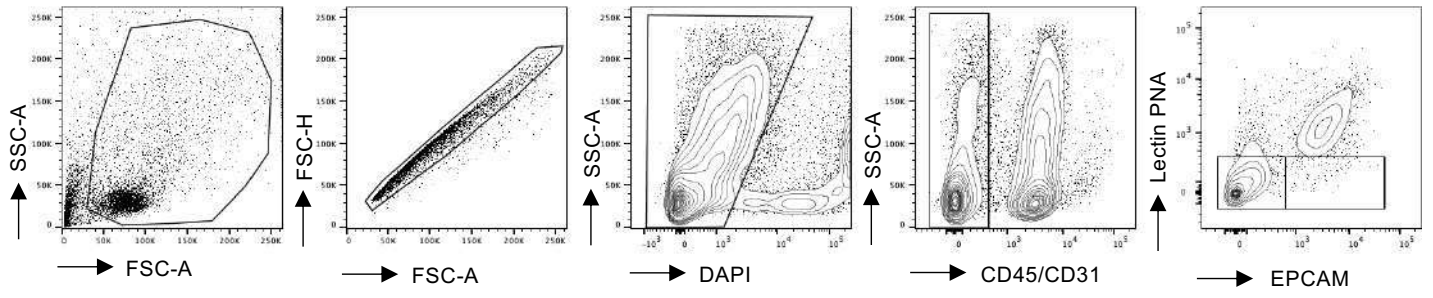
Appendix Figure S1.....	2
Appendix Figure S2 .....	3
Appendix Figure S3 .....	4-5
Appendix Figure S4 .....	6
Appendix Figure S5 .....	7-9
Appendix Figure S6 .....	10
Appendix Figure S7 .....	11
Appendix Table S1 .....	12

# Appendix Figure S1

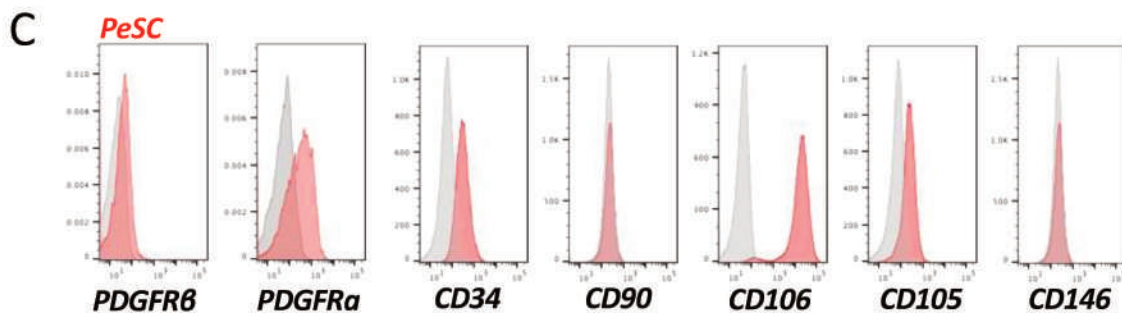
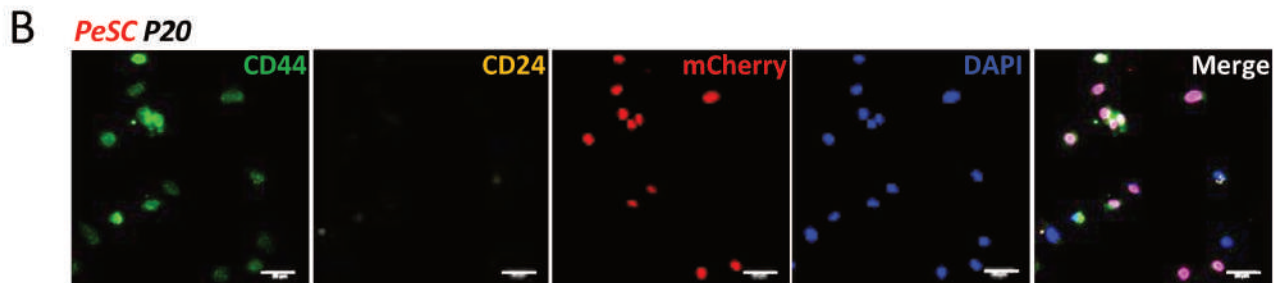
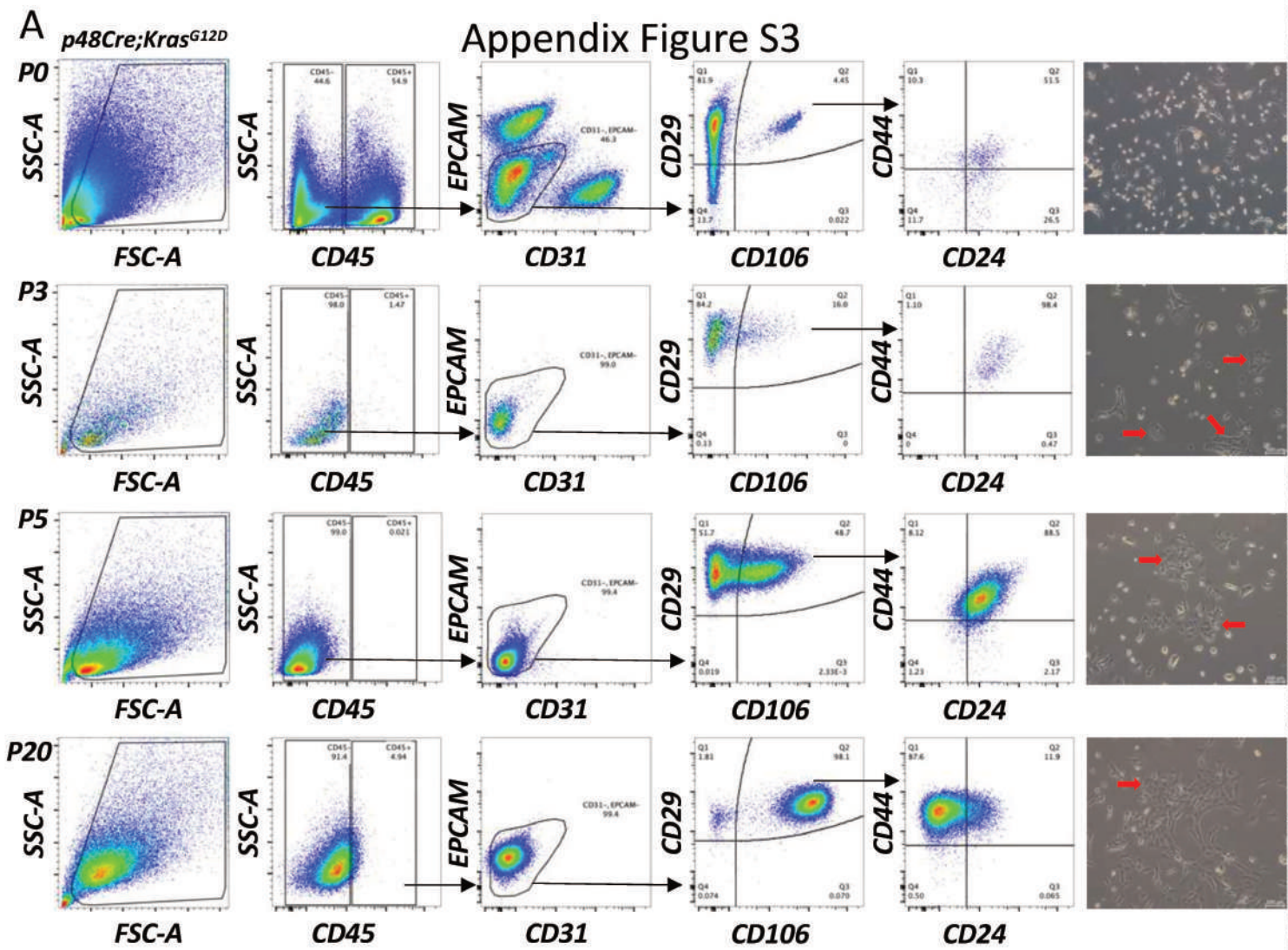


Appendix Figure S1: The CD106<sup>+</sup> population is uniquely localized in pancreatic injury and precancerous lesions. Representative IHC staining of tumor core and adjacent region in PDAC patient (stage III) for CD106<sup>+</sup>. The corresponding magnification insets of tumor core (red dotted line) or adjacent region (green dotted line) are displayed below the gross figure. Scale bar, 500  $\mu\text{m}$  in gross, 20  $\mu\text{m}$  in magnification.

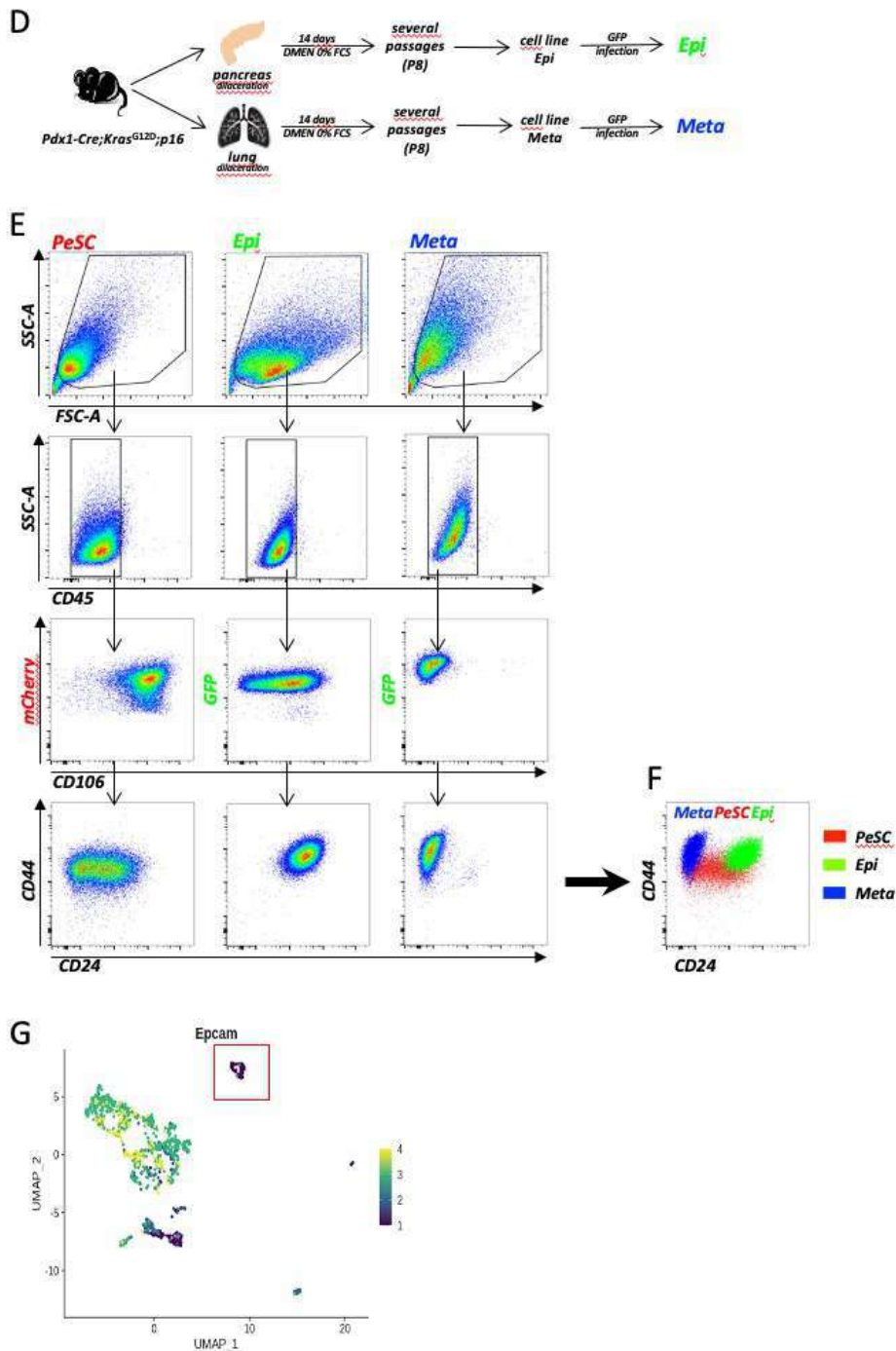
## Appendix Figure S2



Appendix Figure S2: Gating strategy for FACS sorting and single cell RNAseq.

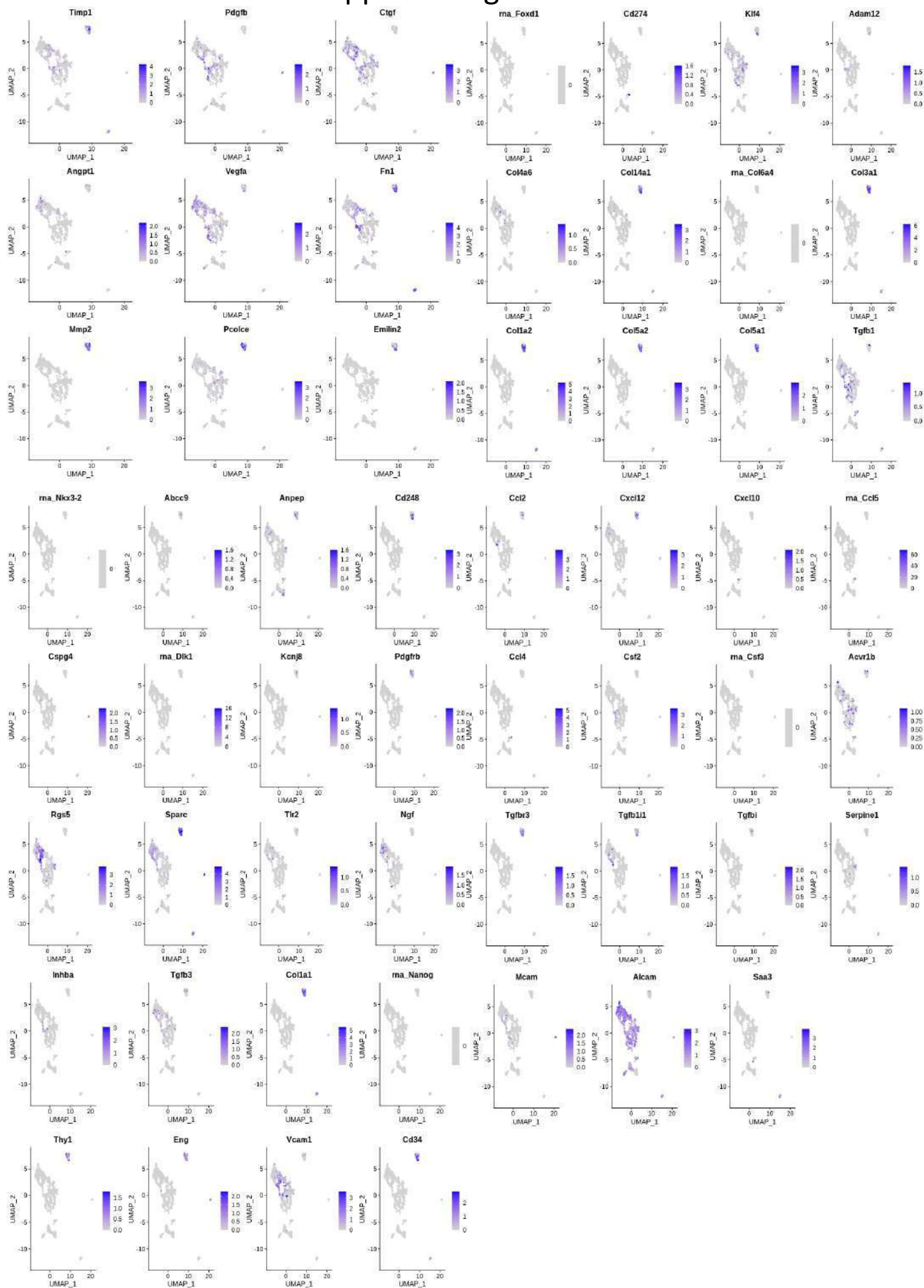


## Appendix Figure S3



Appendix Figure S3: Generation of the PeSC line and its phenotype. (A) Gating strategy for the identification and kinetic phenotype-progression of the  $CD45^+EPCAM^+CD31^+CD106^+CD24^{low}CD44^{high}$  population after cell line generation at P0, P3, P5 and P20. The red arrows indicate morphologically similar PeSC population clusters. Scale bar, 100  $\mu$ m. (B) Representative IF staining of the PeSC cell line on coverslip at P20 for CD44 (green), CD24 (yellow), mCherry (red), DAPI (blue). Scale bar, 50  $\mu$ m. (C) Representative histogram analysis of PDGFR $\beta$ , PDGFR $\alpha$ , CD34, CD90, CD106, CD105, and CD146 by FACS staining in PeSCs. Generation of the Epi and Meta cell lines and their phenotypes. (D) Schematic representation of the experimental setting for Epi and Meta cell line generation. (E) Gating strategy for PeSCs, Epi cells and Meta cells based on CD45, mCherry/GFP, CD106, CD24 and CD44 staining. (F) Representative merged dot plots of PeSCs, Epi cells and Meta cells for CD24 and CD44 staining. (G) Single cell analysis UMAP plots shows that cluster 7 (PeSC fraction) had no expression of EPCAM.

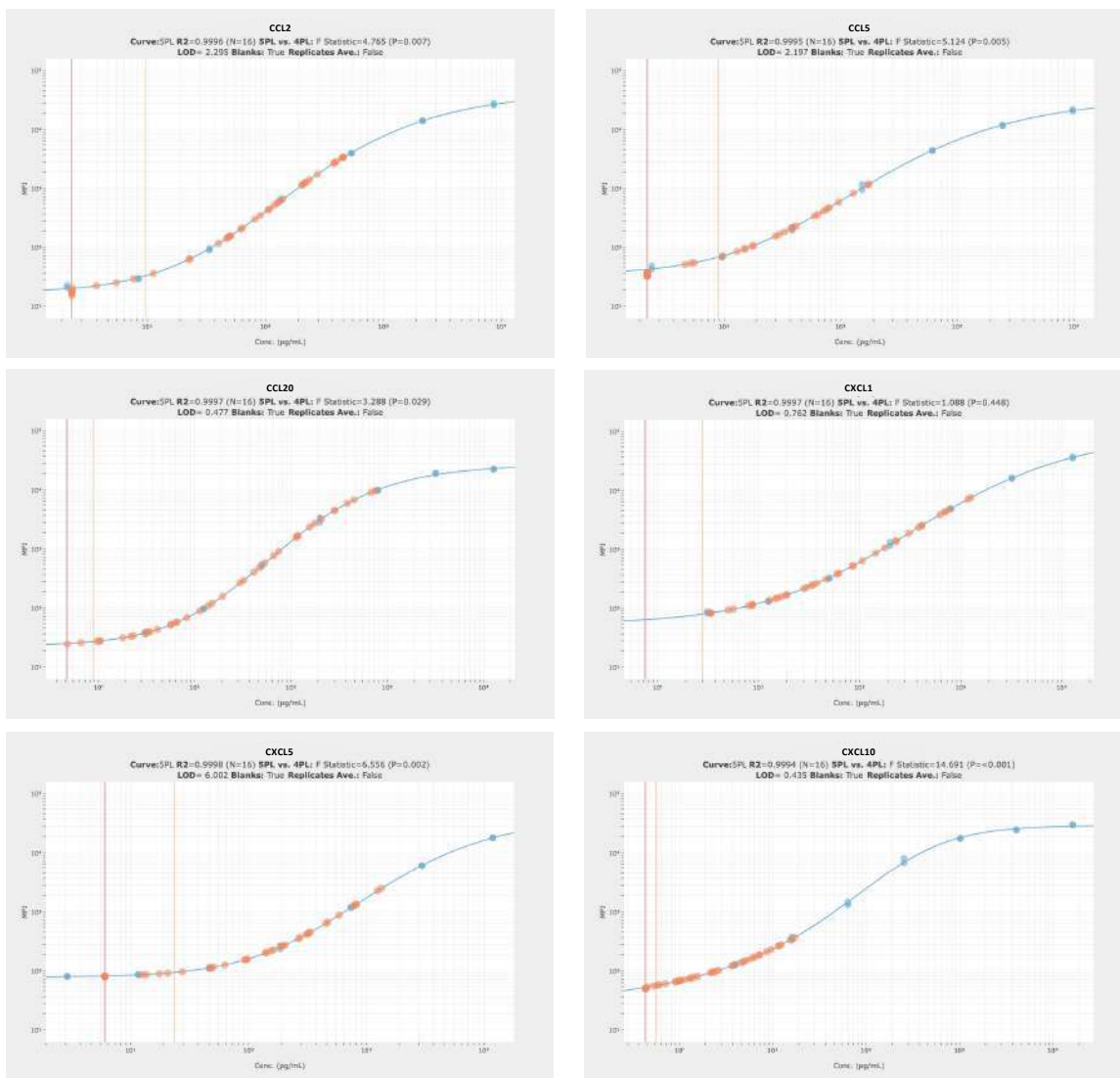
# Appendix Figure S4



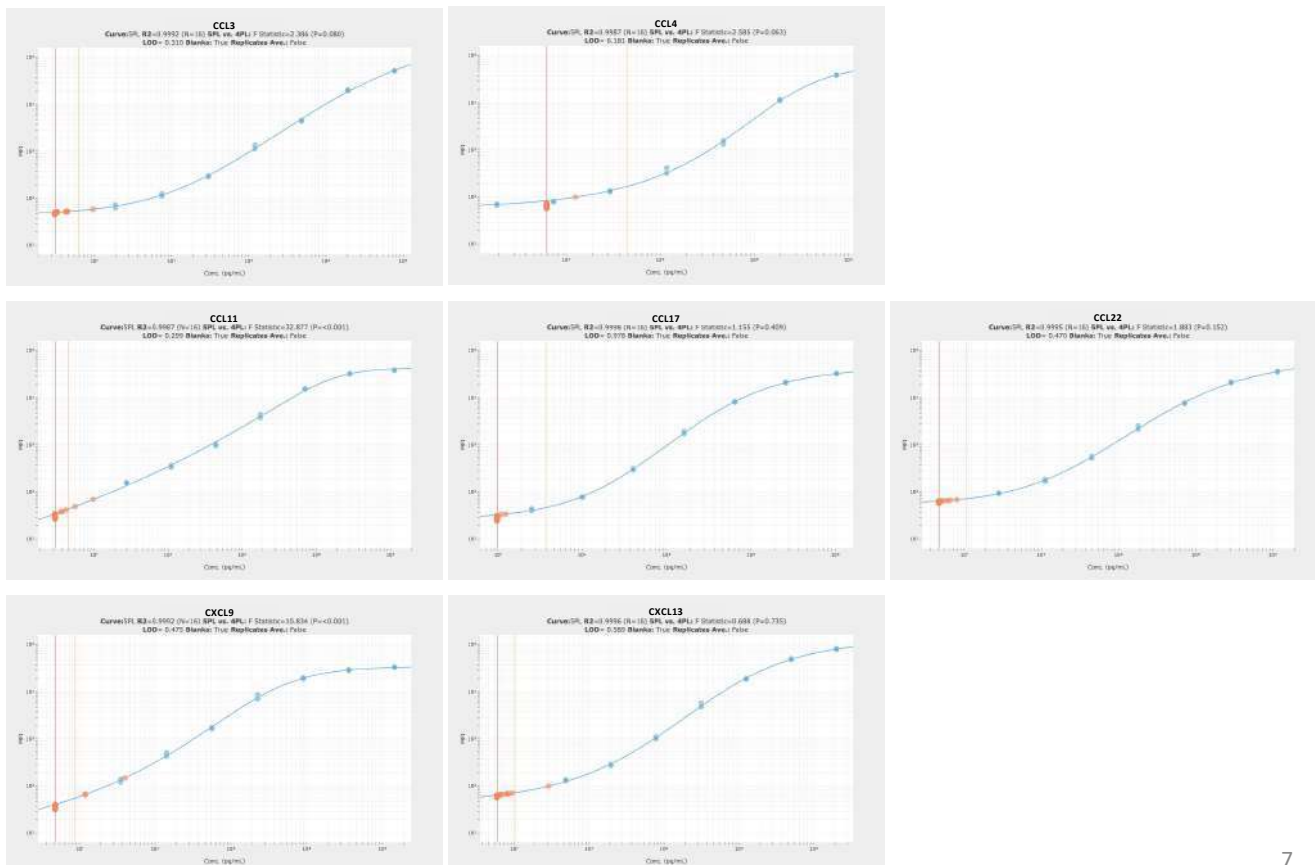
Appendix Figure S4: Single cell analysis reveals a distinct cluster 7 with PeSC signature. Single cell analysis UMAP plots of the PeSC signature genes extracted from the bulk RNAseq analysis and applied to the single cell analysis UMAP dots.

# Appendix Figure S5

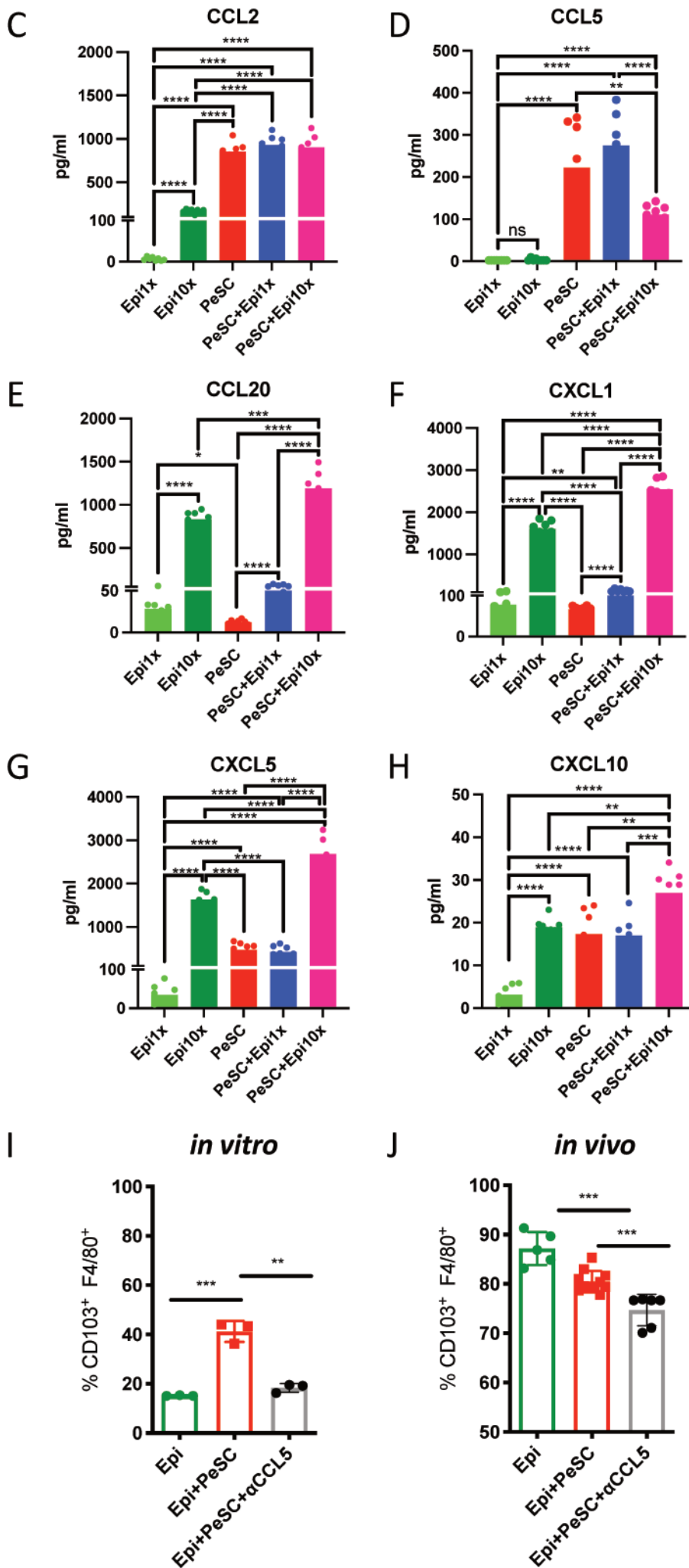
**A**



**B**



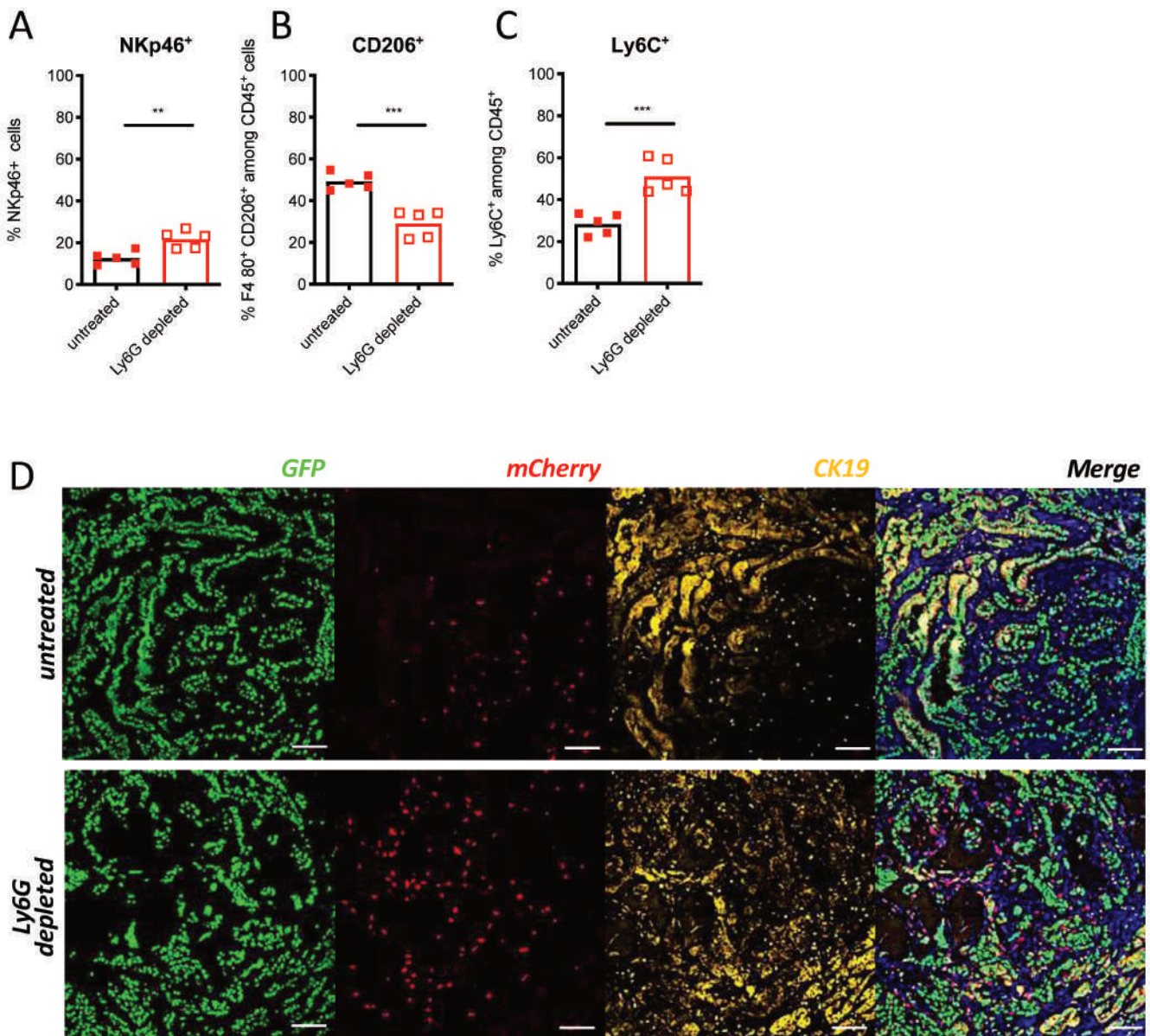
# Appendix Figure S5



## Appendix Figure S5

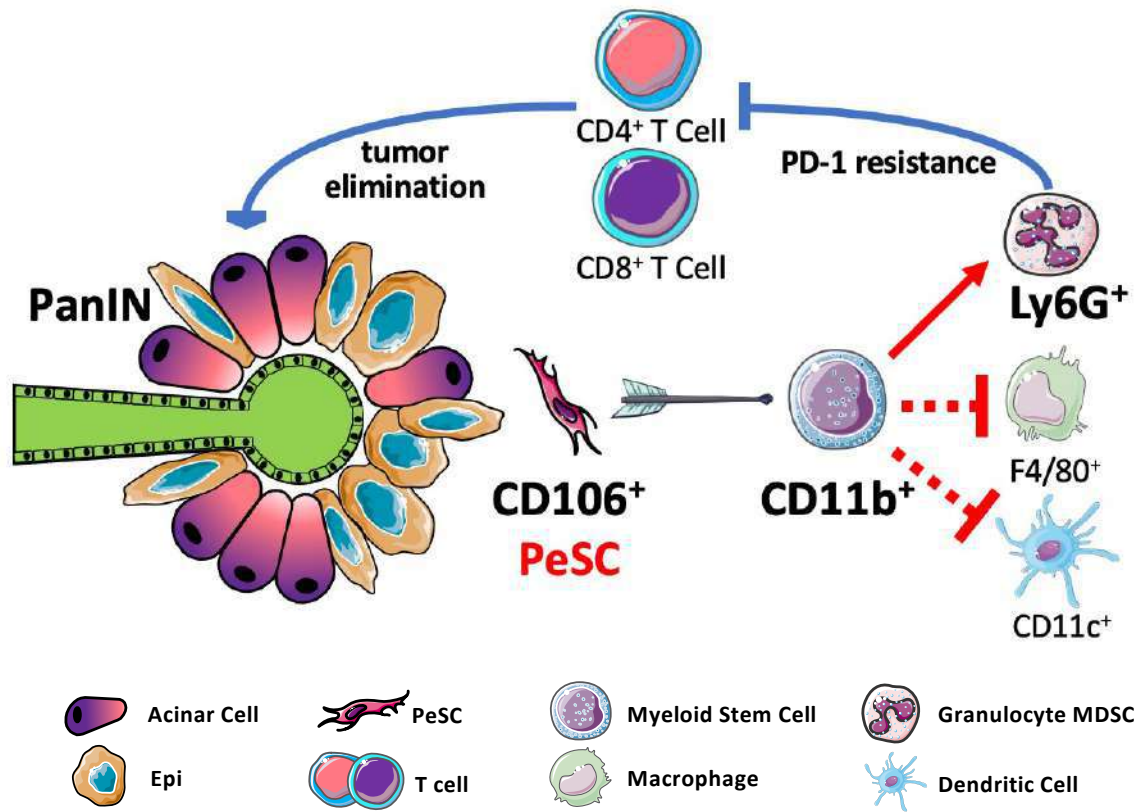
Appendix Figure S5: Tumor-PeSC crosstalk affects the immune system. (A and B) The standard curve of each chemokine is derived from the LEGENDplex<sup>TM</sup> data analysis software (blue dots and curves). All non-zero standard curve points are displayed as blue dots on the graph. All logistic regression line derived by the curve fitting algorithm is performed by 5-parameter logistic regression (5PL), displaying on the graph as a solid blue line. The theoretical limit of detection (LOD) and limit of quantification (LOQ) are depicted as red and orange vertical lines, respectively. Chemokine CCL2, CCL5, CCL20, CXCL1, CXCL5, and CXCL10 can be detected from the cell culture supernatant in condition of Epi1x, Epi10x, PeSC, PeSC + Epi1x and PeSC + Epi10x, as showed by the orange dots in line with the curve which were mostly above the LOD and LOQ (A). Chemokine CCL3, CCL4, CCL11, CCL17, CCL22, CXCL19 and CXCL13 are not detected from the cell culture supernatant in condition of Epi1x, Epi10x, PeSC, PeSC + Epi1x and PeSC + Epi10x, as all the sample dots (orange) were below the LOD and LOQ (B). Quantification of chemokine CCL2 (C), CCL5 (D), CCL20 (E), CXCL1 (F), CXCL5 (G), and CXCL10 (H) detected from the cell culture supernatant in conditions of Epi1x, Epi10x, PeSC, PeSC + Epi1x and PeSC + Epi10x, respectively. The LEGENDplex assays have been performed twice. The displayed results are extracted from the second experiment. Biological duplicates were applied in each culture condition and the supernatant of each condition was then distributed into 4 different dilutions for FACS analysis quantified as technical replicates. (I) *In vitro* FACS analysis of the percentage of CD103<sup>+</sup>F4/80<sup>+</sup> cells among CD45<sup>+</sup> cells under the indicated culture conditions (biological triplicates in each condition). (J) *In vivo* FACS analysis of the percentage of CD103<sup>+</sup>F4/80<sup>+</sup> cells among CD45<sup>+</sup> cells under the indicated graft and treatment conditions. Each dot represents 1 grafted mouse, 5-6 mice in each group. \*\*P < 0.01, \*\*\*P < 0.001, \*\*\*\*P < 0.0001 The P-values were calculated using Student's t-test with GraphPad Prism.

## Appendix Figure S6



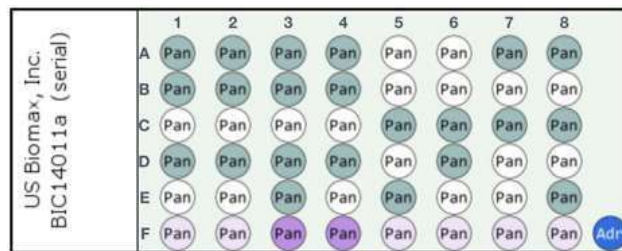
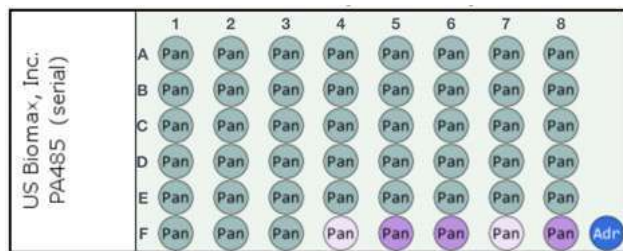
Appendix Figure S6: *In vivo* depletion of Ly6G<sup>+</sup> MDSCs diminishes tumor growth. FACS analysis of the percentage of NKp46<sup>+</sup> cells (A), CD206<sup>+</sup>F4/80<sup>+</sup> cells (B), and Ly6C<sup>+</sup> cells (C). \*\*P < 0.01 and \*\*\* P < 0.001. The P-values were calculated using Student's t-test with GraphPad Prism. (D) Representative IF staining of the implanted tumor graft in Rag2KO mouse for GFP (green), mCherry (red), CK19 (yellow) and DAPI (blue). Scale bar, 50µm. 8 mice in each group, 5 for FACS analysis and 3 for histological analysis. Each dot represents 1 mouse.

# Appendix Figure S7



Appendix Figure S7: Interaction of CD106<sup>+</sup> PeSCs with CD11b<sup>+</sup> myeloid stem cells in the neoplastic microenvironment of PDAC

# Appendix Table S1



No.	Age	Sex	Organ/ Anatomic Site	Pathological diagnosis	TNM	Grade	Stage	Type
A1	68	M	Pancreas	AP	-	-	-	Inf
A2	47	M	Pancreas	AP	-	-	-	Inf
A3	60	M	Pancreas	AP	-	-	-	Inf
A4	44	M	Pancreas	CP	-	-	-	Inf
A5	49	F	Pancreas	CP	-	-	-	Inf
A6	62	M	Pancreas	CP	-	-	-	Inf
A7	40	M	Pancreas	CP	-	-	-	Inf
A8	51	F	Pancreas	CP	-	-	-	Inf
B1	58	M	Pancreas	CP	-	-	-	Inf
B2	47	M	Pancreas	CP	-	-	-	Inf
B3	51	M	Pancreas	RCP	-	-	-	Inf
B4	39	M	Pancreas	RCP	-	-	-	Inf
B5	59	M	Pancreas	RCP	-	-	-	Inf
B6	50	F	Pancreas	RCP	-	-	-	Inf
B7	51	M	Pancreas	RCP	-	-	-	Inf
B8	61	M	Pancreas	RCP	-	-	-	Inf
C1	51	F	Pancreas	RCP	-	-	-	Inf
C2	50	F	Pancreas	RCP	-	-	-	Inf
C3	67	M	Pancreas	RCP	-	-	-	Inf
C4	60	M	Pancreas	RCP	-	-	-	Inf
C5	67	M	Pancreas	RCP	-	-	-	Inf
C6	53	F	Pancreas	RCP	-	-	-	Inf
C7	33	F	Pancreas	RCP	-	-	-	Inf
C8	47	F	Pancreas	RCP	-	-	-	Inf
D1	57	M	Pancreas	RCP	-	-	-	Inf
D2	33	F	Pancreas	RCP	-	-	-	Inf
D3	49	M	Pancreas	RCP	-	-	-	Inf
D4	46	F	Pancreas	RCP	-	-	-	Inf
D5	59	M	Pancreas	RCP	-	-	-	Inf
D6	66	F	Pancreas	RCP	-	-	-	Inf
D7	66	F	Pancreas	RCP	-	-	-	Inf
D8	65	F	Pancreas	RCP	-	-	-	Inf
E1	55	M	Pancreas	RCP	-	-	-	Inf
E2	76	M	Pancreas	RCP	-	-	-	Inf
E3	35	F	Pancreas	RCP	-	-	-	Inf
E4	60	M	Pancreas	RCP	-	-	-	Inf
E5	49	M	Pancreas	RCP	-	-	-	Inf
E6	47	F	Pancreas	RCP	-	-	-	Inf
E7	61	M	Pancreas	RCP	-	-	-	Inf
E8	76	F	Pancreas	RCP	-	-	-	Inf
F1	53	M	Pancreas	RCP	-	-	-	Inf
F2	55	F	Pancreas	RCP	-	-	-	Inf
F3	68	M	Pancreas	RCP	-	-	-	Inf
F4	60	M	Pancreas	PDAC	T2N0M0	2	IB	Mal
F5	49	M	Pancreas	PDAC	T3N0M0	3	II	Mal
F6	47	F	Pancreas	PDAC	T2N0M0	2	IIB	Mal
F7	61	M	Pancreas	PDAC	T2N0M0	2	IB	Mal
F8	76	F	Pancreas	PDAC	T3N0M0	1	I	Mal
-	42	M	Adrenal gland	PCC	-	-	-	Mal

AP = Acute Pancreatitis  
 CP = Chronic Pancreatitis  
 RCP = Reactive Chronic Pancreatitis  
 PCC = Pheochromocytoma  
 Inf = Inflammation  
 Mal = Malignant

<https://www.biomax.us/tissue-arrays/pancreas/PA485>

No.	Age	Sex	Organ/ Anatomic Site	Pathologica l diagnosis	TMN	Grade	Stage	Type
A1	42	M	Pancreas	CP	-	-	-	Inf
A2	42	M	Pancreas	CP	-	-	-	Inf
A3	50	F	Pancreas	CP	-	-	-	Inf
A4	50	F	Pancreas	CP	-	-	-	Inf
A5	66	F	Pancreas	PanIN2	-	-	-	PanIN
A6	66	F	Pancreas	PanIN2	-	-	-	PanIN
A7	70	F	Pancreas	CP	-	-	-	Inf
A8	70	F	Pancreas	CP	-	-	-	Inf
B1	51	M	Pancreas	CP	-	-	-	Inf
B2	51	M	Pancreas	CP	-	-	-	Inf
B3	57	M	Pancreas	CP	-	-	-	Inf
B4	57	M	Pancreas	CP	-	-	-	Inf
B5	33	F	Pancreas	PanIN1	-	-	-	PanIN
B6	33	F	Pancreas	PanIN1	-	-	-	PanIN
B7	44	M	Pancreas	PanIN1	-	-	-	PanIN
B8	44	M	Pancreas	PanIN1	-	-	-	PanIN
C1	53	M	Pancreas	PanIN1	-	-	-	PanIN
C2	53	M	Pancreas	PanIN1	-	-	-	PanIN
C3	51	F	Pancreas	PanIN1	-	-	-	PanIN
C4	51	F	Pancreas	PanIN1	-	-	-	PanIN
C5	51	M	Pancreas	CP	-	-	-	Inf
C6	51	M	Pancreas	CP	-	-	-	Inf
C7	55	F	Pancreas	CP	-	-	-	Inf
C8	55	F	Pancreas	CP	-	-	-	Inf
D1	53	M	Pancreas	CP	-	-	-	Inf
D2	53	M	Pancreas	CP	-	-	-	Inf
D3	67	M	Pancreas	CP	-	-	-	Inf
D4	67	M	Pancreas	CP	-	-	-	Inf
D5	73	F	Pancreas	PanIN1	-	-	-	PanIN
D6	73	F	Pancreas	CP	-	-	-	Inf
D7	65	M	Pancreas	PanIN2	-	-	-	PanIN
D8	65	M	Pancreas	PanIN2	-	-	-	PanIN
E1	64	M	Pancreas	PanIN2	-	-	-	PanIN
E2	64	M	Pancreas	PanIN2	-	-	-	PanIN
E3	76	M	Pancreas	CP	-	-	-	Inf
E4	76	M	Pancreas	PanIN1	-	-	-	PanIN
E5	15	F	Pancreas	CP	-	-	-	Inf
E6	15	F	Pancreas	PanIN2	-	-	-	PanIN
E7	55	F	Pancreas	PanIN2	-	-	-	PanIN
E8	55	F	Pancreas	CP	-	-	-	Inf
F1	54	F	Pancreas	PDAC	T2N0M0	1	I	Mal
F2	54	F	Pancreas	PDAC	T2N0M0	1	I	Mal
F3	51	M	Pancreas	PDAC	T3N1M0	1	IIB	Mal
F4	51	M	Pancreas	PDAC	T3N1M0	1	IIB	Mal
F5	68	F	Pancreas	PDAC	T2N0M0	2	IB	Mal
F6	68	F	Pancreas	PDAC	T2N0M0	2	IB	Mal
F7	55	F	Pancreas	PDAC	T2N0M0	2	IB	Mal
F8	55	F	Pancreas	PDAC	T2N0M0	-	IB	Mal
-	42	M	Adrenal gland	PCC	-	-	-	Mal

PanIN = Pancreatic Intraepithelial Neoplasia  
 PDAC = Pancreatic Duct Adenocarcinoma

<https://www.biomax.us/tissue-arrays/pancreas/BIC14011a>

Appendix Table S1: TMA characteristics.

## II. CD169<sup>+</sup> macrophages orchestrate immune reaction and matrix deposition in pancreatic cancer.

The following study is originated from the part 1 given that we questioned the role of PeSC and macrophages communication. This study was part of my whole PhD and is under reviewing in Cancer Immunology Research. I participated in the conceptualization of the experiments, writing the original draft, *in vitro*, *ex-vivo* and *in vivo* analysis. All *in-silico* analysis were performed in collaboration with Dr. Hernandez-Vargas.

Based on our previous results showing that PeSC establish a communication with freshly recruited CD11b<sup>+</sup> monocytes to promote MDSC accumulation, we questioned whether PeSC could shape other myeloid cells: macrophages. Macrophages represent one of the most prominent immune populations in PDAC TME. They are usually considered to be pro-tumoral as they integrate an accumulation of signals that are send by other actors in the TME. We therefore decided to study the cellular niche between macrophages and other cell types in PDAC independently of macrophages origin.

We observed that CD106<sup>+</sup> PeSC were capable of shaping macrophages phenotype defined by the expression of CD169, CD206, PD-L1 and Arg1. We showed *ex vivo* that CD169<sup>+</sup> macrophages expressing tumour associated macrophages markers (CD206 and CD163) are found in both PanIN and PDAC murine model. This observation was confirmed in human by single cell RNAseq analysis using published data set of PDAC patients. Functionally, we showed that PeSC-educated macrophages were capable of releasing  $\beta$ ig-h3 to activate CXCL12 secretion from PeSC and inactivate CD8 T cells. Finally, we showed *in vivo* that CD169<sup>+</sup> depletion impairs both CD8 and CD4 T cells recruitment. Additionally, CD169<sup>+</sup> macrophages depletion was associated with a significant decrease of the tumour weight and a total reshaping of the TME by impacting both cellular (CD31<sup>+</sup> endothelial cells, PDPN<sup>+</sup> CAFs) and acellular components ( $\beta$ ig-h3 and collagen deposition).

This work may open new therapeutic avenue given that we demonstrated that cellular niche found in other disease and/or at steady state in other tissues can be found in pancreatic cancer tissue.

**(See submitted paper next page)**

# CD169<sup>+</sup> macrophages orchestrate immune reaction and matrix deposition in pancreatic cancer

Kevin Thierry<sup>1,2,3\*</sup>, Zhichong Wu<sup>1,2,3\*</sup>, Sophie Bachy<sup>1,2,3</sup>, Pia Gamradt<sup>1,2,3</sup>, Hector Hernandez-Vargas<sup>1,2,3</sup> and Ana Hennino<sup>1,2,3</sup>

<sup>1</sup>Cancer Research Center of Lyon, UMR INSERM 1052, CNRS 5286, Lyon, F-69373, France

<sup>2</sup>Université Lyon 1, Lyon, F-69000, France

<sup>3</sup>Centre Léon Bérard, Lyon, F-69008, France

\* Equally contributed to this work

SB, HHV and AH are employees of StromaCare. Other authors declare no potential conflicts of interest.

**Correspondence:** Ana Hennino, 28 rue Laennec, Lyon 69008 France; Tel: +33469166669, E-mail: [ana.hennino@inserm.fr](mailto:ana.hennino@inserm.fr)

## A. Summary

Macrophages are an important component of the tumor microenvironment in pancreatic cancer. We identified that CD169<sup>+</sup> macrophages were very abundant in pancreatic cancer in human and mice settings. We described previously the identification of a pericyte stem cells (PeSC) population with immunosuppressive properties. We show here that PeSC were able to polarize macrophages CD11b<sup>+</sup>F4/80<sup>+</sup> towards an immunosuppressive phenotype expressing CD169. CD169<sup>+</sup> macrophages were able to produce large amounts of stromal big-h3/TGFBI that directly stimulated CXCL12 production by PeSC that attracted CD8<sup>+</sup> T cells. Invalidation of CD169 by a DTR-approach in orthotopic pancreatic cancer model led to diminished matrix deposition and CD8<sup>+</sup> T cell infiltration cells within the tumor microenvironment. These data suggest that CD169 macrophages play an important role in sustaining the stromal reaction in pancreatic cancer.

## B. Material and methods

### Mice

All male and female mice p48-Cre;LSL-Kras<sup>G12D</sup>,Acvr1b<sup>flox/flox</sup> (4KC), Pdx1-Cre; LSL-Kras<sup>G12D</sup>;Ink4a/Arf<sup>flox/flox</sup> (KIC) and Pdx1-Cre;LSL-Kras<sup>G12D</sup>;LSL-Trp53<sup>R172H</sup> (KPC) Siglec1<sup>tm1(HBEGF)Mtk</sup> (CD169<sup>DTR</sup>)<sup>1-4</sup> were bred and maintained in the Cancer Research Center of Lyon mouse facility (P-PAC, Lyon, France) under specific pathogen free conditions and a 12 hours light/12hours dark cycle; water and food were available ad libitum. C57BL/6J mice (6 weeks of age) were purchased from Charles River Laboratories (L'Arbresle, France). In all experiments, mice were sacrificed by cervical dislocation. All experimental procedures were performed according to the European Community rules on animal care with permission and ethical approval from the local institutional review board (Comité Régional d'Ethique sur l'Expérimentation Animale CECCAPP) and the French Authorities (APAFIS #35125-2022020214089191)

### Cell lines and macrophages differentiation

PeSC and TC primary cell line were generated as previously described<sup>5</sup>. All incubations were carried out at 37°C in a 5% CO<sub>2</sub> atmosphere using DMEM (10% FCS, 1% penicillin/streptomycin) (Gibco). Femur and tibia were obtained from C57BL6 mice, the bone marrow was flushed and bone marrow derived cells (BMDC) (B were cultured using 80%DMEM+ 20% of L929 cell line (ATCC #CCL-1) supernatant containing M-CSF for 7 days. Co-culture experiments were performed in a 96-well plate. In each well, 5x10<sup>3</sup> previously mitomycin (10µg/mL) treated PeSC or TC were incubated with 1x10<sup>5</sup> BMDC. After 48 hours, cells were harvested and stain for flow cytometer analysis. Supernatant were stored at -20°C for ELISA analysis. For qRT-PCR experiments, 3.3x10<sup>4</sup> PeSC and/or TC were co-cultured with 10x10<sup>6</sup> Bone marrow derived macrophages cells (BMDM). For βig-h3 PeSC stimulation, recombinant protein was added at different timepoint in culture media.

### Single Cell analysis

Single cell analysis were performed using a scRNAseq dataset specific for pancreas that was recently compiled (Chijimatsu et al., 2022). The dataset is comprising over 70 samples and > 130.000 cells, most of them from cancer samples (> 110.000 cells). The dataset was normalized and quality controlled.

### DT treatment

Mice were treated with 10µg/kg of diphtheria toxin (Sigma, D2918) or 1x PBS by intra-peritoneal injection 24 hours before surgical day and every 4 days after surgical procedures.

### CD8+ T cell proliferation assay

Spleen and lymph node were harvested from C57Bl6, or PD-1 KO mice. Both organs were filtered through a 100µm cell strainer (VWR). Blood cell lysis was performed by incubating cells for 3 minutes in NH<sub>4</sub> (concentration). Cells were counted and incubated 15 minutes at 4°C in the dark with anti-CD8 microbeads (CD8a (Ly-2) MicroBeads, mouse, miltenyi 130-117-044) to further perform a magnetic-activated cell sorting (MACS). MACS were performed using magnetic column (MS Columns miltenyi 130-042-201). Cells were then stained with CFSE as described by the manufacturer. CD8 purified cells were then mixed with CD3/CD28 beads (ThermoFisher, 11452D) and plate with or without macrophages and or TC and or PeSC in an 8:1 ratio (T:M) for 48hours.

### **Transwell assay**

Transwell permeable support of 6,5mm insert composed of 5.0µm polycarbonate membrane (Corning) were used to perform cell attraction assay. PeSC alone or co-cultured with BMDM were incubated for 48h in the lower wells, Mesenteric lymph nodes of 6 weeks old C57Bl6 were harvested and filtered using a 100µm cell strainer. Cells were then stained with CFSE according to the manufacturer.  $8 \times 10^4$  cells were incubated for 4 hours in the upper wells. Cells in the lower well were harvested and CFSE<sup>+</sup> cells were counted using flow cytometer.

### **ELISA**

ELISA assays were performed on co-cultured cells supernatant. The level of βig-h3 and CXCL12 (SDF-1) were determined by using Mouse beta IG-H3 DuoSet ELISA kit (R&D systems and LEGEND MAX™ Mouse CXCL12 (SDF-1β) ELISA Kit (Biolegend®), respectively, according to the manufacturer's instructions.

### **Orthotopic injection**

24 hours before surgical procedures, mice were shaved at the upper quadrant. 30 minutes before the surgical procedure, mice were given buprenorphine subcutaneously (0.1mg/kg). Mice were put under anesthesia using 4% isoflurane for induction and 2.5% isoflurane for maintenance. By performing a laparotomy at the upper quadrant with an 1cm wide incision, pancreas was injected with 30µl of cells mixed with 50% of matrigel (Corning, 354248). Peritoneal muscle was sutured using a Ethibond® non-absorbable braided suture, 3/0 (Ethicon, X31037), skin was sutured using Ethibond® non-absorbable braided suture, 4/0 (Ethicon, E6943H). Mice were weighted once a week and sacrificed after 10 or 30 days. Both pancreatic tumor and spleen were weighted, mesenteric lymph node were harvested for further analysis.

## qPCR

RNA was extracted from pelleted cells issued from different conditions using RNeasy kits according to the manufacturer's instructions (Qiagen, Valencia, USA). RNA concentrations were determined using a nanodrop spectrophotometer (Thermo Scientific) and reverse transcription (RT) was assessed using equivalent quantities of extracted RNAs (> 8µg). The obtained cDNA was used to perform quantitative polymerase chain reaction (qPCR) analysis with Power SYBR® Master Mix (Life Technologies) with the following primer sequences:

<b>Table 1. qPCR primers</b>		
<i>Genes</i>	Forward	Reverse
<i>Hprt</i>	5' TGA CAC TGG CAA AAC AAT GCA 3'	5'GGT CCT TTT CAC CAG CAA GCT 3'
<i>Sdf-1</i>	5' CGCCAAGGTCGTCGCCG 3'	5' CGCCAAGGTCGTCGCCG 3'
Hprt Hypoxanthine Phosphoribosyl transferase 1, Sdf-1 stromal cell-derived factor 1		

## Immunofluorescence staining

Mouse pancreata, spleen and lymph node were snap freeze in liquid nitrogen. Sample were embedded in optimal cutting temperature (OCT) to perform cryosection using a Cryostat (NX50, Leica). 8 to 10µm thick section were sectioned and then stored at -80°C. Cryosection were fixed with 4% PFA for 5min, permeabilized with 0.2% Triton for 5 min and blocked with a blocking reagent (Invitrogen, 003118). Cryosection were incubated with directly coupled antibodies or primary antibodies overnight at 4°C in a wet chamber. Secondary antibodies were added for 2h at room temperature. Each section was mounted with Vectashield mounting (VECTASHIELD, H-1900). Cryosection were imaged using a LSM-880 or -980 (Zeiss) microscope with a plan-apochromat 20x objective. Individual images resolution can be found in the supplementary methods.

Table 2.		IF antibodies		
Specificity	Clone	Host/Isotype	Producer	Reference
CD206	Polyclonal	Goat/IgG	R&D Systems	AF2535
CD169	3D6.112	Rat/ IgG2ak	Biologend	142419
F4/80	BM8	Rat/ IgG2ak	Biologend	123140
CXCL12	79018	Mouse / IgG	R&D Systems	MAB350
a-amylase	Polyclonal	Rabbit	Sigma	A8273
VCAM1	EPR5047	Rabbit	Abcam	ab134047
CD3e	145-2C11	Armenia hamster/IgG	Biologend	100302
DAPI	N/A	N/A	ThermoFisher	D1306

### Flow cytometry analysis

For *in vitro* analysis, cells were harvested and incubated with staining antibodies for 20 at 4°C protected from light. Intracellular staining was performed using Cytofix/Cytoperm solution (BD, 554722). Cells were fixed with 0.4% PFA at 4°C for 20minutes and then stored in flow cytometer buffer at 4°C protected from light until data acquisition.

For *in vivo* analysis, pancreatic tumor or pancreas were harvested to be both mechanically and enzymatically dissociated by incubating chopped pancreas with collagenase (10mg/mL, Roche) at 37°C for 30min. Pancreata was filtered into 100µm cell strainer (VWR) to obtain single cell suspension. Live cells were stained following manufacturer's instructions (Biologend, 423113). Cells were then incubated with surface staining antibodies for 20min at 4°C protected from light. If necessary, cells were then permeabilized using cytofix/cytoperm kit and incubated with intracellular staining antibodies for 20min at 4°C protected from light.

<b>Table 3.</b>		<b>FACS antibodies</b>		
<b>Specificity</b>	<b>Clone</b>	<b>Fluorochrome</b>	<b>Producer</b>	<b>Reference</b>
<b>CD11b</b>	M1/70	PerCP	Biolegend	101229
<b>CD45</b>	30-F11	APC/Cy7	Biolegend	103116
<b>CD206</b>	C068C2	Bv650/Bv605	Biolegend	141721
<b>CD169</b>	3D6.112	Bv421	Biolegend	142421
<b>CD163</b>	TNKUPJ	PE	ThermoFisher	12-1631-82
<b>CD69</b>	H1.2F3	PerCP-Cy5.5	BD Biosciences	551113
<b>MHC-II</b>	M5/114.15.2	PE	ThermoFisher	12-5321-81
<b>TIM4</b>	RMT4654	APC	Biolegend	130008
<b>LAP-TGFβ</b>	TW7-16B4	Bv421	Biolegend	141408
<b>F4/80</b>	BM8	PECy7	Biolegend	123114
<b>CD8a</b>	53-6.7	Bv421	Biolegend	100738
<b>PD-L1</b>	10F.9G2	PerCP-Cy5.5	Biolegend	124334
<b>Ly6G</b>	1A8	AF700	Biolegend	127622
<b>CD184 (CXCR4)</b>	L276F12	PE	Biolegend	146506
<b>Zombie Violet</b>	N/A	BV421	Biolegend	423113
<b>CD8β</b>	30-F11	APC	Biolegend	140410
<b>CD4</b>	RM4-5	Bv510	Biolegend	100553
<b>IFNγ</b>	XMG1.2	Bv650	Biolegend	505831
<b>Granzyme B</b>	16G6	Biotin	ThermoFisher	13-8822-80
<b>Arginase 1</b>	Polyclonal	APC	R&D Systems	IC5868A
<b>Streptavidin</b>	N/A	PE	Biolegend	405203

Data were acquired using a BD Fortessa Flow Cytometer (BD Biosciences) and analysed using either BD FACS Diva software v5.0.1 or FlowJo (Tree Star, Inc).

## Immunohistochemistry staining (IHC)

FFPE mouse tumor were sectioned between 4 and 5  $\mu\text{m}$  using a microtome (Micro Microtech, HM 340E). Samples were rehydrated by heating slides at 55°C for 30 minutes, two baths of xylene (Sigma, 214736) and successive ethanol bath (100%, 95%, 70%, 0%). Endogenous peroxidase was inactivated with a 3% H<sub>2</sub>O<sub>2</sub> incubation for 30 at room temperature. IHC staining were performed following a heat mediated antigen retrieval using an antigen-unmasking solution (Vector Laboratories, H-3300). The sections were incubated with a blocking reagent (Invitrogen, 003118) for 1 hour at room temperature and incubating at 4°C with suitable primary antibodies overnight in a wet chamber. Next, the sections were incubated with biotinylated secondary antibodies for 1 h at room temperature. IHC staining was visualized using 3,3'-diaminobenzidine (Vector Laboratories, SK-4100) and the sections were counterstained with hematoxylin (DiaPath, C0303). IHC was imaged using a Carl Zeiss microscope Axioscan 7 with a x20 objective. Qupath (0.4) imaging software was used for visualization and analysis of IHC staining. Analysis parameter can be found in the supplementary methods table. The following antibodies have been used for IHC staining;

Specificity	Clone	Host/Isotype	Producer	Reference
Arg1	Polyclonal	Rabbit/IgG	GeneTex	GTX109242
GFP	Polyclonal	Goat/IgG	Abcam	ab6673
mCherry	Polyclonal	Rabbit/IgG	Abcam	ab167453
Collagen 1	3G3	Mouse/IgG3	Abcam	ab88147
$\alpha$ -SMA	Polyclonal	Rabbit/IgG	GeneTex	GTX100034
$\beta$ ig-h3	Polyclonal	Rabbit/IgG	Sigma-Aldrich	HPA008612
CD3e	145-2C11	Armenia hamster/IgG	Biolegend	100302
DAPI	N/A	N/A	ThermoFisher	D1306

## Statistical analysis

P values were calculated using Student's t-test or One-way anova and Tukey's multiple comparisons test (GraphPad Prism 9.5.1) as indicated in the figure legends. \*P<0.05; \*\*p<0.01; \*\*\*P<0.001 and \*\*\*\*p<0.0001.

## C. Introduction

Despite major findings in the field of immunotherapy during the past 20 years<sup>6</sup>, pancreatic cancer is listed among the cancers where immunotherapy showed no efficiency<sup>7,8</sup>. Many studies revealed that immunotherapy failure in pancreatic cancer can be explained by a variety of reasons such as desmoplasia and immune suppression occurring in the tumor microenvironment (TME)<sup>9</sup>. Macrophages and T lymphocyte are the most abundant immune cells in the TME alongside mesenchymal-derived cells (CAFs, Pericyte) for non-immune cells<sup>10,11</sup>. On one hand, T lymphocytes are infiltrated within the tissue but excluded from the tumor and are not effective to eliminate the tumor<sup>12,13</sup>. On the other hand, both recruited and resident macrophages are infiltrated in the tumor and play numerous roles in fibrosis and immune modulation<sup>14</sup>. CD169<sup>+</sup> macrophages are a subset of tissue-resident macrophages that express the marker of CD169, also known as sialoadhesin or Siglec-1. Several roles have been described for CD169<sup>+</sup> macrophages (e.g., modulating hematopoietic stem cell niche, regulating apoptotic cell clearance)<sup>4,15</sup>. CD169<sup>+</sup> macrophages play different roles in cancer progression. Specifically, resident CD169<sup>+</sup> macrophages have been shown to support tumor growth in non-small cell lung carcinoma and breast cancer<sup>16-18</sup> but to have an anti-tumoral role in glioblastoma<sup>19</sup>. However, up to date, there is currently no assigned function of CD169<sup>+</sup> macrophages in pancreatic cancer. On top of that, CAFs and/or macrophages can secrete extracellular matrix deposit to develop the desmoplasia within the TME. While type I collagen from  $\alpha$ SMA<sup>+</sup> cells has been shown to protect the tissue<sup>20</sup>, collagen is generally assumed to play a role in tumor development. Recently, we characterized a mesenchymal-derived cell called pericyte stem cell (PeSC)<sup>5</sup>. Given the data that we accumulated showing the communication between PeSC and CD11b<sup>+</sup> cells as well as the plasticity of intra-tumoral macrophages<sup>21</sup>, we hypothesized that PeSC were reprogramming macrophages in a specific subtype. Several reports revealed the importance of macrophages reprogramming in pancreatic cancer<sup>11,22</sup>. Therefore, understanding the communication leading to pro or anti-tumoral macrophages may be the keystone to unleash the potential of immunotherapy in pancreatic cancer. To this end, we generated a co-culture model between PeSC and macrophages as well as an *in vivo* orthotopic model of tumor development. We show that CD169<sup>+</sup> macrophages that are present in both human and murine model PDAC and neoplasia can be polarized by PeSC to express CD169<sup>+</sup> and induce CXCL12 secretion by PeSC allowing T lymphocytes recruitment. Finally, we show that *in vivo* CD169<sup>+</sup> macrophages depletion is significantly reducing stroma development.

## D. Results

### **CD169 macrophages are highly expressed in both human and mouse pancreatic cancer**

First, we evaluated the expression of *siglec1* gene in normal pancreas and in primary tumor by comparing TCGA and GTEX data bases. We detected a significant increase of the *siglec1* transcript in primary tumors in pancreas (**Fig. 1a**). Next, we determine which cell population specifically expressed CD169 in pancreatic cancer. Therefore, we analysed a pancreas specific scRNAseq dataset that was recently compiled<sup>10</sup>, comprising over 70 samples and > 130.000 cells, most of them from cancer samples (> 110.000 cells). *Siglec1* expression was solely limited to a fraction of macrophage cluster (**Fig 1b, Supplementary Fig. 1a**). Approximately 23k cells were present in the macrophage cluster. These cells were taken for further unsupervised clustering, resulting in 9 different sub-clusters (**Fig. 1c**), most of them represented in the non-tumor samples (**Supplementary Fig. 1b and Supplementary Table 1**). We applied a 37-genes signature that was previously published defining tumor associated macrophages (TAMs) in breast cancer<sup>18</sup> to the 9 sub-cluster representation. We observed that the TAMs score had the highest intensity in cluster 0 (**Fig. 1d**). This cluster expressed CD169 as well as other known TAM markers as CD68 and CD163 (**Fig. 1e-g**). In attempt to place CD169<sup>+</sup> macrophages in the spectrum of macrophages polarization we looked for the expression of *siglec1* in M0, M1 and M2 macrophages in different solid cancers (**Supplementary Fig. 1c**). We found that *siglec1* was mainly expressed by defined M2 macrophages across different cancers, but also that *siglec1* was positively correlated to known TAMs markers namely *mrc1* and *cd163* (**Supplementary Fig. 1d, e**) in human pancreatic cancer. Next, we determined the localization of CD169<sup>+</sup> macrophages in human PDAC and neoplastic sections by performing immunohistochemistry staining. In PDAC lesions, CD169 was highly expressed in the stroma of tumor (**Fig. 1h**). In neoplastic lesions, the majority of the CD169 staining was localized around the blood vessels (**Fig. 1h**). We aimed to determine if CD169<sup>+</sup> macrophages were also present in pancreatic tumor and neoplasia mouse model based on the expression of *Kras*<sup>G12D 2,23</sup>. We confirmed that CD169<sup>+</sup> macrophages are present in both PDAC and neoplasia of mouse model (**Fig. 1i**). More importantly, we determined by immunofluorescence on tissue section that F4/80<sup>+</sup> CD169<sup>+</sup>CD206<sup>+</sup> macrophages infiltrated the tumoral bed (**Fig. 1j**) and particularly in the stroma close to transforming acini going through acinar to ductal metaplasia (ADM). We confirmed this observation by analysing WT and 4KC mouse pancreata by flow cytometry. We noticed that 4KC mouse pancreata were infiltrated in a higher proportion by CD169<sup>+</sup> macrophages than WT mice (**Fig. 1k**). This might indicate that CD169<sup>+</sup> TAMs in 4KC could be a resident population differentiating from CD169<sup>+</sup> macrophages in WT mice by acquiring CD206 and/or CD163 (**Supplementary Fig. 1f-j**). Altogether, these findings suggest that CD169<sup>+</sup> macrophages are eminently expressed in human and mouse pancreatic cancer and neoplastic stroma.

### Pericyte stem cells induce CD169 expression on macrophages

The localization of CD169<sup>+</sup> macrophages around blood vessel was reminiscent of a previously identified cell population of pericyte stem cells (PeSC)<sup>5</sup>. We previously reported that CD106<sup>+</sup> PeSC were able to structure blood vessels in early pancreatic cancer lesions. Hence, we stained for both CD169 and CD106 population and showed a closed vicinity between the 2 cell types in mouse model (**Fig. 2a**).

Macrophages and mesenchymal-derived cells such as fibroblasts, stem cells or pericytes are known to communicate with each other through cell-cell interaction in pancreatic cancer and other diseases<sup>24</sup>. Since we detected the presence of macrophages in proximity to PeSC in mouse pancreatic cancer, we sought to determine if the macrophage's phenotype was dependent on PeSCs presence. To this purpose, we generated BMDM as previously described<sup>25</sup> and co-cultured them with PeSC. In the presence of PeSC, we documented that F4/80<sup>+</sup> macrophages downregulated MHC-cIII and CD107a (**Fig. 2b, c**) suggesting a lower antigen-presentation capacity. Subsequently, we showed that macrophages upregulated the expression of Arg1, CD206, PD-L1 and CD169 (**Fig. 2d-g**). These results suggest that PeSC induced polarization of macrophages towards a CD169<sup>+</sup> phenotype with M2-like features. We could not replicate these observations when macrophages were cultured with conditioned media generated from PeSC (**Supplementary Fig. 2a**), illustrating that cell-cell interaction is mandatory for the macrophage polarization. In summary, we confirmed our *ex vivo* findings showing that CD169<sup>+</sup> macrophages express M2-like markers and that PeSC were able to drive this phenotype in a cell-contact manner.

### PeSC-CD169<sup>+</sup> macrophage crosstalk induces big-h3 and CXCL12 production

Although this communication may be true, we proposed that it was not limited to a one-way exchange. It has been reported that TAMs were adept of secreting extracellular matrix cues in various cancer types<sup>21</sup>. We recently illustrated that TAMs secreted the immunosuppressive protein big-h3 (Tgfbi) in ovarian cancer<sup>26</sup>. This discovery was also confirmed in glioblastoma<sup>27</sup>. In pancreas, we showed that big-h3 can be found in the stroma of early and late human PDAC and was secreted by CAFs<sup>28</sup>. In line with these findings, we checked for *tgfbi* expression in macrophages using the human pancreas scRNAseq dataset<sup>10</sup>. Our results indicate that *tgfbi* was expressed in the same cluster as *siglec1* (**Fig. 3a**). We also observed that *tgfbi* was mainly expressed in defined M2 macrophages in PDAC supporting a perhaps pro-tumoral role of this population (**Supplementary Fig. 3a**). Consequently, we hypothesized that PeSC–macrophages communication resulted in big-h3 secretion by macrophages. To this end, we quantified the release of big-h3 in the supernatant of PeSC–macrophages coculture. Both PeSC and macrophage released a limited amount of big-h3 when cultured separately (**Fig. 3b**). In co-culture condition, a significant increased production of big-h3 was detected (**Fig. 3b**). At **steady** state

conditions, CD169<sup>+</sup> macrophages–stromal stem cell communication has been investigated in the bone marrow<sup>15</sup>. The authors showed that CD169<sup>+</sup> macrophages were activating stromal stem cell to secrete CXCL12 to retain hematopoietic stem cell through an un-identified protein factor<sup>15</sup>. Therefore, we measured the level of released CXCL12 in the supernatant of PeSC-macrophages coculture. Similar to big-h3 level, CXCL12 level was relatively low when macrophages and PeSC were cultured separately although PeSC were found to secrete CXCL12 in a greater amount than macrophages (**Fig. 3c**), confirming the mesenchymal source of CXCL12<sup>29</sup>. CXCL12 released was significantly higher when both PeSC and macrophages were cultured together (**Fig. 3c**). To verify if CXCL12 and big-h3 releasing was connected, we stimulated PeSC with recombinant  $\beta$ ig-h3 (r $\beta$ ig-h3) protein. Consequently, a similar level of CXCL12 was observed between stimulated PeSC and the coculture (**Fig. 3c**), indicating that  $\beta$ ig-h3 release may promote CXCL12 secretion from PeSC. To ensure that  $\beta$ ig-h3 was responsible for CXCL12 secretion by PeSC, we stimulated PeSC kinetic wise with r $\beta$ ig-h3 and quantified CXCL12 transcript *sdf-1*. We noticed that *sdf-1* transcript was significantly expressed following 30 minutes of stimulation with r $\beta$ ig-h3 and was maintained up to 3 hours of stimulation compared to unstimulated PeSC (**Fig. 3d**). Furthermore, we confirmed that  $\beta$ ig-h3 was inducing CXCL12 release from PeSC in a dose-response manner (**Fig. 3e**). Altogether, our observations support that macrophages and PeSC upon interaction release a large amount of  $\beta$ ig-h3 and CXCL12, respectively. Next, we evaluated the relevance of this finding *ex vivo*. We checked the localisation of  $\beta$ ig-h3 and CD169<sup>+</sup> macrophages in mouse pancreatic cancer. As shown in **Fig. 3f**,  $\beta$ ig-h3 is closely localized near CD169<sup>+</sup> CD206<sup>+</sup> confirming our *in vitro* results. A similar observation was made by staining CXCL12 and CD169<sup>+</sup> macrophages (**Fig. 3f**). Since CXCL12 was described to attract CXCR4 positive lymphocytes<sup>15</sup>, we investigated the potential migration of CD8<sup>+</sup> T cells upon PeSC–macrophages interaction. To explore this hypothesis, we used Boyden chambers in which we incubated in the lower chamber either macrophages and PeSC separately or cocultured. We incubated in the upper chamber CFSE stained CD8<sup>+</sup> T cell (**Fig. 3g**). We measured the number of migrating CD8<sup>+</sup> T cells in the lower chamber and observed a significant fold increased migration in the coculture condition compared to macrophages or PeSC cultured separately (**Fig. 3h**). This data suggests that PeSC-macrophage communication impact the recruitment of CD8<sup>+</sup> T cells through CXCL12 secretion.

Next, we investigated if PeSC-instructed macrophages impacted the proliferation and activation of CD8<sup>+</sup> T cell beside the recruitment. Since CD169<sup>+</sup> displayed increased PD-L1 expression, we tested whether the impact of PeSC instructed macrophages on the proliferation and activation of CD8<sup>+</sup> T cells was dependent on PD-1/PD-L1 axis. To that purpose, magnetically WT or PD-1 KO purified CD8<sup>+</sup> T cells were cultured with PeSC instructed macrophages and activated with anti-CD3/CD28 beads (**Fig. 3i**). On one hand, we noticed that CD8<sup>+</sup> T cells proliferated similarly in the presence of PeSC and macrophages in PD-1 WT or KO condition (**Fig. 3j**). On the other hand, we depicted a lower activation status in PD-

1WT CD8<sup>+</sup> T cells as they maintained both CD62L and CD69 expression through the division in contrast to PD-1KO CD8<sup>+</sup> T cells that escaped PeSC-instructed macrophages inhibition (**Fig. 3 k-n**). Consequently, these results suggest that PeSC–macrophages communication leads to CD8<sup>+</sup> T cell attraction and activation inhibition through PD1-PD-L1 axis.

### **CD169<sup>+</sup> macrophages are mandatory for CD8<sup>+</sup> T cell recruitment**

Since our *in vitro* data showed that PeSCs potentiated the emergence of CD169<sup>+</sup> macrophages, we subsequently sought to investigate the impact of PeSCs – macrophages communication *in vivo*. To explore this issue, we orthotopically injected tumor cells alone (TC)<sup>5</sup> or in the presence of PeSCs (TC+PeSC) at a 1:1 ratio in C57Bl6 recipient mice. The co-injection TC+PeSC led to increased tumor weight (**Supplementary Fig. 4a**) and accumulation of Ly6G<sup>+</sup> population (**Supplementary Fig. 4b, c**) compared to TC injection alone as previously described in subcutaneous context<sup>5</sup>. More importantly, we detected an increased level of CD169<sup>+</sup> macrophages in tumoral tissue when both TC and PeSC were injected (**Supplementary Fig. 4b**). These data demonstrates that PeSC may induced CD169 expression on macrophages *in vivo*. Additionally, we investigated the question of CD169<sup>+</sup> macrophages role in tumor progression by taking advantage of CD169<sup>DTR</sup> mice. This model allows the specific depletion of CD169<sup>+</sup> macrophages but preserve dendritic cells and other myeloid populations<sup>4</sup>. Therefore, we orthotopically co-injected TC and PeSC in diphtheria toxin (DT) treated or untreated CD169<sup>DTR</sup> mice (**Fig. 4a**). To better understand the model, we evaluated the efficiency of CD169<sup>+</sup> macrophages depletion from DT treatment. DT treatment significantly depleted CD169<sup>+</sup> macrophages in the pancreas after 2 days. Kinetically wise, we detected a re-emergence of CD169<sup>+</sup> macrophages around day 9 after treatment (**Supplementary Fig. 4d**). DT treatment was also efficient in cancer condition as we barely detected F4/80<sup>+</sup>CD169<sup>+</sup> macrophages in the tumoral, splenic and lymphoid tissue compared to untreated mice (**Supplementary Fig. 4g, h**).

First, we show that the amount of hematopoietic cell stained by CD45<sup>+</sup> was equivalent in both conditions (control and depleted) in tumoral tissue (**Fig. 4b**) and secondary lymphoid organ (**Supplementary Fig. 4i**). Specifically, the percentage of F4/80<sup>+</sup> macrophages was reduced in depleted condition in tumor (**Fig. 4c**) but not in secondary lymphoid organ (**Supplementary Fig. 4j**) emphasizing the fact that the DT treatment solely depleted CD169<sup>+</sup> macrophages rather than all macrophages. In the meantime, F4/80<sup>+</sup>CD206<sup>+</sup> macrophages were significantly reduced (**Fig. 4d**) confirming our previous observations that CD169 is mainly co-expressed with CD206. These macrophages expressed reduced MHC-cl II molecules on their surface (**Fig. 4e**) although the treatment did not show differences of Arginase 1 expression compared to control (**Supplementary Fig. 4l, m**). Concomitantly, we observed increased proportions of Ly6G<sup>+</sup> cells in depleted conditions compared to control one in tumoral tissue (**Fig. 4f**) and secondary lymphoid organ (**Supplementary Fig. 4n**). We next evaluated the proportions of CD8<sup>+</sup> and CD4<sup>+</sup> T cells among CD45<sup>+</sup> hematopoietic cells. We pinpointed a significant reduction of

CD8 $\beta$ <sup>+</sup> T lymphocytes infiltration within the tumor microenvironment (**Fig. 4g, h**) as well as CD4<sup>+</sup> T lymphocytes in treated condition (**Fig. 4i**). However, we observed an increased level of CD8 $\beta$ <sup>+</sup> cells in the lymph nodes in depleted condition (**Supplementary Fig. 4p**) suggesting that priming of T cells occurs but there a default of migration towards the tumor site. We further evaluated their functional capacity (e.g.: cytotoxic activities) *in situ*. Both IFN $\gamma$ <sup>+</sup> and GrZB<sup>+</sup> CD8 $\beta$ <sup>+</sup> levels were similar in control and depleted conditions (**Fig. 4j-m**). Given the role of macrophages in shaping the extracellular matrix in both PDAC<sup>14</sup> and other diseases, we analysed by IHC staining tumoral tissue of control and depleted mice. We detected more GFP<sup>+</sup> cells (i.e.: cancer cells) in depleted condition than in control (**Fig. 5a**) (**Supplementary Fig. 5a, b**). More precisely, the stroma area defined by non-cancer cells was largely reduced in depleted condition (**Fig. 5b, c**). Nevertheless, we observed a lower tumor weight in depleted condition (**Fig. 5d**) and this finding was not related to differences in mCherry<sup>+</sup> PeSCs cells level. Indeed, we did not detect any difference between control and depleted mice in both FACS analysis (**Fig. 5c, d**) or IHC quantification (**Supplementary Fig. 5e**). Consequently, we analysed extracellular matrix deposit (e.g.: collagen,  $\beta$ ig-h3). We noticed a slight but significant reduction of  $\beta$ ig-h3 deposit in the extracellular matrix of depleted mice (**Fig. 5e**) confirming  $\beta$ ig-h3 is not uniquely produced by macrophages but also other cells (e.g.: CAFs, Pericytes). We also observed that  $\alpha$ SMA<sup>+</sup> cells (i.e., CAFs) level remained the same between control or depleted condition while the level of PDPN<sup>+</sup> CAFs were significantly reduced in the depleted condition. Finally, to assess the full spectrum of the TME, we analysed CD31<sup>+</sup> cells in the TME characterizing endothelial cells. We observed a significant reduction of CD31<sup>+</sup> positive signal in the TME of depleted tumor. These results indicate that CD169<sup>+</sup> macrophages depletion in PDAC reshape diverse components of the TME. Given our observations and the importance of type 1 collagen in PDAC, we assessed the level of type I collagen in the TME of the orthotopic tumor. Interestingly, we observed a drastic reduction of type I collagen deposit (**Fig. 6a**). We confirmed this observation with a picrosirius red staining (**Fig. 6b**). Despite that there were much less collagen fibers in the absence of CD169<sup>+</sup> macrophages, we measured the length and width of individuals fibers in the TME. While the length of each fibers appears to be similar, collagen fibers are thinner in the absence of CD169<sup>+</sup> macrophages (**Fig. 6c, d**). More importantly, the fibers in the TME have a different orientation in space when CD169<sup>+</sup> macrophages are depleted (**Fig. 6e, f**)

In summary, these data show that CD169<sup>+</sup> macrophages orchestrate the immune and stromal reaction in pancreatic tumor microenvironment.

## E. Discussion

The immune response is playing a critical role in regulating the tumor progression. Macrophages are master regulators of adaptive immune but also capable of regulating the development of many tissues, providing repair functions upon tissue injury and maintaining homeostasis<sup>30</sup>. Macrophages are a major components of the stromal cell infiltrate playing a key role in shaping the tumor immunity and response to immunotherapy<sup>31</sup>. Their phenotype and function are highly plastic depending on the exchanging signals within the transforming tissue leading to anti- or pro-tumoral roles. We show here for the first time that CD169<sup>+</sup> macrophages are playing an important role in pancreatic tumor microenvironment by promoting the stromal reaction with extensive collagen deposition and CXCL12 production. The use of CD169-DTR mouse allowed us to show that specific depletion of CD169<sup>+</sup> macrophages in pancreatic cancer led to reduced collagen deposition and CD8 T lymphocytes infiltration in the tumor microenvironment.

What drives the emergence of CD169<sup>+</sup> macrophages in the tumor microenvironment? Previous reports show that cooperation between endothelial and marginal reticular stromal cells was responsible of the CD169 macrophage differentiation via RANK-RANKL axis<sup>32</sup>. Our study highlights that PeSC can induce CD169<sup>+</sup> macrophages suggesting that similar interactions between pericytes and macrophages might be at the origin of their differentiation. The interaction between PeSC and macrophages led to the expression of CD169 on the surface of macrophages as well as CD206 and PD-L1 upregulation. The upregulation of PD-L1 upon PeSC–macrophages communication led to CD8<sup>+</sup> T cell activation inhibition through PD1-PD-L1 axis.

In several cancer types, including malignant melanoma, colorectal cancer, endometrial carcinoma, prostate cancer, bladder cancer, breast cancer, and oesophageal cancer, high density of CD169<sup>+</sup> macrophages in lymph nodes is associated with better clinical outcome and longer survival. CD169<sup>+</sup> macrophages located in the paracortical region of lymph node phagocytose dead tumor cells transported via lymphatic flow and subsequently cross present tumor antigens to CD8<sup>+</sup> T cells. On the other hand, CD169 in the TME is linked with worse prognosis in breast and bladder cancer, lung carcinoma and better prognosis in glioma. However, little is known about CD169<sup>+</sup> macrophages in pancreatic cancer. Cooperation between pancreatic tumor and immune cells occurs very early in pancreatic cancer as macrophages has been shown to promote both ADM and PanIN formation<sup>33</sup>. Our study highlighted that that depleting CD169<sup>+</sup> macrophages in pancreatic cancer was associated with both reduce collagen deposition and CD8 T lymphocytes infiltration in the tumor microenvironment alongside a reduce tumor growth. By depleting CD169<sup>+</sup> macrophages, we diminished the production of CXCL12 and inhibited CD8<sup>+</sup> T cell recruitment in the tumor microenvironment. CXCL12 – CXCR4 axis is currently being evaluated as potential therapeutic target in pancreatic cancer<sup>34,35</sup>.

In line with this data, *in vivo* study in CD169-DTR transgenic mouse model for breast cancer, demonstrates that CD169 macrophage depletion enhances the infiltration of CD8<sup>+</sup> T cells<sup>17</sup>. Here we unveil an unknown role of CD169 macrophages in promoting matrix deposition and orchestrating stromal response in pancreatic cancer. We demonstrate that the cross talk between PeSC and macrophages is essential for the production of collagen I and big-h3. Our results are also in line with a recent study conducted by DeNardo group who showed that depleting resident macrophages was associated with a higher tumor cell percentage and a reduced stroma in both Kras mutated or pancreatitis context<sup>11</sup>. Based on these results we propose the following hypothetical model (**Fig. 6.**)

## F. Figure legend

### Fig. 1. CD169<sup>+</sup> macrophages are expressed in both human and mouse pancreatic cancer.

**a** Relative expression of *siglec1* in normal pancreas or primary tumor (Normal tissue n=165, Primary tumor n=178). **b** UMAP projection of the full scRNAseq dataset highlighting *siglec1* expression. **c** UMAP projection of macrophage cells after subsetting and re-clustering from cluster 0 to 8. **d** UMAP projection of top Cassetta's TAM score in pancreas macrophages subset. **e, f, g** Density UMAP projection of *siglec1* (**e**), *cd68* (**f**), *cd163* (**g**) in macrophages cells after subsetting and re-clustering. **h** Representative pictures of immunohistochemistry (IHC) staining against CD169 in FFPE section of human pancreatic specimen of PDAC (left panel) and pancreatic neoplasia (right panel). Scale bar is 100µm. **i** Representative pictures of CD169 and EPCAM double staining in PDAC or neoplasia lesions Pdx1-Cre; LSL-Kras<sup>G12D</sup>; Ink4a/Arf<sup>flox/flox</sup> (KIC) (Upper panel) or p48-Cre; LSL-Kras<sup>G12D</sup>, Acvr1b<sup>flox/flox</sup> (4KC) cryosection (Lower panel). The yellow dashed lines surround PDAC or neoplastic lesions. Scale bar is 50µm. **j** Representative pictures of F4/80, CD169, CD206 triple staining in 4KC cryosection. Scale bar is 50µm. **k** Quantification by flow cytometry of CD45<sup>+</sup> CD169<sup>+</sup> in wild type (WT, n=7) or 4KC (n=6) mice. The p-value was determined by an unpaired two-tailed t-test. Error bars show the mean ± SEM. \*\*, p<0.01, student t-test.

### Fig.2. Pericyte stem cells potentiate CD169 expression on macrophages *in vitro*.

**a** Representative picture of IHC staining against CD169 (left panel) and CD106 (right panel) in human PDAC. Scale bar is 100µm. **b** Representative pictures of double staining of CD169 and CD106 in 4KC cryosection. 2-fold zoomed in picture of individual and merge channels are indicated with a white square. White arrow show CD106 vicinity with CD169. Scale bar is 50µm. **c-h** BMDM were cultured alone (M) or co-cultured with PeSC for 48 hours (PeSC+M) and macrophages (F4/80<sup>+</sup>) were analyzed by flow cytometry. Quantification among F4/80<sup>+</sup> cells of MHC-clII<sup>+</sup> (**c**), CD107a<sup>+</sup> (**d**), ARG1<sup>+</sup> (**e**), CD206<sup>+</sup> (**f**), PD-L1<sup>+</sup> (**g**), CD169<sup>+</sup> (**h**), representative of 3 independent experiments with technical triplicates in each condition. The p-value was determined by an unpaired two-tailed t-test. Error bar show the mean ± SEM. \*, p<0.05; \*\*, p<0.01; \*\*\*, p<0.001; \*\*\*\*, p<0.0001, student t-test. M, Macrophages; PeSC, Pericyte Stem Cells.

### Fig. 3. βig-h3 secreted by macrophages activate PeSC to attract and inhibit CD8<sup>+</sup> T cells.

**a** Density UMAP projection of *siglec1* and *tgfb1* in macrophages subset. **b-c** ELISA assay of the different cells culture supernatant (M, PeSC, PeSC+M, PeSC+rβig-h3) against βig-h3 (**b**) and CXCL12 (**c**). PeSC were treated with 10µg/mL of rβig-h3 for 48 hours, representative of 2 independent experiments. **d** Quantitative reverse transcription PCR analysis of *sdf-1* in tumoral cell or βig-h3 stimulated PeSC. *Sdf-*

1 was normalized against HPRT1 expression. Stimulation duration (h = hour) is indicated in axis. PeSC were treated with 10µg/mL of rβig-h3. Unstimulated PeSC and TC were cultured for 3 hours. Representative of 3 independent experiments. **e** ELISA assay against CXCL12 in βig-h3 stimulated PeSC supernatant. PeSC were treated with different concentration of rβig-h3 indicated in X axis. Representative of 2 independent experiments. **f** Representative pictures of βig-h3, CD169, CD206 (upper panel) and CXCL12, CD169 (lower panel) staining in p48-Cre;LSL-Kras<sup>G12D</sup>,Acvr1b<sup>fllox/fllox</sup> (4KC) pancreas cryosection. Scale bar is 50µm. **g** Experimental design of the transwell assay. **h** Analysis of lymphoid cells migration from the upper well to the lower well containing either M, PeSC or PeSC+M by flow cytometry. CFSE<sup>+</sup> cells were quantified and normalized to spontaneous migration from the upper to the lower well. Representative of 3 independent experiments with triplicates in each condition. **i** Experimental design of CD8<sup>+</sup> purification and activation assay. CD8<sup>+</sup> were purified from wt or PD1<sup>-/-</sup> mice secondary lymphoid organs, stained with CFSE and activated with CD3/CD28 beads. CD8<sup>+</sup> were then cultured with the different co-culture condition for 48 hours. CFSE dilution were followed by flow-cytometry. **j** % of cell population throughout the CD8<sup>+</sup> division was determined by flow cytometry in both PeSC+M culture condition. **k-l** Gating strategy of CD62L (**k**) and CD69 (**l**) in PeSC+M with wild type (left panel) or PD-1 KO (right panel) CD8<sup>+</sup> cells condition. **m-n** CD62L (**m**) and CD69 (**n**) mean fluorescent intensity (MFI) in WT or PD1-KO CD8<sup>+</sup> T cell cultured with PeSC+M. P-values were calculated with an unpaired two-tailed t-test. Representative of 3 independent experiment, student t-test. All error bars of Fig. 3 represent mean ± SEM. All p-values were calculated with a one-way anova statistical test unless mentioned otherwise. \*, p<0.05; \*\*, p<0.01; \*\*\*, p<0.001; \*\*\*\*, p<0.0001. TC, Tumoral cells; rβig-h3, recombinant βig-h3; CFSE, Carboxyfluorescein succinimidyl ester.

**Fig. 4. Depletion of CD169<sup>+</sup> macrophages inhibit CD8<sup>+</sup> T cell recruitment in the tumor microenvironment.**

**a** TC and PeSC were co-injected orthotopically in the pancreas of Siglec1<sup>tm1(HBEGF)Mtk</sup> (CD169<sup>DTR</sup>) mice treated or not with diphtheria toxin (DT<sup>+/-</sup>). At day 10 post-surgery, tumoral, spleen and lymph nodes were harvested. **b-f** Scatterplot showing the % of CD45<sup>+</sup> (**b**), F4/80<sup>+</sup> in CD45<sup>+</sup> (**c**), CD206<sup>+</sup> in F4/80<sup>+</sup> (**d**), MCH cIII<sup>hi</sup> in F4/80<sup>+</sup> (**e**), Ly6G<sup>+</sup> in CD45<sup>+</sup> (**f**). **g** Representative dot-plot of CD8β and CD45 of tumoral tissue. **h-k** Scatterplot showing the % of CD8β<sup>+</sup> in CD45<sup>+</sup> (**h**), CD4<sup>+</sup> in CD45<sup>+</sup> (**i**), IFNγ<sup>+</sup> in CD8β<sup>+</sup> (**j**), GrzB<sup>+</sup> in CD8β<sup>+</sup> (**k**). **l** Representative picture of IHC staining against GrzB of FFPE tumoral tissue, scale bar 250µm. **m** Scatterplot showing the number of GrzB<sup>+</sup> per high power field in tumoral tissue. All p-values of figure 4 were calculated with an unpaired two-tailed t-test and is representative of 3 independent experiments. All error bars of Fig. 4 represent mean ± SEM. \*, p<0.05; \*\*\*\*, p<0.0001. GrzB, Granzyme

B

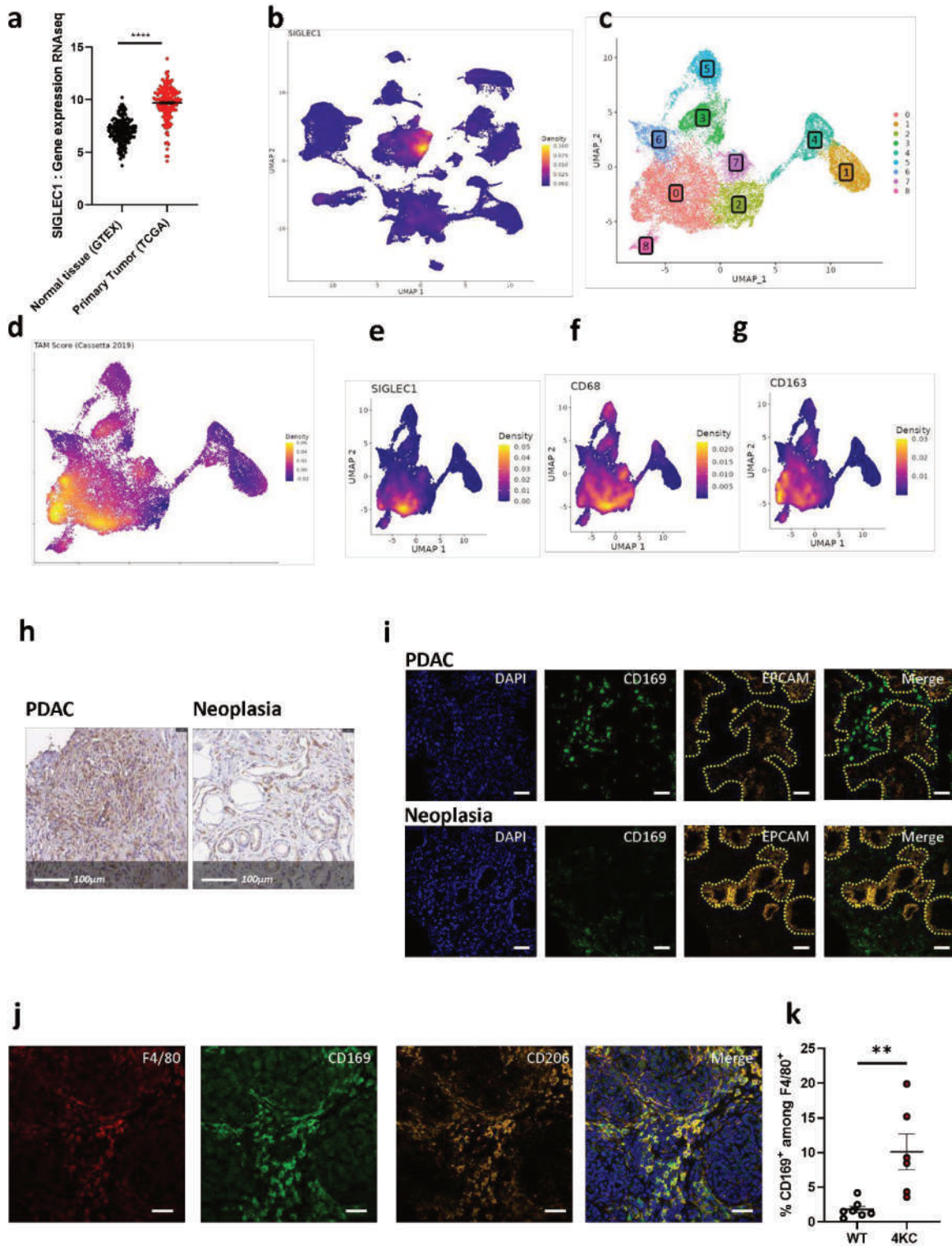
**Fig. 5. Depletion of CD169<sup>+</sup> macrophages reshape the extracellular matrix in the tumor microenvironment.**

**a** Representative picture of IHC staining against GFP of FFPE tumoral tissue of control or DT treated mice. **b** Pie chart of relative proportions between tumoral area and stromal area. **c** Scatterplot showing the % of tumoral area in the TME, mean  $\pm$  SEM, student t-test  $\pm$  SEM. **d** Scatterplot showing the tumor weight in control or treated mice, representative of 3 independent experiments. P-values was calculated with an unpaired two-tailed t-test. **e-h** Representative pictures of IHC staining against  $\beta$ ig-h3 (**e**),  $\alpha$ -SMA (**f**), PNP (**g**), CD31 (**h**) and their associated scatterplot showing the % of  $\beta$ ig-h3<sup>+</sup>,  $\alpha$ -SMA<sup>+</sup>, PNP<sup>+</sup> and CD31<sup>+</sup> respectively in tumoral tissue. All error bars of Fig. 5 represent the mean  $\pm$  SEM. ns,  $p > 0.05$ ; \*,  $p < 0.01$ ; \*\*\*\*,  $p < 0.0001$ .

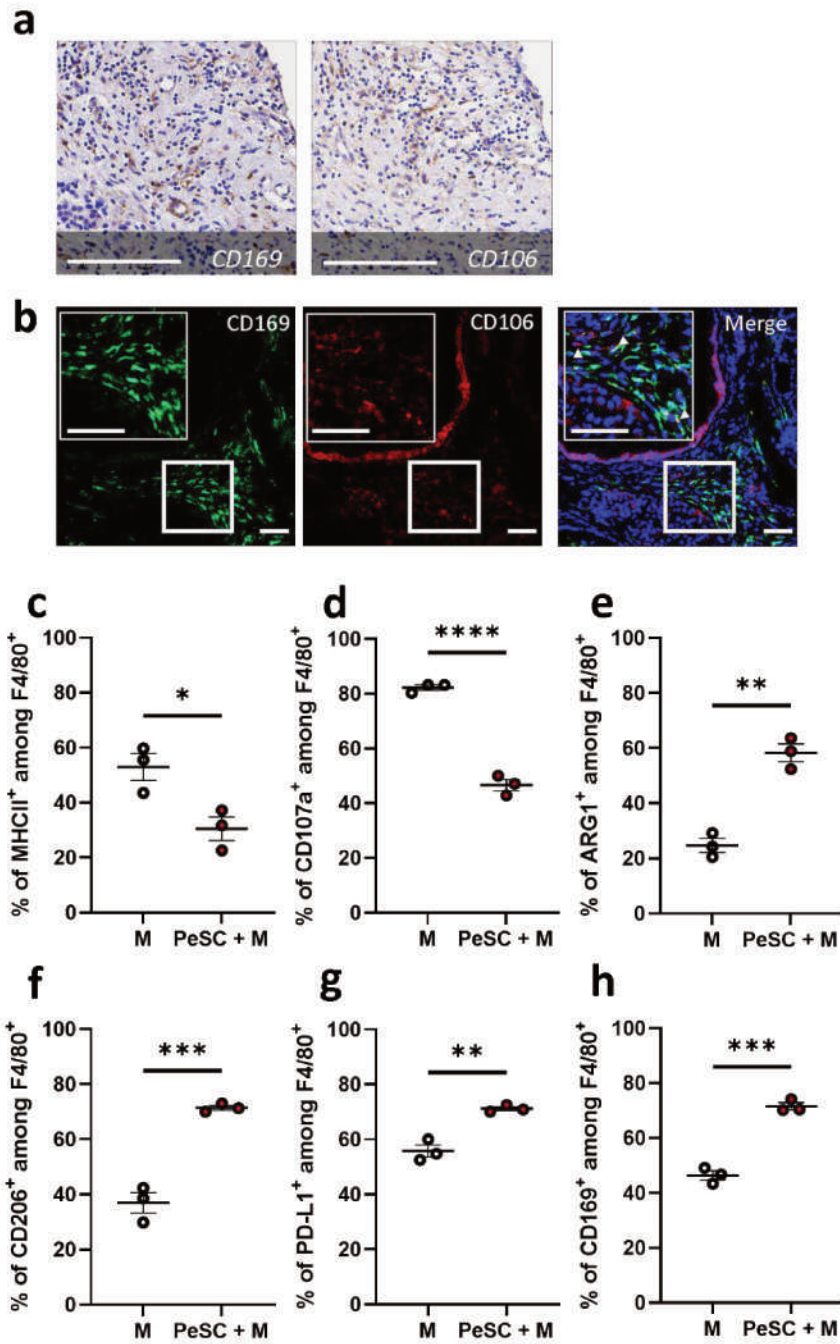
**Fig.6 CD169<sup>+</sup> macrophages allow collagen deposition and architecture**

**a** Representative picture of IHC staining against type I collagen and the associated scatterplot showing the % of Collagen 1<sup>+</sup> in control or DT treated mice TME. **b** Representative picture of picrosirius red staining through brightfield. **c-d** Quantification of collagen fibers length and width. **e** Representative picture of picrosirius red staining through polarized light. **f** Quantification of collagen fibers orientation and frequency in control of depleted mice.

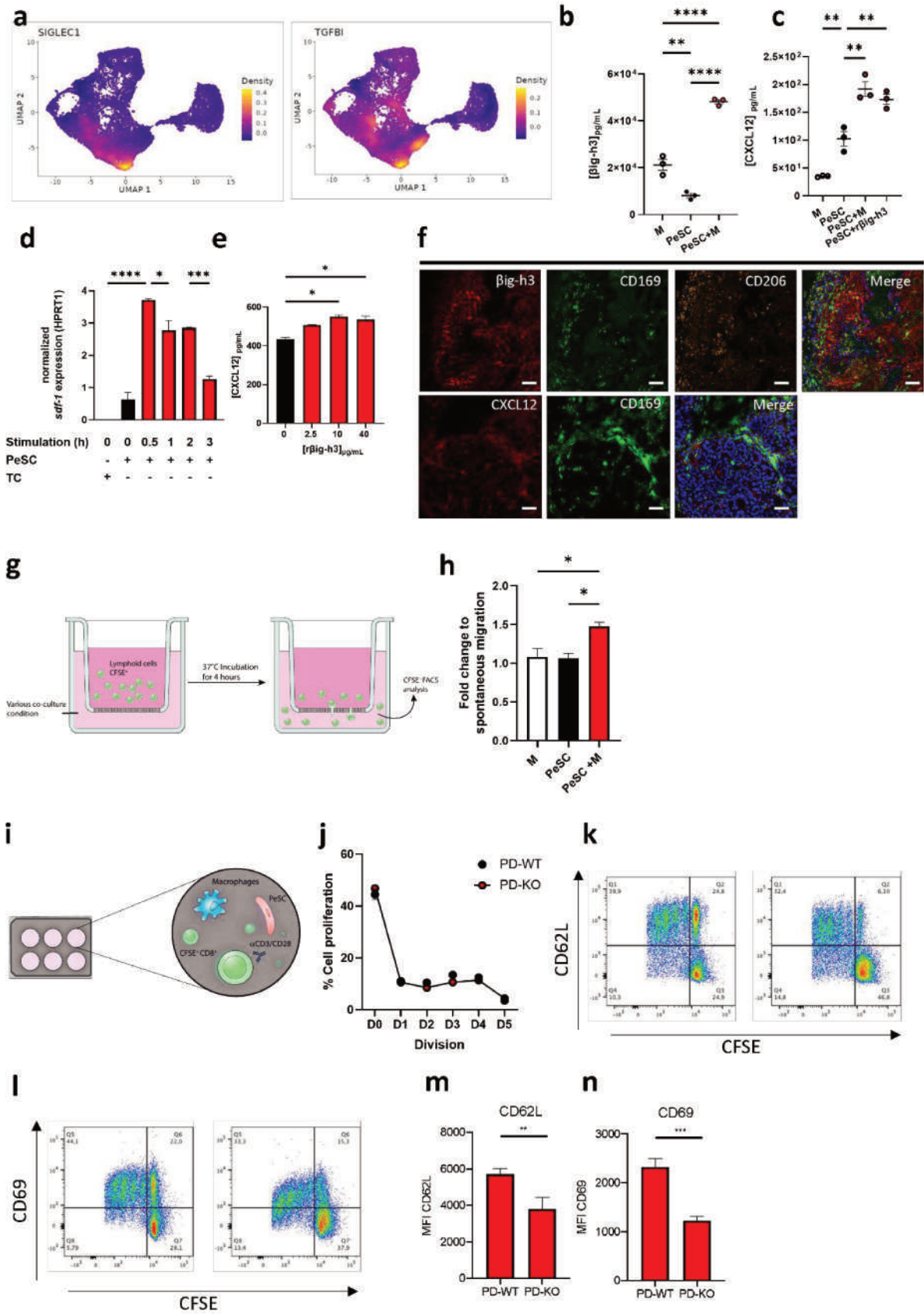
G. Figure



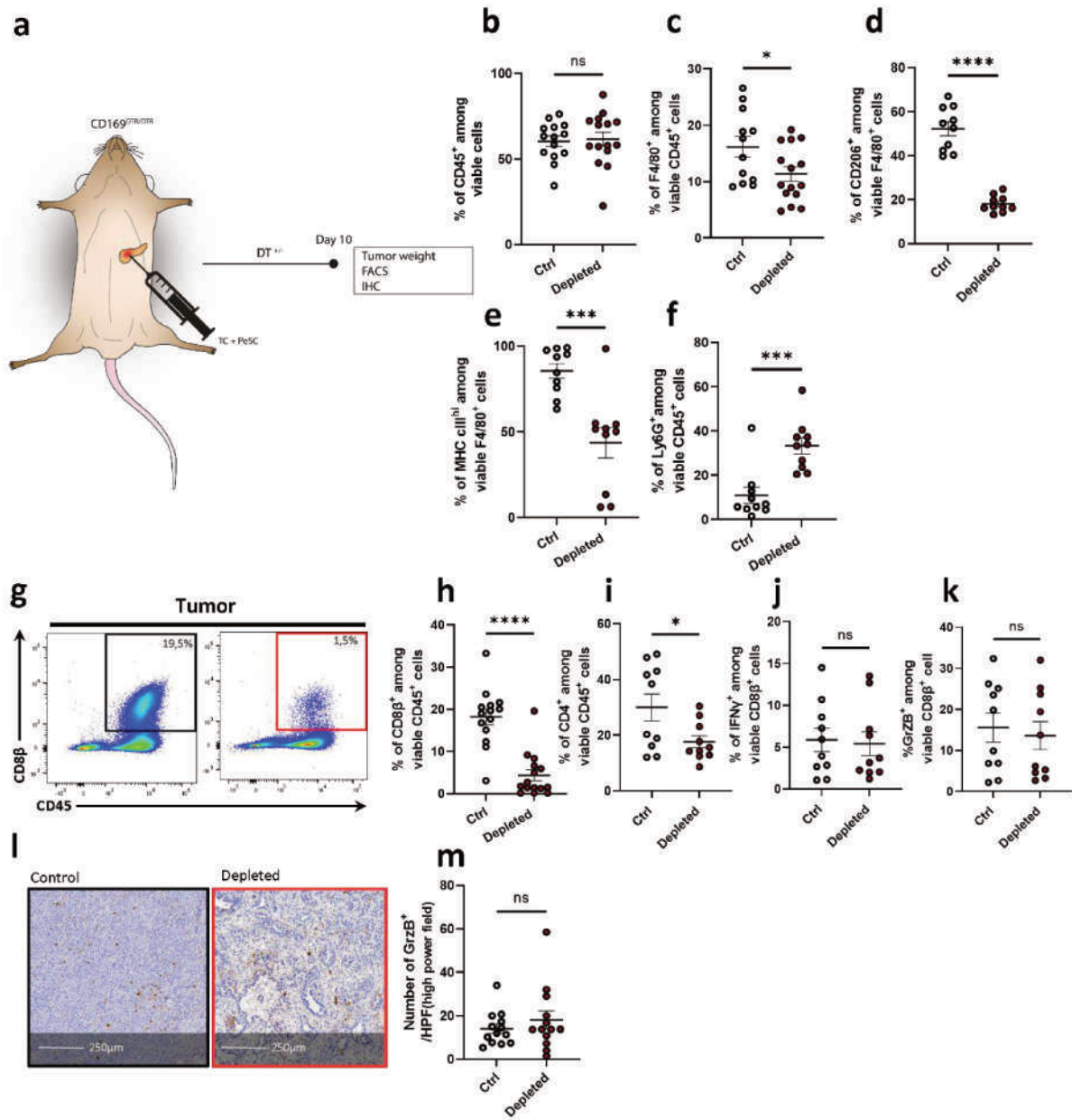
Result II Fig. 1 CD169<sup>+</sup> macrophages are expressed in both human and mouse pancreatic cancer



Result II Fig. 2 Pericyte stem cells potentiate CD169 expression on macrophages *in vitro*.



Result II Fig. 3 βig-h3 secreted by macrophages activate PeSC to attract and inhibit CD8<sup>+</sup> T cells.

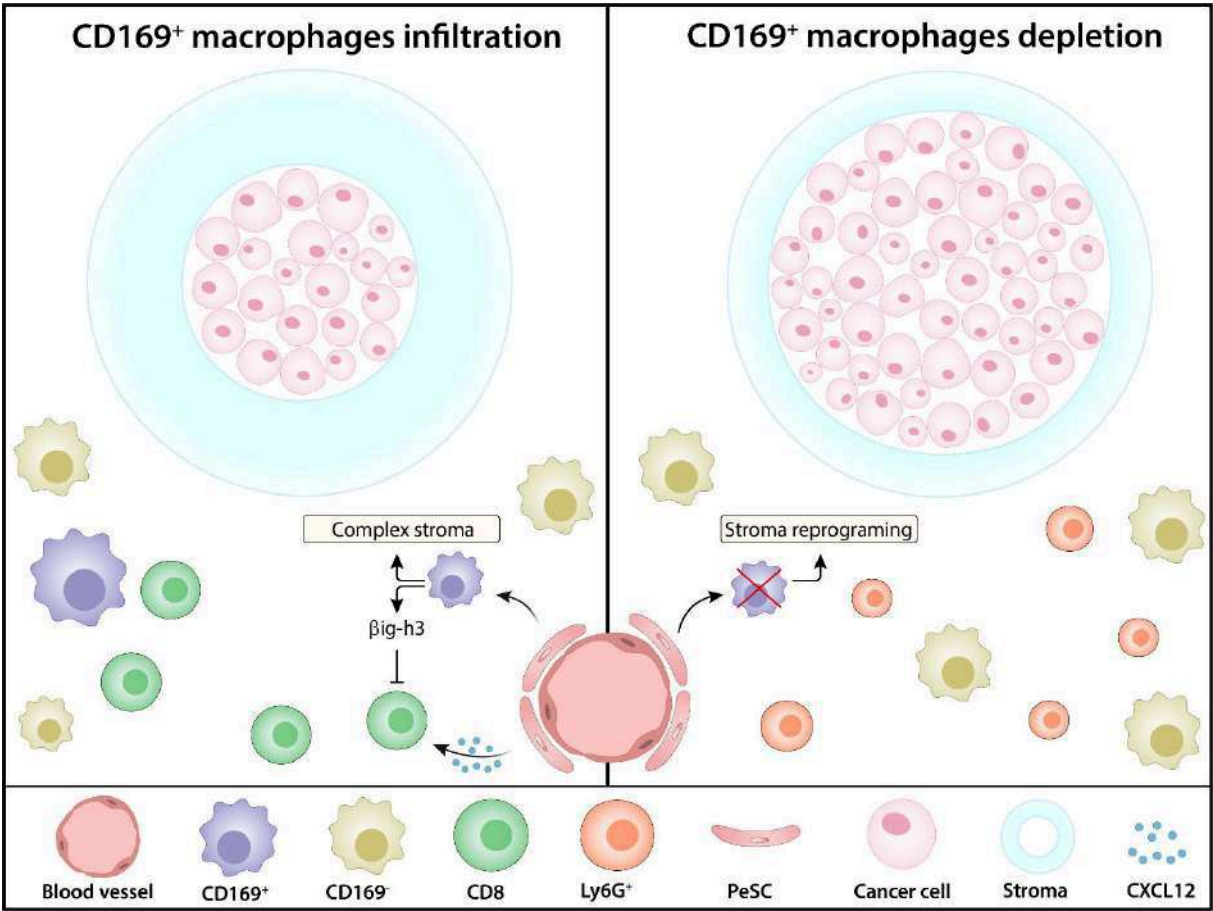


Result II Fig. 4 Depletion of CD169<sup>+</sup> macrophages inhibit CD8<sup>+</sup> T cell recruitment in the tumor microenvironment.









Result II Fig. 7 CD169<sup>+</sup> macrophages structure the fibrotic response in PDAC

## Supplementary figure legend

### **Supplementary Fig.1. CD169<sup>+</sup> macrophages are expressed in both human and mouse pancreatic cancer.**

**a** UMAP projection of the full *scRNAseq* data. **b** Projection of macrophages cells after subsetting and re-clustering in normal and tumor tissue. **c** mRNA expression level of *siglec1* in different macrophages subset (M0, M1, M2) using CIBERSORT deconvolution in Skin Cutaneous Melanoma (SKCM, n=469), Pancreatic adenocarcinoma (PAAD, n= 179), Colon adenocarcinoma (COAD, n=290), Breast invasive carcinoma (BRCA, n=1099), Ovarian serous cystadenocarcinoma (OV, n=427). **d, e** Correlation analysis between *siglec1* and *mrc1* (**d**), *cd163* (**e**) in human PDAC (n=177). P-value was calculated with a two-tailed Pearson correlation analysis. **f** t-SNE analysis of CD45<sup>+</sup> F4/80<sup>+</sup> cells from WT (n=3) or 4KC (n=3) mice pancreata. **g-i** relative expression of CD169 (**g**), CD163 (**h**) and CD206 (**i**) is shown by the heatmap.

### **Supplementary Fig. 3. CD169<sup>+</sup> macrophages express $\beta$ ig-h3 and arise from pericyte stem cells communication.**

**a** mRNA expression level of *tgfb1* in different macrophages subset (M0, M1, M2) using CIBERSORT deconvolution Pancreatic adenocarcinoma (PAAD, n= 179). P-values were calculated with a one-way anova test.

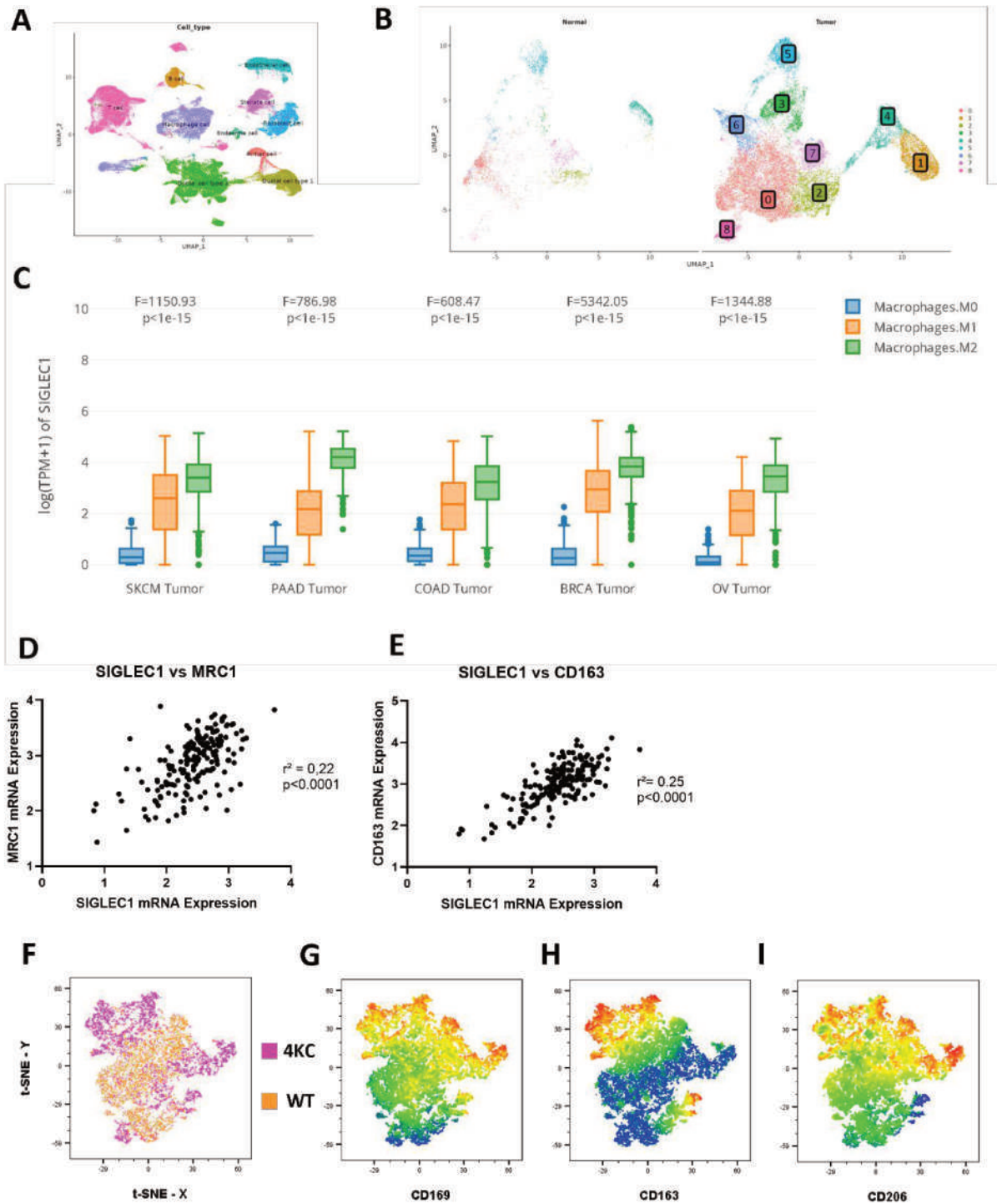
### **Supplementary Fig. 4. Depletion of CD169<sup>+</sup> macrophages inhibit CD8<sup>+</sup> T cell recruitment in the tumor microenvironment.**

**a** TC or TC + PeSC were injected orthotopically in the pancreas for 30 days and tumor weight were analyzed. Representative of 1 experiment (n=4 in each condition). P-value was calculated with an unpaired two-tailed t-test. **b** Histogram analysis of CD169 (left panel) and CD206 (right panel) expression in pancreatic tumor of TC vs TC + PeSC injected mice. **c** Scatterplot of CD45<sup>+</sup> Ly6G<sup>+</sup>. P-value was calculated with an unpaired two-tailed t-test. **d** Representative picture of immunofluorescent staining against CD169 (green), CD3e (red), DAPI (blue) of CD169<sup>DTR/DTR</sup> spleen untreated (day 0) and treated (Day 4 and 9) with DT. Scale bar is 50 $\mu$ m. **e** Scatterplot showing the % of CD8 $\beta$ <sup>+</sup> in CD45<sup>+</sup> cells in normal pancreas, lymph nodes and spleen following 4 days after treatment with DT. **f** Spleen from treated and untreated CD169<sup>DTR/DTR</sup> were weighted at day 0, day 4 and 6. Representative of 1 experiment. **g-h** Scatterplot showing the % of CD169<sup>+</sup> in F4/80<sup>-</sup> (**g**) or F4/80<sup>+</sup> (**h**) in tumoral tissue, spleen, and lymph nodes. **i-k** Scatterplot showing the following population in spleen and lymph nodes: % of CD45<sup>+</sup> (i) F4/80<sup>+</sup> in CD45<sup>+</sup> (j), % of CD206<sup>+</sup> in F4/80<sup>+</sup> (k). **l** Scatterplot showing the % of Arg1 in the TME. P-value were calculated with an unpaired two-tailed t-test. **m** Representative pictures of IHC staining against Arg1 of FFPE tumoral tissue, scale bar 250 $\mu$ m. **n-p** Scatterplot showing the following population in spleen and lymph nodes: % of Ly6G<sup>+</sup> in CD45<sup>+</sup> (n), MHC cIII<sup>hi</sup> in F4/80<sup>+</sup> (o), % of CD8 $\beta$  in CD45<sup>+</sup> (p). All p-values of figure S4 were calculated with one-way anova test and is representative of 3 independent experiments unless mentioned otherwise. All error bars of Fig. S4 represent the mean  $\pm$  SEM. ns, p>0.05; \*, p<0.05; \*\*, p<0.01; \*\*\*\*, p<0.0001.

**Supplementary Fig. 5. Depletion of CD169<sup>+</sup> macrophages reshape the extracellular matrix in the tumor microenvironment.**

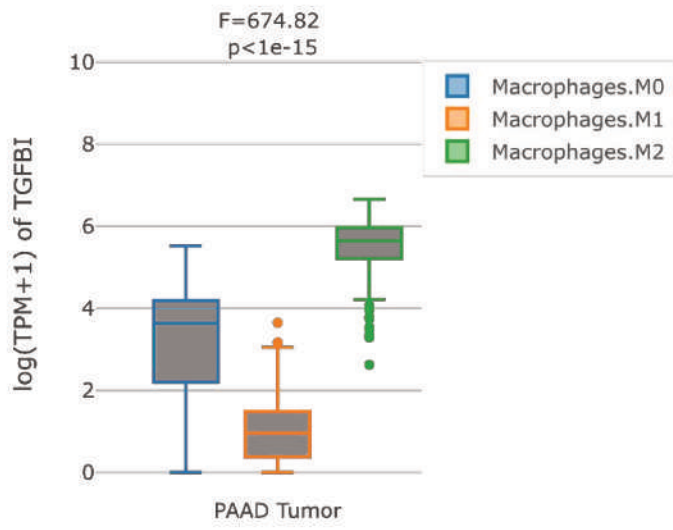
**a** Representative dot plot of FSC-H and GFP in control (left panel) and treated (right panel) mice. **b** Scatterplot showing the % of GFP<sup>+</sup> in control or treated mice in tumoral tissue (n=15 per condition, representative of 3 independent experiments). **c** Representative dot plot of FSC-H and mCherry in control (left panel) and treated (right panel) mice. **d** Scatterplot showing the % of mCherry<sup>+</sup> in control or treated mice in tumoral tissue (n=15 per condition, representative of 3 independent experiments). All p-values of figure S5 were calculated with an unpaired two-tailed t-test is representative of 3 independent experiments. All error bars of Fig. S5 represent the mean  $\pm$  SEM. ns, p>0.05; \*\*\*\*, p<0.0001.

## H. Supplementary figure

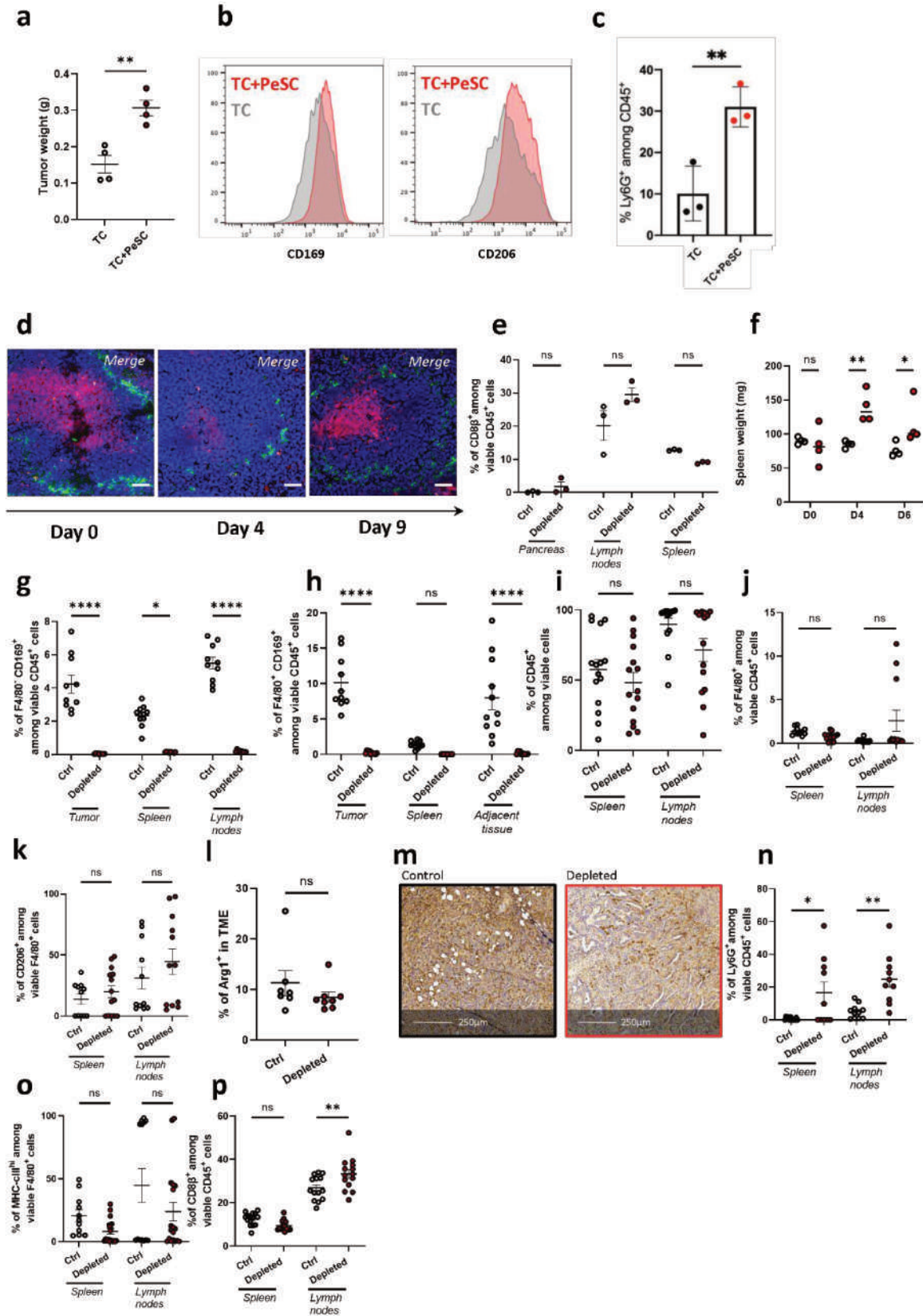


Result II supplementary Fig. 1 CD169+ macrophages are expressed in both human and mouse pancreatic cancer

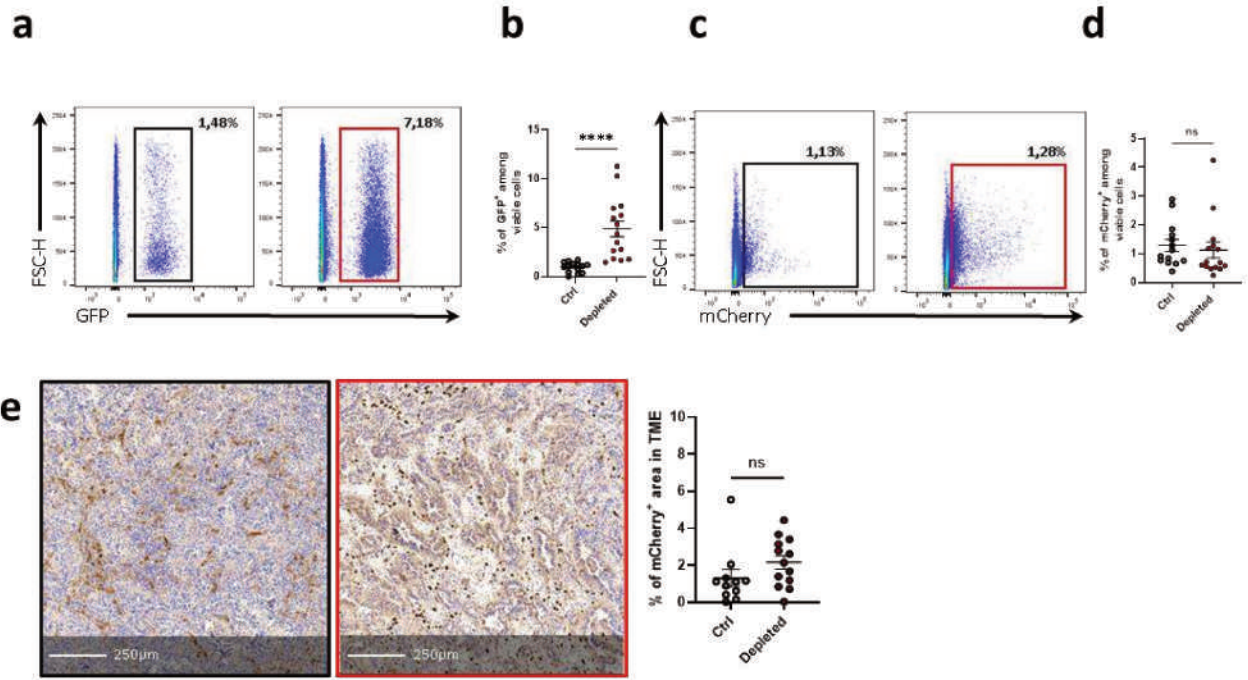
**a**



Result II supplementary Fig. 2  $\beta$ ig-h3 secreted by macrophages activate PeSC to attract and inhibit CD8+ T cells.



Result II supplementary Fig. 4 Depletion of CD169<sup>+</sup> macrophages inhibit CD8<sup>+</sup> T cell recruitment in the tumor microenvironment.



Result II supplementary Fig. 5 Depletion of CD169<sup>+</sup> macrophages reshape the extracellular matrix in the tumor microenvironment.

## I. References

1. Aguirre, A.J., *et al.* Activated Kras and Ink4a/Arf deficiency cooperate to produce metastatic pancreatic ductal adenocarcinoma. *Genes Dev* **17**, 3112-3126 (2003).
2. Hingorani, S.R., *et al.* Preinvasive and invasive ductal pancreatic cancer and its early detection in the mouse. *Cancer Cell* **4**, 437-450 (2003).
3. Hingorani, S.R., *et al.* Trp53R172H and KrasG12D cooperate to promote chromosomal instability and widely metastatic pancreatic ductal adenocarcinoma in mice. *Cancer Cell* **7**, 469-483 (2005).
4. Miyake, Y., *et al.* Critical role of macrophages in the marginal zone in the suppression of immune responses to apoptotic cell-associated antigens. *J Clin Invest* **117**, 2268-2278 (2007).
5. Wu, Z., *et al.* Pericyte stem cells induce Ly6G(+) cell accumulation and immunotherapy resistance in pancreatic cancer. *EMBO Rep*, e56524 (2023).
6. Dagher, O.K., Schwab, R.D., Brookens, S.K. & Posey, A.D., Jr. Advances in cancer immunotherapies. *Cell* **186**, 1814-1814 e1811 (2023).
7. Royal, R.E., *et al.* Phase 2 trial of single agent Ipilimumab (anti-CTLA-4) for locally advanced or metastatic pancreatic adenocarcinoma. *J Immunother* **33**, 828-833 (2010).
8. Wainberg, Z.A., *et al.* Open-label, Phase I Study of Nivolumab Combined with nab-Paclitaxel Plus Gemcitabine in Advanced Pancreatic Cancer. *Clin Cancer Res* **26**, 4814-4822 (2020).
9. Torphy, R.J., *et al.* Stromal Content Is Correlated With Tissue Site, Contrast Retention, and Survival in Pancreatic Adenocarcinoma. *JCO Precis Oncol* **2018**(2018).
10. Chijimatsu, R., *et al.* Establishment of a reference single-cell RNA sequencing dataset for human pancreatic adenocarcinoma. *iScience* **25**, 104659 (2022).
11. Zuo, C., *et al.* Stromal and therapy-induced macrophage proliferation promotes PDAC progression and susceptibility to innate immunotherapy. *J Exp Med* **220**(2023).
12. Ene-Obong, A., *et al.* Activated pancreatic stellate cells sequester CD8+ T cells to reduce their infiltration of the juxtatumoral compartment of pancreatic ductal adenocarcinoma. *Gastroenterology* **145**, 1121-1132 (2013).
13. Hartmann, N., *et al.* Prevailing role of contact guidance in intrastromal T-cell trapping in human pancreatic cancer. *Clin Cancer Res* **20**, 3422-3433 (2014).
14. Zhu, Y., *et al.* Tissue-Resident Macrophages in Pancreatic Ductal Adenocarcinoma Originate from Embryonic Hematopoiesis and Promote Tumor Progression. *Immunity* **47**, 323-338 e326 (2017).
15. Chow, A., *et al.* CD169(+) macrophages provide a niche promoting erythropoiesis under homeostasis and stress. *Nat Med* **19**, 429-436 (2013).

16. Casanova-Acebes, M., *et al.* Tissue-resident macrophages provide a pro-tumorigenic niche to early NSCLC cells. *Nature* **595**, 578-584 (2021).
17. Jing, W., *et al.* Breast cancer cells promote CD169(+) macrophage-associated immunosuppression through JAK2-mediated PD-L1 upregulation on macrophages. *Int Immunopharmacol* **78**, 106012 (2020).
18. Cassetta, L., *et al.* Human Tumor-Associated Macrophage and Monocyte Transcriptional Landscapes Reveal Cancer-Specific Reprogramming, Biomarkers, and Therapeutic Targets. *Cancer Cell* **35**, 588-602 e510 (2019).
19. Kim, H.J., *et al.* Blood monocyte-derived CD169(+) macrophages contribute to antitumor immunity against glioblastoma. *Nat Commun* **13**, 6211 (2022).
20. Chen, Y., *et al.* Type I collagen deletion in alphaSMA(+) myofibroblasts augments immune suppression and accelerates progression of pancreatic cancer. *Cancer Cell* **39**, 548-565 e546 (2021).
21. Kloosterman, D.J. & Akkari, L. Macrophages at the interface of the co-evolving cancer ecosystem. *Cell* **186**, 1627-1651 (2023).
22. Comito, G., *et al.* Cancer-associated fibroblasts and M2-polarized macrophages synergize during prostate carcinoma progression. *Oncogene* **33**, 2423-2431 (2014).
23. Ripoché, D., *et al.* Generation of a conditional mouse model to target *Acvr1b* disruption in adult tissues. *Genesis* **51**, 120-127 (2013).
24. Buechler, M.B., Fu, W. & Turley, S.J. Fibroblast-macrophage reciprocal interactions in health, fibrosis, and cancer. *Immunity* **54**, 903-915 (2021).
25. Bachy, S., *et al.* beta1g-h3-structured collagen alters macrophage phenotype and function in pancreatic cancer. *iScience* **25**, 103758 (2022).
26. Lecker, L.S.M., *et al.* TGFBI Production by Macrophages Contributes to an Immunosuppressive Microenvironment in Ovarian Cancer. *Cancer Res* **81**, 5706-5719 (2021).
27. Peng, P., *et al.* TGFBI secreted by tumor-associated macrophages promotes glioblastoma stem cell-driven tumor growth via integrin alpha5beta1-Stat3 signaling. *Theranostics* **12**, 4221-4236 (2022).
28. Goehrig, D., *et al.* Stromal protein beta1g-h3 reprogrammes tumour microenvironment in pancreatic cancer. *Gut* **68**, 693-707 (2019).
29. Agarwal, P., *et al.* Mesenchymal Niche-Specific Expression of *Cxcl12* Controls Quiescence of Treatment-Resistant Leukemia Stem Cells. *Cell Stem Cell* **24**, 769-784 e766 (2019).
30. Wynn, T.A., Chawla, A. & Pollard, J.W. Macrophage biology in development, homeostasis and disease. *Nature* **496**, 445-455 (2013).

31. Mantovani, A., Marchesi, F., Malesci, A., Laghi, L. & Allavena, P. Tumour-associated macrophages as treatment targets in oncology. *Nat Rev Clin Oncol* **14**, 399-416 (2017).
32. Camara, A., *et al.* Lymph Node Mesenchymal and Endothelial Stromal Cells Cooperate via the RANK-RANKL Cytokine Axis to Shape the Sinusoidal Macrophage Niche. *Immunity* **50**, 1467-1481 e1466 (2019).
33. Liou, G.Y. & Storz, P. Inflammatory macrophages in pancreatic acinar cell metaplasia and initiation of pancreatic cancer. *Oncoscience* **2**, 247-251 (2015).
34. Feig, C., *et al.* Targeting CXCL12 from FAP-expressing carcinoma-associated fibroblasts synergizes with anti-PD-L1 immunotherapy in pancreatic cancer. *Proc Natl Acad Sci U S A* **110**, 20212-20217 (2013).
35. Biasci, D., *et al.* CXCR4 inhibition in human pancreatic and colorectal cancers induces an integrated immune response. *Proc Natl Acad Sci U S A* **117**, 28960-28970 (2020).

### III. Stiffness-induced cancer-associated fibroblasts are responsible for immunosuppression in a PDGF ligand-dependent manner

The 3<sup>rd</sup> study was mainly conducted by Dr. Gamradt and lasted during my whole PhD. I participated in the conceptualization of experiments and writing a large part of the accepted paper in PNAS journal. I performed the majority of *in vivo* experiments for anti-PDGF-AA treatment. I also took part in the reviewing process by performing atomic force microscopy in collaboration with a private company as well as other *in vitro* and *ex vivo* experiments. All transcriptomic analysis was performed in collaboration with Dr. Gamradt and Dr. Hernandez-Vargas.

This study was conducted based on the observation that throughout pancreatic cancer progression, mechanical changes are observed in the tumoral tissue. Specifically, it was observed that the desmoplastic response was responsible for drug delivery impairment. Our objective was to find mechanisms inducing both tissue stiffness and immune response impairment in pancreatic cancer from the beginning of the transformation.

We previously established an *in vivo* model named 4KC and we observed a massive collagen deposition associated with an increase tissue stiffness measured by atomic force microscopy compared to KC mouse model. We therefore evaluated the difference in CAFs populations and found by flow cytometry that PDGFRa<sup>Hi</sup>CD61<sup>+</sup> shift to PDGFRa<sup>Low</sup>CD61<sup>+</sup> in a kinetic wise manner in 4KC mouse. Additionally, PDGFRa<sup>Hi</sup>CD61<sup>+</sup> were prominent in KC mouse model compared to 4KC mouse model. Therefore, we hypothesized that PDGFRa<sup>Low</sup>CD61<sup>+</sup> were associated with tissue stiffness and named them stiffness induced CAFs (siCAF). We confirmed *in vitro* that siCAF were responsible for collagen deposition. Through ligand-receptor analysis, we observed that ductal cells and CAFs had more interactions. Specifically, we observed that ductal cells in 4KC were secreting PDGF ligands (A and B) binding to PDGFRa<sup>Hi</sup>CD61<sup>+</sup> CAFs to become PDGFRa<sup>Low</sup>CD61<sup>+</sup> CAFs through the internalization of PDGFRa.

We showed treatment of CD8 T cell with siCAF conditioned media led to decreased proliferation and GrzB production. Finally, we showed that treating 4KC mice with anti-PDGF-AA Ab decreased tumour weight and reprogrammed siCAF to PDGFRa<sup>Hi</sup>CD61<sup>+</sup> CAFs. CAFs in pancreatic cancer are mostly categorized into myCAF, iCAF or apCAF family. We established a 29 gene signature of siCAF and we show that this signature is distributed among all described types of CAFs suggesting that despite the origin of the cells, the mechanical constraint together with the secretion of soluble factors breaks the heterogeneity of CAFs into a binary classification according to their “microenvironment sensing”, namely, PDGFRa<sup>Hi</sup>.

**(See accepted paper next page)**

# Stiffness-induced cancer-associated fibroblasts are responsible for immunosuppression in a platelet-derived growth factor ligand-dependent manner

Pia Gamradt<sup>a,b,c</sup>, Kevin Thierry<sup>d,a,b,c,1</sup>, Melissa Masmoudi<sup>a,b,c,d,1</sup>, Zhichong Wu<sup>e,a,b,c,e</sup>, Hector Hernandez-Vargas<sup>d,a,b,c</sup>, Sophie Bachy<sup>a,b,c,d</sup>, Tiffanie Antonio<sup>a,b,c</sup>, Berkan Savas<sup>a,b,c</sup>, Zainab Hussain<sup>f</sup>, Richard Tomasini<sup>d,f</sup>, Pascale Milani<sup>g</sup>, Philippe Bertolino<sup>d,a,b,c</sup> and Ana Hennino<sup>d,a,b,c,d,\*</sup>

<sup>a</sup>Tumor Escape, Resistance and Immunity, Cancer Research Center of Lyon, UMR INSERM 1052, CNRS 5286, Lyon F-69373, France

<sup>b</sup>Université Lyon 1, Lyon F-69000, France

<sup>c</sup>Centre Léon Bérard, Lyon F-69008, France

<sup>d</sup>StromaCare, Lyon F-69008, France

<sup>e</sup>Department of General Surgery, Pancreatic Disease Center, Ruijin Hospital, Shanghai Jiao Tong University School of Medicine, Shanghai 200025, China

<sup>f</sup>INSERM 1068, CRCM, Marseille F-30059, France

<sup>g</sup>Ecole Normale Supérieure de Lyon, Lyon F-69008, France

\*To whom correspondence should be addressed: Email: [ana.hennino@inserm.fr](mailto:ana.hennino@inserm.fr)

<sup>1</sup>K.T. and M.M. contributed equally to this work.

**Edited By:** David Brenner

## Abstract

Pancreatic ductal adenocarcinoma (PDAC) is associated with a vast stromal reaction that arises mainly from cancer-associated fibroblasts (CAFs) and promotes both immune escape and tumor growth. Here, we used a mouse model with deletion of the activin A receptor ALK4 in the context of the *Kras*<sup>G12D</sup> mutation, which strongly drives collagen deposition that leads to tissue stiffness. By ligand–receptor analysis of single-cell RNA-sequencing data, we identified that, in stiff conditions, neoplastic ductal cells instructed CAFs through sustained platelet-derived growth factor (PDGF) signaling. Tumor-associated tissue rigidity resulted in the emergence of stiffness-induced CAFs (siCAFs) in vitro and in vivo. Similar results were confirmed in human data. siCAFs were able to strongly inhibit CD8<sup>+</sup> T-cell responses in vitro and in vivo, promoting local immunosuppression. More importantly, targeting PDGF signaling led to diminished siCAF and reduced tumor growth. Our data show for the first time that early paracrine signaling leads to profound changes in tissue mechanics, impacting immune responses and tumor progression. Our study highlights that PDGF ligand neutralization can normalize the tissue architecture independent of the genetic background, indicating that finely tuned stromal therapy may open new therapeutic avenues in pancreatic cancer.

**Keywords:** pancreatic adenocarcinoma (PDAC), cancer-associated fibroblasts (CAFs), tissue remodeling, PDGFR/PDGF signaling

## Significance Statement

Here, we report the identification of a cell population of cancer-associated fibroblast (CAF)-stiffness-induced CAFs (siCAFs) that is instructed by tumor cell through sustained platelet-derived growth factor (PDGF) signaling and that is able to strongly inhibit CD8<sup>+</sup> T-cell response in vitro and in vivo. Our study provides support for the translational potential of using a PDGF ligand trap strategy in pancreatic cancer therapy.

## Introduction

Pancreatic ductal adenocarcinoma (PDAC) is currently the fourth leading cause of cancer-related death in the industrialized world and is predicted to become the second leading cause of cancer-related death by 2030 (1). PDAC develops through the preceding formation of acinar-to-duct metaplasia (ADM) and pancreatic intraepithelial neoplasia (PanIN), which are primarily driven by oncogenic *Kras* activation (2). In addition, PDAC is associated

with an abundant stromal reaction that usually surrounds islands of cancer cells and accounts for 50–80% of the tumor volume (3, 4).

The pancreatic tumor stroma consists of a variety of cellular and noncellular components. A broad range of extracellular matrix (ECM) proteins, such as collagens, fibrous and nonfibrous glycoproteins, and proteoglycans contribute to the structural formation of the noncellular stromal compartment. In addition, the ECM also contains nonstructural components, such as growth

**Competing Interest:** M.M., S.B., H.H.V., and A.H. are employees of StromaCare. Other authors declare no potential conflicts of interest.  
**Received:** May 4, 2023. **Accepted:** November 2, 2023

© The Author(s) 2023. Published by Oxford University Press on behalf of National Academy of Sciences. This is an Open Access article distributed under the terms of the Creative Commons Attribution License (<https://creativecommons.org/licenses/by/4.0/>), which permits unrestricted reuse, distribution, and reproduction in any medium, provided the original work is properly cited.

factors and matricellular proteins (4–6). The cellular compartment of the stroma includes immune cells, such as lymphocytes, macrophages, mast cells, and myeloid-derived suppressor cells (MDSCs), along with vascular and neural elements (endothelial cells and neurons, respectively) (7–9).

Accumulating evidence indicates the presence of close and complex paracrine interactions mediating bidirectional crosstalk between tumor cells and the cellular and noncellular stroma that facilitates cancer progression (5). While the stroma might provide a barrier limiting the dissemination and metastasis of pancreatic cancer cells, it also stimulates aggressive behaviors in pancreatic cancer cells and helps these cells escape host immune surveillance (10, 11). Mechanical tissue stiffness is associated with poor survival in PDAC patients (12–14). It is now a well-established fact that activated pancreatic stellate cells (PSCs) are primarily responsible for the development of the stroma (15). PSCs represent ~4% of all pancreatic cells in the steady state. Upon inflammation, PSCs are activated and converted into cancer-associated fibroblasts (CAFs), which are the main source of ECM proteins and growth factors (16). Several mouse studies have shown that CAF depletion abolishes immune suppression (17). Surprisingly, contrary to the initial preclinical results (18), several publications have shown that the stromal response mediated by hedgehog signaling inhibits tumor progression and that its ablation would be harmful in PDAC. However, it has been shown that high stromal activity, as represented by  $\alpha$ -smooth muscle actin ( $\alpha$ -SMA) expression, is associated with a poor prognosis in patients with pancreatic cancer (3). All these results show that tumor–stroma interactions are complex. Indeed, several populations of CAFs with different functions related to antitumor immune responses have been described in both breast cancer (19) and pancreatic cancer (20, 21), indicating that the modulation of stromal activity rather than overall depletion of the stroma would be a therapeutic approach of choice.

Members of the Transforming Growth Factor (TGF)- $\beta$  superfamily, including TGF- $\beta$ , activins, inhibins, bone morphogenic proteins, growth and differentiation factors and nodal, have growth-stimulatory or growth-inhibitory effects in different types of tumors (22). Inactivating mutations in ALK4, the receptor of activin A, have been identified in pancreatic cell lines derived from patients (23, 24). These mutations are associated with increased tumor aggressiveness and a poor survival prognosis (23). Recently, our group discovered that activin A secreted by neoplastic cells acts as a protective senescence-associated secretory phenotype protein that limits tumor progression even during the early stage of ADM by preventing massive ECM deposition (25). Here, we aimed to investigate the role of early tissue mechanical alterations in driving CAF differentiation and the consequent impact on the immune response.

## Methods

### Mouse models

All animal protocols were reviewed and approved in accordance with the guidelines provided by the CRCL Animal Care Committee (CECCAPP\_CLB\_2019\_002). The generation of  $Acvr1b^{flox/flox}$  mutant mice has been previously described (26).  $Acvr1b^{flox/flox}$ ; LSL-Kras<sup>G12D/+</sup>; Ptf1a-Cre mice (termed 4KC mice) were generated by crossing  $Acvr1b^{flox/flox}$  mice with previously established LSL-Kras<sup>G12D/+</sup>; Ptf1a-Cre mice (termed KC mice) (27).

### Atomic force microscopy

Detailed information about atomic force microscopy (AFM) analysis is given in [supplementary methods](#).

### Flow cytometric analysis

Detailed information about the flow cytometric analysis are given in [supplementary methods](#).

### Single-cell RNA sequencing

Detailed information about single-cell RNA sequencing (scRNAseq) are given in [supplementary methods](#).

### LEGENDplex custom array

The experiment has been carried out according to the provider's protocol.

### Statistical analysis

GraphPad Prism was used for the graphical representation of the data and statistical analysis. P-values were calculated using Student's test. For multiple comparisons, a one-way analysis of variance with Tukey's post hoc test was used. Significance was indicated as follows: \* $P < 0.05$ , \*\* $P < 0.01$ , \*\*\* $P < 0.001$ , and \*\*\*\* $P < 0.0001$ .

## Results

### ALK4 signaling disruption in neoplastic cells leads to early increased collagen deposition and tissue rigidity

Given that ablation of protective activin A signaling promotes the formation of ADM lesions (25), we sought to further evaluate the effect of ALK4 signaling disruption in neoplastic cells on the structural and mechanical qualities of the pancreatic tumor microenvironment (TME). Although oncogenic KRAS<sup>G12D</sup> expression occurs during the prenatal state in both KC mice and 4KC mice (28), ADM lesions develop only at or shortly after the time of weaning. While no difference in pancreas weight was observed at 3 weeks of age, at 6 weeks of age, the pancreata of 4KC mice were already significantly enlarged than those of KC mice (Fig. S1A and B). Histological analysis revealed significantly expanded areas of pancreatic lesions in 4KC mice compared with KC mice at 6 weeks of age, and while this expansion was mainly mediated by stroma formation, ADM formation was also accelerated in 4KC mice at this age (Fig. S1C and D). In both KC and 4KC pancreata, collagen deposition was observed in the stromal compartment of lesions, as determined by histological analysis of Sirius red staining (Fig. 1A), and as expected, the total collagen amount was significantly higher in the 4KC pancreata (Fig. 1B), which was accompanied by palpable tissue induration. Interestingly, although more collagen was detected in 4KC pancreata than in KC pancreata, evaluation of Sirius red staining under polarized light revealed no change in the thickness of the collagen fibers for either genotype (Fig. 1B).

To compare the rigidity within distinct tissue compartments between KC and 4KC pancreata, we performed AFM analysis in combination with immunofluorescence (IF) microscopy. Stromal and ADM regions were identified by the expression of  $\alpha$ -SMA and CK19, respectively, and the elastic modulus was measured in three different regions per sample (Fig. 1C and D). The data revealed increased tissue rigidity in the stroma of 4KC mice compared with that of age-matched KC mice (Fig. 1D), which could be explained by increased deposition of collagen fibers that most likely form more interfiber connections, which create tissue stiffness (Fig. 1A and B). Of note, we also detected an increase in tissue stiffness in the neoplastic compartment of 4KC mice compared with that of KC mice (Fig. 1D). Taken together, the results indicate

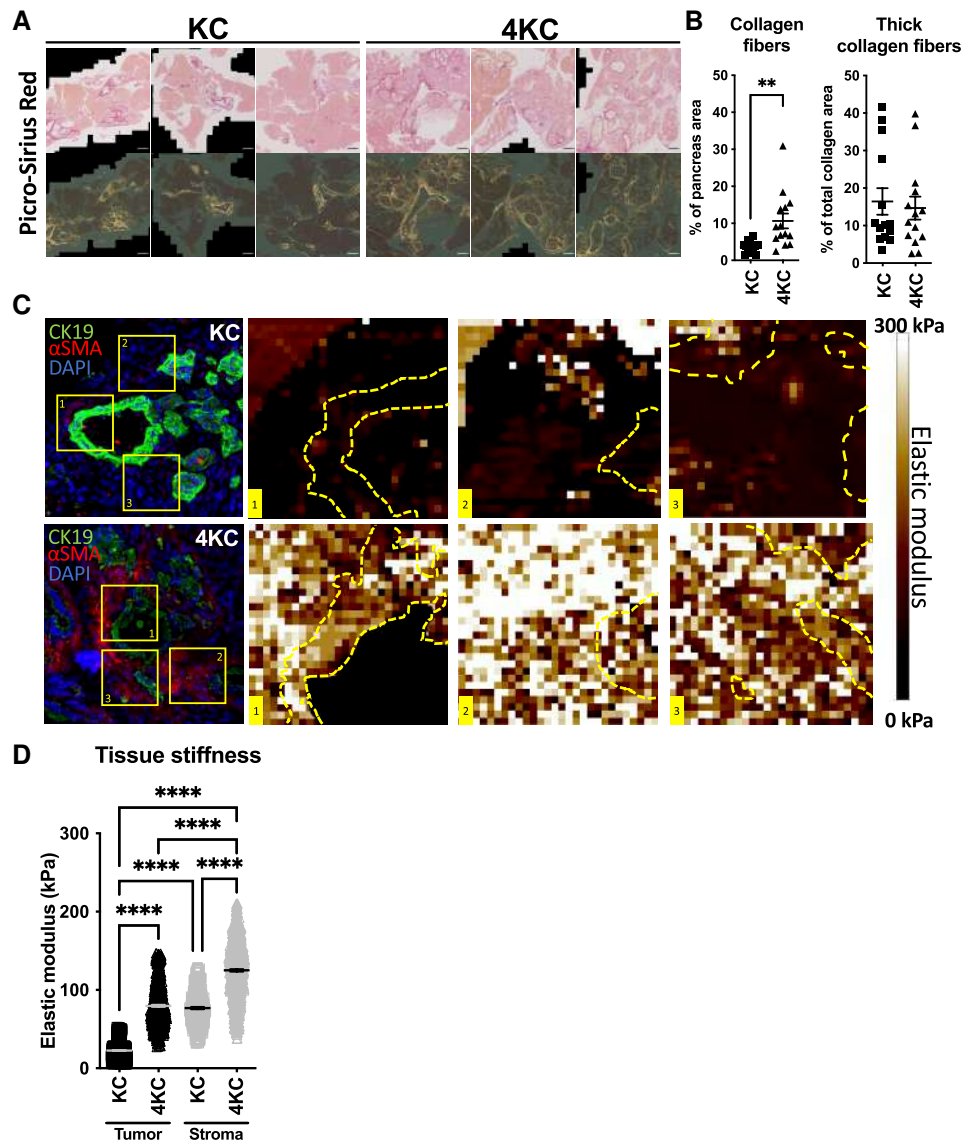


**Fig. 1.** ALK4 signaling disruption in tumor cells alters the tissue mechanics of the pancreatic TME. A) Representative photographs of pancreata from 6-week-old KC (left panel) and 4KC mice (right panel) stained with Picrosirius red. Total collagen (top: transmitted light) and thick collagen fibers (bottom: polarized light) are shown. B) Quantification of the total collagen (left) and thick collagen fiber (right) content in the pancreata of KC and 4KC mice. Cumulative data from three individual experiments with four to five mice per group are shown. C) IF staining of pancreata from 6-week-old KC and 4KC mice for CK19 (green),  $\alpha$ -SMA (red; KC mice), and 4',6-Diamidino-2-PhenylIndole (DAPI) (blue). Stiffness topography measured by AFM of selected regions (1, 2, or 3 as indicated on the IF staining images) in pancreata from KC and 4KC mice. D) Quantification of the elastic modulus (kPa) measured by AFM in tumor or stromal regions of KC and 4KC pancreata. Cumulative data from three independent mice per group are shown. One hundred force curves per zone of interest were measured. B and D) The mean values  $\pm$  SEMs are displayed. \*\* $P < 0.01$ ; \*\*\*\* $P < 0.0001$ .

that disruption of ALK4 signaling in neoplastic cells not only overcomes protective antitumorigenic mechanisms as previously shown (25) but also produces a strong paracrine effect at the early stage of ADM, resulting in excessive ECM secretion within the TME.

### Sustained PDGF signaling is increased in stiff tissue conditions

Recently, the complex heterogeneity of CAFs has been revealed by other studies, indicating the existence of CAF subpopulations equipped with pro- and antitumorigenic qualities (19–21, 29). Although CAFs have been determined to be the main ECM producers, to our knowledge, there is no data available linking stromal tissue stiffness to the phenotypic and functional properties of CAFs after their initial instruction/activation by neoplastic

cells. Thus, we took advantage of the KC and 4KC mouse models representing opposing ends of the tissue stiffness scale and performed scRNAseq analysis of pancreatic CAFs and neoplastic enriched cell fractions. Fluorescence activated cell sorting (FACS) was used to exclude hematopoietic and endothelial cells based on their expression of CD45 and CD31, respectively. Next, lectin peanut agglutinin (PNA)<sup>+</sup> acinar cells were excluded (30) to enrich for CAFs (CD45<sup>-</sup>CD31<sup>-</sup>Lectin PNA-EpCAM<sup>-</sup>) or neoplastic ductal cells (CD45<sup>-</sup>CD31<sup>-</sup>Lectin PNA<sup>-</sup>EpCAM<sup>+</sup>; (Fig. 2A and S2A). Importantly, in 4KC mice, CAFs, and ductal cells were present at significantly higher frequencies among pancreatic CD45-CD31 cells (Fig. 2B), but equal numbers of single cells from each sample (KC or 4KC) and each fraction (CAF or duct) were captured and sequenced using a droplet-based approach.

In the CAFs-enriched fraction, nine main clusters (CAF 0–8) were identified in both KC mice and 4KC mice and the cluster

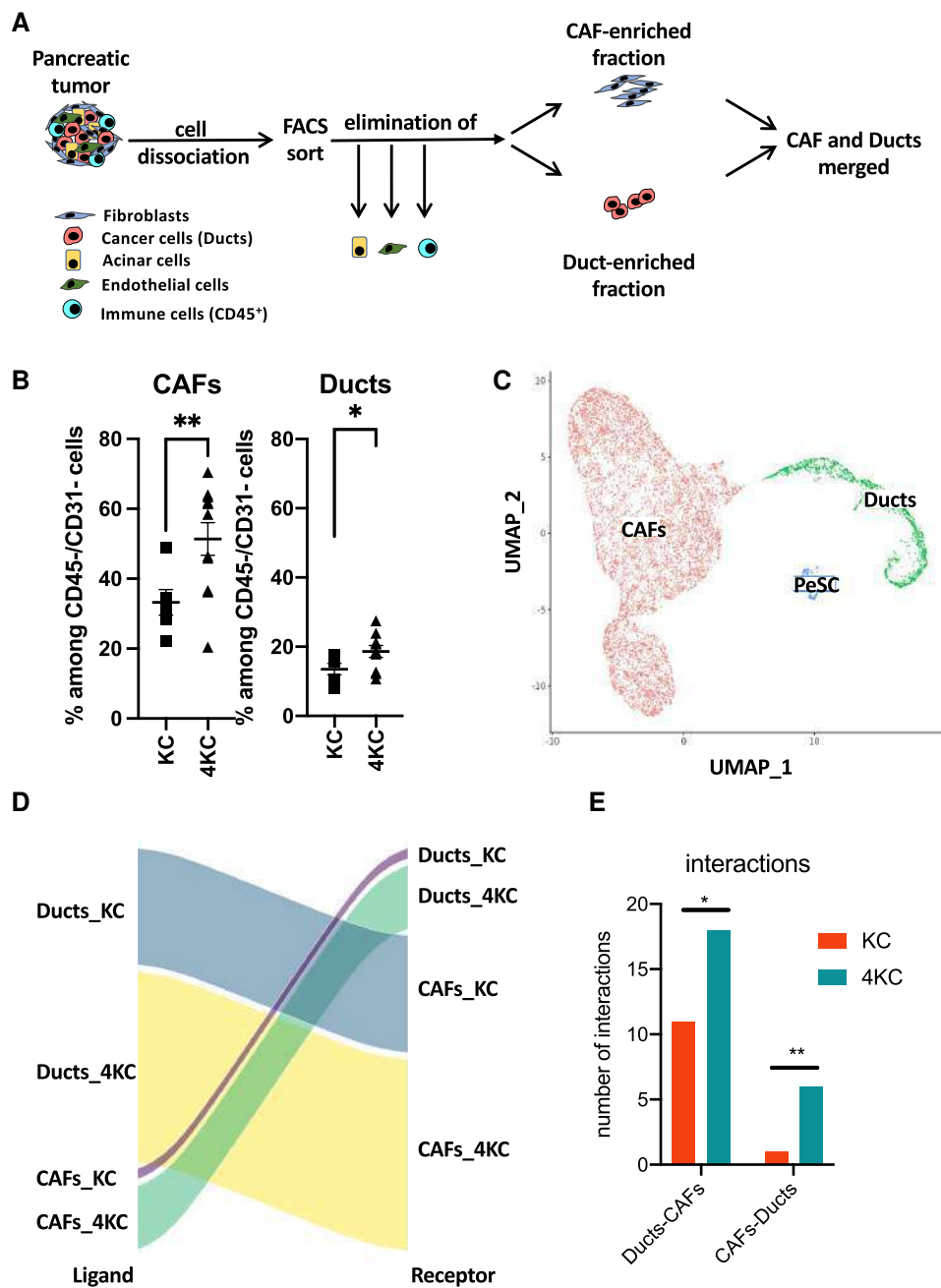


**Fig. 2.** Identification of increased interactions between components in stiff conditions. (A) Graphical scheme representing the workflow for CAF and duct isolation from the pancreata of 6-week-old KC and 4KC mice by FACS sorting. Both sorted fractions were further subjected to single-cell capture, barcoding, and reverse transcription using the 10× genomics platform. (B) Frequencies of CAFs (lectin PNA-EpCAM<sup>-</sup>) and ductal cells (Lectin PNA-EpCAM<sup>+</sup>) among viable CD45<sup>-</sup>CD31<sup>-</sup> cells detected by FACS analysis. The mean values ± SEMs are displayed. \**P* < 0.05, \*\**P* < 0.01. (C) Uniform Manifold Approximation and Projection (UMAP) plot of merged sorted fractions illustrating the CAF, duct, and PeSC fractions. (D) Ligand:Receptor network maps were obtained from scRNAseq data using “SingleCellSignalR.” Alluvial plot representing the interactions between ducts and CAFs separately for the two conditions (i.e. KC and 4KC). Paracrine signals flow from ligands (left column) to receptors (right column), with the width of the connecting streams indicating the number of interactions. (E) Number of interactions (ducts-CAFs and CAFs-ducts) in 4K and 4KC conditions. \**P* < 0.05; \*\**P* < 0.01, two-sided test of proportions.

proportions are indicated (Fig. S2B). We identified cluster 7 as being pericyte stem cells (PeSCs) that we recently identified in neoplasia (31). Previously described myofibroblast CAFs (myCAFs), inflammatory CAFs (iCAFs), and antigen-presenting CAFs (apCAFs) (21) signatures were identified as clusters 6, 3, and 8 in both conditions (Fig. S2C–E). All of the previously identified populations of CAFs were significantly increased in proportions in the 4KC condition compared with KC (Fig. S2B).

In order to identify any particular interactions between the CAF and duct cell population associated with increased tissue stiffness, we merged the two fractions and obtained three major clusters: CAFs, ducts (tumor), and in addition, a small fraction of PeSCs (Fig. 2C). To determine how these three populations interact, we performed ligand-receptor-based SingleCellSignalR algorithms (32) analysis among the CAFs, ducts, and PeSCs in the KC and 4KC conditions. The algorithm was used in “paracrine”

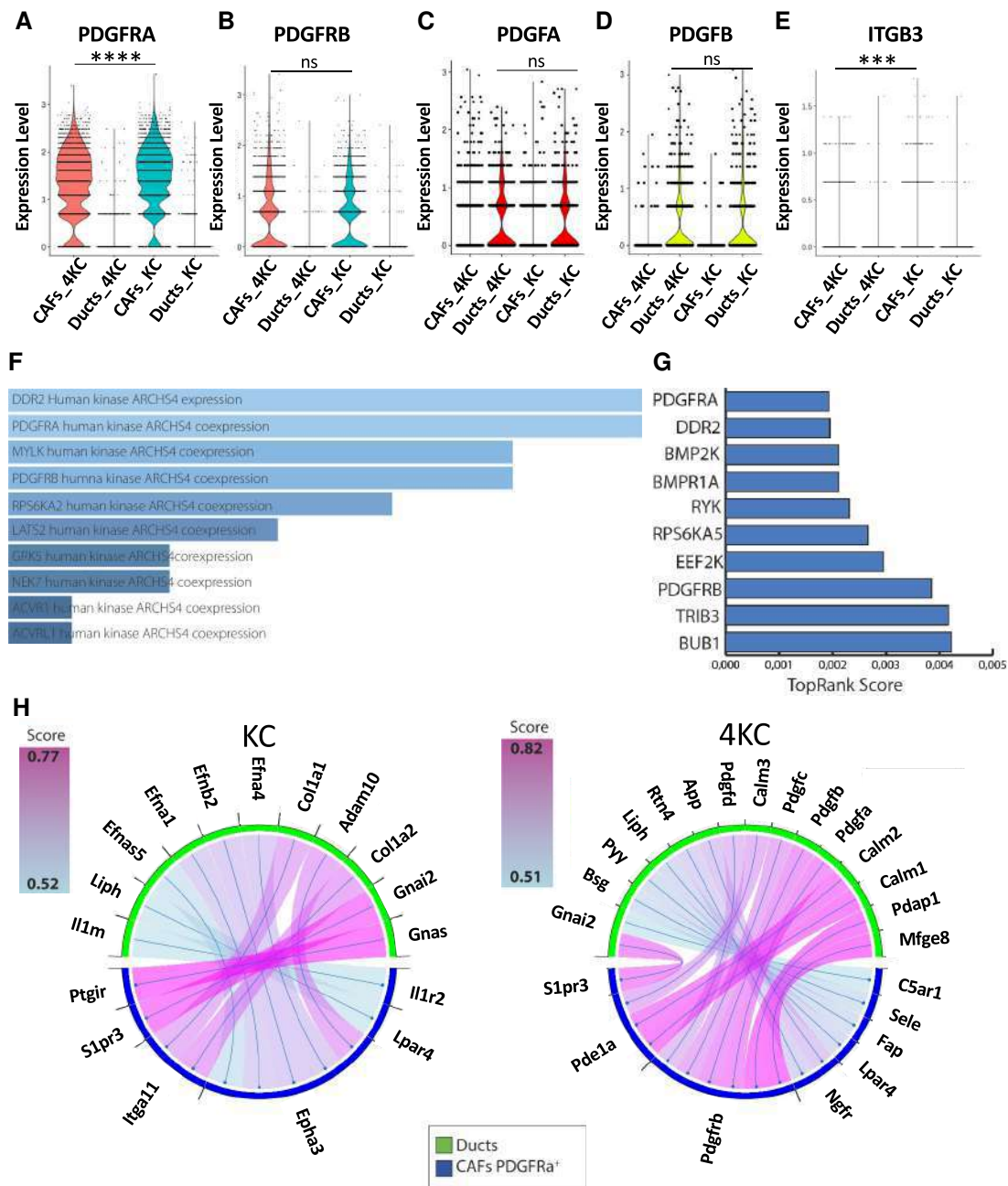


**Fig. 3.** Identification of PDGF signaling signature associated with tissue stiffness. A–E) Violin plots displaying the gene expression of PDGFRA, PDGFRB, PDGFA, PDGFB, and ITGB3 by CAFs and ducts obtained from 6-week-old KC and 4KC mice determined by scRNAseq (C–G). \*\*\*\* $P < 0.0001$ ; \*\*\*\* $P < 0.0001$ ; ns, not significant. F) Top signaling term enrichment of the 29-gene siCAF signature according to the massive mining of publicly available RNA-Seq data from human and mouse ARCH54 database (<https://maayanlab.cloud/arch54/>). G) Top signaling term enrichment of the 29-gene siCAF signature according to the kinase enrichment analysis version 3 (KEA3) database. (<https://maayanlab.cloud/kea3/>). H) Receptor–ligand interactions (as assessed with SingleCellSignalR) from ductal to PDGFRA + CAFs in KC (left) and 4KC (right) conditions.

mode with a large receptor:ligand database specific for mouse, as previously described (32). Our analysis revealed that there were increased number of interactions among the 3 clusters in the KC soft condition than in the 4KC stiff condition (Fig. S2F) and the specific top 50 interactions are represented (Fig. S2H). To test the hypothesis that early instruction from duct cells to CAFs contributes to the establishment of stiff phenotype, we analyzed the interactions between ducts and CAFs in both soft (KC) and stiff conditions (4KC). As shown in Fig. 2D and E, we determined an increased number of interactions either from ducts toward CAFs or from CAFs toward ducts in 4KC condition.

We analyzed in detail the most upregulated interactions in both KC and 4KC conditions (Fig. S2H). We identified platelet-derived growth factor (PDGF)-dependent interactions from ducts to CAFs to be prevalent in 4KC while absent in KC. As PDGFs are considered fibrogenic growth factors, we next sought to determine the expression of PDGFRA, PDGFRB, PDGFA, and PDGFB in merged scRNAseq data. While the two major receptors, PDGFRA and PDGFRB, were exclusively expressed in the CAF compartment, the ligands PDGFA and PDGFB were exclusively expressed in the duct compartment (Fig. 3A–D). In addition, we analyzed the expression of the integrin (ITG)  $\beta 3$ /CD61, which has been

shown to be key in CAF-mediated tumor cell invasion via the assembly of the ECM protein fibronectin (33) and thereby might promote tissue stiffness. Moreover, CD61 is known to interact with the ECM protein  $\beta$ ig-h3/TGF- $\beta$ i (34), which has been described as a key ECM protein in the pancreatic TME hampering conventional (35, 36) and unconventional T-cell responses (37). We observed that CD61 was also expressed in the CAF compartment (Fig. 3E).

As shown in Fig. 3A, most CAFs expressed PDGFRA in both KC and 4KC conditions (82 and 74% of CAFs, respectively). Therefore, we performed differential expression analysis in 4KC vs. KC, using only PDGFRA<sup>+</sup> CAFs. This analysis resulted in 72 differentially expressed genes (DEGs), 29 of them upregulated, and 43 downregulated in 4KC CAFs. DEGs were tested for enrichment in Gene Ontology, Kyoto Encyclopedia of Genes and Genomes (KEGG), and REACTOME pathway terms showing significant differences in ECM organization, assembly of collagen fibrils, and collagen formation (Fig. S3A–C) in the 4KC stiff relative to KC soft condition. Furthermore, most of the ECM pathways from several repositories were enriched in the DEGs of the PDGFRA<sup>+</sup> vs. PDGFRA<sup>-</sup>, suggesting these pathways exhibit dependence on PDGFRA expression (Fig. S3D–F). Based on the 29 4KC upregulated genes (Table S1) we generated a stiffness CAF signature. To specifically test for potential signaling activity, we interrogated the 29-gene CAF signature for kinase activity enrichment using 2 different kinase databases. In both cases, PDGFRA was among the top kinase activities significantly enriched in the CAF signature (Fig. 3F and G). Furthermore, ligand-receptor interaction analysis was also performed separately for PDGFRA<sup>+</sup> positive CAFs. More PDGF-related interactions from ducts to CAFs were detected in the 4KC condition, relative to the KC condition (Fig. 3H). We further looked for the distribution of stiffness-induced CAFs (siCAF) signature across the nine CAF clusters. We applied the 29-gene siCAF signature using the AUCell method to calculate a score for every single cell (38). As shown in Fig. S3G, all clusters displayed at least one fraction of cells with relatively high score with the exception of cluster 7, previously identified as PeSC (31). Altogether, these results indicate that PDGF–PDGFR interactions play a key role in the early establishment of tissue stiffness independent of CAF origin and subtype.

### Increased tissue stiffness is associated with the loss of PDGFRA surface expression on CAFs

Based on these observations, we sought to further examine the TME of 4KC and KC mice by determining the phenotype of CAFs by multicolor flow cytometry. Therefore, we applied the same gating strategy as that used in FACS sorting and focused on the CAF populations. FACS analysis of the two markers PDGFRA and CD61 identified a CAF population that was positive for both markers (PDGFRA<sup>+</sup>CD61<sup>+</sup>) and present in both KC mice and 4KC mice at frequencies of 75.8 and 52.9%, respectively (Fig. 4A and B). In addition, we detected a PDGFRA<sup>-</sup>CD61<sup>+</sup> CAF population that was significantly increased in 4KC pancreata (18.5%) compared with KC pancreata (6.1%; Fig. 4A and B). Given the association of these 2 CAF populations with the opposing tissue stiffness explored in KC and 4KC mice, we termed them siCAF and PDGFRA<sup>+</sup> CAFs. The fact that we did not detect the siCAF population by scRNAseq analysis highlighted that the disruption of ALK4 signaling in 4KC mice might be a result of continuous signaling through the PDGF–PDGFR system at the protein level.

In addition to PDGFRA and CD61, we further evaluated the expression of the established CAF markers  $\alpha$ -SMA, Fibroblast

activation protein (FAP)1, FSP1/S100-A4, and PDGFRA, as well as CD29/ITG $\beta$ 1 (19, 39). Interestingly,  $\alpha$ -SMA and FSP1, which are both considered activated CAF markers (40, 41), were expressed on siCAF and PDGFRA<sup>+</sup> CAFs, respectively. While no differences in the expression of  $\alpha$ -SMA were found between KC and 4KC siCAF, FSP1 expression was significantly increased on PDGFRA<sup>+</sup> CAFs from 4KC mice (Fig. 4C). Moreover, the expression of the integrins CD61 and CD29 was significantly higher on PDGFRA<sup>+</sup> CAFs obtained from KC mice. In contrast, the mean fluorescence intensity (MFI) of CD61 was significantly higher on PDGFRA<sup>+</sup> CAFs from 4KC mice (Fig. 4C). Unsupervised t-distributed stochastic neighbor embedding analysis of siCAF and PDGFRA<sup>+</sup> CAFs revealed an increased siCAF population in the high-stiffness conditions (Fig. 4D). Of note, we also detected a PDGFRA<sup>-</sup>CD61<sup>-</sup> CAF population in both KC and 4KC pancreata, representing 16.8 and 26.7% of all CAFs, respectively (Fig. S4A). However, since this population did not express any of the other evaluated CAF markers (Fig. S4B), we excluded it from this study. Nevertheless, given the relatively high frequency, this population should be subject to future analysis.

Spatial analysis by immunohistochemistry (IHC) displayed an almost exclusive site of PDGFRA<sup>+</sup> stromal cells at the outer edge of pancreatic lesions that was more pronounced in 4KC than in KC pancreata (Fig. 4E). We detected a diminished staining for PDGFRA protein in 4KC although the PDGFRA mRNA detected by RNAscope was similar in both conditions (Fig. S4C–E). Linking the spatial distribution of PDGFRA and CD61 expression with the phenotype determined by FACS analysis, we concluded that PDGFRA<sup>+</sup> CAFs were located at the edge of lesions, whereas siCAF were mainly found within 4KC lesion centers. To compare the rigidity within distinct PDGFRA<sup>+</sup> and PDGFRA<sup>-</sup> regions between KC and 4KC pancreata, we performed AFM analysis in combination with IF microscopy. We detected increased elastic modulus in PDGFRA<sup>-</sup> stromal area in 4KC mice. In KC mice, PDGFRA<sup>+</sup> area had a significant diminished elastic modulus compared with the PDGFRA<sup>-</sup> area (Fig. 4F). These results demonstrate that siCAF are localized in the stiff regions in mouse pancreata. Taken together, our data demonstrate that stiffness-promoting ductal cells lead to specific instruction of CAFs, characterized by a unique phenotypic signature based on two markers: PDGFRA and CD61.

### Loss of PDGFRA surface expression on siCAF is a tumor cell-driven early event accompanied by PDGF ligand accumulation

To better understand the instruction of CAFs by ductal cells and the contribution of CAFs to altered tissue mechanics, we determined the kinetics of PDGFRA<sup>+</sup> and siCAF emergence in KC and 4KC mice by FACS performed at 1, 1.5, 2, 3, 4, and 6 months of age. In KC mice, the frequencies of PDGFRA<sup>+</sup> CAFs and siCAF stably represented ~66.9 and 5.6% of all CAFs, respectively (Fig. 4A and B). In contrast, although the frequencies in 4KC mice were comparable with those in KC mice at 1 month of age, a significant decrease and increase in PDGFRA<sup>+</sup> CAFs and siCAF, respectively, could be observed as early as 1.5 months of age. Moreover, these changes in the CAF populations of 4KC mice stabilized until the end of the experiment at 6 months of age, with PDGFRA<sup>+</sup> CAFs representing 36.9% and siCAF representing 27.1% of all CAFs (Fig. 5A and B). Notably, the previously mentioned PDGFRA<sup>-</sup>CD61-CAF population remained unchanged in both KC and 4KC mice over the course of the experiment (Fig. S5A). These results indicate that early CAF instruction was maintained and that PDGFRA<sup>+</sup> CAFs and siCAF most likely represented two different CAF

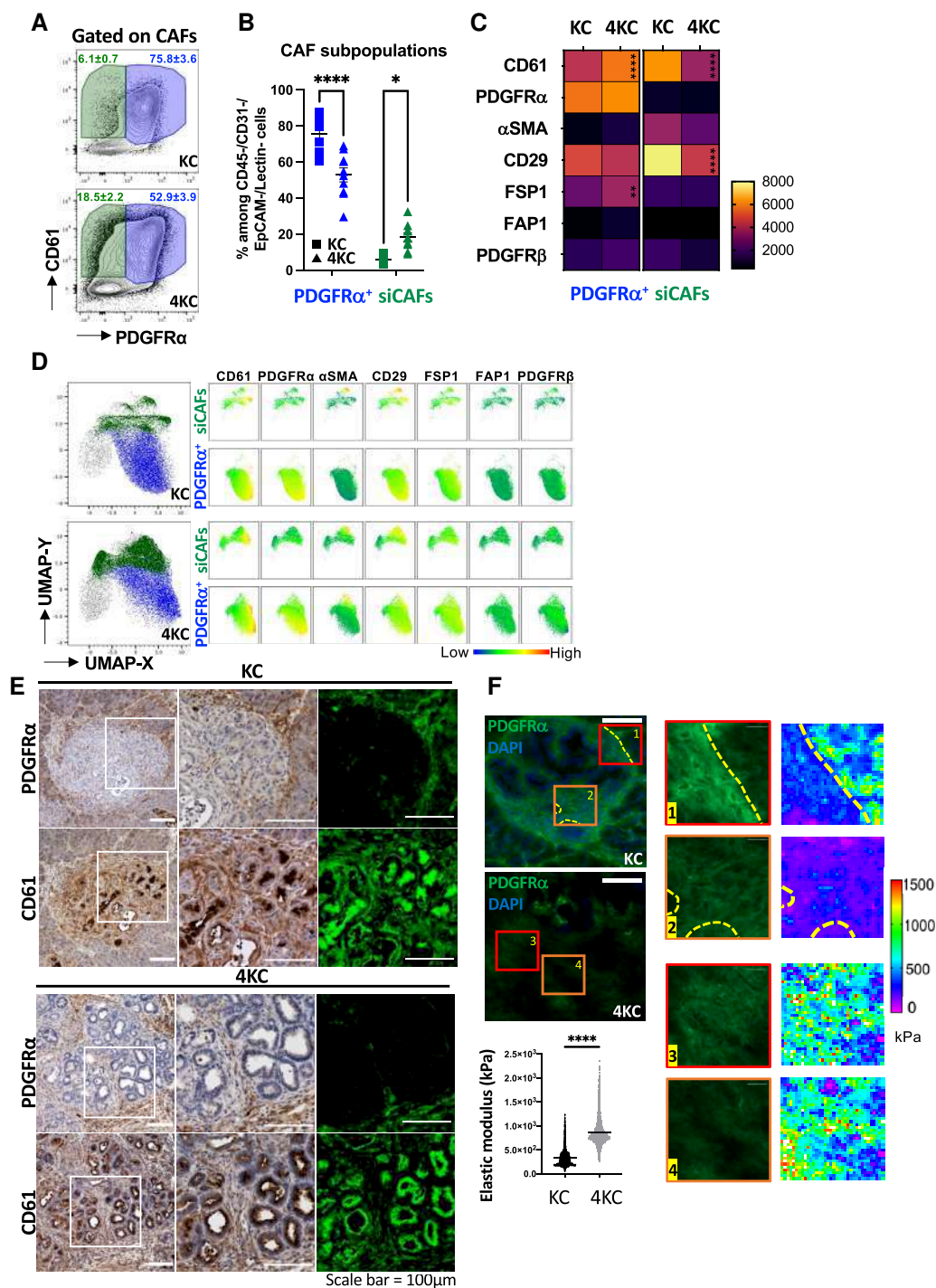


**Fig. 4.** Increased tissue stiffness favors the accumulation of siCAFs. **A**) Representative FACS dot plots showing the surface expression of PDGFR $\alpha$  and CD61 on PDGFR $\alpha$ <sup>+</sup> CAFs and siCAFs (PDGFR $\alpha$ <sup>-</sup>) in pancreata from 6-week-old KC (top) and 4KC (bottom) mice. Cells were gated on viable CD45<sup>+</sup>CD31<sup>-</sup>Lectin PNA<sup>-</sup>EpcAM<sup>-</sup> CAFs. **B**) Frequencies of PDGFR $\alpha$ <sup>+</sup> CAFs and siCAFs among CD45<sup>+</sup>CD31<sup>-</sup>Lectin PNA<sup>-</sup>EpcAM<sup>-</sup> CAFs in pancreata from 6-week-old KC (squares) and 4KC mice (triangles). **C**) Heatmap of the MFIs of CAF markers on PDGFR $\alpha$ <sup>+</sup> CAFs and siCAFs from KC and 4KC pancreata. **D**) Unsupervised UMAP analysis of CAFs from KC (top) and 4KC (bottom) pancreata, with PDGFR $\alpha$ <sup>+</sup> CAFs and siCAFs highlighted in blue and green, respectively, and corresponding multigraph mapping of CAF markers for each cell population. **E**) Representative images of IHC staining for PDGFR $\alpha$  (top) and CD61 (bottom) in serial sections of pancreata from 6-week-old KC (left panel) and 4KC (right panel) mice. White squares indicate the magnified regions of each panel. The images on the right of each panel show pseudocolored positive cells for the indicated marker (green). **F**) Stiffness topography measured by AFM of selected regions (1–4 as indicated on the IF staining images) in pancreata from KC and 4KC mice. Quantification of the elastic modulus (kPa) measured by AFM in stromal regions of KC and 4KC pancreata. Scale bars 100 and 20 μm. **A–F**) Cumulative data from three individual experiments with three to four mice per group are shown. The mean values  $\pm$  SEMs are displayed. \**P* < 0.05; \*\**P* < 0.01; \*\*\*\**P* < 0.0001.

activation states associated with the opposing tissue stiffness phenotypes of KC and 4KC mice. In line with these findings, we observed that siCAFs had significantly lower expression of the qPSC

marker glia fibrillary acidic protein (GFAP) than PDGFR $\alpha$ <sup>+</sup> CAFs (Fig. 5C), further highlighting the different activation statuses of these two cell populations.

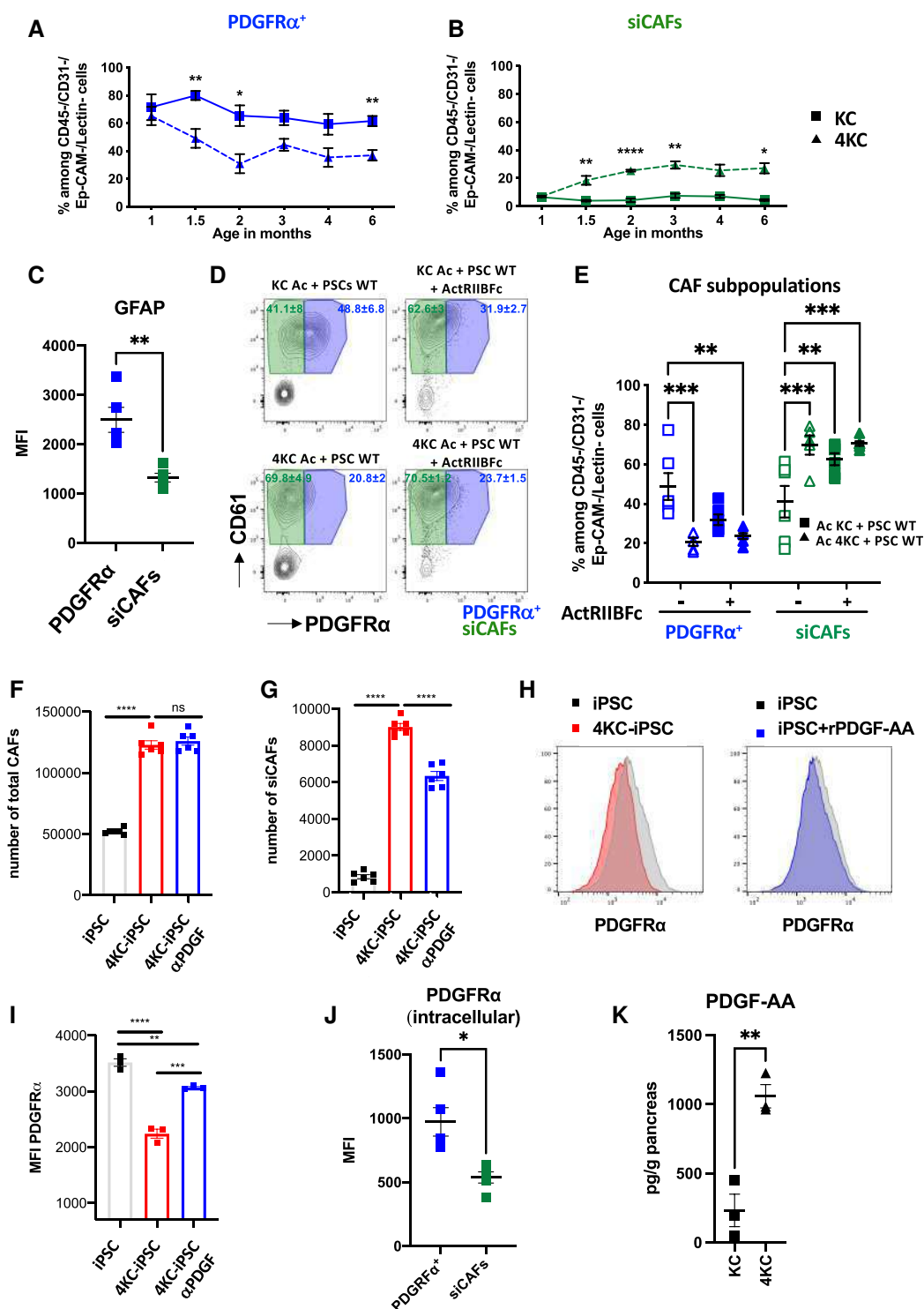


**Fig. 5.** Neoplastic cells instruct the emergence of siCAFs at early tumor stages. A and B) Frequencies of (A) PDGFR $\alpha$ <sup>+</sup> CAFs and (B) siCAFs among CD45<sup>-</sup>CD31<sup>-</sup>Lectin PNA<sup>-</sup>EpCAM<sup>-</sup> CAFs determined by FACS analysis of pancreata from KC (squares) and 4KC mice (triangles) harvested at 1, 1.5, 3, 4, and 6 months of age. C) MFI of intracellular GFAP in PDGFR $\alpha$ <sup>+</sup> CAFs and siCAFs determined by FACS analysis. D) Representative FACS dot plots showing the surface expression of PDGFR $\alpha$  and CD61 on PDGFR $\alpha$ <sup>+</sup> CAFs and siCAFs generated by coculturing WT PSCs with acinar cells (Ac) from KC or 4KC mice in the absence or presence of the soluble activin A inhibitor ActRIIBFc. E) Frequencies of PDGFR $\alpha$ <sup>+</sup> CAFs and siCAFs generated in the absence or presence of ActRIIBFc. F and G) siCAFs were generated by coculturing iPSCs with 4KC cell line in the absence or presence of  $\alpha$ PDGF Ab for 7 days. F) Number of iPSC and total CAFs and (G) number of siCAFs determined by FACS analysis. H and I) siCAFs were generated by coculturing iPSCs with 4KC cell line or in the presence of rPDGF-AA for 7 days. H) Histograms of PDGFR $\alpha$  expression. I) MFI of extracellular PDGFR $\alpha$  determined by FACS analysis. J) MFI of intracellular PDGFR $\alpha$  in PDGFR $\alpha$ <sup>+</sup> CAFs and siCAFs determined by FACS analysis. K) Tissue levels of PDGF-AA (pg/g) determined by ELISA analysis of pancreata from 6-week-old KC and 4KC mice. A and B) Results from five mice per group and time point are shown. C and F) Representative data from two individual experiments with five mice are shown. G) Representative data from two individual experiments with three mice and technical triplicates are shown. F-J) Representative data from two individual experiments and technical triplicates are shown. The mean values  $\pm$  SEMs are displayed. \*P < 0.05; \*\*P < 0.01; \*\*\*P < 0.001; \*\*\*\*P < 0.0001.

We next aimed to verify that the instruction of PDGFR $\alpha$ <sup>+</sup> CAFs into siCAF in 4KC mice is driven through altered signals mediated by neoplastic ductal cells lacking ALK4 signaling rather than by increased release and/or availability of the ALK4 ligand activin A, which is still produced in ALK4-knock out (KO) tumor cells. Therefore, we differentiated PSCs isolated from wild-type (WT) mice into CAFs in the presence of neoplastic cells from KC or 4KC pancreata and added ActRIIBFc, a soluble inhibitor of activin A. Previously, injection of ActRIIBFc into KC mice has been shown to result in a 4KC-like phenotype (25). Similar to our previous *in vivo* data, even in the absence of ActRIIBFc, PSCs differentiated into more siCAF when cocultured with 4KC acinar cells rather than KC acinar cells, which produced significantly more PDGFR $\alpha$ <sup>+</sup> CAFs (Fig. 5D, left panel, and E). However, when ActRIIBFc was added to the coculture containing KC acinar cells, the frequency of siCAF was similar to that observed in the coculture containing 4KC acinar cells. The addition of ActRIIBFc to the coculture containing 4KC acinar cells did not affect the expression of CD61 or PDGFR $\alpha$  on CAFs (Fig. 5D, right panel, and E).

We next aimed to investigate the reason for the downregulation of PDGFR $\alpha$  surface expression in 4KC CAFs as an indicator of CAF activation. PDGFRs are internalized after binding to their ligands. First, we verified that PDGFR $\alpha$  was phosphorylated in PSCs after ligand binding *in vitro*. As neoplastic primary cells from 4KC mice as well as primary PSC from WT are difficult to generate in high numbers, we used alternatively immortalized PSC (iPSC) previously described (20) as well as 4KC-green fluorescent protein (GFP) primary cell line generated as previously described (31). iPSC displayed increased phosphorylation upon 4KC culture media or recombinant PDGRF-AA binding (Fig. 55D and E). Next, we performed *in vitro* generation of siCAF for 7 days in presence or absence of a neutralizing polyclonal anti-PDGF antibody. As shown in Fig. 55F and G the use of anti-PDGF neutralizing Ab was able to significantly reduce the phosphorylation of PDGFR $\alpha$ . Moreover, the number of siCAF diminished in the presence of anti-PDGF neutralizing Ab (Fig. 5F and G). Adding recombinant PDGRF-AA induced PDGRF $\alpha$  surface expression downregulation on the surface of CAFs, although to a lesser extent than in the presence of a 4KC-GFP cell line (Fig. 5H and I). Ultimately, most internalized PDGFRs are subjected to lysosomal or proteasomal degradation (42). FACS analysis revealed that siCAF had lower intracellular PDGFR $\alpha$  expression than PDGFR $\alpha$ <sup>+</sup> CAFs (Fig. 5J) and the use of MG-132 proteasome inhibitor increased the accumulation of PDGFR $\alpha$  (Fig. 55H and I). We speculated that the increased availability of PDGF ligands in 4KC mice results in receptor internalization, which in turn promotes cell proliferation and ECM deposition (43–45). Although PDGF ligand expression was not different between KC and 4KC mice on a per-cell basis (Fig. 3D) we hypothesized that in 4KC mice, higher overall PDGF ligand levels must be found due to the increased presence of ductal cells (Fig. 2B). Indeed, Enzyme-linked immunosorbent assay (ELISA) analysis revealed significantly increased levels of the ligand PDGF-AA per gram of 4KC mouse pancreas (Fig. 5K).

### siCAF hamper antitumor immune responses

Next, we investigated whether the siCAF signature associated with high tissue stiffness was also linked to immune suppression. We did not observe altered frequencies of infiltrating hematopoietic CD45<sup>+</sup> cells, including CD8<sup>+</sup> T cells (Fig. 6A and B), CD4<sup>+</sup> T cells, CD4<sup>+</sup>/Foxp3<sup>+</sup> regulatory T cells (Tregs), NK-p46 natural killer cells, T-cell receptor (TCR) $\gamma\delta$  T cells or neutrophils (Fig. S6A–D),

between KC and 4KC pancreata. Further analysis of CD8<sup>+</sup> T cells revealed a significant reduction in T-cell activation in pancreata from 4KC mice, as indicated by the lower frequencies of CD62L<sup>low</sup> (Fig. 6C). In contrast, CD8<sup>+</sup> T-cell activation was significantly increased in the spleen of 4KC mice (Fig. 6D). Taken together, these data indicate that although peripheral T-cell activation appears to be efficient in 4KC mice and CD8<sup>+</sup> T cells are recruited into the pancreas at similar frequencies in KC and 4KC mice, T-cell responses are hampered within the pancreatic TME.

To determine whether the two CAF populations affect CD8<sup>+</sup> T-cell activation within the pancreas of 4KC mice, we isolated PDGFR $\alpha$ <sup>+</sup> CAFs and siCAF from 4KC mice by FACS and cocultured them with a primary tumor cell line (35) to generate CAF-conditioned medium. Next, WT CD8<sup>+</sup> T cells were cocultured in the presence of bone marrow derived dendritic cells (BMDC)s and CD3/CD28 activation beads using the obtained PDGFR $\alpha$ <sup>+</sup> CAF- or siCAF-conditioned medium. Reduced proliferation rates were detected with the siCAF-conditioned medium, as indicated by less CarboxyFluorescein Succinimidyl Ester (CFSE) staining dilution compared with that achieved with the PDGFR $\alpha$ <sup>+</sup> CAF-conditioned medium (Fig. 6E and F). Moreover, the production of Granzyme B (GrzB) was reduced in proliferating CD8<sup>+</sup> T cells when they were cultured in the siCAF-conditioned medium (Fig. 5G). Similar results were obtained with KC PDGFR $\alpha$ <sup>+</sup> CAF- and siCAF-conditioned medium (Fig. S6E and F). T cells cocultured in KC or 4KC PDGFR $\alpha$ <sup>+</sup> CAF-conditioned medium showed proliferation and GrzB production similar to those cultured in control conditioned medium obtained from tumor cells alone (Fig. S6E and F). In order to determine which soluble factors could be responsible for T-cell-mediated inhibition, we performed a customized LegendPlex array for cytokines and chemokines that have been previously reported to be produced by CAFs (Fig. 6H). We detected a significant increase of Vascular endothelial growth factor (VEGF), CCL2, and CXCL12 amount siCAF condition media compared with PDGFR $\alpha$ <sup>+</sup> CAFs condition media. Low quantities of IL-6, TGF- $\beta$ 1, and IL-10 were detected in both conditions. VEGF was previously shown to have a direct immunosuppressive effect on T-cell proliferation and activation (46) suggesting that siCAF T-cell activation inhibition might be at least in part mediated by VEGF.

### PDGF neutralization reduces tumor growth and favors CD8<sup>+</sup> T-cell response

Our results show that the instruction of siCAF in 4KC mice occurs early between 1 and 1.5 months after birth and it develops in a PDGF/PDGFR signaling-dependent manner. Moreover, siCAF prevent an efficient CD8<sup>+</sup> T-cell immune response, which is a key for tumor elimination (47–49). Thus, we hypothesized that the prevention of siCAF development in 4KC mice could improve the course of the disease. Therefore, we intraperitoneally (ip) injected 4KC mice at 3, 4, and 5 weeks of age with a neutralizing polyclonal anti-PDGF antibody, which recognizes PDGF-AA, PDGF-AB, and PDGF-BB dimers. Control age-matched littermates were injected with 1 $\times$  Phosphate-buffered saline (PBS). At 6 weeks of age, we analyzed pancreata collected from anti-PDGF- and PBS-injected mice (Fig. 7A). First, we observed a decrease in pancreas weight in 4KC mice injected with anti-PDGF, indicating diminished tumor growth (Fig. 7B and S7A). We next performed FACS analysis and evaluated the frequencies of siCAF and PDGFR $\alpha$ <sup>+</sup> CAFs among total CAFs. We observed decreased siCAF in anti-PDGF-injected 4KC mice compared with PBS-injected 4KC mice (Fig. 7C and D). In addition, we observed an increased percentage of activated CD8<sup>+</sup> T cells (CD44<sup>+</sup>CD8<sup>+</sup> T cells) pancreas

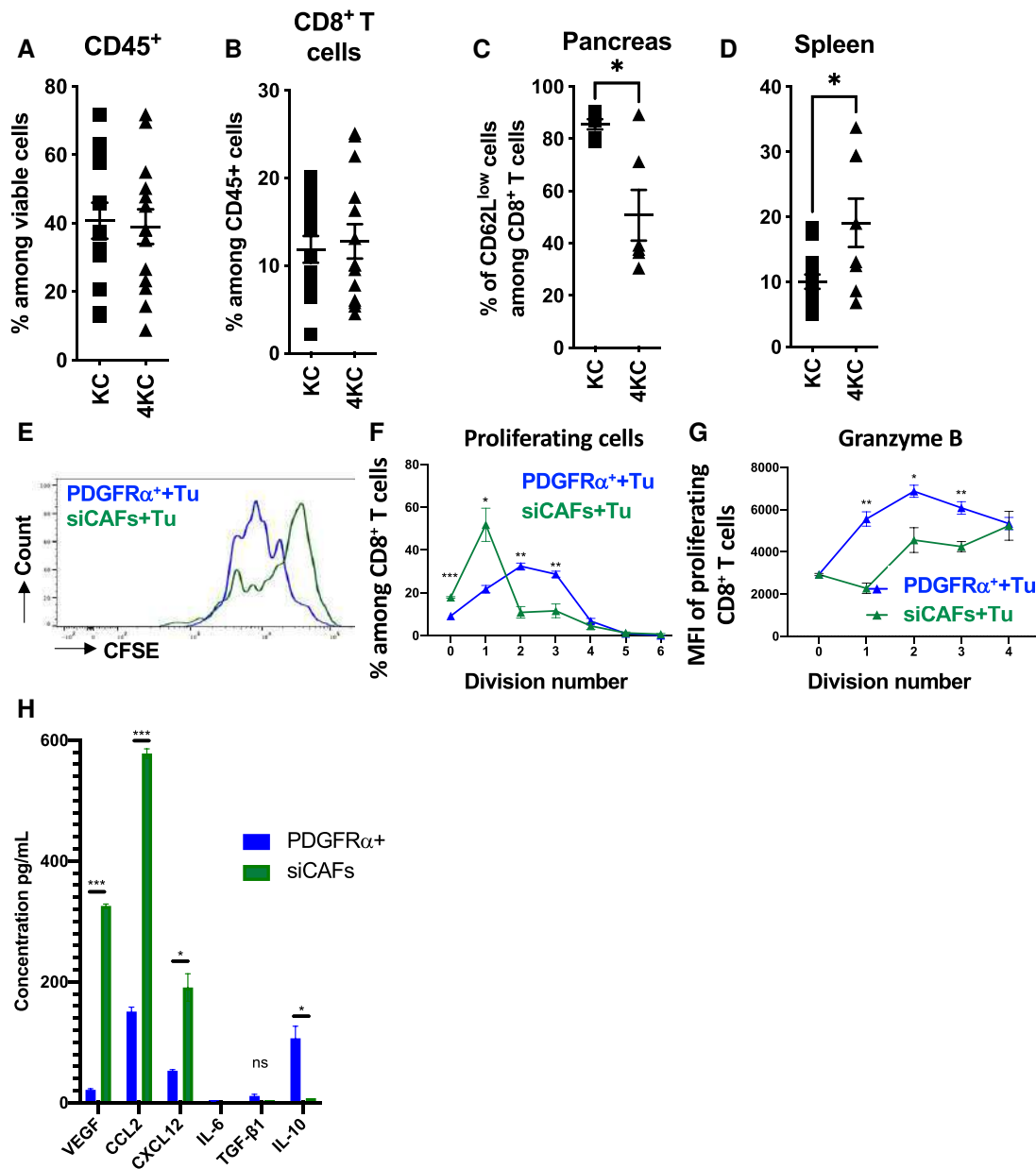


**Fig. 6.** siCAFs prevent efficient T-cell activation. A and B) FACS analysis of the frequencies of CD45<sup>+</sup> and CD8 $\alpha$ <sup>+</sup> cells in the pancreata of 6-week-old KC and 4KC mice. C and D) Frequencies of CD62L<sup>low</sup> cells among CD45<sup>+</sup>/CD8 $\alpha$ <sup>+</sup>/CD11c<sup>-</sup> T cells in the spleen and pancreata of KC and 4KC mice. E) CFSE dilution in CD8<sup>+</sup> T cells cocultured with BMDCs and CD3/CD28 activation beads in PDGFR $\alpha$ <sup>+</sup> CAF/tumor cell (blue line) or siCAF/tumor cell-conditioned medium (green line). F and G) Proliferating (F) and GrzB (G) producing CD8<sup>+</sup> T cells at the indicated division numbers after coculture with BMDCs and CD3/CD28 activation beads in PDGFR $\alpha$ <sup>+</sup> CAF/tumor cell-conditioned (blue line) or siCAF/tumor cell-conditioned medium (green line). G) Cytokine and chemokine profiles detected in PDGFR $\alpha$ <sup>+</sup> and siCAF in conditioned media used in E–G. A–D) Cumulative data from at least two individual experiments with three to four mice per group are shown. E–G) Representative data from two individual experiments with technical replicates are shown. PDGFR $\alpha$ <sup>+</sup> CAFs and siCAFs were isolated from three 6-week-old 4KC mice. \**P* < 0.05; \*\**P* < 0.01; \*\*\**P* < 0.001, unpaired t test.

in the anti-PDGF-treated conditions (Fig. 7E). Furthermore, we observed increased CD31<sup>+</sup> endothelial cells (Fig. 7F), decreased lesions (Fig. 7G), and increased EPCAM expression (Fig. 7H) in lesions, suggesting an early tumor phenotype. CD8<sup>+</sup> T-cell activation, indicated by the upregulation of CD44 and CD69 as well as the downregulation of CD62L, was similar in the spleen of anti-PDGF- or PBS-injected 4KC mice (Fig. S6B–D). In addition, IHC analyses revealed the prevention of PDGFR $\alpha$  downregulation in pancreatic lesions by anti-PDGF injection (Fig. 7I), as well as a reduced number of advanced lesions. Furthermore, Sirius red staining showed decreased collagen fiber deposition in

anti-PDGF condition (Fig. 7J). Taken together, our data show that PDGF neutralization leads to the reprogramming of the tumor environment.

### Identification of siCAFs in the human setting

To relate our findings to human PDAC patients, we performed FACS analysis of primary pancreatic CAFs obtained from four different donors. Similar to our mouse results, we detected an abundant siCAF population correlated with a reduced PDGFR $\alpha$ <sup>+</sup> CAF population, indicating a differentiation-dependent connection

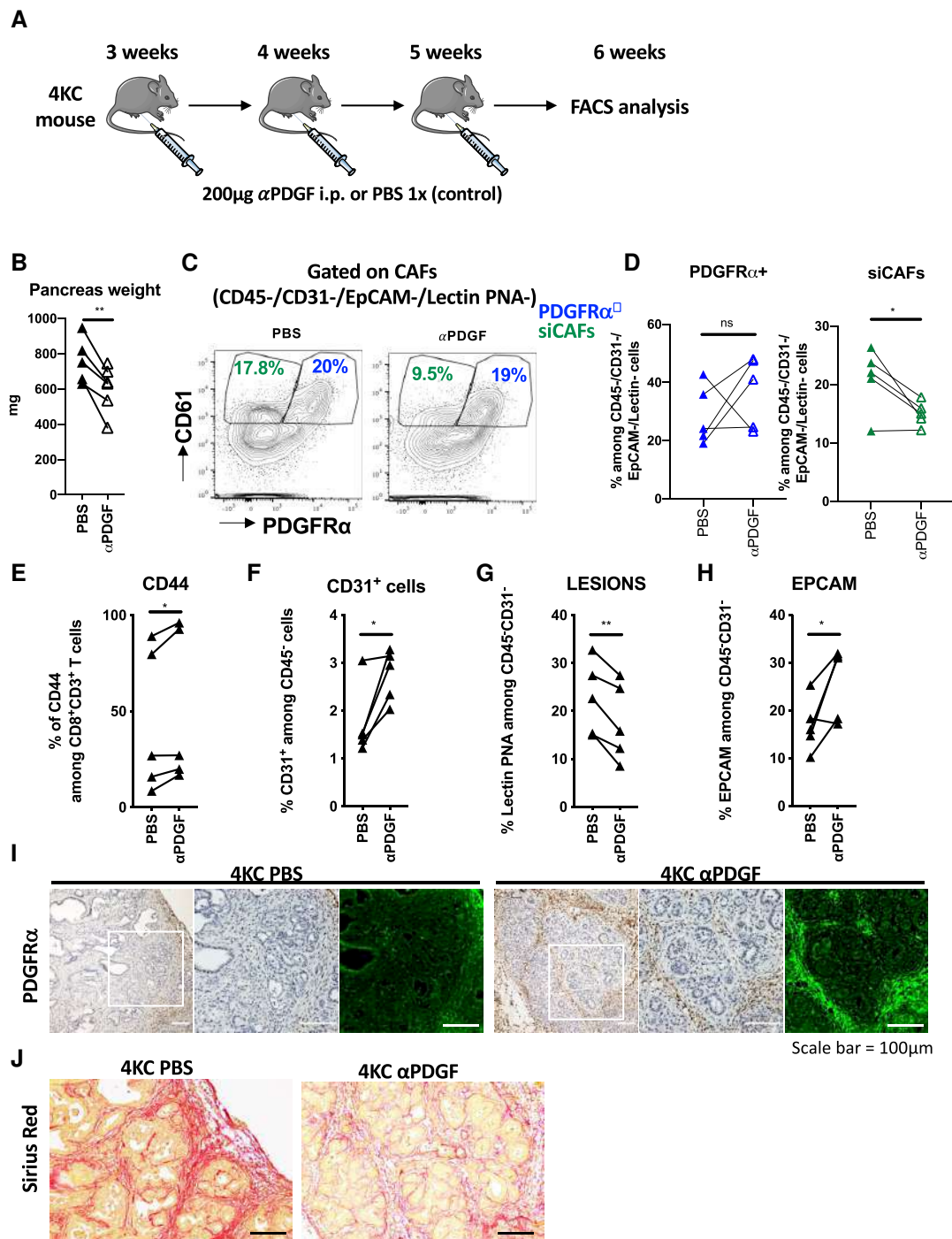


**Fig. 7.** PDGF neutralization reduces stromal activation and promotes PDGFR $\alpha$  surface expression. A) Graphical scheme representing the treatment schedule for 4KC mice: at 3, 4, and 5 weeks of age, 200  $\mu$ g of neutralizing anti-PDGF antibody diluted in 100  $\mu$ L of PBS was administered ip; age-matched control mice received PBS alone. One week after the last injection, the mice were sacrificed, and harvested pancreata were subjected to FACS and IHC analyses. B) Weight (mg) of pancreata excised from 6-week-old 4KC mice. Lines connect age-matched littermates treated with the anti-PDGF antibody (white) or PBS alone (black). C) Representative FACS dot plots showing the surface expression of PDGFR $\alpha$  and CD61 on CAFs in pancreata from 6-week-old 4KC mice treated with the anti-PDGF antibody (right) or PBS (left). Cells were gated on viable CD45<sup>-</sup>CD31<sup>-</sup>Lectin PNA<sup>-</sup>EpCAM<sup>-</sup>CAFs. D) Frequencies of PDGFR $\alpha$ <sup>+</sup> CAFs and siCAFs among CD45<sup>-</sup>CD31<sup>-</sup>Lectin PNA<sup>-</sup>EpCAM<sup>-</sup>CAFs in pancreata from 6-week-old 4KC mice treated with the anti-PDGF antibody or PBS. E-H) FACS analysis of the percentages of CD44<sup>+</sup> among CD8<sup>+</sup> T cells (E), CD31<sup>+</sup> cells among CD45<sup>+</sup> cells (F), Lectin PNA<sup>+</sup> (G), and EpcAM<sup>+</sup> (H) cells among CD45<sup>+</sup>CD31<sup>-</sup> cells isolated from the pancreas of 6-week-old 4KC mice treated with the anti-PDGF antibody or PBS. I) Representative images of IHC staining for PDGFR $\alpha$  in sections of pancreata from 6-week-old 4KC mice treated with the anti-PDGF antibody (right panel) or PBS (left panel). White squares indicate the magnified regions of each panel. The images on the right of each panel show pseudocolored PDGFR $\alpha$ <sup>+</sup> cells (green). \* $P$  < 0.05, \*\* $P$  < 0.01.

between these two populations (Fig. 8A). Further analysis showed that the overall expression of the known CAF markers and integrins PDGFR $\alpha$ , CD61, CD29, FAP, and Fibroblast specific protein

(FSP)-1 was significantly lower in siCAFs than in PDGFR $\alpha$ <sup>+</sup> CAFs (Fig. 8B-F). To determine whether it is possible to reprogram siCAFs in the human setting, we performed in vitro coculture of

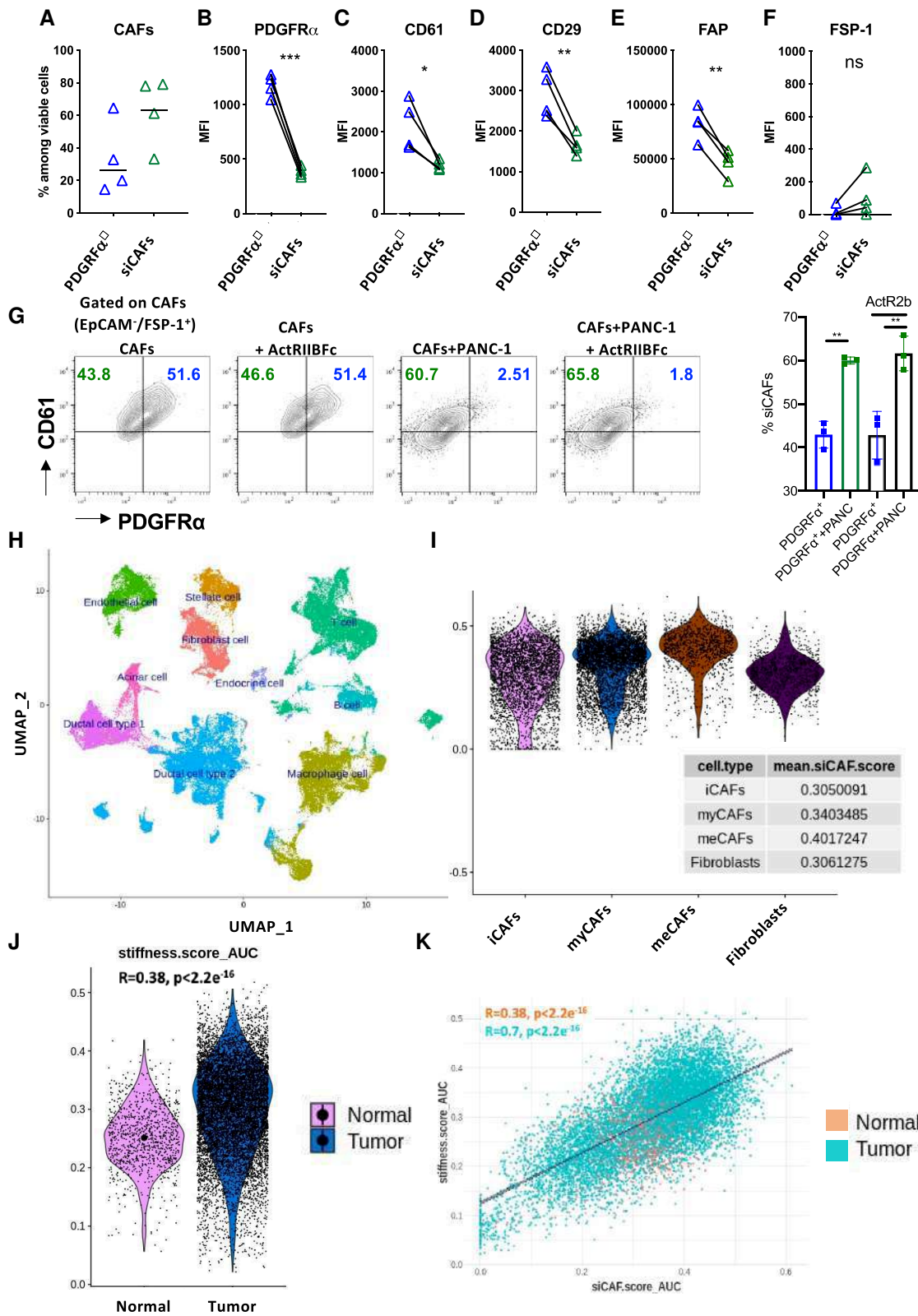


**Fig. 8.** Tumor cells instruct siCAFs in human PDAC. A) FACS analysis of the frequencies of PDGFR $\alpha$ <sup>+</sup> CAFs and siCAFs among viable cells after CAF isolation. B–F) FACS analysis of the MFIs of PDGFR $\alpha$  (B), CD61 (C), CD29 (D), FAP (E), and FSP1 (F) on PDGFR $\alpha$ <sup>+</sup> CAFs and siCAFs. G) Representative FACS dot plots showing the surface expression of PDGFR $\alpha$  and CD61 on EpCAM<sup>+</sup>FSP1<sup>+</sup> CAFs after coculturing with or without PANC-1 tumor cells in the absence or presence of the soluble activin A inhibitor ActRIIBFc. Frequencies of siCAFs generated in the absence or presence of ActRIIBFc. \*P < 0.05; \*\*P < 0.01; \*\*\*P < 0.001, unpaired t test (A–G). H) UMAP projection of PDAC single-cell Atlas comprising over 70 samples and >130,000 cells, most of them from cancer samples (>110,000 cells). I) siCAF signature distribution among fibroblast and described CAF subtypes. J) Previously described stiffness score distribution among tumor CAFs and normal fibroblasts. K) Correlation between the stiffness score and siCAF score.

human CAFs with human pancreatic cancer cell line PANC-1 cells, a human PDAC cell line previously described to express ALK4 (24) and respond to activin A (25), in the presence or absence of ActRIIBFc. FACS analysis showed that in the presence of PANC-1 cells, CAFs lost expression of PDGFR $\alpha$  which was similar to the mouse results and that the addition of ActRIIBFc did not have any effect on the amount of siCAF. To get insight into the existence of siCAF in human setting, we applied siCAF signature to a scRNA dataset specific for pancreas (50). As shown in Fig. 8H, the annotated dataset includes a well-defined “fibroblast” cluster. We extracted 10,953 human fibroblasts (1,037 and 9,916 from non-tumor and tumor tissues, respectively), classified these fibroblasts according to human CAF signatures (51) that distinguish iCAF, myCAF, and meCAF as well as normal fibroblasts and applied the 29-gene siCAF signature (38). As shown in Fig. 8I, the siCAF score was expressed in all three types of CAFs at significantly higher levels than normal fibroblasts. In order to determine whether similar association between siCAF and tissue stiffness exists in human tissues, we took advantage of a previously published stiffness signature (Table S2) (52). This stiffness score was upregulated in tumor CAFs compared with normal fibroblasts (Fig. 8J). Moreover, siCAF and stiffness scores were significantly correlated across all PDAC CAF cells (Fig. 8K). Altogether, these data suggest for the first time that paracrine signaling between tumor cells and CAFs is able to induce siCAF phenotype independent of the genetic background.

## Discussion

In this study, we show for the first time that targeting PDGF signaling through a ligand trap approach is able to inhibit tumor progression by reprogramming the activation status of the CAFs. Despite the previously described heterogeneity of CAF populations (19–21), we showed here that PDGFR $\alpha$  and CD61 were able to define two activation states reflecting the stiffness of the TME and that physical constraint was able to remodel the immune response outcome and the consequent tumor progression.

Enhancement of intrinsic PDGFR signaling induced by mutational activation of PDGFRFA, but not PDGFRFB, systemically induced fibroblastic hyperplasia and increased ECM deposition similar to that observed in collagen diseases (53). PDGFRFA point mutations (gain of function) were reported to be associated with gastrointestinal tumors (54, 55). The secretion of PDGFs by platelets and their effects on fibroblasts play a role in wound healing (56). Exogenous PDGF-BB accelerates ulcer healing in diabetic patients (57). High expression of PDGFA has been reported to predict a poor prognosis in esophageal squamous cell carcinoma (58). Transgenic mice overexpressing PDGFA have been shown to display severe fibrotic reactions in the heart supporting the crucial role of this ligand in ECM deposition (59). PDGF-AA binds primarily to PDGFR $\alpha$ , while PDGF-AB and PDGF-BB bind to PDGFR $\alpha$  as well as other receptor subtypes, such as PDGFR $\beta$  (60). Our results are supported by previous reports showing that stromal constitutive activation of PDGFR $\alpha$  (by using mice that harbor a mutation in the activation loop of PDGFR $\alpha$  tyrosine kinase domain) in the mammary stromal fibroblast compartment led to fibrosis and concomitant increase in collagen deposition (61). We demonstrated here that continuous binding of PDGF-AA to PDGFR $\alpha$  induced receptor downregulation, leading to the emergence of siCAF. Our data are in accordance with previous findings in vascular smooth muscle cells showing that PDGFR $\alpha$  protein was decreased on stiff substrates, indicating internalization and degradation through ligand bound to the receptor (62). Furthermore, previous work highlighted that in PDAC, PDGFRFA expression by CAFs is associated with

an inflammatory phenotype in iCAF and FB1 CAFs (20, 63). The expression analysis of genes encoding CAF markers other than PDGFRFA and PDGFRFB (64, 65) showed that FSP1 expression was significantly increased on PDGFR $\alpha$  CAFs from 4KC mice (stiff conditions). This finding was validated by the high expression of FSP1 observed in a human setting, suggesting that FSP-1 might be a universal bona fide marker of activated CAFs. The expression of integrins, such as CD29/ITGB1 (66, 67) or CD61/ITGB3 (68), on the surface of CAFs has been previously described. Here, we show that CD29 and CD61 expression was downregulated on siCAF in both mouse and human settings, suggesting an active role in signaling. Previous work from our group showed that  $\beta$ ig-h3/TGF- $\beta$ i was able to bind CD61 and phosphorylate Lck at Y505 (35, 36) and Focal adhesion kinase (FAK) (69). We reported that  $\beta$ ig-h3 was highly expressed in stiff conditions and that the use of an anti- $\beta$ ig-h3 antibody was able to reduce TME stiffness (35, 69), suggesting that targeting both PDGF-AA and  $\beta$ ig-h3 might represent a promising therapeutic combination.

Herein, the pro- and anti-inflammatory properties of CAFs are demonstrated to be highly dependent on intratumoral location and less dependent on origin. We demonstrated that PDGFR $\alpha$  CAFs had no potential to inhibit a T-cell response *in vitro* under the loose condition (KC condition). Under stiff conditions, this population had less inhibitory potential than siCAF, highlighting the importance of the mechanical properties of the tissue in the education of CAFs. Several publications have demonstrated that these cells are important for sensing mechanical changes in tissues not only at homeostasis but also in pathological conditions, i.e. fibrosis. The important finding of this study is that despite the origin of the cells, the mechanical constraint together with the secretion of soluble factors breaks the heterogeneity of CAFs into a binary classification according to their “microenvironment sensing,” namely, PDGFR $\alpha$  CAFs and siCAF. This creates the option of targeting a pathway through a ligand trap approach that would reprogram siCAF into PDGFR $\alpha$  CAFs rather than targeting a particular surface marker. This might also be beneficial since the elimination of CAFs by antibody-dependent cytotoxicity has been shown to be deleterious in PDAC (clinical trial failure).

A hallmark of the pathogenesis of solid cancers such as PDAC escapes from efficient antitumor immune responses. It has been demonstrated that the collagenous TME can restrain infiltrating CD8 $^+$  T cells from accessing tumor cells (70, 71). Additionally, the cytotoxic activity of tumor-infiltrating lymphocytes can be reduced by insufficient T-cell priming (72). CD8 $^+$  T-cell exclusion from the tumor bed has been proven to be a key element in the antitumor response (48). We show here that early mechanical and paracrine education through PDGF ligands (PDGF-AA in particular) can skew an effective antitumor response *in situ*. Although we identified potent immune priming of CD4 $^+$  and CD8 $^+$  T-cell responses in the spleen, the number of activated CD8 $^+$  T cells in the stiff pancreas was diminished compared with that in the loose pancreas, indicating that local tissue mechanics are a key element in the outcome of the immune response. Further studies combining spatial detection of activated CD8 $^+$  T cells and tissue rigidity would provide indications of the outcome of immune checkpoint therapy. Interestingly, we also observed an increase in CD31 expression in PDGF-depleted conditions, suggesting that an increase in modified interactions at the level of blood vessels might involve other partners that prevent an efficient T-cell response (i.e. MDSCs or macrophages). Further investigation linking the availability of PDGF-AA to angiogenesis should shed new light on this additional mechanism of action.

Based on our data, we established a model of the mechanism of action. As tumors evolve, they proliferate, produce PDGF ligands, and instruct CAFs via a paracrine effect. PDGFR $\alpha$ <sup>+</sup> CAFs become siCAF capable of inhibiting T-cell responses in situ. By using a PDGF-AA ligand trap approach, neoplastic tissue homeostasis can be restored. Neutralization of the PDGF-AA leads to PDGFR $\alpha$ <sup>+</sup> CAF maintenance associated with soft conditions and an efficient T-cell response. Our study provides support for the translational potential of using a PDGF ligand trap strategy.

## Supplementary Material

Supplementary material is available at PNAS Nexus online.

## Funding

This study was supported by grants Fondation pour la Recherche Médicale (P.G. and A.H.); Ligue contre le cancer, INCA AAP, INSERM TRANSFERT (A.H., 2019); and Ligue contre le cancer (K.T., 2020). Z.W. was supported by a Chinese Scholarship Council (CSC) Fellowship.

## Author Contributions

P.G.: investigation, writing—original draft. K.T., M.M., S.B., T.A., B.S., Z.H., Z.W., and P.M.: investigation. H.H.-V.: formal analysis. R.T.: supervision, funding. P.B.: writing—original draft. A.H.: conceptualization, supervision, funding acquisition, writing—original and revised draft.

## Data Availability

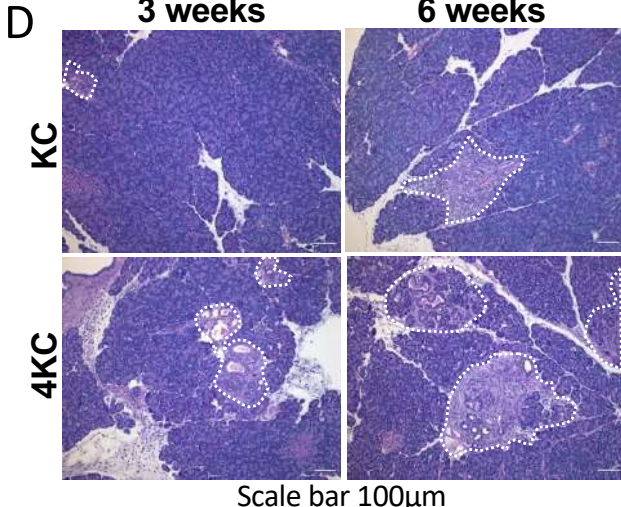
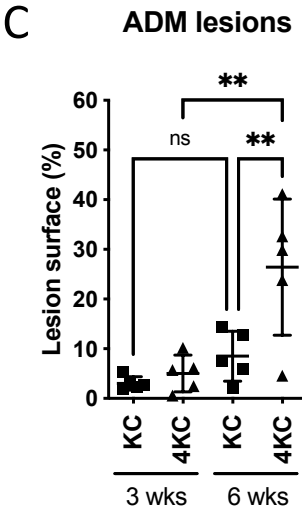
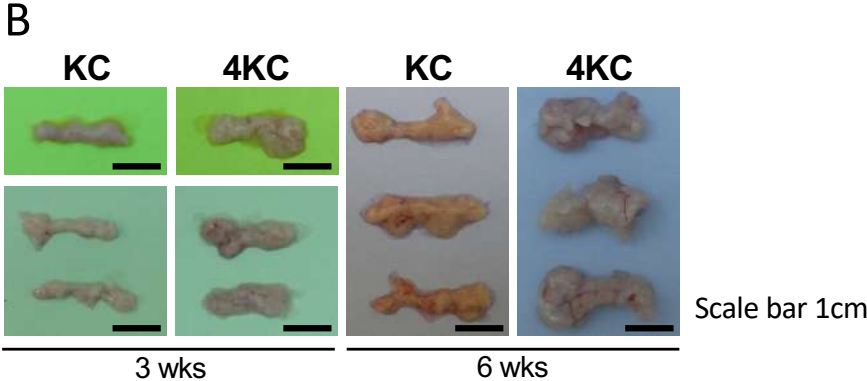
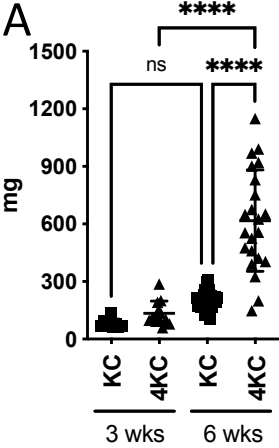
All data will be publicly released. GEO Accession: GSE231348. <https://www.ncbi.nlm.nih.gov/geo/query/acc.cgi?acc=GSE231348>

## References

- Hidalgo M. 2010. Pancreatic cancer. *N Engl J Med.* 362(17):1605–1617.
- Ying H, et al. 2016. Genetics and biology of pancreatic ductal adenocarcinoma. *Genes Dev.* 30(4):355–385.
- Erkan M, et al. 2008. The activated stroma index is a novel and independent prognostic marker in pancreatic ductal adenocarcinoma. *Clin Gastroenterol Hepatol.* 6(10):1155–1161.
- Neesse A, et al. 2011. Stromal biology and therapy in pancreatic cancer. *Gut.* 60(6):861–868.
- Gore J, Korc M. 2014. Pancreatic cancer stroma: friend or foe? *Cancer Cell.* 25(6):711–712.
- Gamradt P, De La Fouchardiere C, Hennino A. 2021. Stromal protein-mediated immune regulation in digestive cancers. *Cancers (Basel).* 13(1):146.
- Pearce OMT, et al. 2018. Deconstruction of a metastatic tumor microenvironment reveals a common matrix response in human cancers. *Cancer Discov.* 8(3):304–319.
- Torphy RJ, Schulick RD, Zhu Y. 2020. Understanding the immune landscape and tumor microenvironment of pancreatic cancer to improve immunotherapy. *Mol Carcinog.* 59(7):775–782.
- Oya Y, Hayakawa Y, Koike K. 2020. Tumor microenvironment in gastric cancers. *Cancer Sci.* 111(8):2696–2707.
- Kai F, Drain AP, Weaver VM. 2019. The extracellular matrix modulates the metastatic journey. *Dev Cell.* 49(3):332–346.
- Pickup MW, Mouw JK, Weaver VM. 2014. The extracellular matrix modulates the hallmarks of cancer. *EMBO Rep.* 15(12):1243–1253.
- Laklai H, et al. 2016. Genotype tunes pancreatic ductal adenocarcinoma tissue tension to induce matricellular fibrosis and tumor progression. *Nat Med.* 22(5):497–505.
- Rice AJ, et al. 2017. Matrix stiffness induces epithelial-mesenchymal transition and promotes chemoresistance in pancreatic cancer cells. *Oncogenesis.* 6(7):e352.
- Perez VM, Kearney JF, Yeh JJ. 2021. The PDAC extracellular matrix: a review of the ECM protein composition, tumor cell interaction, and therapeutic strategies. *Front Oncol.* 11:751311.
- Feig C, et al. 2012. The pancreas cancer microenvironment. *Clin Cancer Res.* 18(16):4266–4276.
- Apte MV, et al. 1998. Periacinar stellate shaped cells in rat pancreas: identification, isolation, and culture. *Gut.* 43(1):128–133.
- Heinemann V, et al. 2014. Tumour-stroma interactions in pancreatic ductal adenocarcinoma: rationale and current evidence for new therapeutic strategies. *Cancer Treat Rev.* 40(1):118–128.
- Olive KP, et al. 2009. Inhibition of hedgehog signaling enhances delivery of chemotherapy in a mouse model of pancreatic cancer. *Science.* 324(5933):1457–1461.
- Costa A, et al. 2018. Fibroblast heterogeneity and immunosuppressive environment in human breast cancer. *Cancer Cell.* 33(3):463–79.e10.
- Ohlund D, et al. 2017. Distinct populations of inflammatory fibroblasts and myofibroblasts in pancreatic cancer. *J Exp Med.* 214(3):579–596.
- Elyada E, et al. 2019. Cross-species single-cell analysis of pancreatic ductal adenocarcinoma reveals antigen-presenting cancer-associated fibroblasts. *Cancer Discov.* 9(8):1102–1123.
- Morianos I, Papadopoulou G, Semitekolou M, Xanthou G. 2019. Activin-A in the regulation of immunity in health and disease. *J Autoimmun.* 104:102314.
- Togashi Y, et al. 2014. Homozygous deletion of the activin A receptor, type IB gene is associated with an aggressive cancer phenotype in pancreatic cancer. *Mol Cancer.* 13(1):126.
- Su GH, et al. 2001. ACVR1B (ALK4, activin receptor type 1B) gene mutations in pancreatic carcinoma. *Proc Natl Acad Sci U S A.* 98(6):3254–3257.
- Zhao Y, et al. 2020. Oncogene-induced senescence limits the progression of pancreatic neoplasia through production of activin A. *Cancer Res.* 80(16):3359–3371.
- Ripoche D, et al. 2013. Generation of a conditional mouse model to target Acvr1b disruption in adult tissues. *Genesis.* 51(2):120–127.
- Hingorani SR, et al. 2003. Preinvasive and invasive ductal pancreatic cancer and its early detection in the mouse. *Cancer Cell.* 4(6):437–450.
- Herreros-Villanueva M, Hijona E, Cosme A, Bujanda L. 2012. Mouse models of pancreatic cancer. *World J Gastroenterol.* 18(12):1286–1294.
- Huang H, et al. 2019. Targeting TGFbeta2-mutant tumors exposes vulnerabilities to stromal TGFbeta blockade in pancreatic cancer. *EMBO Mol Med.* 11(11):e10515.
- Xiao X, et al. 2016. PNA lectin for purifying mouse acinar cells from the inflamed pancreas. *Sci Rep.* 6:21127.
- Wu Z, et al. 2023. Pericyte stem cells induce Ly6G(+) cell accumulation and immunotherapy resistance in pancreatic cancer. *EMBO Rep.* 24(4):e56524.
- Cabello-Aguilar S, et al. 2020. SingleCellSignalR: inference of intercellular networks from single-cell transcriptomics. *Nucleic Acids Res.* 48(10):e55.

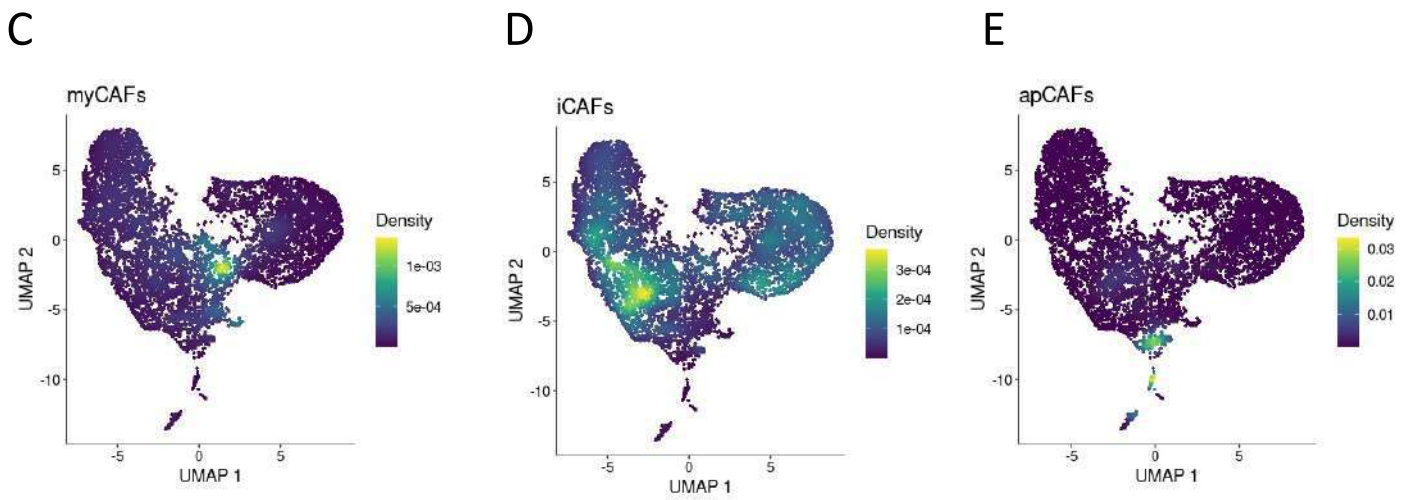
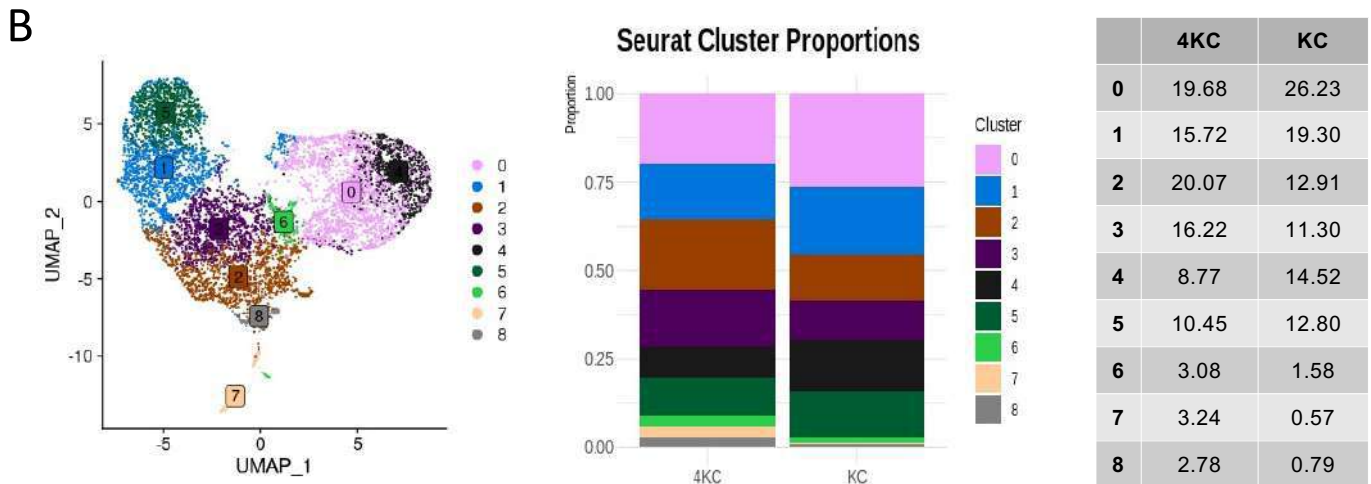
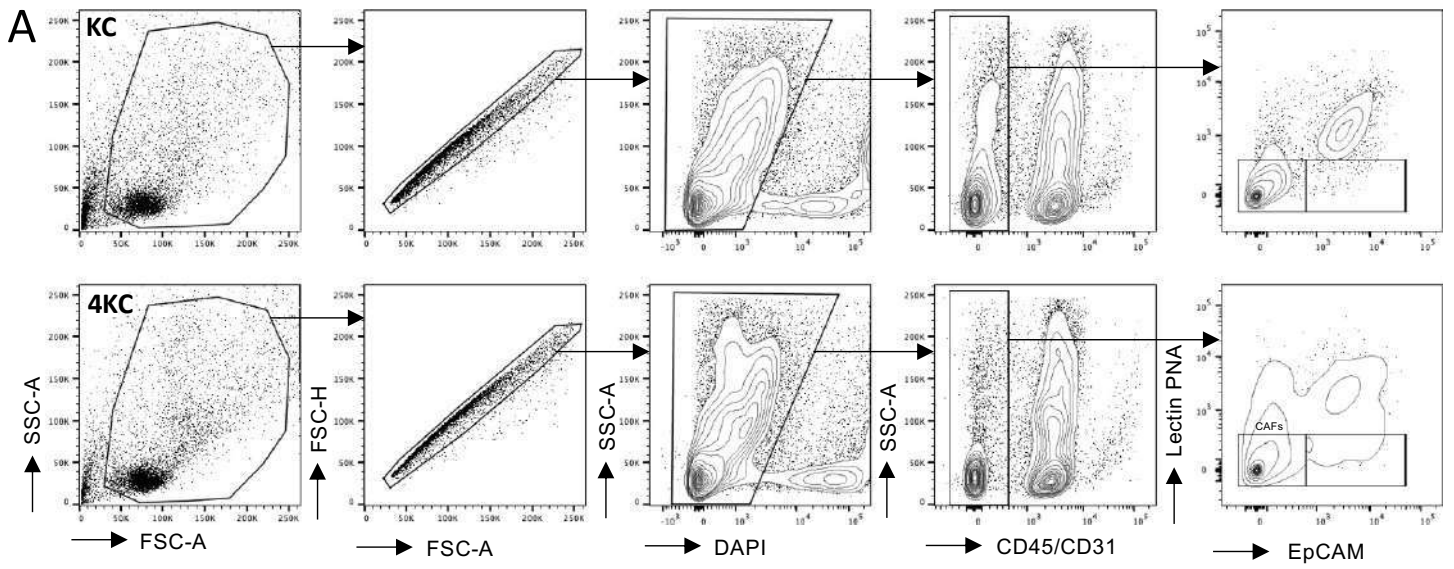
- 33 Attieh Y, et al. 2017. Cancer-associated fibroblasts lead tumor invasion through integrin-beta3-dependent fibronectin assembly. *J Cell Biol.* 216(11):3509–3520.
- 34 Tumbarello DA, Temple J, Brenton JD. 2012.  $\beta 3$  integrin modulates transforming growth factor beta induced (TGFBI) function and paclitaxel response in ovarian cancer cells. *Mol Cancer.* 11:36.
- 35 Goehrig D, et al. 2019. Stromal protein betaig-h3 reprogrammes tumour microenvironment in pancreatic cancer. *Gut.* 68(4):693–707.
- 36 Patry M, et al. 2015.  $\beta$ ig-h3 represses T-cell activation in type 1 diabetes. *Diabetes.* 64(12):4212–4219.
- 37 Lecker LSM, et al. 2021. TGFBI production by macrophages contributes to an immunosuppressive microenvironment in ovarian cancer. *Cancer Res.* 81(22):5706–5719.
- 38 Aibar S, et al. 2017. SCENIC: single-cell regulatory network inference and clustering. *Nat Methods.* 14(11):1083–1086.
- 39 Nurmik M, Ullmann P, Rodriguez F, Haan S, Letellier E. 2020. In search of definitions: cancer-associated fibroblasts and their markers. *Int J Cancer.* 146(4):895–905.
- 40 Omary MB, Lugea A, Lowe AW, Pandol SJ. 2007. The pancreatic stellate cell: a star on the rise in pancreatic diseases. *J Clin Invest.* 117(1):50–59.
- 41 Kalluri R. 2016. The biology and function of fibroblasts in cancer. *Nat Rev Cancer.* 16(9):582–598.
- 42 Rogers MA, Fantauzzo KA. 2020. The emerging complexity of PDGFRs: activation, internalization and signal attenuation. *Biochem Soc Trans.* 48(3):1167–1176.
- 43 Kuo TL, Cheng KH, Shan YS, Chen LT, Hung WC. 2019.  $\beta$ -Catenin-activated autocrine PDGF/Src signaling is a therapeutic target in pancreatic cancer. *Theranostics.* 9(2):324–336.
- 44 Eitner F, et al. 2008. PDGF-C is a proinflammatory cytokine that mediates renal interstitial fibrosis. *J Am Soc Nephrol.* 19(2):281–289.
- 45 Ostendorf T, Eitner F, Floege J. 2012. The PDGF family in renal fibrosis. *Pediatr Nephrol.* 27(7):1041–1050.
- 46 Ziogas AC, et al. 2012. VEGF directly suppresses activation of T cells from ovarian cancer patients and healthy individuals via VEGF receptor type 2. *Int J Cancer.* 130(4):857–864.
- 47 Galon J, et al. 2006. Type, density, and location of immune cells within human colorectal tumors predict clinical outcome. *Science.* 313(5795):1960–1964.
- 48 Ene-Obong A, et al. 2013. Activated pancreatic stellate cells sequester CD8+ T cells to reduce their infiltration of the juxtatumoral compartment of pancreatic ductal adenocarcinoma. *Gastroenterology.* 145(5):1121–1132.
- 49 Raskov H, Orhan A, Christensen JP, Gogenur I. 2021. Cytotoxic CD8(+) T cells in cancer and cancer immunotherapy. *Br J Cancer.* 124(2):359–367.
- 50 Chijimatsu R, et al. 2022. Establishment of a reference single-cell RNA sequencing dataset for human pancreatic adenocarcinoma. *iScience.* 25(8):104659.
- 51 Lavie D, Ben-Shmuel A, Erez N, Scherz-Shouval R. 2022. Cancer-associated fibroblasts in the single-cell era. *Nat Cancer.* 3(7):793–807.
- 52 Brielle S, et al. 2021. Delineating the heterogeneity of matrix-directed differentiation toward soft and stiff tissue lineages via single-cell profiling. *Proc Natl Acad Sci U S A.* 118(19):e2016322118.
- 53 Olson LE, Soriano P. 2009. Increased PDGFRalpha activation disrupts connective tissue development and drives systemic fibrosis. *Dev Cell.* 16(2):303–313.
- 54 Corless CL, et al. 2005. PDGFRA mutations in gastrointestinal stromal tumors: frequency, spectrum and in vitro sensitivity to imatinib. *J Clin Oncol.* 23(23):5357–5364.
- 55 Chompret A, et al. 2004. PDGFRA germline mutation in a family with multiple cases of gastrointestinal stromal tumor. *Gastroenterology.* 126(1):318–321.
- 56 Andrae J, Gallini R, Betsholtz C. 2008. Role of platelet-derived growth factors in physiology and medicine. *Genes Dev.* 22(10):1276–1312.
- 57 Papanas N, Maltezos E. 2008. Becaplermin gel in the treatment of diabetic neuropathic foot ulcers. *Clin Interv Aging.* 3(2):233–240.
- 58 Han N, et al. 2021. High expression of PDGFA predicts poor prognosis of esophageal squamous cell carcinoma. *Medicine (Baltimore).* 100(20):e25932.
- 59 Gallini R, Lindblom P, Bondjers C, Betsholtz C, Andrae J. 2016. PDGF-A and PDGF-B induces cardiac fibrosis in transgenic mice. *Exp Cell Res.* 349(2):282–290.
- 60 Liang M, Wang B, Schneider A, Vainshtein I, Roskos L. 2020. A novel pharmacodynamic biomarker and mechanistic modeling facilitate the development of tovetumab, a monoclonal antibody directed against platelet-derived growth factor receptor alpha, for cancer therapy. *AAPS J.* 23(1):4.
- 61 Hammer AM, et al. 2017. Stromal PDGFR-alpha activation enhances matrix stiffness, impedes mammary ductal development, and accelerates tumor growth. *Neoplasia.* 19(6):496–508.
- 62 Brown XQ, et al. 2010. Effect of substrate stiffness and PDGF on the behavior of vascular smooth muscle cells: implications for atherosclerosis. *J Cell Physiol.* 225(1):115–122.
- 63 Hosein AN, et al. 2019. Cellular heterogeneity during mouse pancreatic ductal adenocarcinoma progression at single-cell resolution. *JCI Insight.* 5(16):e129212.
- 64 Kanzaki R, Pietras K. 2020. Heterogeneity of cancer-associated fibroblasts: opportunities for precision medicine. *Cancer Sci.* 111(8):2708–2717.
- 65 Erez N, Truitt M, Olson P, Arron ST, Hanahan D. 2010. Cancer-associated fibroblasts are activated in incipient neoplasia to orchestrate tumor-promoting inflammation in an NF-kappaB-dependent manner. *Cancer Cell.* 17(2):135–147.
- 66 Sun Q, et al. 2018. Prognostic value of increased integrin-beta 1 expression in solid cancers: a meta-analysis. *Oncotargets Ther.* 11:1787–1799.
- 67 Gharibi A, et al. 2017. ITGA1 is a pre-malignant biomarker that promotes therapy resistance and metastatic potential in pancreatic cancer. *Sci Rep.* 7(1):10060.
- 68 Fuentes P, et al. 2020. ITGB3-mediated uptake of small extracellular vesicles facilitates intercellular communication in breast cancer cells. *Nat Commun.* 11(1):4261.
- 69 Bachy S, et al. 2022.  $\beta$ ig-h3-structured collagen alters macrophage phenotype and function in pancreatic cancer. *iScience.* 25(2):103758.
- 70 Salmon H, et al. 2012. Matrix architecture defines the preferential localization and migration of T cells into the stroma of human lung tumors. *J Clin Invest.* 122(3):899–910.
- 71 Ohno S, et al. 2002. Role of stromal collagen in immunomodulation and prognosis of advanced gastric carcinoma. *Int J Cancer.* 97(6):770–774.
- 72 Kuczek DE, et al. 2019. Collagen density regulates the activity of tumor-infiltrating T cells. *J Immunother Cancer.* 7(1):68.

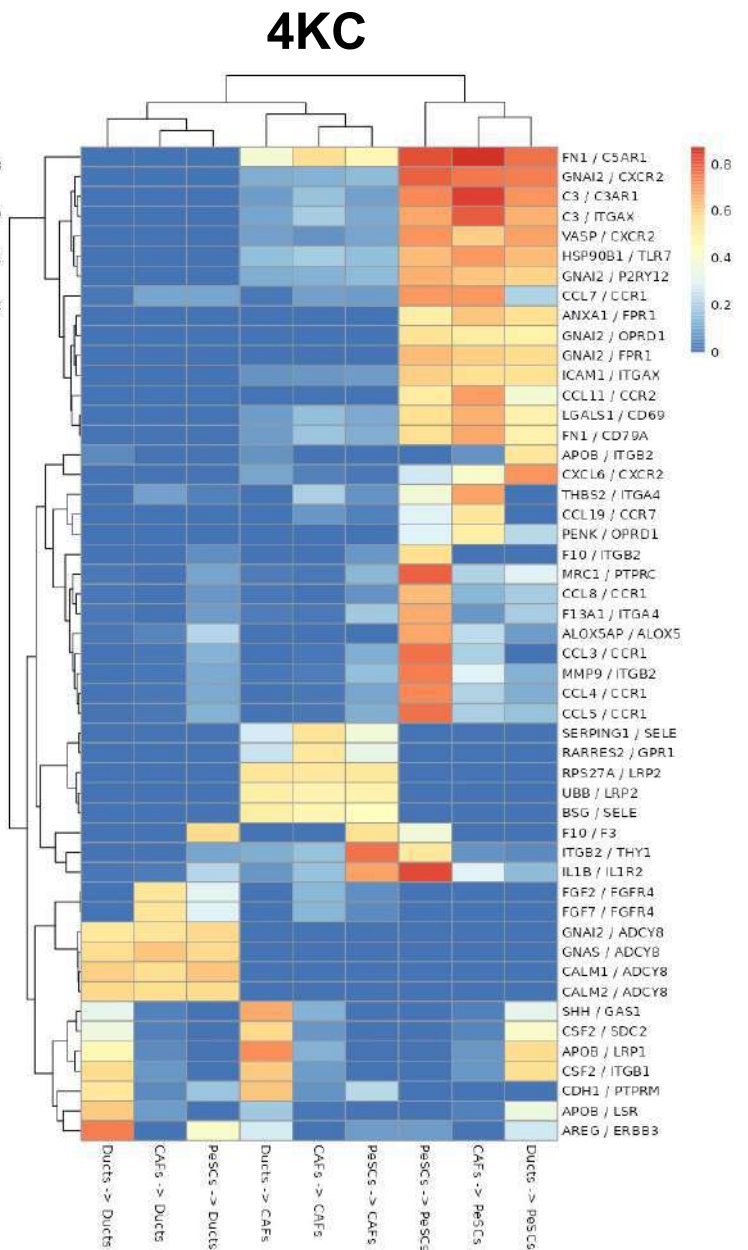
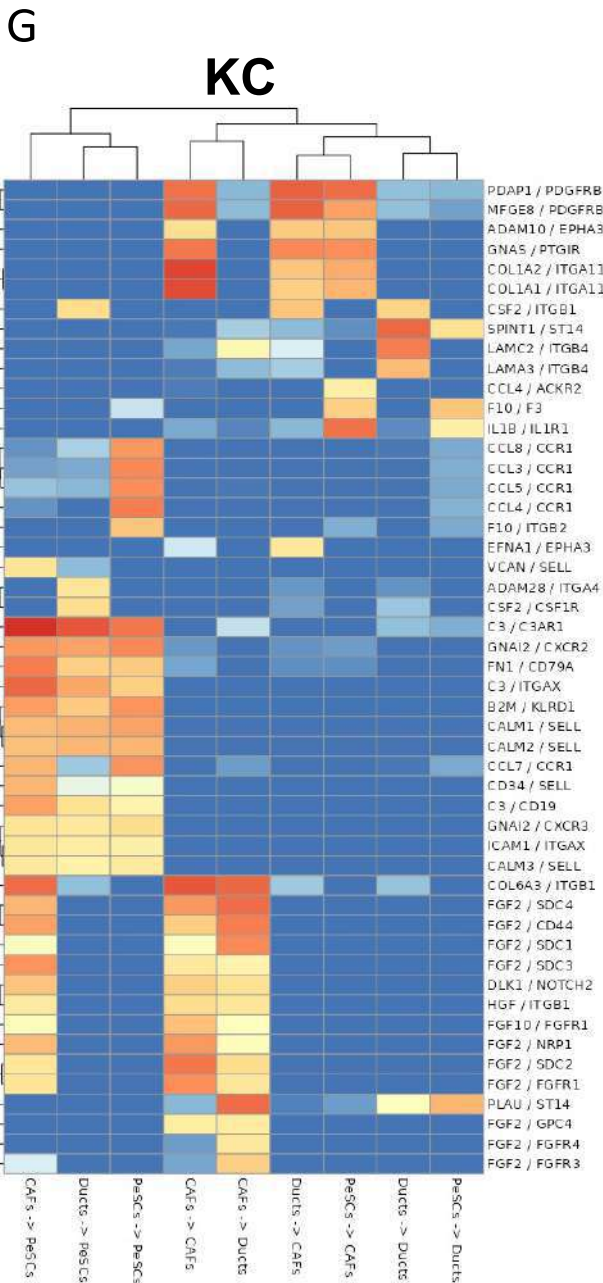
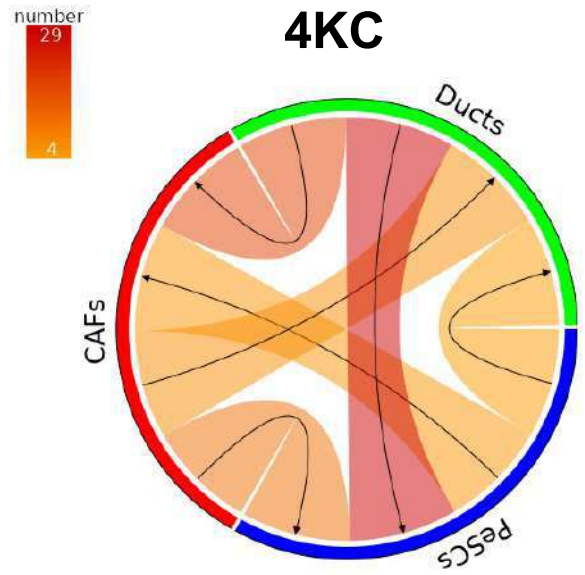
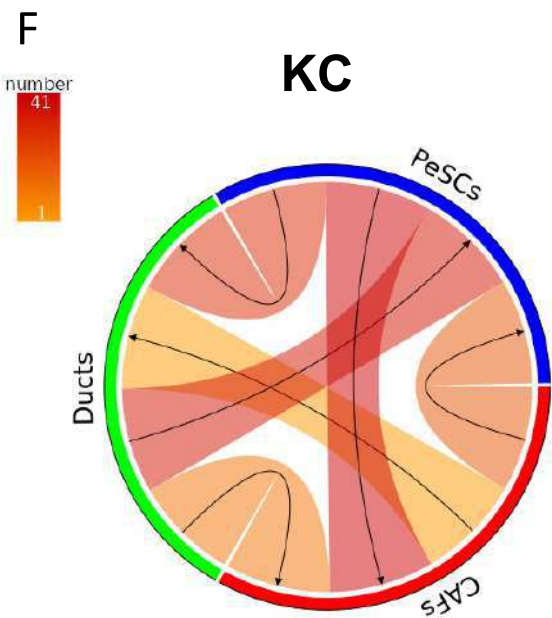
**Pancreas weight**



**Supplementary Figure 1: ALK4 signaling disruption in tumor cells promotes tumor progression and stromal development.**

(A) Weight (mg) of pancreata excised from three- or six-week-old KC and 4KC mice. Cumulative data from three individual experiments with 3-5 mice per group are shown. (B) Representative photographs of pancreata from three- (left panel) or six-week-old (right panel) KC and 4KC mice. (C) Quantification of the lesional pancreatic surface of three- or six-week-old KC and 4KC mice (bottom). Representative data from two individual experiments with 5 mice per group are shown. (D) Representative photographs of pancreata from three- (left panel) or six-week-old (right panel) KC (top) and 4KC mice (bottom); dashed lines mark representative lesions included in the quantification. (A and C) The mean values  $\pm$  SEMs are displayed. \*\* $p < 0.01$ ; \*\*\*\* $p < 0.0001$ .





Supplementary Fig. 2

# H

## KC

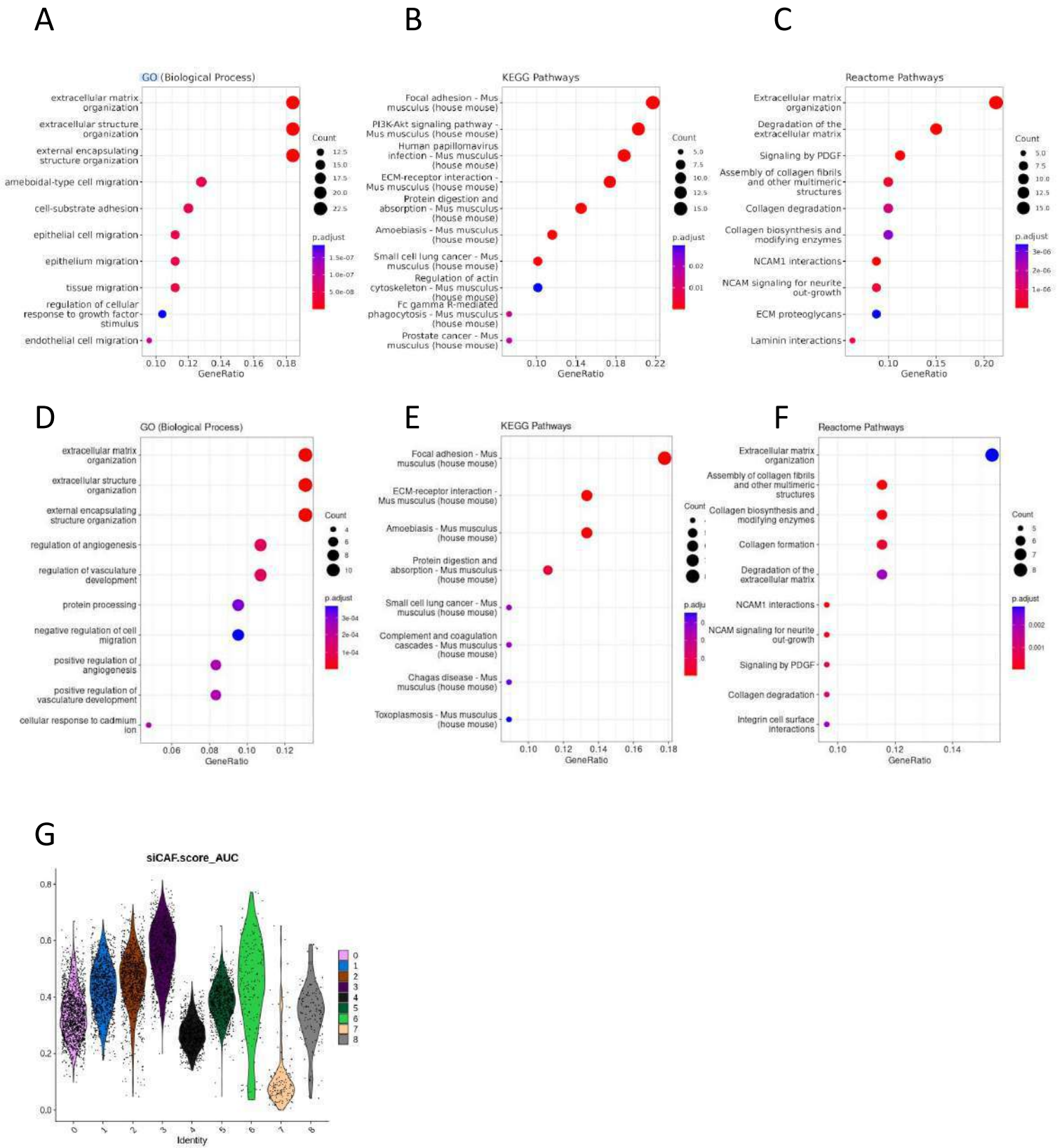
ligand	receptor	interaction.type	LRscore
CAFs.Dcn	Ducts.Erb4	paracrine	0,720650548
Ducts.Gnas	CAFs.Ptgir	paracrine	0,761025074
Ducts.Gnai2	CAFs.S1pr3	paracrine	0,744468335
Ducts.Col1a2	CAFs.Itga11	paracrine	0,660710975
Ducts.Adam10	CAFs.Epha3	paracrine	0,653949874
Ducts.Col1a1	CAFs.Itga11	paracrine	0,644123049
Ducts.Efna4	CAFs.Epha3	paracrine	0,581752451
Ducts.Efnb2	CAFs.Epha3	paracrine	0,580854742
Ducts.Efna1	CAFs.Epha3	paracrine	0,571991179
Ducts.Efna5	CAFs.Epha3	paracrine	0,532367775
Ducts.Liph	CAFs.Lpar4	paracrine	0,521164091
Ducts.Ill1rn	CAFs.Ill1r2	paracrine	0,518848794

## 4KC

ligand	receptor	interaction.type	LRscore
CAFs.Gnas	Ducts.Adcy8	paracrine	0,658399288
CAFs.Dcn	Ducts.Erb4	paracrine	0,656188423
CAFs.Calm1	Ducts.Adcy8	paracrine	0,607756525
CAFs.Calm2	Ducts.Adcy8	paracrine	0,605529211
CAFs.Gnai2	Ducts.Adcy8	paracrine	0,587255586
CAFs.Calm3	Ducts.Adcy8	paracrine	0,512820559
Ducts.Mfge8	CAFs.Pdgfrb	paracrine	0,817461691
Ducts.Pdap1	CAFs.Pdgfrb	paracrine	0,808549034
Ducts.Calm1	CAFs.Pde1a	paracrine	0,796738991
Ducts.Calm2	CAFs.Pde1a	paracrine	0,783743393
Ducts.Pdgfa	CAFs.Pdgfrb	paracrine	0,747897849
Ducts.Gnai2	CAFs.S1pr3	paracrine	0,746085913
Ducts.Pdgfb	CAFs.Pdgfrb	paracrine	0,727260299
Ducts.Pdgfc	CAFs.Pdgfrb	paracrine	0,684227532
Ducts.Calm3	CAFs.Pde1a	paracrine	0,661038708
Ducts.Pdgfd	CAFs.Pdgfrb	paracrine	0,63106737
Ducts.App	CAFs.Ngfr	paracrine	0,610311843
Ducts.Rps27a	CAFs.Lrp2	paracrine	0,582174411
Ducts.Rtn4	CAFs.Ngfr	paracrine	0,579450283
Ducts.Liph	CAFs.Lpar4	paracrine	0,547120748
Ducts.Bsg	CAFs.Sele	paracrine	0,545015849
Ducts.Ubb	CAFs.Lrp2	paracrine	0,53970867
Ducts.Pyy	CAFs.Fap	paracrine	0,538041911
Ducts.Hspa8	CAFs.Lrp2	paracrine	0,505137277

## Supplementary Figure 2: Single-cell RNA sequencing of pancreatic CAFs and ducts.

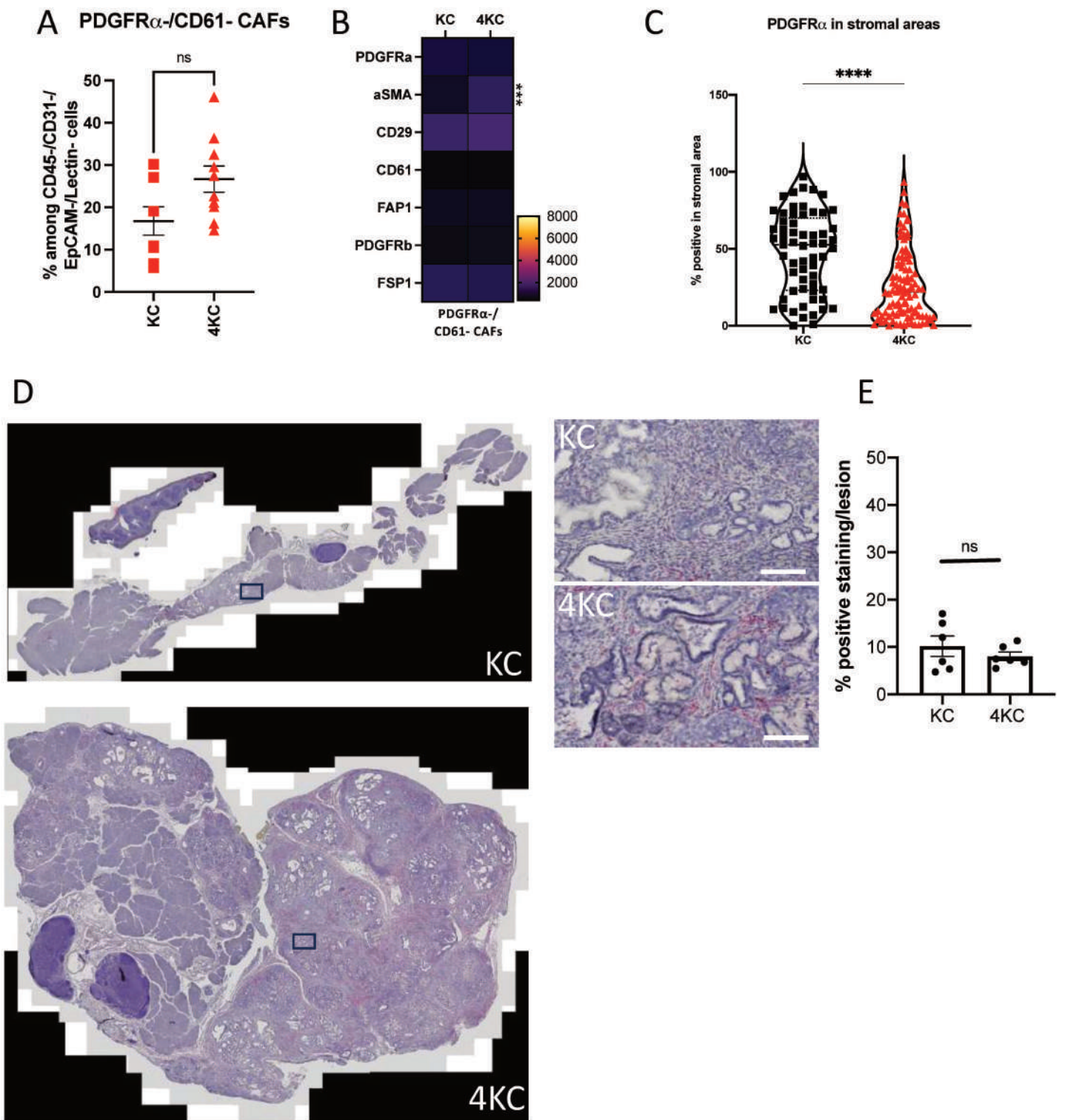
(A) Gating strategy for CAF and ductal cell isolation by FACS sorting. Briefly, after enzymatic/physical dissociation, the cells obtained from the pancreata harvested from five KC (top row) or five 4KC (bottom row) mice were stained with fluorochrome-labeled antibodies and subjected to FACS sorting. After exclusion of cell doublets, DAPI<sup>+</sup> dead cells, CD45<sup>+</sup> hematopoietic cells, and CD31<sup>+</sup> endothelial cells, 5000 Lectin PNA<sup>-</sup> EpCAM<sup>-</sup> CAFs and 1000 Lectin<sup>-</sup> EpCAM<sup>+</sup> ductal cells were sorted and further subjected to single-cell capture, barcoding, and reverse transcription using the 10x Genomics platform. (B) UMAP plot of KC and 4KC CAF enriched fractions (9 clusters) and cluster proportions. (C-E) UMAP plot showing previously reported CAF signatures : myCAFs (myofibroblastic CAFs), iCAFs (inflammatory CAFs) and apCAFs (antigen presenting CAFs). Expression scores for each cell were calculated for known CAF subtypes, using previously described signatures (see Methods). The scores were plotted on the same two-dimensional UMAP representation shown in (B). (F-H) Ligand:receptor interaction network was obtained with SingleCellSignalR. (F) chord plots illustrating the number of all paracrine signals between the major cell subtypes (i.e. ducts, CAFs, and PeSCs). (G) heatmaps showing the most variable receptor:ligand interactions among all clusters in KC (left) and 4KC (right) cells. Direction of all pairwise interactions are used to label the columns at the bottom of each heatmap. (H) Detailed Ligand:receptor interactions in KC and 4KC.



Supplementary Fig. 3

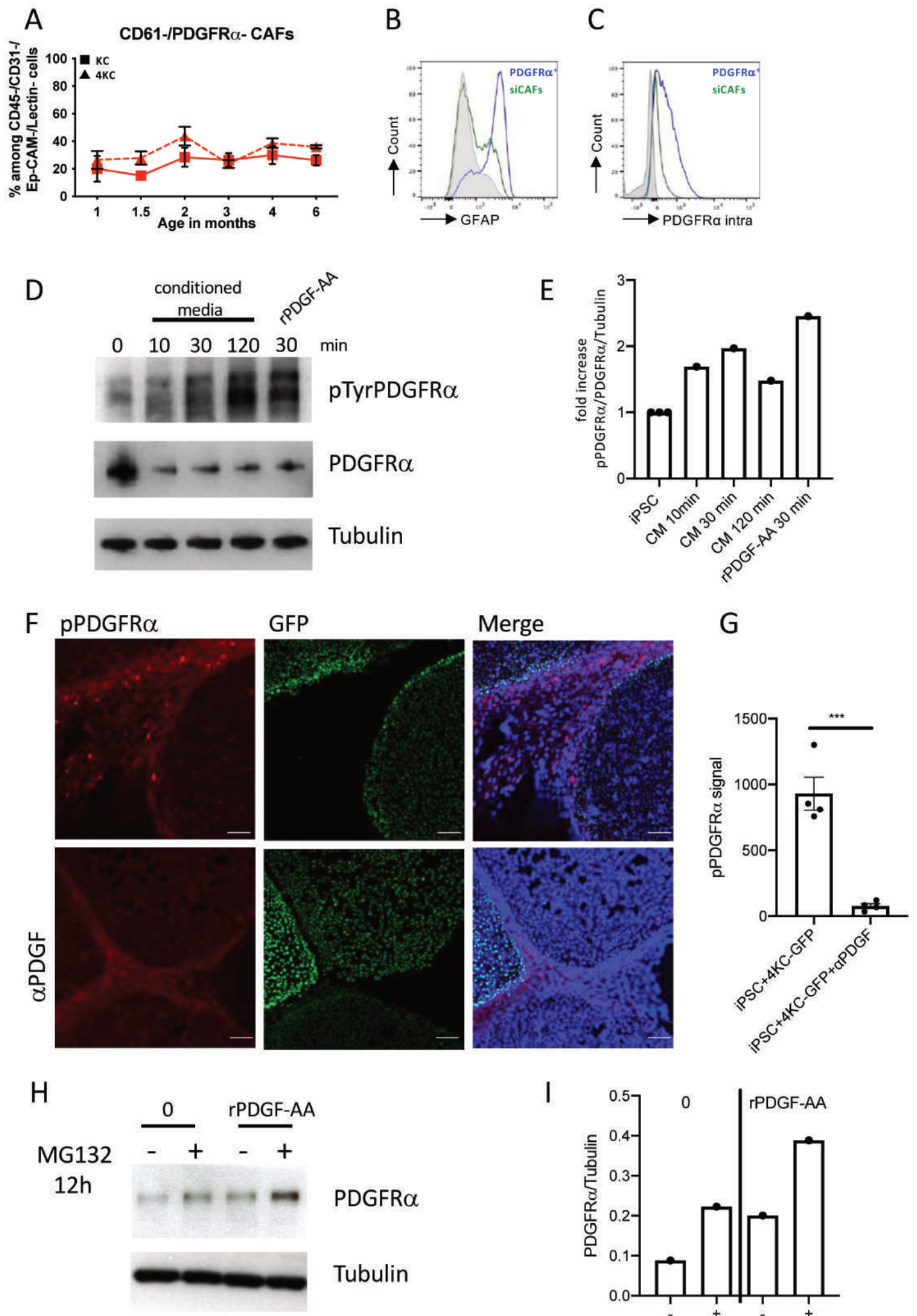
### **Supplementary Figure 3: Pathway enrichment analysis on single cell data.**

(A, B, C). Expression was compared between 4KC and KC condition populations in scRNAseq data subsetted on PDGFRA<sup>+</sup> CAFs. (D, E, F). Expression was compared between PDGFRA<sup>+</sup> and PDGFRA<sup>-</sup> in scRNAseq data subsetted on CAFs. Differentially expressed genes were interrogated for pathway enrichment using different databases (Gene Ontology Biological Process, KEGG and Reactome). The top 10 most significant terms are represented in dotplot charts, where dot color indicates p value and dot size the number of significant genes within each term.



**Supplementary Figure 4: Expression of CAF markers on PDGFR $\alpha$ -CD61<sup>+</sup> CAFs.**

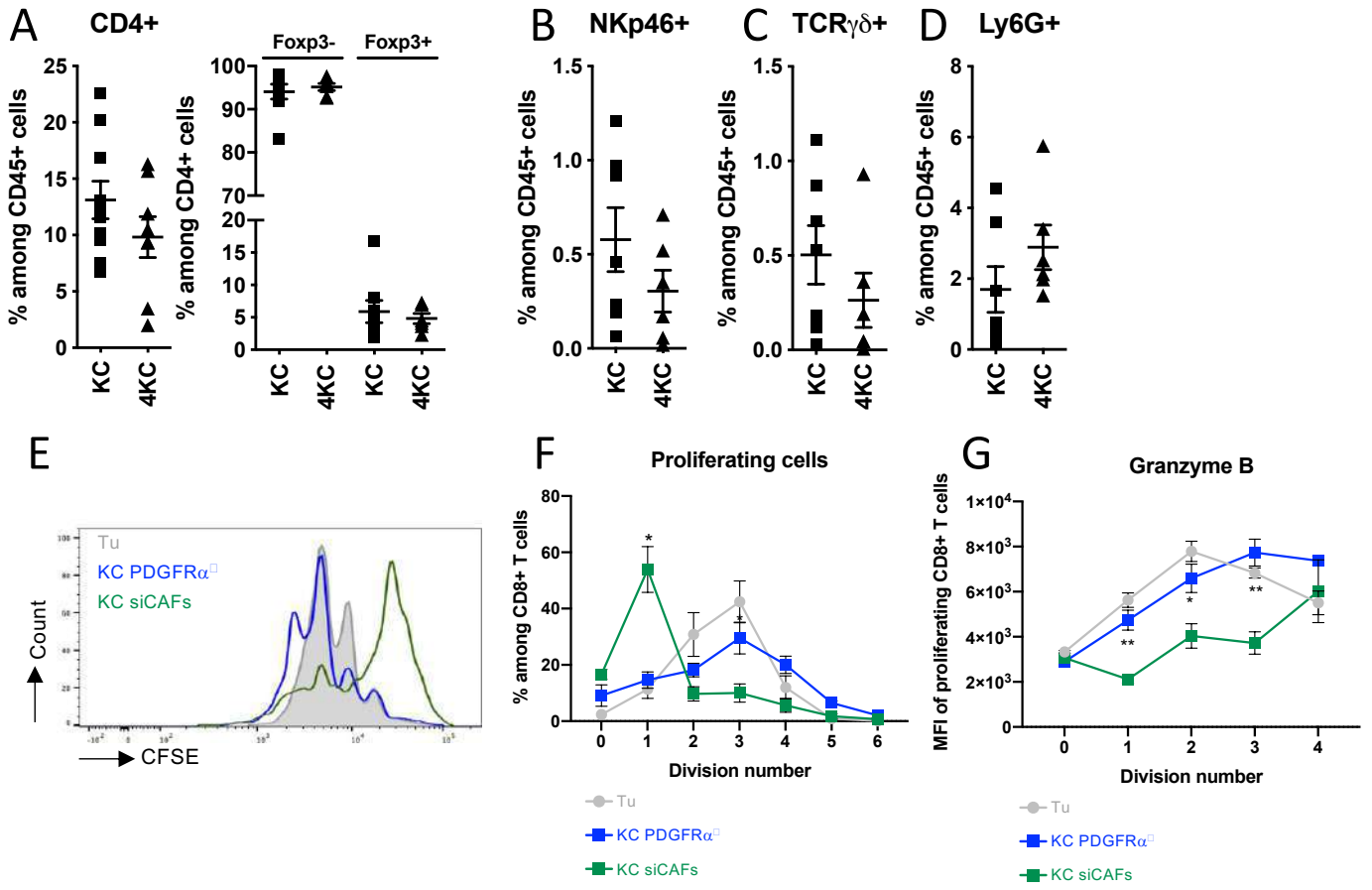
(A) Frequencies of PDGFR $\alpha$ -CD61<sup>+</sup> CAFs among CD45<sup>+</sup>-CD31<sup>-</sup>-Lectin PNA<sup>-</sup>-EpCAM<sup>-</sup> CAFs in pancreata from six-week-old KC (squares) and 4KC mice (triangles). (B) Heatmap of the mean fluorescence intensities (MFIs) of CAF markers on PDGFR $\alpha$ -CD61<sup>+</sup> CAFs from KC and 4KC pancreata. (C) Quantification of the PDGFR $\alpha$  staining in stromal area in six-week-old KC and 4KC mice. Cumulative data from three individual experiments with three to four mice per group are shown. The mean values  $\pm$  SEMs are displayed. \*\*\*\*p <0.0001. (D) Representative scans of PDGFR $\alpha$  RNAscope in sections of pancreata from six-week-old KC and 4KC mice (E) Quantification of the mRNA signal expressed as % per lesion (3 individual mice were used in each group).



Supplementary Fig. 5

**Supplementary Figure 5: ALK4 signaling disruption in tumor cells drives the loss of PDGFR and GFAP expression in siCAFs.**

(A) Frequencies of PDGFR $\alpha$ <sup>-</sup>CD61<sup>-</sup> CAFs among CD45<sup>-</sup>CD31<sup>-</sup>Lectin PNA<sup>-</sup>EpCAM<sup>-</sup> CAFs determined by FACS analysis of pancreata harvested from KC (squares) and 4KC mice (triangles) at 1, 1.5, 3, 4, and 6 months of age. (B,C) FACS analysis of intracellular GFAP (B) and PDGFR $\alpha$  expression (C) in PDGFR $\alpha$ <sup>+</sup> CAFs (blue line) and siCAFs (green line). FMO controls are shown in gray. (A) Results from five mice per group and timepoint are shown. (B, C) Representative data from two individual experiments with five mice are shown. The mean values  $\pm$  SEMs are displayed. (D) iPSC were cultured for the indicated time points and in presence of 4KC-conditioned media or recombinant PDGF-AA and subjected to WB analysis for pPDGFR $\alpha$ , PDGFR $\alpha$  and tubulin expression. (E) Quantification of the WB signal band intensity presented in (D). (F) iPSC were cultured in the presence or absence of MG-132 for 12h (G) Quantification of the WB signal band intensity presented (F). Representative data from two individual experiments. (H) Representative photographs of PDGFR $\alpha$  phosphorylation and (I) signal quantification after 7 days of iPSC and 4KC-GFP cell line coculture.



Supplementary Fig. 6

**Supplementary Figure 6: CD8<sup>+</sup> T-cell activation is impaired by siCAFs.** (A) Frequencies of CD4<sup>+</sup> T cells among CD45<sup>+</sup> cells and Foxp3<sup>-</sup> and Foxp3<sup>+</sup> cells among CD45<sup>+</sup>CD4<sup>+</sup> T cells in pancreata from 6-week-old KC and 4KC mice. (B-D) Frequencies of NKp46<sup>+</sup> (B), TCR $\gamma\delta$ <sup>+</sup> (C), and Ly6G<sup>+</sup> (D) cells among CD45<sup>+</sup> cells in pancreata from KC and 4KC mice. Cumulative data from at least two individual experiments with 3-4 mice per group are shown. (E) CFSE dilution in CD8<sup>+</sup> T cells cocultured with BMDCs and CD3/CD28 activation beads in PDGFR $\alpha$ <sup>+</sup> CAF/tumor cell-(blue line) or siCAF/tumor cell-conditioned medium (green line). The FMO control is shown in gray. (F, G) Proliferating (F) and Granzyme B (G)-producing CD8<sup>+</sup> T cells at the indicated division numbers after coculture with BMDCs and CD3/CD28 activation beads in PDGFR $\alpha$ <sup>+</sup> CAF/tumor cell- (blue line) or siCAF/tumor cell-conditioned medium (green line). The FMO control is shown in gray. Representative data from two individual experiments with technical replicates are shown. PDGFR $\alpha$ <sup>+</sup> CAFs and siCAFs were isolated from three six-week-old 4KC mice. \*p < 0.05; \*\*p < 0.01.



**Supplementary Figure 7: PDGF neutralization reduces tumor growth.**

(A) Representative photographs of pancreata from six-week-old 4KC littermates treated with an anti-PDGF antibody (right panel) or PBS (left panel). (b-d) FACS analysis of MFIs of CD69, (B), CD44 (C) and CD62L (D) and on CD8<sup>+</sup> T cells from the pancreas of six-week-old 4KC mice treated with the anti-PDGF antibody or PBS. ns- not significant.

## **Supplementary Information**

### **Immunohistochemistry (IHC) and immunofluorescence (IF)**

Formalin-fixed paraffin-embedded (FFPE) mouse pancreata were sectioned at 4  $\mu$ m. FFPE samples were rehydrated by heating slides at 55°C for 30 minutes and successive baths of xylene and ethanol (100%, 95%, 70%). In sections submitted for IHC, endogenous peroxidase was inactivated with 3% H<sub>2</sub>O<sub>2</sub>. IHC and IF staining procedures were performed after heat-induced epitope retrieval using an antigen-unmasking solution (Vector Laboratories, US). The sections were incubated with primary antibodies overnight at 4°C in a wet chamber. Next, the sections were incubated with biotinylated (IHC) or fluorochrome-conjugated (IF) secondary antibodies for 1 h at room temperature (RT). IHC staining was visualized using 3,3'-diaminobenzidine (DAB kit; Vector Laboratories, UK), and the sections were counterstained with hematoxylin. IF sections were counterstained by mounting with Vectashield mounting medium with DAPI. Hematoxylin & eosin (H&E) staining was performed using a standard protocol. IHC and H&E staining was imaged using a Carl Zeiss microscope Axioscan 7. IF images were acquired on a Carl Zeiss LSM 880 microscope. FIJI imaging software was used for visualization and/or analysis of IHC, IF, and H&E staining.

### **Flow cytometric analysis**

Single-cell suspensions were stained with fluorochrome-labeled antibodies for 20 minutes at 4°C. Fixable viability dye (BioLegend) or DAPI staining was performed to exclude dead cells from the analysis. The stained cells were fixed directly by incubation in FACS buffer supplemented with 4% paraformaldehyde (PFA) for 20 minutes at 4°C, or intracellular staining was performed using the Fixation/Permeabilization Kit (BD Biosciences). No fixation/permeabilization was performed if the cells were subjected to FACS sorting. Stained cells were acquired on a BD Fortessa flow cytometer (BD Biosciences) for FACS analysis. For CAF and ductal cell isolation, cells were acquired on a BD FACSAria (BD Biosciences), and the sorted cells were collected in DMEM containing 10% (functional assays) or 20% fetal calf serum (FCS) (RNA isolation). FACS data were analyzed using FlowJo software (TreeStar).

A list of the antibodies used for flow cytometry can be found in the Supplementary Methods.

### **Supplemental list of FACS antibodies**

The following antibodies and reagents were used for flow cytometric analysis and FACS sorting of cells freshly isolated from mouse pancreata or spleens:

anti-CD4-BV605 or anti-CD4-PE (RM4-5); anti-CD8 $\alpha$ -PE-Cy7 (53-6.7); anti-CD11c-BV510 (N418); anti-CD29-PerCP-Cy5.5 (HM $\beta$ 1-1); anti-CD31-BV421 (390); anti-CD44-AF700 (IM7); anti-CD45-BV421, anti-CD45-APC-Cy7 or anti-CD45-BV650 (30-F11); anti-CD61-PE-Cy7 (2C9.g2); anti-CD62L-PE or anti-CD62L-BV510 (MEL-14); anti-CD69-BV785 (H1.2F3); anti-CD326/EpCAM-FITC or anti-CD327/EpCAM-BV421 (G8.8); anti-CD355/NKp46-BV421 (29.A1.4); anti-Foxp3-AF647 (MF-14); anti-Granzyme B-AF647 (GB11); and anti-Ly6G-AF700 (1A8) were obtained from BioLegend. Anti- $\alpha$ SMA-eF660 (1A4), anti-CD11c-AF700 (N418), anti-CD31-SuperBright 645 (390), anti-CD45-APC (30-F11), anti-FSP1/S100-Biotin (4C4.9), anti-GFAP-AF488 (GA5), anti-PDGFR $\alpha$ /CD140a-APC-eF780 or anti-PDGR $\alpha$ /CD140a-SuperBright 600 (APA5), anti-PDGFR $\beta$ /CD140b-SuperBright780 (APB5), and anti-TCR $\gamma\delta$ -APC (eBioGL3) were obtained from ThermoFisher. Anti-FAP1-AF488 (Polyclonal) was obtained from Bioss Antibodies/CliniSciences, anti-CD44-PE (KM18) was obtained from Immuno Tools, and anti-CD69-PerCP-Cy5.5 (H1.2F3) was obtained from BD Biosciences. Anti-Lectin PNA-AF568 or anti-Lectin PNA-AF647 was obtained from ThermoFisher. Streptavidin-BV510 was obtained from BioLegend.

Antibodies against the following markers were used for flow cytometric analysis of primary PDAC patient-derived CAFs:

CD29, CD61, FAP1, PDGFR $\alpha$ /CD140a, and PDGFR $\beta$ /CD140b.

### **Supplemental list of IHC and IF antibodies**

The following antibodies were used for IHC or IF staining:

Purified anti-CD61/ITG $\beta$ 3 (EPR20825) obtained from Abcam and anti-PDGFR $\alpha$ /CD140a (16A1) obtained from BioLegend were revealed with biotinylated horse- $\alpha$ -rabbit and goat- $\alpha$ -mouse secondary antibodies, respectively. Purified anti-CK19 (TROMA-III) obtained from Developmental Studies Hybridoma Bank (DSHB) and anti- $\alpha$ SMA (polyclonal) obtained from GeneTex were revealed with donkey  $\alpha$ -rat-AF488 and donkey  $\alpha$ -rabbit-Cy3 secondary antibodies, respectively.

### **AFM: protocol application**

The mechanical properties of pancreatic tissue areas were determined by AFM as described previously (34). Briefly, in AFM, the tip of a cantilever is pushed against sample tissue, and its deflection is monitored. Based on the stiffness constant of the cantilever, the deflection indicates the resisting force of the sample (34). The applied protocol allows the measurement of tissue stiffness very locally in a minimally invasive manner by deforming the sample down to a depth of 100 nm.

The stiffness patterns of different regions within a pancreatic lesion (stromal compartment and tumor cells) were determined at high resolution by applying quantitative nanomechanical mapping and force volume protocols (Bruker). In these protocols, the AFM probe oscillates at a low frequency while horizontally scanning the sample and generating a force curve each time the probe contacts the sample. The elastic modulus reflecting the stiffness of the sample is extracted from each curve by applying the Sneddon (Hertz) model, resulting in a 2D stiffness map in which each pixel represents one force curve.

### **Cell isolation from mouse tissues**

Excised mouse pancreata were washed in phosphate-buffered saline (PBS) and minced into small fragments, followed by incubation in a collagenase solution (1 mg/ml collagenase P obtained from Sigma-Merck in HBSS) at 37°C for 20 minutes. A single-pancreatic cell suspension was obtained by sequentially filtering the digested tissue through a 100-µm cell strainer followed by a 70-µm cell strainer. Spleens were homogenized by filtration through a 100-µm cell strainer to obtain single-cell suspensions. Red blood cells were lysed using NH<sub>4</sub>Cl lysis buffer.

### **scRNAseq: quality control and data analysis**

FACS-purified CAFs and ductal tumor cells from a pool of five KC or 4KC mice were partitioned into nanoliter-scale gel bead-in-emulsions (GEMs) with the Chromium Single Cell Controller (10x Genomics) at the in-house Single Cell Platform (CLB/CRCL). After cell encapsulation and barcoding, library preparation followed the standard 10x Genomics 3'scRNAseq protocol comprising reverse transcription, amplification, and indexing. Sequencing was performed using a NovaSeq Illumina device (Illumina). Illumina bcl files were basecalled, demultiplexed and aligned to the mouse mm10 genome using CellRanger software (10x Genomics).

Count data (filtered barcode matrices) were obtained with CellRanger (10xGenomics). All downstream analyses were performed using R/Bioconductor/CRAN packages, R version 4.2.2 (2022-11-10) [<https://cran.r-project.org/>; <http://www.bioconductor.org/>; <https://cran.r-project.org/>] on a Linux platform (x86\_64-pc-linux-gnu [64-bit]). Filtered barcoded matrices were used to create Seurat objects (81) for each condition that were subsequently merged (package 'Seurat' v.4.1.1).

A total of 8878 cells (3638 4KC CAFs, 3664 KC CAFs, 901 4KC Ducts, and 675 KC Ducts) remained after filtering for quality parameters (number of features per cell between 1000 and 6000, fraction of mitochondrial genes < 10%). The Seurat SCTransform function was used to

simultaneously normalize, identify variable features and scale the data. Following dimension reduction with principal component analysis (PCA), the first 30 dimensions were used to construct a shared nearest neighbor (SNN) graph using the FindNeighbors function. Clusters were identified with a resolution of 0.1 and projected in two-dimensional plots using UMAP [arXiv: 1802.03426v3]. The markers of each cluster and DEGs in pairwise comparisons were identified using the FindAllMarkers and FindMarkers functions, respectively (main parameters: only.pos = F, min.pct = 0.25, and logfc.threshold = 0.25), with an adjusted p value threshold of 0.05. Fibroblasts (CAFs) were identified and re-clustered with a higher resolution (0.5). Known CAF markers(23, 24) were used to score each cell according to their myofibroblastic (myCAFs), inflammatory (iCAFs), and antigen-presenting (apCAFs) signatures, using the AUCell package (v.1.18.1). Pathway analyses were performed with the enrichment functions of the 'ClusterProfiler' package (v.4.7.1). Pathway scores were estimated with the Seurat AddModuleScore function using 100 control features after downloading relevant pathways with the R packages enrichR v.3.1 (82, 83) and pathfindR v.1.6.3 (84). 'SingleCellSignalR' v.1.8.0 was used to study cell interaction networks on Seurat preprocessed data, using the major cell type labels (i.e. ducts, CAFs ), independently for the two study conditions (i.e. KC and 4KC). All receptor:ligand analyses were done in "paracrine" mode and visualized with the chord plot and heatmap functions of the same package. siCAF signature using the AUCell method to calculate a score for every single cell (46).

### **CAF differentiation assay: coculture of isolated PSCs and acinar cells**

PSCs were isolated from wild-type (WT) C57BL/6 mice as previously described (17, 23). Briefly, a single-pancreatic cell suspension was resuspended in 9 ml of GBSS containing 0.3% BSA and 43.75% Histodenz (Sigma-Merck), placed into a 15-ml conical tube and overlaid with 6 ml of GBSS containing 0.3% BSA. After gradient centrifugation, the cells within the gray band just above the interface between the GBSS and Histodenz layers were harvested and used for CAF differentiation.

Acinar cells (Acs) were isolated from KC and 4KC pancreata after digestion in a collagenase/soybean trypsin inhibitor solution (1 mg/ml collagenase P and 25 µg/ml soybean trypsin inhibitor, both obtained from Sigma-Merck, in HBSS).

PSCs and acinar cells were labeled using a CellTrace-CFSE or CellTrace-Violet proliferation kit (Invitrogen), respectively, and cocultured in DMEM (Gibco) containing 10% FCS, penicillin/streptomycin, and 0.2 mg/ml soybean trypsin inhibitor (Sigma-Merck) at a ratio of

1:2 in 24-well plates equipped with discs made of rat tail collagen (Sigma-Merck). For certain conditions, the activin A inhibitor ActRIIBFc (gift from Olli Ritvos, Helsinki, Finland) was added at a final concentration of 0.5 µg/ml. After six days, the cells and collagen plates were recovered, and FACS analysis was performed to evaluate the differentiation of WT PSCs into CAFs.

### **Mouse cells lines**

The isolation and culture of cells were performed using a protocol adapted from previously published protocol (35). Tumor primary cell line 4KC was obtained from the pancreas of 2.5-months old 4KC mice using the same protocol. After several passages, the cells were infected with a lentivector expressing H2B GFP as previously described (36). Immortalized mouse pancreatic stellate cells (iPSCs) were obtained from Tuveson DA (23).

### **Human CAF generation**

Small pancreatic tissue blocks were obtained from patients with resectable PDAC during pancreatic surgery. The experimental procedure relating to the use of patient-derived pancreatic tumor pieces was performed after approval by the South Mediterranean Personal Protection Committee under reference 2011-A01439-32. Primary CAFs were isolated as previously described (37). Briefly, tumors were cut into small pieces (1 mm<sup>3</sup>) using a razor blade. The tissue pieces were dissociated using the Tumor Dissociation Kit (Miltenyi Biotec; 130-095-929) according to the manufacturer's recommendations. The cells were then resuspended, passed through a cell strainer (100 µM), and plated. Primary CAFs were used between passages 4 and 8. Primary CAF features were verified by flow cytometry with positive  $\alpha$ -SMA and FAP staining. Immortalized CAFs were generated from primary CAFs of limited passage via retrovirus-mediated expression of human telomerase reverse transcriptase (hTERT).

Human primary CAFs were cultured in Dulbecco's modified Eagle's medium (DMEM)/F-12 supplemented with 10% fetal bovine serum (Biosera FB-1001/500), 2 mmol/l l-glutamine (Invitrogen; 25030-024), 1% antibiotic-antimycotic (Invitrogen; 15240-062), and 0.5% sodium pyruvate (Invitrogen; 11360-039). Human immortalized CAFs were cultured in DMEM/F-12 supplemented with 10% fetal bovine serum and 1% antibiotic-antimycotic. The pancreatic cancer cell line PANC-1 was obtained from ATCC and cultured in DMEM GlutaMAX (Gibco 10566016) supplemented with 10% fetal bovine serum and 1% antibiotic-antimycotic. For coculture experimental conditions, primary CAF medium was used. Cells were authenticated through an STR profile report (LGC Standard) and confirmed to be mycoplasma free (Lonza, LT07-318).

PANC-1 cells were plated 24 h before coculture with CAFs in triplicate for each experimental condition and treated with 0.5 µg/ml ActRIIbFc inhibitor. The following day, human primary or immortalized CAFs were plated in monoculture or coculture according to the experimental conditions at a 2:1 ratio with PANC-1 cells and were treated with 0.5 µg/ml ActRIIbFc inhibitor. Half of the cell culture medium was refreshed every 48 h with the addition of 0.5 µg/ml ActRIIbFc inhibitor until day 6 of culture. Cells were detached using StemPro Accutase cell dissociation reagent (Gibco A1110501) and washed once with PBS. Samples were resuspended in FACS buffer (0.5% BSA and 2 mM EDTA in PBS) and surface stained with the following fluorochrome-coupled antibodies: anti-CD61 (BioLegend 370010), anti-CD140a/PDGFR $\alpha$  (BD Biosciences 742666), anti-FAP (R&D Biotechne FAB3715R), and anti-EpCAM (BioLegend 324204). Intracellular staining using anti- $\alpha$ -SMA (R&D Biotechne IC1420P) and anti-FSP-1 (BioLegend 370010) antibodies was performed following fixation and permeabilization with BD Cytotfix/Cytoperm (554714). Samples were analyzed on a BD LSRFortessa X20 cell analyzer.

#### **PDGFR $\alpha$ tyrosine phosphorylation and Western blot**

iPSCs were seeded onto 6 wells plate ( $4.0 \times 10^5$  cells per wells). Treatments of various lengths (10min, 30min, 2h) were done with 4KC conditioned medium or mouse recombinant PDGF-AA protein (Biolegend,776304) at 50ng/mL. For proteasome inhibition, cells were starved and treated with the proteasome inhibitor MG-132 (Sigma Aldrich, M8699-1MG) at 10µM for 12h. Cell extracts were prepared from cultured cells lysed by scratching at 4°C in 80uL RIPA (ThermoFisher, 89900) supplemented with protease (Roche, 04693159001) and phosphatase inhibitors (Roche, 04906837001). Obtained lysates were sonicated and centrifugated at 13,000g for 15min at 4°C. Equal amount of proteins were separated by SDS-PAGE then transferred onto Immune-Blot PVDF membrane. Membranes were incubated in blocking buffer containing 5% milk or Bovine Serum Albumine (BSA) (Sigma Aldrich, A2153-100G) in Tris Buffered Saline/Tween 20 (TBST). The blots were then probed overnight at 4°C with the appropriate primary antibodies. The membranes were revealed with the appropriate secondary antibodies for 1h at RT. Detection was performed by enhanced chemiluminescence using Pierce™ ECL Western Blotting Substrate (Thermo Scientific, 32106) according to the manufacturer's protocol. Tubulin was used as a loading control. Antibodies and dilutions were as follows: anti-p-Ty754 Ab (Thermo Fisher, TF441008G), 1:1000; anti-PDGFR $\alpha$  (Cell Signalling Technology, 3174S),1:1000; anti-Tubulin (GenTex, GTX628802), 1:1000.Secondary HRP-

conjugated anti-rabbit Ab (Jackson Immuno Research, 711-035-152) or anti-mouse Ab (Jackson Immuno Research, 715-035-150).

#### **CAF and 4KC-conditioned medium**

For the generation of conditioned medium, CAF subpopulations isolated by FACS were cocultured with cells from the KIC tumor cell line (35) at a ratio of 1:1 in DMEM containing 10% FCS. After a 48-h incubation at 37°C and 5% CO<sub>2</sub>, the supernatants were collected and stored at -20°C until further use. For the generation of conditioned medium, 4KC cells (1.5 x10<sup>4</sup> cells per wells) were seeded onto 6 wells plate in DMEM containing 10% FCS. After 7 days of incubation at 37°C and 5% CO<sub>2</sub>, the supernatants were collected and stored at -20°C until further use.

#### **Bone marrow-derived dendritic cell (BMDC) generation**

To generate bone marrow-derived monocytes, bone marrow cell suspensions were isolated by flushing the femurs and tibias of 8- to 12-week-old C57BL/6 mice (Charles River) with DMEM containing 10% FCS as previously described (36). Cell aggregates were dislodged by passing the suspension through a 70-µm cell strainer. Lysis of red blood cells was performed with ammonium-chloride-potassium (AKC) lysis buffer. The obtained cells were incubated for 6 days at 37°C and 5% CO<sub>2</sub>, and every other day, fresh DMEM containing 10% FCS and GM-CSF was added.

#### **T-cell proliferation assay**

Spleen and lymph nodes from 8 to 12-weeks old C57BL/6 mice were harvested, mechanically dissociated and cell suspension was incubated with anti-CD8α magnetic beads following manufacturer's protocol (Miltenyi Biotec). MACS-purified CD8<sup>+</sup> T cells were labeled with a CellTrace-CFSE proliferation kit (Life Technologies) according to the manufacturer's protocol. The CFSE-labeled CD8<sup>+</sup> T cells were cultured for 2 days in the presence of BMDCs (T cells:BMDCs=16:1). Mouse T-Cell-Activator CD3/CD28 Dynabeads (Gibco) were added to the coculture (T cells:Beads=1:1). The proliferation of the CD8<sup>+</sup> T cells was evaluated at the end of the culture period by analyzing CFSE dilution using flow cytometry.

#### **Enzyme-linked immunosorbent assay (ELISA)**

To determine the amount of PDGF-AA in tissue samples, freshly excised mouse pancreata were weighed and finely minced. Then, 500 µl of 1x PBS was added to the tissue fragments of each pancreas and thoroughly mixed. After centrifugation for 5 minutes at 300 g, the supernatant was collected, and a mouse PDGF AA ELISA kit obtained from Abcam was used according to the manufacturer's protocol.

# DISCUSSION

## I. The discovery of CD169<sup>+</sup> and PeSC in PDAC

The first objective of my thesis was to decipher the role of the communication between two compartments : the stromal compartment and macrophages. Our results provide for the first time in pancreatic cancer the existence of PeSC population and CD169<sup>+</sup> macrophages that have an interdependence and communicate during disease progression.

Indeed, we observed the infiltration of both PeSCs and CD169<sup>+</sup> macrophages during PanIN stage. While we showed that PeSCs were bone-marrow originated, we have no certitude about the origin of CD169<sup>+</sup> macrophages in pancreatic cancer. Our results are consistent with another study (Chittezhath et al., 2019) showing that CD169<sup>+</sup> macrophages infiltrate normal pancreatic tissue in young aged mice (<8 weeks). It was proposed that the pancreas may be a “slow” organ where circulating monocytes from the bone-marrow (HSCs derived) contribute to the vast majority of resident macrophages in adult mice (>8 weeks). The presence of CD169<sup>+</sup> macrophages in young-aged mice indicates that they may derive from embryonic stage. However, we showed that CD169<sup>+</sup> macrophages can also be detected in old-aged mice developing PDAC supporting the idea that CD169<sup>+</sup> macrophages can be maintained in pancreatic tissue. Their maintenance may be fed by circulating monocytes or by the auto-renewal of resident CD169<sup>+</sup> macrophages already infiltrated in normal pancreatic tissue through mitosis.

Very recently, it was brought up that in the KPC model, around 10% of TAMs are proliferative (Zuo et al., 2023). These TAMs were only proliferative in contact of fibroblasts in a CSF-1 dependant manner and through p21 signalling (Zuo et al., 2023) which is a reminiscent of the hypothesis stating that both macrophages and fibroblasts show inter-dependence by secreting growth factors (Zhou et al., 2018).

In a recent study, the use of a Yellow Fluorescent Protein (YFP) based cell lineage tracing showed that *siglec1* was more expressed in YFP<sup>-</sup> (embryonic macrophages) than YFP<sup>+</sup> (HSC-derived) macrophages in normal pancreas, pancreatitis condition and PDAC stage alongside with other tissue-remodelling macrophages markers (Baer et al., 2023). Our results indicate that PeSCs are capable of inducing the differentiation bone-marrow derived macrophages to acquire CD169 marker *in vitro*. Furthermore, the PeSC *in vivo* injection in orthotopic context induced increased CD169<sup>+</sup> percentage among F4/80 macrophages. However, the latter observation could not be replicated in a subcutaneous context indicating that circulating monocyte may need pancreatic environment to differentiate into CD169<sup>+</sup> macrophages. More importantly, PeSC are capable of secreting CCL2 chemokine which is the main chemokine responsible of macrophages recruitment in PDAC.

It was recently shown CD169<sup>+</sup> macrophages can be differentiated through cytokine signalling. Indeed, endothelial cells and marginal reticular stromal cells cooperate to differentiate CD169<sup>+</sup> macrophages in the spleen through RANK-RANKL axis (Camara et al., 2019). Also, TNF $\alpha$  can differentiate CD169<sup>+</sup> macrophages in breast cancer (Cassetta et al., 2019). CD169 expression on macrophages cannot be considered a marker of residency or recruitment as CD169<sup>+</sup> macrophages have been shown to be embryonically derived in the lung and recruited from circulating blood monocytes in the brain (Casanova-Acebes et al., 2021; Kim et al., 2022).

In the context of subcutaneous injection of PeSC and tumor cells, PeSC induced bone-marrow derived cells to become CD11b<sup>+</sup> Ly6G<sup>+</sup> MDSCs in favour of macrophages. In the orthotopic injection context, we showed CD11b<sup>+</sup> Ly6G<sup>+</sup> MDSCs increase as well as CD11b<sup>+</sup>F4/80 macrophages. In both subcutaneous and orthotopic model, PeSCs represent around 1% of the total population indicating that differences of macrophages infiltration do not come from PeSC proliferation capacities in the 2 contexts. We propose that observed differences might be explained by the fact that in the orthotopic model, blood vessels are already present in the pancreas facilitating the monocyte recruitment while in the subcutaneous graft blood vessel need time to develop. Interestingly, we observed that Ly6G<sup>+</sup> MDSCs were significantly upregulated when CD169<sup>+</sup> macrophages were depleted suggesting that a part of CD169<sup>+</sup> macrophages are recruited through CCL2/CCL5 production by the PeSC. The depletion of CD169<sup>+</sup> macrophages may re-induce Ly6G<sup>+</sup> MDSCs differentiation as a compensatory effect. However, in the pancreatic tissue, PeSCs may be in contact with resident CD169<sup>+</sup> macrophages orchestrating the redirection of CD11b<sup>+</sup> progenitor differentiation into macrophages differentiation rather than MDSCs. This hypothesis is in line with our observation showing that although all CD169<sup>+</sup> macrophages are depleted, around 10% of F4/80<sup>+</sup> macrophages remain in the microenvironment that are not capable of instructing PeSC. These remaining F4/80<sup>+</sup> macrophages express low level of CD206 suggesting an inflammatory role.

As deeply discussed in chapter II of the introduction, pancreatic cancer faces a great challenge to immunotherapy resistance. We showed that PeSC play an important role in this process. Indeed, in a subcutaneous context, PeSC induced an anti-PD1 resistance by the recruitment of PD-L1 expressing MDSCs inhibiting CD8<sup>+</sup> T cells. More importantly, CD169<sup>+</sup> macrophages also expressed PD-L1 on their surface allowing CD8<sup>+</sup> T cells inhibition in a PD-1 -PD-L1 dependent manner. These observations point out the fact that PeSC – CD169<sup>+</sup> macrophages – MDSCs establish an immunosuppressive niche in PDAC TME.

Beyond the direct effect on CD8<sup>+</sup> T cells function, CD169<sup>+</sup> macrophages depletion is associated with a significant reduction of intra-tumoral CD8<sup>+</sup> T cells. This results correlated with an increase infiltration

of CD8<sup>+</sup> T cells in pancreas draining lymph nodes which indicate that CD8<sup>+</sup> T cells recruitment to the tumor site is impaired when CD169<sup>+</sup> macrophages are depleted. In a pivotal study, it was proposed that the combination of  $\alpha$ PD-L1 and AMD3100 (CXCL12 – CXCR4 inhibitor) was efficient to reduce tumor progression through the recruitment of CD8<sup>+</sup> T cells (Feig et al., 2013). While they propose that the inhibition of CXCL12 allows for the recruitment of CD8<sup>+</sup> T cells, we proposed that the recruitment of CD8<sup>+</sup> T cells is CXCL12 dependent. This observation could indicate that mesenchymal cells and CD169<sup>+</sup> macrophages replicate the bone-marrow niche in the pancreatic TME (Chow et al., 2011).

## II. The Janus-faced of PDAC stroma

Both CD106<sup>+</sup> PeSC and CD169<sup>+</sup> may represent promising targets in pancreatic cancer. We showed that the specific targeting of CD106<sup>+</sup> cells with a monoclonal antibody showed a reduced tumor weight and tumor cells. However, one of the limitations of our approach is that CD106 is not specific to PeSC as CD106 can be secreted soluble form or expressed by endothelial cells (Sano et al., 2021). CD106 better survival, less high grade PanIN and F4/80<sup>+</sup> macrophages infiltration decrease (Sano et al., 2021).

On the other hand, the specific depletion of CD169<sup>+</sup> macrophages showed a reduced tumor weight with an increase of tumor cells and no difference of PeSC infiltration. Alongside with these observations, depletion of CD169<sup>+</sup> macrophages were associated with less stroma. This observation indicate that macrophages can shape the fibrotic response as previously reported in PDAC (Zhu et al., 2017). The exact mechanism by which CD169<sup>+</sup> macrophages shape the fibrotic response is still unknown and represents one of the weak point of our study. However, we showed that there is a reduction of PDPN<sup>+</sup> cells in the TME when CD169<sup>+</sup> macrophages are depleted which could indicate that PDPN<sup>+</sup> cells regulate collagen deposition. However, given that most of type I collagen in PDAC is secreted by myCAFs (Chen et al., 2021) that are  $\alpha$ SMA<sup>+</sup>, it is very likely that CD169<sup>+</sup> macrophages either impair CAFs development or CAFs signalling. We observed no difference in  $\alpha$ SMA<sup>+</sup> content in depleted vs control condition which may indicate that the signalling is impaired rather than the development or the maintenance of CAFs in the TME. On the other hand, we observed a reduced level of PDPN<sup>+</sup> cells which is a pan-marker for CAFs in PDAC. This observation may indicate that PDPN<sup>+</sup> CAFs communicate with  $\alpha$ SMA<sup>+</sup> CAFs in order to induce collagen secretion. More importantly, it has recently been demonstrated that CD169<sup>+</sup> macrophages can communicate with MSC to induce fibrosis in a context of graft versus host disease in the bone marrow (Zhang et al., 2023). Specifically, CD169<sup>+</sup> macrophages secrete TGF- $\beta$ 1 to activate Nestin<sup>+</sup> MSC through SMAD pathway and increase tissue fibrosis. This is a reminiscent of a pioneer study showing the communication between CD169<sup>+</sup> macrophages and MSC in the bone marrow to retain HSC progenitor through CXCL12 secretion (Chow et al., 2011). These observations strongly suggest that CD169<sup>+</sup> macrophages in contact with bone marrow originated PeSC might mimic the bone marrow niche context.

It was shown very recently that pancreatic resident macrophages (not CD169<sup>+</sup> macrophages specifically) infiltrate both pancreatitis and PDAC environment (Baer et al., 2023). Through single-cell analysis, they showed that resident macrophages were associated with ECM protein deposit and PDGF signalling. Resident macrophages depletion in a chronic pancreatitis context was associated with a reduced number of pre-neoplastic cells (CK19<sup>+</sup>) and a lighter fibrotic response (Less PDPN, PDGFR $\alpha$ , Fibronectin and collagen)(Baer et al., 2023). More importantly, in an induced Kras and KPC model, the

depletion of resident macrophages was associated with a decrease of relative pancreas weight while the number of CK19<sup>+</sup> cells (i.e., transformed cells) increased that is in line with our observations (Baer et al., 2023).

CD169<sup>+</sup> macrophages have been proposed to be either pro or anti-tumoral in many other tumors as discussed in chapter III. However, given their role in shaping the fibrotic response in the pancreas and the current controversy about the role of the stroma in pancreatic cancer (See chapter II), the definitive role of CD169<sup>+</sup> macrophages in PDAC is difficult to conclude. CD8<sup>+</sup> T cells infiltration is usually a sign of anti-tumoral response and lower tumor weight. Our observations indicate that despite a reduced tumor weight and stroma when CD169<sup>+</sup> macrophages are depleted, CD8<sup>+</sup> T cells are absent.

Our results brought us back to question the role of the stroma in pancreatic cancer. Is stroma good or bad in PDAC ? Answering this question is not easy as there are many parameters influencing the role of the stroma in PDAC. As discussed in the introduction, we absolutely must not entirely disrupt the stroma in its wholeness as there is an equilibrium between stroma supportive and stroma restricting parameters in pancreatic cancer. Among these parameters are :

- CAFs heterogeneity
- ECM protein deposition including collagen
- Tissue stiffness

Tissue stiffness is not commonly considered in previously reported studies in mouse and human PDAC. Tissue stiffness refers to the property of a tissue to easily be compressed or stretched. In a tumoral tissue, there are several mechanical forces taking place : Solid Stress, IFP and ECM stiffness. Solid stress denotes the mechanical pressure exerted by the cancer cells that undergo expansion. This mechanical force, in conjunction with the stiffness generated by the ECM and stromal cells, contributes to the elevation of IFP. We generated a genetical model developing early lesions of pancreatic cancer with a higher tissue stiffness than conventional KC model. We hypothesized that solid stress occurring in high stiff model induces paracrine communication between cancer cell and CAFs allowing their differentiation into stiffness-induced CAFs (siCAF). Our results show that in a softer solid stress model, less paracrine interactions are detected from ductal cells to CAFs. Among those paracrine interactions PDGF signalling allows for the trans differentiation of CAFs into siCAF. Targeting PDGF-ligand allows for reprogramming of siCAF back to "normal" CAFs further reducing collagen deposition and relative pancreas weight. The number of lesions was lower while the number of CD31 endothelial cells was higher allowing for effector T cell recruitment. One of the limitations of our study is the lack of direct mechanistic data showing that tissue stiffness can impair CD8<sup>+</sup> T cells response although CD8<sup>+</sup> T cells have been shown to be highly sensitive to their mechanical environment (Adu-Berchie et al., 2023).

Further investigations should look into the mechano-receptor of CD8<sup>+</sup> T cells and how they are regulated in our two different *in vivo* model.

Our results are in line with recent data demonstrating that targeting PDGFR $\alpha/\beta$  reprogram the stroma in fibrotic tumors (Akiyama et al., 2023). However, there are differences between targeting the ligand and the receptor signalling. Indeed, by targeting the receptor with an inhibitor as Akiyama and colleagues did, they also deplete CAFs which has been shown not to be benefit in human setting. More importantly, the use of kinase inhibitors may induce off target effects. Further investigations are necessary to evaluate the therapeutic potential of PDGF signalling to reshape the stroma but also to evaluate if PDGF signalling targeting can be combined with another stroma-based therapy.

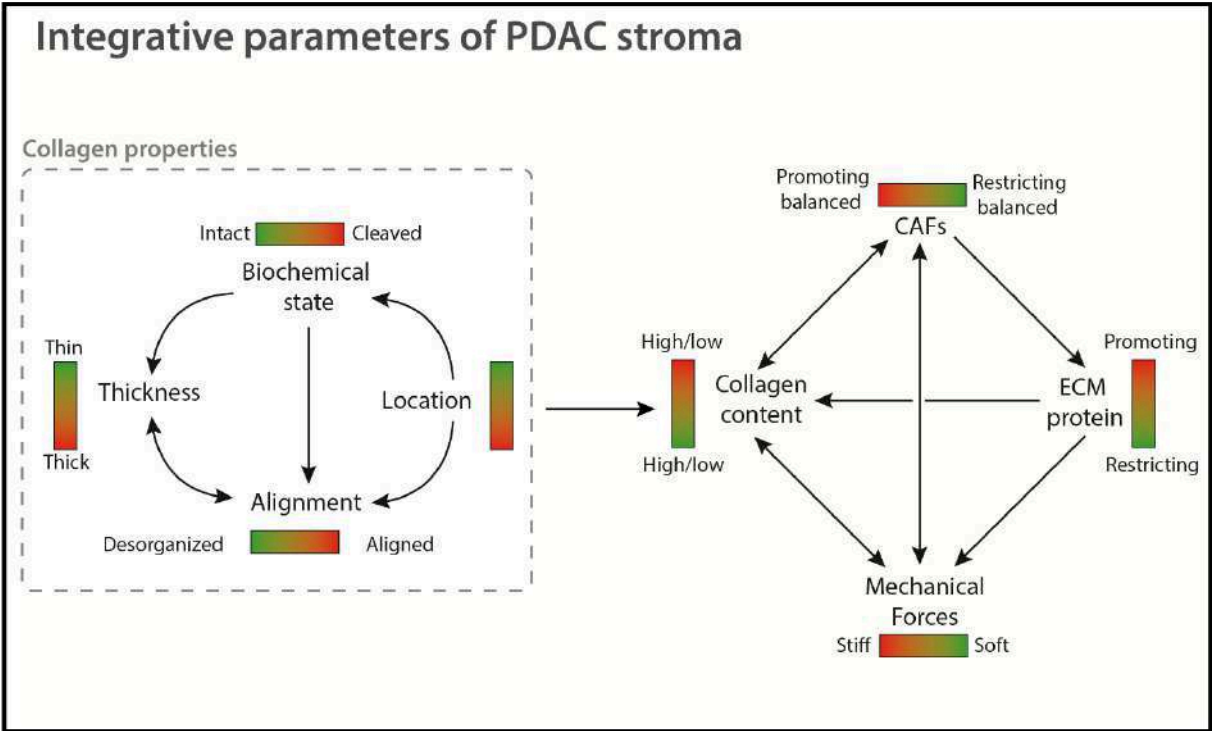


**Figure 20** Determinant parameters of stroma role in PDAC

The stroma has controversial role in PDAC due to the lack of integration of different parameter in clinical practice and at diagnosis. Graduate scale red mean tumor promoting while green mean tumor restricting.

Theses stromal parameters are interdependent and studying the causality of each separated parameter is utterly difficult but also do not necessarily reflect the physiological phenomena in the disease as many of the parameters are independent. Therefore, it is important to always consider the model in which one parameter has been evaluated.

The collagen content is one such parameter. Unfortunately, looking at the collagen content only may be an oversimplification of collagen role in PDAC. Indeed, we and others showed that there are

accumulated evidence showing that independently of collagen content level, there are other crucial parameters dictating PDAC progression (biochemical state, thickness, alignment, location) (Alonso-Nocelo et al., 2023; Bachy et al., 2022; Chen et al., 2022; Laklai et al., 2016; Su et al., 2022). In our study, we observed that CD169<sup>+</sup> macrophages depletion changed collagen fibers thickness and orientation. These results are in line with recently published study (Alonso-Nocelo et al., 2023). The reduced thickness of collagen fibers when CD169<sup>+</sup> macrophages are depleted can be explained by our results showing that  $\beta$ ig-h3 can structure collagen fibers in a thicker structure (See Appendices) (Bachy et al., 2022). One of the limitation of our study regarding the effect of CD169<sup>+</sup> macrophages depletion is the absence of collagen biochemical state analysis which appear to be important in PDAC. These parameters can be kinetic sensitive but also may vary between patients. It goes without saying that there may be additional parameters of stroma role in PDAC that are still unknown. Each patients have a different set up of stroma parameters that may be regulated by intrinsic factors (Age, sex, genetical background) and extrinsic factors (TME).

As the stroma is an essential component of how the immune response operate in the pancreatic TME, the stroma parameters diversity make direct (CAFs depletion, collagen degradation...) and indirect stroma-based (Immunotherapy) therapy difficult. Although the combination between immunotherapy and stroma-based therapies are currently being evaluated in PDAC, preliminary results failed to show benefit in some studies (Zhen et al., 2022). These observation may indicate that despite the promising data that are observed in pre-clinical studies, a barrier is always observed when brought to human.

### III. Personalized medicine in pancreatic cancer

Contrary to others cancer that transferred pre-clinical immunotherapy results in a rather successful manner, it is not the case in PDAC. Indeed, conventional approaches to treat PDAC failed to show benefits. PDAC therapies are often based on specific actors (e.g., CAFs, protein ...) which mean that patient selection is crucial for such therapeutical avenues. More importantly, while PDAC is a deadly cancer, the incidence is relatively low compared to other cancers (e.g., Lungs, Breast, Melanoma). Additionally, as discussed in the introduction, patients are often diagnosed very late, which means that they have a lower probability of responding to any treatment. Finally, it was commonly known that very few patients are enrolled in clinical trials (between 5 to 10%). Altogether, these observation may explain why we have such difficulties to transfer immunotherapies in clinical practice. However, although it may sound unrealistic from an economical and logistical perspective, personalized medicine in PDAC may be applicable and beneficial to improve clinical outcomes in the future for PDAC patients. Indeed, I do think that personalized medicine with an integrative evaluation of as many parameters as possible is the way. My work and the ones of many others showed that PDAC is a highly complex disease in which many parameters can influence the progress of the disease. Therefore, patients selection before treatment may be the best options so far to unleash the full potential of immunotherapy in PDAC.

Recently, a programme titled “ Know Your Tumor “ enrolled more than 600 patients to evaluate the benefits “actionable molecular alterations” consideration in the treatment in PDAC. Patient’s biopsies were sequenced to identified “actionable molecular alterations” (e.g., Mutation of DNA damage response and repair protein, High microsatellite instability, Protein fusion or amplification...) for which there is clinical or pre-clinical evidence of efficient therapy targeting those specific molecular alterations. Of the 677 patients, 189 had actionable molecular alterations with 46 who received a matched therapy and 143 who did not receive a matched therapy. The matched therapy group showed a significant long survival compared to other patients (no marker and unmatched)(Pishvaian et al., 2020). This was the first large, scaled study in human evaluating the potential of personalized medicine in pancreatic cancer.

Our results show that PDAC is far from being a single-hit disease as the TME support tumor progression and therapeutic resistance in many way. Therefore, additionally to molecular sequencing of patients biopsies, TME should be considered by deeply analysing the immune and stromal profile. The rise of single cell and spatial transcriptomic analysis on patient biopsies would facilitate the evaluation of all known key parameters (**Figure 21**). Indeed, spatial transcriptomic analysis has been validated as a method to classify PDAC subtype since small specimen can recapitulate large tumor state (Williams et al., 2023). The evaluation of immune profile is currently transferred to clinical practice with the Immunoscore concept but has not been evaluated in PDAC yet (**Figure 21**).

We also showed that specific CAFs population (i.e., siCAF) can impair the immune response in PDAC and therefore, the evaluation of CAFs populations content is crucial. For example, some patients harbour a FAP<sup>+</sup> dominant stroma while some do not. These patients would highly benefit from CAFs balance evaluation and  $\alpha$ FAP therapy. Meanwhile, while we do show that macrophages are the most infiltrating population and can also support cancer progression from initiation the metastatic phase, some patients may not express immune checkpoint on macrophages or specific chemokine at the time of diagnosis and treatment.

Finally, it is not unreasonable to think that in cooperation with the immunoscore that is currently evaluated in PDAC, the establishment of a stromal score composed of : tissue stiffness, CAFs subpopulation, ECM deposit and collagen state could improve how patients are diagnosed.

# Sine qua non personalized medicine to treat PDAC

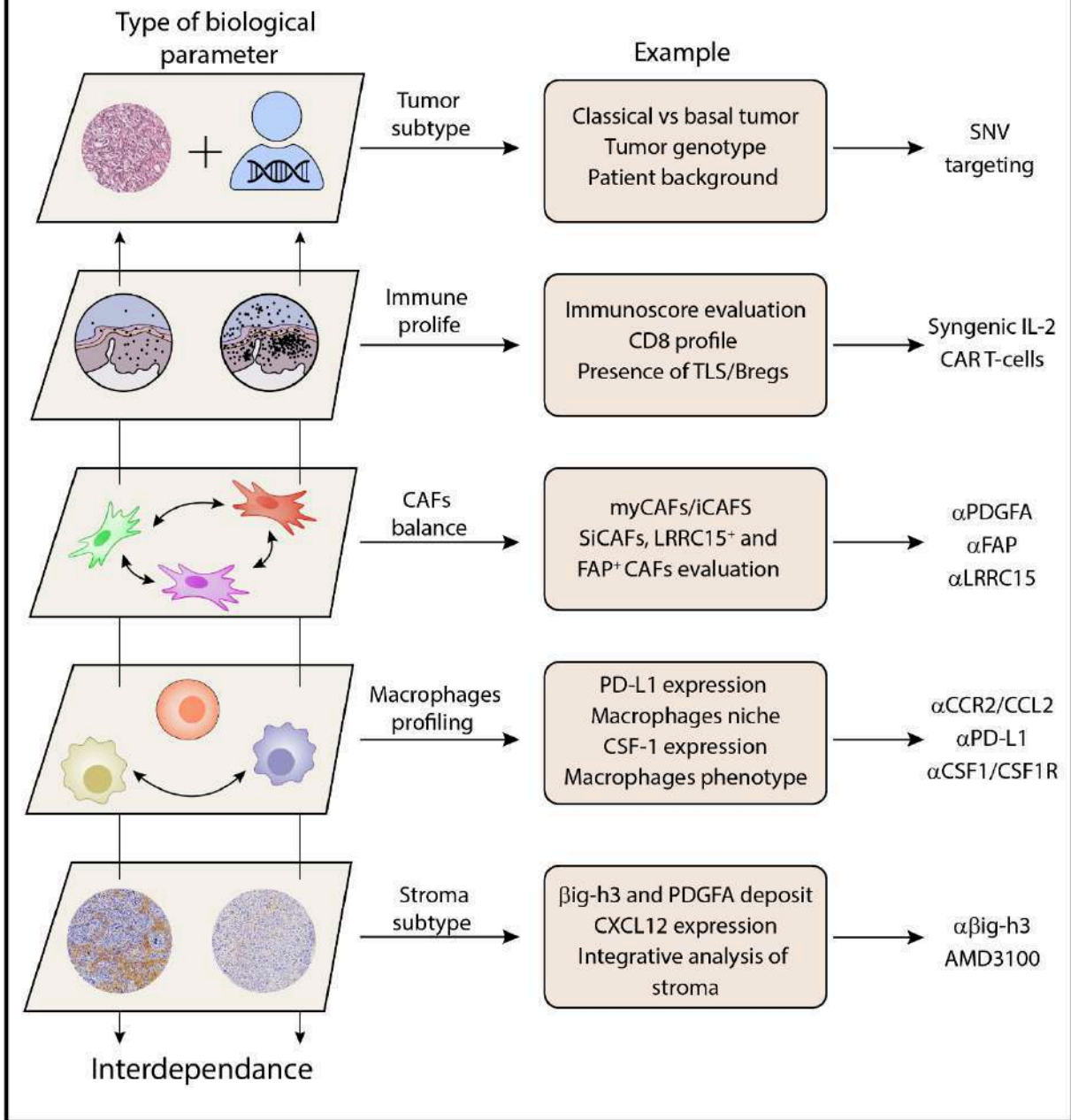


Figure 21 Personalized medicine to treat PDAC

## CONCLUSION

First, I participated in the identification of a new stromal population called PeSC. We showed that PeSC share both stem and pericyte properties and express CD106 receptor (VCAM1). We showed that PeSC were able to differentiate into multiple cells type but also to structure vessels as they express both pericyte and stem signature. We observed *in vivo* that PeSC were responsible for the recruitment in a CCL5/CCL2 dependent manner of MDSCs that impair the CD8<sup>+</sup> T cells anti tumoral immune response. Finally, we showed that PeSC were necessary for the resistance to anti-PD1 therapy.

Secondly, I analysed the role of a specific macrophages population expressing CD169 and how CD169<sup>+</sup> macrophages communicate with PeSC. We observed that macrophages expressing CD169 were expressed in both PDAC and neoplastic stage in human and murine model. We observed that PeSC were capable of differentiating macrophages into CD169<sup>+</sup> macrophages both *in vitro* and *in vivo*. We showed that macrophages were responsible of secreting immunosuppressive protein such as  $\beta$ ig-h3 to activate the secretion of CXCL12 from PeSC. Finally, we showed that *in vivo* depletion of CD169<sup>+</sup> macrophages was associated with a reduced stroma deposit as less type I collagen was detected. More importantly, although the number of cancer cells in the depleted condition was higher, the tumor weight was smaller indicating that CD169<sup>+</sup> macrophages may regulate the fibrotic response and stromal complexity in PDAC.

Lastly, I participated in the identification of mechanisms regulating tissue stiffness in PDAC. With the use of two different *in vivo* model of neoplastic lesions of PDAC, one with low stiffness and one with high stiffness, we observed differential interactions between ductal cells and CAFs with higher interactions in the stiff model. Specifically, we showed that in the stiff model, ductal cells secrete PDGF ligand to differentiate CAFs into siCAF. We showed that siCAF were associated with higher tissue stiffness and CD8<sup>+</sup> T cells inhibition. More importantly, we observed that the targeting of PDGF ligand allow the regression of neoplastic lesions development and the reprogramming of siCAF.

# Appendices

## A. Posters

**Thierry, K.,** Wu, Z., Bachy, S., Gamradt, P., Hennino, A., 2021. Crosstalk between stromal compartment and macrophages lead to CD169<sup>+</sup> macrophages in pancreatic ductal adenocarcinoma. 6<sup>th</sup> European Congress of Immunology, September 1-4 2021, **Virtual edition**.

**Thierry, K.,** Wu, Z., Bachy, S., Gamradt, P., Hennino, A., 2022. Crosstalk between stromal compartment and macrophages lead to CD169<sup>+</sup> macrophages in pancreatic ductal adenocarcinoma. 4<sup>th</sup> International conference on Stem cells, Development and Cancer, May 16-17 2022, **Lyon – France**.

**Thierry, K.,** Wu, Z., Bachy, S., Gamradt, P., Hennino, A., 2022. Crosstalk between stromal compartment and macrophages lead to CD169<sup>+</sup> macrophages in pancreatic ductal adenocarcinoma. Immune Response in Cancer and Infection, June 15-17 2022, **Lyon – France**.

**Thierry, K.,** Wu, Z., Bachy, S., Gamradt, P., Hennino, A., 2022. Crosstalk between stromal compartment and macrophages lead to CD169<sup>+</sup> macrophages in pancreatic ductal adenocarcinoma. 5<sup>th</sup> International Cancer Symposium, November 2-4 2022, **Lyon – France**.

**Thierry, K.,** Wu, Z., Bachy, S., Gamradt, P., Hennino, A., 2022. Crosstalk between stromal compartment and macrophages lead to CD169<sup>+</sup> macrophages in pancreatic ductal adenocarcinoma. Young European Federation of Immunological Societies (yEFIS) 1<sup>st</sup> symposium, November 10-11 2022, **Berlin – Germany**.

**Thierry, K.,** Wu, Z., Bachy, S., Gamradt, P., Hennino, A., 2022. Crosstalk between stromal compartment and macrophages lead to CD169<sup>+</sup> macrophages in pancreatic ductal adenocarcinoma. Joint meeting SFI&DGFI, September 26-29 2023, **Strasbourg – France**.

## B. Oral Presentations

**Thierry, K.,** Crosstalk between stromal compartment and macrophages lead to CD169<sup>+</sup> macrophages in pancreatic ductal adenocarcinoma. 6<sup>e</sup> Journée Scientifique de l'Association pour la Recherche sur le Cancer du Pancréas (AFRCP), November 6 2021, Hopital Beaujon, **Clichy – France**.

**Thierry, K.,** Crosstalk between stromal compartment and macrophages lead to CD169<sup>+</sup> macrophages in pancreatic ductal adenocarcinoma. Joint Congress of the 26th Meeting of International Association of Pancreatology and the 53rd Annual Meeting of Japan Pancreas Society, Kyoto International Conference Center, July 7-9 2022, **Kyoto – Japan**.

**Thierry, K.,** Pancreatic cancer and stromal reaction. Cérémonie Annuelle de la Recherche / Ligue contre le cancer de Savoie, september 19 2023, **Chambéry – France**.

**Thierry, K.** CD169<sup>+</sup> macrophages orchestrate immune reaction and matrix deposition in pancreatic cancer. Pancreatic cancer symposium, October 16-18 2023, **Talences – France**.

## C. List of publications

### a. Published manuscript

Gamradt, P., **Thierry, K\***, Masmoudi, M\*, Wu, Z., Hernandez-Vargas, H., Bachy, S., Antonio, T., Savas, B., Hussain, Z., Tomasini, R., Milani, P., Bertolino, P., Hennino, A., 2023. Stiffness-induced cancer-associated fibroblasts are responsible for immunosuppression in a platelet-derived growth factor ligand-dependent manner. *PNAS Nexus* 2, pgad405.

<https://doi.org/10.1093/pnasnexus/pgad405>

Wu, Z\*, **Thierry, K\***, Bachy, S., Zhang, X., Gamradt, P., Hernandez-Vargas, H., Mikaelian, I., Tonon, L., Pommier, R., Zhao, Y., Bertolino, P., Hennino, A., 2023. Pericyte stem cells induce Ly6G<sup>+</sup> cell accumulation and immunotherapy resistance in pancreatic cancer. *EMBO reports* 24, e56524.

<https://doi.org/10.15252/embr.202256524>

Bachy, S., Wu, Z., Gamradt, P., **Thierry, K.**, Milani, P., Chlasta, J., Hennino, A., 2022.  $\beta$ ig-h3-structured collagen alters macrophage phenotype and function in pancreatic cancer. *iScience* 25, 103758.

<https://doi.org/10.1016/j.isci.2022.103758>

**Thierry, K.**, Ménétrier-Caux, C., 2020. Le rôle des lymphocytes T régulateurs dans l'activité antitumorale des anticorps anti-CTLA-4. *Med Sci (Paris)* 36, 73–76.

<https://doi.org/10.1051/medsci/2019260>

### b. Submitted manuscript

**Thierry, K\***, Wu, Z\*, Bachy, S., Gamradt, P., Hernandez-Vargas, H., Hennino, A., 2023. CD169<sup>+</sup> macrophages orchestrate immune reaction and matrix deposition in pancreatic cancer

Chen, J., Sobecki, M., Krzywinska E., **Thierry, K.**, Nagarajan, S., Fan, Z., Nelius, E., Seehusen, F., Gotthardt, D., Takeda, N., Sommer, L., Sexl, V., Münz, C., DeNardo, D.G., Hennino, A., Stockmann C., 2023. Fibrolytic vaccination against ADAM12 reduces desmoplasia in preclinical pancreatic adenocarcinomas.

### c. Published abstract

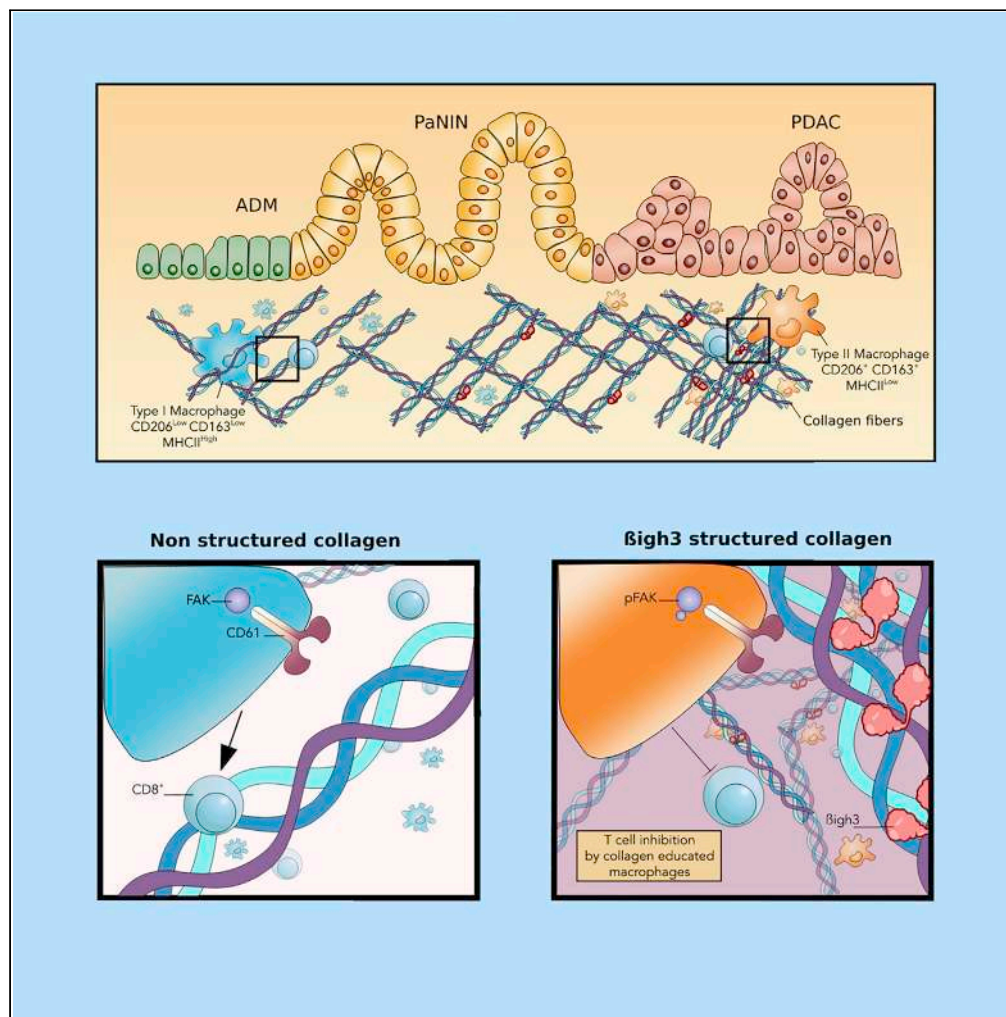
**Thierry, K.**, Wu, Z., Bachy, S., Gamradt, P., Hennino, A., 2021. Crosstalk between stromal compartment and macrophages lead to CD169<sup>+</sup> macrophages in pancreatic ductal adenocarcinoma. *Eur. J. Immunol.* 51, 326–326.

## D. Participant paper results

(See published paper next page)

Article

# $\beta$ ig-h3-structured collagen alters macrophage phenotype and function in pancreatic cancer



Sophie Bachy, Zhichong Wu, Pia Gamradt, Kevin Thierry, Pascale Milani, Julien Chlasta, Ana Hennino

ana.hennino@inserm.fr

**Highlights**

Atomic force microscopy of  $\beta$ ig-h3-structured collagen

*In vitro* and *in vivo* macrophage education on structured collagen

*In vitro* macrophage phenotype imprinting is stable *in vivo*

Bachy et al., iScience 25, 103758  
February 18, 2022 © 2022 The Authors.  
<https://doi.org/10.1016/j.isci.2022.103758>

## Article

# $\beta$ ig-h3-structured collagen alters macrophage phenotype and function in pancreatic cancer

Sophie Bachy,<sup>1,2,3,5</sup> Zhichong Wu,<sup>1,2,3,5</sup> Pia Gamradt,<sup>1,2,3</sup> Kevin Thierry,<sup>1,2,3</sup> Pascale Milani,<sup>4</sup> Julien Chlasta,<sup>4</sup> and Ana Hennino<sup>1,2,3,6,\*</sup>

**SUMMARY**

**Macrophages play an important role in immune and matrix regulation during pancreatic adenocarcinoma (PDAC). Collagen deposition massively contributes to the physical and functional changes of the tissue during pathogenesis. We investigated the impact of thick collagen fibers on the phenotype and function of macrophages. We recently demonstrated that the extracellular protein  $\beta$ ig-h3/TGF $\beta$ i (Transforming growth factor- $\beta$ -induced protein) plays an important role in modulating the stiffness of the pancreatic stroma. By using atomic force microscopy, we show that  $\beta$ ig-h3 binds to type I collagen and establishes thicker fibers. Macrophages cultured on  $\beta$ ig-h3-structured collagen layers display a different morphology and a pro-tumoral M2 phenotype and function compared to those cultured on non-structured collagen layers. *In vivo* injection of those instructed CD206<sup>+</sup>CD163<sup>+</sup> macrophages was able to suppress T cell responses. These results reveal for the first time that the collagen structure impacts the phenotype and function of macrophages by potentiating their immunosuppressive features.**

**INTRODUCTION**

We have recently demonstrated that the extracellular matrix protein  $\beta$ ig-h3/TGF $\beta$ i (Transforming growth factor- $\beta$ -induced protein) plays an important role in modulating the stiffness of tumor microenvironment (TME) in pancreatic adenocarcinoma (PDAC) (Goehrig et al., 2019). Previous studies established that  $\beta$ ig-h3 binds to type I, II, and IV collagens as well as to biglycan and decorin thereby influencing cell-to-cell, cell-to-collagen, and cell-to-matrix interactions (Bae et al., 2002; Hashimoto et al., 1997). The *tgfb1* gene encodes a 683-amino acid protein that contains a secretory signal sequence, an N-terminal cysteine-rich EMI domain, four fasciclin 1 domains, and an RGD (Arg-Gly-Asp) motif (Skonier et al., 1992, 1994).

Though the pancreas is a soft tissue at homeostasis, collagen deposition massively contributes to the “physical and functional” changes of the tissue that occur during pathogenesis. This process results in a stiffened pancreatic parenchyma and represents a significant risk factor for developing PDAC (Laklai et al., 2016). Because collagen fibers adjacent to pancreatic lesions are significantly thicker in patients with the shortest survival, we investigated the impact of thick collagen fibers on the phenotype and function of macrophages during PDAC. We previously showed that, aside from its role in modulating collagen stiffness,  $\beta$ ig-h3 has immunosuppressive properties hampering T cell activation and is able to reprogram macrophages (Goehrig et al., 2019; Patry et al., 2015). It is well-known that macrophages play an important role in the immune responses in pancreatic fibrosis, a risk factor for PDAC, and we thus speculated that  $\beta$ ig-h3 may affect macrophage properties by modulating collagen fibers.

**RESULTS****Matrix protein  $\beta$ ig-h3 structures collagen I in thicker fibers**

We first investigated the localization of  $\beta$ ig-h3 and collagen I by performing immunofluorescence (IF) microscopy on pancreatic samples obtained from the *p48-Cre*, *Kras*<sup>G12D</sup> (KC) mouse model, which develops pancreatic intraepithelial neoplasias (PanINs) from the age of 1.5 months old (Hingorani et al., 2003). As shown in Figure 1A, we observed that both proteins co-localized around pancreatic neoplastic lesions. Moreover, F4/80<sup>+</sup> macrophages were localized in close proximity to  $\beta$ ig-h3 around PanIN lesions

<sup>1</sup>Cancer Research Center of Lyon, UMR INSERM1052, CNRS5286, 69373 Lyon, France

<sup>2</sup>Université Lyon 1, 69000 Lyon, France

<sup>3</sup>Centre Léon Bérard, 69008 Lyon, France

<sup>4</sup>Biomeca, 69007 Lyon, France

<sup>5</sup>These authors contributed equally

<sup>6</sup>Lead contact

\*Correspondence:

ana.hennino@inserm.fr

<https://doi.org/10.1016/j.isci.2022.103758>



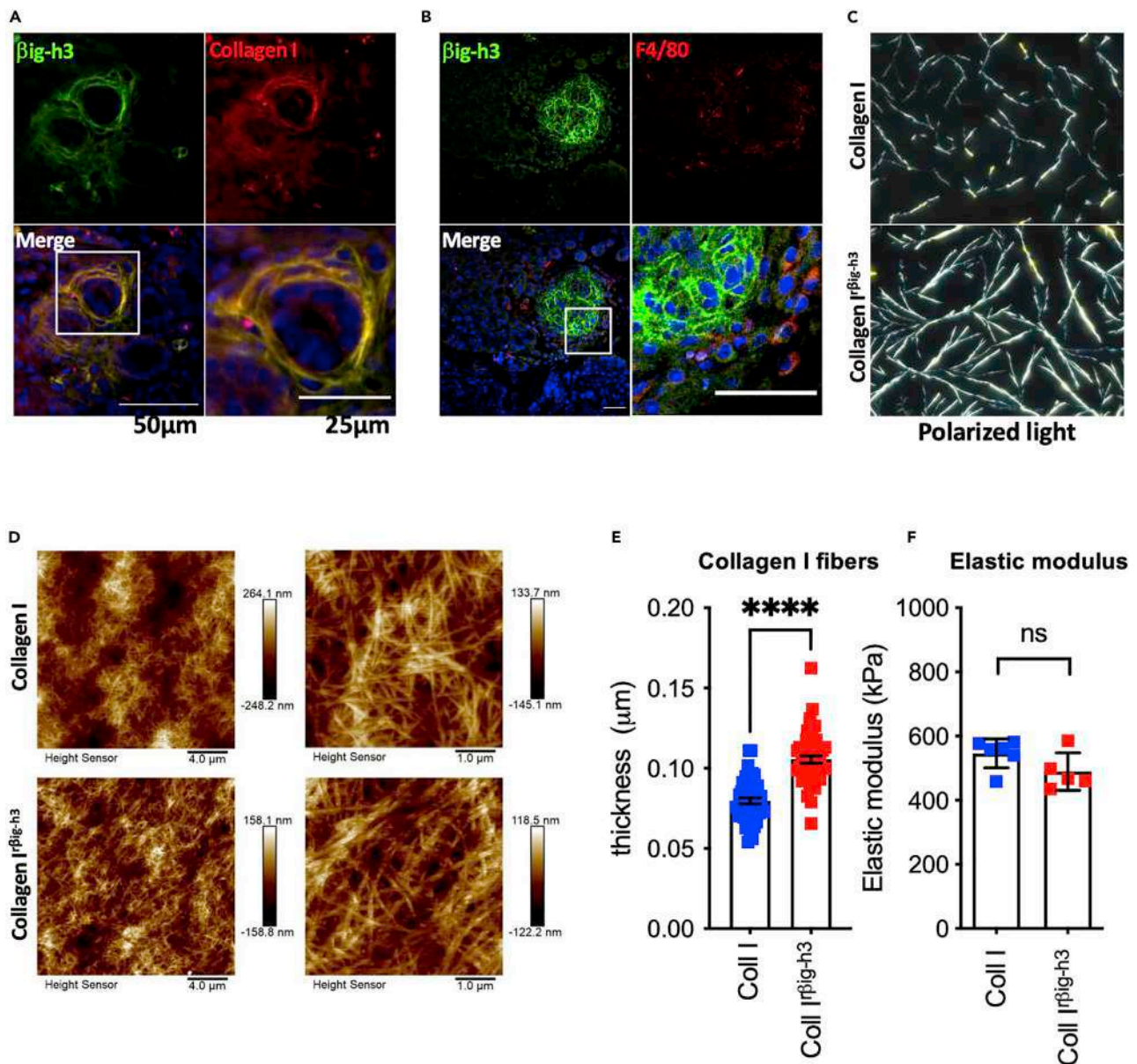


**Figure 1. rβig-h3 structures collagen I into thick fibers**

(A and B): Representative micrographs of immunofluorescence staining in pancreata from three-months-old KC mice for (A) βig-h3 (green), collagen I (red) or (B) βig-h3 (green) and F4/80 (red); (A, B) nuclear counterstaining in DAPI (blue).

(C) Representative micrographs taken with polarized light of collagen I structured in the absence (top) or presence (bottom) of rβig-h3 and stained with Sirius Red.

(D) Thickness topography measured by AFM of representative regions of collagen I structured in the absence (up) or presence (bottom) of rβig-h3. Two different magnifications are shown.

(E) Quantification of collagen I fiber thickness measured by AFM.

(F) Quantification of the Elastic modulus measured by AFM. Student's t-test \*\*\*\* $p < 0.0001$ , ns - not significant. Error bars 50 μm, 25 μm.

(Figure 1B). A previous study having shown that βig-h3 was able to interact with collagen (Hashimoto et al., 1997), we generated collagen I matrices in the presence or absence of human recombinant βig-h3 (rβig-h3). Analysis of Sirius Red-stained collagen I matrices under polarized light allowed us to evaluate the effect of rβig-h3 on their microarchitecture (Figure 1C). In the presence of rβig-h3, the structure of the collagen I matrices developed into a network with higher density with thicker collagen fibers. In order to confirm these results, we performed quantitative topological analysis by atomic force microscopy which revealed that the

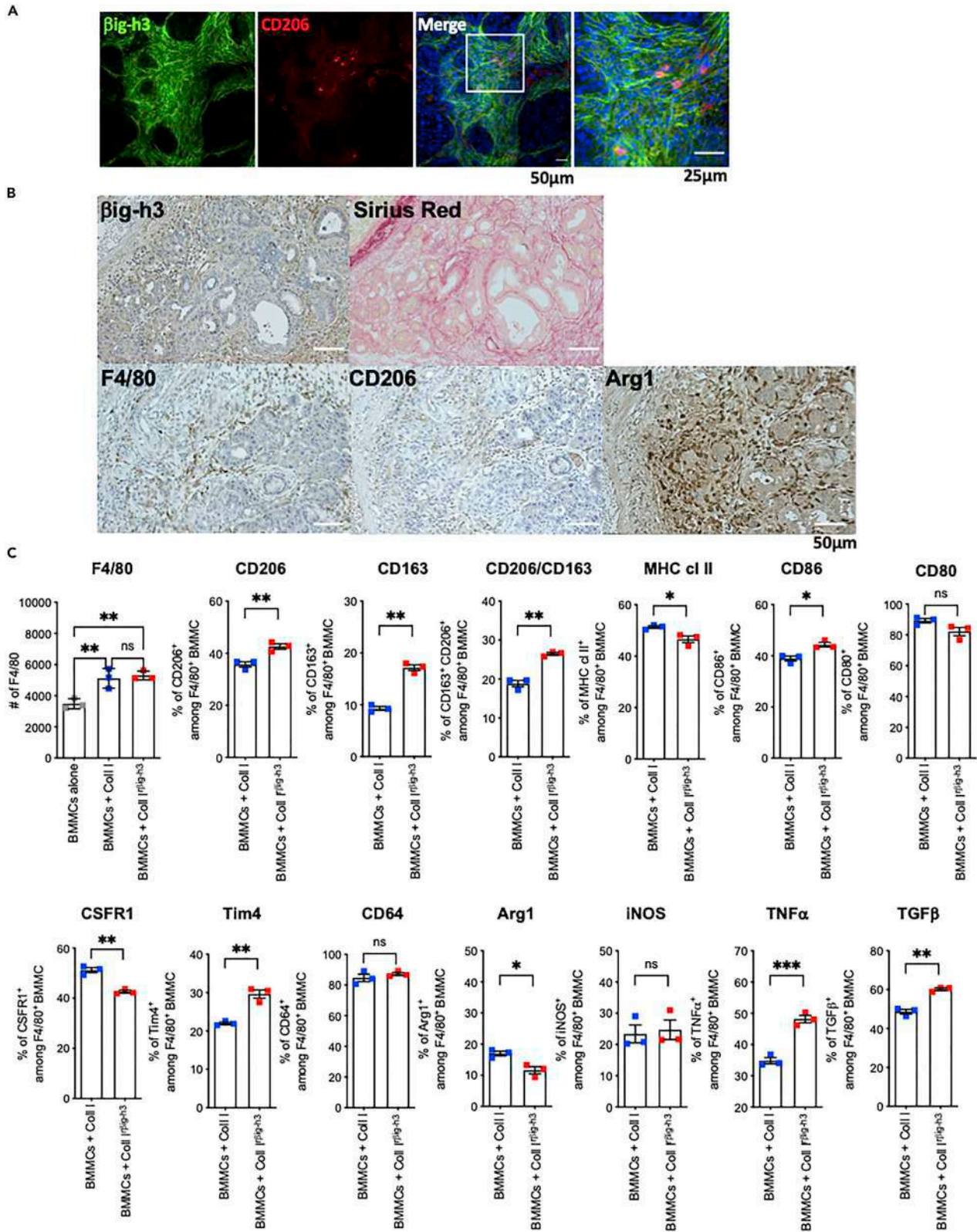


### Figure 2. rβig-h3-structured collagen I fibers modulate the phenotype and function of macrophages

(A) Representative photographs of immunofluorescence staining of pancreata from three-months-old KC mice stained for βig-h3 (green) and CD206 (red). Nuclear counterstaining in DAPI (blue).  
 (B) Representative photographs of βig-h3, F4/80, CD206, and Arg1 staining on serial section of pancreata from three-months-old KC mice.  
 (C) FACS analysis of BMMCs cultured alone or on collagen I structured in the absence (BMMCs + Col I) or presence of rβig-h3 (BMMCs + Col I<sup>rβig-h3</sup>). Representative data of three independent experiments with three in vitro replicates per group are shown. \*p<0.05, \*\*p<0.01. Error bars 50 μm, 25 μm.

diameter of collagen fibers had increased in the presence of rβig-h3 (Figure 1E) whereas the elastic modulus measurements were similar in both conditions (Figure 1F). These results show that βig-h3 plays a role in structuring collagen I during fibrillogenesis.

### rβig-h3-structured collagen I fibers modulate the phenotype and function of macrophages

Having detected the presence of macrophages in close proximity to PanIN lesions in mouse pancreatic cancer, we sought to determine the phenotype of macrophages in contact with endogenous βig-h3 within these tissues. We observed that macrophages in close contact with βig-h3 were positive for CD206 (Figure 2A), a well described marker associated with an M2 phenotype. To further characterize the phenotype of these macrophages *in situ*, we performed immunohistochemistry on serial sections of pancreatic tumors from KC mice stained for βig-h3, F4/80, CD206, and Arg1 as well as Sirius Red. We thereby confirmed M2 phenotype of F4/80<sup>+</sup> macrophages in close proximity to βig-h3 and collagen I, as they co-expressed CD206 and Arg1 (Figure 2B).

Next, we attempted to determine the direct effect of βig-h3-structured collagen fibers on the phenotype and function of macrophages. To achieve this, we cultured bone marrow-derived mononuclear cells (BMMCs) for 48 h on collagen I matrices generated in the presence or absence of rβig-h3. Flow cytometric analysis of recovered BMMCs revealed that rβig-h3-structured collagen I decreased MHC cl II and CSFR1 expression but increased CD206, CD163, CD86, and Tim4 surface expression (Figure 2C). The expression of CD80 and CD64 was similar in both conditions. We detected a small but significant decrease in Arg1 in the presence of rβig-h3-structured collagen I. We further detected increased TNFα and TGFβ cytokine production. Overall, these results indicate that βig-h3-structured collagen I in the TME might promote a pro-tumorigenic macrophage phenotype, displaying an M2 signature associated with increased CD206 and CD163 surface expression as well as augmented TGFβ cytokine production.

### rβig-h3-structured collagen I fibers activate FAK signaling pathway in macrophages

Because the thickness of the collagen fibers was increased in the presence of βig-h3, we next investigated whether culturing BMMCs on collagen I structured in the absence or presence of rβig-h3 would have any impact on the cellular morphology. Morphological analysis of BMMCs revealed more spherical macrophages with fewer processes when cultured for 48 h on rβig-h3-structured collagen I compared to those on non-structured collagen I after 48 h of culture (Figures 3A and 3B). We then performed western blot analysis of FAK, phosphorylated FAK (pFAK) on macrophages cultured on plastic or on structured collagen I in the absence or presence of rβig-h3 for 48 h. BMMCs cultured on rβig-h3-structured collagen I displayed a greater increase in pFAK compared to non-structured collagen I (Figure 3C). These results indicate that rβig-h3-structured collagen I is able to not only modulate the cellular morphology of the cells but also induce FAK phosphorylation and hence its stronger activation in this condition. To verify whether the FAK phosphorylation mediated the change in the BMMC morphology, we added the pFAK inhibitor (Y15) to cell cultures. This restored the morphology of macrophages grown on rβig-h3-structured collagen I that resembled to those grown on non-structured collagen I (Figures 3D–3F). Furthermore, we evaluated their phenotype by flow cytometric analysis and revealed that pFAK treatment downregulated the CD163 and CD206 expression (Figure 3G). Altogether, these results suggest that rβig-h3-structured collagen I modulates the morphology of macrophages and subsequently their phenotype and function.

### rβig-h3-structured collagen I promotes an immunosuppressive macrophage phenotype

Having established that culturing BMMCs on collagen I structured in the absence or presence of rβig-h3 affected the functional and morphological phenotype, we next evaluated its effect on T cell activation. We co-cultured CD8<sup>+</sup> T cells with BMMCs generated on plastic on collagen I or rβig-h3-structured collagen I at indicated ratios (4:1 or 2:1 or 1:1) and determined their proliferation by CFSE dilution as well as their activation based on the surface expression of CD69 and CD44. Whereas CFSE dilution revealed four to five cell divisions of CD8<sup>+</sup> T cells co-cultured with BMMCs generated on plastic or non-structured collagen

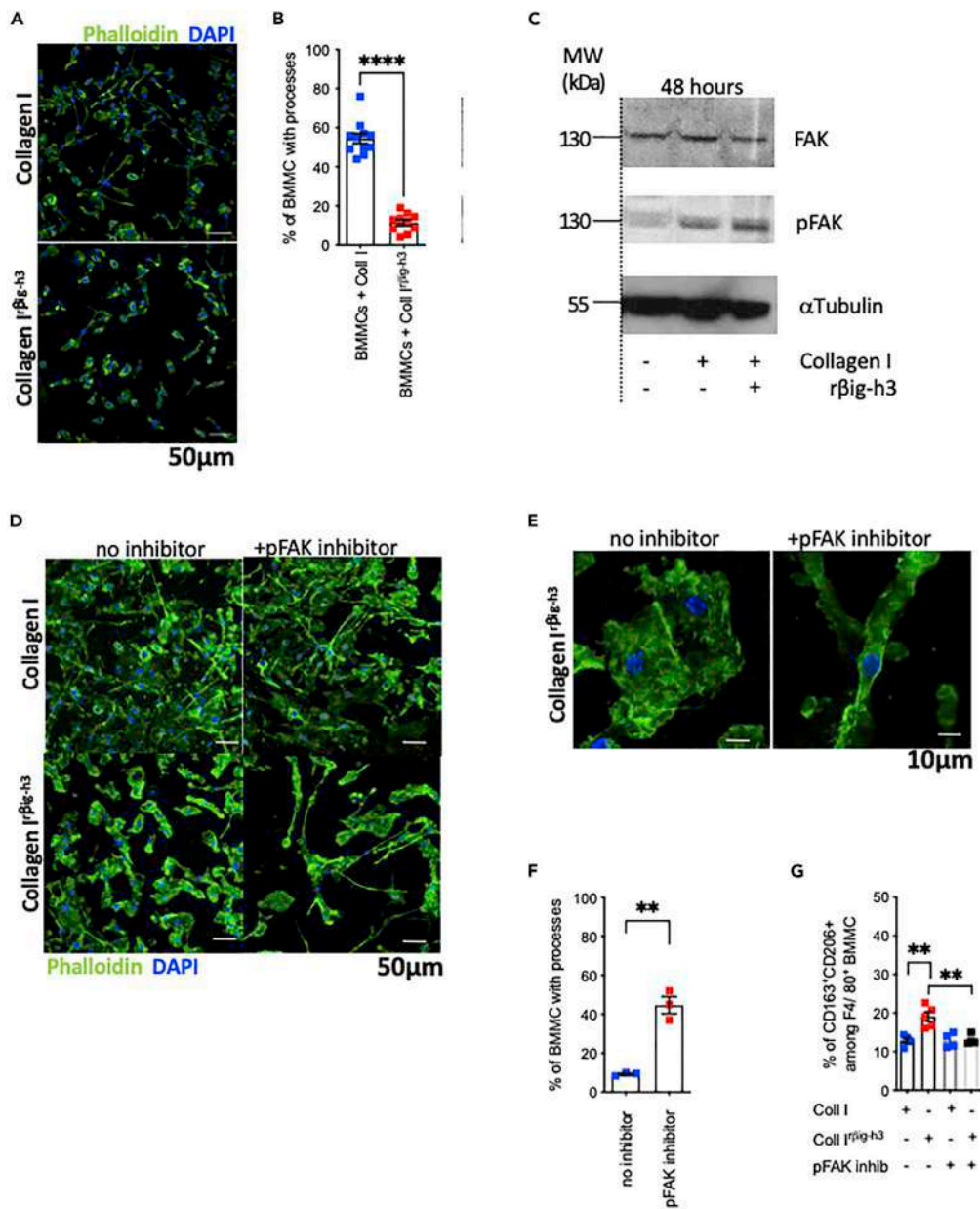


**Figure 3. rβig-h3-structured collagen I fibers activate the FAK signaling pathway in macrophages**

(A) Representative photographs of phalloidin immunofluorescence staining of BMMCs cultured on collagen I structured in the absence (left) or presence (right) of rβig-h3.

(B) Quantification of the processes of BMMCs cultured on collagen I structured in the absence or presence of rβig-h3.

(C) Western blot analysis of FAK, pFAK, and tubulin of BMMCs cultured on plastic, collagen I, or βig-h3-structured collagen I.

(D) Representative micrographs of phalloidin immunofluorescence staining of BMMCs cultured on collagen I structured in the absence (up) or presence (down) of rβig-h3 and with (left) or without (right) Y15.

(E) High-magnification micrographs of BMMCs cultured on rβig-h3-structured collagen in the absence (left) or presence (right) of Y15 inhibitor.

(F) Quantification of the processes detected in E. Each point represents an individual in vitro replicate.

(G) FACS analysis of % of CD163<sup>+</sup>CD206<sup>+</sup> cells among F4/80<sup>+</sup> BMMCs cultured on collagen I structured in the absence (BMMCs + Col I) or presence of rβig-h3 (BMMCs + Col I<sup>rβig-h3</sup>) in absence or presence of pFAK inhibitor. Representative data of two independent experiments with five replicates per condition are shown. \*\*p < 0.01, \*\*\*\*p < 0.0001. Error bars 50 μm, 25 μm.

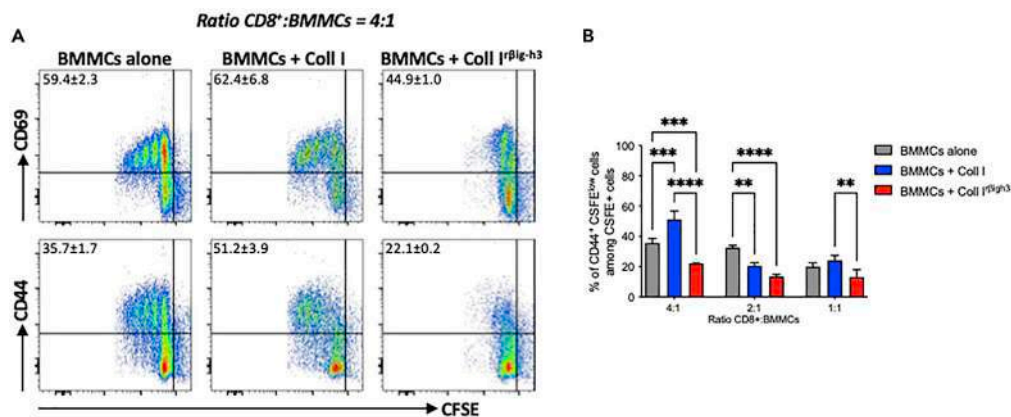


**Figure 4. rβig-h3-structured collagen I fibers instruct macrophages with immunosuppressive properties**

(A) Representative dot plots of CFSE and CD69 or CFSE and CD44 staining of CD8<sup>+</sup>T cells that have been cultured with BMMCs (ratio CD8:BMMC 4:1) grown on plastic (BMMC alone), collagen I (BMMC+ coll I), or on βig-h3-structured collagen I (BMMC+ Coll I rβig-h3).

(B) Quantification of the proliferating CD44<sup>+</sup> CD8<sup>+</sup> T in different ratios (4:1, 2:1, and 1:1). Representative of two independent experiments with three in vitro replicates per group. \*\*p<0.01, \*\*\*p< 0.001, and \*\*\*\*p< 0.0001.

I, CD8<sup>+</sup> T cell proliferation was arrested after two divisions when co-cultured with BMMCs generated on rβig-h3-structured collagen I (Figure 4A). CD44 and CD69 expression of CD8<sup>+</sup> T cells was also significantly reduced when they were co-cultured with BMMCs generated on rβig-h3-structured collagen I confirming their immunosuppressive capacity (Figures 4A and 4B). In addition, this immunosuppressive effect of educated BMMC was dependent on the contact with CD8<sup>+</sup> T cells, because the use of condition media generated from different condition (plastic, on collagen I or rβig-h3-structured collagen I) displayed limited impact in CD8<sup>+</sup> T cell activation (Figure S1).

### βig-h3-structured collagen I educated macrophages are immunosuppressive *in vivo*

In order to determine whether the structuration of collagen I in the absence or presence of rβig-h3 affects recruitment and phenotype of macrophages *in vivo*, we subcutaneously injected the GFP-tagged primary KIC (GFP<sup>+</sup> KIC) tumor cell line, which was generated from the pancreas of GEMM mice as previously described (Goehrig et al., 2019), embedded in non-structured or rβig-h3-structured collagen I into the flanks of Rag2KO mice. Five days after the injection, we evaluated the phenotype of recruited macrophages (Figure 5A). As shown in Figure S2, the non-structured collagen I and rβig-h3-structured collagen I were still detected in the subcutaneous plugs at day 5. We show that although less F4/80<sup>+</sup> macrophages were recruited when tumor cells were embedded in rβig-h3-structured collagen I (Figure 5B), the macrophages displayed increased CD206 expression as well as increased production of TGF-β and TNF-α cytokines suggesting an M2 phenotype (Figure 5B).

In order to investigate if the phenotype acquired by the macrophages was stable, we performed subcutaneously injection of C57BL/6 (WT) mice with GFP<sup>+</sup> KIC tumor cells and BMMCs generated on plastic, collagen I, or rβig-h3-structured collagen I. Five days later, we evaluated the number of tumor cells within the graft and the BMMC phenotype (Figure 6A). While the co-injection of BMMCs generated on plastic and non-structured collagen I resulted in equivalent number of tumor cells, this number was significantly increased, when GFP<sup>+</sup> KIC cells were co-injected with BMMCs generated on rβig-h3-structured collagen I (Figure 6B). Moreover, FACS analysis revealed that after the co-injection of BMMCs generated on rβig-h3-structured collagen I, the number of F4/80<sup>+</sup> BMMC was higher suggesting a better survival *in vivo*. In addition, these BMMCs were conserving CD206 expression and acquired CD163. These results indicate that education of BMMC on βig-h3-structured collagen I results in a stable phenotype that is preserved after *in vivo* injection.

### βig-h3 depletion reprograms M2 macrophages phenotype *in vivo*

In order to determine if the modulation of βig-h3 *in vivo* affects the macrophage phenotype, WT mice were subcutaneously injected with GFP<sup>+</sup> KIC tumor cells. Starting from day 10, the mice were treated

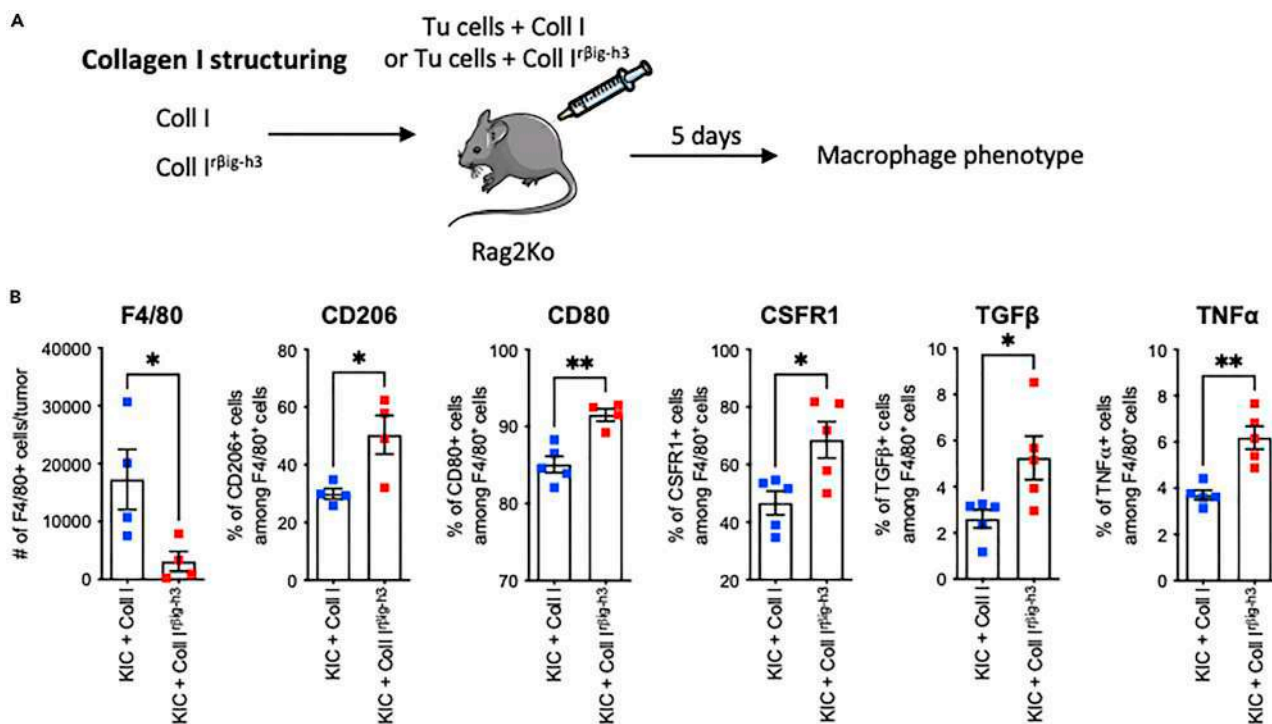


**Figure 5. rβig-h3-structured collagen I fibers are able to instruct immunosuppressive macrophage phenotype in vivo**

(A) Experimental setting.

(B) FACS analysis of the percentages of F4/80<sup>+</sup>CD45<sup>+</sup>, CD206<sup>+</sup>F4/80<sup>+</sup>, CD80<sup>+</sup>F4/80<sup>+</sup>, CSFR1<sup>+</sup>F4/80<sup>+</sup>, TGFβ<sup>+</sup>F4/80<sup>+</sup>, and TNFα<sup>+</sup>F4/80<sup>+</sup> cells collected in A. \*p<0.05, \*\*p<0.01. Representative of two independent experiments with five mice per group.

with anti-βig-h3 monoclonal Ab (clone 18B3) twice a week for two weeks. At day 24, the mice were sacrificed, the tumor weight was evaluated, and flow cytometry analysis was performed in order to establish the impact on macrophages phenotype (Figure 7A). We evaluated the efficiency of the anti-βig-h3 mAb treatment by IHC staining of the tumor graft and shown decreased βig-h3 staining in the treated condition compared to control IgG1 Ab (FigureS3A). We show that mice treated with anti-βig-h3 exhibit diminished tumor weight compared to control IgG1 Ab-treated mice (Figure 7B). Furthermore, FACS analysis showed similar recruitment of CD45<sup>+</sup> total hematopoietic cells as well as F4/80 macrophages in the two conditions (Figures 7C and 7D). More importantly, the recruited macrophages express less CD206 and Arg1 (Figures 7E and 7F), suggesting a diminished M2 phenotype in the absence of βig-h3. Furthermore, we detected more CD8<sup>+</sup> cells that present a non-exhausted phenotype associated with reduced PD-1 expression (Figures S3B and S3C).

## DISCUSSION

We report here for the first time that the matrix protein βig-h3 is able to structure collagen I into thicker fibers. These fibers are able to induce changes in morphology of macrophages that are accompanied by FAK phosphorylation. More importantly, we showed that these fibers skew the polarization of the macrophages toward an M2 phenotype associated with CD206 expression and MHC cl II and CSFR1 downregulation. Furthermore, these M2 macrophages acquired an immunosuppressive phenotype because they were able to reduce CD8<sup>+</sup> T cells proliferation and activation upon co-culture *in vitro*. This phenotype is stable *in vivo* because the injection of those macrophages led to increased number of tumor cells and to the maintenance of CD206 expression and acquisition of CD163 marker.

Tumor-associated macrophages are one of the most abundant immune cell populations in the TME representing up to 50% of all CD45<sup>+</sup> cells (Diskin et al., 2020). Macrophages represent a plastic cell population that can be polarized into several phenotypes depending on the cytokine environment. On one hand, there are M1 macrophages that are associated with Th1 responses, high phagocytic activity, and inflammatory cytokine secretion. On the other hand, there are M2 macrophages associated with Th2 responses,

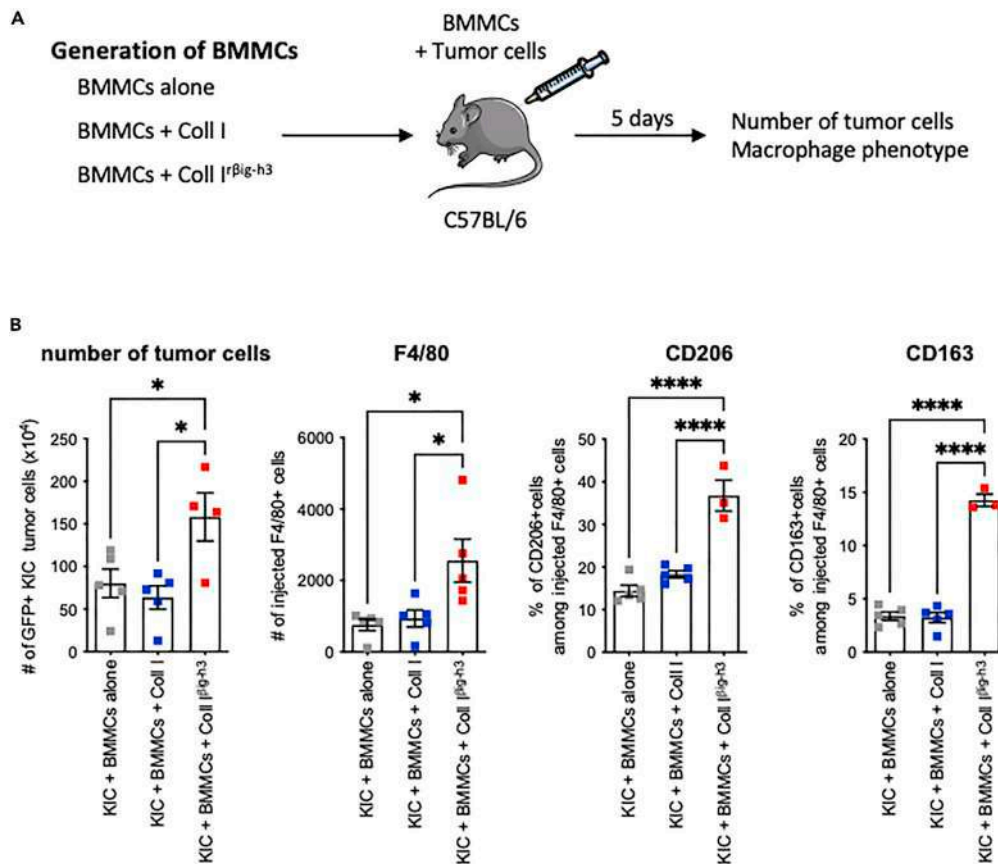


**Figure 6. rβig-h3-structured collagen I educated macrophages maintain their phenotype after *in vivo* injection** (A and B) Experimental setting (B) FACS analysis of the number of tumor cells (GFP tagged), and the percentages of F4/80<sup>+</sup>CD45<sup>+</sup>, CD206<sup>+</sup>F4/80<sup>+</sup>, and CD163<sup>+</sup>F4/80<sup>+</sup>. \*p<0.05, \*\*\*\*p< 0.0001. Representative of two independent experiments with five mice per group.

extracellular matrix remodeling, and immunosuppressive cytokine secretion (Mantovani et al., 2004). In PDAC, tumor-associated macrophages are associated with a lower overall survival and fibrosis in both pre-clinical mouse models and patients (Hu et al., 2016; Zhu et al., 2017). In addition, they have been shown to promote tumor growth by different mechanisms such as epithelial to mesenchymal transition of tumor cells (Liu et al., 2013), secretion of immunosuppressive cues (TGFβ, CCL22, CCL2, and CCL18), and, more generally, the re-shaping of the TME due to M2 functions. In the present study, we initially demonstrated that βig-h3-structured collagen plays an important role in educating macrophages toward an M2 phenotype. We show that this phenotype is associated with a morphological change from an originally spindle shape toward a more spherical appearance with reduced processes. Of note, other studies characterized M2 macrophages as elongated rather than spherical (Ruiz-Valdepenas et al., 2011), which seems to contrast with our data. We hypothesize that the acquisition of an M2 phenotype was previously achieved by adding soluble factors (*i. e.* Interleukin-4 and -13) to the differentiation medium, which differs from our own experimental approach based on substrate “education” through different collagen matrices structured in the absence or presence of rβig-h3. In our setting, rβig-h3-structured collagen I increased FAK phosphorylation and thereby augmented the adhesion points to the substrate facilitating a spherical shape with higher surface contact. Furthermore, the acquired phenotype was conserved after *in vivo* injection indicating that *in vitro* education induced a highly stable macrophage signature.

Aside from macrophages, the critical role of CD8<sup>+</sup> T cells in tumor clearance is undisputed. CD8<sup>+</sup> T cell tumor infiltration is thought to reflect a good prognosis (Galon et al., 2006). Our findings suggest that βig-h3-structured collagen I educated macrophages play an important immunosuppressive role because they inhibited the CD8<sup>+</sup> T cell proliferation *in vitro*. We show that these macrophages induced a CD8<sup>+</sup>

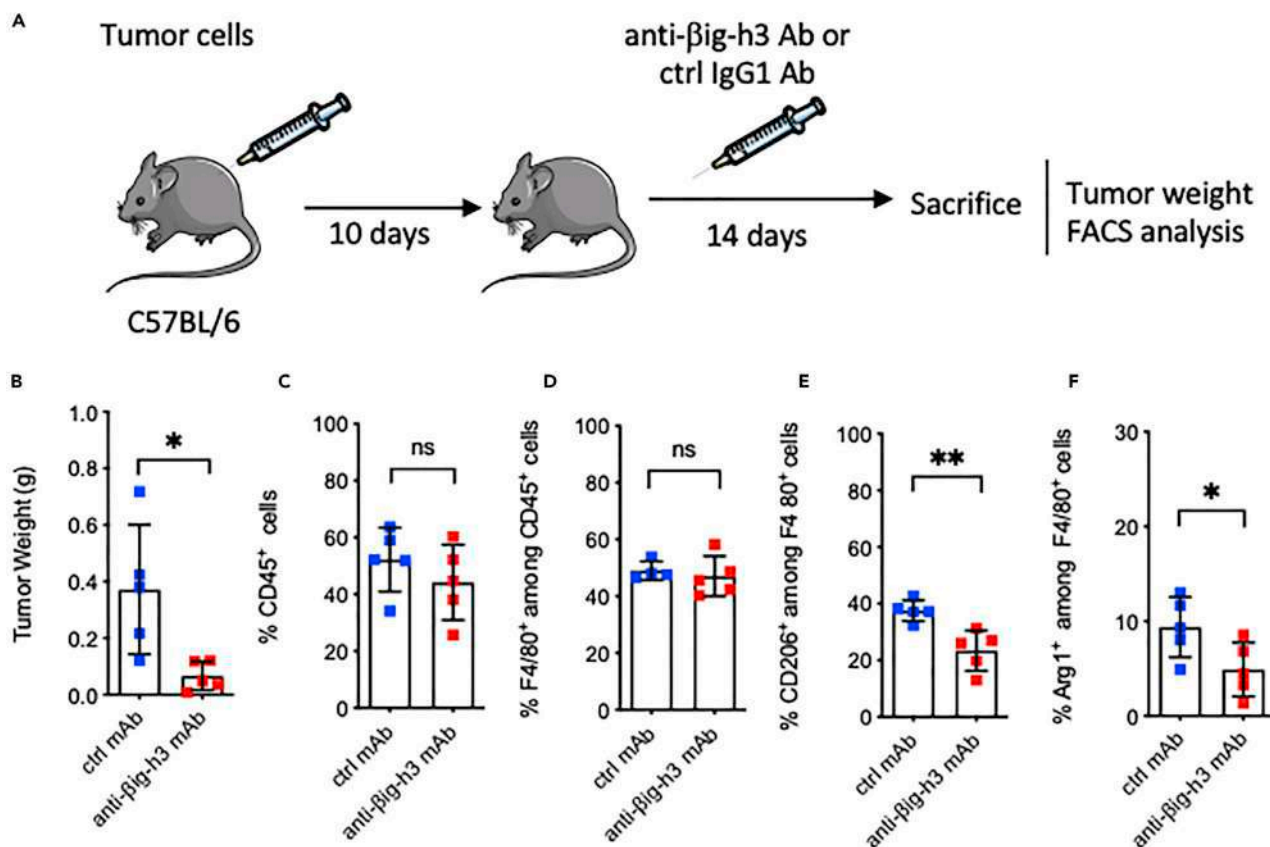


**Figure 7. βig-h3 Ab depletion in vivo reprograms macrophage phenotype in the tumor microenvironment**

(A) Experimental setting.

(B) Tumor weight of mice treated in A.

(C-F) FACS analysis of the percentages of CD45<sup>+</sup> (C), F4/80<sup>+</sup>CD45<sup>+</sup> (D), CD206<sup>+</sup>F4/80<sup>+</sup> (E), and Arg1<sup>+</sup>F4/80<sup>+</sup> (F) cells collected in A. \*p<0.05, \*\*p<0.01. Representative of two independent experiments with five mice per group.

T cell proliferation arrest accompanied with reduced expression of well-known activation markers such as CD69 and CD44. Previous findings demonstrated that bone marrow grown in a high-density collagen matrix compared with a low-density collagen matrix had higher immunosuppressive capacities inhibiting the proliferation of CD8<sup>+</sup> T cell *in vitro* (Kuczek et al., 2019; Larsen et al., 2020). Our findings highlight a new dimension of collagen organization in addition to matrix density structured in the presence of other extracellular matrix molecules, namely βig-h3 resulting in an immunosuppressive macrophage phenotype.

Furthermore, we revealed that this “M2 education” of macrophages can occur *in vivo* upon injection of tumor cells embedded in βig-h3-structured collagen because recruited macrophages also displayed an immunosuppressive phenotype.

This phenotype imprinted *in vitro* the macrophage phenotype imprinted *in vitro* by the βig-h3-structured collagen was highly stable, as “M2 characteristics” were maintained even after injection *in vivo* in combination with tumoral cells. Our results provide the first demonstration that the architecture of stromal collagen has a significant impact on the outcome of anti-tumoral immune responses because it alters the phenotype of macrophages toward a sustained M2 phenotype with immunosuppressive properties. These physical and functional modifications of the collagen in the context of pancreatic cancer might lead to the “reprogramming” of the TME by instructing F4/80<sup>+</sup> macrophages to become immunosuppressive. Importantly, our findings also show that *in vivo* depletion of the βig-h3 protein by a mAb approach diminishes the M2 phenotype macrophages. Further investigations should address how to disrupt βig-h3 binding to collagen, as this may lead to macrophages reprogramming in the pancreatic cancer TME with a potential therapeutic effect.

## STAR★METHODS

Detailed methods are provided in the online version of this paper and include the following:

- **KEY RESOURCES TABLE**
- **RESOURCE AVAILABILITY**
  - Lead contact
  - Materials availability
  - Data availability
- **METHOD DETAILS**
  - Mice
  - Generation of collagen matrices
  - BMMC generation and education
  - KIC tumor cell line
  - Atomic force microscopy measurements and collagen fibrils analysis
  - Immunofluorescence staining
  - Confocal microscopy
  - Western blot
  - FACS analysis
  - T cell activation assay
  - Short term tumor implantation assay
- **QUANTIFICATION AND STATISTICAL ANALYSIS**

## SUPPLEMENTAL INFORMATION

Supplemental information can be found online at <https://doi.org/10.1016/j.isci.2022.103758>.

## ACKNOWLEDGMENTS

The authors thank the staff of ANICAN (Cancer Research Center of Lyon) staff for the maintenance of the mouse strains and Christophe Vanbelle for the helpful assistance with the confocal microscopy experiments. We also thank Brigitte Manship for proofreading the manuscript. This study was supported by grants from La Ligue Contre le Cancer (A.H.), Bristol Meyers Squibb Foundation (A.H.), Inserm Transfert (A.H.), Sanofi iAward (A.H.), INCaAAP 2019 (A.H.), and Fondation de France (A.H. and P.G.), WZC was supported by a Chinese Scholarship Council (CSC) Fellowship.

## AUTHOR CONTRIBUTIONS

S.B performed the experiments and analyzed the data. Z.W., P.G., and K.T. performed the experiments. P.M. and J.C. performed the AFM experiments and analysis. A.H. designed the experiments, analyzed the data, and wrote the manuscript. A.H. is the guarantor of this work and thus had full access to all the data obtained in the study and takes responsibility for the integrity of the data and the accuracy of the data analysis.

## DECLARATION OF INTERESTS

The authors have no conflicts of interest to disclose.

Received: July 20, 2021

Revised: October 27, 2021

Accepted: January 7, 2022

Published: February 18, 2022

## REFERENCES

- Bae, J.S., Lee, S.H., Kim, J.E., Choi, J.Y., Park, R.W., Yong Park, J., Park, H.S., Sohn, Y.S., Lee, D.S., Bae Lee, E., and Kim, I.S. (2002). Betaig-h3 supports keratinocyte adhesion, migration, and proliferation through alpha3beta1 integrin. *Biochem.biophysicalRes.Communic.* 294, 940–948.
- Bayne, L.J., Beatty, G.L., Jhala, N., Clark, C.E., Rhim, A.D., Stanger, B.Z., and Vonderheide, R.H. (2012). Tumor-derived granulocyte-macrophage colony-stimulating factor regulates myeloid inflammation and T cell immunity in pancreatic cancer. *Cancer cell* 21, 822–835.
- Diskin, B., Adam, S., Cassini, M.F., Sanchez, G., Liria, M., Aykut, B., Buttar, C., Li, E., Sundberg, B., Salas, R.D., et al. (2020). PD-L1 engagement on T cells promotes self-tolerance and suppression of neighboring macrophages and effector T cells in cancer. *Nat. Immunol.* 21, 442–454.
- Galon, J., Costes, A., Sanchez-Cabo, F., Kirilovsky, A., Mlecnik, B., Lagorce-Pages, C., Tosolini, M., Camus, M., Berger, A., Wind, P., et al. (2006). Type, density, and location of immune cells within human colorectal tumors predict clinical outcome. *Science* 313, 1960–1964.

Goehrig, D., Nigri, J., Samain, R., Wu, Z., Cappello, P., Gabiane, G., Zhang, X., Zhao, Y., Kim, I.S., Chanal, M., et al. (2019). Stromal protein betaig-h3 reprogrammes tumour microenvironment in pancreatic cancer. *Gut* 68, 693–707.

Hashimoto, K., Noshiro, M., Ohno, S., Kawamoto, T., Satakeda, H., Akagawa, Y., Nakashima, K., Okimura, A., Ishida, H., Okamoto, T., et al. (1997). Characterization of a cartilage-derived 66-kDa protein (RGD-CAP/beta ig-h3) that binds to collagen. *Biochim.Biophys. Acta* 1355, 303–314.

Hingorani, S.R., Petricoin, E.F., Maitra, A., Rajapakse, V., King, C., Jacobetz, M.A., Ross, S., Conrads, T.P., Veenstra, T.D., Hitt, B.A., et al. (2003). Preinvasive and invasive ductal pancreatic cancer and its early detection in the mouse. *Cancer cell* 4, 437–450.

Hu, H., Hang, J.J., Han, T., Zhuo, M., Jiao, F., and Wang, L.W. (2016). The M2 phenotype of tumor-associated macrophages in the stroma confers a poor prognosis in pancreatic cancer. *Tumour Biol.* 37, 8657–8664.

Kuczek, D.E., Larsen, A.M.H., Thorseth, M.L., Carretta, M., Kalvisa, A., Siersbaek, M.S., Simoes, A.M.C., Roslind, A., Engelholm, L.H., Noessner, E., et al. (2019). Collagen density regulates the activity of tumor-infiltrating T cells. *J. Immunother.Cancer* 7, 68.

Laklai, H., Miroshnikova, Y.A., Pickup, M.W., Collisson, E.A., Kim, G.E., Barrett, A.S., Hill, R.C.,

Lakins, J.N., Schlaepfer, D.D., Mouw, J.K., et al. (2016). Genotype tunes pancreatic ductal adenocarcinoma tissue tension to induce matricellular fibrosis and tumor progression. *Nat.Med.* 22, 497–505.

Larsen, A.M.H., Kuczek, D.E., Kalvisa, A., Siersbaek, M.S., Thorseth, M.L., Johansen, A.Z., Carretta, M., Grontved, L., Vang, O., and Madsen, D.H. (2020). Collagen density modulates the immunosuppressive functions of macrophages. *J. Immunol.* 205, 1461–1472.

Liu, C.Y., Xu, J.Y., Shi, X.Y., Huang, W., Ruan, T.Y., Xie, P., and Ding, J.L. (2013). M2-polarized tumor-associated macrophages promoted epithelial-mesenchymal transition in pancreatic cancer cells, partially through TLR4/IL-10 signaling pathway. *Lab.Invest.* 93, 844–854.

Mantovani, A., Sica, A., Sozzani, S., Allavena, P., Vecchi, A., and Locati, M. (2004). The chemokine system in diverse forms of macrophage activation and polarization. *Trends Immunol.* 25, 677–686.

Milani, P., Mirabet, V., Cellier, C., Rozier, F., Hamant, O., Das, P., and Boudaoud, A. (2014). Matching patterns of gene expression to mechanical stiffness at cell resolution through quantitative tandem epifluorescence and nanoindentation. *Plant Physiol.* 165, 1399–1408.

Patry, M., Teinturier, R., Goehrig, D., Zetu, C., Ripoche, D., Kim, I.S., Bertolino, P., and Hennino, A. (2015). betaig-h3 represses T-cell activation in type 1 diabetes. *Diabetes* 64, 4212–4219.

Ruiz-Valdepenas, L., Martinez-Orgado, J.A., Benito, C., Millan, A., Tolon, R.M., and Romero, J. (2011). Cannabidiol reduces lipopolysaccharide-induced vascular changes and inflammation in the mouse brain: an intravital microscopy study. *J. Neuroinflammation* 8, 5.

Schneider, C.A., Rasband, W.S., and Eliceiri, K.W. (2012). NIH Image to ImageJ: 25 years of image analysis. *Nat. Methods* 9, 671–675.

Skonier, J., Bennett, K., Rothwell, V., Kosowski, S., Plowman, G., Wallace, P., Edelhoff, S., Disteche, C., Neubauer, M., Marquardt, H., et al. (1994). Beta ig-h3: a transforming growth factor-beta-responsive gene encoding a secreted protein that inhibits cell attachment in vitro and suppresses the growth of CHO cells in nude mice. *DNA Cell Biol* 13, 571–584.

Skonier, J., Neubauer, M., Madisen, L., Bennett, K., Plowman, G.D., and Purchio, A.F. (1992). cDNA cloning and sequence analysis of beta ig-h3, a novel gene induced in a human adenocarcinoma cell line after treatment with transforming growth factor-beta. *DNA Cell Biol.* 11, 511–522.

Zhu, Y., Herndon, J.M., Sojka, D.K., Kim, K.W., Knolhoff, B.L., Zuo, C., Cullinan, D.R., Luo, J., Bearden, A.R., Lavine, K.J., et al. (2017). Tissue-resident macrophages in pancreatic ductal adenocarcinoma originate from embryonic hematopoiesis and promote tumor progression. *Immunity* 47, 597.

**STAR★METHODS**

**KEY RESOURCES TABLE**

REAGENT or RESOURCE	SOURCE	IDENTIFIER
<b>Antibodies</b>		
Rabbit polyclonal anti-βig-h3	Sigma-Aldrich	Cat# HPA008612, RRID:AB_1857970
Mouse monoclonal anti-collagen I (clone 3G3)	Abcam	Cat# ab88147, RRID:AB_2081873
Rat monoclonal to F4/80 (clone Cl:A3-1)	Abcam	Cat#ab6640 RRID:AB_1140040
Mouse monoclonal anti-CD206 (Mannose receptor) (clone 15-2)	Abcam	Cat# ab8918, RRID:AB_306860
Donkey polyclonal Anti-Rabbit IgG (H + L), Alexa Fluor 647-conjugated	Invitrogen/Thermo Fisher Scientific	Cat# A-31573, RRID:AB_2536183
Donkey polyclonal anti-Mouse IgG (H + L), Alexa Fluor 555-conjugated	Invitrogen/Thermo Fisher Scientific	Cat# A-31570, RRID:AB_2536180
Donkey polyclonal anti-Rat IgG (H + L), Cy3-conjugated	Jackson ImmunoResearch	Cat#712-166-150 RRID:AB_2340668
Phalloidin, Alexa Fluor 488-conjugated	Cell Signaling Technology	Cat#8878S RRID:AB_2315147
Rabbit monoclonal anti-Phospho-FAK (Tyr397) (clone 31H5L17)	Invitrogen/Thermo Fisher Scientific	Cat# 700,255, RRID:AB_2532307
Rabbit polyclonal anti-FAK	Cell signaling Technology	Cat#3285 RRID: AB 2269034
Anti-tubulin	GeneTex	Cat#GTX628802
anti-pERK	Cell Signaling	Cat#4695
Donkey polyclonal Anti-Rabbit IgG (H + L), HRP-conjugated	Jackson ImmunoResearch Labs	Cat# 711-035-152, RRID:AB_10015282
Rat monoclonal anti-F4/80 (clone BM8), PE-Cy7-conjugated	Biolegend	Cat# 123114, RRID:AB_893478
Rat monoclonal anti-F4/80 (clone BM8), PerCP-Cy5.5-conjugated	Biolegend	Cat# 123128, RRID:AB_893484
Rat monoclonal anti-MHC Clas II (I-A/I-E) (clone M5/114.15.2), PE-Cy7-conjugated	eBioscience/Thermo Fisher Scientific	Cat# 12-5321-81, RRID:AB_465927
Rat monoclonal anti-CD206 (clone C068C2), Brilliant Violet 650-conjugated	Biolegend	Cat# 141723, RRID:AB_2562445
Rat monoclonal anti-CD86 (clone GL-1), APC-Cy7-conjugated	Biolegend	Cat# 105030, RRID:AB_2244452
Armenian hamster monoclonal anti-CD80 (clone 16-10A1), Brilliant Violet 605-conjugated	Biolegend	Cat# 104729, RRID:AB_11126141
Rat monoclonal anti-CD115 (CSF-1R) (clone AFS98), APC-Cy7-conjugated	Biolegend	Cat# 135511, RRID:AB_11218605
Rat monoclonal anti-iNOS (clone CXNFT), PE-conjugated	Life Technologies/Thermo Fisher Scientific	Cat# 12-5920-82, RRID:AB_2572642
Sheep polyclonal anti-Arginase 1/ARG1, APC-conjugated	R&D Systems	Cat# IC5868A, RRID:AB_2810265
Mouse monoclonal anti-LAP (TGF-beta-a) (clone TW7-16B4), Brilliant Violet 421-conjugated	Biolegend	Cat# 141408, RRID:AB_2650898
Human/mouse monoclonal anti-Granzyme B (clone GB11), Alexa Fluor 647 conjugated	Biolegend	Cat#515406 RRID:AB 2566333

(Continued on next page)

**Continued**

REAGENT or RESOURCE	SOURCE	IDENTIFIER
Rat monoclonal anti-IFN gamma (clone XMG1.2), Brilliant Violet 650-conjugated	Biologend	Cat#505831 RRID:AB_11142685
Rat monoclonal anti-TNF-alpha (clone MP6-XT22), Brilliant Violet 605-conjugated	Biologend	Cat# 506329, RRID:AB_11123912
Hamster anti-mouse CD69 (clone H1.2F3), PerCP-Cy5.5-conjugated	BD Biosciences	Cat#551113 RRID:AB_394051
Rat anti-human/mouse CD44 (clone IM7), Alexa Fluor 700 conjugated	Biologend	Cat#103025 RRID:AB_493712
Rat anti-mouse CD163 (clone TNKUPJ), PE conjugated	eBioscience/Thermo Fisher Scientific	Cat#12-1631-82 RRID:AB_2716924
anti-βig-h3 18B3	(Goehrig et al., 2019)	(Goehrig et al., 2019)
IgG1 control Ab	BioXcell, USA	BE0083

**Chemicals, peptides, and recombinant proteins**

Collagen I	Gibco/Thermo Fisher Scientific	Cat#A10483-01
Phosphate-buffered saline (PBS) 10x	Gibco/Thermo Fisher Scientific	Cat#14190-144
Phosphate-buffered saline (PBS) 1x	Gibco/Thermo Fisher Scientific	Cat#14190-144
Human recombinant βig-h3 protein	Bio-Techne/RD	Cat#3409-BG
Dulbecco's Modified Eagle Medium (DMEM)	Gibco/Thermo Fisher Scientific	Cat#61965059
Fetal calf serum (FCS)	Eurobio	Cat#CVFSVF00-01
Penicillin-Streptomycin (P/S)	Gibco/Thermo Fisher Scientific	Cat#15140-122
Collagenase P	Roche/Sigma-Aldrich	Cat#11213865001
Triton X-100	Sigma-Aldrich	Cat#T8787
16% Formaldehyde solution (PFA)	Termo Fisher	Cat#28908
Antigen Unmasking Solution, Citrate-Based	Vector/Eurobio	Cat#H-3300
Antibody diluent Reagent	Life Techno/Thermo Fisher	Cat#003218
Vectashield mounting medium with DAPI	Vector/Eurobio	Cat#H-1200
NuPAGE 4-12% Bis-Tris polyacrylamide gel	Invitrogen/Thermo fischer	Cat#NP0335BOX
Immun-Blot PVDF membrane	Biorad	Cat#1620177
Tris buffered saline (TBS)	Euromedex	Cat#ET220
Tween 20	VWR	Cat#28829.296
Bovine serum albumin (BSA)	Sigma	Cat#A2153-100G
RIPA buffer	Pierce/Thermo Fisher	Cat#89900
Protease complete EDTA-free	Roche/Sigma-Aldrich	Cat#04 693 159 001
Phosphatase phoSTOP	Roche/Sigma-Aldrich	Cat#04 906 837 001
Brefeldin A solution	Biologend	Cat#420601
Dynabeads™ Mouse T-Activator CD3/CD28 for T-Cell Expansion and Activation	Gibco/Thermo Fisher Scientific	Cat#11452D
Corning® Matrigel® Basement Membrane Matrix High Concentration	Corning	Cat#354248
CD8a (Ly-2) microbeads mouse	Miltenyi Biotec	Cat#130-117-044
FAK Inhibitor 14	Sigma-Aldrich	Cat#SML0837

**Critical commercial assays**

ECL chemiluminescence kit	Pierce Chemical/Thermo Fisher Scientific	Cat#32106
Fixation/permeabilisation kit	BD	Cat#554714
CellTrace™ Violet Cell Proliferation Kit	Invitrogen/Thermo Fisher Scientific	Cat#C34557
CellTrace™ CFSE Cell Proliferation Kit	Invitrogen/Thermo Fisher Scientific	Cat#C34554

(Continued on next page)

**Continued**

REAGENT or RESOURCE	SOURCE	IDENTIFIER
<i>Experimental models: Cell lines</i>		
L929 cells	ATCC CCL-1	ATCC CCL-1
Tumoral cells Epi	(Goehrig et al., 2019)	(Goehrig et al., 2019)
<i>Experimental models: Organisms/strains</i>		
C57BL/6 (WT) mice	Envigo	C57BL/6J0laHsd
P48 <sup>+/Cre</sup> ;Kras <sup>G12D</sup> (KC) mice	(Hingorani et al., 2003)	Hingorani et al. (2003)
<i>Software and algorithms</i>		
ImageJ	Schneider et al., 2012(Schneider et al., 2012)	<a href="https://imagej.net">https://imagej.net</a>
BD FACSDiva™ Software	BD Biosciences	<a href="https://www.bdbiosciences.com">https://www.bdbiosciences.com</a>
FlowJo	Becton, Dickinson and Company, 2019	<a href="https://www.flowjo.com">https://www.flowjo.com</a>
Python 3.0 processing	BIOMECA	<a href="https://www.bio-meca.com">https://www.bio-meca.com</a>
Nanoscope software 9.1.R.3	BIOMECA	<a href="https://www.bio-meca.com">https://www.bio-meca.com</a>

**RESOURCE AVAILABILITY**

**Lead contact**

Further information and requests for resources and reagents should be directed to and will be fulfilled by the lead contact Ana Hennino ([ana.hennino@inserm.fr](mailto:ana.hennino@inserm.fr)).

**Materials availability**

This study did not generate new unique reagents.

**Data availability**

- All data reported in this paper will be shared by the lead contact upon request.
- This paper does not report original code.
- Any additional information required to reanalyze the data reported in this paper is available from the lead contact upon request.

**METHOD DETAILS**

**Mice**

C57BL/6 mice (WT) were obtained from Envigo (Indianapolis/Indiana/USA). KC mice, KIC mice and Rag2-KO mice were bred in house (males and females). All mice were kept under specific pathogen-free conditions at the Animale en Cancérologie (AniCan) platform at the Cancer Research Center of Lyon (CRCL). All animal procedures and experiments were performed in compliance with the ethical guidelines of the CRCL Animal Care and Use Committee, with approval of the Experimental Animal Ethics Committee of the Rhône-Alpes region (CECCAPP) (CECCAPP\_CLB\_2019\_002).

**Generation of collagen matrices**

Collagen I matrix was prepared by carefully mixing 800 µL of collagen I (Gibco; Amarillo/TX/USA) with 7,000 µL of 1x PBS (Gibco; Amarillo/TX/USA), 100 µL of 10x PBS and 100 µL of NaOH 0.1M. 8 mL of collagen I matrix at 300 µg/mL was added on a 10 cm<sup>2</sup> Petri dish and allowed to solidify at 37°C for at least 1 h. For βig-h3 structured collagen, rβig-h3 (Bio-Techne; Minneapolis/Minnesota/USA) was added to the collagen I matrix mix at a final concentration of 2.5 µg/mL prior to the solidification.

**BMMC generation and education**

In order to generate bone marrow-derived monocytes, bone marrow cell suspensions were isolated by flushing femurs and tibias of 8-12 week-old C57BL/6 mice with Dulbecco's Modified Eagle Medium (DMEM) (Gibco; Amarillo/TX/USA) containing 10% of foetal calf serum (FCS) (Eurobio; Evry-France) and 1% penicilin/streptomycin (P/S) (10,000 U/mL penicillin and 10 mg/mL of streptomycine; Gibco; Amarillo/TX/USA) (DMEM-c). Cell aggregates were dislodged by passing the suspension through a 100µm

cell strainer. Lysis of red blood cells was performed with in house-made ammonium-chloride-potassium (AKC) lysis buffer. 10 millions cells obtained were resuspended in 10 mL of DMEM-c supplemented with 20% of supernatant from L292 cells containing M-CSF plated on a 10 cm<sup>2</sup> tissue culture dish, and incubated for 6 days at 37°C, CO<sub>2</sub> 5%. Every other day, 10 mL of medium was removed and fresh DMEM-c supplemented with 20% M-CSF was added to the cells. Cells were harvested at day 7. For BMMC education, 10<sup>7</sup> cells were seeded onto 10 cm<sup>2</sup> tissue culture dish coated with collagen or collagen+βig-h3 matrices previously described for 48 hat 37°C.

### KIC tumor cell line

The isolation and culture of KIC pancreatic tumor cells from KIC mice, which were generated on a C57BL/6 background, was performed by modifying a previously published protocol (Bayne et al., 2012; Goehrig et al., 2019). Briefly, the excised pancreas of a 2.5-month-old KIC mouse was minced into small fragments and then incubated in 1x PBS containing collagenase V (1 mg/mL; Roche; Basel/Switzerland) at 37°C for 20 minutes. The digested tissue was homogenized by passage through a 100 μm cell strainer and the obtained cells were plated into 6-well plates with serum-free DMEM. After 2 weeks, the medium was changed to DMEM-c. After three to six passages, the cells were infected with lentiviral vector expressing H2B GFP (Addgene no 25999).

### Atomic force microscopy measurements and collagen fibrils analysis

AFM measurements were performed in the BIOMECA laboratory (ENS, Lyon) with a Resolve Bioscope (Bruker Nano Surface, Santa Barbara, CA) mounted on an inverted optical DMI8 (Leica). AFM measurements were performed using a conical tip located on a flexible cantilever with a 0.35 N/m spring constant (DNP-10A, Bruker AFM probes). Before each experiment, the deflexional sensitivity of the cantilever was calibrated against a sapphire wafer and spring constant was measured using the thermal tune method. All experiments were conducted on sample sections immersed in PBS (Capricorn-scientific) at room temperature and the standard cantilever holder for operation in liquid was used. Data acquisition was made with the Nanoscope software, 9.1.R.3 version, on AFM QNM mode (Quantitative Nanomechanical Mapping), in fluid condition. Experiments consisted in acquiring topographic images (5 μm × 5 μm, 20nN of force, 8μm ramp size and 1.0 Hz ramp rate). Collagen fibrils thickness was analyzed using a BIOMECA's analysis script on PYTHON 3.0 processing. The AFM images were converted to a binary black and white image and analyzed by a skeletonized approach to extract collagen fibril thickness. Using the stiffness constant of the lever, the deflection indicates the resistance of the sample. Our protocol (Milani et al., 2014) allows us to measure the local stiffness of the matrices in a minimally invasive manner, by deforming the samples down to a depth of 100 nm. In order to investigate the stiffness patterns at high resolution we used the quantitative nanomechanical mapping and the force volume protocols (Bruker). In these protocols, the AFM probe oscillates at low frequency while horizontally scanning the sample and a force curve is generated each time the probe enters in contact with the sample. The elastic modulus of the sample, which reflects the stiffness, is then extracted from each curve applying the Sneddon (Hertz) model, yielding two-dimensional stiffness maps, where each pixel represents one force curve.

### Immunofluorescence staining

Paraffin embedded mouse tissue was sectioned at a thickness of 4 μm thick on a Microtome (Leica; Wet-zlar/Germany). The sections were deparaffinized and rehydrated before antigen unmasking was performed using unmasking solution Vector H 3300 (Eurobio; Evry-France). The sections were saturated with antibody (Ab) diluent (Dako/Agilent; Santa Clara/CA/USA) for 30 min and then incubated overnight at 4 °C with primary Abs that were appropriately diluted in Ab diluent. The next day, the sections were incubated with specific secondary Abs that were diluted in Ab diluent. Finally, the sections were mounted in Vectashield mounting medium containing DAPI (Eurobio; Evry-France) for nuclear counterstaining.

For phalloidin staining 4 × 10<sup>5</sup> BMMC were cultured in P12 plates equipped with circular cover slips coated with collagen or collagen + rβig-h3 for 24 h. The cover slips were recovered and washed in PBS. Attached cells were fixed with PFA 4% for 5 min and permeabilized in PBS 0.2% Triton for 6minat RT. Cells were stained with phalloidin overnight at 4 °C and then mounted in Vectashield mounting medium containing DAPI (Eurobio; Evry-France) for nuclear counterstaining.

### Confocal microscopy

All samples were visualized under an LSM 880 inverted confocal microscope (Zeiss/Provenance). Series of images were collected and processed using ImageJ software. For the analysis of BMMC processes 10 regions of interest (ROI) were analyzed.

### Western blot

Educated BMMCs were collected by scratching in 10 mL of PBS. After centrifugation, the proteins were isolated using RIPA buffer supplemented with protease and phosphatase inhibitors. 20 $\mu$ L of the obtained lysate were separated by NUPAGE 4-12% Bis-Tris Gel electrophoresis (SDS- PAGE) (Gibco; Amarillo/TX/USA) and transferred to a Immune-Blot PVDF membrane (Biorad; Hercules/California/USAs). After transfer, the immune-blot were blocked by incubating with 5% BSA in Tris buffered saline (TBS) (Euromedex; Souffelweyersheim/France) containing 0.05% Tween 20 (VWR; Radnor/Pennsylvanie/USA). The blots were then probed overnight with appropriately diluted primary Abs. After washing in TBS-Tween 0.05%, the membranes were revealed with secondary antibodies for 1 hour at room temperature. After washing, the blots were developed using the ECL chemiluminescence method according to the manufacturer's protocol (Pierce Chemical; Waltham/MA/USA).

The following antibodies were used to detect their corresponding substrates: anti-pFAK from Invitrogen, FAK from Cell Signalling, pERK from Cell Signaling and anti-tubulin obtained from GeneTex. Either HRP-conjugated anti-rabbit or anti-mouse Abs (Jackson Immunoresearch; Ely/United Kingdom) were used for primary antibody binding.

### FACS analysis

Educated BMMCs were collected by scratching into 10 mL of PBS and centrifuged. In case of tumor implantation, the tumor grafts were excised, weighed and measured. The tumor grafts were then digested in PBS (Gibco; Amarillo/TX/USA) supplemented with collagenase (1 mg/mL; Roche; Basel/Switzerland) for 20 min at 37°C. The digested tissue was homogenized by passage through a 100 $\mu$ m cell strainer. Single cell suspensions from BMMCs or tumor grafts were stained with fluorescently labelled antibodies for 20 min at 4°C. For cytokine analysis single cell suspensions were incubated with Brefeldin A (Biolegend; San Diego/CA/USA) for 2h at 37°C prior to surface staining in order to retain intracellular proteins. After surface staining, cells were fixed and permeabilized using the Fixation/Permeabilization kit according to the manufacturer's protocol (BD; New Jersey/USA) and intracellular staining was performed for 30 min at 4°C. Fluorescently labelled cells were acquired on a BD Fortessa Flow Cytometer (BD; Franklin Lakes/NJ/USA) and analyzed using either BD FACS Diva software V.5.0.1 (BD; Franklin Lakes/NJ/USA) or FlowJo (Tree Star/BD; Franklin Lakes/NJ/USA).

The following monoclonal Abs were used in flow cytometry: anti-F4/80 Pe-Cy7 (clone BM8-Biolegend, 123114) or PerCP Cy5.5 (clone BM8-Biolegend, 123128), anti-MHCII PE (clone M5/114.15.2- eBioscience, 12-5321-81), anti-CD206 BV650 (clone C068C2-Biolegend, 141723), anti-CD86 BV605 (clone GL-1- Biolegend, 105029), anti-CD80 APC-Cy7 (clone 16-10A1-Biolegend, 104729), anti-CSFRI AF488 (clone AFS98- Biolegend, 135511), anti-INOS PE (clone CXNFT, Life Techno, 12-5920-82), anti-Arginase1 APC (RD, IC5868A), anti-TGF- $\beta$  B421 (clone TW7-16B4-Biolegend, 141408) and anti-TNF $\alpha$  BV605 (clone MP6-XT22-Biolegend, 506329).

### T cell activation assay

CD8<sup>+</sup>T cells were purified from the spleens and lymph nodes of female C57BL/6 mice by column-based magnetic activated cells sorting (MACS) according to the manufacturer's protocol (Miltenyi Biotec; Bergisch Gladbach/Germany). Purified CD8<sup>+</sup>T cells were then labelled with 5 $\mu$ M CFSE at 37 °C for 20min in PBS according to the manufacturer's protocol (Invitrogen; Amarillo/TX/USA). Following, CFSE-labelled CD8<sup>+</sup>T cells were then cultured for two days in the presence of BMMCs respecting the T cell:BMMC ratios of 4:1, 2:1 and 1:1. Dynabeads<sup>TM</sup> Mouse T-Activator CD3/CD28 for T-cell expansion and Activation (Gibco; Amarillo/TX/USA) were added to the co-culture respecting at a T cell:bead ratio of 1:1. Proliferation of CD8<sup>+</sup>T cells was evaluated at the end of the culture period by analysing CFSE dilution using flow cytometry.

### Short term tumor implantation assay

BMMCs were generated *in vitro* and educated for 48 h at 37 °C on collagen matrices structured in the presence or absence of rh $\beta$ ig-h3 as described above. BMMCs were then harvested using trypsin action, and

labelled with 5 $\mu$ M Cell Trace Violet at 37 °C for 20min according to the manufacturer's protocol (Invitrogen; Amarillo/TX/USA).

Tumor cells line were generated in the lab like as described previously. The cells were routinely cultured in DMEM-c and recovered by trypsinization.

Next,  $1 \times 10^6$  cells BMMCs and  $5 \times 10^5$  tumor cells were resuspended in a Matrigel 1:1 mix (Matrigel Matrix HC Cat 354248 Corning; Glendale/Arizona/USA) and subcutaneously injected as plugs into the flank of C57BL/6 mice.

For some experiments,  $5 \times 10^5$  cells tumor cells were resuspended in a collagen I mix (300  $\mu$ g/mL) with or without rh $\beta$ ig-h3 (2.5  $\mu$ g/mL) and subcutaneously injected as plugs into the flank of Rag2KO mice. In both experimental setups, the mice were monitored on a daily basis. Five days after the engraftments, the mice were sacrificed and the tumor plugs were recovered.

Alternatively KIC cells ( $5 \times 10^5$ ) were subcutaneously injected into C57BL/6 mice. Ten days later, mice were treated twice a week for two weeks with an anti- $\beta$ ig-h3 depleting Ab (6  $\mu$ g) or isotype control Ab (6  $\mu$ g, Biocell). Mice were then monitored for 14 days and then sacrificed. The tumor grafts were then weighed, measured and processed for flow cytometric analysis.

#### QUANTIFICATION AND STATISTICAL ANALYSIS

The p-values were calculated using Student's t-test with GraphPad Prism as indicated in the figure legends: \*p < 0.05, \*\*p < 0.01, \*\*\*p < 0.001 and \*\*\*\*p < 0.0001. One-way ANOVA with Tukey's post hoc test was used for multiple comparisons.

## REFERENCES

- Adu-Berchie, K., Liu, Y., Zhang, D.K.Y., Freedman, B.R., Brockman, J.M., Vining, K.H., Nerger, B.A., Garmilla, A., Mooney, D.J., 2023. Generation of functionally distinct T-cell populations by altering the viscoelasticity of their extracellular matrix. *Nat. Biomed. Eng.* <https://doi.org/10.1038/s41551-023-01052-y>
- Ajami, B., Bennett, J.L., Krieger, C., Tetzlaff, W., Rossi, F.M.V., 2007. Local self-renewal can sustain CNS microglia maintenance and function throughout adult life. *Nat Neurosci* 10, 1538–1543. <https://doi.org/10.1038/nn2014>
- Akiyama, T., Yasuda, T., Uchihara, T., Yasuda-Yoshihara, N., Tan, B.J.Y., Yonemura, A., Semba, T., Yamasaki, J., Komohara, Y., Ohnishi, K., Wei, F., Fu, L., Zhang, J., Kitamura, F., Yamashita, K., Eto, K., Iwagami, S., Tsukamoto, H., Umemoto, T., Masuda, M., Nagano, O., Satou, Y., Saya, H., Tan, P., Baba, H., Ishimoto, T., 2023. Stromal Reprogramming through Dual PDGFR $\alpha$ / $\beta$  Blockade Boosts the Efficacy of Anti-PD-1 Immunotherapy in Fibrotic Tumors. *Cancer Research* 83, 753–770. <https://doi.org/10.1158/0008-5472.CAN-22-1890>
- Allavena, P., Chieppa, M., Bianchi, G., Solinas, G., Fabbri, M., Laskarin, G., Mantovani, A., 2010. Engagement of the mannose receptor by tumoral mucins activates an immune suppressive phenotype in human tumor-associated macrophages. *Clin Dev Immunol* 2010, 547179. <https://doi.org/10.1155/2010/547179>
- Allen, G.M., Frankel, N.W., Reddy, N.R., Bhargava, H.K., Yoshida, M.A., Stark, S.R., Purl, M., Lee, J., Yee, J.L., Yu, W., Li, A.W., Garcia, K.C., El-Samad, H., Roybal, K.T., Spitzer, M.H., Lim, W.A., 2022. Synthetic cytokine circuits that drive T cells into immune-excluded tumors. *Science* 378, eaba1624. <https://doi.org/10.1126/science.aba1624>
- Alonso-Nocelo, M., Ruiz-Cañas, L., Sancho, P., Görgülü, K., Alcalá, S., Pedrero, C., Vallespinos, M., López-Gil, J.C., Ochando, M., García-García, E., David Trabulo, S.M., Martinelli, P., Sánchez-Tomero, P., Sánchez-Palomo, C., Gonzalez-Santamaría, P., Yuste, L., Wörmann, S.M., Kabacaoğlu, D., Earl, J., Martin, A., Salvador, F., Valle, S., Martin-Hijano, L., Carrato, A., Erkan, M., García-Bermejo, L., Hermann, P.C., Algül, H., Moreno-Bueno, G., Heeschen, C., Portillo, F., Cano, A., Sainz, B., 2023. Macrophages direct cancer cells through a LOXL2-mediated metastatic cascade in pancreatic ductal adenocarcinoma. *Gut* 72, 345–359. <https://doi.org/10.1136/gutjnl-2021-325564>
- Amrutkar, M., Aasrum, M., Verbeke, C.S., Gladhaug, I.P., 2019. Secretion of fibronectin by human pancreatic stellate cells promotes chemoresistance to gemcitabine in pancreatic cancer cells. *BMC Cancer* 19, 596. <https://doi.org/10.1186/s12885-019-5803-1>

- Apte, M.V., Haber, P.S., Applegate, T.L., Norton, I.D., McCaughan, G.W., Korsten, M.A., Pirola, R.C., Wilson, J.S., 1998. Periacinar stellate shaped cells in rat pancreas: identification, isolation, and culture. *Gut* 43, 128–133. <https://doi.org/10.1136/gut.43.1.128>
- Apte, M.V., Park, S., Phillips, P.A., Santucci, N., Goldstein, D., Kumar, R.K., Ramm, G.A., Buchler, M., Friess, H., McCarroll, J.A., Keogh, G., Merrett, N., Pirola, R., Wilson, J.S., 2004. Desmoplastic reaction in pancreatic cancer: role of pancreatic stellate cells. *Pancreas* 29, 179–187. <https://doi.org/10.1097/00006676-200410000-00002>
- Asano, K., Takahashi, N., Ushiki, M., Monya, M., Aihara, F., Kuboki, E., Moriyama, S., Iida, M., Kitamura, H., Qiu, C.-H., Watanabe, T., Tanaka, M., 2015. Intestinal CD169(+) macrophages initiate mucosal inflammation by secreting CCL8 that recruits inflammatory monocytes. *Nat Commun* 6, 7802. <https://doi.org/10.1038/ncomms8802>
- Auciello, F.R., Bulusu, V., Oon, C., Tait-Mulder, J., Berry, M., Bhattacharyya, S., Tumanov, S., Allen-Petersen, B.L., Link, J., Kendsersky, N.D., Vringer, E., Schug, M., Novo, D., Hwang, R.F., Evans, R.M., Nixon, C., Dorrell, C., Morton, J.P., Norman, J.C., Sears, R.C., Kamphorst, J.J., Sherman, M.H., 2019. A Stromal Lysolipid-Autotaxin Signaling Axis Promotes Pancreatic Tumor Progression. *Cancer Discov* 9, 617–627. <https://doi.org/10.1158/2159-8290.CD-18-1212>
- Bachem, M.G., Schünemann, M., Ramadani, M., Siech, M., Beger, H., Buck, A., Zhou, S., Schmid-Kotsas, A., Adler, G., 2005. Pancreatic carcinoma cells induce fibrosis by stimulating proliferation and matrix synthesis of stellate cells. *Gastroenterology* 128, 907–921. <https://doi.org/10.1053/j.gastro.2004.12.036>
- Bachy, S., Wu, Z., Gamradt, P., Thierry, K., Milani, P., Chlasta, J., Hennino, A., 2022.  $\beta$ ig-h3-structured collagen alters macrophage phenotype and function in pancreatic cancer. *iScience* 25, 103758. <https://doi.org/10.1016/j.isci.2022.103758>
- Baer, J.M., Zuo, C., Kang, L.-I., de la Lastra, A.A., Borchering, N.C., Knolhoff, B.L., Bogner, S.J., Zhu, Y., Yang, L., Laurent, J., Lewis, M.A., Zhang, N., Kim, K.-W., Fields, R.C., Yokoyama, W.M., Mills, J.C., Ding, L., Randolph, G.J., DeNardo, D.G., 2023. Fibrosis induced by resident macrophages has divergent roles in pancreas inflammatory injury and PDAC. *Nat Immunol* 1–15. <https://doi.org/10.1038/s41590-023-01579-x>
- Bailey, J.M., Swanson, B.J., Hamada, T., Eggers, J.P., Singh, P.K., Caffery, T., Ouellette, M.M., Hollingsworth, M.A., 2008. Sonic hedgehog promotes desmoplasia in pancreatic cancer. *Clin Cancer Res* 14, 5995–6004. <https://doi.org/10.1158/1078-0432.CCR-08-0291>
- Bailey, P., Chang, D.K., Nones, K., Johns, A.L., Patch, A.-M., Gingras, M.-C., Miller, D.K., Christ, A.N., Bruxner, T.J.C., Quinn, M.C., Nourse, C., Murtaugh, L.C., Harliwong, I., Idrisoglu, S., Manning, S., Nourbakhsh, E., Wani, S., Fink, L., Holmes, O., Chin, V., Anderson, M.J., Kazakoff, S., Leonard, C., Newell, F., Waddell, Nick, Wood, S., Xu, Q., Wilson, P.J., Cloonan, N., Kassahn, K.S., Taylor,

- D., Quek, K., Robertson, A., Pantano, L., Mincarelli, L., Sanchez, L.N., Evers, L., Wu, J., Pinese, M., Cowley, M.J., Jones, M.D., Colvin, E.K., Nagrial, A.M., Humphrey, E.S., Chantrill, L.A., Mawson, A., Humphris, J., Chou, A., Pajic, M., Scarlett, C.J., Pinho, A.V., Giry-Laterriere, M., Rooman, I., Samra, J.S., Kench, J.G., Lovell, J.A., Merrett, N.D., Toon, C.W., Epari, K., Nguyen, N.Q., Barbour, A., Zeps, N., Moran-Jones, K., Jamieson, N.B., Graham, J.S., Duthie, F., Oien, K., Hair, J., Grützmann, R., Maitra, A., Iacobuzio-Donahue, C.A., Wolfgang, C.L., Morgan, R.A., Lawlor, R.T., Corbo, V., Bassi, C., Rusev, B., Capelli, P., Salvia, R., Tortora, G., Mukhopadhyay, D., Petersen, G.M., Munzy, D.M., Fisher, W.E., Karim, S.A., Eshleman, J.R., Hruban, R.H., Pilarsky, C., Morton, J.P., Sansom, O.J., Scarpa, A., Musgrove, E.A., Bailey, U.-M.H., Hofmann, O., Sutherland, R.L., Wheeler, D.A., Gill, A.J., Gibbs, R.A., Pearson, J.V., Waddell, Nicola, Biankin, A.V., Grimmond, S.M., 2016. Genomic analyses identify molecular subtypes of pancreatic cancer. *Nature* 531, 47–52. <https://doi.org/10.1038/nature16965>
- Bain, C.C., Bravo-Blas, A., Scott, C.L., Perdiguero, E.G., Geissmann, F., Henri, S., Malissen, B., Osborne, L.C., Artis, D., Mowat, A.M., 2014. Constant replenishment from circulating monocytes maintains the macrophage pool in the intestine of adult mice. *Nat Immunol* 15, 929–937. <https://doi.org/10.1038/ni.2967>
- Balachandran, V.P., Łuksza, M., Zhao, J.N., Makarov, V., Moral, J.A., Remark, R., Herbst, B., Askan, G., Bhanot, U., Senbabaoglu, Y., Wells, D.K., Cary, C.I.O., Grbovic-Huezo, O., Attiyeh, M., Medina, B., Zhang, J., Loo, J., Saglimbeni, J., Abu-Akeel, M., Zappasodi, R., Riaz, N., Smoragiewicz, M., Kelley, Z.L., Basturk, O., Australian Pancreatic Cancer Genome Initiative, Garvan Institute of Medical Research, Prince of Wales Hospital, Royal North Shore Hospital, University of Glasgow, St Vincent’s Hospital, QIMR Berghofer Medical Research Institute, University of Melbourne, Centre for Cancer Research, University of Queensland, Institute for Molecular Bioscience, Bankstown Hospital, Liverpool Hospital, Royal Prince Alfred Hospital, Chris O’Brien Lifehouse, Westmead Hospital, Fremantle Hospital, St John of God Healthcare, Royal Adelaide Hospital, Flinders Medical Centre, Envoi Pathology, Princess Alexandria Hospital, Austin Hospital, Johns Hopkins Medical Institutes, ARC-Net Centre for Applied Research on Cancer, Gönen, M., Levine, A.J., Allen, P.J., Fearon, D.T., Merad, M., Gnjatic, S., Iacobuzio-Donahue, C.A., Wolchok, J.D., DeMatteo, R.P., Chan, T.A., Greenbaum, B.D., Merghoub, T., Leach, S.D., 2017. Identification of unique neoantigen qualities in long-term survivors of pancreatic cancer. *Nature* 551, 512–516. <https://doi.org/10.1038/nature24462>
- Ballehaninna, U.K., Chamberlain, R.S., 2012. The clinical utility of serum CA 19-9 in the diagnosis, prognosis and management of pancreatic adenocarcinoma: An evidence based appraisal. *J Gastrointest Oncol* 3, 105–119. <https://doi.org/10.3978/j.issn.2078-6891.2011.021>

- Barral, P., Polzella, P., Bruckbauer, A., van Rooijen, N., Besra, G.S., Cerundolo, V., Batista, F.D., 2010. CD169(+) macrophages present lipid antigens to mediate early activation of iNKT cells in lymph nodes. *Nat. Immunol.* 11, 303-U48. <https://doi.org/10.1038/ni.1853>
- Basturk, O., Hong, S.-M., Wood, L.D., Adsay, N.V., Albores-Saavedra, J., Biankin, A.V., Brosens, L.A.A., Fukushima, N., Goggins, M., Hruban, R.H., Kato, Y., Klimstra, D.S., Klöppel, G., Krasinskas, A., Longnecker, D.S., Matthaei, H., Offerhaus, G.J.A., Shimizu, M., Takaori, K., Terris, B., Yachida, S., Esposito, I., Furukawa, T., 2015. A REVISED CLASSIFICATION SYSTEM AND RECOMMENDATIONS FROM THE BALTIMORE CONSENSUS MEETING FOR NEOPLASTIC PRECURSOR LESIONS IN THE PANCREAS. *Am J Surg Pathol* 39, 1730–1741. <https://doi.org/10.1097/PAS.0000000000000533>
- Bayne, L.J., Beatty, G.L., Jhala, N., Clark, C.E., Rhim, A.D., Stanger, B.Z., Vonderheide, R.H., 2012. Tumor-derived granulocyte-macrophage colony-stimulating factor regulates myeloid inflammation and T cell immunity in pancreatic cancer. *Cancer Cell* 21, 822–835. <https://doi.org/10.1016/j.ccr.2012.04.025>
- Beatty, G.L., Winograd, R., Evans, R.A., Long, K.B., Luque, S.L., Lee, J.W., Clendenin, C., Gladney, W.L., Knoblock, D.M., Guirnalda, P.D., Vonderheide, R.H., 2015. Exclusion of T Cells From Pancreatic Carcinomas in Mice Is Regulated by Ly6C(low) F4/80(+) Extratumoral Macrophages. *Gastroenterology* 149, 201–210. <https://doi.org/10.1053/j.gastro.2015.04.010>
- Bellomo, A., Mondor, I., Spinelli, L., Lagueyrie, M., Stewart, B.J., Brouilly, N., Malissen, B., Clatworthy, M.R., Bajénoff, M., 2020. Reticular Fibroblasts Expressing the Transcription Factor WT1 Define a Stromal Niche that Maintains and Replenishes Splenic Red Pulp Macrophages. *Immunity* 53, 127-142.e7. <https://doi.org/10.1016/j.immuni.2020.06.008>
- Bensch, F., Knoblock, D.M., Liu, A., McAllister, F., Beatty, G.L., 2017. CTLA-4/CD80 pathway regulates T cell infiltration into pancreatic cancer. *Cancer Immunol Immunother* 66, 1609–1617. <https://doi.org/10.1007/s00262-017-2053-4>
- Benzel, J., Fendrich, V., 2018. Familial Pancreatic Cancer. *Oncol Res Treat* 41, 611–618. <https://doi.org/10.1159/000493473>
- Bernard, V., Semaan, A., Huang, J., San Lucas, F.A., Mulu, F.C., Stephens, B.M., Guerrero, P.A., Huang, Y., Zhao, J., Kamyabi, N., Sen, S., Scheet, P.A., Taniguchi, C.M., Kim, M.P., Tzeng, C.-W., Katz, M.H., Singhi, A.D., Maitra, A., Alvarez, H.A., 2019. Single-Cell Transcriptomics of Pancreatic Cancer Precursors Demonstrates Epithelial and Microenvironmental Heterogeneity as an Early Event in Neoplastic Progression. *Clin Cancer Res* 25, 2194–2205. <https://doi.org/10.1158/1078-0432.CCR-18-1955>

- Bernhard, C.A., Ried, C., Kochanek, S., Brocker, T., 2015. CD169(+) macrophages are sufficient for priming of CTLs with specificities left out by cross-priming dendritic cells. *Proc. Natl. Acad. Sci. U. S. A.* 112, 5461–5466. <https://doi.org/10.1073/pnas.1423356112>
- Bhattacharjee, S., Hamberger, F., Ravichandra, A., Miller, M., Nair, A., Affo, S., Filliol, A., Chin, L., Savage, T.M., Yin, D., Wirsik, N.M., Mehal, A., Arpaia, N., Seki, E., Mack, M., Zhu, D., Sims, P.A., Kalluri, R., Stanger, B.Z., Olive, K.P., Schmidt, T., Wells, R.G., Mederacke, I., Schwabe, R.F., 2021. Tumor restriction by type I collagen opposes tumor-promoting effects of cancer-associated fibroblasts. *Journal of Clinical Investigation* 131, e146987. <https://doi.org/10.1172/JCI146987>
- Biffi, G., Oni, T.E., Spielman, B., Hao, Y., Elyada, E., Park, Y., Preall, J., Tuveson, D.A., 2019. IL1-Induced JAK/STAT Signaling Is Antagonized by TGF $\beta$  to Shape CAF Heterogeneity in Pancreatic Ductal Adenocarcinoma. *Cancer Discov* 9, 282–301. <https://doi.org/10.1158/2159-8290.CD-18-0710>
- Bissell, M.J., Hines, W.C., 2011. Why don't we get more cancer? A proposed role of the microenvironment in restraining cancer progression. *Nat Med* 17, 320–329. <https://doi.org/10.1038/nm.2328>
- Bochet, L., Lehuédé, C., Dauvillier, S., Wang, Y.Y., Dirat, B., Laurent, V., Dray, C., Guiet, R., Maridonneau-Parini, I., Le Gonidec, S., Couderc, B., Escourrou, G., Valet, P., Muller, C., 2013. Adipocyte-derived fibroblasts promote tumor progression and contribute to the desmoplastic reaction in breast cancer. *Cancer Res* 73, 5657–5668. <https://doi.org/10.1158/0008-5472.CAN-13-0530>
- Bonapace, L., Coissieux, M.-M., Wyckoff, J., Mertz, K.D., Varga, Z., Junt, T., Bentires-Alj, M., 2014. Cessation of CCL2 inhibition accelerates breast cancer metastasis by promoting angiogenesis. *Nature* 515, 130–133. <https://doi.org/10.1038/nature13862>
- Bowman, R.L., Klemm, F., Akkari, L., Pyonteck, S.M., Sevenich, L., Quail, D.F., Dhara, S., Simpson, K., Gardner, E.E., Iacobuzio-Donahue, C.A., Brennan, C.W., Tabar, V., Gutin, P.H., Joyce, J.A., 2016. Macrophage Ontogeny Underlies Differences in Tumor-Specific Education in Brain Malignancies. *Cell Rep* 17, 2445–2459. <https://doi.org/10.1016/j.celrep.2016.10.052>
- Bruni, D., Angell, H.K., Galon, J., 2020. The immune contexture and Immunoscore in cancer prognosis and therapeutic efficacy. *Nat Rev Cancer* 20, 662–680. <https://doi.org/10.1038/s41568-020-0285-7>
- Buechler, M.B., Pradhan, R.N., Krishnamurty, A.T., Cox, C., Calviello, A.K., Wang, A.W., Yang, Y.A., Tam, L., Caothien, R., Roose-Girma, M., Modrusan, Z., Arron, J.R., Bourgon, R., Müller, S., Turley, S.J., 2021. Cross-tissue organization of the fibroblast lineage. *Nature* 593, 575–579. <https://doi.org/10.1038/s41586-021-03549-5>
- Calderon, B., Carrero, J.A., Ferris, S.T., Sojka, D.K., Moore, L., Epelman, S., Murphy, K.M., Yokoyama, W.M., Randolph, G.J., Unanue, E.R., 2015. The pancreas anatomy conditions the origin and

- properties of resident macrophages. *Journal of Experimental Medicine* 212, 1497–1512. <https://doi.org/10.1084/jem.20150496>
- Camara, A., Cordeiro, O.G., Alloush, F., Sponcel, J., Chypre, M., Onder, L., Asano, K., Tanaka, M., Yagita, H., Ludewig, B., Flacher, V., Mueller, C.G., 2019. Lymph Node Mesenchymal and Endothelial Stromal Cells Cooperate via the RANK-RANKL Cytokine Axis to Shape the Sinusoidal Macrophage Niche. *Immunity* 50, 1467-1481.e6. <https://doi.org/10.1016/j.immuni.2019.05.008>
- Canel, M., Sławińska, A.D., Lonergan, D.W., Kallor, A.A., Upstill-Goddard, R., Davidson, C., Kriegsheim, A. von, Biankin, A.V., Byron, A., Alfaro, J., Serrels, A., 2023. FAK suppresses antigen processing and presentation to promote immune evasion in pancreatic cancer. *Gut*. <https://doi.org/10.1136/gutjnl-2022-327927>
- Carpenter, E.S., Elhossiny, A.M., Kadiyala, P., Li, J., McGue, J., Griffith, B.D., Zhang, Y., Edwards, J., Nelson, S., Lima, F., Donahue, K.L., Du, W., Bischoff, A.C., Alomari, D., Watkoske, H.R., Mattea, M., The, S., Espinoza, C.E., Barrett, M., Sonnenday, C.J., Olden, N., Chen, C.-T., Peterson, N., Gunchick, V., Sahai, V., Rao, A., Bednar, F., Shi, J., Frankel, T.L., Pasca di Magliano, M., 2023. Analysis of Donor Pancreata Defines the Transcriptomic Signature and Microenvironment of Early Neoplastic Lesions. *Cancer Discovery* 13, 1324–1345. <https://doi.org/10.1158/2159-8290.CD-23-0013>
- Casanova-Acebes, M., Dalla, E., Leader, A.M., LeBerichel, J., Nikolic, J., Morales, B.M., Brown, M., Chang, C., Troncoso, L., Chen, S.T., Sastre-Perona, A., Park, M.D., Tabachnikova, A., Dhainaut, M., Hamon, P., Maier, B., Sawai, C.M., Agulló-Pascual, E., Schober, M., Brown, B.D., Reizis, B., Marron, T., Kenigsberg, E., Mousson, C., Benaroch, P., Aguirre-Ghiso, J.A., Merad, M., 2021. Tissue-resident macrophages provide a pro-tumorigenic niche to early NSCLC cells. *Nature* 595, 578–584. <https://doi.org/10.1038/s41586-021-03651-8>
- Casazza, A., Laoui, D., Wenes, M., Rizzolio, S., Bassani, N., Mambretti, M., Deschoemaeker, S., Van Genderachter, J.A., Tamagnone, L., Mazzone, M., 2013. Impeding macrophage entry into hypoxic tumor areas by Sema3A/Nrp1 signaling blockade inhibits angiogenesis and restores antitumor immunity. *Cancer Cell* 24, 695–709. <https://doi.org/10.1016/j.ccr.2013.11.007>
- Cassetta, L., Fragkogianni, S., Sims, A.H., Swierczak, A., Forrester, L.M., Zhang, H., Soong, D.Y.H., Cotechini, T., Anur, P., Lin, E.Y., Fidanza, A., Lopez-Yrigoyen, M., Millar, M.R., Urman, A., Ai, Z., Spellman, P.T., Hwang, E.S., Dixon, J.M., Wiechmann, L., Coussens, L.M., Smith, H.O., Pollard, J.W., 2019. Human Tumor-Associated Macrophage and Monocyte Transcriptional Landscapes Reveal Cancer-Specific Reprogramming, Biomarkers, and Therapeutic Targets. *Cancer Cell* 35, 588-602.e10. <https://doi.org/10.1016/j.ccell.2019.02.009>

- Castino, G.F., Cortese, N., Capretti, G., Serio, S., Di Caro, G., Mineri, R., Magrini, E., Grizzi, F., Cappello, P., Novelli, F., Spaggiari, P., Roncalli, M., Ridolfi, C., Gavazzi, F., Zerbi, A., Allavena, P., Marchesi, F., 2016. Spatial distribution of B cells predicts prognosis in human pancreatic adenocarcinoma. *Oncoimmunology* 5, e1085147. <https://doi.org/10.1080/2162402X.2015.1085147>
- Catenacci, D.V.T., Junttila, M.R., Karrison, T., Bahary, N., Horiba, M.N., Nattam, S.R., Marsh, R., Wallace, J., Kozloff, M., Rajdev, L., Cohen, D., Wade, J., Sleckman, B., Lenz, H.-J., Stiff, P., Kumar, P., Xu, P., Henderson, L., Takebe, N., Salgia, R., Wang, X., Stadler, W.M., de Sauvage, F.J., Kindler, H.L., 2015. Randomized Phase Ib/II Study of Gemcitabine Plus Placebo or Vismodegib, a Hedgehog Pathway Inhibitor, in Patients With Metastatic Pancreatic Cancer. *J Clin Oncol* 33, 4284–4292. <https://doi.org/10.1200/JCO.2015.62.8719>
- Cecchini, M.G., Dominguez, M.G., Mocci, S., Wetterwald, A., Felix, R., Fleisch, H., Chisholm, O., Hofstetter, W., Pollard, J.W., Stanley, E.R., 1994. Role of colony stimulating factor-1 in the establishment and regulation of tissue macrophages during postnatal development of the mouse. *Development* 120, 1357–1372. <https://doi.org/10.1242/dev.120.6.1357>
- Chauhan, V.P., Boucher, Y., Ferrone, C.R., Roberge, S., Martin, J.D., Stylianopoulos, T., Bardeesy, N., DePinho, R.A., Padera, T.P., Munn, L.L., Jain, R.K., 2014. Compression of pancreatic tumor blood vessels by hyaluronan is caused by solid stress and not interstitial fluid pressure. *Cancer Cell* 26, 14–15. <https://doi.org/10.1016/j.ccr.2014.06.003>
- Chauhan, V.P., Martin, J.D., Liu, H., Lacorre, D.A., Jain, S.R., Kozin, S.V., Stylianopoulos, T., Mousa, A.S., Han, X., Adstamongkonkul, P., Popović, Z., Huang, P., Bawendi, M.G., Boucher, Y., Jain, R.K., 2013. Angiotensin inhibition enhances drug delivery and potentiates chemotherapy by decompressing tumour blood vessels. *Nat Commun* 4, 2516. <https://doi.org/10.1038/ncomms3516>
- Chen, D.S., Mellman, I., 2013. Oncology Meets Immunology: The Cancer-Immunity Cycle. *Immunity* 39, 1–10. <https://doi.org/10.1016/j.immuni.2013.07.012>
- Chen, Y., Kim, J., Yang, S., Wang, H., Wu, C.-J., Sugimoto, H., LeBleu, V.S., Kalluri, R., 2021. Type I collagen deletion in  $\alpha$ SMA<sup>+</sup> myofibroblasts augments immune suppression and accelerates progression of pancreatic cancer. *Cancer Cell* 39, 548-565.e6. <https://doi.org/10.1016/j.ccell.2021.02.007>
- Chen, Y., Yang, S., Tavormina, J., Tampe, D., Zeisberg, M., Wang, H., Mahadevan, K.K., Wu, C.-J., Sugimoto, H., Chang, C.-C., Jenq, R.R., McAndrews, K.M., Kalluri, R., 2022. Oncogenic collagen I homotrimers from cancer cells bind to  $\alpha$ 3 $\beta$ 1 integrin and impact tumor microbiome and immunity to promote pancreatic cancer. *Cancer Cell* 40, 818-834.e9. <https://doi.org/10.1016/j.ccell.2022.06.011>

- Chijimatsu, R., Kobayashi, S., Takeda, Y., Kitakaze, M., Tatekawa, S., Arao, Y., Nakayama, M., Tachibana, N., Saito, T., Ennishi, D., Tomida, S., Sasaki, K., Yamada, D., Tomimaru, Y., Takahashi, H., Okuzaki, D., Motooka, D., Ohshiro, T., Taniguchi, M., Suzuki, Y., Ogawa, K., Mori, M., Doki, Y., Eguchi, H., Ishii, H., 2022. Establishment of a reference single-cell RNA sequencing dataset for human pancreatic adenocarcinoma. *iScience* 25, 104659. <https://doi.org/10.1016/j.isci.2022.104659>
- Chittezhath, M., Gunaseelan, D., Zheng, X., Hasan, R., Tay, V.S.Y., Lim, S.T., Wang, X., Berggren, P.-O., Bornstein, S., Boehm, B., Ruedl, C., Ali, Y., 2019. Islet macrophages are associated with islet vascular remodeling and compensatory hyperinsulinemia during diabetes. *Am. J. Physiol.-Endocrinol. Metab.* 317, E1108–E1120. <https://doi.org/10.1152/ajpendo.00248.2019>
- Chow, A., Huggins, M., Ahmed, J., Hashimoto, D., Lucas, D., Kunisaki, Y., Pinho, S., Leboeuf, M., Noizat, C., van Rooijen, N., Tanaka, M., Zhao, Z.J., Bergman, A., Merad, M., Frenette, P.S., 2013. CD169+ macrophages provide a niche promoting erythropoiesis under homeostasis, myeloablation and in JAK2V617F-induced polycythemia vera. *Nat Med* 19, 429–436. <https://doi.org/10.1038/nm.3057>
- Chow, A., Lucas, D., Hidalgo, A., Méndez-Ferrer, S., Hashimoto, D., Scheiermann, C., Battista, M., Leboeuf, M., Prophete, C., van Rooijen, N., Tanaka, M., Merad, M., Frenette, P.S., 2011. Bone marrow CD169+ macrophages promote the retention of hematopoietic stem and progenitor cells in the mesenchymal stem cell niche. *Journal of Experimental Medicine* 208, 261–271. <https://doi.org/10.1084/jem.20101688>
- Chow, A., Perica, K., Klebanoff, C.A., Wolchok, J.D., 2022. Clinical implications of T cell exhaustion for cancer immunotherapy. *Nat Rev Clin Oncol* 19, 775–790. <https://doi.org/10.1038/s41571-022-00689-z>
- Chronopoulos, A., Robinson, B., Sarper, M., Cortes, E., Auernheimer, V., Lachowski, D., Attwood, S., García, R., Ghassemi, S., Fabry, B., del Río Hernández, A., 2016. ATRA mechanically reprograms pancreatic stellate cells to suppress matrix remodelling and inhibit cancer cell invasion. *Nat Commun* 7, 12630. <https://doi.org/10.1038/ncomms12630>
- Clark, C.E., Hingorani, S.R., Mick, R., Combs, C., Tuveson, D.A., Vonderheide, R.H., 2007. Dynamics of the Immune Reaction to Pancreatic Cancer from Inception to Invasion. *Cancer Research* 67, 9518–9527. <https://doi.org/10.1158/0008-5472.CAN-07-0175>
- Cloyd, J.M., Wang, H., Egger, M.E., Tzeng, C.-W.D., Prakash, L.R., Maitra, A., Varadhachary, G.R., Shroff, R., Javle, M., Fogelman, D., Wolff, R.A., Overman, M.J., Koay, E.J., Das, P., Herman, J.M., Kim, M.P., Vauthey, J.-N., Aloia, T.A., Fleming, J.B., Lee, J.E., Katz, M.H.G., 2017. Association of Clinical Factors With a Major Pathologic Response Following Preoperative Therapy for

- Pancreatic Ductal Adenocarcinoma. *JAMA Surg* 152, 1048–1056.  
<https://doi.org/10.1001/jamasurg.2017.2227>
- Collisson, E.A., Sadanandam, A., Olson, P., Gibb, W.J., Truitt, M., Gu, S., Cooc, J., Weinkle, J., Kim, G.E., Jakkula, L., Feiler, H.S., Ko, A.H., Olshen, A.B., Danenberg, K.L., Tempero, M.A., Spellman, P.T., Hanahan, D., Gray, J.W., 2011. Subtypes of pancreatic ductal adenocarcinoma and their differing responses to therapy. *Nat Med* 17, 500–503. <https://doi.org/10.1038/nm.2344>
- Conroy, T., Desseigne, F., Ychou, M., Bouché, O., Guimbaud, R., Bécouarn, Y., Adenis, A., Raoul, J.-L., Gourgou-Bourgade, S., de la Fouchardière, C., Bennouna, J., Bachet, J.-B., Khemissa-Akouz, F., Péré-Vergé, D., Delbaldo, C., Assenat, E., Chauffert, B., Michel, P., Montoto-Grillot, C., Ducreux, M., Groupe Tumeurs Digestives of Unicancer, PRODIGE Intergroup, 2011. FOLFIRINOX versus gemcitabine for metastatic pancreatic cancer. *N Engl J Med* 364, 1817–1825. <https://doi.org/10.1056/NEJMoa1011923>
- Costanza, B., Rademaker, G., Tiamiou, A., De Tullio, P., Leenders, J., Blomme, A., Bellier, J., Bianchi, E., Turtoi, A., Delvenne, P., Bellahcène, A., Peulen, O., Castronovo, V., 2019. Transforming growth factor beta-induced, an extracellular matrix interacting protein, enhances glycolysis and promotes pancreatic cancer cell migration. *Int J Cancer* 145, 1570–1584. <https://doi.org/10.1002/ijc.32247>
- Costa-Silva, B., Aiello, N.M., Ocean, A.J., Singh, S., Zhang, H., Thakur, B.K., Becker, A., Hoshino, A., Mark, M.T., Molina, H., Xiang, J., Zhang, T., Theilen, T.-M., García-Santos, G., Williams, C., Ararso, Y., Huang, Y., Rodrigues, G., Shen, T.-L., Labori, K.J., Lothe, I.M.B., Kure, E.H., Hernandez, J., Doussot, A., Ebbesen, S.H., Grandgenett, P.M., Hollingsworth, M.A., Jain, M., Mallya, K., Batra, S.K., Jarnagin, W.R., Schwartz, R.E., Matei, I., Peinado, H., Stanger, B.Z., Bromberg, J., Lyden, D., 2015. Pancreatic cancer exosomes initiate pre-metastatic niche formation in the liver. *Nat Cell Biol* 17, 816–826. <https://doi.org/10.1038/ncb3169>
- Crocker, P.R., Paulson, J.C., Varki, A., 2007. Siglecs and their roles in the immune system. *Nat Rev Immunol* 7, 255–266. <https://doi.org/10.1038/nri2056>
- D’Addio, M., Frey, J., Tacconi, C., Commerford, C.D., Halin, C., Detmar, M., Cummings, R.D., Otto, V.I., 2021. Sialoglycans on lymphatic endothelial cells augment interactions with Siglec-1 (CD169) of lymph node macrophages. *The FASEB Journal* 35, e22017. <https://doi.org/10.1096/fj.202100300R>
- Dai, X.-M., Ryan, G.R., Hapel, A.J., Dominguez, M.G., Russell, R.G., Kapp, S., Sylvestre, V., Stanley, E.R., 2002. Targeted disruption of the mouse colony-stimulating factor 1 receptor gene results in osteopetrosis, mononuclear phagocyte deficiency, increased primitive progenitor cell frequencies, and reproductive defects. *Blood* 99, 111–120. <https://doi.org/10.1182/blood.v99.1.111>

- Daley, D., Mani, V.R., Mohan, N., Akkad, N., Ochi, A., Heindel, D.W., Lee, K.B., Zambirinis, C.P., Pandian, G.S.B., Savadkar, S., Torres-Hernandez, A., Nayak, S., Wang, D., Hundeyin, M., Diskin, B., Aykut, B., Werba, G., Barilla, R.M., Rodriguez, R., Chang, S., Gardner, L., Mahal, L.K., Ueberheide, B., Miller, G., 2017. Dectin 1 activation on macrophages by galectin 9 promotes pancreatic carcinoma and peritumoral immune tolerance. *Nat Med* 23, 556–567. <https://doi.org/10.1038/nm.4314>
- Das, S., Shapiro, B., Vucic, E.A., Vogt, S., Bar-Sagi, D., 2020. Tumor Cell-Derived IL1 beta Promotes Desmoplasia and Immune Suppression in Pancreatic Cancer. *Cancer Res.* 80, 1088–1101. <https://doi.org/10.1158/0008-5472.CAN-19-2080>
- de la Fouchardière, C., Gamradt, P., Chabaud, S., Raddaz, M., Blanc, E., Msika, O., Treilleux, I., Bachy, S., Cattey-Javouhey, A., Guibert, P., Sarabi, M., Rochefort, P., Funk-Debleds, P., Coutzac, C., Ray-Coquard, I., Peyrat, P., Meeus, P., Rivoire, M., Dupré, A., Hennino, A., 2022. A Promising Biomarker and Therapeutic Target in Patients with Advanced PDAC: The Stromal Protein  $\beta$ ig-h3. *Journal of Personalized Medicine* 12, 623. <https://doi.org/10.3390/jpm12040623>
- DeNardo, D.G., Ruffell, B., 2019. Macrophages as regulators of tumour immunity and immunotherapy. *Nat Rev Immunol* 19, 369–382. <https://doi.org/10.1038/s41577-019-0127-6>
- Diskin, B., Adam, S., Cassini, M.F., Sanchez, G., Liria, M., Aykut, B., Buttar, C., Li, E., Sundberg, B., Salas, R.D., Chen, R., Wang, J., Kim, M., Farooq, M.S., Nguy, S., Fedele, C., Tang, K.H., Chen, T., Wang, W., Hundeyin, M., Rossi, J.A.K., Kurz, E., Haq, M.I.U., Karlen, J., Kruger, E., Sekendiz, Z., Wu, D., Shadaloey, S.A.A., Baptiste, G., Werba, G., Selvaraj, S., Loomis, C., Wong, K.-K., Leinwand, J., Miller, G., 2020. PD-L1 engagement on T cells promotes self-tolerance and suppression of neighboring macrophages and effector T cells in cancer. *Nat Immunol* 21, 442–454. <https://doi.org/10.1038/s41590-020-0620-x>
- Dixit, A., Sarver, A., Zettervall, J., Huang, H., Zheng, K., Brekken, R.A., Provenzano, P.P., 2022. Targeting TNF- $\alpha$ -producing macrophages activates antitumor immunity in pancreatic cancer via IL-33 signaling. *JCI Insight* 7, e153242. <https://doi.org/10.1172/jci.insight.153242>
- Dolberg, D.S., Hollingsworth, R., Hertle, M., Bissell, M.J., 1985. Wounding and its role in RSV-mediated tumor formation. *Science* 230, 676–678. <https://doi.org/10.1126/science.2996144>
- Dominguez, C.X., Müller, S., Keerthivasan, S., Koeppen, H., Hung, J., Gierke, S., Breart, B., Foreman, O., Bainbridge, T.W., Castiglioni, A., Senbabaoglu, Y., Modrusan, Z., Liang, Y., Junttila, M.R., Klijn, C., Bourgon, R., Turley, S.J., 2020. Single-Cell RNA Sequencing Reveals Stromal Evolution into LRRC15+ Myofibroblasts as a Determinant of Patient Response to Cancer Immunotherapy. *Cancer Discov* 10, 232–253. <https://doi.org/10.1158/2159-8290.CD-19-0644>
- Dunn, G.P., Old, L.J., Schreiber, R.D., 2004. The immunobiology of cancer immunosurveillance and immunoediting. *Immunity* 21, 137–148. <https://doi.org/10.1016/j.immuni.2004.07.017>

- Dutta, P., Hoyer, F.F., Grigoryeva, L.S., Sager, H.B., Leuschner, F., Courties, G., Borodovsky, A., Novobrantseva, T., Ruda, V.M., Fitzgerald, K., Iwamoto, Y., Wojtkiewicz, G., Sun, Y., Da Silva, N., Libby, P., Anderson, D.G., Swirski, F.K., Weissleder, R., Nahrendorf, M., 2015. Macrophages retain hematopoietic stem cells in the spleen via VCAM-1. *J. Exp. Med.* 212, 497–512. <https://doi.org/10.1084/jem.20141642>
- Dvorak, H.F., 1986. Tumors: wounds that do not heal. Similarities between tumor stroma generation and wound healing. *N Engl J Med* 315, 1650–1659. <https://doi.org/10.1056/NEJM198612253152606>
- Elyada, E., Bolisetty, M., Laise, P., Flynn, W.F., Courtois, E.T., Burkhart, R.A., Teinor, J.A., Belleau, P., Biffi, G., Lucito, M.S., Sivajothi, S., Armstrong, T.D., Engle, D.D., Yu, K.H., Hao, Y., Wolfgang, C.L., Park, Y., Preall, J., Jaffee, E.M., Califano, A., Robson, P., Tuveson, D.A., 2019. Cross-Species Single-Cell Analysis of Pancreatic Ductal Adenocarcinoma Reveals Antigen-Presenting Cancer-Associated Fibroblasts. *Cancer Discov* 9, 1102–1123. <https://doi.org/10.1158/2159-8290.CD-19-0094>
- Ene-Obong, A., Clear, A.J., Watt, J., Wang, J., Fatah, R., Riches, J.C., Marshall, J.F., Chin-Aleong, J., Chelala, C., Gribben, J.G., Ramsay, A.G., Kocher, H.M., 2013. Activated Pancreatic Stellate Cells Sequester CD8+ T Cells to Reduce Their Infiltration of the Juxtatumoral Compartment of Pancreatic Ductal Adenocarcinoma. *Gastroenterology* 145, 1121–1132. <https://doi.org/10.1053/j.gastro.2013.07.025>
- Epelman, S., Lavine, K.J., Beaudin, A.E., Sojka, D.K., Carrero, J.A., Calderon, B., Brija, T., Gautier, E.L., Ivanov, S., Satpathy, A.T., Schilling, J.D., Schwendener, R., Sergin, I., Razani, B., Forsberg, E.C., Yokoyama, W.M., Unanue, E.R., Colonna, M., Randolph, G.J., Mann, D.L., 2014. Embryonic and adult-derived resident cardiac macrophages are maintained through distinct mechanisms at steady state and during inflammation. *Immunity* 40, 91–104. <https://doi.org/10.1016/j.immuni.2013.11.019>
- Erkan, M., Michalski, C.W., Rieder, S., Reiser-Erkan, C., Abiatari, I., Kolb, A., Giese, N.A., Esposito, I., Friess, H., Kleeff, J., 2008. The activated stroma index is a novel and independent prognostic marker in pancreatic ductal adenocarcinoma. *Clin Gastroenterol Hepatol* 6, 1155–1161. <https://doi.org/10.1016/j.cgh.2008.05.006>
- Fahrman, J.F., Schmidt, C.M., Mao, X., Irajizad, E., Loftus, M., Zhang, Jinming, Patel, N., Vykoukal, J., Dennison, J.B., Long, J.P., Do, K.-A., Zhang, Jianjun, Chabot, J.A., Kluger, M.D., Kastrinos, F., Brais, L., Babic, A., Jajoo, K., Lee, L.S., Clancy, T.E., Ng, K., Bullock, A., Genkinger, J., Yip-Schneider, M.T., Maitra, A., Wolpin, B.M., Hanash, S., 2021. Lead-Time Trajectory of CA19-9 as an Anchor Marker for Pancreatic Cancer Early Detection. *Gastroenterology* 160, 1373-1383.e6. <https://doi.org/10.1053/j.gastro.2020.11.052>

- Fang, H.-Y., Hughes, R., Murdoch, C., Coffelt, S.B., Biswas, S.K., Harris, A.L., Johnson, R.S., Imityaz, H.Z., Simon, M.C., Fredlund, E., Greten, F.R., Rius, J., Lewis, C.E., 2009. Hypoxia-inducible factors 1 and 2 are important transcriptional effectors in primary macrophages experiencing hypoxia. *Blood* 114, 844–859. <https://doi.org/10.1182/blood-2008-12-195941>
- Feig, C., Jones, J.O., Kraman, M., Wells, R.J.B., Deonarine, A., Chan, D.S., Connell, C.M., Roberts, E.W., Zhao, Q., Caballero, O.L., Teichmann, S.A., Janowitz, T., Jodrell, D.I., Tuveson, D.A., Fearon, D.T., 2013. Targeting CXCL12 from FAP-expressing carcinoma-associated fibroblasts synergizes with anti-PD-L1 immunotherapy in pancreatic cancer. *Proc Natl Acad Sci U S A* 110, 20212–20217. <https://doi.org/10.1073/pnas.1320318110>
- Feng, Z., Diao, B., Wang, R., Wang, G., Wang, Chenhui, Tan, Y., Liu, L., Wang, Changsong, Liu, Ying, Liu, Yueping, Yuan, Z., Ren, L., Wu, Y., Chen, Y., 2020. The Novel Severe Acute Respiratory Syndrome Coronavirus 2 (SARS-CoV-2) Directly Decimates Human Spleens and Lymph Nodes. <https://doi.org/10.1101/2020.03.27.20045427>
- Fogg, D.K., Sibon, C., Miled, C., Jung, S., Aucouturier, P., Littman, D.R., Cumano, A., Geissmann, F., 2006. A clonogenic bone marrow progenitor specific for macrophages and dendritic cells. *Science* 311, 83–87. <https://doi.org/10.1126/science.1117729>
- Franklin, R.A., Liao, W., Sarkar, A., Kim, M.V., Bivona, M.R., Liu, K., Pamer, E.G., Li, M.O., 2014. The cellular and molecular origin of tumor-associated macrophages. *Science* 344, 921–925. <https://doi.org/10.1126/science.1252510>
- Fridman, W.H., Zitvogel, L., Sautès-Fridman, C., Kroemer, G., 2017. The immune contexture in cancer prognosis and treatment. *Nat Rev Clin Oncol* 14, 717–734. <https://doi.org/10.1038/nrclinonc.2017.101>
- Galon, J., Bruni, D., 2020. Tumor Immunology and Tumor Evolution: Intertwined Histories. *Immunity* 52, 55–81. <https://doi.org/10.1016/j.immuni.2019.12.018>
- Gamradt, P., De La Fouchardière, C., Hennino, A., 2021. Stromal Protein-Mediated Immune Regulation in Digestive Cancers. *Cancers* 13, 146. <https://doi.org/10.3390/cancers13010146>
- Garcia, P.E., Adoumie, M., Kim, E.C., Zhang, Y., Scales, M.K., El-Tawil, Y.S., Shaikh, A.Z., Wen, H.-J., Bednar, F., Allen, B.L., Wellik, D.M., Crawford, H.C., Pasca di Magliano, M., 2020. Differential Contribution of Pancreatic Fibroblast Subsets to the Pancreatic Cancer Stroma. *Cell Mol Gastroenterol Hepatol* 10, 581–599. <https://doi.org/10.1016/j.jcmgh.2020.05.004>
- Gatti, A., Fassini, P., Mazzone, A., Rusconi, S., Brando, B., Mistraretti, G., 2023. Kinetics of CD169, HLA-DR, and CD64 expression as predictive biomarkers of SARS-CoV2 outcome. *J Anesth Analg Crit Care* 3, 6. <https://doi.org/10.1186/s44158-023-00090-x>
- Gautier, E.L., Shay, T., Miller, J., Greter, M., Jakubzick, C., Ivanov, S., Helft, J., Chow, A., Elpek, K.G., Gordonov, S., Mazloom, A.R., Ma'ayan, A., Chua, W.-J., Hansen, T.H., Turley, S.J., Merad, M.,

- Randolph, G.J., Immunological Genome Consortium, 2012. Gene-expression profiles and transcriptional regulatory pathways that underlie the identity and diversity of mouse tissue macrophages. *Nat Immunol* 13, 1118–1128. <https://doi.org/10.1038/ni.2419>
- Ginhoux, F., Greter, M., Leboeuf, M., Nandi, S., See, P., Gokhan, S., Mehler, M.F., Conway, S.J., Ng, L.G., Stanley, E.R., Samokhvalov, I.M., Merad, M., 2010. Fate mapping analysis reveals that adult microglia derive from primitive macrophages. *Science* 330, 841–845. <https://doi.org/10.1126/science.1194637>
- Ginhoux, F., Williams, M., 2016. Tissue-Resident Macrophage Ontogeny and Homeostasis. *Immunity* 44, 439–449. <https://doi.org/10.1016/j.immuni.2016.02.024>
- Goehrig, D., Nigri, J., Samain, R., Wu, Z., Cappello, P., Gabiane, G., Zhang, X., Zhao, Y., Kim, I.-S., Chanal, M., Curto, R., Hervieu, V., de La Fouchardière, C., Novelli, F., Milani, P., Tomasini, R., Bousquet, C., Bertolino, P., Hennino, A., 2019. Stromal protein  $\beta$ ig-h3 reprogrammes tumour microenvironment in pancreatic cancer. *Gut* 68, 693–707. <https://doi.org/10.1136/gutjnl-2018-317570>
- Gomez Perdiguero, E., Klapproth, K., Schulz, C., Busch, K., Azzoni, E., Crozet, L., Garner, H., Trouillet, C., de Bruijn, M.F., Geissmann, F., Rodewald, H.-R., 2015. Tissue-resident macrophages originate from yolk-sac-derived erythro-myeloid progenitors. *Nature* 518, 547–551. <https://doi.org/10.1038/nature13989>
- Gordon, S., Plüddemann, A., Mukhopadhyay, S., 2015. Sinusoidal Immunity: Macrophages at the Lymphohematopoietic Interface. *Cold Spring Harb Perspect Biol* 7, a016378. <https://doi.org/10.1101/cshperspect.a016378>
- Greter, M., Lelios, I., Pelczar, P., Hoeffel, G., Price, J., Leboeuf, M., Kündig, T.M., Frei, K., Ginhoux, F., Merad, M., Becher, B., 2012. Stroma-Derived Interleukin-34 Controls the Development and Maintenance of Langerhans Cells and the Maintenance of Microglia. *Immunity* 37, 1050–1060. <https://doi.org/10.1016/j.immuni.2012.11.001>
- Groot, V.P., Rezaee, N., Wu, W., Cameron, J.L., Fishman, E.K., Hruban, R.H., Weiss, M.J., Zheng, L., Wolfgang, C.L., He, J., 2018. Patterns, Timing, and Predictors of Recurrence Following Pancreatectomy for Pancreatic Ductal Adenocarcinoma. *Annals of Surgery* 267, 936. <https://doi.org/10.1097/SLA.0000000000002234>
- Groth, C., Hu, X., Weber, R., Fleming, V., Altevogt, P., Utikal, J., Umansky, V., 2019. Immunosuppression mediated by myeloid-derived suppressor cells (MDSCs) during tumour progression. *Br J Cancer* 120, 16–25. <https://doi.org/10.1038/s41416-018-0333-1>
- Guerra, C., Schuhmacher, A.J., Cañamero, M., Grippo, P.J., Verdaguer, L., Pérez-Gallego, L., Dubus, P., Sandgren, E.P., Barbacid, M., 2007. Chronic pancreatitis is essential for induction of pancreatic

- ductal adenocarcinoma by K-Ras oncogenes in adult mice. *Cancer Cell* 11, 291–302. <https://doi.org/10.1016/j.ccr.2007.01.012>
- Guilliams, M., De Kleer, I., Henri, S., Post, S., Vanhoutte, L., De Prijck, S., Deswarte, K., Malissen, B., Hammad, H., Lambrecht, B.N., 2013. Alveolar macrophages develop from fetal monocytes that differentiate into long-lived cells in the first week of life via GM-CSF. *J Exp Med* 210, 1977–1992. <https://doi.org/10.1084/jem.20131199>
- Guilliams, M., Mildner, A., Yona, S., 2018. Developmental and Functional Heterogeneity of Monocytes. *Immunity* 49, 595–613. <https://doi.org/10.1016/j.immuni.2018.10.005>
- Guilliams, M., Thierry, G.R., Bonnardel, J., Bajenoff, M., 2020. Establishment and Maintenance of the Macrophage Niche. *Immunity* 52, 434–451. <https://doi.org/10.1016/j.immuni.2020.02.015>
- Gulhati, P., Schalck, A., Jiang, S., Shang, X., Wu, C.-J., Hou, P., Ruiz, S.H., Soto, L.S., Parra, E., Ying, H., Han, J., Dey, P., Li, J., Deng, P., Sei, E., Maeda, D.Y., Zebala, J.A., Spring, D.J., Kim, M., Wang, H., Maitra, A., Moore, D., Clise-Dwyer, K., Wang, Y.A., Navin, N.E., DePinho, R.A., 2023. Targeting T cell checkpoints 41BB and LAG3 and myeloid cell CXCR1/CXCR2 results in antitumor immunity and durable response in pancreatic cancer. *Nat Cancer* 4, 62–80. <https://doi.org/10.1038/s43018-022-00500-z>
- Gunderson, A.J., Kaneda, M.M., Tsujikawa, T., Nguyen, A.V., Affara, N.I., Ruffell, B., Gorjestani, S., Liudahl, S.M., Truitt, M., Olson, P., Kim, G., Hanahan, D., Tempero, M.A., Sheppard, B., Irving, B., Chang, B.Y., Varner, J.A., Coussens, L.M., 2016. Bruton Tyrosine Kinase-Dependent Immune Cell Cross-talk Drives Pancreas Cancer. *Cancer Discov* 6, 270–285. <https://doi.org/10.1158/2159-8290.CD-15-0827>
- Gunnarsdottir, F.B., Briem, O., Lindgren, A.Y., Källberg, E., Andersen, C., Grenthe, R., Rosenqvist, C., Millrud, C.R., Wallgren, M., Viklund, H., Bexell, D., Johansson, M.E., Hedenfalk, I., Hagerling, C., Leandersson, K., 2023. Breast cancer associated CD169+ macrophages possess broad immunosuppressive functions but enhance antibody secretion by activated B cells. *Front Immunol* 14, 1180209. <https://doi.org/10.3389/fimmu.2023.1180209>
- Hakim, N., Patel, R., Devoe, C., Saif, M.W., 2019. Why HALO 301 Failed and Implications for Treatment of Pancreatic Cancer. *Pancreas (Fairfax)* 3, e1–e4. <https://doi.org/10.17140/POJ-3-e010>
- Han, B., Luo, H., Raelson, J., Huang, J., Li, Y., Tremblay, J., Hu, B., Qi, S., Wu, J., 2014. TGFBI ( $\beta$ IG-H3) is a diabetes-risk gene based on mouse and human genetic studies. *Hum Mol Genet* 23, 4597–4611. <https://doi.org/10.1093/hmg/ddu173>
- Han, B., Qi, S., Hu, B., Luo, H., Wu, J., 2011. TGF-beta 1 promotes islet beta-cell function and regeneration. *J Immunol* 186, 5833–5844. <https://doi.org/10.4049/jimmunol.1002303>
- Han, L., Wu, Y., Fang, K., Sweeney, S., Roesner, U.K., Parrish, M., Patel, K., Walter, T., Piermattei, J., Trimboli, A., Lefler, J., Timmers, C.D., Yu, X.-Z., Jin, V.X., Zimmermann, M.T., Mathison, A.J.,

- Urrutia, R., Ostrowski, M.C., Leone, G., 2023. The splanchnic mesenchyme is the tissue of origin for pancreatic fibroblasts during homeostasis and tumorigenesis. *Nat Commun* 14, 1. <https://doi.org/10.1038/s41467-022-34464-6>
- Hanahan, D., 2022. Hallmarks of Cancer: New Dimensions. *Cancer Discovery* 12, 31–46. <https://doi.org/10.1158/2159-8290.CD-21-1059>
- Hanahan, D., Weinberg, R.A., 2011. Hallmarks of Cancer: The Next Generation. *Cell* 144, 646–674. <https://doi.org/10.1016/j.cell.2011.02.013>
- Hanahan, D., Weinberg, R.A., 2000. The hallmarks of cancer. *Cell* 100, 57–70. [https://doi.org/10.1016/s0092-8674\(00\)81683-9](https://doi.org/10.1016/s0092-8674(00)81683-9)
- Hartmann, N., Giese, N.A., Giese, T., Poschke, I., Offringa, R., Werner, J., Ryschich, E., 2014. Prevailing Role of Contact Guidance in Intrastromal T-cell Trapping in Human Pancreatic Cancer. *Clinical Cancer Research* 20, 3422–3433. <https://doi.org/10.1158/1078-0432.CCR-13-2972>
- Hashimoto, D., Chow, A., Noizat, C., Teo, P., Beasley, M.B., Leboeuf, M., Becker, C.D., See, P., Price, J., Lucas, D., Greter, M., Mortha, A., Boyer, S.W., Forsberg, E.C., Tanaka, M., van Rooijen, N., García-Sastre, A., Stanley, E.R., Ginhoux, F., Frenette, P.S., Merad, M., 2013. Tissue-resident macrophages self-maintain locally throughout adult life with minimal contribution from circulating monocytes. *Immunity* 38, 792–804. <https://doi.org/10.1016/j.immuni.2013.04.004>
- Hashimoto, K., Noshiro, M., Ohno, S., Kawamoto, T., Satakeda, H., Akagawa, Y., Nakashima, K., Okimura, A., Ishida, H., Okamoto, T., Pan, H., Shen, M., Yan, W., Kato, Y., 1997. Characterization of a cartilage-derived 66-kDa protein (RGD-CAP/beta ig-h3) that binds to collagen. *Biochim Biophys Acta* 1355, 303–314. [https://doi.org/10.1016/s0167-4889\(96\)00147-4](https://doi.org/10.1016/s0167-4889(96)00147-4)
- Hegde, S., Krisnawan, V.E., Herzog, B.H., Zuo, C., Breden, M.A., Knolhoff, B.L., Hogg, G.D., Tang, J.P., Baer, J.M., Mpoy, C., Lee, K.B., Alexander, K.A., Rogers, B.E., Murphy, K.M., Hawkins, W.G., Fields, R.C., DeSelm, C.J., Schwarz, J.K., DeNardo, D.G., 2020. Dendritic Cell Paucity Leads to Dysfunctional Immune Surveillance in Pancreatic Cancer. *Cancer Cell* 37, 289–307.e9. <https://doi.org/10.1016/j.ccell.2020.02.008>
- Helms, E.J., Berry, M.W., Chaw, R.C., DuFort, C.C., Sun, D., Onate, M.K., Oon, C., Bhattacharyya, S., Sanford-Crane, H., Horton, W., Finan, J.M., Sattler, A., Makar, R., Dawson, D.W., Xia, Z., Hingorani, S.R., Sherman, M.H., 2022. Mesenchymal Lineage Heterogeneity Underlies Nonredundant Functions of Pancreatic Cancer-Associated Fibroblasts. *Cancer Discov* 12, 484–501. <https://doi.org/10.1158/2159-8290.CD-21-0601>
- Hettinger, J., Richards, D.M., Hansson, J., Barra, M.M., Joschko, A.-C., Krijgsveld, J., Feuerer, M., 2013. Origin of monocytes and macrophages in a committed progenitor. *Nat Immunol* 14, 821–830. <https://doi.org/10.1038/ni.2638>

- Hilton, D.J., Nicola, N.A., Metcalf, D., 1988. Purification of a murine leukemia inhibitory factor from Krebs ascites cells. *Anal Biochem* 173, 359–367. [https://doi.org/10.1016/0003-2697\(88\)90200-x](https://doi.org/10.1016/0003-2697(88)90200-x)
- Hiraoka, N., Ino, Y., Yamazaki-Itoh, R., Kanai, Y., Kosuge, T., Shimada, K., 2015. Intratumoral tertiary lymphoid organ is a favourable prognosticator in patients with pancreatic cancer. *Br J Cancer* 112, 1782–1790. <https://doi.org/10.1038/bjc.2015.145>
- Hodi, F.S., Chiarion-Sileni, V., Gonzalez, R., Grob, J.-J., Rutkowski, P., Cowey, C.L., Lao, C.D., Schadendorf, D., Wagstaff, J., Dummer, R., Ferrucci, P.F., Smylie, M., Hill, A., Hogg, D., Marquez-Rodas, I., Jiang, J., Rizzo, J., Larkin, J., Wolchok, J.D., 2018. Nivolumab plus ipilimumab or nivolumab alone versus ipilimumab alone in advanced melanoma (CheckMate 067): 4-year outcomes of a multicentre, randomised, phase 3 trial. *Lancet Oncol* 19, 1480–1492. [https://doi.org/10.1016/S1470-2045\(18\)30700-9](https://doi.org/10.1016/S1470-2045(18)30700-9)
- Honke, N., Shaabani, N., Cadeddu, G., Sorg, U.R., Zhang, D.-E., Trilling, M., Klingel, K., Sauter, M., Kandolf, R., Gailus, N., van Rooijen, N., Burkart, C., Baldus, S.E., Grusdat, M., Löhning, M., Hengel, H., Pfeffer, K., Tanaka, M., Häussinger, D., Recher, M., Lang, P.A., Lang, K.S., 2012. Enforced viral replication activates adaptive immunity and is essential for the control of a cytopathic virus. *Nat Immunol* 13, 51–57. <https://doi.org/10.1038/ni.2169>
- Hosaka, K., Yang, Y., Seki, T., Fischer, C., Dubey, O., Fredlund, E., Hartman, J., Religa, P., Morikawa, H., Ishii, Y., Sasahara, M., Larsson, O., Cossu, G., Cao, R., Lim, S., Cao, Y., 2016. Pericyte-fibroblast transition promotes tumor growth and metastasis. *Proc Natl Acad Sci U S A* 113, E5618–5627. <https://doi.org/10.1073/pnas.1608384113>
- Hosein, A.N., Huang, H., Wang, Z., Parmar, K., Du, W., Huang, J., Maitra, A., Olson, E., Verma, U., Brekken, R.A., 2019. Cellular heterogeneity during mouse pancreatic ductal adenocarcinoma progression at single-cell resolution. *JCI Insight* 4, e129212. <https://doi.org/10.1172/jci.insight.129212>
- Houbracken, I., de Waele, E., Lardon, J., Ling, Z., Heimberg, H., Rooman, I., Bouwens, L., 2011. Lineage tracing evidence for transdifferentiation of acinar to duct cells and plasticity of human pancreas. *Gastroenterology* 141, 731–741, 741.e1–4. <https://doi.org/10.1053/j.gastro.2011.04.050>
- Hoves, S., Ooi, C.-H., Wolter, C., Sade, H., Bissinger, S., Schmittnaegel, M., Ast, O., Giusti, A.M., Wartha, K., Runza, V., Xu, W., Kienast, Y., Cannarile, M.A., Levitsky, H., Romagnoli, S., De Palma, M., Rüttinger, D., Ries, C.H., 2018. Rapid activation of tumor-associated macrophages boosts preexisting tumor immunity. *J Exp Med* 215, 859–876. <https://doi.org/10.1084/jem.20171440>
- Huang, H., Wang, Z., Zhang, Y., Pradhan, R.N., Ganguly, D., Chandra, R., Murimwa, G., Wright, S., Gu, X., Maddipati, R., Müller, S., Turley, S.J., Brekken, R.A., 2022. Mesothelial cell-derived antigen-

- presenting cancer-associated fibroblasts induce expansion of regulatory T cells in pancreatic cancer. *Cancer Cell* 40, 656-673.e7. <https://doi.org/10.1016/j.ccell.2022.04.011>
- Hutton, C., Heider, F., Blanco-Gomez, A., Banyard, A., Kononov, A., Zhang, X., Karim, S., Paulus-Hock, V., Watt, D., Steele, N., Kemp, S., Hogg, E.K.J., Kelly, J., Jackstadt, R.-F., Lopes, F., Menotti, M., Chisholm, L., Lamarca, A., Valle, J., Sansom, O.J., Springer, C., Malliri, A., Marais, R., Pasca di Magliano, M., Zelenay, S., Morton, J.P., Jørgensen, C., 2021. Single-cell analysis defines a pancreatic fibroblast lineage that supports anti-tumor immunity. *Cancer Cell* 39, 1227-1244.e20. <https://doi.org/10.1016/j.ccell.2021.06.017>
- Hwang, W.L., Jagadeesh, K.A., Guo, J.A., Hoffman, H.I., Yadollahpour, P., Reeves, J.W., Mohan, R., Drokhlyansky, E., Van Wittenberghe, N., Ashenberg, O., Farhi, S.L., Schapiro, D., Divakar, P., Miller, E., Zollinger, D.R., Eng, G., Schenkel, J.M., Su, J., Shiau, C., Yu, P., Freed-Pastor, W.A., Abbondanza, D., Mehta, A., Gould, J., Lambden, C., Porter, C.B.M., Tsankov, A., Dionne, D., Waldman, J., Cuoco, M.S., Nguyen, L., Delorey, T., Phillips, D., Barth, J.L., Kem, M., Rodrigues, C., Ciprani, D., Roldan, J., Zelga, P., Jorgji, V., Chen, J.H., Ely, Z., Zhao, D., Fuhrman, K., Fropf, R., Beechem, J.M., Loeffler, J.S., Ryan, D.P., Weekes, C.D., Ferrone, C.R., Qadan, M., Aryee, M.J., Jain, R.K., Neuberg, D.S., Wo, J.Y., Hong, T.S., Xavier, R., Aguirre, A.J., Rozenblatt-Rosen, O., Mino-Kenudson, M., Castillo, C.F., Liss, A.S., Ting, D.T., Jacks, T., Regev, A., 2022. Single-nucleus and spatial transcriptome profiling of pancreatic cancer identifies multicellular dynamics associated with neoadjuvant treatment. *Nat Genet* 54, 1178–1191. <https://doi.org/10.1038/s41588-022-01134-8>
- Iannaccone, M., Moseman, E.A., Tonti, E., Bosurgi, L., Junt, T., Henrickson, S.E., Whelan, S.P., Guidotti, L.G., von Andrian, U.H., 2010. Subcapsular sinus macrophages prevent CNS invasion on peripheral infection with a neurotropic virus. *Nature* 465, 1079-U143. <https://doi.org/10.1038/nature09118>
- Ino, Y., Yamazaki-Itoh, R., Shimada, K., Iwasaki, M., Kosuge, T., Kanai, Y., Hiraoka, N., 2013. Immune cell infiltration as an indicator of the immune microenvironment of pancreatic cancer. *Br J Cancer* 108, 914–923. <https://doi.org/10.1038/bjc.2013.32>
- Ivanov, S.V., Ivanova, A.V., Salnikow, K., Timofeeva, O., Subramaniam, M., Lerman, M.I., 2008. Two novel VHL targets, TGFBI (BIGH3) and its transactivator KLF10, are up-regulated in renal clear cell carcinoma and other tumors. *Biochem Biophys Res Commun* 370, 536–540. <https://doi.org/10.1016/j.bbrc.2008.03.066>
- Jacobetz, M.A., Chan, D.S., Nesses, A., Bapiro, T.E., Cook, N., Frese, K.K., Feig, C., Nakagawa, T., Caldwell, M.E., Zecchini, H.I., Lolkema, M.P., Jiang, P., Kultti, A., Thompson, C.B., Maneval, D.C., Jodrell, D.I., Frost, G.I., Shepard, H.M., Skepper, J.N., Tuveson, D.A., 2013. Hyaluronan impairs

- vascular function and drug delivery in a mouse model of pancreatic cancer. *Gut* 62, 112–120. <https://doi.org/10.1136/gutjnl-2012-302529>
- Jaiswal, S., Jamieson, C.H.M., Pang, W.W., Park, C.Y., Chao, M.P., Majeti, R., Traver, D., van Rooijen, N., Weissman, I.L., 2009. CD47 is upregulated on circulating hematopoietic stem cells and leukemia cells to avoid phagocytosis. *Cell* 138, 271–285. <https://doi.org/10.1016/j.cell.2009.05.046>
- Jakubzick, C., Gautier, E.L., Gibbings, S.L., Sojka, D.K., Schlitzer, A., Johnson, T.E., Ivanov, S., Duan, Q., Bala, S., Condon, T., van Rooijen, N., Grainger, J.R., Belkaid, Y., Ma'ayan, A., Riches, D.W.H., Yokoyama, W.M., Ginhoux, F., Henson, P.M., Randolph, G.J., 2013. Minimal differentiation of classical monocytes as they survey steady-state tissues and transport antigen to lymph nodes. *Immunity* 39, 599–610. <https://doi.org/10.1016/j.immuni.2013.08.007>
- Jiang, H., Hegde, S., Knolhoff, B.L., Zhu, Y., Herndon, J.M., Meyer, M.A., Nywening, T.M., Hawkins, W.G., Shapiro, I.M., Weaver, D.T., Pachter, J.A., Wang-Gillam, A., DeNardo, D.G., 2016. Targeting focal adhesion kinase renders pancreatic cancers responsive to checkpoint immunotherapy. *Nat Med* 22, 851–860. <https://doi.org/10.1038/nm.4123>
- Jiang, Z., Sun, H., Yu, J., Tian, W., Song, Y., 2021. Targeting CD47 for cancer immunotherapy. *Journal of Hematology & Oncology* 14, 180. <https://doi.org/10.1186/s13045-021-01197-w>
- Jing, W., Guo, X., Wang, G., Bi, Y., Han, L., Zhu, Q., Qiu, C., Tanaka, M., Zhao, Y., 2020. Breast cancer cells promote CD169+ macrophage-associated immunosuppression through JAK2-mediated PD-L1 upregulation on macrophages. *International Immunopharmacology* 78, 106012. <https://doi.org/10.1016/j.intimp.2019.106012>
- Junt, T., Moseman, E.A., Iannaccone, M., Massberg, S., Lang, P.A., Boes, M., Fink, K., Henrickson, S.E., Shayakhmetov, D.M., Di Paolo, N.C., Van Rooijen, N., Mempel, T.R., Whelan, S.P., von Andrian, U.H., 2007. Subcapsular sinus macrophages in lymph nodes clear lymph-borne viruses and present them to antiviral B cells. *Nature* 450, 110–+. <https://doi.org/10.1038/nature06287>
- Kalbasi, A., Komar, C., Tooker, G.M., Liu, M., Lee, J.W., Gladney, W.L., Ben-Josef, E., Beatty, G.L., 2017. Tumor-Derived CCL2 Mediates Resistance to Radiotherapy in Pancreatic Ductal Adenocarcinoma. *Clin. Cancer Res.* 23, 137–148. <https://doi.org/10.1158/1078-0432.CCR-16-0870>
- Kaneda, M.M., Cappello, P., Nguyen, A.V., Ralainirina, N., Hardamon, C.R., Foubert, P., Schmid, M.C., Sun, P., Mose, E., Bouvet, M., Lowy, A.M., Valasek, M.A., Sasik, R., Novelli, F., Hirsch, E., Varner, J.A., 2016. Macrophage PI3K gamma Drives Pancreatic Ductal Adenocarcinoma Progression. *Cancer Discov.* 6, 870–885. <https://doi.org/10.1158/2159-8290.CD-15-1346>
- Keklikoglou, I., De Palma, M., 2014. Metastasis risk after anti-macrophage therapy. *Nature* 515, 46–47. <https://doi.org/10.1038/nature13931>

- Kheir, V., Cortés-González, V., Zenteno, J.C., Schorderet, D.F., 2019. Mutation update: TGFBI pathogenic and likely pathogenic variants in corneal dystrophies. *Human Mutation* 40, 675–693. <https://doi.org/10.1002/humu.23737>
- Kim, E.J., Sahai, V., Abel, E.V., Griffith, K.A., Greenson, J.K., Takebe, N., Khan, G.N., Blau, J.L., Craig, R., Balis, U.G., Zalupski, M.M., Simeone, D.M., 2014. Pilot clinical trial of hedgehog pathway inhibitor GDC-0449 (vismodegib) in combination with gemcitabine in patients with metastatic pancreatic adenocarcinoma. *Clin Cancer Res* 20, 5937–5945. <https://doi.org/10.1158/1078-0432.CCR-14-1269>
- Kim, H.-J., Park, J.H., Kim, H.C., Kim, C.W., Kang, I., Lee, H.K., 2022. Blood monocyte-derived CD169+ macrophages contribute to antitumor immunity against glioblastoma. *Nat Commun* 13, 6211. <https://doi.org/10.1038/s41467-022-34001-5>
- Kinker, G.S., Vitiello, G.A.F., Diniz, A.B., Cabral-Piccin, M.P., Pereira, P.H.B., Carvalho, M.L.R., Ferreira, W.A.S., Chaves, A.S., Rondinelli, A., Gusmão, A.F., Defelicibus, A., Santos, G.O. dos, Nunes, W.A., Claro, L.C.L., Bernardo, T.M., Nishio, R.T., Pacheco, A.M., Laus, A.C., Arantes, L.M.R.B., Fleck, J.L., Jesus, V.H.F. de, Moricz, A. de, Weinlich, R., Coimbra, F.J.F., Lima, V.C.C. de, Medina, T. da S., 2023. Mature tertiary lymphoid structures are key niches of tumour-specific immune responses in pancreatic ductal adenocarcinomas. *Gut*. <https://doi.org/10.1136/gutjnl-2022-328697>
- Klichinsky, M., Ruella, M., Shestova, O., Lu, X.M., Best, A., Zeeman, M., Schmierer, M., Gabrusiewicz, K., Anderson, N.R., Petty, N.E., Cummins, K.D., Shen, F., Shan, X., Veliz, K., Blouch, K., Yashiro-Ohtani, Y., Kenderian, S.S., Kim, M.Y., O'Connor, R.S., Wallace, S.R., Kozlowski, M.S., Marchione, D.M., Shestov, M., Garcia, B.A., June, C.H., Gill, S., 2020. Human chimeric antigen receptor macrophages for cancer immunotherapy. *Nat Biotechnol* 38, 947–953. <https://doi.org/10.1038/s41587-020-0462-y>
- Klug, F., Prakash, H., Huber, P.E., Seibel, T., Bender, N., Halama, N., Pfirschke, C., Voss, R.H., Timke, C., Urnansky, L., Klapproth, K., Schaekel, K., Garbi, N., Jaeger, D., Weitz, J., Schmitz-Winnenthal, H., Haemmerling, G.J., Beckhove, P., 2013. Low-Dose Irradiation Programs Macrophage Differentiation to an iNOS(+)/M1 Phenotype that Orchestrates Effective T Cell Immunotherapy. *Cancer Cell* 24, 589–602. <https://doi.org/10.1016/j.ccr.2013.09.014>
- Kopp, J.L., von Figura, G., Mayes, E., Liu, F.-F., Dubois, C.L., Morris, J.P., Pan, F.C., Akiyama, H., Wright, C.V.E., Jensen, K., Hebrok, M., Sander, M., 2012. Identification of Sox9-dependent acinar-to-ductal reprogramming as the principal mechanism for initiation of pancreatic ductal adenocarcinoma. *Cancer Cell* 22, 737–750. <https://doi.org/10.1016/j.ccr.2012.10.025>
- Kraman, M., Bambrough, P.J., Arnold, J.N., Roberts, E.W., Magiera, L., Jones, J.O., Gopinathan, A., Tuveson, D.A., Fearon, D.T., 2010. Suppression of Antitumor Immunity by Stromal Cells

- Expressing Fibroblast Activation Protein- $\alpha$ . *Science* 330, 827–830.  
<https://doi.org/10.1126/science.1195300>
- Kramann, R., Schneider, R.K., DiRocco, D.P., Machado, F., Fleig, S., Bondzie, P.A., Henderson, J.M., Ebert, B.L., Humphreys, B.D., 2015. Perivascular Gli1+ progenitors are key contributors to injury-induced organ fibrosis. *Cell Stem Cell* 16, 51–66.  
<https://doi.org/10.1016/j.stem.2014.11.004>
- Krishnamurthy, A.T., Shyer, J.A., Thai, M., Gandham, V., Buechler, M.B., Yang, Y.A., Pradhan, R.N., Wang, A.W., Sanchez, P.L., Qu, Y., Breart, B., Chalouni, C., Dunlap, D., Ziai, J., Elstrott, J., Zacharias, N., Mao, W., Rowntree, R.K., Sadowsky, J., Lewis, G.D., Pillow, T.H., Nabet, B.Y., Banachereau, R., Tam, L., Caothien, R., Bacarro, N., Roose-Girma, M., Modrusan, Z., Mariathasan, S., Müller, S., Turley, S.J., 2022. LRRC15+ myofibroblasts dictate the stromal setpoint to suppress tumour immunity. *Nature* 611, 148–154. <https://doi.org/10.1038/s41586-022-05272-1>
- Lachowski, D., Cortes, E., Pink, D., Chronopoulos, A., Karim, S.A., P. Morton, J., del Río Hernández, A.E., 2017. Substrate Rigidity Controls Activation and Durotaxis in Pancreatic Stellate Cells. *Sci Rep* 7, 2506. <https://doi.org/10.1038/s41598-017-02689-x>
- Laklai, H., Miroshnikova, Y.A., Pickup, M.W., Collisson, E.A., Kim, G.E., Barrett, A.S., Hill, R.C., Lakins, J.N., Schlaepfer, D.D., Mouw, J.K., LeBleu, V.S., Roy, N., Novitskiy, S.V., Johansen, J.S., Poli, V., Kalluri, R., Iacobuzio-Donahue, C.A., Wood, L.D., Hebrok, M., Hansen, K., Moses, H.L., Weaver, V.M., 2016. Genotype tunes pancreatic ductal adenocarcinoma tissue tension to induce matricellular fibrosis and tumor progression. *Nat Med* 22, 497–505.  
<https://doi.org/10.1038/nm.4082>
- LaRue, M.M., Parker, S., Puccini, J., Cammer, M., Kimmelman, A.C., Bar-Sagi, D., 2022. Metabolic reprogramming of tumor-associated macrophages by collagen turnover promotes fibrosis in pancreatic cancer. *Proc. Natl. Acad. Sci. U.S.A.* 119, e2119168119.  
<https://doi.org/10.1073/pnas.2119168119>
- Laumont, C.M., Banville, A.C., Gilardi, M., Hollern, D.P., Nelson, B.H., 2022. Tumour-infiltrating B cells: immunological mechanisms, clinical impact and therapeutic opportunities. *Nat Rev Cancer* 22, 414–430. <https://doi.org/10.1038/s41568-022-00466-1>
- Lazarov, T., Juarez-Carreño, S., Cox, N., Geissmann, F., 2023. Physiology and diseases of tissue-resident macrophages. *Nature* 618, 698–707. <https://doi.org/10.1038/s41586-023-06002-x>
- Leach, D.R., Krummel, M.F., Allison, J.P., 1996. Enhancement of antitumor immunity by CTLA-4 blockade. *Science* 271, 1734–1736. <https://doi.org/10.1126/science.271.5256.1734>
- Lecker, L.S., Berlato, C., Maniati, E., Delaine-Smith, R., Pearce, O.M.T., Heath, O., Nichols, S.J., Trevisan, C., Novak, M., McDermott, J., Brenton, J.D., Cutillas, P.R., Rajeeve, V., Hennino, A., Drapkin, R., Loessner, D., Balkwill, F.R., 2021. TGF $\beta$ 1 production by macrophages contributes to an

- immunosuppressive microenvironment in ovarian cancer. *Cancer Res.* <https://doi.org/10.1158/0008-5472.CAN-21-0536>
- Lee, J.J., Perera, R.M., Wang, H., Wu, D.-C., Liu, X.S., Han, S., Fitamant, J., Jones, P.D., Ghanta, K.S., Kawano, S., Nagle, J.M., Deshpande, V., Boucher, Y., Kato, T., Chen, J.K., Willmann, J.K., Bardeesy, N., Beachy, P.A., 2014. Stromal response to Hedgehog signaling restrains pancreatic cancer progression. *Proc Natl Acad Sci U S A* 111, E3091-3100. <https://doi.org/10.1073/pnas.1411679111>
- Leidner, R., Sanjuan Silva, N., Huang, H., Sprott, D., Zheng, C., Shih, Y.-P., Leung, A., Payne, R., Sutcliffe, K., Cramer, J., Rosenberg, S.A., Fox, B.A., Urba, W.J., Tran, E., 2022. Neoantigen T-Cell Receptor Gene Therapy in Pancreatic Cancer. *N Engl J Med* 386, 2112–2119. <https://doi.org/10.1056/NEJMoa2119662>
- Li, C., Luo, X., Lin, Y., Tang, X., Ling, L., Wang, L., Jiang, Y., 2015. A Higher Frequency of CD14(+)CD169(+) Monocytes/Macrophages in Patients with Colorectal Cancer. *PLoS One* 10, e0141817. <https://doi.org/10.1371/journal.pone.0141817>
- Li, J.-Q., Yu, X.-J., Wang, Y.-C., Huang, L.-Y., Liu, C.-Q., Zheng, L., Fang, Y.-J., Xu, J., 2017. Distinct patterns and prognostic values of tumor-infiltrating macrophages in hepatocellular carcinoma and gastric cancer. *J. Transl. Med.* 15, 37. <https://doi.org/10.1186/s12967-017-1139-2>
- Liao, J., Zeng, D.-N., Li, J.-Z., Hua, Q.-M., Huang, C.-X., Xu, J., Wu, C., Zheng, L., Wen, W.-P., Wu, Y., 2022. Type I IFNs repolarized a CD169+ macrophage population with anti-tumor potentials in hepatocellular carcinoma. *Mol Ther* 30, 632–643. <https://doi.org/10.1016/j.ymthe.2021.09.021>
- Linde, N., Casanova-Acebes, M., Sosa, M.S., Mortha, A., Rahman, A., Farias, E., Harper, K., Tardio, E., Reyes Torres, I., Jones, J., Condeelis, J., Merad, M., Aguirre-Ghiso, J.A., 2018. Macrophages orchestrate breast cancer early dissemination and metastasis. *Nat Commun* 9, 21. <https://doi.org/10.1038/s41467-017-02481-5>
- Liou, G.-Y., Döppler, H., Braun, U.B., Panayiotou, R., Scotti Buzhardt, M., Radisky, D.C., Crawford, H.C., Fields, A.P., Murray, N.R., Wang, Q.J., Leitges, M., Storz, P., 2015a. Protein kinase D1 drives pancreatic acinar cell reprogramming and progression to intraepithelial neoplasia. *Nat Commun* 6, 6200. <https://doi.org/10.1038/ncomms7200>
- Liou, G.-Y., Döppler, H., Necela, B., Edenfield, B., Zhang, L., Dawson, D.W., Storz, P., 2015b. Mutant KRAS–Induced Expression of ICAM-1 in Pancreatic Acinar Cells Causes Attraction of Macrophages to Expedite the Formation of Precancerous Lesions. *Cancer Discovery* 5, 52–63. <https://doi.org/10.1158/2159-8290.CD-14-0474>
- Liu, C.-Y., Xu, J.-Y., Shi, X.-Y., Huang, W., Ruan, T.-Y., Xie, P., Ding, J.-L., 2013. M2-polarized tumor-associated macrophages promoted epithelial–mesenchymal transition in pancreatic cancer

- cells, partially through TLR4/IL-10 signaling pathway. *Laboratory Investigation* 93, 844–854. <https://doi.org/10.1038/labinvest.2013.69>
- Liu, K., Victora, G.D., Schwickert, T.A., Guermonprez, P., Meredith, M.M., Yao, K., Chu, F.-F., Randolph, G.J., Rudensky, A.Y., Nussenzweig, M., 2009. In vivo analysis of dendritic cell development and homeostasis. *Science* 324, 392–397. <https://doi.org/10.1126/science.1170540>
- Lo, A., Wang, L.-C.S., Scholler, J., Monslow, J., Avery, D., Newick, K., O'Brien, S., Evans, R.A., Bajor, D.J., Clendenin, C., Durham, A.C., Buza, E.L., Vonderheide, R.H., June, C.H., Albelda, S.M., Puré, E., 2015. Tumor-Promoting Desmoplasia Is Disrupted by Depleting FAP-Expressing Stromal Cells. *Cancer Research* 75, 2800–2810. <https://doi.org/10.1158/0008-5472.CAN-14-3041>
- Loyher, P.-L., Hamon, P., Laviron, M., Meghraoui-Kheddar, A., Goncalves, E., Deng, Z., Torstensson, S., Bercovici, N., Baudesson de Chanville, C., Combadière, B., Geissmann, F., Savina, A., Combadière, C., Boissonnas, A., 2018. Macrophages of distinct origins contribute to tumor development in the lung. *J Exp Med* 215, 2536–2553. <https://doi.org/10.1084/jem.20180534>
- Ludewig, B., Cervantes-Barragan, L., 2012. CD169+ macrophages take the bullet. *Nat Immunol* 13, 13–14. <https://doi.org/10.1038/ni.2189>
- Łuksza, M., Sethna, Z.M., Rojas, L.A., Lihm, J., Bravi, B., Elhanati, Y., Soares, K., Amisaki, M., Dobrin, A., Hoyos, D., Guasp, P., Zebboudj, A., Yu, R., Chandra, A.K., Waters, T., Odgerel, Z., Leung, J., Kappagantula, R., Makohon-Moore, A., Johns, A., Gill, A., Gigoux, M., Wolchok, J., Merghoub, T., Sadelain, M., Patterson, E., Monasson, R., Mora, T., Walczak, A.M., Cocco, S., Iacobuzio-Donahue, C., Greenbaum, B.D., Balachandran, V.P., 2022. Neoantigen quality predicts immunoediting in survivors of pancreatic cancer. *Nature* 606, 389–395. <https://doi.org/10.1038/s41586-022-04735-9>
- Luo, H., Xia, X., Huang, L.-B., An, H., Cao, M., Kim, G.D., Chen, H.-N., Zhang, W.-H., Shu, Y., Kong, X., Ren, Z., Li, P.-H., Liu, Yang, Tang, H., Sun, R., Li, C., Bai, B., Jia, W., Liu, Yi, Zhang, W., Yang, L., Peng, Y., Dai, L., Hu, H., Jiang, Y., Hu, Y., Zhu, J., Jiang, H., Li, Z., Caulin, C., Park, J., Xu, H., 2022. Pan-cancer single-cell analysis reveals the heterogeneity and plasticity of cancer-associated fibroblasts in the tumor microenvironment. *Nat Commun* 13, 6619. <https://doi.org/10.1038/s41467-022-34395-2>
- Mace, T.A., Ameen, Z., Collins, A., Wojcik, S., Mair, M., Young, G.S., Fuchs, J.R., Eubank, T.D., Frankel, W.L., Bekaii-Saab, T., Bloomston, M., Lesinski, G.B., 2013. Pancreatic Cancer-Associated Stellate Cells Promote Differentiation of Myeloid-Derived Suppressor Cells in a STAT3-Dependent Manner. *Cancer Res.* 73, 3007–3018. <https://doi.org/10.1158/0008-5472.CAN-12-4601>

- MacKie, R.M., Reid, R., Junor, B., 2003. Fatal Melanoma Transferred in a Donated Kidney 16 Years after Melanoma Surgery. *N Engl J Med* 348, 567–568. <https://doi.org/10.1056/NEJM200302063480620>
- Mantovani, A., Sica, A., Sozzani, S., Allavena, P., Vecchi, A., Locati, M., 2004. The chemokine system in diverse forms of macrophage activation and polarization. *Trends Immunol* 25, 677–686. <https://doi.org/10.1016/j.it.2004.09.015>
- Martínez-Jiménez, F., Movasati, A., Brunner, S.R., Nguyen, L., Priestley, P., Cuppen, E., Van Hoeck, A., 2023. Pan-cancer whole-genome comparison of primary and metastatic solid tumours. *Nature* 618, 333–341. <https://doi.org/10.1038/s41586-023-06054-z>
- Mathew, E., Brannon, A.L., Del Vecchio, A., Garcia, P.E., Penny, M.K., Kane, K.T., Vinta, A., Buckanovich, R.J., di Magliano, M.P., 2016. Mesenchymal Stem Cells Promote Pancreatic Tumor Growth by Inducing Alternative Polarization of Macrophages. *Neoplasia* 18, 142–151. <https://doi.org/10.1016/j.neo.2016.01.005>
- Matsuda, Y., Furukawa, T., Yachida, S., Nishimura, M., Seki, A., Nonaka, K., Aida, J., Takubo, K., Ishiwata, T., Kimura, W., Arai, T., Mino-Kenudson, M., 2017. The Prevalence and Clinicopathological Characteristics of High-Grade Pancreatic Intraepithelial Neoplasia: Autopsy Study Evaluating the Entire Pancreatic Parenchyma. *Pancreas* 46, 658–664. <https://doi.org/10.1097/MPA.0000000000000786>
- Maude, S.L., Frey, N., Shaw, P.A., Aplenc, R., Barrett, D.M., Bunin, N.J., Chew, A., Gonzalez, V.E., Zheng, Z., Lacey, S.F., Mahnke, Y.D., Melenhorst, J.J., Rheingold, S.R., Shen, A., Teachey, D.T., Levine, B.L., June, C.H., Porter, D.L., Grupp, S.A., 2014. Chimeric Antigen Receptor T Cells for Sustained Remissions in Leukemia. *New England Journal of Medicine* 371, 1507–1517. <https://doi.org/10.1056/NEJMoa1407222>
- McWhorter, F.Y., Wang, T., Nguyen, P., Chung, T., Liu, W.F., 2013. Modulation of macrophage phenotype by cell shape. *Proceedings of the National Academy of Sciences* 110, 17253–17258. <https://doi.org/10.1073/pnas.1308887110>
- Meng, K.P., Majedi, F.S., Thauland, T.J., Butte, M.J., 2020. Mechanosensing through YAP controls T cell activation and metabolism. *Journal of Experimental Medicine* 217. <https://doi.org/10.1084/jem.20200053>
- Merad, M., Manz, M.G., Karsunky, H., Wagers, A., Peters, W., Charo, I., Weissman, I.L., Cyster, J.G., Engleman, E.G., 2002. Langerhans cells renew in the skin throughout life under steady-state conditions. *Nat Immunol* 3, 1135–1141. <https://doi.org/10.1038/ni852>
- Meyer, M.A., Baer, J.M., Knolhoff, B.L., Nywening, T.M., Panni, R.Z., Su, X., Weilbaecher, K.N., Hawkins, W.G., Ma, C., Fields, R.C., Linehan, D.C., Challen, G.A., Faccio, R., Aft, R.L., DeNardo, D.G., 2018. Breast and pancreatic cancer interrupt IRF8-dependent dendritic cell development to

- overcome immune surveillance. *Nat Commun* 9, 1250. <https://doi.org/10.1038/s41467-018-03600-6>
- Miller, B.W., Morton, J.P., Pinese, M., Saturno, G., Jamieson, N.B., McGhee, E., Timpson, P., Leach, J., McGarry, L., Shanks, E., Bailey, P., Chang, D., Oien, K., Karim, S., Au, A., Steele, C., Carter, C.R., McKay, C., Anderson, K., Evans, T.R.J., Marais, R., Springer, C., Biankin, A., Erler, J.T., Sansom, O.J., 2015. Targeting the LOX/hypoxia axis reverses many of the features that make pancreatic cancer deadly: inhibition of LOX abrogates metastasis and enhances drug efficacy. *EMBO Molecular Medicine* 7, 1063–1076. <https://doi.org/10.15252/emmm.201404827>
- Mills, C.D., Kincaid, K., Alt, J.M., Heilman, M.J., Hill, A.M., 2000. M-1/M-2 Macrophages and the Th1/Th2 Paradigm. *The Journal of Immunology* 164, 6166–6173. <https://doi.org/10.4049/jimmunol.164.12.6166>
- Mirlekar, B., Michaud, D., Lee, S.J., Kren, N.P., Harris, C., Greene, K., Goldman, E.C., Gupta, G.P., Fields, R.C., Hawkins, W.G., DeNardo, D.G., Rashid, N.U., Yeh, J.J., McRee, A.J., Vincent, B.G., Vignali, D.A.A., Pylayeva-Gupta, Y., 2020. B cell-Derived IL35 Drives STAT3-Dependent CD8+ T-cell Exclusion in Pancreatic Cancer. *Cancer Immunol Res* 8, 292–308. <https://doi.org/10.1158/2326-6066.CIR-19-0349>
- Mirlekar, B., Michaud, D., Searcy, R., Greene, K., Pylayeva-Gupta, Y., 2018. IL35 Hinders Endogenous Antitumor T-cell Immunity and Responsiveness to Immunotherapy in Pancreatic Cancer. *Cancer Immunol Res* 6, 1014–1024. <https://doi.org/10.1158/2326-6066.CIR-17-0710>
- Mirlekar, B., Wang, Y., Li, S., Zhou, M., Entwistle, S., De Buyscher, T., Morrison, A., Herrera, G., Harris, C., Vincent, B.G., Ting, J.P.-Y., Rashid, N., Kim, W.Y., Yeh, J.J., Pylayeva-Gupta, Y., 2022. Balance between immunoregulatory B cells and plasma cells drives pancreatic tumor immunity. *Cell Rep Med* 3, 100744. <https://doi.org/10.1016/j.xcrm.2022.100744>
- Miyake, Y., Asano, K., Kaise, H., Uemura, M., Nakayama, M., Tanaka, M., 2007. Critical role of macrophages in the marginal zone in the suppression of immune responses to apoptotic cell-associated antigens. *J. Clin. Invest.* 117, 2268–2278. <https://doi.org/10.1172/JCI31990>
- Miyamoto, Y., Maitra, A., Ghosh, B., Zechner, U., Argani, P., Iacobuzio-Donahue, C.A., Sriuranpong, V., Iso, T., Meszoely, I.M., Wolfe, M.S., Hruban, R.H., Ball, D.W., Schmid, R.M., Leach, S.D., 2003. Notch mediates TGF alpha-induced changes in epithelial differentiation during pancreatic tumorigenesis. *Cancer Cell* 3, 565–576. [https://doi.org/10.1016/s1535-6108\(03\)00140-5](https://doi.org/10.1016/s1535-6108(03)00140-5)
- Moffitt, R.A., Marayati, R., Flate, E.L., Volmar, K.E., Loeza, S.G.H., Hoadley, K.A., Rashid, N.U., Williams, L.A., Eaton, S.C., Chung, A.H., Smyla, J.K., Anderson, J.M., Kim, H.J., Bentrem, D.J., Talamonti, M.S., Iacobuzio-Donahue, C.A., Hollingsworth, M.A., Yeh, J.J., 2015. Virtual microdissection identifies distinct tumor- and stroma-specific subtypes of pancreatic ductal adenocarcinoma. *Nat Genet* 47, 1168–1178. <https://doi.org/10.1038/ng.3398>

- Molawi, K., Wolf, Y., Kandalla, P.K., Favret, J., Hagemeyer, N., Frenzel, K., Pinto, A.R., Klapproth, K., Henri, S., Malissen, B., Rodewald, H.-R., Rosenthal, N.A., Bajenoff, M., Prinz, M., Jung, S., Sieweke, M.H., 2014. Progressive replacement of embryo-derived cardiac macrophages with age. *J Exp Med* 211, 2151–2158. <https://doi.org/10.1084/jem.20140639>
- Moo-Young, T.A., Larson, J.W., Belt, B.A., Tan, M.C., Hawkins, W.G., Eberlein, T.J., Goedegebuure, P.S., Linehan, D.C., 2009. Tumor-derived TGF-beta mediates conversion of CD4+Foxp3+ regulatory T cells in a murine model of pancreas cancer. *J Immunother* 32, 12–21. <https://doi.org/10.1097/CJI.0b013e318189f13c>
- Movahedi, K., Laoui, D., Gysemans, C., Baeten, M., Stangé, G., Van den Bossche, J., Mack, M., Pipeleers, D., In't Veld, P., De Baetselier, P., Van Ginderachter, J.A., 2010. Different Tumor Microenvironments Contain Functionally Distinct Subsets of Macrophages Derived from Ly6C(high) Monocytes. *Cancer Research* 70, 5728–5739. <https://doi.org/10.1158/0008-5472.CAN-09-4672>
- Murphy, K.M., Weaver, C., 2016. *Janeway's Immunobiology: Ninth International Student Edition*. Garland Science.
- Murray, P.J., Allen, J.E., Biswas, S.K., Fisher, E.A., Gilroy, D.W., Goerdt, S., Gordon, S., Hamilton, J.A., Ivashkiv, L.B., Lawrence, T., Locati, M., Mantovani, A., Martinez, F.O., Mege, J.-L., Mosser, D.M., Natoli, G., Saeij, J.P., Schultze, J.L., Shirey, K.A., Sica, A., Suttles, J., Udalova, I., van Ginderachter, J.A., Vogel, S.N., Wynn, T.A., 2014. Macrophage activation and polarization: nomenclature and experimental guidelines. *Immunity* 41, 14–20. <https://doi.org/10.1016/j.immuni.2014.06.008>
- Neuhöfer, P., Roake, C.M., Kim, S.J., Lu, R.J., West, R.B., Charville, G.W., Artandi, S.E., 2021. Acinar cell clonal expansion in pancreas homeostasis and carcinogenesis. *Nature* 597, 715–719. <https://doi.org/10.1038/s41586-021-03916-2>
- Neuzillet, C., Nicolle, R., Raffenne, J., Tijeras-Raballand, A., Brunel, A., Astorgues-Xerri, L., Vacher, S., Arbateraz, F., Fanjul, M., Hilmi, M., Samain, R., Klein, C., Perraud, A., Rebours, V., Mathonnet, M., Bièche, I., Kocher, H., Cros, J., Bousquet, C., 2022. Periostin- and podoplanin-positive cancer-associated fibroblast subtypes cooperate to shape the inflamed tumor microenvironment in aggressive pancreatic adenocarcinoma. *J Pathol* 258, 408–425. <https://doi.org/10.1002/path.6011>
- Nielsen, S.R., Quaranta, V., Linford, A., Emeagi, P., Rainer, C., Santos, A., Ireland, L., Sakai, T., Sakai, K., Kim, Y.-S., Engle, D., Campbell, F., Palmer, D., Ko, J.H., Tuveson, D.A., Hirsch, E., Mielgo, A., Schmid, M.C., 2016. Macrophage-secreted granulin supports pancreatic cancer metastasis by inducing liver fibrosis. *Nat Cell Biol* 18, 549–560. <https://doi.org/10.1038/ncb3340>

- Northey, J.J., Przybyla, L., Weaver, V.M., 2017. Tissue Force Programs Cell Fate and Tumor Aggression. *Cancer Discov* 7, 1224–1237. <https://doi.org/10.1158/2159-8290.CD-16-0733>
- Nywening, T.M., Wang-Gillam, A., Sanford, D.E., Belt, B.A., Panni, R.Z., Cusworth, B.M., Toriola, A.T., Nieman, R.K., Worley, L.A., Yano, M., Fowler, K.J., Lockhart, A.C., Suresh, R., Tan, B.R., Lim, K.-H., Fields, R.C., Strasberg, S.M., Hawkins, W.G., DeNardo, D.G., Goedegebuure, S.P., Linehan, D.C., 2016. Targeting tumour-associated macrophages with CCR2 inhibition in combination with FOLFIRINOX in patients with borderline resectable and locally advanced pancreatic cancer: a single-centre, open-label, dose-finding, non-randomised, phase 1b trial. *Lancet Oncol* 17, 651–662. [https://doi.org/10.1016/S1470-2045\(16\)00078-4](https://doi.org/10.1016/S1470-2045(16)00078-4)
- Ogawa, Y., Masugi, Y., Abe, T., Yamazaki, K., Ueno, A., Fujii-Nishimura, Y., Hori, S., Yagi, H., Abe, Y., Kitago, M., Sakamoto, M., 2021. Three Distinct Stroma Types in Human Pancreatic Cancer Identified by Image Analysis of Fibroblast Subpopulations and Collagen. *Clinical Cancer Research* 27, 107–119. <https://doi.org/10.1158/1078-0432.CCR-20-2298>
- Öhlund, D., Handly-Santana, A., Biffi, G., Elyada, E., Almeida, A.S., Ponz-Sarvisé, M., Corbo, V., Oni, T.E., Hearn, S.A., Lee, E.J., Chio, I.I.C., Hwang, C.-I., Tiriác, H., Baker, L.A., Engle, D.D., Feig, C., Kultti, A., Egeblad, M., Fearon, D.T., Crawford, J.M., Clevers, H., Park, Y., Tuveson, D.A., 2017. Distinct populations of inflammatory fibroblasts and myofibroblasts in pancreatic cancer. *Journal of Experimental Medicine* 214, 579–596. <https://doi.org/10.1084/jem.20162024>
- Olive, K.P., Jacobetz, M.A., Davidson, C.J., Gopinathan, A., McIntyre, D., Honess, D., Madhu, B., Goldgraben, M.A., Caldwell, M.E., Allard, D., Frese, K.K., Denicola, G., Feig, C., Combs, C., Winter, S.P., Ireland-Zecchini, H., Reichelt, S., Howat, W.J., Chang, A., Dhara, M., Wang, L., Rückert, F., Grützmann, R., Pilarsky, C., Izeradjene, K., Hingorani, S.R., Huang, P., Davies, S.E., Plunkett, W., Egorin, M., Hruban, R.H., Whitebread, N., McGovern, K., Adams, J., Iacobuzio-Donahue, C., Griffiths, J., Tuveson, D.A., 2009. Inhibition of Hedgehog signaling enhances delivery of chemotherapy in a mouse model of pancreatic cancer. *Science* 324, 1457–1461. <https://doi.org/10.1126/science.1171362>
- Onai, N., Obata-Onai, A., Schmid, M.A., Ohteki, T., Jarrossay, D., Manz, M.G., 2007. Identification of clonogenic common Flt3+M-CSFR+ plasmacytoid and conventional dendritic cell progenitors in mouse bone marrow. *Nat Immunol* 8, 1207–1216. <https://doi.org/10.1038/ni1518>
- Oosterhof, N., Chang, I.J., Karimiani, E.G., Kuil, L.E., Jensen, D.M., Daza, R., Young, E., Astle, L., van der Linde, H.C., Shivaram, G.M., Demmers, J., Latimer, C.S., Keene, C.D., Loter, E., Maroofian, R., van Ham, T.J., Hevner, R.F., Bennett, J.T., 2019. Homozygous Mutations in CSF1R Cause a Pediatric-Onset Leukoencephalopathy and Can Result in Congenital Absence of Microglia. *Am J Hum Genet* 104, 936–947. <https://doi.org/10.1016/j.ajhg.2019.03.010>

- Opperman, K.S., Vandyke, K., Clark, K.C., Coulter, E.A., Hewett, D.R., Mrozik, K.M., Schwarz, N., Evdokiou, A., Croucher, P.I., Psaltis, P.J., Noll, J.E., Zannettino, A.C.W., 2019. Clodronate-Liposome Mediated Macrophage Depletion Abrogates Multiple Myeloma Tumor Establishment In Vivo. *Neoplasia* 21, 777–787. <https://doi.org/10.1016/j.neo.2019.05.006>
- O'Reilly, E.M., Oh, D.-Y., Dhani, N., Renouf, D.J., Lee, M.A., Sun, W., Fisher, G., Hezel, A., Chang, S.-C., Vlahovic, G., Takahashi, O., Yang, Y., Fitts, D., Philip, P.A., 2019. Durvalumab With or Without Tremelimumab for Patients With Metastatic Pancreatic Ductal Adenocarcinoma: A Phase 2 Randomized Clinical Trial. *JAMA Oncol* 5, 1431–1438. <https://doi.org/10.1001/jamaoncol.2019.1588>
- Özdemir, B.C., Pentcheva-Hoang, T., Carstens, J.L., Zheng, X., Wu, C.-C., Simpson, T.R., Laklai, H., Sugimoto, H., Kahlert, C., Novitskiy, S.V., De Jesus-Acosta, A., Sharma, P., Heidari, P., Mahmood, U., Chin, L., Moses, H.L., Weaver, V.M., Maitra, A., Allison, J.P., LeBleu, V.S., Kalluri, R., 2014. Depletion of Carcinoma-Associated Fibroblasts and Fibrosis Induces Immunosuppression and Accelerates Pancreas Cancer with Reduced Survival. *Cancer Cell* 25, 719–734. <https://doi.org/10.1016/j.ccr.2014.04.005>
- Padrón, L.J., Maurer, D.M., O'Hara, M.H., O'Reilly, E.M., Wolff, R.A., Wainberg, Z.A., Ko, A.H., Fisher, G., Rahma, O., Lyman, J.P., Cabanski, C.R., Yu, J.X., Pfeiffer, S.M., Spasic, M., Xu, J., Gherardini, P.F., Karakunnel, J., Mick, R., Alanio, C., Byrne, K.T., Hollmann, T.J., Moore, J.S., Jones, D.D., Tognetti, M., Chen, R.O., Yang, X., Salvador, L., Wherry, E.J., Dugan, U., O'Donnell-Tormey, J., Butterfield, L.H., Hubbard-Lucey, V.M., Ibrahim, R., Fairchild, J., Bucktrout, S., LaVallee, T.M., Vonderheide, R.H., 2022. Sotigalimab and/or nivolumab with chemotherapy in first-line metastatic pancreatic cancer: clinical and immunologic analyses from the randomized phase 2 PRINCE trial. *Nat Med* 28, 1167–1177. <https://doi.org/10.1038/s41591-022-01829-9>
- Pagès, F., Mlecnik, B., Marliot, F., Bindea, G., Ou, F.-S., Bifulco, C., Lugli, A., Zlobec, I., Rau, T.T., Berger, M.D., Nagtegaal, I.D., Vink-Börger, E., Hartmann, A., Geppert, C., Kolwelter, J., Merkel, S., Grützmann, R., Van den Eynde, M., Jouret-Mourin, A., Kartheuser, A., Léonard, D., Remue, C., Wang, J.Y., Bavi, P., Roehrl, M.H.A., Ohashi, P.S., Nguyen, L.T., Han, S., MacGregor, H.L., Hafezi-Bakhtiari, S., Wouters, B.G., Masucci, G.V., Andersson, E.K., Zavadova, E., Vocka, M., Spacek, J., Petruzella, L., Konopasek, B., Dunder, P., Skalova, H., Nemejcova, K., Botti, G., Tatangelo, F., Delrio, P., Ciliberto, G., Maio, M., Laghi, L., Grizzi, F., Fredriksen, T., Buttard, B., Angelova, M., Vasaturo, A., Maby, P., Church, S.E., Angell, H.K., Lafontaine, L., Bruni, D., El Sissy, C., Haicheur, N., Kirilovsky, A., Berger, A., Lagorce, C., Meyers, J.P., Paustian, C., Feng, Z., Ballesteros-Merino, C., Dijkstra, J., van de Water, C., van Lent-van Vliet, S., Knijn, N., Muşină, A.-M., Scripcariu, D.-V., Popivanova, B., Xu, M., Fujita, T., Hazama, S., Suzuki, N., Nagano, H., Okuno, K., Torigoe, T., Sato, N., Furuhashi, T., Takemasa, I., Itoh, K., Patel, P.S., Vora, H.H., Shah, B., Patel, J.B., Rajvik,

- K.N., Pandya, S.J., Shukla, S.N., Wang, Y., Zhang, G., Kawakami, Y., Marincola, F.M., Ascierto, P.A., Sargent, D.J., Fox, B.A., Galon, J., 2018. International validation of the consensus Immunoscore for the classification of colon cancer: a prognostic and accuracy study. *The Lancet* 391, 2128–2139. [https://doi.org/10.1016/S0140-6736\(18\)30789-X](https://doi.org/10.1016/S0140-6736(18)30789-X)
- Paget, S., 1889. THE DISTRIBUTION OF SECONDARY GROWTHS IN CANCER OF THE BREAST. *The Lancet*, Originally published as Volume 1, Issue 3421 133, 571–573. [https://doi.org/10.1016/S0140-6736\(00\)49915-0](https://doi.org/10.1016/S0140-6736(00)49915-0)
- Palma, A., Jarrah, A.S., Tieri, P., Cesareni, G., Castiglione, F., 2018. Gene Regulatory Network Modeling of Macrophage Differentiation Corroborates the Continuum Hypothesis of Polarization States. *Frontiers in Physiology* 9.
- Palma, M.D., Venneri, M.A., Galli, R., Sergi, L.S., Politi, L.S., Sampaolesi, M., Naldini, L., 2005. Tie2 identifies a hematopoietic lineage of proangiogenic monocytes required for tumor vessel formation and a mesenchymal population of pericyte progenitors. *Cancer Cell* 8, 211–226. <https://doi.org/10.1016/j.ccr.2005.08.002>
- Pan, Y., Lu, F., Fei, Q., Yu, Xingxing, Xiong, P., Yu, Xunbin, Dang, Y., Hou, Z., Lin, W., Lin, X., Zhang, Z., Pan, M., Huang, H., 2019. Single-cell RNA sequencing reveals compartmental remodeling of tumor-infiltrating immune cells induced by anti-CD47 targeting in pancreatic cancer. *Journal of Hematology & Oncology* 12, 124. <https://doi.org/10.1186/s13045-019-0822-6>
- Patry, M., Teinturier, R., Goehrig, D., Zetu, C., Ripoche, D., Kim, I.-S., Bertolino, P., Hennino, A., 2015.  $\beta$ ig-h3 Represses T-Cell Activation in Type 1 Diabetes. *Diabetes* 64, 4212–4219. <https://doi.org/10.2337/db15-0638>
- Peng, P., Zhu, H., Liu, D., Chen, Z., Zhang, X., Guo, Z., Dong, M., Wan, L., Zhang, P., Liu, G., Zhang, S., Dong, F., Hu, F., Cheng, F., Huang, S., Guo, D., Zhang, B., Yu, X., Wan, F., 2022. TGFBI secreted by tumor-associated macrophages promotes glioblastoma stem cell-driven tumor growth via integrin  $\alpha\beta$ 5- $\text{Src-Stat3}$  signaling. *Theranostics* 12, 4221–4236. <https://doi.org/10.7150/thno.69605>
- Perez, O.A., Yeung, S.T., Vera-Licona, P., Romagnoli, P.A., Samji, T., Ural, B.B., Maher, L., Tanaka, M., Khanna, K.M., 2017. CD169(+) macrophages orchestrate innate immune responses by regulating bacterial localization in the spleen. *Sci. Immunol.* 2, eaah5520. <https://doi.org/10.1126/sciimmunol.aah5520>
- Peto, R., Roe, F.J., Lee, P.N., Levy, L., Clack, J., 1975. Cancer and ageing in mice and men. *Br J Cancer* 32, 411–426. <https://doi.org/10.1038/bjc.1975.242>
- Pishvaian, M.J., Blais, E.M., Brody, J.R., Lyons, E., DeArbeloa, P., Hendifar, A., Mikhail, S., Chung, V., Sahai, V., Sohal, D.P.S., Bellakbira, S., Thach, D., Rahib, L., Madhavan, S., Matrisian, L.M., Petricoin, E.F., 2020. Overall survival in patients with pancreatic cancer receiving matched

- therapies following molecular profiling: a retrospective analysis of the Know Your Tumor registry trial. *Lancet Oncol* 21, 508–518. [https://doi.org/10.1016/S1470-2045\(20\)30074-7](https://doi.org/10.1016/S1470-2045(20)30074-7)
- Pommier, A., Anaparthi, N., Memos, N., Kelley, Z.L., Gouronnet, A., Yan, R., Auffray, C., Albregues, J., Egeblad, M., Iacobuzio-Donahue, C.A., Lyons, S.K., Fearon, D.T., 2018. Unresolved endoplasmic reticulum stress engenders immune-resistant, latent pancreatic cancer metastases. *Science* 360, eaao4908. <https://doi.org/10.1126/science.aao4908>
- Provenzano, P.P., Cuevas, C., Chang, A.E., Goel, V.K., Von Hoff, D.D., Hingorani, S.R., 2012. Enzymatic targeting of the stroma ablates physical barriers to treatment of pancreatic ductal adenocarcinoma. *Cancer Cell* 21, 418–429. <https://doi.org/10.1016/j.ccr.2012.01.007>
- Puleo, F., Nicolle, R., Blum, Y., Cros, J., Marisa, L., Demetter, P., Quertinmont, E., Svrcek, M., Elarouci, N., Iovanna, J., Franchimont, D., Verset, L., Galdon, M.G., Devière, J., de Reyniès, A., Laurent-Puig, P., Van Laethem, J.-L., Bachet, J.-B., Maréchal, R., 2018. Stratification of Pancreatic Ductal Adenocarcinomas Based on Tumor and Microenvironment Features. *Gastroenterology* 155, 1999–2013.e3. <https://doi.org/10.1053/j.gastro.2018.08.033>
- Pylayeva-Gupta, Y., Das, S., Handler, J.S., Hajdu, C.H., Coffre, M., Koralov, S.B., Bar-Sagi, D., 2016. IL35-Producing B Cells Promote the Development of Pancreatic Neoplasia. *Cancer Discovery* 6, 247–255. <https://doi.org/10.1158/2159-8290.CD-15-0843>
- Pyonteck, S.M., Akkari, L., Schuhmacher, A.J., Bowman, R.L., Sevenich, L., Quail, D.F., Olson, O.C., Quick, M.L., Huse, J.T., Teijeiro, V., Setty, M., Leslie, C.S., Oei, Y., Pedraza, A., Zhang, J., Brennan, C.W., Sutton, J.C., Holland, E.C., Daniel, D., Joyce, J.A., 2013. CSF-1R inhibition alters macrophage polarization and blocks glioma progression. *Nat Med* 19, 1264–1272. <https://doi.org/10.1038/nm.3337>
- Pyonteck, S.M., Gadea, B.B., Wang, H.-W., Gocheva, V., Hunter, K.E., Tang, L.H., Joyce, J.A., 2012. Deficiency of the macrophage growth factor CSF-1 disrupts pancreatic neuroendocrine tumor development. *Oncogene* 31, 1459–1467. <https://doi.org/10.1038/onc.2011.337>
- Qian, B.-Z., Li, J., Zhang, H., Kitamura, T., Zhang, J., Campion, L.R., Kaiser, E.A., Snyder, L.A., Pollard, J.W., 2011. CCL2 recruits inflammatory monocytes to facilitate breast-tumour metastasis. *Nature* 475, 222–225. <https://doi.org/10.1038/nature10138>
- Quaranta, V., Rainer, C., Nielsen, S.R., Raymant, M.L., Ahmed, M.S., Engle, D.D., Taylor, A., Murray, T., Campbell, F., Palmer, D.H., Tuveson, D.A., Mielgo, A., Schmid, M.C., 2018. Macrophage-Derived Granulin Drives Resistance to Immune Checkpoint Inhibition in Metastatic Pancreatic Cancer. *Cancer Res* 78, 4253–4269. <https://doi.org/10.1158/0008-5472.CAN-17-3876>
- Rademakers, R., Baker, M., Nicholson, A.M., Rutherford, N.J., Finch, N., Soto-Ortolaza, A., Lash, J., Wider, C., Wojtas, A., DeJesus-Hernandez, M., Adamson, J., Kouri, N., Sundal, C., Shuster, E.A., Aasly, J., MacKenzie, J., Roeber, S., Kretschmar, H.A., Boeve, B.F., Knopman, D.S., Petersen,

- R.C., Cairns, N.J., Ghatti, B., Spina, S., Garbern, J., Tselis, A.C., Uitti, R., Das, P., Van Gerpen, J.A., Meschia, J.F., Levy, S., Broderick, D.F., Graff-Radford, N., Ross, O.A., Miller, B.B., Swerdlow, R.H., Dickson, D.W., Wszolek, Z.K., 2011. Mutations in the colony stimulating factor 1 receptor (CSF1R) gene cause hereditary diffuse leukoencephalopathy with spheroids. *Nat Genet* 44, 200–205. <https://doi.org/10.1038/ng.1027>
- Rahib, L., Wehner, M.R., Matrisian, L.M., Nead, K.T., 2021. Estimated Projection of US Cancer Incidence and Death to 2040. *JAMA Netw Open* 4, e214708. <https://doi.org/10.1001/jamanetworkopen.2021.4708>
- Ramanathan, R.K., McDonough, S.L., Philip, P.A., Hingorani, S.R., Lacy, J., Kortmansky, J.S., Thumar, J., Chiorean, E.G., Shields, A.F., Behl, D., Mehan, P.T., Gaur, R., Seery, T., Guthrie, K.A., Hochster, H.S., 2019. Phase IB/II Randomized Study of FOLFIRINOX Plus Pegylated Recombinant Human Hyaluronidase Versus FOLFIRINOX Alone in Patients With Metastatic Pancreatic Adenocarcinoma: SWOG S1313. *J Clin Oncol* 37, 1062–1069. <https://doi.org/10.1200/JCO.18.01295>
- Razak, A.R., Cleary, J.M., Moreno, V., Boyer, M., Calvo Aller, E., Edenfield, W., Tie, J., Harvey, R.D., Rutten, A., Shah, M.A., Olszanski, A.J., Jäger, D., Lakhani, N., Ryan, D.P., Rasmussen, E., Juan, G., Wong, H., Soman, N., Smit, M.-A.D., Nagorsen, D., Papadopoulos, K.P., 2020. Safety and efficacy of AMG 820, an anti-colony-stimulating factor 1 receptor antibody, in combination with pembrolizumab in adults with advanced solid tumors. *J Immunother Cancer* 8, e001006. <https://doi.org/10.1136/jitc-2020-001006>
- Rice, A.J., Cortes, E., Lachowski, D., Cheung, B.C.H., Karim, S.A., Morton, J.P., del Río Hernández, A., 2017. Matrix stiffness induces epithelial–mesenchymal transition and promotes chemoresistance in pancreatic cancer cells. *Oncogenesis* 6, e352–e352. <https://doi.org/10.1038/oncsis.2017.54>
- Rivera, L.B., Bergers, G., 2013. Location, Location, Location: Macrophage Positioning within Tumors Determines Pro- or Antitumor Activity. *Cancer Cell* 24, 687–689. <https://doi.org/10.1016/j.ccr.2013.11.014>
- Roussel, M., Ferrant, J., Reizine, F., Le Gallou, S., Dulong, J., Carl, S., Lesouhaitier, M., Gregoire, M., Bescher, N., Verdy, C., Latour, M., Bézier, I., Cornic, M., Vinit, A., Monvoisin, C., Sawitzki, B., Leonard, S., Paul, S., Feuillard, J., Jeannet, R., Daix, T., Tiwari, V.K., Tadié, J.M., Cogné, M., Tarte, K., 2021. Comparative immune profiling of acute respiratory distress syndrome patients with or without SARS-CoV-2 infection. *Cell Reports Medicine* 2, 100291. <https://doi.org/10.1016/j.xcrm.2021.100291>
- Royal, R.E., Levy, C., Turner, K., Mathur, A., Hughes, M., Kammula, U.S., Sherry, R.M., Topalian, S.L., Yang, J.C., Lowy, I., Rosenberg, S.A., 2010. Phase 2 trial of single agent Ipilimumab (anti-CTLA-

- 4) for locally advanced or metastatic pancreatic adenocarcinoma. *J Immunother* 33, 828–833.  
<https://doi.org/10.1097/CJI.0b013e3181eec14c>
- Ryschich, E., Nötzel, T., Hinz, U., Autschbach, F., Ferguson, J., Simon, I., Weitz, J., Fröhlich, B., Klar, E., Büchler, M.W., Schmidt, J., 2005. Control of T-cell-mediated immune response by HLA class I in human pancreatic carcinoma. *Clin Cancer Res* 11, 498–504.
- Sanford, D.E., Belt, B.A., Panni, R.Z., Mayer, A., Deshpande, A.D., Carpenter, D., Mitchem, J.B., Plambeck-Suess, S.M., Worley, L.A., Goetz, B.D., Wang-Gillam, A., Eberlein, T.J., Denardo, D.G., Goedegebuure, S.P., Linehan, D.C., 2013. Inflammatory Monocyte Mobilization Decreases Patient Survival in Pancreatic Cancer: A Role for Targeting the CCL2/CCR2 Axis. *Clin. Cancer Res.* 19, 3404–3415. <https://doi.org/10.1158/1078-0432.CCR-13-0525>
- Sano, M., Takahashi, R., Ijichi, H., Ishigaki, K., Yamada, T., Miyabayashi, K., Kimura, G., Mizuno, S., Kato, H., Fujiwara, H., Nakatsuka, T., Tanaka, Y., Kim, J., Masugi, Y., Morishita, Y., Tanaka, M., Ushiku, T., Nakai, Y., Tateishi, K., Ishii, Y., Isayama, H., Moses, H.L., Koike, K., 2021. Blocking VCAM-1 inhibits pancreatic tumour progression and cancer-associated thrombosis/thromboembolism. *Gut* 70, 1713–1723. <https://doi.org/10.1136/gutjnl-2020-320608>
- Sautès-Fridman, C., Petitprez, F., Calderaro, J., Fridman, W.H., 2019. Tertiary lymphoid structures in the era of cancer immunotherapy. *Nat Rev Cancer* 19, 307–325.  
<https://doi.org/10.1038/s41568-019-0144-6>
- Schäfer, M., Werner, S., 2008. Cancer as an overhealing wound: an old hypothesis revisited. *Nat Rev Mol Cell Biol* 9, 628–638. <https://doi.org/10.1038/nrm2455>
- Schorderet, D.F., Menasche, M., Morand, S., Bonnel, S., Büchillier, V., Marchant, D., Auderset, K., Bonny, C., Abitbol, M., Munier, F.L., 2000. Genomic characterization and embryonic expression of the mouse *Bigh3* (*Tgfb1*) gene. *Biochem Biophys Res Commun* 274, 267–274.  
<https://doi.org/10.1006/bbrc.2000.3116>
- Schuh, A.C., Keating, S.J., Monteclaro, F.S., Vogt, P.K., Breitman, M.L., 1990. Obligatory wounding requirement for tumorigenesis in v-jun transgenic mice. *Nature* 346, 756–760.  
<https://doi.org/10.1038/346756a0>
- Schulz, C., Gomez Perdiguero, E., Chorro, L., Szabo-Rogers, H., Cagnard, N., Kierdorf, K., Prinz, M., Wu, B., Jacobsen, S.E.W., Pollard, J.W., Frampton, J., Liu, K.J., Geissmann, F., 2012. A lineage of myeloid cells independent of Myb and hematopoietic stem cells. *Science* 336, 86–90.  
<https://doi.org/10.1126/science.1219179>
- Schuster, S.J., Bishop, M.R., Tam, C.S., Waller, E.K., Borchmann, P., McGuirk, J.P., Jäger, U., Jaglowski, S., Andreadis, C., Westin, J.R., Fleury, I., Bachanova, V., Foley, S.R., Ho, P.J., Mielke, S., Magenau, J.M., Holte, H., Pantano, S., Pacaud, L.B., Awasthi, R., Chu, J., Anak, Ö., Salles, G., Maziarz, R.T., JULIET Investigators, 2019. Tisagenlecleucel in Adult Relapsed or Refractory

- Diffuse Large B-Cell Lymphoma. *N Engl J Med* 380, 45–56.  
<https://doi.org/10.1056/NEJMoa1804980>
- Seifert, L., Werba, G., Tiwari, S., Ly, N.N.G., Allothman, S., Alqunaibit, D., Avanzi, A., Barilla, R., Daley, D., Greco, S.H., Torres-Hernandez, A., Pergamo, M., Ochi, A., Zambirinis, C.P., Pansari, M., Rendon, M., Tippens, D., Hundeyin, M., Mani, V.R., Hajdu, C., Engle, D., Miller, G., 2016. The necrosome promotes pancreatic oncogenesis via CXCL1 and Mincle-induced immune suppression. *Nature* 532, 245–+. <https://doi.org/10.1038/nature17403>
- Shankaran, V., Ikeda, H., Bruce, A.T., White, J.M., Swanson, P.E., Old, L.J., Schreiber, R.D., 2001. IFN $\gamma$  and lymphocytes prevent primary tumour development and shape tumour immunogenicity. *Nature* 410, 1107–1111. <https://doi.org/10.1038/35074122>
- Sherman, M.H., Yu, R.T., Engle, D.D., Ding, N., Atkins, A.R., Tiriach, H., Collisson, E.A., Connor, F., Van Dyke, T., Kozlov, S., Martin, P., Tseng, T.W., Dawson, D.W., Donahue, T.R., Masamune, A., Shimosegawa, T., Apte, M.V., Wilson, J.S., Ng, B., Lau, S.L., Gunton, J.E., Wahl, G.M., Hunter, T., Drebin, J.A., O'Dwyer, P.J., Liddle, C., Tuveson, D.A., Downes, M., Evans, R.M., 2014. Vitamin D Receptor-Mediated Stromal Reprogramming Suppresses Pancreatitis and Enhances Pancreatic Cancer Therapy. *Cell* 159, 80–93. <https://doi.org/10.1016/j.cell.2014.08.007>
- Shi, G., Zhu, L., Sun, Y., Bettencourt, R., Damsz, B., Hruban, R.H., Konieczny, S.F., 2009. Loss of the acinar-restricted transcription factor Mist1 accelerates Kras-induced pancreatic intraepithelial neoplasia. *Gastroenterology* 136, 1368–1378. <https://doi.org/10.1053/j.gastro.2008.12.066>
- Shields, C.W., Evans, M.A., Wang, L.L.-W., Baugh, N., Iyer, S., Wu, D., Zhao, Z., Pusuluri, A., Ukidve, A., Pan, D.C., Mitragotri, S., 2020. Cellular backpacks for macrophage immunotherapy. *Sci Adv* 6, eaaz6579. <https://doi.org/10.1126/sciadv.aaz6579>
- Sierra, J.R., Corso, S., Caione, L., Cepero, V., Conrotto, P., Cignetti, A., Piacibello, W., Kumanogoh, A., Kikutani, H., Comoglio, P.M., Tamagnone, L., Giordano, S., 2008. Tumor angiogenesis and progression are enhanced by Sema4D produced by tumor-associated macrophages. *J Exp Med* 205, 1673–1685. <https://doi.org/10.1084/jem.20072602>
- Skonier, J., Neubauer, M., Madisen, L., Bennett, K., Plowman, G.D., Purchio, A.F., 1992. cDNA cloning and sequence analysis of beta ig-h3, a novel gene induced in a human adenocarcinoma cell line after treatment with transforming growth factor-beta. *DNA Cell Biol* 11, 511–522. <https://doi.org/10.1089/dna.1992.11.511>
- Solis, A.G., Bielecki, P., Steach, H.R., Sharma, L., Harman, C.C.D., Yun, S., de Zoete, M.R., Warnock, J.N., To, S.D.F., York, A.G., Mack, M., Schwartz, M.A., Dela Cruz, C.S., Palm, N.W., Jackson, R., Flavell, R.A., 2019. Mechanosensation of cyclical force by PIEZO1 is essential for innate immunity. *Nature* 573, 69–74. <https://doi.org/10.1038/s41586-019-1485-8>

- Steele, N.G., Carpenter, E.S., Kemp, S.B., Sirihorachai, V.R., The, S., Delrosario, L., Lazarus, J., Amir, E.D., Gunchick, V., Espinoza, C., Bell, S., Harris, L., Lima, F., Irizarry-Negron, V., Paglia, D., Macchia, J., Chu, A.K.Y., Schofield, H., Wamsteker, E.-J., Kwon, R., Schulman, A., Prabhu, A., Law, R., Sondhi, A., Yu, J., Patel, A., Donahue, K., Nathan, H., Cho, C., Anderson, M.A., Sahai, V., Lyssiotis, C.A., Zou, W., Allen, B.L., Rao, A., Crawford, H.C., Bednar, F., Frankel, T.L., Pasca di Magliano, M., 2020. Multimodal mapping of the tumor and peripheral blood immune landscape in human pancreatic cancer. *Nat Cancer* 1, 1097–1112. <https://doi.org/10.1038/s43018-020-00121-4>
- Stein, M., Keshav, S., Harris, N., Gordon, S., 1992. Interleukin 4 potently enhances murine macrophage mannose receptor activity: a marker of alternative immunologic macrophage activation. *J Exp Med* 176, 287–292. <https://doi.org/10.1084/jem.176.1.287>
- Stromnes, I.M., Brockenbrough, J.S., Izeradjene, K., Carlson, M.A., Cuevas, C., Simmons, R.M., Greenberg, P.D., Hingorani, S.R., 2014. Targeted depletion of an MDSC subset unmasks pancreatic ductal adenocarcinoma to adaptive immunity. *Gut* 63, 1769–1781. <https://doi.org/10.1136/gutjnl-2013-306271>
- Su, H., Yang, F., Fu, R., Trinh, B., Sun, N., Liu, J., Kumar, A., Baglieri, J., Siruno, J., Le, M., Li, Y., Dozier, S., Nair, A., Filliol, A., Sinchai, N., Rosenthal, S.B., Santini, J., Metallo, C.M., Molina, A., Schwabe, R.F., Lowy, A.M., Brenner, D., Sun, B., Karin, M., 2022. Collagenolysis-dependent DDR1 signalling dictates pancreatic cancer outcome. *Nature* 610, 366–372. <https://doi.org/10.1038/s41586-022-05169-z>
- Sung, H., Ferlay, J., Siegel, R.L., Laversanne, M., Soerjomataram, I., Jemal, A., Bray, F., 2021. Global Cancer Statistics 2020: GLOBOCAN Estimates of Incidence and Mortality Worldwide for 36 Cancers in 185 Countries. *CA Cancer J Clin* 71, 209–249. <https://doi.org/10.3322/caac.21660>
- Tamoutounour, S., Guilliams, M., Montanana Sanchis, F., Liu, H., Terhorst, D., Malosse, C., Pollet, E., Ardouin, L., Luche, H., Sanchez, C., Dalod, M., Malissen, B., Henri, S., 2013. Origins and functional specialization of macrophages and of conventional and monocyte-derived dendritic cells in mouse skin. *Immunity* 39, 925–938. <https://doi.org/10.1016/j.immuni.2013.10.004>
- Tcymbarevich, I., Richards, S.M., Russo, G., Kühn-Georgijevic, J., Cosin-Roger, J., Baebler, K., Lang, S., Bengs, S., Atrott, K., Bettoni, C., Gruber, S., Frey-Wagner, I., Scharl, M., Misselwitz, B., Wagner, C.A., Seuwen, K., Rogler, G., Ruiz, P.A., Spalinger, M., de Vallière, C., 2019. Lack of the pH-sensing Receptor TDAG8 [GPR65] in Macrophages Plays a Detrimental Role in Murine Models of Inflammatory Bowel Disease. *J Crohns Colitis* 13, 245–258. <https://doi.org/10.1093/ecco-jcc/jjy152>

Thapa, N., Lee, B.-H., Kim, I.-S., 2007. TGF $\beta$ 1/ $\beta$ ig-h3 protein: A versatile matrix molecule induced by TGF- $\beta$ . *The International Journal of Biochemistry & Cell Biology* 39, 2183–2194. <https://doi.org/10.1016/j.biocel.2007.06.004>

Thorsson, Vésteinn, Gibbs, D.L., Brown, S.D., Wolf, D., Bortone, D.S., Yang, T.-H.O., Porta-Pardo, E., Gao, G.F., Plaisier, C.L., Eddy, J.A., Ziv, E., Culhane, A.C., Paull, E.O., Sivakumar, I.K.A., Gentles, A.J., Malhotra, R., Farshidfar, F., Colaprico, A., Parker, J.S., Mose, L.E., Vo, N.S., Liu, Jianfang, Liu, Y., Rader, J., Dhankani, V., Reynolds, S.M., Bowlby, R., Califano, A., Cherniack, A.D., Anastassiou, D., Bedognetti, D., Mokrab, Y., Newman, A.M., Rao, A., Chen, K., Krasnitz, A., Hu, H., Malta, T.M., Noushmehr, H., Pedomallu, C.S., Bullman, S., Ojesina, A.I., Lamb, A., Zhou, W., Shen, H., Choueiri, T.K., Weinstein, J.N., Guinney, J., Saltz, J., Holt, R.A., Rabkin, C.S., Caesar-Johnson, S.J., Demchok, J.A., Felau, I., Kasapi, M., Ferguson, M.L., Hutter, C.M., Sofia, H.J., Tarnuzzer, R., Wang, Z., Yang, L., Zenklusen, J.C., Zhang, J. (Julia), Chudamani, S., Liu, Jia, Lolla, L., Naresh, R., Pihl, T., Sun, Q., Wan, Y., Wu, Y., Cho, J., DeFreitas, T., Frazer, S., Gehlenborg, N., Getz, G., Heiman, D.I., Kim, J., Lawrence, M.S., Lin, P., Meier, S., Noble, M.S., Saksena, G., Voet, D., Zhang, Hailei, Bernard, B., Chambwe, N., Dhankani, V., Knijnenburg, T., Kramer, R., Leinonen, K., Liu, Y., Miller, M., Reynolds, S., Shmulevich, I., Thorsson, Vesteynn, Zhang, W., Akbani, R., Broom, B.M., Hegde, A.M., Ju, Z., Kanchi, R.S., Korkut, A., Li, J., Liang, H., Ling, S., Liu, W., Lu, Y., Mills, G.B., Ng, K.-S., Rao, A., Ryan, M., Wang, Jing, Weinstein, J.N., Zhang, J., Abeshouse, A., Armenia, J., Chakravarty, D., Chatila, W.K., Bruijn, I. de, Gao, J., Gross, B.E., Heins, Z.J., Kundra, R., La, K., Ladanyi, M., Luna, A., Nissan, M.G., Ochoa, A., Phillips, S.M., Reznik, E., Sanchez-Vega, F., Sander, C., Schultz, N., Sheridan, R., Sumer, S.O., Sun, Y., Taylor, B.S., Wang, Jioajiao, Zhang, Hongxin, Anur, P., Peto, M., Spellman, P., Benz, C., Stuart, J.M., Wong, C.K., Yau, C., Hayes, D.N., Parker, J.S., Wilkerson, M.D., Ally, A., Balasundaram, M., Bowlby, R., Brooks, D., Carlsen, R., Chuah, E., Dhalla, N., Holt, R., Jones, S.J.M., Kasaian, K., Lee, D., Ma, Y., Marra, M.A., Mayo, M., Moore, R.A., Mungall, A.J., Mungall, K., Robertson, A.G., Sadeghi, S., Schein, J.E., Sipahimalani, P., Tam, A., Thiessen, N., Tse, K., Wong, T., Berger, A.C., Beroukhi, R., Cherniack, A.D., Cibulskis, C., Gabriel, S.B., Gao, G.F., Ha, G., Meyerson, M., Schumacher, S.E., Shih, J., Kucherlapati, M.H., Kucherlapati, R.S., Baylin, S., Cope, L., Danilova, L., Bootwalla, M.S., Lai, P.H., Maglinte, D.T., Berg, D.J.V.D., Weisenberger, D.J., Auman, J.T., Balu, S., Bodenheimer, T., Fan, C., Hoadley, K.A., Hoyle, A.P., Jefferys, S.R., Jones, C.D., Meng, S., Mieczkowski, P.A., Mose, L.E., Perou, A.H., Perou, C.M., Roach, J., Shi, Y., Simons, J.V., Skelly, T., Soloway, M.G., Tan, D., Veluvolu, U., Fan, H., Hinoue, T., Laird, P.W., Shen, H., Zhou, W., Bellair, M., Chang, K., Covington, K., Creighton, C.J., Dinh, H., Doddapaneni, H., Donehower, L.A., Drummond, J., Gibbs, R.A., Glenn, R., Hale, W., Han, Y., Hu, J., Korchina, V., Lee, S., Lewis, L., Li, W., Liu, X., Morgan, M., Morton, D., Muzny, D., Santibanez, J., Sheth, M., Shinbrot, E.,

Wang, L., Wang, M., Wheeler, D.A., Xi, L., Zhao, F., Hess, J., Appelbaum, E.L., Bailey, M., Cordes, M.G., Ding, L., Fronick, C.C., Fulton, L.A., Fulton, R.S., Kandoth, C., Mardis, E.R., McLellan, M.D., Miller, C.A., Schmidt, H.K., Wilson, R.K., Crain, D., Curley, E., Gardner, J., Lau, K., Mallery, D., Morris, S., Paulauskis, J., Penny, R., Shelton, C., Shelton, T., Sherman, M., Thompson, E., Yena, P., Bowen, J., Gastier-Foster, J.M., Gerken, M., Leraas, K.M., Lichtenberg, T.M., Ramirez, N.C., Wise, L., Zmuda, E., Corcoran, N., Costello, T., Hovens, C., Carvalho, A.L., Carvalho, A.C. de, Fregnani, J.H., Longatto-Filho, A., Reis, R.M., Scapulatempo-Neto, C., Silveira, H.C.S., Vidal, D.O., Burnette, A., Eschbacher, J., Hermes, B., Noss, A., Singh, R., Anderson, M.L., Castro, P.D., Ittmann, M., Huntsman, D., Kohl, B., Le, X., Thorp, R., Andry, C., Duffy, E.R., Lyadov, V., Paklina, O., Setdikova, G., Shabunin, A., Tavobilov, M., McPherson, C., Warnick, R., Berkowitz, R., Cramer, D., Feltmate, C., Horowitz, N., Kibel, A., Muto, M., Raut, C.P., Malykh, A., Barnholtz-Sloan, J.S., Barrett, W., Devine, K., Fulop, J., Ostrom, Q.T., Shimmel, K., Wolinsky, Y., Sloan, A.E., Rose, A.D., Giuliante, F., Goodman, M., Karlan, B.Y., Hagedorn, C.H., Eckman, J., Harr, J., Myers, J., Tucker, K., Zach, L.A., Deyarmin, B., Hu, H., Kvecher, L., Larson, C., Mural, R.J., Somiari, S., Vicha, A., Zelinka, T., Bennett, J., Iacocca, M., Rabeno, B., Swanson, P., Latour, M., Lacombe, L., Têtu, B., Bergeron, A., McGraw, M., Staugaitis, S.M., Chabot, J., Hibshoosh, H., Sepulveda, A., Su, T., Wang, T., Potapova, O., Voronina, O., Desjardins, L., Mariani, O., Roman-Roman, S., Sastre, X., Stern, M.-H., Cheng, F., Signoretti, S., Berchuck, A., Bigner, D., Lipp, E., Marks, J., McCall, S., McLendon, R., Secord, A., Sharp, A., Behera, M., Brat, D.J., Chen, A., Delman, K., Force, S., Khuri, F., Magliocca, K., Maithel, S., Olson, J.J., Owonikoko, T., Pickens, A., Ramalingam, S., Shin, D.M., Sica, G., Meir, E.G.V., Zhang, Hongzheng, Eijckenboom, W., Gillis, A., Korpershoek, E., Looijenga, L., Oosterhuis, W., Stoop, H., Kessel, K.E. van, Zwarthoff, E.C., Calatozzolo, C., Cuppini, L., Cuzzubbo, S., DiMeco, F., Finocchiaro, G., Mattei, L., Perin, A., Pollo, B., Chen, C., Houck, J., Lohavanichbutr, P., Hartmann, A., Stoehr, C., Stoehr, R., Taubert, H., Wach, S., Wullich, B., Kycler, W., Murawa, D., Wiznerowicz, M., Chung, K., Edenfield, W.J., Martin, J., Baudin, E., Bublely, G., Bueno, R., Rienzo, A.D., Richards, W.G., Kalkanis, S., Mikkelsen, T., Noushmehr, H., Scarpacci, L., Girard, N., Aymerich, M., Campo, E., Giné, E., Guillermo, A.L., Bang, N.V., Hanh, P.T., Phu, B.D., Tang, Y., Colman, H., Evason, K., Dottino, P.R., Martignetti, J.A., Gabra, H., Juhl, H., Akeredolu, T., Stepa, S., Hoon, D., Ahn, K., Kang, K.J., Beuschlein, F., Breggia, A., Birrer, M., Bell, D., Borad, M., Bryce, A.H., Castle, E., Chandan, V., Cheville, J., Copland, J.A., Farnell, M., Flotte, T., Giama, N., Ho, T., Kendrick, M., Kocher, J.-P., Kopp, K., Moser, C., Nagorney, D., O'Brien, D., O'Neill, B.P., Patel, T., Petersen, G., Que, F., Rivera, M., Roberts, L., Smallridge, R., Smyrk, T., Stanton, M., Thompson, R.H., Torbenson, M., Yang, J.D., Zhang, L., Brimo, F., Ajani, J.A., Gonzalez, A.M.A., Behrens, C., Bondaruk, J., Broaddus, R., Czerniak, B., Esmali, B., Fujimoto, J., Gershenwald, J., Guo, C., Lazar, A.J.,

Logothetis, C., Meric-Bernstam, F., Moran, C., Ramondetta, L., Rice, D., Sood, A., Tamboli, P., Thompson, T., Troncoso, P., Tsao, A., Wistuba, I., Carter, C., Haydu, L., Hersey, P., Jakrot, V., Kakavand, H., Kefford, R., Lee, K., Long, G., Mann, G., Quinn, M., Saw, R., Scolyer, R., Shannon, K., Spillane, A., Stretch, O., Synott, M., Thompson, J., Wilmott, J., Al-Ahmadie, H., Chan, T.A., Ghossein, R., Gopalan, A., Levine, D.A., Reuter, V., Singer, S., Singh, B., Tien, N.V., Broudy, T., Mirsaidi, C., Nair, P., Drwiega, P., Miller, J., Smith, J., Zaren, H., Park, J.-W., Hung, N.P., Kebebew, E., Linehan, W.M., Metwalli, A.R., Pacak, K., Pinto, P.A., Schiffman, M., Schmidt, L.S., Vocke, C.D., Wentzensen, N., Worrell, R., Yang, H., Moncrieff, M., Goparaju, C., Melamed, J., Pass, H., Botnariuc, N., Caraman, I., Cernat, M., Chemencedji, I., Clipca, A., Doruc, S., Gorincioi, G., Mura, S., Pirtac, M., Stancul, I., Tcaciuc, D., Albert, M., Alexopoulou, I., Arnaout, A., Bartlett, J., Engel, J., Gilbert, S., Parfitt, J., Sekhon, H., Thomas, G., Rassl, D.M., Rintoul, R.C., Bifulco, C., Tamakawa, R., Urba, W., Hayward, N., Timmers, H., Antenucci, A., Facciolo, F., Grazi, G., Marino, M., Merola, R., Krijger, R. de, Gimenez-Roqueplo, A.-P., Piché, A., Chevalier, S., McKercher, G., Birsoy, K., Barnett, G., Brewer, C., Farver, C., Naska, T., Pennell, N.A., Raymond, D., Schilero, C., Smolenski, K., Williams, F., Morrison, C., Borgia, J.A., Liptay, M.J., Pool, M., Seder, C.W., Junker, K., Omberg, L., Dinkin, M., Manikhas, G., Alvaro, D., Bragazzi, M.C., Cardinale, V., Carpino, G., Gaudio, E., Chesla, D., Cottingham, S., Dubina, M., Moiseenko, F., Dhanasekaran, R., Becker, K.-F., Janssen, K.-P., Slotta-Huspenina, J., Abdel-Rahman, M.H., Aziz, D., Bell, S., Cebulla, C.M., Davis, A., Duell, R., Elder, J.B., Hilty, J., Kumar, B., Lang, J., Lehman, N.L., Mandt, R., Nguyen, P., Pilarski, R., Rai, K., Schoenfield, L., Senecal, K., Wakely, P., Hansen, P., Lechan, R., Powers, J., Tischler, A., Grizzle, W.E., Sexton, K.C., Kastl, A., Henderson, J., Porten, S., Waldmann, J., Fassnacht, M., Asa, S.L., Schadendorf, D., Couce, M., Graefen, M., Huland, H., Sauter, G., Schlomm, T., Simon, R., Tennstedt, P., Olabode, O., Nelson, M., Bathe, O., Carroll, P.R., Chan, J.M., Disaia, P., Glenn, P., Kelley, R.K., Landen, C.N., Phillips, J., Prados, M., Simko, J., Smith-McCune, K., VandenBerg, S., Roggin, K., Fehrenbach, A., Kendler, A., Sifri, S., Steele, R., Jimeno, A., Carey, F., Forgie, I., Mannelli, M., Carney, M., Hernandez, B., Campos, B., Herold-Mende, C., Jungk, C., Unterberg, A., Deimling, A. von, Bossler, A., Galbraith, J., Jacobus, L., Knudson, M., Knutson, T., Ma, D., Milhem, M., Sigmund, R., Godwin, A.K., Madan, R., Rosenthal, H.G., Adebamowo, C., Adebamowo, S.N., Boussioutas, A., Beer, D., Giordano, T., Mes-Masson, A.-M., Saad, F., Bocklage, T., Landrum, L., Mannel, R., Moore, K., Moxley, K., Postier, R., Walker, J., Zuna, R., Feldman, M., Valdivieso, F., Dhir, R., Luketich, J., Pinero, E.M.M., Quintero-Aguilo, M., Carlotti, C.G., Santos, J.S.D., Kemp, R., Sankarankuty, A., Tirapelli, D., Catto, J., Agnew, K., Swisher, E., Creaney, J., Robinson, B., Shelley, C.S., Godwin, E.M., Kendall, S., Shipman, C., Bradford, C., Carey, T., Haddad, A., Moyer, J., Peterson, L., Prince, M., Rozek, L., Wolf, G., Bowman, R., Fong, K.M., Yang, I., Korst, R., Rathmell, W.K., Fantacone-

- Campbell, J.L., Hooke, J.A., Kovatich, A.J., Shriver, C.D., DiPersio, J., Drake, B., Govindan, R., Heath, S., Ley, T., Tine, B.V., Westervelt, P., Rubin, M.A., Lee, J.I., Aredes, N.D., Mariamidze, A., Lazar, A.J., Serody, J.S., Demicco, E.G., Disis, M.L., Vincent, B.G., Shmulevich, I., 2018. The Immune Landscape of Cancer. *Immunity* 48, 812-830.e14. <https://doi.org/10.1016/j.immuni.2018.03.023>
- Tian, C., Clauser, K.R., Öhlund, D., Rickelt, S., Huang, Y., Gupta, M., Mani, D.R., Carr, S.A., Tuveson, D.A., Hynes, R.O., 2019. Proteomic analyses of ECM during pancreatic ductal adenocarcinoma progression reveal different contributions by tumor and stromal cells. *Proc Natl Acad Sci U S A* 116, 19609–19618. <https://doi.org/10.1073/pnas.1908626116>
- Tian, H., Callahan, C.A., DuPree, K.J., Darbonne, W.C., Ahn, C.P., Scales, S.J., de Sauvage, F.J., 2009. Hedgehog signaling is restricted to the stromal compartment during pancreatic carcinogenesis. *Proc Natl Acad Sci U S A* 106, 4254–4259. <https://doi.org/10.1073/pnas.0813203106>
- Toda, G., Yamauchi, T., Kadowaki, T., Ueki, K., 2021. Preparation and culture of bone marrow-derived macrophages from mice for functional analysis. *STAR Protocols* 2, 100246. <https://doi.org/10.1016/j.xpro.2020.100246>
- Toole, B.P., 2004. Hyaluronan: from extracellular glue to pericellular cue. *Nat Rev Cancer* 4, 528–539. <https://doi.org/10.1038/nrc1391>
- Tsai, C.-H., Chuang, Y.-M., Li, X., Yu, Y.-R., Tzeng, S.-F., Teoh, S.T., Lindblad, K.E., Di Matteo, M., Cheng, W.-C., Hsueh, P.-C., Kao, K.-C., Imrichova, H., Duan, L., Gallart-Ayala, H., Hsiao, P.-W., Mazzone, M., Ivanesevic, J., Liu, X., de Visser, K.E., Lujambio, A., Lunt, S.Y., Kaech, S.M., Ho, P.-C., 2023. Immunoediting instructs tumor metabolic reprogramming to support immune evasion. *Cell Metabolism* 35, 118-133.e7. <https://doi.org/10.1016/j.cmet.2022.12.003>
- Tu, M., Klein, L., Espinet, E., Georgomanolis, T., Wegwitz, F., Li, X., Urbach, L., Danieli-Mackay, A., Küffer, S., Bojarczuk, K., Mizi, A., Günesdogan, U., Chapuy, B., Gu, Z., Neesse, A., Kishore, U., Ströbel, P., Hessmann, E., Hahn, S.A., Trumpp, A., Papantonis, A., Ellenrieder, V., Singh, S.K., 2021. TNF- $\alpha$ -producing macrophages determine subtype identity and prognosis via AP1 enhancer reprogramming in pancreatic cancer. *Nat Cancer* 2, 1185–1203. <https://doi.org/10.1038/s43018-021-00258-w>
- Turaga, R.C., Sharma, M., Mishra, F., Krasinskas, A., Yuan, Y., Yang, J.J., Wang, S., Liu, C., Li, S., Liu, Z.-R., 2021. Modulation of Cancer-Associated Fibrotic Stroma by An Integrin  $\alpha\beta3$  Targeting Protein for Pancreatic Cancer Treatment. *Cell Mol Gastroenterol Hepatol* 11, 161–179. <https://doi.org/10.1016/j.jcmgh.2020.08.004>
- Ural, B.B., Yeung, S.T., Damani-Yokota, P., Devlin, J.C., de Vries, M., Vera-Licona, P., Samji, T., Sawai, C.M., Jang, G., Perez, O.A., Pham, Q., Maher, L., Loke, P., Dittmann, M., Reizis, B., Khanna, K.M., 2020. Identification of a nerve-associated, lung-resident interstitial macrophage subset with

- distinct localization and immunoregulatory properties. *Sci Immunol* 5, eaax8756. <https://doi.org/10.1126/sciimmunol.aax8756>
- Van Cutsem, E., Tempero, M.A., Sigal, D., Oh, D.-Y., Fazio, N., Macarulla, T., Hitre, E., Hammel, P., Hendifar, A.E., Bates, S.E., Li, C.-P., Hingorani, S.R., de la Fouchardiere, C., Kasi, A., Heinemann, V., Maraveyas, A., Bahary, N., Layos, L., Sahai, V., Zheng, L., Lacy, J., Park, J.O., Portales, F., Oberstein, P., Wu, W., Chondros, D., Bullock, A.J., HALO 109-301 Investigators, 2020. Randomized Phase III Trial of Pegvorhyaluronidase Alfa With Nab-Paclitaxel Plus Gemcitabine for Patients With Hyaluronan-High Metastatic Pancreatic Adenocarcinoma. *J Clin Oncol* 38, 3185–3194. <https://doi.org/10.1200/JCO.20.00590>
- van Dinther, D., Veninga, H., Iborra, S., Borg, E.G.F., Hoogterp, L., Olesek, K., Beijer, M.R., Schetters, S.T.T., Kalay, H., Garcia-Vallejo, J.J., Franken, K.L., Cham, L.B., Lang, K.S., van Kooyk, Y., Sancho, D., Crocker, P.R., den Haan, J.M.M., 2018. Functional CD169 on Macrophages Mediates Interaction with Dendritic Cells for CD8(+) T Cell Cross-Priming. *Cell Reports* 22, 1484–1495. <https://doi.org/10.1016/j.celrep.2018.01.021>
- van Furth, R., Cohn, Z.A., Hirsch, J.G., Humphrey, J.H., Spector, W.G., Langevoort, H.L., 1972. The mononuclear phagocyte system: a new classification of macrophages, monocytes, and their precursor cells. *Bull World Health Organ* 46, 845–852.
- Vantourout, P., Hayday, A., 2013. Six-of-the-best: unique contributions of  $\gamma\delta$  T cells to immunology. *Nat Rev Immunol* 13, 88–100. <https://doi.org/10.1038/nri3384>
- von Figura, G., Morris, J.P., Wright, C.V.E., Hebrok, M., 2014. Nr5a2 maintains acinar cell differentiation and constrains oncogenic Kras-mediated pancreatic neoplastic initiation. *Gut* 63, 656–664. <https://doi.org/10.1136/gutjnl-2012-304287>
- Von Hoff, D.D., Ervin, T., Arena, F.P., Chiorean, E.G., Infante, J., Moore, M., Seay, T., Tjulandin, S.A., Ma, W.W., Saleh, M.N., Harris, M., Reni, M., Dowden, S., Laheru, D., Bahary, N., Ramanathan, R.K., Taberero, J., Hidalgo, M., Goldstein, D., Van Cutsem, E., Wei, X., Iglesias, J., Renschler, M.F., 2013. Increased survival in pancreatic cancer with nab-paclitaxel plus gemcitabine. *N Engl J Med* 369, 1691–1703. <https://doi.org/10.1056/NEJMoa1304369>
- Wainberg, Z.A., Hochster, H.S., Kim, E.J., George, B., Kaylan, A., Chiorean, E.G., Waterhouse, D.M., Guitierrez, M., Parikh, A., Jain, R., Carrizosa, D.R., Soliman, H.H., Lila, T., Reiss, D.J., Pierce, D.W., Bhore, R., Banerjee, S., Lyons, L., Louis, C.U., Ong, T.J., O'Dwyer, P.J., 2020. Open-label, Phase I Study of Nivolumab Combined with nab-Paclitaxel Plus Gemcitabine in Advanced Pancreatic Cancer. *Clin Cancer Res* 26, 4814–4822. <https://doi.org/10.1158/1078-0432.CCR-20-0099>
- Wang, H., Liu, J., Xia, G., Lei, S., Huang, Xiuyan, Huang, Xinyu, 2020. Survival of pancreatic cancer patients is negatively correlated with age at diagnosis: a population-based retrospective study. *Sci Rep* 10, 7048. <https://doi.org/10.1038/s41598-020-64068-3>

- Ween, M.P., Oehler, M.K., Ricciardelli, C., 2012. Transforming Growth Factor-Beta-Induced Protein (TGFBI)/( $\beta$ ig-H3): A Matrix Protein with Dual Functions in Ovarian Cancer. *International Journal of Molecular Sciences* 13, 10461–10477. <https://doi.org/10.3390/ijms130810461>
- Wei, D., Wang, L., Yan, Y., Jia, Z., Gagea, M., Li, Z., Zuo, X., Kong, X., Huang, S., Xie, K., 2016. KLF4 Is Essential for Induction of Cellular Identity Change and Acinar-to-Ductal Reprogramming during Early Pancreatic Carcinogenesis. *Cancer Cell* 29, 324–338. <https://doi.org/10.1016/j.ccell.2016.02.005>
- Williams, H.L., Dias Costa, A., Zhang, J., Raghavan, S., Winter, P.S., Kapner, K.S., Ginebaugh, S.P., Väyrynen, S.A., Väyrynen, J.P., Yuan, C., Navia, A.W., Wang, Junning, Yang, A., Bosse, T.L., Kalekar, R.L., Lowder, K.E., Lau, M.C., Elganainy, D., Morales-Oyarvide, V., Rubinson, D.A., Singh, H., Perez, K., Cleary, J.M., Clancy, T.E., Wang, Jiping, Mancias, J.D., Brais, L.K., Hill, E.R., Kozak, M.M., Linehan, D.C., Dunne, R.F., Chang, D.T., Koong, A.C., Hezel, A.F., Hahn, W.C., Shalek, A.K., Aguirre, A.J., Nowak, J.A., Wolpin, B.M., 2023. Spatially Resolved Single-Cell Assessment of Pancreatic Cancer Expression Subtypes Reveals Co-expressor Phenotypes and Extensive Intratumoral Heterogeneity. *Cancer Research* 83, 441–455. <https://doi.org/10.1158/0008-5472.CAN-22-3050>
- Wouters, M.C.A., Nelson, B.H., 2018. Prognostic Significance of Tumor-Infiltrating B Cells and Plasma Cells in Human Cancer. *Clinical Cancer Research* 24, 6125–6135. <https://doi.org/10.1158/1078-0432.CCR-18-1481>
- Yamamoto, K., Venida, A., Yano, J., Biancur, D.E., Kakiuchi, M., Gupta, S., Sohn, A.S.W., Mukhopadhyay, S., Lin, E.Y., Parker, S.J., Banh, R.S., Paulo, J.A., Wen, K.W., Debnath, J., Kim, G.E., Mancias, J.D., Fearon, D.T., Perera, R.M., Kimmelman, A.C., 2020. Autophagy promotes immune evasion of pancreatic cancer by degrading MHC-I. *Nature* 581, 100–105. <https://doi.org/10.1038/s41586-020-2229-5>
- Yáñez, A., Coetzee, S.G., Olsson, A., Muench, D.E., Berman, B.P., Hazelett, D.J., Salomonis, N., Grimes, H.L., Goodridge, H.S., 2017. Granulocyte-monocyte progenitors and monocyte-dendritic cell progenitors independently produce functionally distinct monocytes. *Immunity* 47, 890-902.e4. <https://doi.org/10.1016/j.immuni.2017.10.021>
- Yang, L., Cui, R., Li, Y., Liang, K., Ni, M., Gu, Y., 2020. Hypoxia-Induced TGFBI as a Serum Biomarker for Laboratory Diagnosis and Prognosis in Patients with Pancreatic Ductal Adenocarcinoma. *Lab Med* 51, 352–361. <https://doi.org/10.1093/labmed/lmz063>
- Zaghdoudi, S., Decaup, E., Belhabib, I., Samain, R., Cassant-Sourdy, S., Rochotte, J., Brunel, A., Schlaepfer, D., Cros, J., Neuzillet, C., Strehaiano, M., Alard, A., Tomasini, R., Rajeeve, V., Perraud, A., Mathonnet, M., Pearce, O.M., Martineau, Y., Pyronnet, S., Bousquet, C., Jean, C., 2020. FAK activity in cancer-associated fibroblasts is a prognostic marker and a druggable key

- metastatic player in pancreatic cancer. *EMBO Molecular Medicine* 12, e12010. <https://doi.org/10.15252/emmm.202012010>
- Zeisberg, E.M., Potenta, S., Xie, L., Zeisberg, M., Kalluri, R., 2007. Discovery of endothelial to mesenchymal transition as a source for carcinoma-associated fibroblasts. *Cancer Res* 67, 10123–10128. <https://doi.org/10.1158/0008-5472.CAN-07-3127>
- Zeng, X., Wei, Y.-L., Huang, J., Newell, E.W., Yu, H., Kidd, B.A., Kuhns, M.S., Waters, R.W., Davis, M.M., Weaver, C.T., Chien, Y., 2012.  $\gamma\delta$  T cells recognize a microbial encoded B cell antigen to initiate a rapid antigen-specific interleukin-17 response. *Immunity* 37, 524–534. <https://doi.org/10.1016/j.immuni.2012.06.011>
- Zhang, F., Parayath, N.N., Ene, C.I., Stephan, S.B., Koehne, A.L., Coon, M.E., Holland, E.C., Stephan, M.T., 2019. Genetic programming of macrophages to perform anti-tumor functions using targeted mRNA nanocarriers. *Nat Commun* 10, 3974. <https://doi.org/10.1038/s41467-019-11911-5>
- Zhang, H., Liu, J., Sun, Y., Huang, J., Qi, H., Shao, R., Wu, Q., Jiang, Q., Fu, R., Liu, Q., Jin, H., 2023. Nestin+ Mesenchymal Stromal Cells Fibrotic Transition Mediated by CD169+ Macrophages in Bone Marrow Chronic Graft-versus-Host Disease. *The Journal of Immunology* ji2200558. <https://doi.org/10.4049/jimmunol.2200558>
- Zhang, Y., Lazarus, J., Steele, N.G., Yan, W., Lee, H.-J., Nwosu, Z.C., Halbrook, C.J., Menjivar, R.E., Kemp, S.B., Sirihorachai, V.R., Velez-Delgado, A., Donahue, K., Carpenter, E.S., Brown, K.L., Irizarry-Negron, V., Nevison, A.C., Vinta, A., Anderson, M.A., Crawford, H.C., Lyssiotis, C.A., Frankel, T.L., Bednar, F., Pasca di Magliano, M., 2020. Regulatory T-cell Depletion Alters the Tumor Microenvironment and Accelerates Pancreatic Carcinogenesis. *Cancer Discov* 10, 422–439. <https://doi.org/10.1158/2159-8290.CD-19-0958>
- Zhang, Y., Li, J.-Q., Jiang, Z.-Z., Li, L., Wu, Y., Zheng, L., 2016. CD169 identifies an anti-tumour macrophage subpopulation in human hepatocellular carcinoma. *J. Pathol.* 239, 231–241. <https://doi.org/10.1002/path.4720>
- Zhang, Y., Velez-Delgado, A., Mathew, E., Li, D., Mendez, F.M., Flannagan, K., Rhim, A.D., Simeone, D.M., Beatty, G.L., Pasca di Magliano, M., 2017. Myeloid cells are required for PD-1/PD-L1 checkpoint activation and the establishment of an immunosuppressive environment in pancreatic cancer. *Gut* 66, 124–136. <https://doi.org/10.1136/gutjnl-2016-312078>
- Zhen, D.B., Whittle, M., Ritch, P.S., Hochster, H.S., Coveler, A.L., George, B., Hendifar, A.E., Dragovich, T., Green, S., Dion, B., Stoll-D’Astice, A.C., Lee, A., Thorsen, S.M., Rosenthal, A., Hingorani, S.R., Chiorean, E.G., 2022. Phase II study of PEGPH20 plus pembrolizumab for patients (pts) with hyaluronan (HA)-high refractory metastatic pancreatic adenocarcinoma (mPC): PCRT16-001. *JCO* 40, 576–576. [https://doi.org/10.1200/JCO.2022.40.4\\_suppl.576](https://doi.org/10.1200/JCO.2022.40.4_suppl.576)

- Zhou, X., Franklin, R.A., Adler, M., Jacox, J.B., Bailis, W., Shyer, J.A., Flavell, R.A., Mayo, A., Alon, U., Medzhitov, R., 2018. Circuit Design Features of a Stable Two-Cell System. *Cell* 172, 744-757.e17. <https://doi.org/10.1016/j.cell.2018.01.015>
- Zhu, Y., Herndon, J.M., Sojka, D.K., Kim, K.-W., Knolhoff, B.L., Zuo, C., Cullinan, D.R., Luo, J., Bearden, A.R., Lavine, K.J., Yokoyama, W.M., Hawkins, W.G., Fields, R.C., Randolph, G.J., DeNardo, D.G., 2017. Tissue-Resident Macrophages in Pancreatic Ductal Adenocarcinoma Originate from Embryonic Hematopoiesis and Promote Tumor Progression. *Immunity* 47, 323-338.e6. <https://doi.org/10.1016/j.immuni.2017.07.014>
- Zhu, Y., Knolhoff, B.L., Meyer, M.A., Nywening, T.M., West, B.L., Luo, J., Wang-Gillam, A., Goedegebuure, S.P., Linehan, D.C., DeNardo, D.G., 2014. CSF1/CSF1R blockade reprograms tumor-infiltrating macrophages and improves response to T-cell checkpoint immunotherapy in pancreatic cancer models. *Cancer Res* 74, 5057–5069. <https://doi.org/10.1158/0008-5472.CAN-13-3723>
- Zitvogel, L., Perreault, C., Finn, O.J., Kroemer, G., 2021. Beneficial autoimmunity improves cancer prognosis. *Nat Rev Clin Oncol* 18, 591–602. <https://doi.org/10.1038/s41571-021-00508-x>
- Zuo, C., Baer, J.M., Knolhoff, B.L., Belle, J.I., Liu, X., Alarcon De La Lastra, A., Fu, C., Hogg, G.D., Kingston, N.L., Breden, M.A., Dodhiawala, P.B., Zhou, D.C., Lander, V.E., James, C.A., Ding, L., Lim, K.-H., Fields, R.C., Hawkins, W.G., Weber, J.D., Zhao, G., DeNardo, D.G., 2023. Stromal and therapy-induced macrophage proliferation promotes PDAC progression and susceptibility to innate immunotherapy. *Journal of Experimental Medicine* 220, e20212062. <https://doi.org/10.1084/jem.20212062>